

A11103 070622

NAT'L INST OF STANDARDS & TECH R.I.C.



A1103070622

Informal Conference / 12th Informal Confe
QC100 .U57 NO.526, 1978 C.2 NBS-PUB-C 19



NBS SPECIAL PUBLICATION 526

U.S. DEPARTMENT OF COMMERCE / National Bureau of Standards

12th Informal Conference on Photochemistry

QC
100
U57
NO.526
1978
C.2

NATIONAL BUREAU OF STANDARDS

The National Bureau of Standards¹ was established by an act of Congress March 3, 1901. The Bureau's overall goal is to strengthen and advance the Nation's science and technology and facilitate their effective application for public benefit. To this end, the Bureau conducts research and provides: (1) a basis for the Nation's physical measurement system, (2) scientific and technological services for industry and government, (3) a technical basis for equity in trade, and (4) technical services to promote public safety. The Bureau's technical work is performed by the National Measurement Laboratory, the National Engineering Laboratory, and the Institute for Computer Sciences and Technology.

THE NATIONAL MEASUREMENT LABORATORY provides the national system of physical and chemical and materials measurement; coordinates the system with measurement systems of other nations and furnishes essential services leading to accurate and uniform physical and chemical measurement throughout the Nation's scientific community, industry, and commerce; conducts materials research leading to improved methods of measurement, standards, and data on the properties of materials needed by industry, commerce, educational institutions, and Government; provides advisory and research services to other Government Agencies; develops, produces, and distributes Standard Reference Materials; and provides calibration services. The Laboratory consists of the following centers:

Absolute Physical Quantities² — Radiation Research — Thermodynamics and Molecular Science — Analytical Chemistry — Materials Science.

THE NATIONAL ENGINEERING LABORATORY provides technology and technical services to users in the public and private sectors to address national needs and to solve national problems in the public interest; conducts research in engineering and applied science in support of objectives in these efforts; builds and maintains competence in the necessary disciplines required to carry out this research and technical service; develops engineering data and measurement capabilities; provides engineering measurement traceability services; develops test methods and proposes engineering standards and code changes; develops and proposes new engineering practices; and develops and improves mechanisms to transfer results of its research to the ultimate user. The Laboratory consists of the following centers:

Applied Mathematics — Electronics and Electrical Engineering² — Mechanical Engineering and Process Technology² — Building Technology — Fire Research — Consumer Product Technology — Field Methods.

THE INSTITUTE FOR COMPUTER SCIENCES AND TECHNOLOGY conducts research and provides scientific and technical services to aid Federal Agencies in the selection, acquisition, application, and use of computer technology to improve effectiveness and economy in Government operations in accordance with Public Law 89-306 (40 U.S.C. 759), relevant Executive Orders, and other directives; carries out this mission by managing the Federal Information Processing Standards Program, developing Federal ADP standards guidelines, and managing Federal participation in ADP voluntary standardization activities; provides scientific and technological advisory services and assistance to Federal Agencies; and provides the technical foundation for computer-related policies of the Federal Government. The Institute consists of the following divisions:

Systems and Software — Computer Systems Engineering — Information Technology.

¹Headquarters and Laboratories at Gaithersburg, Maryland, unless otherwise noted; mailing address Washington, D.C. 20234.

²Some divisions within the center are located at Boulder, Colorado, 80303.

OCT 18 1978

NBS 526 - ARC

12th Informal Conference on Photochemistry

Special Publication

NBS 526

U.S.A.

NBS 526

10-78

L 2

Proceedings of the
12th Informal Conference on Photochemistry
Held at the National Bureau of Standards
Gaithersburg, Maryland

June 28-July 1, 1976

Edited by

Michael J. Kurylo

and

Walter Braun

Center for Thermodynamics and Molecular Science
National Measurement Laboratory
National Bureau of Standards
Washington, D.C. 20234

Sponsored by

National Bureau of Standards
Department of Transportation
Department of Energy
National Science Foundation



U.S. DEPARTMENT OF COMMERCE, Juanita M. Kreps, Secretary

Dr. Sidney Harman, Under Secretary

Jordan J. Baruch, Assistant Secretary for Science and Technology

US NATIONAL BUREAU OF STANDARDS, Ernest Ambler, Director

Issued October 1978

NATIONAL BUREAU OF STANDARDS

The National Bureau of Standards¹ was established by an act of Congress March 3, 1901. The Bureau's overall goal is to strengthen and advance the Nation's science and technology and facilitate their effective application for public benefit. To this end, the Bureau conducts research and provides: (1) a basis for the Nation's physical measurement system, (2) scientific and technological services for industry and government, (3) a technical basis for equity in trade, and (4) technical services to promote public safety. The Bureau's technical work is performed by the National Measurement Laboratory, the National Engineering Laboratory, and the Institute for Computer Sciences and Technology.

THE NATIONAL MEASUREMENT LABORATORY provides the national system of physical and chemical and materials measurement; coordinates the system with measurement systems of other nations and furnishes essential services leading to accurate and uniform physical and chemical measurement throughout the Nation's scientific community, industry, and commerce; conducts materials research leading to improved methods of measurement, standards, and data on the properties of materials needed by industry, commerce, educational institutions, and Government; provides advisory and research services to other Government Agencies; develops, produces, and distributes Standard Reference Materials; and provides calibration services. The Laboratory consists of the following centers:

Absolute Physical Quantities² — Radiation Research — Thermodynamics and Molecular Science — Analytical Chemistry — Materials Science.

THE NATIONAL ENGINEERING LABORATORY provides technology and technical services to users in the public and private sectors to address national needs and to solve national problems in the public interest; conducts research in engineering and applied science in support of objectives in these efforts; builds and maintains competence in the necessary disciplines required to carry out this research and technical service; develops engineering data and measurement capabilities; provides engineering measurement traceability services; develops test methods and proposes engineering standards and code changes; develops and proposes new engineering practices; and develops and improves mechanisms to transfer results of its research to the ultimate user. The Laboratory consists of the following centers:

Applied Mathematics — Electronics and Electrical Engineering² — Mechanical Engineering and Process Technology² — Building Technology — Fire Research — Consumer Product Technology — Field Methods.

THE INSTITUTE FOR COMPUTER SCIENCES AND TECHNOLOGY conducts research and provides scientific and technical services to aid Federal Agencies in the selection, acquisition, application, and use of computer technology to improve effectiveness and economy in Government operations in accordance with Public Law 89-306 (40 U.S.C. 759), relevant Executive Orders, and other directives; carries out this mission by managing the Federal Information Processing Standards Program, developing Federal ADP standards guidelines, and managing Federal participation in ADP voluntary standardization activities; provides scientific and technological advisory services and assistance to Federal Agencies; and provides the technical foundation for computer-related policies of the Federal Government. The Institute consists of the following divisions:

Systems and Software — Computer Systems Engineering — Information Technology.

¹Headquarters and Laboratories at Gaithersburg, Maryland, unless otherwise noted; mailing address Washington, D.C. 20234.

²Some divisions within the center are located at Boulder, Colorado, 80303.

OCT 18 1978

12th Informal Conference on Photochemistry

Special Publication

NO. 526

Proceedings of the
12th Informal Conference on Photochemistry
Held at the National Bureau of Standards
Gaithersburg, Maryland

June 28-July 1, 1976

Edited by

Michael J. Kurylo

and

Walter Braun

Center for Thermodynamics and Molecular Science
National Measurement Laboratory
National Bureau of Standards
Washington, D.C. 20234

Sponsored by

National Bureau of Standards
Department of Transportation
Department of Energy
National Science Foundation



U.S. DEPARTMENT OF COMMERCE, Juanita M. Kreps, Secretary

Dr. Sidney Harman, Under Secretary

Jordan J. Baruch, Assistant Secretary for Science and Technology

US NATIONAL BUREAU OF STANDARDS, Ernest Ambler, Director

Issued October 1978

Library of Congress Catalog Card Number: 78-600105

National Bureau of Standards Special Publication 526

Nat. Bur. Stand. (U.S.), Spec. Publ. 526, 411 pages (Oct. 1978)

CODEN: XNBSAV

U.S. GOVERNMENT PRINTING OFFICE
WASHINGTON: 1978

ABSTRACT

The 12th Informal Conference on Photochemistry was held at the National Bureau of Standards Laboratories in Gaithersburg, Maryland, from June 28-July 1, 1976. Nearly 300 members of the international scientific community attended the 123 individual research papers presented. Extended abstracts of these presentations (many revised after the Conference) comprise the present proceedings. The wide range of highly specialized topics include Environmental Chemistry (both Photochemical Smog and Upper Atmosphere/Ozone Layer), Laser Photochemistry, Photochemical Isotope Separation, Photochemical Conversion of Solar Energy, Actinometric and Radiometric Measurements, Chemiluminescent Processes, Primary Photochemical and Photophysical Processes, Inorganic Photochemistry, and Elementary Reaction Processes.

Key words: Chemical kinetics; energy transfer; fluorescence; lasers; photochemistry; solar energy; spectra

CONTENTS

<u>Section</u>	<u>Page</u>
Abstract	iii
M. J. Kurylo and W. Braun	
SESSION A: ACTINOMETRIC AND RADIOMETRIC MEASUREMENT	
A Modern Approach to Accurate Radiometry	1
E. Zalewski	
Temperature Dependence of the Fluorescence Quantum Yields of Rhodamine Derivatives	3
R. E. Schwerzel and N. E. Klosterman	
NBS Ultraviolet Radiometric Standards	5
W. R. Ott	
New Methods of Measuring Light Intensities	8
D. G. Taylor, J. N. Demas, W. D. Bowman, E. W. Harris and R. P. McBride	
Infrared Photography at 5 and 10 μm ¹	11
G. F. Frazier, T. D. Wilkerson and J. M. Lindsay	
SESSION B: CHEMILUMINESCENT PROCESSES	
Kinetics of the Chemiluminescence Accompanying Metal Atom Oxidation Reactions	14
W. Felder and A. Fontijn	
A Study of the Chemiluminescence of the Pb + O ₃ Reactions	18
M. J. Kurylo, W. Braun, S. Abramowitz and M. Krauss	
Chemiluminescence in Reactions of Ozone	21
S. Toby, F. S. Toby and B. Kaduk	
Dioxetane Chemistry in the Gas Phase UV-Visible Chemiluminescence from the Reactions of O ₂ (¹ Δ_g) with Olefins	24
D. J. Bogan and J. ⁹ L. Durant, Jr.	
SESSION C: PHOTOCHEMICAL ISOTOPE SEPARATION	
Molecular Dissociation by High-Intensity Infrared Laser Radiation	31
K. H. Welge	
Photochemistry of Formaldehydes: Past and Present	32
E. K. C. Lee, R. S. Lewis and R. G. Miller	
Decomposition of Formic Acid Vapor by Infrared Laser Radiation	35
R. Corkum, C. Willis, M. H. Back and R. A. Back	
The Laser Augmented Decomposition of D ₃ B Adducts	37
K. R. Chien and S. H. Bauer	
Infrared Laser Isotope Separation	40
J. L. Lyman and S. D. Rockwood	
CO ₂ TE Laser Induced Photochemical Enrichment of Carbon Isotopes	43
J. J. Ritter and S. M. Freund	
Measurement of Mean Lives in Atomic Uranium	45
J. Z. Klose	

Principles of Photochemical Separation of Isomeric Nuclides	49
G. C. Baldwin, H. M. Clark, D. Hakala and R. R. Reeves	

SESSION D: PRIMARY PHOTOCHEMICAL PROCESSES (LARGE MOLECULES AND ENERGY TRANSFER)

The Early Years of Photochemistry in the Vacuum Ultraviolet	51
W. Groth	
Fluorescence and Decomposition of Tertiary Amines in a Glow Discharge	53
F. Lahmani and R. Srinivasan	
Photochemistry and Flash Photolysis of 5-Nitroquinoline	55
A. C. Testa and A. Cu	
Photochemistry and Photophysics of Nitrogen Heterocycles	57
M. S. Henry and M. Z. Hoffman	
The Photophysics of Several Condensed Ring Heteroaromatic Compounds	60
F. S. Wettack, R. Klapthor, A. Shedd, M. Koeppe, K. Janda, P. Dwyer and K. Stratton	
Molecular Weight Dependence of Triplet-Triplet Processes in Polyo(2-Vinylnaphthalene).	63
N. F. Pasch and S. E. Webber	
Singlet and Triplet Precursors of $O_2^1\Delta_g$	66
B. Stevens and J. A. Ors	
The Heavy Atom Effect on the Photochemical Cycloaddition Processes of Acenaphthylene.	70
B. F. Plummer and L. J. Scott	

SESSION E: PHOTOCHEMISTRY WITH LASERS

Laser Induced Fluorescence Emission Spectroscopy of $H_2CO(A,^1A_2)$	72
K. Y. Tang and E. K. C. Lee	
Laser Excited NO_2 Fluorescence Lifetime Studies in the 600 NM Region	75
V. M. Donnelly and F. Kaufman	
Laser Fluorescence Studies, including the $B^3\Pi(0^+)$ States of BrF, IF and ICl	77
M. A. A. Clyne, A. H. Curran and I. S. McDermid	
Laser-Induced Fluorescence of CN Radicals Produced by Photodissociation of RCN	79
R. J. Cody, M. J. Sabety-Dzvonik	
Photofragment Spectroscopy of the $A\leftrightarrow X$ Transition in CN Using Two Pulsed Lasers	82
A. Baronavski and J. R. McDonald	
Spectroscopic and Photochemical Studies of Gaseous Ions Using Tunable Dye Lasers	86
J. R. Eyler	
Photodissociation Spectra of Positive Ions with Time-Of-Flight Analysis	88
T. F. Thomas and J. F. Paulson	
Vibrational States of Molecules in the Visible Region by Thermo-Optical Spectroscopy and the Local Mode Model	92
A. C. Albrecht	
Mechanism of High Intensity I.R. Photodecomposition of Molecules	94
W. Braun and W. Tsang	

SESSION F: ENVIRONMENTAL PHOTOCHEMISTRY (UPPER ATMOSPHERE)

The In-Situ Measurement of Atoms and Radicals in the Upper Atmosphere	99
J. G. Anderson	
The O(¹ S) Airglow - New Laboratory Results	102
T. Slanger and G. Black	
A Quantum Yield Determination for O(¹ D) Production from Ozone Via Laser Flash Photolysis	105
D. L. Philen, R. T. Watson and D. D. Davis	
Absence of N ₂ O Photolysis in the Troposphere	108
D. H. Stedman, R. J. Cicerone, W. L. Chameides and R. B. Harvey	
Temperature Dependence of O(¹ D) Reactions of Atmospheric Importance	111
J. A. Davidson and H. I. Schiff, G. E. Streit, A. L. Schmeltekopf and C. J. Howard	
Modeling Stratospheric Photochemistry and Kinetics	114
J. McAfee and P. J. Crutzen	
The Rate Constant for O + NO + M from 217-500K in Five Heat Bath Gases	115
J. V. Michael, W. A. Payne and D. A. Whytock	
Determination by the Phase Shift Technique of the Temperature Dependence of the Reactions of O(³ P) with HCl, HBr, and HI	117
D. L. Singleton and R. J. Cvetanovic	

SESSION G: INORGANIC PHOTOCHEMISTRY

High Energy Pulsed Laser Photolysis of Some Chromium (III) and Cobalt (III) Complexes	120
A. W. Adamson, A. R. Gutierrez, R. E. Wright and R. T. Walters	
Studies Using a Combination of Flash Photolysis and Pulsed Magnetic Induction: Application to the NO ₃ Radical in Aqueous Acid Solution at 25°C	126
T. W. Martin and M. V. Stevens	
Luminescence of Some Metal Trisdithioacetylacetonate Complexes	130
M. K. DeArmond and J. T. Merrill	
Luminescent Transition Metal Complex Photosensitizers	134
J. N. Demas, J. W. Addington, R. P. McBride, W. E. Harris and S. Peterson	
Picosecond Studies of Transition Metal Complexes	137
P. E. Hoggard, A. D. Kirk, G. B. Porter, M. G. Rockley and M. W. Windsor	
Electron Transfer Properties of Excited States of Transition Metal Complexes	139
V. Balzani, F. Bolletta, M. Maestri, A. Juris and N. Serpone	
A Comparison of the Excited-State Electron-Transfer Reactions of RU(BIPY) ₃ ²⁺ and OS(BIPY) ₃ ²⁺	142
P. Fisher, E. Finkenberg and H. D. Gafney	

SESSION H: PRIMARY PHOTOCHEMICAL PROCESSES (SMALL MOLECULES)

Photodissociation of Simple Polyatomic Molecules	145
J. P. Simons	
Energy Distribution in the Photodissociation of Methylketene at 215 NM	147
M. E. Umstead, R. G. Shortridge and M. C. Lin	
The Production and Reactions of Vibrationally Excited 1,1,2,2-Tetrachloroethane . .	150
M. H. J. Wijnen	
Measurement of Branching Ratios for the $O + CS_2 \rightarrow OCS + S$ Reaction	152
R. E. Graham and D. Gutman	
Photodissociation of Molecular Beams of Metallic Iodides	155
M. Kawasaki, H. Litvak, S.-J. Lee and R. Bersohn	
The Photochemistry of 2-Furaldehyde in the Gas Phase	157
A. Gandini, P. A. Hackett, J. M. Parsons and R. A. Back	
Photoinitiated Decomposition of Monosilane	160
E. R. Austin and F. W. Lampe	
Excitation of HNO by $O_2(^1\Delta_g)$	163
T. Ishiwata, H. Akimoto and I. Tanaka	
Solar Photodissociation Rates for $ClONO_2$; An Estimate of Current Levels of $ClONO_2$ in the Stratosphere	167
J. P. Jesson, L. C. Glasgow and P. Meakin	
The Tropospheric Lifetime of $CFCI_3$	174
J. P. Jesson, P. Meakin and L. C. Glasgow	
The Gas Kinetic and Photochemical Degradation of Chlorine Nitrate	176
A. R. Ravishankara, G. Smith, G. Tesi and D. D. Davis	

SESSION I: PHOTOCHEMICAL CONVERSION OF SOLAR ENERGY

Photogalvanic Cells	177
M. D. Archer, M. I. C. Ferreira, W. J. Albery and W. R. Bowen	
The Importance of Intermediate Partitioning in Energy Storing Photoreactions	180
G. Jones, II, W. R. Bergmark and M. Santhanam	
Optimization of the Iron-Thionine Photogalvanic Cell; Photochemical Aspects	183
P. D. Wildes, N. N. Lichtin and M. Z. Hoffman	
A Biomimetic Approach to Solar Energy Conversion	186
T. R. Janson and J. J. Katz	
Light Energy Conversion via Photoredox Processes in Micellar Systems	189
M. Grätzel	
Photoelectrolysis of Water by Solar Energy	191
D. I. Tchernev	

SESSION J: PHOTOPHYSICAL PROCESSES

Recent Work in Exciplex Photophysics	193
D. V. O'Connor and W. R. Ware	

Charge Transfer and Hydrogen Atom Transfer Reactions of Excited Aromatic Hydrocarbon-Amine Systems	196
N. Mataga, T. Okada and T. Mori	
Protolysis Equilibria of Lumichrome (6,7-Dimethyl-Alloxazine) in the Lowest Excited Singlet State	199
B. Holmström, S. Bergström and H. B. Larson	
Photochemistry of Pheophytins and Porphyrins	204
D. C. Brune, J. Fajer and S. P. Van	
SESSION K: ENVIRONMENTAL PHOTOCHEMISTRY (PHOTOCHEMICAL SMOG)	
A Kinetic Study of CH_3O_2 and $(\text{CH}_3)_3\text{CO}_2$ Radical Reactions by Kinetic Flash Spectroscopy	212
M. R. Whitbeck, J. W. Bottenheim, S. Z. Levine and J. G. Calvert	
The Reaction of OH Radicals with C_3H_6 and C_2H_4	215
R. Overend and G. Paraskevopoulos	
On the Triplet State(s) of Sulphur Dioxide	219
J. W. Böttenheim, F. Su, D. L. Thorsell, J. G. Calvert and E. Damon	
The $\text{SO}_2(^3\text{B}_1)$ Photosensitized Isomerization of Cis and Trans-1,2-Dichloroethylene . .	224
F. B. Wampler and J. W. Böttenheim	
Gas Phase Photochemical Synthesis of Peroxyacyl Nitrates via Chlorine-Aldehyde Reaction	227
B. W. Gay, Jr., R. C. Noonan, J. J. Bufalini, P. L. Hanst	
Chemical Control of Photochemical Smog	230
J. Heicklen	
Photochemically Induced Free Radical Reactions in Nitrogen Dioxide-Acetaldehyde Mixtures	233
E. R. Allen	
Photo-Oxidation of Toluene- NO_2 - O_2 - N_2 System in Gas Phase	243
H. Akimoto, M. Hoshino, G. Inoue, M. Okuda and N. Washida	
Effects of Solar Energy Distribution on Photochemical Smog Formation	247
G. Z. Whitten, J. P. Killus, H. Hogo and M. C. Dodge	
SESSION L: PHOTOCHEMICAL AND PHOTOPHYSICAL PROCESSES (CONDENSED PHASES)	
Photophysics of Bound and Dissociative States of Small Molecules in Condensed Phases. .	251
L. E. Brus and V. E. Bondybey	
Spectroscopy and Photochemistry of Matrix Isolated Metal Hexafluorides	253
W. F. Coleman, R. T. Paine, R. B. Lewis, R. S. McDowell, L. H. Jones and L. B. Asprey	
Mercury Photosensitized Production of Trapped Radicals in Organic Glasses at $<77\text{ K}$	256
N. Bremer, B. J. Brown, G. H. Morine and J. E. Willard	
Magnetic Field Effects on Triplet-Triplet Annihilation in Crystals	259
S. H. Tedder and S. E. Webber	
The Contribution of the Physical and Chemical Defects to the Photochemistry of Crystalline Durene at Very Low Temperatures	262
A. Despres, V. Lejeune and E. Migirdicyan	

Photochemistry of Electrons Trapped in Organic Glasses	267
G. C. Dismukes, S. L. Hager, D. P. Lin, G. H. Morine and J. E. Willard	

Spin Labels and the Mechanism of the $S_1 \rightarrow T_1$ Nonradiative Process in Duraldehyde; Possible Manifestation of Pseudo Jahn-Teller Forces on Nonradiative Processes	271
A. Campion and M. A. El-Sayed	

Photodesorption from Metals: Measured Desorption Rates in Comparison with a Mo-Treatment	274
N. Trappen	

Matrix Isolation Spectroscopic Studies of Free Radicals and Molecular Ions Produced by Collisions of Molecules with Excited Argon Atoms	276
M. E. Jacox	

SESSION M: ENVIRONMENTAL PHOTOCHEMISTRY (UPPER ATMOSPHERE)

Atmospheric Chemistry of Chlorofluorocarbons	280
M. J. Molina	

Ultraviolet Photoabsorption Cross-Sections of CF_2Cl_2 and $CFCl_3$ as a Function of Temperature	282
A. M. Bass and A. E. Ledford, Jr.	

Photodissociation of CCl_4	285
R. E. Rebert and P. Ausloos	

The Photolysis of ClO_2	287
S. Jaffe and W. B. DeMore	

Stratospheric Reactions of Chlorofluoromethanes	290
R. J. Donovan, H. M. Gillespie, J. Wolfrum and K. Kaufmann	

SESSION N: ENVIRONMENTAL PHOTOCHEMISTRY (PHOTOCHEMICAL SMOG)

Some Fundamental and Applied Aspects of the Atmospheric Reactivity of Organic Molecules	294
J. N. Pitts, Jr., R. Atkinson, A. M. Winer, K. R. Darnall, A. C. Lloyd and R. A. Perry	

IR Fourier-Transform Spectroscopic Studies of Atmospheric Reactions	300
H. Niki, P. Maker, C. Savage and L. Breitenbach	

Photochemically Generated Ozone from Isolated Strong Point Sources	303
D. D. Davis and W. Keifer	

Evidence for Alkoxy Radical Isomerization in C_4 - C_6 Alkanes in NO_x -Air Systems . . .	305
W. P. L. Carter, K. R. Darnall, A. C. Lloyd, A. M. Winer and J. N. Pitts, Jr.	

SESSION O: PHOTOPHYSICAL PROCESSES

Collisional Destruction of Rovibronic Levels in S_1 Glyoxal: Electronic, Vibrational and Rotational State Changes	309
L. G. Anderson, A. E. W. Knight and C. S. Parmenter	

The Vibronic Dependence of Glyoxal Photodissociation	311
G. H. Atkinson and C. G. Venkatesh	

Behavior of Benzene in Low Vibrational Levels	314
S. A. Lee, J. M. White and W. A. Noyes, Jr.	
Dual Lifetime Fluorescence from Pyrimidine	316
K. G. Spears and M. El-Manguch	
Time Resolved Emission Spectra of Low Pressure Aromatic Molecules	318
M. D. Swords, A. W. Sloman and D. P. Phillips	
Studies in the Mechanism of Radiationless Conversion of Electronic Energy	321
T. A. Gregory and S. Lipsky	
Photosensitization of the 2-Butenes by Benzaldehyde in the Gas Phase	323
A. J. Yarwood, G. R. De Mare and M. Termonia	

SESSION P: ELEMENTARY REACTION PROCESSES (THERMAL SYSTEMS)

Near Infrared Detection of Peroxyl Radicals in Mercury Photosensitized Reactions .	326
H. E. Hunziker	
Reactions of Hydrogen Atoms with Fluorinated Ketones	327
D. W. Grattan and K. O. Kutschke	
The Reaction of NH_2 with Olefins Studied by Flash Photolysis	331
R. Lesclaux and P. V. Khê	
Detection and Reactions of $\text{NH}(\text{X}^3\Sigma^-)$ Radicals in the Vacuum UV Flash Photolysis of NH_3 Using Resonance Fluorescence	334
I. Hansen, K. Hoinghaus, C. Zetzsch and F. Stuhl	
Interpretation of the Arrhenius Plots for Reactions of Oxygen Atoms with Olefins .	337
R. J. Cvetanovic	
Absolute Rate of the Reaction of $\text{O}(\text{P})$ with Hydrogen Sulphide	339
D. A. Whytock, R. B. Timmons, J. H. Lee, J. V. Michael, W. A. Payne and L. J. Stief	
Kinetics of the Reaction: $\text{OH} + \text{NO}_2 (+\text{M}) \rightarrow \text{HNO}_3 (+\text{M})$ Over a Wide Range of Temperature and Pressure	342
C. Anastasi, I. W. M. Smith and R. Zellner	
Vacuum UV Flash Photolysis of Phosphine: Rate of the Reaction $\text{H} + \text{PH}_3$ and Implications for the Photochemistry of the Atmosphere of Jupiter	345
J. H. Lee, J. V. Michael, W. A. Payne, D. A. Whytock and L. J. Stief	

SESSION Q: ENERGY TRANSFER

Energy-Dependent Cross Sections for Quenching of $\text{Li}(\text{P})$ and $\text{Na}(\text{P})$	348
J. R. Barker, S.-M. Lin and R. E. Weston, Jr.	
Electronic-to-Vibrational Energy Transfer Reactions: $\text{Na}(3^2\text{P}) + \text{CO}(\text{X}^1\text{S}^+, v=0)$. . .	351
D. S. Y. Hsu and M. C. Lin	
Energy Transfer in the Collision of Metastable Excited Ar^3P_2 Atoms with Ground State H^2S Atoms	354
P. B. Monkhouse, K. D. Bayes and M. A. A. Clyne	
Quenching Rate Constants for $\text{Ar}(^3\text{P}_2)$, $\text{Kr}(^3\text{P}_2)$ and $\text{Xe}(^3\text{P}_2)$ by Halogen-Containing Molecules, and Branching Ratios for XeF and KrF Formation	359
J. E. Velazco, H. E. Kolts and D. W. Setser	

V-V Energy Transfer in H_2 - Additive Gas Mixtures Using a Stimulated Raman Excitation Technique	364
R. G. Miller and J. K. Hancock	

SESSION R: ELEMENTARY REACTION PROCESSES
(EXCITED STATE DYNAMICS AND ENERGY TRANSFER)

Experiments Concerning the Laser Enhanced Reaction between O_3^+ and NO	368
K.-K. Hui and T. A. Cool	
Infrared Laser Enhanced Reactions: Chemistry of NO($v=1$) with O_3	370
J. C. Stephenson and S. M. Freund	
Kinetic Energy - and Internal State Dependence of the $NO + O_3 \rightarrow NO_2^* + O_2$ Reaction.	373
A. E. Redpath and M. Mensinger	
The Effect of Infrared Laser Excitation on Reaction Dynamics: $O + C_2H_4^+$ and $O + OCS^+$	376
R. G. Manning, W. Braun and M. J. Kurylo	
Reaction of Flash Photolytically Produced $CN(X^2\Sigma^+, v)$ Radicals with $O(^3P)$ Atoms	380
K. J. Schmatjko and J. Wolfrum	
Vibrational Photochemistry: The Relaxation of $HCl(v=1)$ and $DCl(v=1)$ by Bromine Atoms	384
R. D. H. Brown, I. W. M. Smith and S. W. J. Van der Merwe	
Vibrational Relaxation of $HF(v = 1,2,3)$ in the Presence of H_2 , N_2 , and CO_2	388
J. F. Bott	
Quenching of $NO(B^2\Pi_r)_{v=0}$ Produced by the Reaction of $N(^2D)$ with N_2O	390
G. Black, R. L. Sharpless and T. G. Slanger	
CW Infrared Laser Isotope Separation: $Cl + CH_3Br(v_6) \rightarrow HCl + CH_2Br$	395
T. J. Manuccia, M. D. Clark and E. R. Lory	

APPENDIX I

Author Index	397
------------------------	-----

A MODERN APPROACH TO ACCURATE RADIOMETRY

Edward Zalewski

National Bureau of Standards
Washington, DC 20234

The many recent advances in electro-optic technology have produced several new and very powerful tools for accurate photon flux measurements. The two advancements that have the greatest immediate impact on photochemistry are the electro-optic amplitude stabilization of high-powered cw lasers and the electrically calibrated pyroelectric null radiometer. The first has provided a high intensity radiant power source that is monochromatic, highly collimated and very stable--long-term drifts of less than 0.05 percent have been obtained. Such amplitude stabilized lasers facilitate precise control of the number of photons entering a chemical reaction. The second advancement, the electrically calibrated pyroelectric null radiometer, has brought a new order of accuracy, sensitivity and convenience to the measurement of radiant power, thereby facilitating the accurate measurement of photon flux.

The tremendous improvement in amplitude stabilization of cw lasers has been accomplished by using a stable solid state photodetector to monitor the laser beam and, in turn control the transmittance of an electro-optic modulator. A block diagram of a laser amplitude stabilization system is shown in figure 1. The box labeled "beam uniformity optics" refers to apertures, a spatial filter and a beam expanding telescope used to obtain a uniform photon density in the cross section of the beam. Such a beam shaping system does result in a considerable loss of radiant power but is sometimes necessary to avoid saturation effects in certain experiments.

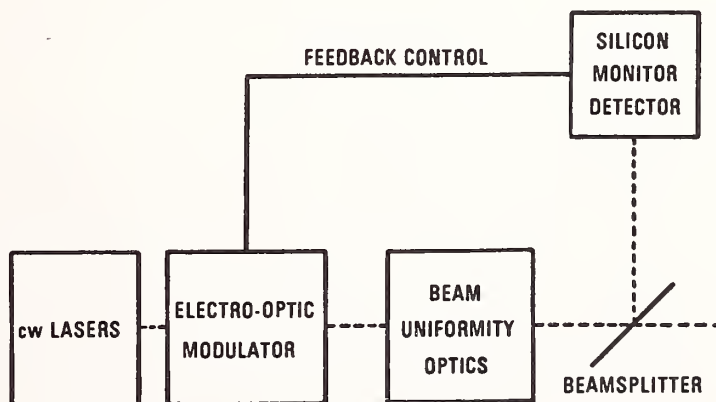


Figure 1: Block diagram of a cw laser stabilization system. The silicon monitor detector supplies a sense signal to a feedback loop. This controls the transmittance of the electrooptic modulator to reduce the fluctuations in the amplitude of the cw laser beam.

The fundamental principle of the electrically calibrated pyroelectric null radiometer is illustrated in figure 2. The idea of electrically calibrating a thermal detector is not new. The new features are the pyroelectric detector material and the ac null-balance approach to the measurements. The pyroelectric, like a thermopile or a bolometer, is a thermal detector. However, it is an ac device rather than dc, responding to temperature changes instead of the steady-state value. This property permits the use of synchronous amplification, increasing the signal-to-noise of the measurements, and consequently improving the sensitivity over that of previous types of electrically calibrated detector radiometers. It also allows the electrical heating pulses to be applied to the detector alternately with the radiant heating pulses. Alternate pulses in the output signal are electronically inverted and amplified by a wide-band, lock-in amplifier. The amplitude of the electrical heating pulses are adjusted to match the effect of the radiant heating pulses in order to obtain a zero value for the dc component of the amplifier output. That is, when the null condition is reached the areas under the electrical and radiant heating pulses are equal.

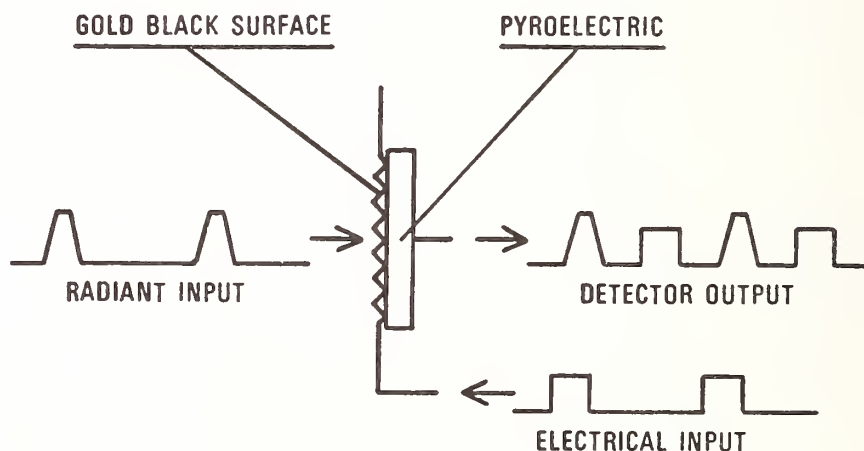


Figure 2. Schematic diagram of the principle of operation of the electrically calibrated pyroelectric null radiometer. The pyroelectric material is alternately heated by radiant and electrical input pulses. The areas under the two types of pulses in the resulting wave train are equal when the heating from the two modes is equivalent.

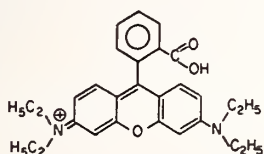
The question of whether the electrical and radiant heating modes in the detector are really equivalent can be answered without recourse to blackbody measurements. From a study of the physics of these detectors it is found that several types of inequivalences occur between the two different heating modes. From the physics, one also obtains the methods whereby the magnitudes of the inequivalences can be evaluated in auxiliary experiments. With a knowledge of the magnitudes of these effects, it is then possible to apply the appropriate correction factors to assure the accuracy of the measurement. With presently existing electrically calibrated pyroelectric null radiometers the best accuracies obtainable are between 0.5 and 1 percent. This is over a range of power from 10 μ W to 100 mW and a wavelength range from 200 to 10,000 nm.

TEMPERATURE DEPENDENCE OF THE FLUORESCENCE QUANTUM YIELDS OF RHODAMINE DERIVATIVES

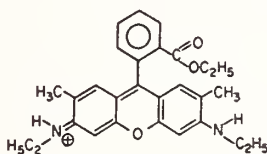
Robert E. Schwerzel and Nancy E. Klosterman

Battelle Columbus Laboratories
505 King Avenue
Columbus, OH 43201

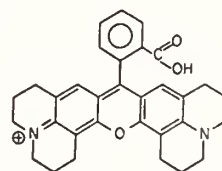
The measurement of absolute fluorescence quantum yields is often a difficult and tedious task which can pose a number of potential sources of error [1,2]¹. While the fluorescence yields of powdered samples or monolayer assemblies can best be obtained by absolute measurements (and several relatively straightforward procedures have recently been developed for this purpose [1-4]), the fluorescence yields of solutions are most easily obtained by relative measurements in which the fluorescence intensity of the sample solution is compared to that of a standard solution. The convenience and widespread popularity of the relative measurement technique make it essential that fluorescence standards be well characterized, both in terms of purity and fluorescence quantum yield under the experimental conditions used. This paper examines the fluorescence behavior of one commonly used fluorescence standard, rhodamine B, and two closely related derivatives, rhodamine 6G and rhodamine 101.



Rhodamine B



Rhodamine 6G



Rhodamine 101

Rhodamine B is an attractive candidate for use as a fluorescence standard for several reasons. It has a constant quantum yield over a wide wavelength range and is not quenched by oxygen [5]. Further, it strongly absorbs the mercury 546 nm line, making it particularly convenient for measurements in the yellow and red portions of the visible spectrum.

The quantum yield of rhodamine B is poorly defined, however, with reported values ranging from 0.69 [6] to 0.97 [5]. Some of this spread may result from calibration errors [1]. It appears likely, however, that an additional contributing factor is the change of the quantum yield as a function of temperature and solvent viscosity [7-9]. Drexhage [9] has reported that the fluorescence quantum yield of rhodamine B in ethanol is approximately 0.40 at 25 C, and that the value increases to nearly 1.00 when the temperature is lowered. Conversely, the quantum yield drops to only a few percent when the solution is heated to 78 C. This behavior has been explained by an activated radiationless decay mechanism involving the hindered rotation of the diethylamino groups. This view is supported by the lower temperature dependence of rhodamine 6G and the even lower temperature dependence of rhodamine

¹Figures in brackets indicate the literature references at the end of this paper.

101 (which has a quantum yield of nearly 1.00 over a wide temperature range) [9]. Our results are generally consistent with those of Drexhage. The paper will elaborate on these results and their relevance to the selection of a suitable yellow-red fluorescence quantum yield standard.

References

- [1] Demas, J. N., and Crosby, G. A., *J. Phys. Chem.*, 75, 991 (1971) references cited within.
- [2] Billon, D., Laine-Böszörményi, M., and Fallot, P., Meures Du Rendement Quantique De Fluorescence Des Poudres Et Des Solutions Au Moyen De Spectrofluorimètres Associés Ou Non A Une Sphere Intégrante, Commissariat A L'Energie Atomique Rapport CEA-R-4466, July 1973 (Available from the Service de Documentation, C.E.N.-Saclay, B.P. n° 2, 91-GIF-sur-YVETTE, France).
- [3] Wrighton, M. S., Ginley, D. S., and Morse, D. L., *J. Phys. Chem.*, 78, 2229 (1974).
- [4] Möbius, D., and Debuch, G., *Chem. Phys. Lett.*, 28, 17 (1974).
- [5] Weber, G., and Teale, F. W. J., *Trans. Faraday Soc.*, 53, 646 (1957); 54, 640 (1958).
- [6] Parker, C. A., and Rees, W. T., *Analyst (London)*, 85, 587 (1960).
- [7] Huth, B. G., Farmer, G. I., and Kagan, M. R., *J. Appl. Phys.*, 40, 5145 (1969).
- [8] Drexhage, K. H., *Laser Focus*, 9 (3), 35 (1973).
- [9] Drexhage, K. H., in *Dye Lasers*, Schäfer, F. P., ed., Springer-Verlag, New York, 1973, Chapter 4.

NBS ULTRAVIOLET RADIOMETRIC STANDARDS

W. R. Ott

National Bureau of Standards
Washington, DC 20234

1. Introduction

In the wavelength region between 5 and 400 nm, the National Bureau of Standards offers a variety of standard sources and detectors which may be used to calibrate the radiant power of unknown sources or the response of radiation detectors and spectral radiometers. The energy range corresponding to these wavelengths spans from about 3 eV to 300 eV. This energetic radiation is of great interest not only in basic photochemistry research, *e.g.*, in photo-absorption and fluorescence studies, but also in industrial applications of photochemistry and photobiology. For example, extreme doses of ultraviolet radiation can cause skin cancer; controlled doses can heal. Continuous exposure to ultraviolet radiation results in the fading of paints and dyes; controlled exposures in specific processes are used to produce protective coatings on materials. Some documented examples of the various applications of ultraviolet radiation as both a natural and artificial element in our home and work environment are shown in table 1.

Table 1. List of applications requiring ultraviolet radiation measurements

Photochemistry

Thin film production
Tooth decay prevention
Textile dyes
Paint curing
Industrial finishes
Cast hardening
Instant oscillographs
Material degradation
UV photosensitive paper
Counterfeit money detection

Bacteriological

Germicidal lamps in hospitals,
schools, and offices
Germicidal lamps in industry

Environmental Studies

Atmospheric sciences
Ecology and the ozone layer
Oil spill identification
Water purification
Smog gauge

Fusion Research

National controlled thermonuclear
fusion efforts

Space Science

Communications
Astrophysics
Skylab
Space shuttle
Reentry and rocket exhaust

VUV and X-Ray Lasers

Integrated circuits
Plasma probes
Isotope separation
Molecular synthesis
High resolution holography
Tumor therapy
Laser fusion

Photobiology

NBS benchmark experiments

Medical and Therapeutic

Jaundice treatments
Calcium deficiency
Skin disease treatments
Wrinkling
Drug detection

Plasma Chemistry

Thin film deposition
Plasma arc steel furnace
Recycling of alloys in steel production

2. Radiometric Quantities

In general, there are two ways to determine the radiant power of an unknown light source: (a) through the use of standard sources, and (b) through the use of standard detectors. Standard sources are most useful when it is desired to know the emission characteristics of an unknown source. Standard detectors are most useful, on the other hand, when it is desired to know the radiant power at the location of a detector. For example, if the quantity of interest is spectral radiance [$\text{watts cm}^{-2}\text{nm}^{-1}\text{sr}^{-1}$], that is, if one is concerned with the power radiated by a specified emitting surface (cm^2) in a certain wavelength band (nm) at a given solid angle (sr), then the light source to be investigated as well as the standard source may be set up in such a manner that the radiation from both passes through the same optical-spectrometric arrangement, thereby eliminating all geometric and other specific factors of the instrumentation. In short the calibration is effected by a simple substitution of sources in the experimental arrangement. On the other hand, if the quantity of interest is spectral irradiance [$\text{watts cm}^{-2}\text{nm}^{-1}$], that is, if one is concerned with the radiant power incident on a specified surface area (cm^2) in a certain wavelength band (nm), then ideally a standard detector and filter arrangement is placed at the location of the irradiated surface to measure the power. Alternatively, if such a standard radiometer is not available, a standard source of spectral irradiance may be used in conjunction with a suitable diffusing element (to account for variations in the geometries of the standard and the unknown sources) to determine the response function of the user's diffuser-radiometer system.

At NBS, standard sources of both ultraviolet spectral radiance and spectral irradiance are available. In the case of NBS standard detectors for the ultraviolet, the calibrated quantity is the absolute quantum efficiency [photoelectrons per incident photon] as a function of wavelength.

3. Standard Sources

The three primary source standards being used at NBS are the gold point blackbody cavity for which the spectral radiance is given by Planck's law, the wall-stabilized hydrogen arc for which the spectral radiance is given by accurately known quantum mechanical absorption coefficients for atomic hydrogen, and the electron storage ring facility for which the spectral radiance is given by the theory of electron synchrotron radiation. The selection of one of these standards for a calibration application is influenced mostly by the specified wavelength region.

The primary standards are most often used to calibrate secondary or transfer standards of spectral radiance which can then be issued to customers. The secondary radiance standards are also used to generate spectral irradiance standards. The following ultraviolet standard sources, listed in order of decreasing wavelength, are available from NBS: the tungsten filament quartz-halogen lamp (above 250 nm); the tungsten strip lamp (above 225 nm); the low pressure mercury vapor lamp (253.7 nm); the deuterium arc lamp (165-350 nm); the argon "mini-arc" (115-400 nm); and the synchrotron radiation source, SURF-II (5-400 nm). The relative strengths and limitations of these radiometric standards with respect to accuracy, reliability, convenience, and intensity and wavelength range will be discussed in the presented paper.

4. Standard Detectors

The primary standard for ultraviolet detector calibrations at NBS is a double-ionization chamber, a gas-filled detector in which each photon absorbed produces one electron-ion pair which is collected by a simple arrangement of parallel plates used to set up the collecting field. The transfer to the actual photodiodes, which are available to customers, is accomplished through the use of a uniformly grey (percent of radiation absorbed is independent of wavelength) thermopile, whose efficiency has been calibrated with the ionization chamber at short wavelengths and checked with a spectral irradiance standard source at 253.7 nm. Windowed photodiodes calibrated in this manner have been used to evaluate the response of other detectors, such as photomultipliers, and the response of radiometers, such as "hazard meters", which are designed to have a spectral response equivalent to a specified erythemal curve. Calibrated photodiodes are available throughout the wavelength region 20-320 nm.

NEW METHODS OF MEASURING LIGHT INTENSITIES

D. G. Taylor, J. N. Demas, W. D. Bowman, E. W. Harris and R. P. McBride

Chemistry Department
University of Virginia
Charlottesville, VA 22901

An inexpensive, easily constructed large area bolometer has been developed. The proto-type has a 1 inch x 1 inch sensitive surface, but smaller sizes could be easily built to give greater sensitivity and faster response times. The 1 inch x 1 inch version has a maximum deviation of sensitivity of 3 percent from the center to the edge and is considerably more uniform over the central 3/4 inch diameter. Sensitivity is $\sim 5 \mu\text{W}$ ($< 1 \mu\text{W}/\text{cm}^2$) with an ~ 45 second time constant. The detector uses a positive temperature coefficient thermistor in a dc bridge; it is mounted on the back of a carefully designed copper plate which smooths out temperature anisotropy on the sensing plate before detection. To minimize drift, the detector is held in an insulated massive aluminum head. The aluminum head is stabilized to $\sim 100 \mu\text{K}$ by means of a solid state proportional controller. Although our current version is only a relative bolometer, we have also made an absolute version using a manganin resistance wire calibration heater. A better arrangement would be to use a distributive heater over the entire surface of the plate, and it could be easily fabricated.

A simple, inexpensive but extremely precise luminescence quantum counter comparator has been developed. The system gives part-per-thousand reproducibility and accuracy for the intercomparison of optically dense quantum counters. It can easily detect the small, but significant variations in spectral sensitivity between rhodamine B under the following conditions: 8 g/l in ethylene glycol; 8 g/l, 5 g/l and 2 g/l in methanol. We have also begun calibration of nile blue A and methylene blue. These dyes promise to give spectral sensitivity to $\sim 700 \text{ nm}$, although in the 340-590 nm region they are not as flat in response as rhodamine B. We have calibrated rhodamine B (5 g/l) in methanol against our large area bolometer. The absolute sensitivities of a number of systems are given in table 1; the data are references to the large area bolometer via the 5 g/l rhodamine B calibration. The relative

Table 1. Absolute spectral sensitivity of quantum counters^a

	Rhodamine B 5 g/l ethylene glycol	Rhodamine B 8 g/l MeOH	Methylene Blue 1 g/l MeOH	Nile Blue A 2 g/l MeOH
$\lambda \text{ nm}$				
590	1.001 .999	.973 1.001	.983 .992	1.010 1.012
570	.996 1.000	1.005 1.010	.996 .997	1.019 1.028
550	.996 1.000	.999 1.002	.994 .992	1.021 1.014
530	.990 .999	.995 1.000	.987 .996	1.003 1.001

Table 1. Absolute spectral sensitivity of quantum counters^a (continued)

λ nm	Rhodamine B 5 g/l ethylene glycol	Rhodamine B 8 g/l MeOH	Methylene Blue 1 g/l MeOH	Nile Blue A 2 g/l MeOH
510	1.001 .998	.999 .997	1.002 1.005	.988 .970
490	1.007 1.015	1.005 1.008	1.016 1.023	.963 .957
470	1.016 1.006	1.001 .996	1.024 1.029	.948 .970
450	1.003 1.002	.982 .982	1.042 1.053	1.002 1.008
430	1.005 1.012	.996 1.001	1.053 .984	1.016 1.015
410	1.007 1.004	.999 1.000	.921 1.006	1.019 1.011
390	.999 .987	.991 .980	.991 .980	1.002 .988
370	.989 .977	.982 .980	.982 .965	1.001 1.000

^aRelative to bolometer, measured via rhodamine B (5 g/l) MeOH calibrated counter.

sensitivities of the quantum counter systems are given in table 2; the detector was an RCA 7164R equipped with a Corning C.S. 2-62 filter.

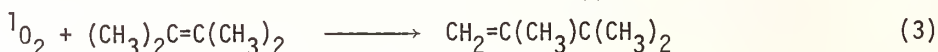
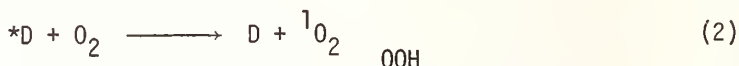
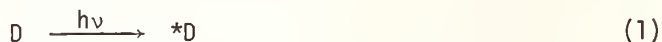
Table 2. Relative sensitivity of quantum counters^{a,b}

Rhodamine B (2 g/l) MeOH	1.71
Rhodamine B (5 g/l) MeOH	1.00 ^a
Rhodamine B (8 g/l) MeOH	0.49
Rhodamine B (5 g/l) Ethylene Glycol	0.92
Rhodamine B (8 g/l) Ethylene Glycol	0.61
Rhodamine 6G (5 g/l) MeOH	1.67
Methylene Blue (1 g/l) MeOH	0.064
Nile Blue A (2 g/l) MeOH	0.15

^aMean sensitivity 360-590 nm compared to standard (Rhodamine B (5 g/l) MeOH) counter.

^bAll counters viewed from rear.

Based on our photooxygenation work with transition metal complexes [1,2]¹ we have developed the first chemical actinometer specifically designed for use with high power laser sources [3,4]. The system is the Ru(bipy)₃²⁺ (bipy = 2,2'-bipyridine) photooxygenation of tetramethylethylene (TME) in methanol. The key reactions are



where D is Ru(bipy)₃²⁺ and ¹O₂ is singlet oxygen. The net effect of absorption of radiation by Ru(bipy)₃²⁺ is consumption of O₂. The actinometer system is closed and O₂ consumption is monitored on a gas buret.

The effective quantum yield for oxygen uptake, ϕ'_{obs} , is given by

$$\phi'_{\text{obs}} = 0.855 \frac{K_{\text{SV}}[O_2]}{1 + K_{\text{SV}}[O_2]} \frac{[TME]}{[TME] + \beta} \quad (4)$$

where K_{SV} is the Stern-Volmer quenching constant for O₂ quenching of ^{*}Ru(bipy)₃²⁺ and equals 1400 M⁻¹, $\beta = 0.0027$ M, and $[O_2]$ and $[TME]$ are the average O₂ and TME concentrations during the photolysis. The actinometer is intrinsically quantum flat and usable for $\lambda \leq \sim 520$ nm, which makes it ideal for use with the ionized Ar laser lines.

An apparently previously unreported artifact with the ferrioxalate actinometer has been discovered [5]. With aged phenanthroline developing reagent and following the recommended procedure, intensity errors of -40 to + 20 percent can result if the phenanthroline is added before the buffer. If the buffer is added before the phenanthroline, the errors are smaller but can still be significant (~ 5 percent). If fresh (≤ 3 weeks) phenanthroline solutions are used, however, development is instantaneous (< 5 min) and independent of the order of addition of reagents.

A preliminary calibration of the 0.15 F ferrioxalate at the 458 nm ionized Ar laser line indicates that the true yield may be ~ 10 percent lower (0.86) than the accepted one (~ 0.96) [6]. A cooperative effort now in progress with the NBS (Gaithersburg) radiometry group will supply a definitive answer to this question by the time of the conference.

References

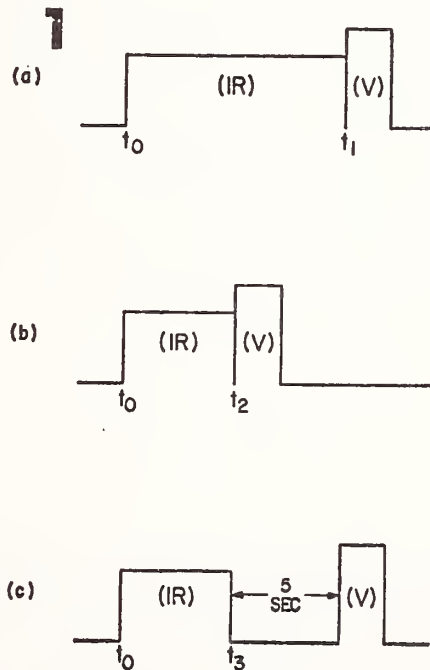
- [1] Demas, J. N., Harris, E. W., Flynn, C. M., Jr., and Diemente, D., *J. Amer. Chem. Soc.*, **97**, 3838 (1975).
- [2] Demas, J. N., Harris, E. W., and McBride, R. P., in preparation.
- [3] Demas, J. N., Harris, E. W., and McBride, R. P., *Lasers in Physical Chemistry and Biophysics*, p. 477 (Elsevier, 1975).
- [4] Demas, J. N., McBride, R. P., and Harris, E. W., submitted for publication.
- [5] Bowman, W. D., and Demas, J. N., submitted for publication.
- [6] Hatchard, C. G., and Parker, C. A., *Proc. Roy. Soc. (London)*, **235A**, 518 (1956).

¹Figures in brackets indicate literature references at the end of this paper.

Gene F. Frazier, T. D. Wilkerson² and J. M. Lindsay³Versar Incorporated
Springfield, VA 22151

A new technique for infrared photography is described involving the sensitization and desensitization of silver halide films by IR irradiation. Since a visible exposure follows the IR exposure, the time order is opposite to the well known Herschel effect. Also, we record images at much longer wavelengths, 5 and 10 μm , even though the films are conventional commercial types such as Polaroid 55 P/N. This film is particularly useful for quantitative densitometry, some of which is reported here. For the image power density range 0.1-1 W/cm², IR exposure times are about 10-1 second, respectively. CO and CO₂ lasers (cw) have been the principal IR light sources, and the visible flash is variable (.001-1 s) and is chosen to fog the film to a modest level of density. Exposure times of 1/10-1/100 second are possible at higher power density, opening up the possibility of inexpensive IR cinematography of the transient behavior of high power laser mode patterns.

Exposure time sequences are indicated in figure 1. The long IR exposure (a) yields *desensitization* of a negative and blackened print. The short IR exposure (b) can give the opposite or the same effects, depending, for example, on the color of the visible flash V. A delay of order 5 seconds or more (c) yields no IR effect on the latent image subsequently formed by V.

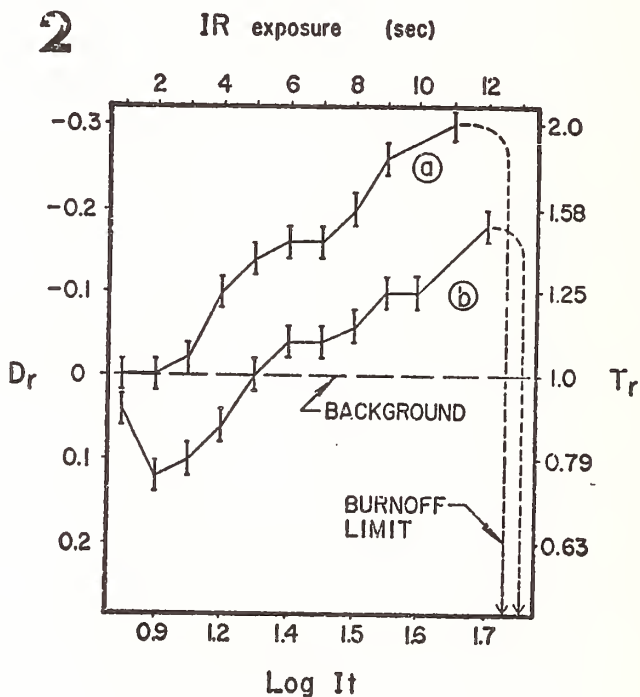


¹ Research supported by AFOSR under Contract No. F44620-72-C-0076.

² Permanent address: Institute for Fluid Dynamics and Applied Mathematics, University of Maryland, College Park, MD 20742.

³ Permanent address: Chesapeake Biological Laboratory, Solomons, MD 20668.

Figure 2 shows a type of characteristic curve (2 cases) for which IR exposure is varied by changing its duration at constant power density (0.3 W/cm^2). Curve (a) shows only *desensitization*, relative to the imposed visible fogging, when the visible light is *green* ($0.56\text{--}0.57 \mu\text{m}$). Curve (b) for white light shows reversal from sensitization to desensitization as IR exposure is increased.



In ongoing work, we want to develop a better understanding of the mechanisms of IR influence on the latent image and, if possible, improve the sensitivity and dynamic range of the IR response. Two main lines of inquiry seem to be the most promising: (A) better delineating the interaction between IR radiation and the gelatin (*i.e.* non-silver halide materials) contained in the emulsion, and (B) estimating the net influence of IR irradiation on the drift mobility and lifetimes of photogenerated species within the grains. Progress on these topics will be discussed in the context of prior work [1-4]⁴.

⁴ Figures in brackets indicate literature references at the end of this paper.

References

- [1] Malinowski, J., *Photogr. Sci. Eng.*, 14, 112 (1970).
- [2] Brown, F. C., and Kobayashi, K., *J. Phys. Chem. Solids*, 8, 300 (1959).
- [3] Wei, J. S., and Brown, F. C., *Photogr. Sci. Eng.*, 17, 197 (1973).
- [4] Babcock, T. A., Lewis, W. C., McCue, P. A., and James, T. H., *Photogr. Sci. Eng.*, 16, 104 (1972).

William Felder and Arthur Fontijn
 AeroChem Research Laboratories, Inc.
 P.O. Box 12
 Princeton, NJ 08540

The search for electronic transition chemical lasers has led to major interest in the chemiluminescence accompanying many metal atom oxidation reactions. Since most of the metals of potential interest are highly refractory, the AeroChem high-temperature fast-flow reactors (HTFFR) (see, *e.g.*, references [1-3]¹), which allow for independent control of temperatures, total pressure, reactant and quencher concentration, are uniquely suited to the study of their kinetics. These reactors are designed for study of metal atom and metal monoxide species over the 300 to near 2000 K temperature range. Independent control of heating zones allows a high temperature (*e.g.*, ~ 1700 K for Sn) source section to be combined with a reaction zone which can be at any desired temperature within this range. Here, we discuss excited state formation and quenching kinetics in the Sn/N₂O system.

1. Experimental

Figure 1 shows the HTFFR used in this work which was modified to cover the intermediate temperature ($\sim 400 - \sim 1400$ K) range; it consists of three sections, an upstream ~ 30 cm.

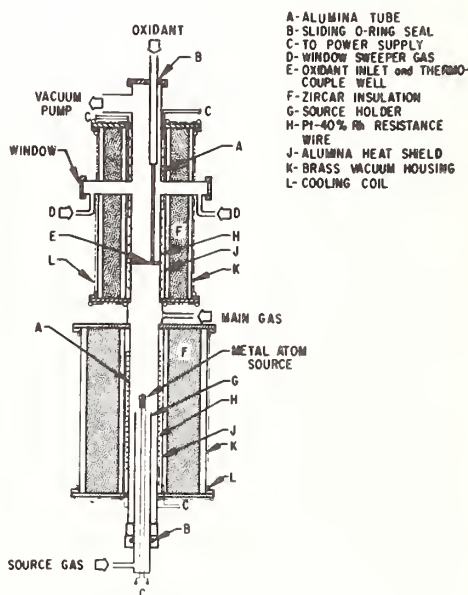


Figure 1. HTFFR for kinetic studies in the intermediate (*ca* 400 - 1400 K) temperature range.

long heated alumina flow tube source section, a short temperature transition region tube and a reaction zone section which is a ~ 30 cm long heated alumina flow tube. Sn is vaporized from a separately heated source placed in the upstream end of the reactor. The vapor is entrained in a bath gas flow and transported to the reaction zone where the second re-

¹ Figures in brackets indicate literature references at the end of this paper.

agent (e.g., N_2O) is added through a traversable inlet (fig. 1). Fixed viewing ports at the downstream end of the reaction zone allow optical observations [3,4] of chemiluminescence intensity and spectral distribution and of $[Sn]$ as functions of the reaction time (flow velocity and distance of inlet from observation port), $[N_2O]$, total pressure, and temperature. Figure 2 shows the optical layout and a cross-section of the reactor in the observation plane.

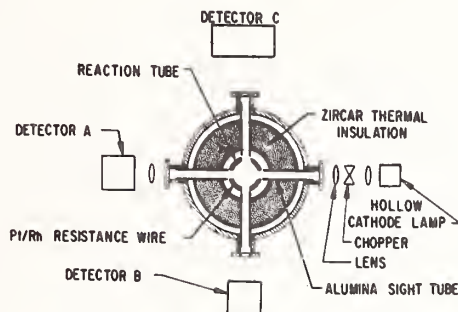


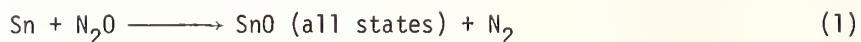
Figure 2. Optical arrangement and cross-section of HTFFR. Detectors A and B are spectrometers used for metal atom absorption and chemiluminescence spectral measurements, respectively. Detector C is a PMT filter combination for chemiluminescence intensity and titration measurements. Reaction tube 2.5 cm i.d., reaction tube observation ports 1 cm diam.

Photon yields are obtained by measuring: (i) the absolute chemiluminescence intensity, integrated both over wavelength and the extent of the glow in the flow tube, and (ii) the absolute $[Sn]$. Absolute wavelength-dependent intensity is determined by calibrating the detection system against the O/NO glow [5] and integration is accomplished by traversing the N_2O inlet to allow construction of intensity vs. distance (time in the flow tube) plots, the area of which gives the integrated intensity. Absolute $[Sn]$ is calculated from absorption measurements at $\lambda = 286.3$ nm using a hollow cathode lamp and the best literature value [6] for the absorption f-number. Experimentally, this measurement is limited to $3 \times 10^{10} < [Sn] < 3 \times 10^{11} \text{ ml}^{-1}$ where the absorption intensity can be accurately measured; the calculated $[Sn]$ absolute are probably accurate to within a factor of ~ 2 . Work is in progress to increase the accuracy of these $[Sn]$ determinations by a titration technique using NO_2 as titrant and N_2O as chemiluminescence indicator. Such titrations, at the $\geq 10 \text{ m s}^{-1}$ flow velocities required for Sn transport, demand $[Sn] > 10^{13} \text{ ml}^{-1}$. We have already successfully titrated $[Sn]$ in the $10^{13} - 10^{14} \text{ ml}^{-1}$ range as part of the Sn quenching measurements.

The overall rate coefficient of the Sn/N_2O reaction is obtained from 286.3 nm absorption measurements of the rate of change of the relative $[Sn]$ as a function of reaction time and $[N_2O]$ using standard techniques which are reviewed in detail in references [2] and [3]. Quenching rate coefficients are obtained from the observed variations in photon yield as a function of quencher concentrations via Stern-Volmer type analyses. Quenching by reagents is a problem inherent to excited species produced by chemi-excitation and required the development of methods suitable for the corresponding rate coefficient measurements, which will be briefly described.

2. Results

The reaction



has been found to be strongly temperature dependent. A cursory determination yielded $k_1 = (1.0 \pm 4) \times 10^{-11} \exp[(-3000 + 1000/T)] \text{ ml molecule}^{-1} \text{ s}^{-1}$ over the 500-390 K range. In this range, only SnO (a-X) and (A-X) band system emission could be definitely established. The total photon yield, Φ , defined as the fraction of Sn oxidation events that leads to emission of a photon, increases by a factor of only ~ 1.25 between 500-930 K, *i.e.*, from ~ 0.54 to 0.69. This increase is essentially all due to an increase in the A-X system intensity ($\Phi(\text{A-X})$ increases from 0.04 to 0.16 over this range), while $\Phi(\text{a-X})$ remains constant at ~ 0.5 . The rate coefficient for photon emission --defined by $dh_\nu/dt = k_{h\nu}[\text{Sn}][\text{N}_2\text{O}]$ --is a strong function of T, since $k_{h\nu}(T) = k_1(T)\Phi(T)$. The large $\Phi(\text{a-X})$ makes SnO ($\text{a}^3\Sigma$) particularly attractive as a candidate for the upper state in a potential electronic transition chemical laser.

Quenching experiments have concentrated on SnO($\text{a}^3\Sigma$). The following upper limit rate coefficients (based on the estimate [7] radiative lifetime of $\sim 1 \times 10^{-3} \text{ s}$) were measured:

$$\begin{aligned} k_Q^{\text{Sn}} &\leq 1.2 \times 10^{-12}; & k_Q^{\text{N}_2\text{O}} &\leq 1 \times 10^{-14}; \\ k_Q^{\text{N}_2} &\leq 0.6 \times 10^{-16}; & k_Q^{\text{Ar}} &\leq 1.0 \times 10^{-16} \end{aligned}$$

in $\text{ml molecule}^{-1} \text{ s}^{-1}$ units.

3. Discussion

The magnitudes of the observed rate coefficients differ strongly from those observed in several other simple metal atom oxidation reaction systems, *e.g.*, Ba/ N_2O [8-12]. Probable reasons for these differences will be discussed. It will be shown that these differences make Sn/ N_2O a very attractive electronic transition chemical laser candidate system.

Work sponsored by the Defense Advanced Research Projects Agency (ARPA) and monitored by the Air Force Weapons Laboratory, Air Force Systems Command, United States Air Force, Kirtland Air Force Base, New Mexico 87117.

References

- [1] Fontijn, A., Kurzius, S. C., Houghton, J. J., and Emerson, J. A., *Rev. Sci. Instr.*, **43**, 726 (1971).
- [2] Fontijn, A., Felder, W., and Houghton, J. J., *Fifteenth Symposium (International) on Combustion*, p. 775 (The Combustion Institute, Pittsburgh, 1975).
- [3] Fontijn, A., *AIAA Paper 76-131* (January 1976).
- [4] Felder, W., and Fontijn, A., *Chem. Phys. Lett.*, **34**, 398 (1975).
- [5] Fontijn, A., Meyer, C. B., and Schiff, H. I., *J. Chem. Phys.*, **40**, 64 (1964).
- [6] DeZafra, R. L., and Marshall, A., *Phys. Rev.*, **A170**, 28 (1968).

- [7] Meyer, B., Smith, J. J., and Spitzer, K., *J. Chem. Phys.*, 53, 3616 (1970).
- [8] Jonah, C. D., Zare, R. N., and Ottinger, Ch., *J. Chem. Phys.*, 56, 263 (1972).
- [9] Jones, C. R., and Broida, H. P., *J. Chem. Phys.*, 60, 4369 (1974).
- [10] Palmer, H. B., Krugh, W. D., and Hsu, C. J., *Fifteenth Symposium (International) on Combustion*, p. 951 (The Combustion Institute, Pittsburgh, 1975).

A STUDY OF THE CHEMILUMINESCENCE OF THE $\text{Pb} + \text{O}_3$ REACTIONS

M. J. Kurylo, W. Braun, S. Abramowitz , and M. Krauss

National Bureau of Standards
Washington, DC 20234

1. Introduction

Recent studies on laser enhanced reactions have shown that vibrational energy in a reactant triatomic molecule can appear as excitation in a product triatomic molecular species. Because of the spectroscopic complexities of triatomic molecules, we are investigating a chemiluminescent reaction producing a diatomic product. The metal atom-oxidant systems represent a class of such reactions which have been investigated because of their potential as chemical lasers. We report herein some observations on the reaction



While the information obtained from studying the infrared laser enhanced reaction component is minimized by the overall reaction complexity, it does nevertheless provide some additional insight into this reaction system. This information coupled with new high pressure spectroscopic results complement the detailed low pressure investigation by Oldenborg, Dickson, and Zare (ODZ).

2. Experimental

The furnace, reaction cell, fast flow pumping system, CO_2 laser, and spectrometer are shown schematically in figure 1. Lead vapor, produced from a resistively heated crucible

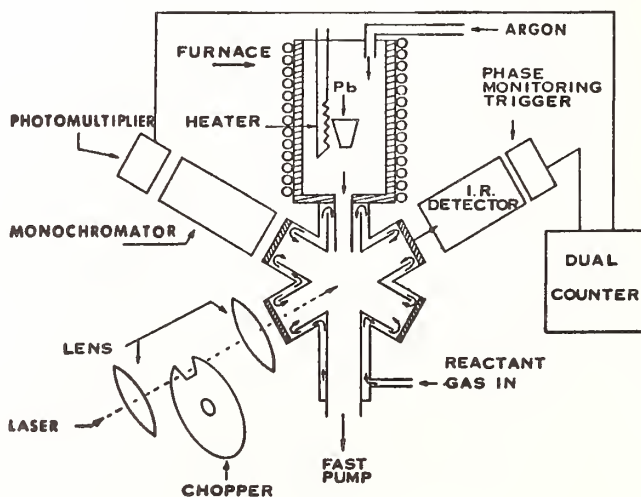


Figure 1. Schematic of the chemiluminescent flow reaction apparatus.

containing lead metal, enters the glass reaction chamber in an Ar diluent stream. The 4 percent O_3 in O_2 effluent from a commercial O_3 generator is mixed with Ar and flows past the cell windows (to eliminate window deposits) into the cell. There it diffusively mixes with the lead-argon flow. The temperature of the crucible (as measured by a thermocouple probe) ranges from 900-1000 K while the temperature in the flame reaction zone varies from 500-600 K. The total pressure in the cell varies from 1 to 5 torr with the flow through the furnace being anywhere from 20 to 50 percent of the total flow.

The 0.5 cm diameter beam from a CO_2 laser tuned to the $9.6\ \mu m$ P(30) transition is square wave chopped and traverses the flame exciting ν_3 , the asymmetric stretching mode of O_3 ($1043\ cm^{-1}$). The chemiluminescence from the $Pb + O_3$ reaction is monitored through a spectrometer-photomultiplier assembly. The photomultiplier output is fed through a series of pulse amplifiers and voltage discriminator into a dual counter, one channel of which records the "laser-on" signal and the other the "laser-off". A printout from these counters is synchronized with the spectrometer wavelength-scan-drive thereby facilitating the recording of the modulation spectrum vs wavelength. The normal spectra ("laser-off") emission is automatically obtained from the "laser-off" counter.

3. Results

In contrast to the spatially sharp diffusion flame observed for the $Ba + O_3$ (or N_2O) reaction, the $Pb - O_3$ flame is quite diffuse (apparently reaction limited). It is brightest in the high temperature zone at the furnace nozzle, diminishes with decreasing temperature (increasing distance from the nozzle), and persists for some time two or three feet into the pumping system. These observations suggest a reaction rate for $Pb + O_3$ which is considerably slower than gas kinetic. The spectrum which we observe at several torr total pressure partly resembles the low pressure spectrum obtained by ODZ and reproduced by us in a similar quasi-beam apparatus. The short wavelength end of the more complete spectrum (fig. 2) can be identified from the low (submicron) pressure spectrum in that it is less diffuse. The long wavelength portion between 480 nm and 595 nm is almost entirely the new state recently characterized by ODZ. At still longer wavelengths, our spectrum differs from that of ODZ in that we observe a series of strong lines which do not agree with a $\rightarrow X$, $A \rightarrow X$, or $B \rightarrow X$, but rather appear to originate from a new state observed via six weak lines by ODZ and identified as b by them. This b state is seen more intensely in our high pressure spectrum. This series of lines in our spectrum can be fit to the expression:

$$\nu(\nu', \nu'') = 16315 + 441.0 \nu' - [717.7 \nu'' - 3.53 \nu'']$$

where the lower state constants have been taken from Rosen's compendium.

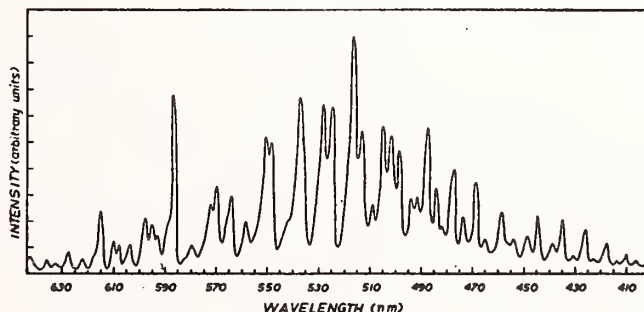


Figure 2. Chemiluminescence spectrum for the $Pb(v) + O_3$ reaction.

Part of the modulation spectrum is reproduced in figure 3. This spectrum, which has been smoothed, represents only that component of the chemiluminescent emission which varies with the laser excitation of O_3 (i.e., only that component which either increases or decreases due to a change in reaction rate with reactant vibrational excitation). Thus, if the emission originated only from a single electronic state, the modulation spectrum would appear as a quasi-continuum with possibly some small structure due to sharp changes in population of one vibrational line relative to an adjacent one. The large amount of structure in figure 3 indicates the presence of emission from at least two electronic states. The peaks (or valleys) in the spectrum do not agree well with either the $a \rightarrow X$ or $b \rightarrow X$ states, but rather with the $A \rightarrow X$ transitions.

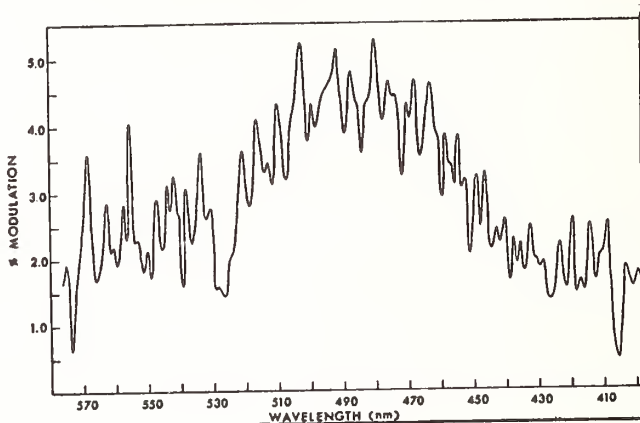


Figure 3. Smoothed modulation spectrum (the component of the emission which varies with laser excitation of O_3) of the $Pb(v) + O_3$ reaction.

The results will be discussed and possible mechanisms proposed taking into account both our results and other investigations of this system.

CHEMILUMINESCENCE IN REACTIONS OF OZONE

S. Toby, F. S. Toby and B. Kaduk

School of Chemistry
Rutgers University
New Brunswick, NJ 08903

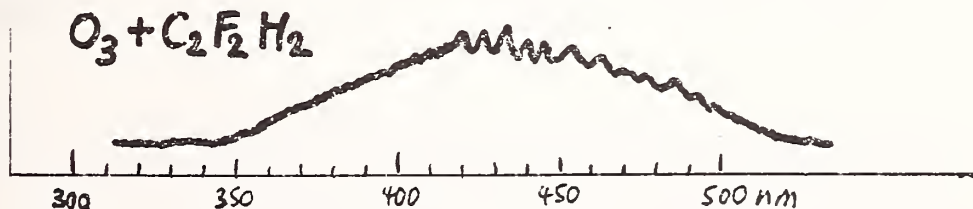
Chemiluminescence (CL) can provide highly sensitive analytical methods for the estimation of reactants, it serves as a unique probe for the identification of intermediates, and it yields data which provide information on energy transfer and partitioning. Gas phase ozone systems have been particularly rich sources of CL, and much work has been done on O_3 + alkenes as an adjunct to kinetic studies. Pitts and co-workers [1]¹ using ozonized oxygen obtained CL from a variety of alkenes and tentatively identified the emissions as from excited formaldehyde and α -diketones. A more extensive investigation [2] confirmed emissions from CH_2O (1A_2) and $(CHO)_2$ (3Au) and reported that in the absence of O_2 Meinel bands ($OH(X^2\Pi)$) were also seen. The presence of O_2 had no effect on the $CH_2O(^1A_2)$ emission in the alkenes studied [2] nor in the case of O_3 + tetramethylethylene and the quenching has been shown to be 10 times as rapid by O_2 as by N_2 [4]. An intriguing parallel is the fact that added O_2 reduces the reaction rate of O_3 + alkenes by about an order of magnitude under conditions normally employed [5]. A similar effect has been noted in the O_3 + C_2F_4 system: added O_2 quenches the CL [6] and also slows the reaction [7].

Reported here are six new CL spectra, measured with apparatus previously described [3, 6]. The spectra were measured at room temperature using a Jarrell-Ash 0.25-m monochromator with a spectral slit width of 3 nm and a cooled EMI 9683QKB photomultiplier. The O_3 flowed in a helium carrier gas at a total pressure of approximately 50 torr.

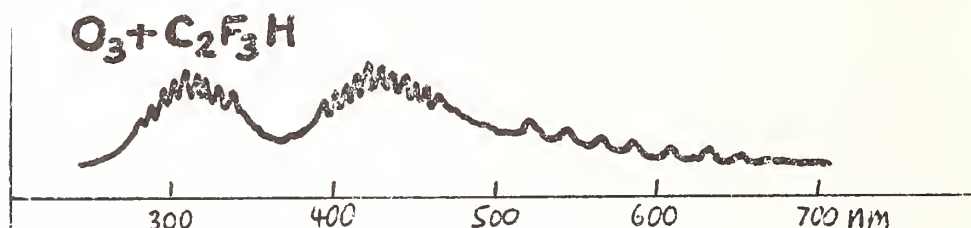
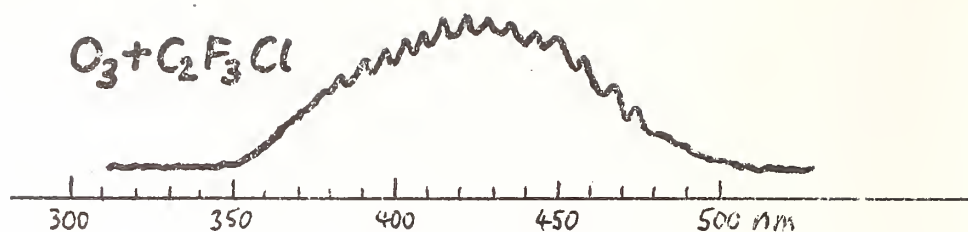
The total intensities uncorrected for spectral response and relative to $C_2H_4 = 1$ are as follows: trans- $C_2F_2H_2$ 30, C_2F_3Cl 350, C_2F_3H 45, thiophene 50, CS_2 540, $HCCCN$ 22.

1. Trans- $C_2F_2H_2$, C_2F_3Cl and C_2F_3H

The CL spectra from the reactions of these fluoroalkenes with O_3 are shown below



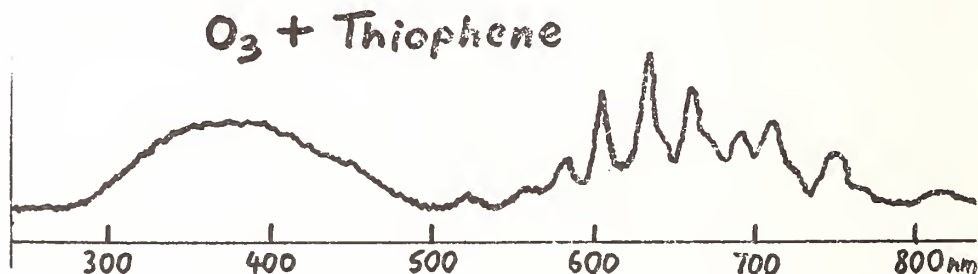
¹ Figures in brackets indicate the literature reference at the end of this paper.



All three substrates give a band from about 350 to 510 nm with a broad maximum at 430 nm and observable fine structure. The species responsible for this emission has not thus far been identified. There is an additional band from $O_3 + C_2F_3H$ in the ultraviolet which we identify as due to singlet excited CF_2 and which is also emitted strongly from $O_3 + C_2F_4$ [6].

2. Thiophene

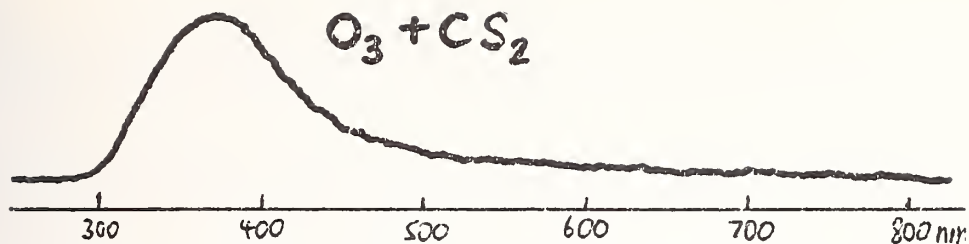
The CL spectrum from $O_3 +$ thiophene is as follows



Two features are seen. The structureless band with a maximum at 370 nm is due to singlet excited SO_2 which has been found in the CL of O_3 with several sulfur-containing compounds [1,8] and which probably arises from the reaction $SO + O_3 \rightarrow O_2 + SO_2^*$. The banded feature from 520 to 810 nm is identical to the longer wave emission from $O_3 + H_2S$ and which has been identified as due to HSO [8], most likely from $SH + O_3 \rightarrow HSO^* + O_2$.

3. Carbon Disulfide

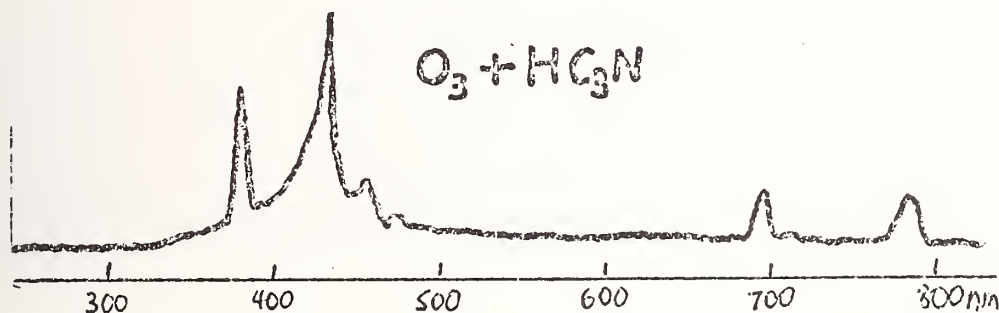
The strong emission from $O_3 + CS_2$ appears as follows:



The emission appears to be entirely due to excited SO_2 . The kinetics of this reaction have been studied by Olszyna and Heicklen [9] who did not report CL but postulated the formation of excited SO_2 from the reaction $\text{CS} + \text{O}_3 \rightarrow \text{CO} + \text{SO}_2^*$.

4. Cyanoacetylene

This unusual spectrum from $\text{O}_3 + \text{HC}_3\text{N}$ extends from 340 to 780 nm and the emission has been identified as due to $\text{CH}(\text{A}^2\Delta \rightarrow \text{X}^2\Pi)$, $\text{CN}(\text{A}^2\Pi \rightarrow \text{X}^2\Sigma)$ and $\text{CN}(\text{B}^2\Sigma \rightarrow \text{A}^2\Pi)$.



The relationship of CL with the kinetics and energetics of some of these reactions is discussed.

References

- [1] Pitts, J. N., Jr., Kummer, W. A., Steer, R. P., and Finlayson, B. J., *Adv. in Chem., (ACS Symposium)* No. 113, 246 (1972).
- [2] Finlayson, B. J., Pitts, J. N., Jr., and Atkinson, R., *J. Am. Chem. Soc.*, 96, 5356 (1974).
- [3] Toby, S., *J. Luminescence*, 8, 94 (1973).
- [4] Schurath, U., Gusten, H., and Penzhorn, R. D., *J. Photochem.*, 5, 33 (1976).
- [5] Toby, F. S., Toby S., and O'Neal, H. E., *Int. J. Chem. Kinet.*, 8, 25 (1976).
- [6] Sheinson, R. S., Toby, F. S., and Toby, S., *J. Am. Chem. Soc.*, 97, 6593 (1975).
- [7] Toby, F. S., and Toby, S., *J. Phys. Chem.*, 80, 0000 (1976).
- [8] Becker, K. H., Inocencio, M., and Schurath, U., *Int. J. Chem. Kinet., Symp.* 1, 205 (1975).
- [9] Olszyna, K. J., and Heicklen, J., *J. Phys. Chem.*, 74, 4188 (1970).

DIOXETANE CHEMISTRY IN THE GAS PHASE UV - VISIBLE CHEMILUMINESCENCE FROM THE REACTIONS OF $O_2(^1\Delta_g)$ WITH OLEFINS

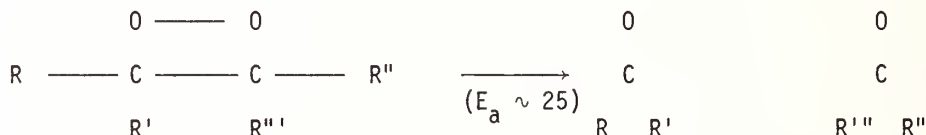
Denis J. Bogan
Chemical Dynamics Branch
Code 6180
Naval Research Laboratory
Washington, DC 20375

and

Joseph L. Durant, Jr.
Chemistry Department
The Catholic University of America
Washington, DC 20064

1. Introduction and Background

Dioxetanes (4 membered cyclic peroxides) are the most notable of a small number of strained cyclic molecules which are known to undergo thermal unimolecular reactions yielding electronically excited products [1,2]¹.

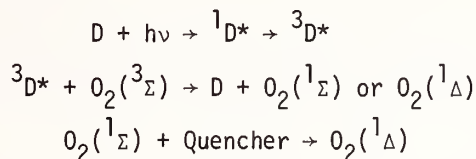


The quantum yields for production of one excited carbonyl product range from 0.01 to perhaps 0.5 with a preferential production of triplet ($n\pi^*$) states [1]. Such quantum yields are orders of magnitude greater than the statistically expected yields based upon equipartitioning of energy to all accessible product states. Recent pervasive interests in chemiluminescence, chemical lasers and electronically non adiabatic reactions have combined to make dioxetane chemistry the subject of considerable attention by both experimentalists [1,2] and theoreticians [3,4].

Previous to our work, studies have involved synthesis of the dioxetane of interest followed by thermal decomposition. The latter has almost always been done in solution where it is complicated by solvent interactions and hence inability to obtain high resolution spectra of the primary excited products. More common than direct chemiluminescence are studies involving energy transfer to dyes which fluoresce efficiently (*e.g.*, 9, 10 dibromo anthracene), and product analysis. Much important information has been gained, for example the singlet-triplet titration experiments of Turro and coworkers [5]; however, the condensed phase techniques, by their very nature, preclude knowledge of the disposition of energy in the primary excited products.

¹Figures in brackets indicate the literature reference at the end of this paper.

Direct 1, 2 cyclo addition of $O_2(^1\Delta)$ to olefins in solution has been used to prepare dioxetanes from mono olefins lacking allylic hydrogen [6,7]. This technique is known as low temperature photosensitized oxygenation and involves production of $O_2(^1\Delta)$ via energy transfer from an organic dye, D.



Only the dioxetanes of electron rich olefins have been made by this technique.

We have found that the reaction of olefins with $O_2(^1\Delta)$ in a low pressure discharge flow system result in the observation of electronically excited products which are expected from the corresponding dioxetanes. The experimental apparatus is shown as figure 1. A microwave discharge through pure O_2 or 3 percent O_2 in He doped with a trace of Hg was used to produce $O_2(^1\Delta)$ free of atomic oxygen. The olefin was added downstream (following 2 light traps) and chemiluminescence was observed axially in a cell of 30 cm path length, with a 1/4 meter grating spectrometer and cooled S-5 photomultiplier in a single photon counting configuration. There is no evidence of complications from atomic oxygen or ozone. Typical pressure and residence time were 4 torr and 0.1 sec. respectively. The results of our experiments with ethyl [8], methyl and n butyl vinyl ethers [8,9], and ethylene [10] have been reported. These and other experiments now underway have centered on two major areas. First, and discussed in Section II, is the dynamics of the reaction, particularly orbital symmetry considerations governing the correlation to excited products and the vibronic motions which serve to promote the reaction. The second main thrust, discussed in Section III, is the production and study of emission spectra which have not been observed previously.

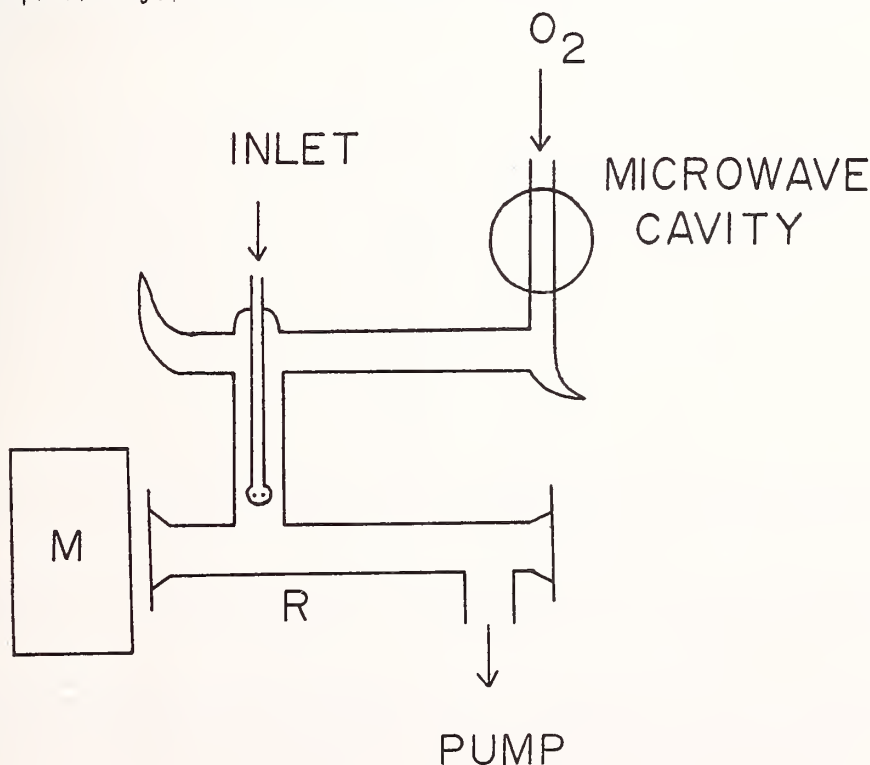


Figure 1. Discharge flow system; R = heated flow reactor with removable quartz windows, M = 1/4 meter monochromator with detector described in text.

2. Dynamics, Capsule Summary

The initial motivation for doing gas phase studies was to obtain high resolution spectra under conditions which would minimize energy transfer and other quenching processes. We soon learned, however, that there is an important fundamental difference between gas phase addition of $O_2(^1\Delta)$ to olefins and liquid phase addition effected by photosensitization. Thermochemistry and chemiluminescence activation energies (Table I) showed that the initially formed adduct of olefin plus $(O_2(^1\Delta))$ contains 45 kcal, or more, of excess vibrational energy [8,10]. Experiments were done measuring the rate of collisional stabilization versus the gas kinetic collision frequency; no stabilization was found and we concluded that the mean lifetime of the vibrationally excited dioxetane was less than 10^{-8} sec. [8,9].

Table I. Data summary for reactions of $O_2(^1\Delta_g)$ with Olefins

Olefin	E_a (kcal/mole)	Emission	$-\Delta H_R^a$ (kcal/mole)
$H_2C=CHOMe$			
$H_2C=CHOEt$	12 ± 1	H_2CO	107
$H_2C=CHOnBu$			
$H_2C=CH_2$	21 ± 1	H_2CO	90.5
$EtOHC=CHOEt$		none ^b	
$H_2C=C=O$	15 ± 1	H_2CO	129
$H_2C=CHF$		H_2CO	136
$H_2C=CF_2$		H_2CO	122
$HFC=CF_2$		$HFCO, F_2CO$	175 ^d
$F_2C=CF_2$		F_2CO	171
$H_2C=CHCl$		H_2CO	129
$H_2C=CCl_2$		H_2CO	103
$Cl_2C=CCl_2$		none ^e	124
$H_2C=CHCHO$		none	
$MeHC=CMe_2$		none ^c	104
$Me_2C=CMe_2$		none ^c	109

^a ΔH_R is calculated for ground state carbonyl products. Thermochemical data are from reference 16, reference 8 for vinyl ethers.

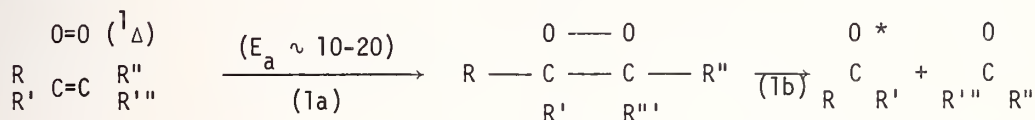
^b $HCOOEt^*$ is believed to rearrange quantitatively to C_2H_4 plus $HCOOH$ via a Norrish Type II process, see reference 16b.

^c The formation of allylic hydroperoxides has $E_a \sim 3-6$ kcal and is favored over dioxetane formation.

^d Our estimate.

^e We infer that Cl_2CO^* is lost completely by predissociation and/or other non radiative processes.

Thus the overall reaction is a chemical activation process (1a), followed by rapid fragmentation (1b).



The chemically activated dioxetane must have a lifetime $> 10^{-12}$ sec., since dioxetanes have been isolated and characterized from low temperature solution photosensitization [7].

Many reactions give formaldehyde ($A \ ^1A_2 \rightarrow X \ ^1A_1$) emission. A hot band representing excitation in ν_4 (the out of plane bend) occurs with intensity which correlates positively with available energy and negatively with the number of vibrational modes of the expected dioxetane. The correlation crudely approximates an RRK relationship. The principal geometry difference between H_2CO in dioxetane and $\text{H}_2\text{CO}^*(^1A_2)$ is in ν_4 , which suggests that chemical Franck-Condon factors are operative and that the hot band intensity is inversely related to the lifetime of the vibrationally excited dioxetane.

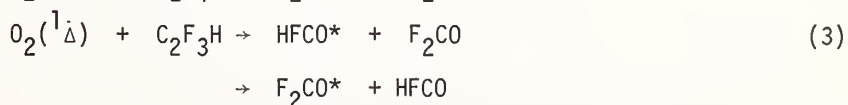
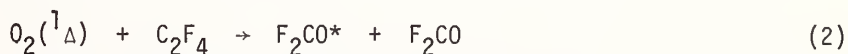
In contrast to the lifetimes, electronic energy partitioning of chemically activated dioxetanes is non statistical. Methyl, ethyl and n-butyl vinyl ethers give only H_2CO^* emission and exhibit equal quantum yields for H_2CO^* emission at all temperatures of study [9]. Many other unsymmetrical olefins give only one of the two possible product emissions. The only apparent exception is $\text{C}_2\text{F}_3\text{H}$ which is discussed in the following section.

The energy partitioning and hot band information (which could not have been obtained from condensed phase studies) are being used to formulate an orbital symmetry - vibronic interaction theory of the dynamics of these reactions [4].

3. Previously Unobserved Emissions

The study of $A - X$ ($n\pi^*$ -ground) electronic transitions of carbonyl compounds has been a subject of major and continuing interest in both photochemistry and molecular spectroscopy. Neither F_2CO nor HFCO ($A-X$) emissions have been characterized. The A ($n\pi^*$) state of HFCO predissociates very readily and HFCO is the basis of a photodissociation chemical laser [12]. The A ($n\pi^*$) state of F_2CO is of interest to atmospheric modellers because F_2CO is a likely secondary product of fluorochlorocarbon photodissociation in the stratosphere and it can in turn, photodissociate to give F atoms which can then destroy ozone [13].

Figure 2 shows spectra which were obtained from the reactions,



We have a complete vibrational assignment of the F_2CO ($A \rightarrow X$) emission; we have not yet assigned HFCO .

The barrier to inversion in the A state of F_2CO has been estimated [14] as 4000^{-1} , hence we expect the behavior of an undoubled well in ν_4 since the lower vibrational levels of 2 deep wells will not communicate effectively. On this basis the reported origin in the absorption spectrum [15] at 42084 cm^{-1} is the energy of the transition 4_0^1 .

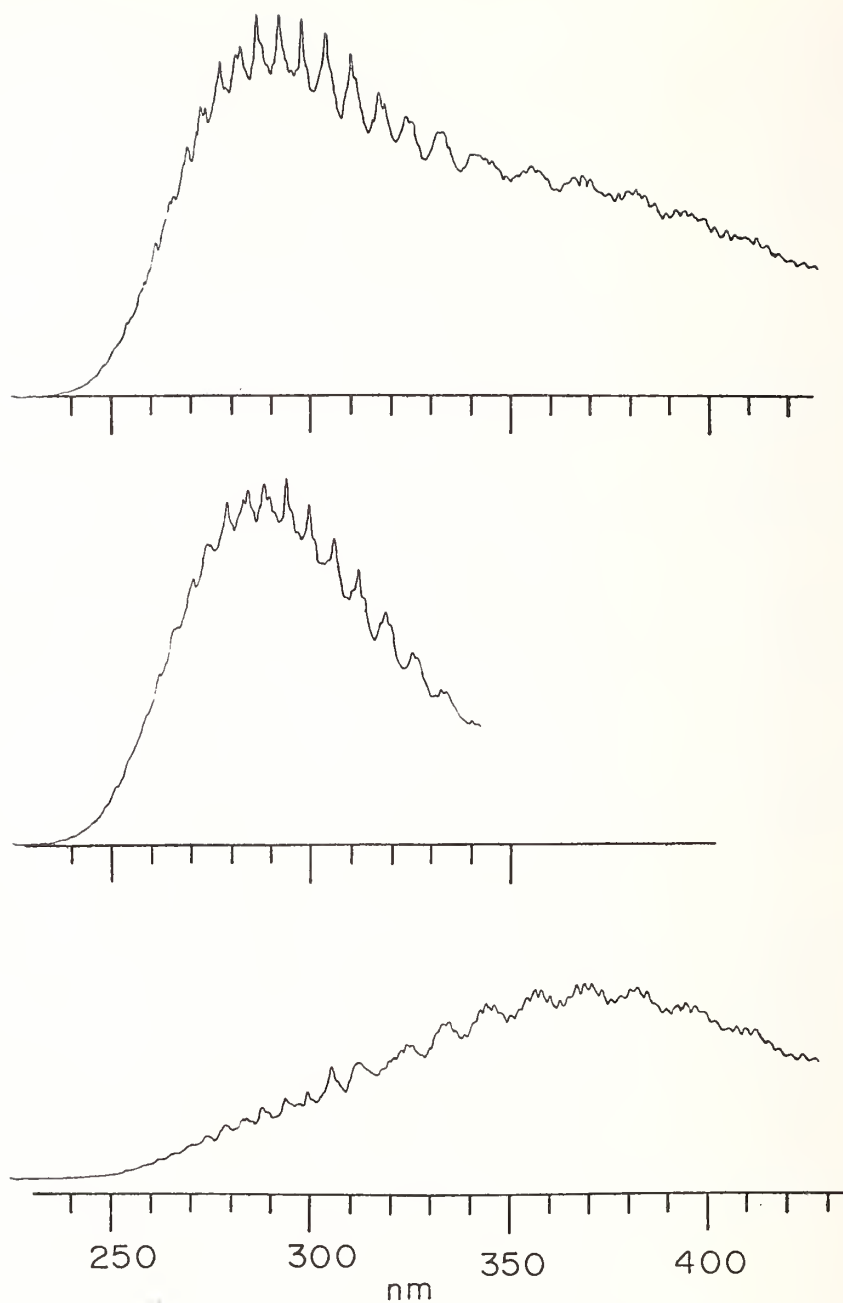


Figure 2. Chemiluminescence spectra from reactions of $O_2(^1\Delta g)$ with fluorinated olefins. Bottom panel is C_2F_3H only, middle panel is C_2F_4 only, top panel is C_2F_3H plus C_2F_4 . Conditions were; $P(\text{total}) = 4.1$ torr (approx. 0.2 of olefin and 3.9 of oxygen), $T = 800$ deg K, reactor residence time = 0.1 sec., spectral slit = 0.4 nm., scan rate = 12.5 nm./min., time constant = 1 sec., full scale intensity = 10K counts/sec.

Plausible assignments have been obtained for 65 lines out of the total of ca. 70 lines in the spectrum. The spectral slit width was 4 Å and line positions have an uncertainty of ca. $\pm 25 \text{ cm}^{-1}$. The observed progressions all obey the vibronic symmetry selection rules for the point group C_{2v} . The fundamental ground state assignments of Neilsen et al [17] (mode numbers redefined in Herzberg convention) were used. These are

- $\nu_1 = 1942 \text{ cm}^{-1} (a_1)$ carbonyl stretch
- $\nu_2 = 965 \text{ cm}^{-1} (a_1)$ totally symmetric stretch
- $\nu_3 = 626 \text{ cm}^{-1} (a_1)$ F-C-F in plane bend
- $\nu_4 = 774 \text{ cm}^{-1} (b_1)$ out of the plane bend
- $\nu_5 = 1249 \text{ cm}^{-1} (b_2)$ asymmetric F-C-F stretch
- $\nu_6 = 584 \text{ cm}^{-1} (b_2)$ wagging

All but 2 (hot band) progressions originate from an electronic origin at 41396 cm^{-1} , hence in the excited state $\nu_4^* = 688 \text{ cm}^{-1}$. Only ν_4 and ν_5 appear as bare progressions; surprisingly ν_1 appears only in concert with promoting modes. Some of the observed progressions are

4_n^0	$n = 1, 3, \dots$	15
5_n^0	$n = 1, 3, \dots$	9
$5_1^0 4_n^0$	$n = 0, 2, \dots$	14
$2_1^0 4_1^0 6_n^0$	$n = 0, 2, \dots$	10
$2_1^0 4_1^0 6_2^0 1_n^0$	$n = 0, 1, \dots$	4
$3_1^0 4_6^0 5_1^0 6_n^0$	$n = 0, 2, \dots$	8

Reasonably convincing indirect evidence that the emission is indeed F_2CO ($A \rightarrow X$) is; a) our emission begins at 235 nm as compared to the known origin of absorption at 237.6, [15]
 b) the observed emission intensity is kinetically first order in both $O_2(^1\Delta)$ and C_2F_4 .
 The spectrum becomes diffuse and steadily diminishes in intensity from 350 to 520 nm., much like the long λ bands of H_2CO ($A-X$).

The spectrum from the reaction of C_2F_3H shows clear evidence that the F_2CO^* emission is present as well as a new very complicated emission. The emission at $\lambda = 400 \pm 25 \text{ nm}$ is first order in C_2F_3H . A spectrum was obtained using C_2F_4 and C_2F_3H both at the concentrations used for their respective pure spectra and this a simple sum of the pure component spectra. This establishes that the postulated $HFCO^*$ emission from reaction 3 is not excited by energy transfer from F_2CO^* .

As a result of these experiments, this chemiluminescence technique is established as a means of characterizing previously unobserved carbonyl ($A-X$) emissions. The region of the excited state phase space which can be reached by light excitation of a polyatomic molecular is severely restricted by the Franck-Condon principle. The volume of phase space accessible by chemical reaction is much less restricted and it is not surprising that regions can be reached from which radiative transitions can be observed. This is particularly significant for excited states which predissociate near the electronic origin.

References

- [1] Turro, N. J., et al, *Accounts Chem. Res.*, 7, 97 (1974).
- [2] Mumford, C., *Chemistry in Britain*, 11, 402 (1975).
- [3] Dewar, M. J. S., and Thiel, W., *J. Am. Chem. Soc.*, 97, 3978 (1975).
- [4] a) Chiu, Y-N., *J. Chem. Phys.*, in press, 64, number 7, (1976).
 b) Chiu, Y-N., Bogan, D. J., and Sheinson, R. S., to be submitted.
- [5] Turro, N. J., and Lechtken, P., *J. Am. Chem. Soc.*, 94, 2886 (1972).
- [6] Adam, W., *Chemiker Zeitung*, 99, 142 (1975).
- [7] Bartlett, P. D., and Schaap, A. P., *J. Am. Chem. Soc.*, 92, 3223 (1970).
- [8] Bogan, D. J., Sheinson, R. S., Gann, R. G., and Williams, F. W., *J. Am. Chem. Soc.*, 97, 2560 (1975).
- [9] Bogan, D. J., Sheinson, R. S., and Williams, F. W., paper F-9, *8th International Conference on Photochem.*, Edmonton, Canada, August 1975; abstract including spectra to be published in *J. Photochem.*
- [10] Bogan, D. J., Sheinson, R. S., and Williams, F. W., *J. Am. Chem. Soc.*, 98, 1034 (1976).
- [11] Berry, M. J., *Chem. Phys. Lett.*, 29, 329 (1974).
- [12] Klimek, D. E., and Berry, M. J., *Chem. Phys. Lett.*, 20, 141 (1973).
- [13] a) Rowland, F. S., and Molina, M. J., *Revs. Geophys. and Space Phys.*, 13, 1 (1975).
 b) Chou, C. C., Ruiz, H. V., Crescentini, G., and Rowland, F. S., paper PHSC 5, *First Chemical Congress of North America* (and 171st National ACS), Mexico City, Mexico, December 1975.
- [14] Condirston, D. A., and Moule, D. C., *Theor. Chim. Acta*, 29, 133 (1973).
- [15] Workman, G. L., and Duncan, A. B. F., *J. Chem. Phys.*, 52, 3204 (1970).
- [16] a) Benson, S. W., in *Thermochemical Kinetics*, Wiley, New York, 1968.
 b) Benson, S. W., and O'Neal, H. E., *Kinetic Data on Gas Phase Unimolecular Reactions*, *NSRDS-NBS 21*, U. S. Dept. of Commerce, 1970.
- [17] Nielsen, A. H., Burke, T. G., Woltz, P. J. H., and Jones, E. A., *J. Chem. Phys.*, 20, 596 (1952).
- [18] Bogan, D. J., and Durant, J. L., Jr., *J. Mol. Spectroscopy*, to be submitted.

MOLECULAR DISSOCIATION BY HIGH-INTENSITY INFRARED LASER RADIATION

K. H. Welge

Fakultät für Physik
Universität Bielefeld
Bielefeld, West Germany

The dissociation of molecules by high-intensity laser radiation in the infrared has recently gained substantial interest, particularly since it has been found that the process is highly state and isotope selective. However these processes have not yet been investigated in any detail and are not yet well understood.

This paper will be concerned with a review of this subject with emphasis on our own studies in this area. We have been concerned with three kinds of experiments using line selected pulsed CO₂-laser radiation at energies ~ 100 Joule/pulse and intensities ~ 10 GWatt/cm²:

1. Dissociation and photolysis of molecules at pressures down to collisionless conditions using laser fluorescence spectroscopy for in-situ diagnostics of fragments. Experiments have been concerned with NH₃ and its isotopic compounds;
2. Crossed molecule/CO₂-laser beam experiments on the kinetics and dynamics of the high-intensity field dissociation process by photodissociation fragment spectroscopy;
3. Experiments on isotope selectivity by measurement of the isotope separation factor as function of parameters such as number of pulses per sample, gas pressure, laser energy etc.. Also, the quantum yield of separation has been investigated.

PHOTOCHEMISTRY OF FORMALDEHYDES: PAST AND PRESENT¹

Edward K. C. Lee, Roger S. Lewis and Richard G. Miller

Department of Chemistry
University of California
Irvine, CA 92717

In the past, photodecomposition of formaldehyde has been studied extensively because of general interest in understanding the primary photochemical processes for the simple carbonyl compounds. Recent interest in its study certainly stems from the need to evaluate the role that formaldehyde plays in photochemical air pollution, particularly due to the formation of H-atoms and consequent reactions in the photooxidation processes [1,2]². More recent and current interest is generated from the suggested practicality of photochemical laser isotope separation of deuterium and other isotopes [3,4]. Since quantum yields of the fluorescence, the radical products (H and HCO) and the molecular elimination products were not known at various single vibronic levels (SVL) earlier, we have undertaken a systematic study in which the mechanism and rates of these primary processes in H₂CO, HDCO, and D₂CO can be established by various photophysical and photochemical techniques.

We have recently reported the observation of a large variation of the radiative lifetimes (τ_R) and the non-radiative lifetimes (τ_{NR}) of selected SVL's of the first excited state of H₂CO (S_1 , \tilde{A}^1A_2) [5]. New results on the fluorescence quantum yields (Φ_F) of H₂CO, HDCO, and D₂CO vs. excitation wavelength (λ_{ex}) have been obtained by fluorescence excitation spectroscopy of these isotopic formaldehydes at low pressures [6], and they are shown in figure 1. The values of Φ_F for the first excited vibrational level (4^1) having one quantum excitation of the out-of-plane wagging mode ($\nu_4' = 1$) are ~ 0.035 for H₂CO, ~ 0.05 for HDCO, and 1.0 for D₂CO, indicating the absence of photochemical activity at the 4^1 level of D₂CO; the fluorescence decay times (τ_F) at low limiting pressures are 0.082, 0.141 and 4.5 μ sec, respectively.

In general, the rates of non-radiative transitions increase exponentially with the increasing excitation energy. The fact that the values of Φ_F and τ_F are slightly higher in HDCO than in H₂CO predicts similar rates of deactivation for this isotopic pair, whereas very different photochemical rates are expected for D₂CO. The rate of non-radiative transition in D₂CO (4^1), showing an extremely large deuterium isotope effect. Furthermore, operational complications in photochemical isotope separation due to collisional electronic quenching and vibrational energy transfer in H₂CO and HDCO should be negligible below 1 torr pressure.

¹This work has been supported by the Office of Naval Research and the National Science Foundation.

²Figures in brackets indicate the literature references at the end of this paper.

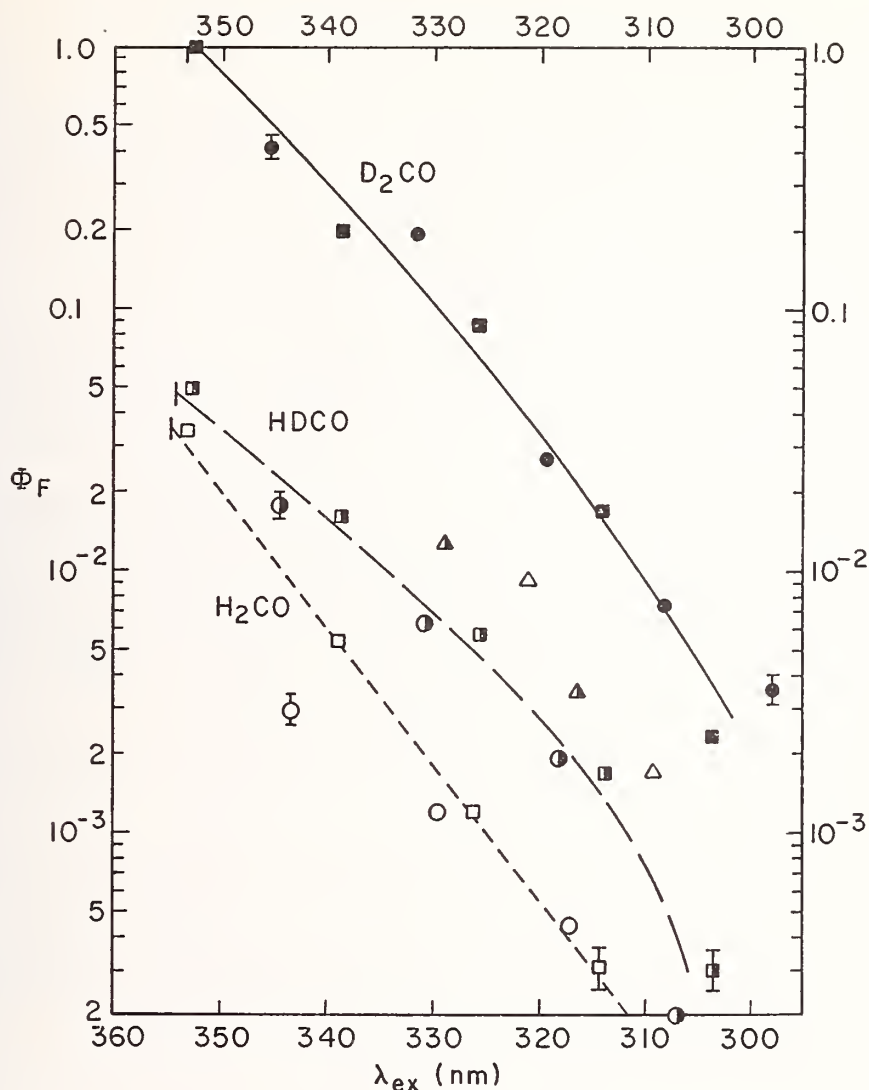


Figure 1. Fluorescence quantum yield vs. excitation wavelength: 0.045 torr D_2CO (filled); 0.20 torr $HDCO$ (half-filled); 0.098 torr H_2CO (open), SVL assignment: squares = 2^n4^1 progression; circles = 2^n4^3 progression; triangle = 2^n5^1 progression where $n = 0, 1, 2, \dots$

It has been well recognized that the radical formation process could seriously lower the isotope separation efficiency [3,4]. In order to evaluate the quantum yield of hydrogen atom formation from various SVL's, we have tried to devise a sensitive, quantitative and convenient spectroscopic method for detecting photochemical H-atoms by observing the near infrared chemiluminescence emission from the HNO^* formed by recombination of $H + NO(+M)$ [7]. We have found that the chemiluminescence photoexcitation spectrum observed in the mixture of H_2CO and NO shows the electronic absorption features of $H_2CO(\tilde{A}^1A_2) \leftarrow \tilde{X}^1A_1$ transition, since the photoexcited H_2CO^* gives off H-atoms by radical decomposition process. The preliminary results are illustrated in figure 2 [8]. The chemiluminescence emission from HNO^*/DNO^* was confirmed by the analysis of the 760 nm emission band from the mixture of $HDCO$ and NO excited with a cadmium laser (325.0 nm) [8]. The threshold for the H-atom formation from H_2CO appears to be near 330 nm. The quantitative implications of the above observation to the atmospheric chemistry and the laser isotope separation will be presented at the conference.

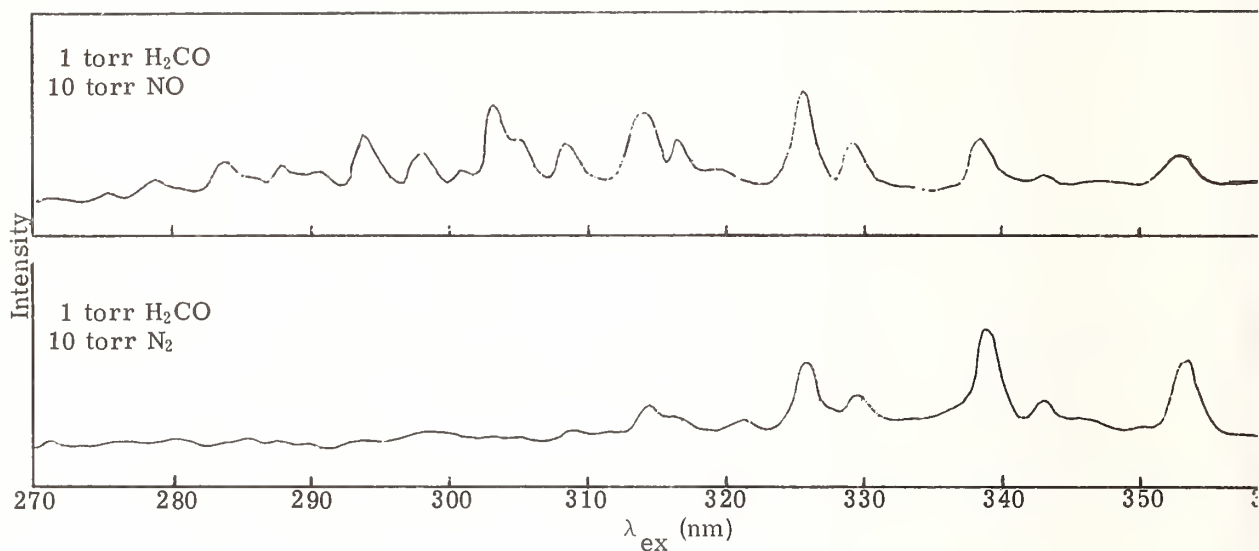


Figure 2. Excitation spectra run with a long pass emission filter (700 nm cut off).

References

- [1] a) DeGraff, B. A., and Calvert, J. G., *J. Amer. Chem. Soc.*, 89, 2247 (1967).
 b) McQuigg, R. D., and Calvert, J. G., *J. Amer. Chem. Soc.*, 91, 1590 (1969).
- [2] Calvert, J. G., Kerr, J. A., Demerjian, K.-L., and McQuigg, R. D., *Science*, 175, 751 (1972).
- [3] a) Yeung, E. S., and Moore, C. B., *J. Chem. Phys.*, 58, 3988 (1973).
 b) Moore, C. B., *Accounts Chem. Res.*, 6, 323 (1973).
- [4] Marling, J. B., *Chem. Phys. Lett.*, 35, 84 (1975).
- [5] Miller, R. G., and Lee, E. K. C., *Chem. Phys. Lett.*, 33, 104 (1975).
- [6] Miller, R. G., and Lee, E. K. C., *Chem. Phys. Lett.*, 00, 0000 (1975).
- [7] a) Clyne, M. A. A., and Thrush, B. A., *Disc. Faraday Soc.*, 33, 139 (1962).
 b) Ishiwata, T., Akimoto, H., and Tanaka, I., *Chem. Phys. Lett.*, 21, 322 (1973).
- [8] Lewis, R. S., Tang, K. Y., and Lee, E. K. C., unpublished results.

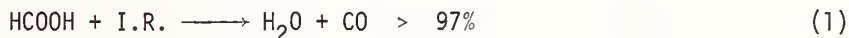
DECOMPOSITION OF FORMIC ACID VAPOR BY INFRARED LASER RADIATION

R. Corkum¹, C. Willis, M. H. Back¹ and R. A. Back

PIE Group Chemistry Division
National Research Council of Canada

The infrared induced decomposition of formic acid vapor has been studied using the P_{18} and P_{28} lines from a line tunable, pulsed HF laser. The study was undertaken both to investigate the parameters involved in the induced decomposition and to assess the potential of the system for photochemical isotope enrichment.

The beam from the laser was focused into a photolysis cell fitted with infrasil quartz windows. After irradiation the cell contents were condensed at -196°C and the non-condensable products measured by gas burette and analysed either by gas chromatography or mass spectrometry. The only non-condensable product observed was CO and in a few experiments it was demonstrated that an equivalent amount of H_2O was formed. Less than 3% of the decomposition led to CO_2 .



and H_2 . Earlier studies have shown (1) that both channels are important in the pyrolysis of formic acid vapor.

The laser beam was focused into the cell with an $f = 7.5$ cm lens. If this was removed no decomposition was detected. Using a long focal length lens, $f = 150$ cm, to focus the beam into the cell gave some decomposition but with a yield of only about 1% of that with the $f = 7.5$ cm lens. These observations are indicative that the decomposition has a relatively sharp intensity threshold. This was confirmed using neutral-density filters in conjunction with the $f = 7.5$ cm lens.

The effect of temperature, pressure, added inert gas and cell path length were investigated. Increasing temperature in the range 25 – 180°C led to a slight increase in yield but this could be attributed to a shift in the dimer-monomer equilibrium, with only the monomer absorbing the HF radiation. Increasing the pressure in the range 10 – 40 Torr led to an almost proportional increase in relative quantum yield. Addition of N_2O or CO_2 did not affect the amount of IR absorbed but dramatically reduced the observed yield of CO. This effect is interpreted as collisional deactivation of vibrationally excited formic acid. Photolysis was performed in cells 10 cm and 1 cm long. The amount of CO formed in the short cell was only slightly smaller than that formed in the long cell, which is consistent with decomposition occurring only close to the focus of the lens. A lower limit of $\phi_{\text{CO}} \geq 6 \times 10^{-2}$ could be set for the quantum yield of the decomposition based on the light absorbed in the short cell. This is a surprisingly large value particularly when it is noted that the activation energy of 29 ± 1 kcal/mole found in the pyrolysis is equivalent to about 3 photons of the incident radiation, and that the quantum yield is still increasing with increasing pressure.

Department of Chemistry, University of Ottawa, Ottawa, Canada.

Figures in brackets indicate the literature references at the end of this paper.

Unfortunately, the formic acid system offers little promise for isotope separation. Since H_2O and not H_2 is the hydrogen-bearing product, any separation in the photolysis would be rapidly lost by re-equilibration with the formic acid substrate. Various mixtures of H^{12}COOH and H^{13}COOH have been irradiated but in each experiment the isotopic ratio in the CO produced faithfully reflected the ratio of the starting material, despite the fact that H^{12}COOH absorbs the P_{18} line nearly twice as effectively as H^{13}COOH .

The laser radiation is absorbed by the OH stretching mode of monomeric formic acid and two limiting mechanisms for the subsequent decomposition can be considered. In the first, individual molecules are excited to levels above their dissociation energy by stepwise absorption of quanta in the O-H stretching vibration. Collisional or power broadening of the higher levels must be invoked to circumvent energy mismatch due to anharmonicity, although since only 3 or 4 quanta are required to exceed the dissociation energy, this problem is not serious. Unimolecular dissociation of vibrationally excited formic acid molecules would follow the usual internal reorganization of vibrational energy into the mode leading to dissociation to $\text{CO} + \text{H}_2\text{O}$ in collisional deactivation.

In the second limiting mechanism collisional relaxation of the initially excited OH stretching vibration is fast enough that stepwise excitation to higher levels is not required. Collisional relaxation into other modes results in a small volume of hot vapor which decomposes through a normal thermal decomposition mechanism in competition with cooling by loss to the surrounding cold vapor.

Either mechanism could probably account for the relatively high quantum efficiency of the decomposition and both would show a strong dependence on intensity as observed. The lack of isotopic selectivity and the pressure dependence suggests that the second mechanism is operative, but uncertainties in the details of the thermal decomposition make it impossible to make a clear choice between the two. The mechanisms suggested are limiting cases, the first favored at low pressure and the second at high pressure. The present experiments may correspond to a mixture of the two with an intermediate degree of relaxation of the OH stretching excitation into other vibrational modes.

References

- [1] Blake, P. G., and Hinshelwood, C., *Proc. Roy. Soc. (London)* A255, 444 (1960).

THE LASER AUGMENTED DECOMPOSITION OF D_3B ADDUCTS

K. R. Chien and S. H. Bauer

Department of Chemistry
Cornell University
Ithaca, NY 14853

We have completed the investigation of the laser augmented decomposition of H_3BPF_3 and extended these studies to D_3BPF_3 . The low power, low pressure absorption coefficients (α_{10}) of D_3BPF_3 for many lines in the CO_2 laser are somewhat larger than the corresponding magnitudes for H_3BPF_3 , and the entire band is shifted to higher frequencies. The band shapes and re-lative positions follow the trends predicted from a normal mode analysis. The P(J) dependence of the augmentation factor is most interesting. For the tri-deutero compound, the highest photolytic yield is produced by the P(24) line; here α_{10} is approximately 1/5 as large as that at the absorption band peak, which occurs at P(4); for the tri-hydrido compound, the most effective line is P(32), where the absorption coefficient (α_{10}) is approximately 1/4 of that at the band peak, which occurs at P(22). The H/D separations are readily achieved by line selection. With P(24) the augmented decomposition of D_3BPF_3 preferentially selects the ^{11}B isotope by $\sim 35\%$ in a 5 minute run. Also, D_3BPF_3 is decomposed preferentially, relative to HD_2BPF_3 ; the H/D separation is substantial, and increases with irradiation time. The (10/11) specificity did not show up in H_3BPF_3 , in agreement with the normal mode analysis.

The augmented rate [H_3BPF_3 at P(32)] is *linearly* dependent on the *pressure* from 2-15 mtorr. At 25 mtorr, and more so at 50 mtorr, the degree of augmentation is increasingly greater. This may be due to the decrease in the mean free path within the reaction cell and consequent v-T heating of the reagent, such that a thermal component is superposed on the photolytic rate. The rate is clearly *not linearly* dependent on the *power*. Plots of $\log (\% \text{ conversion})$ vs $\log (\text{laser intensity})$ gave slopes ~ 3.1 , indicating that at least three photons are required per molecule to augment decomposition. The time dependence of the decomposition, at low % conversion, proved to be unexpected. Whereas the % decomposition is linear with time at the high power levels (120 watts), or for lower powers at higher temperatures (60 w at $36^\circ C$), at low powers (50 watts) the % decomposition is approximately quadratic with time but becomes linear at longer time periods. This is strongly suggestive of a multi-photon process.

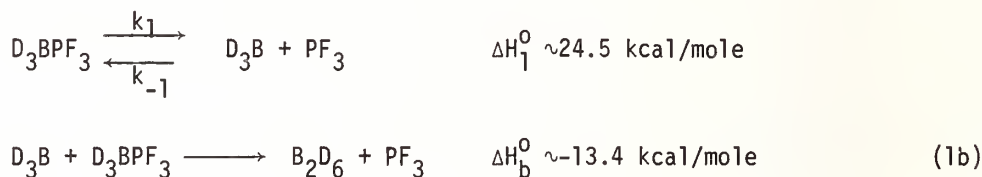
For runs below 15 mtorr the rate constants at several laser powers were calculated on the basis of a first order rate law since these rates are independent of pressure; the reaction time was kept constant at 12 minutes. "Activation energies" (E_a) were deduced from pairs of rate constants at two wall temperatures: $25^\circ C$ and $38^\circ C$. The magnitudes of E_a varied from 2.5 to 5.9 kcal/mole, with a mean value of 3.5 kcal/mole. At this state we assumed that the increment in average gas temperature (which must be somewhat higher than the wall temperature) is equal to the increment in wall temperature.

To determine the photon conversion efficiency we measured changes in laser output levels due to intra-cavity power absorption by the sample, at laser power levels used for the moderate photolysis runs (approximately 60 watts). The *mean* absorption coefficients $\langle \alpha \rangle$ were calculated following the analysis of Kaufman and Oppenheim. They found that laser output decreased essentially linearly with $(1 - e^{-\alpha D})$ until lasing was quenched. Write

$$J_L/J_L^0 = 1 - \beta(1 - e^{-\alpha D}); \quad \alpha D = \ln \left[\frac{\beta}{(\beta - 1) + J_L/J_L^0} \right] \quad \text{where } \beta = 3.33 \text{ for our laser and } \alpha = \langle \alpha \rangle p \text{ at}$$

these low pressures. The $\langle \alpha \rangle$ coefficients for selected lines were thus obtained. The gross photochemical efficiency was then estimated. The laser power extracted by the sample in the cavity per passage through the cell is $20 J_L (1 - e^{-\langle \alpha \rangle pD})$, where J_L is the power read with the monitoring meter, through the output mirror (95% reflecting). The number of photons absorbed is $40 J_L \cdot \langle \alpha \rangle pD \cdot 10^7 \Delta t / h\nu$. The ratio of photons absorbed/molecule decomposed is $\sim 4 \times 10^4$ for 60 w of laser power and $p = 3$ mtorr (298°K). Then $\sim 30\%$ is decomposed in 12 minutes. This low efficiency and the observed low value for E_a^L (mean: 3.5 ± 1.1 kcal/mole), in contrast to the overall thermal value of 29.3 kcal/mole, may be accounted for by considering: (a) the geometry of the reaction cell, (b) the previously estimated thermal activation energy, E_a^{th} (1b) ~ 5 kcal/mole, and (c) the slope of $\log (\% \text{ dec})$ vs $\log (\text{power})$ line. A semi-quantitative account follows.

The two elementary steps which account for the thermal reaction are:



It is plausible to assume that the vibrationally excited adducts do dissociate to a greater extent than *via* the thermal reaction. Under high flux irradiation, the D_3BPF_3 ($\nu_3; \nu_9$) leave the illuminated core and collide with unexcited adducts and dissociation fragments in the larger encompassing volume. However, since BD_3 's recombine to B_2D_6 and D_3BPF_3 with essentially kinetic cross-sections, its concentration level in the encompassing volume is but an order of magnitude higher than under thermal conditions. The upper limit temperature in the encompassing volume is $\approx 45^\circ\text{C}$ because of the absence of detectable decomposition of admixed H_3BCO (in a 12 min. run). The augmented rate we observe is due to D_3BPF_3 which enter the annular region around the illuminated core and there encounter BD_3 's.

A conventional steady-state condition on $[\text{BD}_3]$ leads to:

$$[\text{BD}_3]_{ss} = \left(\frac{k_1}{k_{-1}} \right) \frac{1 - \xi}{\gamma \xi + (k_b/k_{-1})(1 - \xi)} \quad (2)$$

where ξ is the fraction of D_3BPF_3 decomposed at the specified time, and γ ranges from 2 [at early times, when $[\text{BD}_3] \approx [\text{PF}_3]$] to unity, when $[\text{PF}_3] \gg [\text{BD}_3]$.

Under laser irradiation both k_1 and k_b increase. Thus, for those adducts that accumulate $3\nu_3$, about 3 kcal/mole reside in B-P extension. Since $E_b^{th} = 4.8$ kcal/mole and $E_a^{th} = 24.5$ kcal/mole, we postulate that:

$$k_1^{(3\nu_3)} = 2.4 \times 10^{15} \exp\left[-\frac{21,500}{RT}\right] \quad (3)$$

$$k_b^{(3\nu_3)} = 3 \times 10^{12} \exp\left[-\frac{1800}{RT}\right] \quad (4)$$

Application of Eq. (2) gives $[\text{BD}_3]_{ss}^{\dagger} \sim 1.2 \times 10^{-11}$ moles/cc, when $\xi \rightarrow 0.1$, and $T = 318^\circ\text{K}$ for one mfp thick annular region. (Volume = $1.3 \times 10^3 \text{ cm}^3$).

The number of adducts that enter and leave the illuminated core (per sec) is 2.8×10^{20} when the molecule density is 10^{14} cm^{-3} (3 mtorr) [derived from NCA/4]. Their mean exposure time (met) to the radiation is 4×10^{-5} sec. During one such period 1.12×10^{16} D_3BPF_3 enter and leave; concurrently, 1.37×10^{15} photons are absorbed; i.e. *on the average* one out of 8 adducts picks up a single photon. Goodman calculated that 17 of these pick up two, and one out of 79 picks up three in a *coherent sequential* process. Thus, $\sim 1.8 \times 10^{13}$ $\text{D}_3\text{BPF}_3(3\nu_3)$ enter the annular region (1 mfp = 1.5 cm) per *met*. These either get de-excited or react with a D_3B prior to entering the remaining volume.

The total moles of B_2D_6 produced during a 12 min. run, at the 60 watt level, *via*

$$\text{D}_3\text{BFP}_3(3\nu_3) + \text{BD}_3 \xrightarrow{k_b^\ddagger} \text{B}_2\text{D}_6 + \text{PF}_3$$

$$M = \left(\frac{720}{4 \times 10^{-5}} \right) \frac{1.8 \times 10^{13}}{6.02 \times 10^{23}} \frac{1}{1300} [2 \times 10^{11}][\text{BD}_3]_{ss} \quad (5)$$

If we accept the above estimate for $[\text{BD}_3]_{ss}^\ddagger$, $M = 9.9 \times 10^{-7}$ moles, compared with 3.9×10^{-6} moles of the adduct initially present; that is, a conversion of $\sim 25\%$, close to that observed.

INFRARED LASER ISOTOPE SEPARATION

John L. Lyman and Stephen D. Rockwood

Los Alamos Scientific Laboratory
P.O. Box 1663
Los Alamos, NM 87545

It has been established in previous work [1-5]¹ that when SF₆ is irradiated by intense CO₂ laser radiation isotopically selective dissociation occurs. The following points have been established:

1. The reaction is selective when the pressures is less than about 10 torr. [1,2,5]
2. Both reaction yield and selectivity decrease with increasing pressure. [1,2,3,5]
3. A fluorine atom scavenger such as H₂ enhances reaction yield and selectivity [1,2,3,5].
4. The reaction yield increased more rapidly than linear with pulse energy and there appears to be an intensity threshold. [4,5]
5. The reaction yield depends on the laser frequency, but it does not follow the infrared band contour [4].
6. Other molecules also undergo isotopically selective reactions [3].

In a typical experiment a mixture of SF₆ and H₂ is irradiated by focussing the CO₂ pulses into the reaction cell with a short focal length BaF₂ lens [2,3]. If it is assumed that 40 laser photons are required for rapid dissociation (the bond strength is 28 photons), then the photon utilization efficiency is 2.5×10^{-4} for a sample of 0.2 torr of 25% SF₆ in H₂ and 1.0 Joules/pulse.

It has been suggested that this efficiency could be improved by irradiating the gas in reflective cylinders [6]. Several cylindrical cells have been constructed and tested. (See Fig. 1 for cell construction and dimensions.)

¹ Figures in brackets indicate the literature references at the end of this paper.

REFLECTIVE CELL

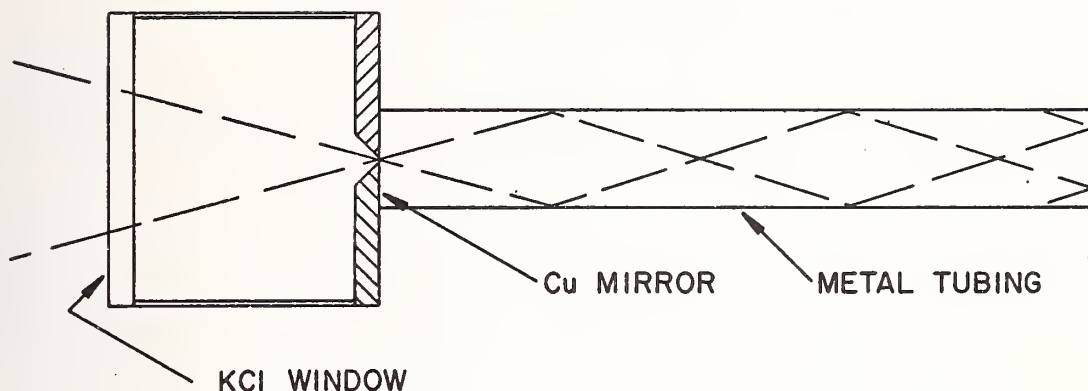


Figure 1. Reflective cell schematic. Light enters from the left through an 8 cm focal length BaF_2 lens. Three types of cylindrical sections (right side) were used. Cell (1), 0.95 cm x 61 cm long, copper. Cell (2), 50 cm i.d. x 20 cm long, gold. Cell (3), 0.23 cm i.d. x 61 cm long, stainless steel.

For any meaningful evaluation of laser-induced chemical reactions occurring in these cells the distribution of laser flux (or intensity) must be known. If, it is assumed that geometrical optics is applicable to this problem then the intensity in a cylinder at a point x centimeters from the entrance end and r centimeters from the cylinder axis is approximately given by

$$\Phi(x, r) = \Phi_0 \frac{b^2}{2ra} R^{\bar{n}} \quad (1)$$

where Φ_0 is the flux of the laser light at the focussing lens and the laser spot is assumed to be of uniform flux with radius b . The cylinder has radius a and wall reflectivity R and \bar{n} is the mean number of times a ray strikes the wall before reaching the point x . \bar{n} is given by

$$\bar{n} = 1/3 \frac{xb}{fa} \quad (2)$$

where f is the lens focal length.

The following table lists some preliminary results for the three cells listed in Fig. 1. All experiments were performed with 25% SF_6 in H_2 irradiated with CO_2 laser pulses at $10.6 \mu\text{m}$ (P(20) line). The equivalent reaction volume, v , is the fraction of the SF_6 that reacts per laser pulse times the total cell volume and is therefore a measure of the reaction yield. The selectivity factor, α , is defined by [3]

$$\frac{d[\text{}^{32}\text{SF}_6]}{d[\text{}^{34}\text{SF}_6]} = \alpha \frac{[\text{}^{32}\text{SF}_6]}{[\text{}^{34}\text{SF}_6]} \quad (3)$$

or as the ratio of equivalent reaction volumes for the two isotopic species.

The isotopic enrichment factor [3] for the residual gas, β , will be given by

$$\ln \beta = (1-1/\alpha) Nv/V \quad (4)$$

where N is the number of laser pulses and V is the cell volume. Equation 3 was used to calculate α from β , v , and N . In experiments where the amount reacted was not determined, α was assumed to be five and Eq. 3 was used to calculate v .

Note from the table that enhancements in reaction yield as high as 50 were obtained, this corresponds to a photon utilization efficiency of 0.5%. This is certainly an improvement over the single focus efficiency. The highest efficiency was obtained with cell 2 which has the highest wall reflectivity (> 0.97). The reflectivity is of cells 1 and 3 respectively 0.87 and 0.70. Experiments are continuing with these cells.

Cell	P(torr)	E(J)	Table 1 α	$v(\text{cm}^3)$	Relative Yield
1	0.1	3.5	5*	6.0	14.2
1	0.5	2.5	6.4	3.1	13.0
1	1.0	3.5	4.5	1.4	6.7
1	2.0	3.9	1.7	2.3	15.6
2	0.1	2.1	5*	16.1	~50
2	0.2	3.4	5*	8.9	13.2
2	1.0	2.8	5*	1.3	3.8
2	0.5	2.7	5*	0.4	1.6

* Assumed; see text

The pulsed CO_2 TEA lasers normally give mode locked pulses. That is, the 200 ns laser pulse is really a train of closely spaced subnanosecond spikes. This mode locking can be suppressed by adding a cw gain cell to the laser cavity. Experiments performed with and without mode locking indicated that the selectivity of the SF_6 laser induced dissociation is not significantly altered by mode locking. However, the reaction yield is greater by 25 to 50% for a mode locked pulse than a non-mode locked pulse of the same total energy.

References

- [1] Ambartzumian, R. V., Gorokhov, Y. A., and Letokhov, V. S., *JETP LETT.* 21, 171 (1975).
- [2] Lyman, J. L., Jensen, R. J., Rink, J. P., Robinson, C. P., and Rockwood, S. D., *Appl. Phys. Lett.* 27, 87 (1975).
- [3] Lyman, J. L., and Rockwood, S. D., *J. Appl. Phys.*, 47, 595 (1976).
- [4] Ambartzumian, R. V., Gorokhov, Y. A., Letokhov, V. S., Makarov, G. N., and Puretskii, A. A., *Zh. ETF. Pis. Red.*, 23, 26 (1976).
- [5] Lyman, J. L., and Rockwood, S. D., *Proceedings of the Laser-Optics International Laser '75 Conference* Nov. 11-13, 1975, Anaheim, CA (to be published).
- [6] Cotter, T. P., (private communication).

CO₂ TE LASER INDUCED PHOTOCHEMICAL ENRICHMENT OF CARBON ISOTOPES

Joseph J. Ritter and Samuel M. Freund¹

National Bureau of Standards
Washington, DC 20234

Several groups have previously reported on the CO₂ laser photolysis of gaseous Cl₂CF₂ [1,2,3]². In one case [3], carbon isotopic perturbations were noted in samples subjected to high energy pulses from a CO₂ transverse excitation (TE) laser. We have studied the CO₂ TE laser-induced chemical reactions of Cl₂CF₂ with several reagents and have noted substantial carbon isotopic enrichments along with evidence for the participation of a reactive intermediate, difluorocarbene.

The systems studied along with the principal products are given below:

Reaction	Reactants	Principal Products
I	Cl ₂ CF ₂ + O ₂	COF ₂ , (ClCF ₂) ₂ , Cl ₂
II	Cl ₂ CF ₂ + NO	C ₂ F ₄ , COF ₂ , ClCFO, NOCl, (ClCF ₂) ₂
III	Cl ₂ CF ₂ + (H ₃ C) ₂ C=CH ₂	C ₂ F ₄ + complex array of other products
IV	Cl ₂ CF ₂ + HCl	HCF ₂ Cl, (ClCF ₂) ₂ , Cl ₂

The reaction mixtures were contained in a 1 l stainless-steel cell and subjected to focussed 929 cm⁻¹ (P-36) radiation from a CO₂ TE laser delivering 300 ns wide pulses, with 0.20 J/pulse at 2 pps.

Chlorine (identified by color and mass spectrometry) was removed by treatment of the crude reaction mixtures with Hg at 25°. The residual gases were then subjected to GLC (10 m, 20% squalane on firebrick). Carbonyl fluoride-containing mixtures were passed over uncoated firebrick to effect a quantitative COF₂ → CO₂ conversion, in order to avoid this conversion by the firebrick support within the GLC column. Separated components were identified by ir and isotope ratios determined by mass spectrometry with a typical relative standard deviation of < 3%. Estimates of halocarbon product recoveries were made from GLC peak area measurement, assuming equivalent TC detector response for all compounds. Other, generally less volatile materials, in amounts too small for unequivocal identification, were noted in all of these systems.

Mass spectrometric examination of the products of reaction I, indicated a depletion of ¹³C while the analysis of recovered, unreacted Cl₂CF₂ indicated its ¹³C content to have changed from an initial 1% to the 16-20% range. This alternation in ¹³C content is sufficient that it is manifested in the ir spectrum of the recovered material with the appearance of two new bands (1131 and 1077 cm⁻¹) as shown in figure 1. Additional experiments performed under identical conditions but with the R-18 (1077 cm⁻¹) line of the TE laser resulted in recovered Cl₂CF₂ which was depleted in ¹³C. Thus the results of the isotopically specific reactions were used to confirm the assignment of the 1077 and 929 cm⁻¹ absorptions to ¹³C and ¹²C species of the Cl₂CF₂ respectively. For II and III, unreacted Cl₂CF₂ enriched in ¹³C, was recovered.

¹Present address: Los Alamos Scientific Laboratories, Los Alamos, New Mexico.

²Figures in brackets indicate the literature references at the end of this paper.



Figure 1. TOP: Cl_2CF_2 prior to laser photolysis. Pressure approximately 10 torr.
 BOTTOM: Cl_2CF_2 recovered after laser photolysis in the presence of O_2 . Pressure approximately 10 torr.

The appearance of ^{12}C enriched COF_2 from reaction I and ^{12}C enriched C_2F_4 from reactions II and III constitutes evidence for the laser induced, isotopically specific formation of difluorocarbene ($:\text{CF}_2$).

Difluorocarbene is also implicated in the formation of HCF_2Cl from reactions with HCl [4]. The fact that C_2F_4 is not also noted in the HCl and O_2 reactions is probably due to the facility of the $\text{O}_2 + :\text{CF}_2 \rightarrow \text{COF}_2 + \text{O}$, $\text{Cl}_2 + :\text{CF}_2 \rightarrow \text{Cl}_2\text{CF}_2$ and $\text{HCl} + :\text{CF}_2 \rightarrow \text{HCF}_2\text{Cl}$ reactions as compared to the dimerization of $:\text{CF}_2$. On the other hand, our results indicate that when Cl_2CF_2 is laser-irradiated in the presence of compounds very reactive toward chlorine such as NO or an olefin, the $\text{Cl}_2 + :\text{CF}_2 \rightarrow \text{Cl}_2\text{CF}_2$ reaction is accordingly less favored and the probability for dimerization of $:\text{CF}_2$ thus improved. Other workers [3] have observed C_2F_4 from the laser photodissociation of Cl_2CF_2 .

Further studies designed to affirm the role of laser-produced difluorocarbene and an assessment of its potential as a reagent in isotopically specific syntheses are currently in progress.

References

- [1] Freeman, M. P., and Travis, D. N., *J. Chem. Phys.*, **60**, 231 (1974).
- [2] Zitter, R. N., Lau, R. A., and Wills, K. S., *J. Amer. Chem. Soc.*, **97**, 2578 (1975).
- [3] Lyman, J. L., and Rockwood, S. D., *J. Appl. Phys.*, **47**, 595 (1976).
- [4] Mahler, W., *Inorg. Chem.*, **2**, 230 (1962).

MEASUREMENT OF MEAN LIVES IN ATOMIC URANIUM¹

Jules Z. Klose

National Bureau of Standards
Washington, DC 20234

During the past several years the availability of tunable dye lasers had led to attempts to develop inexpensive methods of producing isotopically enriched uranium to meet the needs of the expanding nuclear power industry. One of these methods involves isotope separation through stepwise photoionization processes in which selected levels of the isotope of interest are excited with tuned laser light, and the final step of ionization is achieved with a laser or an ultraviolet lamp. The isotope ions are then separated electrostatically from the neutral atoms. Using this method, groups at the Lawrence Livermore Laboratory [1,2]² and the Avco Everett Research Laboratory [3] have done experiments demonstrating the separation of ²³⁵U and ²³⁸U on a small scale.

In selecting a transition to be used in separating ²³⁵U from ²³⁸U, the overriding requirement is that the isotope shift must be large enough to avoid overlapping the unshifted line with the hyperfine structure of the isotope line. Once this requirement has been met, the further criteria of strong absorption and suitable level lifetime must be applied. Thus, selecting transitions requires knowledge of both the absorption cross sections, i.e., transition probabilities, and the excited state lifetimes. Although these two quantities are related, their relationship is usually not a simple one since most excited atomic states have several decay modes. However, in some cases decay branching ratios, i.e., relative transition probabilities, are available from other sources such as arc measurements. In such cases the absolute transition probabilities can be derived from the level lifetimes. To help provide some of this needed lifetime data, the National Bureau of Standards has been carrying on a program of measurements of mean lives of excited levels in the uranium atom [4]. In a complementary program at NBS, relative transition probabilities in uranium are being determined using a stabilized arc [5,6].

At NBS uranium atomic lifetime determinations have been made using low-energy electrons for excitation and a method of delayed coincidence for detection [4]. In order to provide free atoms for the measurements, a Knudsen effusion device especially designed to produce diffuse beams of atoms of heavy elements was constructed and placed in operation [4]. At this writing a result of 7.3 ± 1.1 ns has been obtained for the mean life of the upper level of the 3584.9 Å resonance transition in natural uranium [7]. For ²³⁸U this level has an energy of 27886.99 cm^{-1} . This lifetime was used to place the recently obtained NBS relative transition probabilities and those of Crolliss and Bozman [8] on absolute scales. In addition efforts have been made to measure the mean life of the 16900.39 cm^{-1} level using the 5915.4 Å resonance transition. These efforts were largely thwarted by the very high-intensity scattered light from the source at $\sim 2000^\circ\text{C}$, which gave rise to very poor signal-to-background ratios.

¹This work was supported in part by the U.S. Energy Research and Development Administration through the Lawrence Livermore Laboratory under Interagency Agreement LLL SANL 384-001.

²Figures in brackets indicate the literature references at the end of this paper.

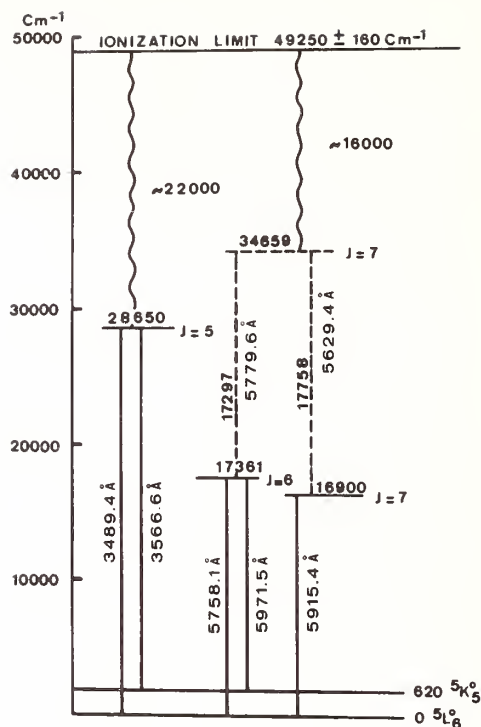


Figure 1. Examples of two- and three-stage ionization processes for separating ^{235}U from ^{238}U . The energies of the levels and transitions are given in wavenumbers (cm^{-1}), and the wavelengths of the transitions are given in angstroms (\AA). The values are for ^{238}U , but differences in energies and wavelengths between ^{235}U and ^{238}U are generally not discernible within the precision of the quantities given in the figure. This figure was reproduced with changes from reference (10).

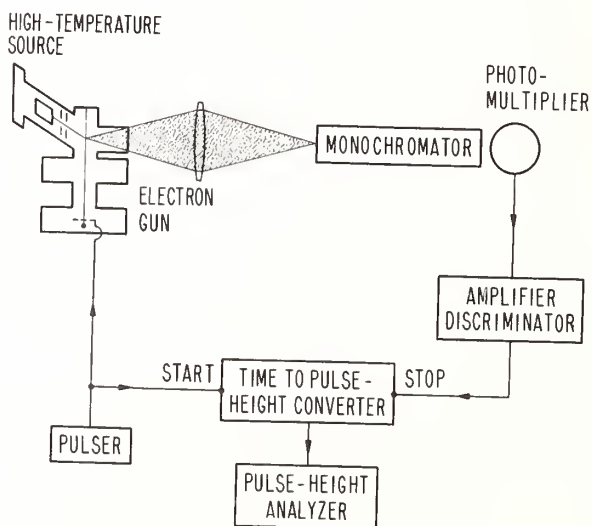


Figure 2. Block diagram of the delayed coincidence experimental setup used for measuring mean lives in heavy elements.

In an attempt to overcome this difficulty of low signal-to-background ratios, a tunable dye laser pumped by a pulsed nitrogen laser is being installed as the source of excitation. The tunable laser will provide such strong decay signals that much more efficient means of detecting the decays can be used. Also, the problem of cascading into the level of interest from simultaneously excited higher levels will be eliminated by selective level excitation with the tunable laser.

The groups at the Avco Everett Research Laboratory [3] and the Lawrence Livermore Laboratory [9] have reported measuring mean lives in UI using their experimental isotope separation setups. In their methods the lifetime of an intermediate level is obtained by observing the yield of isotope ions as a function of the delay between the exciting and ionizing laser pulses.

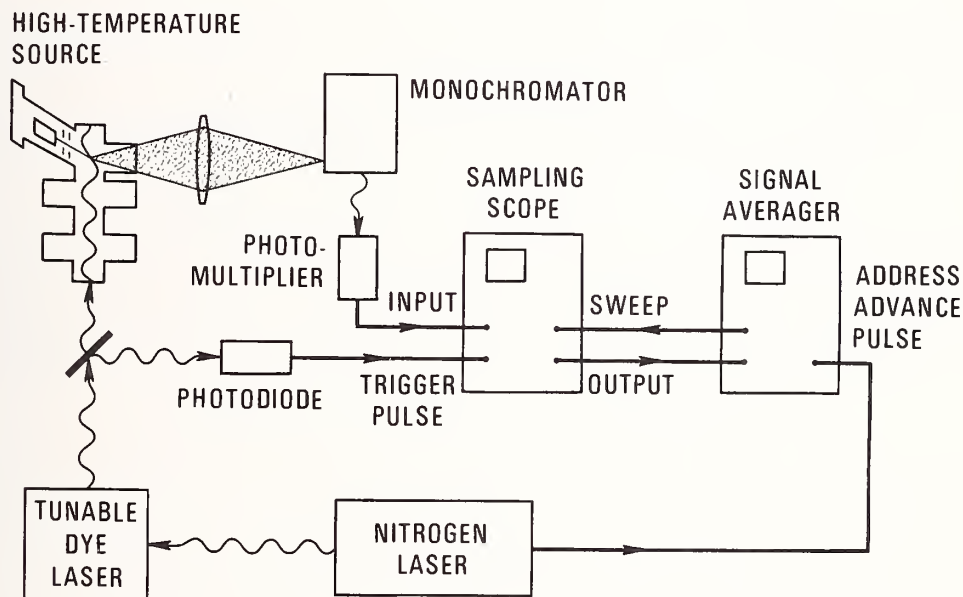


Figure 3. Block diagram of a system for measuring atomic mean lives utilizing the strong decay signal produced by a pulsed tunable dye laser as the source of excitation. Systems similar to this have been described in references (11) and (12).

References

- [1] Tuccion, S. A., Dubrin, J. W., Peterson, O. G., and Snavely, B. B., *IEEE J. Quantum Electron.* QE-10, 790 (1974).
- [2] Tuccion, S. A., Foley, R. J., Dubrin, J. W., and Krikorian, O., *IEEE J. Quantum Electron.*, QE-11, 101D (1974).
- [3] Janes, G. S., Itzkan, I., Pike, C. T., Levy, R. H., and Levin, L., *IEEE J. Quantum Electron.*, QE-12, 111 (1976).
- [4] Klose, J. Z., *Proceedings of the SPIE/SPSE Technical Symposium East*, March 22-25, 1976, Vol. 76 (in press).
- [5] Voigt, P. A., *Phys. Rev.*, A 11, 1845 (1975).

- [6] Voigt, P. A., and Kornblith, R. L., *J. Opt. Soc. Am.*, 66, 492 (1976).
- [7] Klose, J. Z., *Phys. Rev.*, A 11, 1840 (1975).
- [8] Corliss, C. H., *J. Res. Nat. Bur. Stand. (U.S.)*, Sect. A 80, 1 (1976).
- [9] Carlson, L. R., Paisner, J. A., Worden, E. F., Johnson, S. A., May, C. A., and Solarz, R. W., *Lawrence Livermore Laboratory Report UCRL-77832*, 1976 (unpublished).
- [10] Radziemski, L. J., Jr., Gerstenkorn, S., and Luc, P., *Opt. Commun.*, 15, 273 (1974).
- [11] Haroche, S., Paisner, J. A., and Schawlow, A. L., *Phys. Rev. Lett.*, 30, 948 (1973).
- [12] Schenck, P., Hilbron, R. C., and Metcalf, H., *Phys. Rev. Lett.*, 31, 189 (1973).

PRINCIPLES OF PHOTOCHEMICAL SEPARATION OF ISOMERIC NUCLIDES¹

G. C. Baldwin², H. M. Clark, D. Hakala, and R. R. Reeves
Rensselaer Polytechnic Institute

Aside from intrinsic scientific interest, photochemical separation of isomeric states of a single nuclide offers one possibility of achieving a nuclear population inversion, essential to the development of gamma ray lasers [1,2]³. Just as for isotope separation, photochemical methods of isomer separation depend upon the existence and magnitude of spectral differences between the species to be separated exceeding the resolution of tunable optical sources.

Mercury has already been shown to be capable of isotopically-selective photochemical reaction using 254 nm radiation [3]. These studies have been performed on the even mass number stable isotopes (*i.e.* 198 and 202) which have zero nuclear spin and one hyperfine component per isotope within the hyperfine structure of the 254 nm line. Mercury 197 m, the excited nuclear state, has a half-life of 24 hours, with 3 hyperfine components due to the nuclear spin splitting effect [4,5]. The ground state, Hg^{197g}, is also radioactive with a half-life of 64 hours, but the nuclear spin splitting results in a doublet [4,5].

Mass, spin, quadrupole, and nuclear volume effects give rise to shifts and splittings of the optical energy levels of atoms and molecules. In the case of mercury, its optical spectrum has been shown to contain several lines having well-resolved hyperfine structures characteristic of the different isotopic species. The hyperfine structure of the 254 nm has been measured for Hg^{197m} and Hg^{197g}[5]. Isotopes have been separated by chemical reaction of mercury atoms selectively excited at 254 nm by means of a mercury lamp incorporating a single isotope (or enriched in a single isotope). The excited atoms can react with oxygen to produce isotopically enriched HgO which may be recovered [3].

In a similar manner it should be possible to excite and separate the Hg^{197m}. However, a different source of radiation is needed. The specific wavelength required may be obtained by means of a nitrogen laser coupled to a tunable dye laser. The 254 nm line can then be scanned using a nonlinear potassium pentaborate (KPB) doubling crystal. Resolution is in the order of .0008 nm using an incavity etalon with such a laser. One absorption line of the triplet of the Hg^{197m} at 254 nm is almost 0.002 nm from the nearest Hg^{197g} component and about 0.0026 nm from the nearest hyperfine component of any of the stable isotopes [5]. Therefore it should be possible to recover the Hg^{197m} enriched with respect to Hg^{197g} and the other isotopes. The degree of isomer enrichment may be determined by measurement of the characteristic radiations emitted in the decay of the Hg^{197m} and Hg^{197g}. It is noted also that the use of recoil-based radiochemical isotope enrichment (the Szilard-Chalmers process) during the preparation of the isomeric species would facilitate the subsequent photochemical enrichment of the isomeric state.

¹Partially supported by the National Science Foundation.

²On leave to Los Alamos Scientific Laboratory, 1975-1976.

³Figures in brackets indicate the literature references at the end of this paper.

Another element which has been studied for photochemical isotope enrichment [6] and has isomeric states of reasonable lifetime is bromine. Selective excitation of the molecule, Br₂, results in the formation of bromine atoms. Reaction of these atoms with HI can produce isotopic enrichment in the product formed initially. Bromine-80 has a metastable state with a half-life of 4.4 hours and a ground state with a half-life of 17.6 minutes. It should be feasible to separate these isomers by a photochemical process if the molecules containing the isomers has not been measured, but isomer shifts should exist for these species compared to the normal bromine.

References

- [1] Baldwin, G. C., and Khokhlov, R. V., *Physics Today*, 28, (2), 32 (1975).
- [2] Letokhov, V. S., *Science*, 180, 451 (1973), 190, 344 (1975).
- [3] Gunning, H. E., and Strausz, O. P., in *Advances in Photochemistry*, ed. by Noyes, Hammond, and Pitts, Vol. I, p. 209 (1963).
- [4] Lederer, C. M., Hollander, J. M., and Perlman, I., *Table of Isotopes*, John Wiley (1967).
- [5] Mellissinos, A. C., and Davis, S. P., *Phys. Rev.*, 115, 130 (1959).
- [6] Leone, S. R., and Moore, C. B., *Phys. Rev. Letters*, 33, 269 (1974).

THE EARLY YEARS OF PHOTOCHEMISTRY IN THE VACUUM ULTRAVIOLET

Wilhelm Groth

Institut für Physikalische Chemie der Universität Bonn

The wavelength region between 1850 Å and about 1250 Å was opened to spectroscopy around 1900 through the pioneering work of V. Schumann. Photochemistry, which is the younger sister of spectroscopy, reached the Schumann region only after 1930. After shortly describing the importance of photochemistry for the kinetics of thermal reactions, especially for the mechanism of chain reactions, the first spectroscopic investigations in the Schumann ultraviolet with the light of condensed sparks between metal electrodes and with quartz optic are mentioned. Difficulties originated in the transparency of the window materials, the absolute energy measurements and above all in the lack of suitable monochromatic light sources.

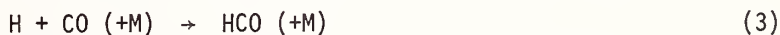
Starting with the development of the high-current low-voltage xenon lamp of Harteck and Oppenheimer the technical improvements of the rare gas lamps are described: the application of low-current glow discharges, micro-wave discharges, and the use of other rare gases xenon, krypton and argon.

In the beginning, the absorption and primary photochemical and total reactions of simple gases were investigated: oxygen, nitrogen, hydrogen, ammonia, carbon dioxide, carbon monoxide, water vapour, and some organic compounds like methane, ethane, and propane.

Remarkable are some experiments carried out by the author and Hans Suess in 1937 who illuminated mixtures of water vapour and carbon dioxide by the xenon resonance wavelengths. The following primary reactions occur:



H atoms react with CO to give formaldehyde or glyoxal according to



This process was assumed to have played an important role in the earth's atmosphere. It would give an explanation for the first appearance of free oxygen in the primitive atmosphere and for the formation of certain carbon compounds that were probably the pre-requisite for the evolution of organic life.

Later on the hypotheses of Oparin, Urey, Kuhn, and Bernal assumed that the earth's primitive atmosphere contained hydrogen, methane, and water vapour. Since the greater part of the energy available in the earth's atmosphere would be contributed by the ultraviolet radiation of the sun, the earlier photochemical experiments were resumed in 1957 by the author and Hanns von Weyssenhoff, using mixtures of methane or ethane with ammonia and water vapour in mercury-sensitized as well as direct photolysis experiments. For irradiation the resonance wave lengths of mercury at 2537 Å and 1849 Å, of xenon at 1469 Å and 1296 Å, and of krypton at 1236 Å and 1165 Å were used. Amino acids (glycine, α -alanine, and α -amino-butyric acid), and fatty acids (formic acid, acetic acid, propionic acid), and hydrocarbons could be detected in several experiments. These results were confirmed in 1959 by Terenin, in 1961 by Dodonova and Siderova, and in 1966 by Ponnampuruma and Flores.

Special photochemical reactions in the Schumann ultraviolet which were carried out in the 1930's with a xenon lamp were concerned with the reactions of O atoms. It could be shown that even at extremely small oxygen partial pressures in mixtures with hydrogen and carbon oxide the ozone formation in a triple collision predominates the primary attack on hydrogen or carbon oxide molecules. It was assumed that the primarily formed energy rich ozone at low O atom concentrations reacts with the molecules before it loses its energy by collisions.

Also the nitrogen oxidation was investigated in the light of the xenon lamp. N_2O could be detected mass-spectrometrically; about 10^{-4} of the O atoms formed N_2O . The small amount of N_2O which is found in the earth's atmosphere can at least partially be produced by this photochemical reaction.

FLUORESCENCE AND DECOMPOSITION OF TERTIARY AMINES IN A GLOW DISCHARGE

Francoise Lahmani¹ and R. Srinivasan

IBM Thomas J. Watson Research Center
Yorktown Heights, New York 10598

1. Introduction

Although electric discharges in gases have been extensively used to produce the excited states of many atoms and small molecules which were subsequently studied by spectroscopy, little attention has been given to large polyatomic, fluorescent molecules (with the exception of benzene and toluene). Tertiary aliphatic amines which have been shown to be strong emitters in the near ultraviolet [1]² should offer an interesting class of compounds for study. We have conducted an investigation of the fluorescence and decomposition of such tertiary amines in a continuous electric discharge in a flow system. In this communication, we shall confine our remarks to diazabicyclo[2.2.2]octane (DABCO) which seems to be typical of these systems.

2. Experimental

The flow system and discharge that were used were unexceptional. The flow rates were about 0.02 mole/hr at the vapor pressure of DABCO which ranged from 0.03 to 0.3 torr. The light emitted from the discharge was analyzed by a 1-meter, Jarrell-Ash spectrometer and detected by a EMI photomultiplier (S-20 response).

3. Results

The following is a summary of the results that were obtained:

1) In pure DABCO vapor (0.3 torr), at the lowest voltage at which a discharge could be sustained (60 V/cm) a purple glow was observed which on spectroscopic analysis was found to be identical to the fluorescence of DABCO vapor that has been reported [1].

2) With an increase in the energy of the discharge, the intensity of the light that was emitted increased. A new emission which consisted of the CN* violet system at 421.6, 388.3, and 359.0 nm was observed. With an increase in voltage, the intensity of CN* emission increased rapidly while the fluorescence of DABCO remained steady or decreased slightly.

3) Addition of helium sharply increased the current as well as the emission from CN*. Argon produced qualitatively the same effect as helium. At a given voltage and a constant ratio of helium to DABCO, the intensity of CN* emission was roughly proportional to the current up to a 20-fold increase. At the same time, the fluorescence of DABCO was only slightly increased or not at all.

¹ On leave from Laboratoire de Photosphysique Moléculaire Université de Paris Sud, Orsay, France.

² Figures in brackets indicate the literature references at the end of this paper.

4) The $\text{CN}^*(\text{B}^2\Sigma) \rightarrow (\text{X}^2\Sigma)$ violet bands $\Delta v=0$ $\Delta v=-1$ were studied under high resolution in order to obtain information on the vibrational and rotational intensity distributions. The weakness or absence of anomalous distributions in the intensities indicated that the first excited electronic state $\text{A}^2\Pi$ of CN was of minor importance relative to $\text{B}^2\Sigma$ in this study.

5) The intensity distribution pattern was the same (within experimental uncertainty) in the presence or absence of helium or argon, with one exception.

6) Under conditions in which only the fluorescence of DABCO was observed, no decomposition products were detected. When CN^* emission was also present, the products that were detected were C_2 hydrocarbons, HCN, and a reactive small molecule which may be $\text{C}_2\text{H}_3\text{N}$.

4. Discussion

Present observations suggest that there are two independent routes to the excitation of DABCO in an electric discharge. These consist of

1) One that leads to excitation to the fluorescent electronic state which has been tentatively identified by Halpern [1] as a low-lying optically forbidden singlet state with a lifetime of 1040 nsec.

2) A second path which induces the dissociation of the molecule. The mechanism by which DABCO dissociates and gives rise to $\text{CN}^* \text{B}^2\Sigma$ cannot be deduced from the present experiments, but it is obvious that CN^* cannot be a *direct* dissociation product of DABCO.

The observation that the distribution of vibrational and rotational energy in the $\text{B}^2\Sigma$ state appears to be normal (without any population inversion) is consistent with other studies on electric discharges. It suggests that either a thermally equilibrated ground state of CN is the precursor to $\text{CN}^*(\text{B}^2\Sigma)$, the excitation being due to collisions between CN and electrons, or that CN^* is produced in a dissociation process from unstable intermediates without much change in the equilibrium C-N bond distance. This kind of intensity distribution in $\text{CN}^*(\text{B}^2\Sigma)$ has been obtained in electron impact induced dissociation of cyanides [3] and in the photodissociation of HCN [4]. It is markedly different from results obtained in the reaction of active nitrogen with hydrocarbons [5] or dissociative excitation of halogen cyanides by collision with metastable argon atoms [6].

The enhancement of the decomposition of DABCO relative to its fluorescence on the addition of helium or argon confirms the existence of two parallel pathways for the excitation of DABCO.

References

- [1] Halpern, A. M., *Mol. Photochem.*, 5, 517 (1973).
- [2] Pearse, R. W. B., and Gaydon, A. G., *The Identification of Molecular Spectra*, John Wiley and Sons, Inc., New York (1963).
- [3] Tokue, I., Urisu, T., and Kuchitsu, K., *J. of Photochem.*, 3, 273 (1974-1975).
- [4] Mele, A., and Okabe, H., *J. Chem. Phys.*, 51, 4798 (1969).
- [5] Kiess, N. H., and Broida, H. P., *7th Symposium on Combustion* 1958, Butterworth (1959), p. 207.
- [6] Coxon, J. A., Setser, D. W., and Duewer, W. H., *J. Chem. Phys.*, 58, 2244 (1973).

PHOTOCHEMISTRY AND FLASH PHOTOLYSIS OF 5-NITROQUINOLINE

A. C. Testa and A. Cu

Department of Chemistry
St. John's University
Jamaica, NY 11439

As an extension of our photochemical studies on aromatic nitro compounds into heterocyclics we have investigated the photochemistry of 5-nitroquinoline, which in the presence of 50% isopropyl alcohol-water solutions containing HCl results in photoreduction to a chlorinated 5-amino-quinoline. The quantum yield of 313 nm photolysis, which proceeds via the triplet state, increases with HCl concentration and levels off at a maximum value of 5.4×10^{-2} when (HCl) > 1 M. Photochemical disappearance is attenuated in sulfuric acid solutions as well as in near isopropyl alcohol, which indicates that the chloride ion serves as an electron donor to the triplet state of the aromatic nitro compound. Measured triplet yields for 1- and 2-nitronaphthalene are 0.63 and 0.83, respectively, and it is reasonable to expect a comparable value for 5-nitroquinoline.

In order to evaluate the importance of the chloride ion as an electron donor we have carried out a flash photolysis study of this molecule in a variety of solvents with the aim of trying to identify triplets, anions and neutral radicals that may account for its photochemical behavior. Although the absorption spectrum of neither the triplet nor the radical anion is known we felt that a comparison of photochemical and flash photolysis data might provide the needed correlation to assign any observed transients.

Flash photolysis of 5-nitroquinoline does not result in any triplet-triplet absorption for any of the solutions studied, which suggests that the triplet is short lived (< 40 usec.). That the triplet is populated can readily be discerned from the phosphorescence yield of 5-nitroquinoline in EPA at 77 °K, which was measured and found to be 0.27. The distinct 0-0 band, vibrational structure and similarity to naphthalene and nitronaphthalene phosphorescence provide evidence that the lowest triplet is π, π^* . The photochemically active medium where reduction occurs with 313 nm photolysis is 50% isopropyl alcohol-water containing HCl, and flash photolysis of these solutions do result in the production of two species absorbing at 550 and 410 nm with lifetimes in the millisecond time range and exhibiting first order decay kinetics. The optical density of the 550 transient increases up to (HCl) ~ 0.5 M, and then decreases rapidly for increasing acidic solutions. In contrast, the optical density of the 410 transient in 50% isopropyl alcohol-water increases continuously from 0.02 M to 6 M HCl, and is also observed in 12 M HCl.

In view of the necessity of HCl and isopropyl alcohol for formation of the 550 transient we assign its absorption spectrum to the radical anion generated by electron transfer from the chloride ion. We have already reported a similar event from nitrobenzene and 4-nitropyridine. Since the first order decay constants for the 550 and 410 transients each remain constant in the acid range 0.5-3 N HCl, we believe that an equilibrium is operating between the anion and its protonated form. Thus, we consider it an attractive possibility to consider the 410 transient as the protonated anion.

Despite the uncertain assignment of the 410 transient, flash photolysis data support the view that the photoreduction of 5-nitroquinoline occurs via two transients. It appears, however, that alcohol is not necessary for the photoreduction of 5-nitroquinoline since the quantum yield in 12 M HCl has been determined to be 5.7×10^{-2} . A summary of the photochemical quantum yields, optical density of the 550 and 410 transients, as a function of HCl concentration are summarized in figure 1. It is seen that the maximum optical density for the 550 transient occurs where the disappearance quantum yield has been observed to achieve its upper limit of 5.4×10^{-2} . That this transient is not present in near isopropyl

alcohol or 50% isopropyl alcohol with 6 N sulfuric acid underlines the importance of the chloride ion as an electron donor. This transient is absent in air-saturated solutions and further supports the view that it is the radical anion generated via electron transfer, i.e., $\text{ArNO}_2^{*3} + \text{Cl}^- \rightarrow \text{ArNO}_2^- + \text{Cl}\cdot$. The lifetime of this transient is 5.3 msec. Since the 410 absorption can be observed in 12 M HCl as well as in 50% isopropyl alcohol-water with 6 N HCl, it appears that the alcohol may not be the predominant species responsible for its formation. The lifetime of the 410 transient is 1.1 msec.

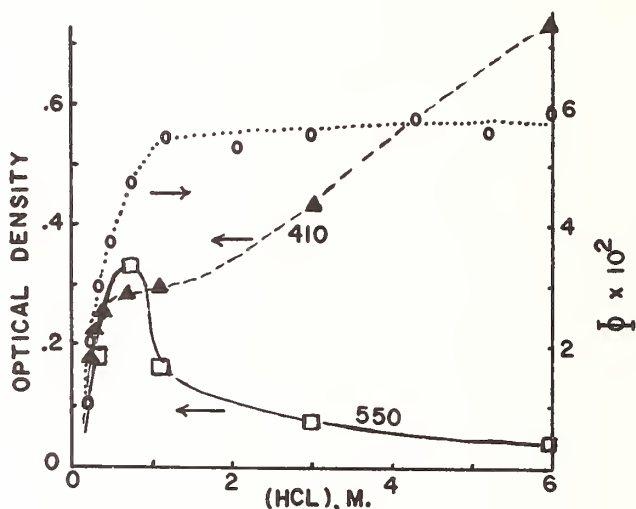


Figure 1. Absorption data for the 410 (Δ) and the 550 nm (□) transient as a function of HCl concentration. (○) = 313 nm quantum yields.

It is evident that for solutions in which $(\text{HCl}) > 0.5 \text{ M}$, the quantum yield remains constant, but the optical density of the 550 nm transient decreases while that of the 410 increases. In the acid range less than 0.5 M the intensity of both species is increasing as is the photochemical quantum yield. It thus seems reasonable to conclude that both transients contribute to the observed photoreduction. The relatively large phosphorescence yield for 5-nitroquinoline suggests that its triplet-triplet absorption should be readily observed in laser flash photolysis.

PHOTOCHEMISTRY AND PHOTOPHYSICS OF NITROGEN HETEROCYCLES

Marian S. Henry and Morton Z. Hoffman

Department of Chemistry
Boston University
Boston, MA 02215

Aromatic N-heterocycle compounds, such as 2,2'-bipyridine (bipy), provide an opportunity to examine the effects of varying molecular structure on the energetics and reactivities of the excited states. The nitrogen heteroatom is an intimate part of the aromatic structure and, being a Lewis base, is subject to protonation and coordination to metal ions. These latter processes, as well as substitution on the aromatic system are expected to have a significant effect on the excited states and their observed photochemistry and photophysics. This research is directed specifically to the establishment of structural-energetic-reactivity relationships for the excited states of these molecules.

The initial phase of this research has involved the characterization of the photophysics and photochemistry of bipy. The ground and flash photolysis transient absorption spectra, and fluorescence excitation and emission spectra have been examined as a function of pH. Acid dissociation constants have been calculated for the ground state (S_0), the fluorescent state (S_1), the flash photolysis transient (T_1), and the species generated from T_1 upon the absorption of light (T_2). The results are given in Table I. Results for S_0 are in agreement with those reported by McBryde [1]¹. Relative fluorescence intensities are 1000:1:5 for bipy, bipyH^+ , and bipyH_2^{2+} respectively. Fluorescence excitation and emission spectra show a good mirror-image relationship for bipy and bipyH_2^{2+} , but not for bipyH^+ .

Table I. pK_a values for bipy

Equilibrium	S_0^a	S_1^b	T_1^a	T_2^c
$\text{bipyH}_2^{2+} \rightleftharpoons \text{bipyH}^+ + \text{H}^+$	-0.5	-7.8	-0.5	-1.4
$\text{bipyH}^+ \rightleftharpoons \text{bipy} + \text{H}^+$	4.5	3.8	5.0	6.7

a. Calculated from pH dependence of absorption spectra.

b. Calculated from pH dependence of emission spectra.

c. Estimated from T_1 absorption and Förster cycle [9,10].

¹ Figures in brackets indicate the literature references at the end of this paper.

In the ground state, bipy is known to be either cis-planar (bipyH^+) or trans-planar (bipyH_2^+ and bipy) [2,3]. The mirror-image relationship between absorption and fluorescence spectra and the small Stokes' shift found for bipyH_2^+ (3.5 kK) and bipy (2.1 kK) suggest a small geometry change upon excitation. Inasmuch as the ground state extinction coefficients are similar [4], the radiative rate constants are expected to be similar. Therefore, the decreased fluorescence intensity of bipy , relative to bipyH_2^+ , is attributed to much faster nonradiative processes, either inter-system crossing or internal conversion. A significantly larger Stokes' shift (5.8 kK) and the lack of a mirror-image relationship for bipyH^+ point to a change in geometry in the $S_0 \rightarrow S_1$ process. The effect may be due to twisting of the two pyridine rings.

The absorption spectrum of the flash photolysis transient T_1 is very similar to that of the biphenyl triplet [5] and is assigned to that of the free base triplet state. Its decay is second-order with no ionic strength dependence. By measurement of the rate of hydrogen atom abstraction from isopropyl alcohol the lowest free base triplet state has been found to be of π, π^* character, in agreement with Gondo and Kanda [6]. In acidic solution, the decay of triplet bipyH^+ is slower but also second-order with an ionic strength dependence consistent with the excited state having a +1 charge. In very acidic solution, triplet bipyH_2^+ decays via first-order kinetics with $k = 3 \times 10^3 \text{ sec}^{-1}$. It is apparent that a competition exists between uni- and bimolecular decay under the relatively high concentration of triplet produced by the flash. Triplet bipy does not react with halide ions but triplet bipyH^+ reactions with I^- and Br^- , but not Cl^- . Finally, we have found that triplet bipyH^+ is quenched by Mn^{2+} but not by Zn^{2+} .

The pK_a values of T_1 and T_2 are similar to those for S_0 while those of S_1 , particularly for bipyH_2^+ , are highly shifted to less positive values. The sensitivity of the S_1 equilibrium $\text{bipyH}^+ \rightleftharpoons \text{bipy} + \text{H}^+$ towards buffer concentration indicates short fluorescence lifetimes [7,8]. Thus the position of the equilibrium is set by pH and the extent to which equilibrium is reached before fluorescence occurs is set by the buffer concentration. It is therefore possible to select the state of protonation of the two excited states, S_1 and T_1 , which most determine the photochemistry (Table II).

Table II. State of Protonation of Excited States

pH range	S_1	T_1
< (-8)	bipyH_2^+	bipyH_2^+
(-7) - (-2)	bipyH^+	bipyH_2^+
0 - 3.5	bipyH^+	bipyH^+
~ 4.8	bipy	bipyH^+
> 6	bipy	bipy

References

- [1] McBryde, W. A. E., *Can. J. Chem.*, 43, 3472 (1965).
- [2] Nakamoto, K., *J. Phys. Chem.*, 64, 1420 (1960).
- [3] Spotswood, T. McL., and Tanzer, C. I., *Aust. J. Chem.*, 20, 1227 (1967).
- [4] Linnell, R. H., and Kaczmarczyk, A., *J. Phys. Chem.*, 65, 1196 (1961).
- [5] Porter, G., and Windsor, M. W., *Proc. Roy. Soc.*, 245A, 238 (1958).
- [6] Gondo, Y., and Kanda, Y., *Bull. Chem. Soc. Jap.*, 38, 1187 (1965).
- [7] Lasser, N., and Feitelson, J., *J. Phys. Chem.*, 77, 1011 (1973); 79, 1334 (1975).
- [8] Schulman, S. G., and Capomacchia, A. C., *J. Phys. Chem.*, 79, 1337 (1975).
- [9] Ireland, J. F., and Wyatt, P. A. H., *J. C. S. Faraday I*, 68, 1053 (1972).
- [10] Jaffe, H. H., and Jones, H. L., *J. Org. Chem.*, 30, 964 (1965).

THE PHOTOPHYSICS OF SEVERAL CONDENSED RING HETEROAROMATIC COMPOUNDS

F. Sheldon Wettack, Robert Klapthor, Allan Shedd, Mary Koeppe, Ken Janda,
Patti Dwyer, and Kathleen Stratton

Department of Chemistry
Hope College
Holland, MI 49423

As a part of our interest in the photophysics of aromatic compounds, we have examined the series of condensed-ring heteroaromatic compounds, indene, indole, benzofuran and benzothiophene. The ring system of these compounds can be considered to be isoelectronic with naphthalene, but with less symmetry and a variable heteroatom. Previous work on absorption [1]¹ and fluorescence [2] and the variation in such properties as weight, aromaticity, and vibrational frequencies combine to yield an ideal series for a photophysical investigation. In particular we have been interested in learning of the role of the heteroatom in radiative and non-radiative processes from both the singlet and triplet states. Although work directed toward this end has been carried out in both the condensed and gas phases, the results reported in this paper will be confined to the condensed phase.

Results at 298 K

In the liquid phase at room temperature the fluorescence of the series varies significantly. Quantum yields are shown in Table I. Also shown are fluorescence lifetimes measured for the same solutions and calculated values of the radiative (k_f) and nonradiative (k_{nr}) rate constants from the excited singlet state.

Compound	ϕ_f	$\tau_f(\text{nsec})$	Table I			
			ϕ_{isc}	$k_f(\times 10^{-7})$	$k_{nr}(\times 10^{-7})$	$k_{isc}(\times 10^{-7})$
Indene	0.073	12	0.67	0.61	7.7	5.9
Indole	0.41	9.0	0.07	4.6	6.6	0.8
Benzofuran	0.23	7.5	0.07	3.1	13	0.9
Benzothiophene	0.014	~ 0.3	0.73	4.7	340	240

We have also measured the intersystem crossing yield (ϕ_{isc}) for these compounds using the sensitized 1,3-pentadiene isomerization technique of Lamola and Hammond [3]. The results are shown in Table I. The triplet yield measurements were carried out with benzene and cyclohexane solutions at concentrations of 10^{-2} - 10^{-3} M whereas the fluorescence measurements were performed at 10^{-5} - 10^{-6} M in cyclohexane.

¹ Figures in brackets indicate the literature references at the end of this paper.

Results at 77 K

Phosphorescence yields at 77 K in 2,2,4-trimethylpentane (isooctane) solvent and lifetimes in EPA are shown in Table II.

Table II

Compound	ϕ_p	τ_p (sec)	$k_p\phi_{isc}$ (sec ⁻¹)
Indole	0.40	5.6	7.1×10^{-2}
Benzofuran	0.34	1.2	28×10^{-2}
Benzothiophene	0.23	0.44	52×10^{-2}

It was found that the most reproducible yields were obtained with isooctane solvent. Cyclohexane, methanol and EPA were also used but problems with solubility, fractured cells and nonreducibility were encountered. The yields shown in Table II are based on naphthalene as a standard ($\phi_p = 0.051$).

Experimental

In all of the work, spectra corrected for emission detector sensitivity were used to calculate the yields. In addition, the effective optical density over the excitation bandwidth was used to account for the relative absorption by standard and unknown. The phosphorescence spectra and lifetimes were obtained using a Farrand spectrofluorometer modified to accept cylindrical cells at liquid nitrogen temperatures. The fluorescence spectra were taken on the same instrument and all absorption measurements were made on a Cary 14. Fluorescent lifetimes were determined by the time-correlated single photon counting technique. Each quantum yield was determined several times in independent experiments. Reproducibilities in the fluorescence yields are better than 10% and the phosphorescence yields are reproducible to 10%.

Discussion

At 298 K sufficient data are available to calculate k_{isc} , the rate constant for intersystem crossing, using $\phi_{isc} = k_{isc} \tau_f$. The results are included in Table I. Clearly the sulfur heteroatom influences the rate of intersystem crossing in benzothiophene. Otherwise k_{isc} goes approximately as the degree of aromaticity in the compounds. It should be noted that the ϕ_{isc} values were determined at higher concentrations than the fluorescence yields and lifetimes. Preliminary work with indole indicates that τ_f is concentration dependent and hence the intersystem crossing yield is a minimum value. It is possible that k_{isc} for indole and, perhaps benzofuran, may be as much as an order of magnitude higher than the values shown in Table I.

At 77 K the relationship $\phi_p = k_p \tau_p \phi_{isc}$ holds. If one assumes that $k_{nr}^3 = 0$, the relationship $\phi_p/\phi_f = k_{isc}/k_f$, known as Kasha intersystem crossing ratio, is obtained. If ϕ_f is taken to be 0.6 for indole [4], k_{isc} is calculated to be 3×10^7 sec⁻¹. If this same value for k_{isc} exists in the liquid phase at 298 K, $\phi_{isc} = 0.3$.

The relationship $\phi_p/\tau_p = k_p \phi_{isc}$ leads to the values of $k_p \phi_{isc}$ shown in Table II. These values imply that k_p and/or ϕ_{isc} are increasing in going from indole to benzothiophene at 77 K. Since the phosphorescence yields indicate that a significant increase in ϕ_{isc} is unlikely, one concludes that k_p is increasing.

We find no evidence of phosphorescence from indene at 77 K in isooctane. Phosphorescence has been reported for EPA solutions. Whether this is an indication that the singlet state photophysics of indene at 77 K in isooctane does not include intersystem crossing or whether all of the energy dissipation from the triplet state is of a radiationless nature is yet unknown. An exhaustive search for phosphorescence in isooctane is continuing.

Benzothiophene, indole, and benzofuran show relatively high phosphorescence yields compared to other hydrocarbon aromatic compounds and the values are consistent with emission yields found for dibenzo condensed-ring heteroaromatic molecules. The fact that indene shows no phosphorescence is consistent with the low yields found in compounds which strictly involve $\pi-\pi^*$ excited triplet states (e.g., naphthalene, benzene).

References

- [1] Hollas, J. M., *Spectrochimica Acta*, 19, 753 (1963).
- [2] Van Duuren, B. L., *Anal. Chem.*, 32, 1436 (1960).
- [3] Lamola, A. M., and Hammond, G. S., *J. Chem. Phys.*, 43, 2129 (1965).
- [4] Eisenger, J., and Navon, G., *J. Chem. Phys.*, 50, 2069 (1969).
- [5] Birks, J.B., *Photophysics of Aromatic Molecules*, Wiley-Interscience, New York, 1970.

MOLECULAR WEIGHT DEPENDENCE OF TRIPLET-TRIPLET PROCESSES IN POLY(2-VINYLNAPHTHALENE)¹

Nicholas F. Pasch and S. E. Webber

Department of Chemistry
University of Texas
Austin, TX 78712

In 1969 Cozzens and Fox [1]² demonstrated the occurrence of triplet-triplet annihilation leading to delayed fluorescence in polymers of 1-vinylnaphthalene (P1VN). Since that time a number of observations of delayed fluorescence in polymer solutions and films for both homopolymers and copolymers have been reported [2-5]. Klotter and Fischer [5] have shown previously that the intensity of delayed fluorescence in poly(vinylcarbazole) increases with \bar{P} , the degree of polymerization. It is our purpose to report some similar experimental observations of delayed fluorescence for solutions of poly(2-vinylnaphthalene) (= P2VN) at 77 °K with \bar{P} values from ~ 100 to ~ 3000 .

All polymers were synthesized using sealed ampules containing freshly sublimed 2-vinylnaphthalene in "spectro" grade benzene (~ 1.5 M) and initiated with AIBN (2×10^{-3} to 1×10^{-2} M). The highest MW samples were obtained by eliminating the solvent from this method. All MW's were determined by viscometry using the results of L. Utrecki, R. Simha, and N. Eliezer [6].

After the initial set of experiments described herein was completed we received from Professor R. Simha two samples of anionically polymerized poly(2-vinylnaphthalene) used in reference 6. These samples were used as received and gave no evidence of any spectroscopically significant contamination.

For all experiments we used a 1:1 THF:Et₂O (tetrahydrofuran:diethyl ether) glass at 77 °K. The THF was freshly distilled from lithium aluminum hydride with triphenylmethyl radical as indicator. Diethyl ether usually was found to give a sufficiently weak phosphorescence (near 500 nm) to be used without further purification. For more recent experiments the diethyl ether was freshly distilled from lithium aluminum hydride.

A solution approximately 10^{-3} M in naphthalene groups was made up with the 1:1 THF:Et₂O mixtures using quartzware that had been recently pyrolyzed with a Meker burner to remove any organic residues. Successive dilutions were made in several cases and the spectra of the 10^{-3} , 10^{-4} and 10^{-5} M solutions were compared. For the highest molecular weight polymers there was a significant ($\sim 15\%$) increase of the delayed fluorescence intensity relative to the naphthalene phosphorescence in the 10^{-4} M solution compared to the 10^{-3} M. No significant change occurred in the next 10-fold dilution except for a diminished signal to noise ratio. Hence the results we report are for $\sim 10^{-4}$ M solutions in naphthalene chromophores.

¹ Supported by the Robert A. Welch Foundation.

² Figures in brackets indicate the literature references at the end of this paper.

A phosphorimeter of our own design was operated in the traditional way. A single chopper alternately exposed the sample to excitation and then exposed a McPherson model 218 monochromator fitted with an EMI 6255S photomultiplier to the delayed emission. Excitation and observation times were approximately 2.35 msec. For long time decay curve experiments a pair of Vincent Associates Uni-blitz shutters was used to cut off excitation and expose the photomultiplier to the long lived emission at a given wavelength, selected on the monochromator. For all decay curve measurements the photomultiplier current was amplified by a Keithley model 427 current to voltage converter and signal averaged by a Fabri-Tek model 1060 instrument computer (manufactured by the Nicolet Instrument Co.). Sample excitation was effected by a 200 watt high pressure Hg lamp filtered by either a Corning 7-54 filter or a 7-54 plus an Oriel 313.0 nm interference filter.

The delayed emission spectrum of these polymers consists of two features: (1) a region to the long wavelength side of 480 nm, typical of naphthalene phosphorescence, and (2) a peak around 340 nm, typical of naphthalene fluorescence. Hence triplet-triplet annihilation leading to delayed fluorescence is present in P2VN. The relative intensity of the delayed fluorescence to the phosphorescence is dependent on the molecular weight (MW) of the polymer. In general the higher the MW the larger the ratio I_{DF}/I_P (intensity of delayed fluorescence to phosphorescence). We have plotted I_{DF}/I_P vs. \bar{P} in figure 1. The choice of \bar{P} for the abscissa is for convenience of display.

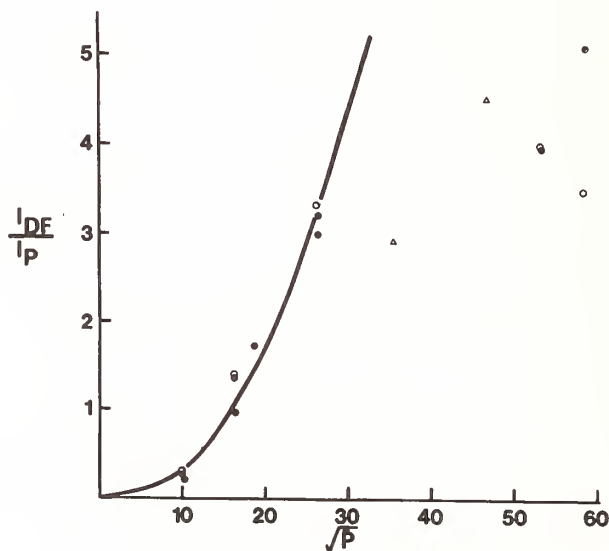


Figure 1. The ratio I_{DF}/I_P vs. \bar{P} . The solid line is from a Poisson distribution of excitons. The closed circles are for our original samples, the open circles for newer samples of our polymers, and the open triangles are the samples provided by Professor Simha.

While the trend of the results is clear, individual differences between polymers of approximately the same MW prevent an unambiguous determination of the functional dependence of I_{DF}/I_P on \bar{P} . Two features worth noting are: (1) the apparent extrapolation of I_{DF}/I_P to zero for $\bar{P} \neq 0$, and (2) the apparent "saturation" of the I_{DF}/I_P ratio for the four polymers with the highest MW. Observation (1) follows if one treats the number of triplets on the polymer as obeying a Poisson distribution where the average number of triplets per polymer chain is small. This treatment yields the solid line in figure 1. Observation (2) is expected when \bar{P} exceeds the average diffusion length of the triplet exciton. However, since two of the high molecular weight polymers were bulk polymerizations, it is not clear if they should be regarded as typical of the solution synthesized polymers.

Certain general features of the decay curves for all polymer samples can be summarized: (1) the delayed fluorescence decays much faster than the phosphorescence for the first 0.5 sec. After the delayed fluorescence has decayed to approximately 0.1 to 0.05 of its initial value, the rate of decay of the delayed fluorescence is approximately twice that of the phosphorescence for polymers with \bar{P} greater than 700. This does not seem to be the case for shorter polymers but poorer signal to noise ratios for delayed fluorescence in these samples prevents a firm statement from being made. (2) Both delayed fluorescence and phosphorescence display highly nonexponential decay for approximately 0.5 to 1.5 sec after cessation of excitation, at which point the former is very weak and the latter appears to be nearly exponential. The non-exponentiality for phosphorescence decay is much more pronounced for longer polymers than short polymers. (3) Only a slight dependence of the decay curves on I_{ex} is observed. This implies that the kinetic behavior of the triplets is dominated by unimolecular processes (emission, trapping, and radiationless transitions). (4) In general the decay of delayed fluorescence is lower as the MW of a polymer increases, although differences in individual samples preclude a clear-cut relation from being derived.

References

- [1] Cozzens, R. F., and Fox, R. B., *J. Chem. Phys.*, 50, 1532 (1969).
- [2] Fox, R. B., Price, T. R., Cozzens, R. F., and Echols, W. H., *Macromolecules*, 7, 937 (1974); Fox, R. B., Price, T. R., Cozzens, R. F., and McDonald, J. R., *J. Chem. Phys.*, 57, 2284 (1972); Fox, R. B., Price, T. R., and Cozzens, R. F., *Ibid.*, 54, 79 (1971).
- [3] Helene, C., and Longworth, J. W., *J. Chem. Phys.*, 57, 399 (1972).
- [4] David, C., Lempereur, M., and Geuskens, G., *Europ. Polymer J.*, 8, 417 (1972) and references therein to earlier work.
- [5] Klover, W., and Fischer, D., *J. Polymer Sci.*, Symposium No. 40, 43, (1973).
- [6] Utracki, L., Simha, R., and Eliezer, N., *Polymer*, 10, 43 (1969).

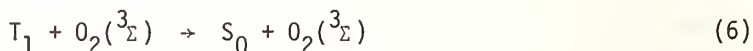
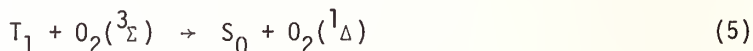
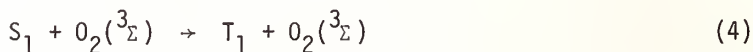
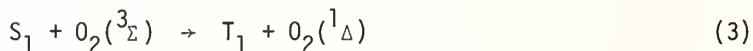
SINGLET AND TRIPLET PRECURSORS OF $O_2(^1\Delta_g)$

B. Stevens and J. A. Ors
Department of Chemistry
University of South Florida
Tampa, FL 33620

The quantum yield γ_{MO_2} of photosensitised addition of molecular oxygen to an organic acceptor M is the product of the quantum yield γ_Δ of $O_2(^1\Delta)$ formation and the efficiency ϕ_{MO_2} of $O_2(^1\Delta)$ addition to the acceptor (process 1) where



$\phi_{MO_2} = k_1[M]/(k_1[M] + k_2)$. Measurements of γ_{MO_2} as a function of dissolved oxygen concentration have been analysed [1]¹ to identify the operative oxygen quenching process of singlet (S_1) and triplet (T_1) states of the sensitiser of which processes 3-6 are spin-allowed and exothermic



if both the singlet-triplet splitting ΔE_{ST} (process 3) and triplet energies E_T (process 5) exceed the excitation energy of $O_2(^1\Delta)$ at 800 cm^{-1} . In terms of the parameters $\alpha = k_3/(k_3 + k_4)$ and $\epsilon = k_5/(k_5 + k_6)$ the overall reaction quantum yield is given by eq. (I) where γ_{IS} is

$$\gamma_{MO_2} = \phi_{MO_2} \{ \epsilon \gamma_{IS} + P_{O_2} [\alpha + \epsilon(1 - \gamma_{IS})] \} \quad (I)$$

¹Figures in brackets indicate the literature references at the end of this paper.

the sensitiser intersystem crossing yield and the probability that S_1 is quenched by $O_2^{1\Delta}$, $P_{O_2} = K[O_2]/(1 + K[O_2])$ is available from independent measurements of the Stern-Volmer fluorescence quenching constant K .

Linear plots of the data $\gamma_{MO_2}(P_{O_2})$ provide the quotients (Table 1)

$$\gamma_{MO_2}(P_{O_2} = 0)/\gamma_{MO_2}(P_{O_2} = 1) = \epsilon\gamma_{IS}/(\alpha + \epsilon) \quad (II)$$

which are close to independent measurements of γ_{IS} (tetracene²) or to values estimated as $1 - \gamma_F$ (DMBA) indicating that $\alpha \ll \epsilon$ for these compounds or that 4 and 5 are the dominant quenching processes. However this conclusion is not unambiguous for those sensitisers with high fluorescence quantum yield (rubrene and DMA) where the estimate of γ_{IS} as $1 - \gamma_F$ is exceeded by the uncertainty in measurement of γ_F .

Table 1. Photoperoxidation Parameters in Benzene at 25°C

Sensitiser	$10^3 \beta (M)$	γ_F^a	γ_{IS}	$10^{-6} k_{IS} (s^{-1})$	$\alpha + \epsilon$
Rubrene	1.0	0.98	≤ 0.02	≤ 3.0	1.9 ± 0.4
DMA	1.2	0.90	≤ 0.10	≤ 1.5	2.0 ± 0.4
Perylene	-	0.89	≤ 0.11	≤ 7.1	2.2 ± 0.3
Tetracene	2.4	0.19	0.68^b	120	1.2 ± 0.2
DMBA	1.6	0.36	≤ 0.64	27	1.0 ± 0.2

^aref. 5

^bref. 2

We have used competitive techniques to determine values for $\beta = k_2/k_1$ for the compounds listed in Table 1. This permits direct evaluation of γ_Δ as $\gamma_{MO_2}/\phi_{MO_2}$ and eq. (I) in the form

$$\gamma_\Delta = \gamma_{MO_2}(1 + \beta/[M]) = \epsilon\gamma_{IS} + P_{O_2}[\alpha + \epsilon(1 - \gamma_{IS})] \quad (III)$$

is used to present the experimental data $\gamma_\Delta(P_{O_2})$. Quantum yields γ_{MO_2} of self-sensitised photoperoxidation of rubrene, tetracene, 9, 10-dimethylanthracene (DMA) and 9,10-dimethyl-1,2,3-benzanthracene (DMBA) were estimated from recordings of the optical density as a function of time at the actinic wavelength and the source intensity at this wavelength determined by ferrioxalate actinometry. In the case of perylene, this was used to sensitise the photoperoxidation of DMA and DMBA at 436 nm where these acceptors are transparent at the concentrations used.

The data presented in figures 1 and 2 illustrate two behavioral patterns, viz

a) $\gamma_\Delta(P_{O_2} = 1) = \alpha + \epsilon \sim 1.0$ for those sensitisers with high intersystem crossing yield. Since $\gamma_\Delta(P_{O_2} = 0) = \epsilon\gamma_{IS} \sim \gamma_{IS}$ for these compounds (tetracene and DMBA), it must be concluded that $\epsilon \sim 1$ and $\alpha \sim 0$ consistent with 4 and 5 as the dominant oxygen quenching process.

b) $\gamma_{\Delta}(P_{O_2} = 1) = \alpha + \epsilon \sim 2.0$ for rubrene, perylene and DMA which exhibit high fluorescence quantum yields (≥ 0.9) and low intersystem crossing efficiencies. Since neither α nor ϵ as defined can exceed unity, it must be concluded that $\alpha \sim \epsilon \sim 1$ or that processes 3 and 5 are largely responsible for oxygen quenching of the singlet and triplet states of these sensitizers. The reverse of process 3 represents the energy pooling process responsible [4] for the oxygen enhancement of fluorescence under conditions where triplet state relaxation is relatively slow.

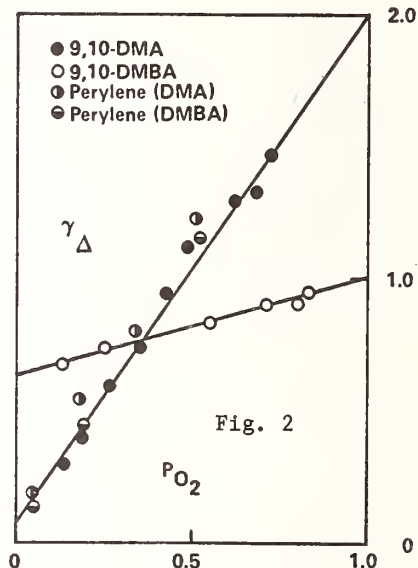
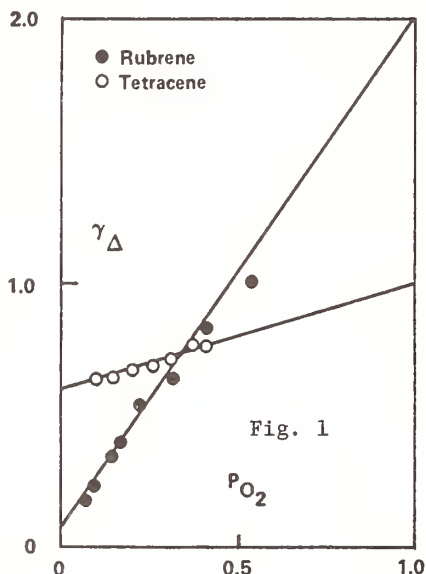


Figure 1.

Since ΔE_{ST} exceeds 8000 cm^{-1} for the sensitizers examined here, the nature of the singlet quenching process is essentially determined by the relative rates of non-radiative transitions from the complex formed initially ${}^3F_i(S_1^3\Sigma)$ to lower energy complex states ${}^3F_f(T_1^1\Delta)$ and ${}^3F_f(T_1^3\Sigma)$. If processes 3 and 4 operate by an exchange mechanism these rates will largely depend on the relative energies of these states viz

$${}^3F_g(T_n^3\Sigma) > {}^3F_i(S_1^3\Sigma) > {}^3F_f(T_1^1\Delta) \quad k_3 \gg k_4$$

$${}^3F_i(S_1^3\Sigma) > {}^3F_g(T_n^3\Sigma) > {}^3F_f(T_1^1\Delta) \quad k_3 \gg k_4$$

which reflect the ordering of molecular states

$$T_n > S_1 > T_1 \quad \gamma_{IS} \sim 0$$

$$S_1 > T_n > T_1 \quad \gamma_{IS} \gg 0$$

expected for sensitizers of high and low fluorescence yields and intersystem crossing rate constants k_{IS} which differ by an order of magnitude (Table 1). The quenching processes 3 and 4 should not therefore be mutually exclusive particularly for sensitizers where $\Delta E_{gf} \sim 0$.

References

- [1] Stevens, B., and Algar, B. E., *Ann. New York Acad. Sci.*, 171, 50 (1970).
- [2] Kearvell, A., and Wilkinson, F., *Chem. Phys. Letters* 11, 472 (1972).
- [3] Stevens, B., Perez, S. R., and Ors, J. A., *J. Amer. Chem. Soc.* 96, 6846 (1974).
- [4] Kenner, R. D., and Khan, A. U., *Chem. Phys. Letters* 36, 643 (1975).
- [5] Stevens, B., and Algar, B. E., *J. Phys. Chem.* 72, 2582 (1968).

THE HEAVY ATOM EFFECT ON THE PHOTOCHEMICAL CYCLOADDITION PROCESSES OF ACENAPHTHYLENE

B. F. Plummer and Lou Jean Scott

Trinity University
San Antonio, TX 78284

Modification of photochemical processes through the influence of heavy atom perturbation continues to be a fruitful area of study [1]¹. Quantum mechanical interpretations satisfactorily rationalize the effect of heavy atom perturbations. However, predictions of specific molecular compounds that will show a measurable change in photochemistry under heavy atom perturbation have not yet materialized [2].

The discovery by Cowan and Drisko that the photodimerization of acenaphthylene (A) showed a dramatic heavy atom effect (HAE) [3] stimulated us to explore the potential of this perturbation when applied to the cycloaddition reactions of other molecules to A. Compounds such as acrylonitrile, α -chloroacrylonitrile, cyclopentadiene (CP) and cis and trans-1,3-pentadiene were found to cycloadd photochemically to A when HA perturbation in the form of brominated solvents was used [4].

The triplet nature of these direct irradiation processes was verified through S-V quenching studies using cyclooctatetraene and ferrocene as quenchers. The triplet energy of these quenchers lies in the range of 30-40 kcal/mole and thus establishes a lower limit for the triplet energy of excited triplet A as near 40 kcal/mol. The product ratios from direct and triplet sensitized radiations were compared for A reacting with CP and found to be similar. The sensitizer used for these studies was the dicyclohexyl 18-crown-6-ether complex of disodium Rose Bengal.

The influence of heavy atom solvents such as bromoethane, 1,2-dibromoethane, and bromobenzene as compared to cyclohexane and acetonitrile was studied. The quantum yield of the reaction was found to vary in a predictable way with a change in the concentration of CP. The mechanism of this reaction was found to conform to the general kinetic expression in equation 1.

$$\frac{1}{\phi_r} = \frac{1}{\alpha \phi_{isc}} + \frac{1}{\alpha \phi_{isc}} \left(\frac{k_d}{k_r} \right) \frac{1}{[D]} \quad (1)$$

[D] + [CP]

The quantum yield of reaction is ϕ_r , α = the fraction of intermediate diradicals forming product, k_d = the rate constant of excited triplet state decay of A and k_r = the rate constant of bimolecular formation of intermediate from A and CP.

Using the reasonable assumption that ϕ_{isc} for A is unity in heavy atom solvents, a value for α of 0.2 was obtained from the kinetic data. Thus, about 20% of the diradicals produced continue on to form products, the remainder apparently dissociating to form A and CP.

¹ Figures in brackets indicate the literature references at the end of this paper.

A comparison of the external perturbation of bromine was made to internal perturbation by studying the photocycloaddition of 5-bromoacenaphthylene (ABr) to CP. Similar kinetic expressions were obeyed for A and ABr reacting with CP. However, it was learned that the internal heavy atom exerts a larger effect upon k_d than does the external heavy atom.

The unique capability of A to magnify heavy atom perturbation in conjunction with its relatively poor fluorescence quantum yield ($\phi_f < 0.001$) and phosphorescence quantum yield ($\phi_p \sim 0$) has led us to explore the photochemistry of the acetyl derivative of A. The new molecule 5-acetoacenaphthylene (aA) was synthesized by acetylating acenaphthene with acetic anhydride and magnesium perchlorate and then subsequently dehydrogenating the saturated precursor with DDQ. Single photon emission studies of aA showed only a very weak fluorescence near 400 nm and no detectable phosphorescence. The absorption spectrum of aA resembled that of A except for a larger absorptivity coefficient at similar regions of maximum absorption. A weak shoulder at 499 nm ($\epsilon = 18$) in cyclohexane that shows a bathochromic shift in ethanol suggests that the $n \rightarrow \pi^*$ transition may occur at this wavelength.

We have studied the excited state cycloaddition of aA to CP in regular and heavy atom solvents. The photoproducts formed are analogous to those formed between A and CP, as verified by gc product distributions, nmr and ir measurements, and mass spectroscopic analysis.

We have studied the direct and sensitized product distributions of the reaction of aA with cP and find that they are similar. Additionally, the direct reaction can be quenched with ferrocene. The kinetic studies of aA reacting with CP have been investigated and data will be reported that suggest an intermediate role of the carbonyl group in aA in effecting spin-orbital perturbation of the reactions of aA.

References

- [1] Plummer, B. F., and Schloman, W. W., Jr., *J. Amer. Chem. Soc.* 98, 3254 (1976).
Cowan, D. O., and Koziar, J. C., *Ibid.*, 98, 1001 (1976).
Gutierrez, A. R., and Whitten, D. G., *Ibid.*, 96, 7128 (1974).
- [2] Giachino, G. A., and Kearns, D. R., *J. Chem. Phys.* 52, 2964 (1970).
- [3] Cowan, D. O., and Drisko, R. L., *Tetrahedron Lett.*, 1255 (1967).
- [4] Plummer, B. F., Ferree, W. I., Jr., and Schloman, W. W., Jr., *J. Amer. Chem. Soc.* 96, 7741 (1974) and references therein.

LASER INDUCED FLUORESCENCE EMISSION SPECTROSCOPY OF $\text{H}_2\text{CO}(\text{A}, {}^1\text{A}_2)^1$

Kenneth Y. Tang and Edward K. C. Lee

Department of Chemistry
University of California
Irvine, CA 92717

The single vibronic level (SVL) radiative lifetimes (τ_R) of the first excited singlet state of $\text{H}_2\text{CO}(\text{A}^1\text{A}_2)$ have been studied recently [1]². The most interesting finding was a large variation of the radiative lifetimes showing a general trend of increasing radiative lifetime with increasing vibrational energy (E_{vib}) and expectedly shorter values of τ_R for the SVL levels with one quantum excitation of the asymmetric C-H stretch mode (ν_5). More specifically, the radiative lifetime of the 5^1 level at $E_{\text{vib}} = 2968 \text{ cm}^{-1}$, $\tau_R(5^1)$ was found to be $\sim 0.7 \times 10^{-6}$ sec, several times shorter than $\tau_R(2^2\text{A}_1^1) = 11 \times 10^{-6}$ sec at $E_{\text{vib}} = 3343 \text{ cm}^{-1}$. Since the non-totally symmetric, out-of-plane puckering mode (ν_4) is much more active than ν_5 in the absorption and in the emission spectra for electric dipole forbidden but vibronically allowed transition (${}^1\text{A}_2 \rightarrow {}^1\text{A}_1$), this behavior of the radiative lifetime is very surprising. In order to establish the extent of the Herzberg-Teller type vibronic coupling in the radiative transitions from the 5^1 level, we have decided to determine quantitatively the activity of the ν_5 mode in the molecular resonance fluorescence spectra from several single vibronic levels at low pressures (nearly collision free). The most interesting results [2] have been obtained with the 5^1 and the 1^1A_1 levels which are nearly degenerate (2.7 cm^{-1}) and perturbed by Coriolis coupling.

For the purpose of illustration, the spectra taken at 3207.0 \AA (vac) and 3215.1 \AA (vac) excitation with 0.5 torr of H_2CO at 23°C are shown in figure 1. The collisionally relaxed spectrum obtained at $\lambda_{\text{ex}}(\text{vac}) = 3207.0 \text{ \AA}$ and 5.0 torr of added N_2 is shown in the middle for comparison. The pumping was achieved with a flashlamp-pumped dye laser equipped with frequency doubling crystals and fine tuning etalons, and the fluorescence was detected with an optical multichannel analyzer.

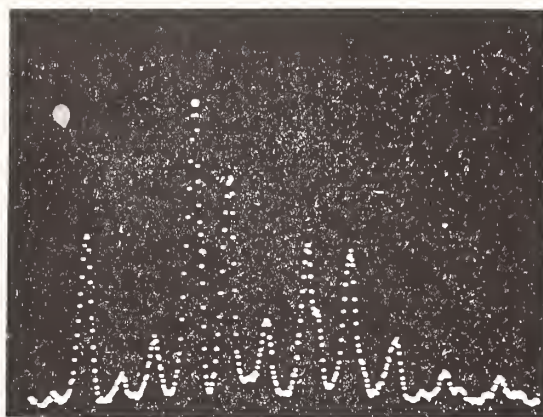
¹This research has been supported by the National Science Foundation and the Office of Naval Research.

²Figures in brackets indicate the literature references at the end of this paper.

5^1 level

$\lambda_{\text{ex}} = 3215.1 \text{ \AA} (\text{vac})$

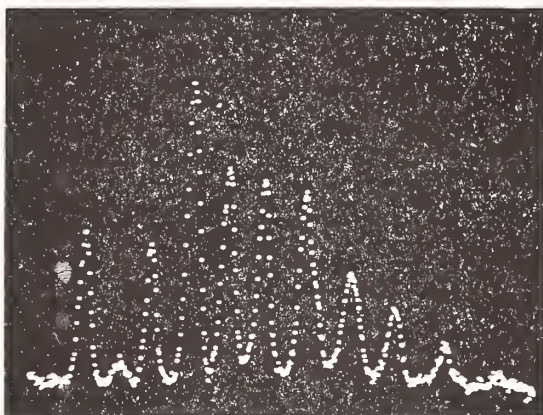
$\text{H}_2\text{CO} = 0.5 \text{ torr}$



$\lambda_{\text{ex}} = 3207.0 \text{ \AA} (\text{vac})$

$\text{H}_2\text{CO} = 0.5 \text{ torr}$

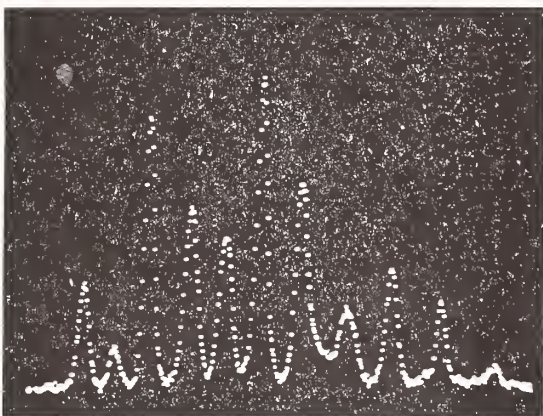
$\text{N}_2 = 5.0 \text{ torr}$



$1^1_4^1$ level

$\lambda_{\text{ex}} = 3207.0 \text{ \AA} (\text{vac})$

$\text{H}_2\text{CO} = 0.5 \text{ torr}$



370 400 430 460 (nm)

Figure 1. Emission spectrum.

Despite our attempt to obtain an SVL spectrum from the "selective" excitation of the pro-vibronic level of either 5^1 or $1^1_4^1$, we were unable to obtain a "level" purity better than 80% as you can see from figure 1. We believe that the 3207.0 Å excitation corresponds to the $1^1_4^1\text{Q}_3(\text{J}' = 13, \text{K}' = 4 \leftarrow \text{J}'' = 13, \text{K}'' = 3)$ transition and 3215.1 Å excitation corresponds to the $5^1\text{P}_3(\text{J}' = 7, \text{K}' = 2 \leftarrow \text{J}'' = 7, \text{K}'' = 3)$ transition and the overlapping $5^1\text{P}_3(\text{J}' = 2, \text{K}' = 2 \leftarrow \text{J}'' = 3, \text{K}'' = 3)$ transition.

In examining the SVL emission spectrum we find that the intense bands in the emission involve the odd quantum number change in the out-of-plane bending mode (ν_4) and the progressions are formed by the C-O stretch mode (ν_2). Hence, the emission spectrum from the 5^1 level is similar to the one from the 4^0 level, showing always the 5_1 contribution as if ν_5 is the "frozen" mode. Likewise, the emission spectrum from the $1^1 4^1$ level is also similar to the one from the 4^1 level, again showing the 1_1 contribution as if ν_1 is the "frozen" mode. The most intense bands from the 5^1 level are $4_1^0 5_1$, $2_1^0 4_1^0 5_1$ and $4_2^0 5_1$, where as the most intense bands from the $1^1 4^1$ level are $1_1^1 4_2^1$ and $1_1^1 2_1^0 4_2^1$.

Fluorescence gives spectra whose distinctive features characterize the emission from the levels 5^1 and $1^1 4^1$. This makes us to believe that the intramolecular energy flow between these two vibronic levels is slow compared to the time scale (10^{-8} sec) of the unimolecular decay processes (mostly non-radiative), although these two states are nearly degenerate with 2.7 cm^{-1} of separation.

The fluorescence intensity I_F from an SVL is proportional to the radiative decay rate constant (k_R) and the population (N). Since the 5^1 and the $1^1 4^1$ levels are $\sim 2.7 \text{ cm}^{-1}$ apart, the Boltzmannized population ratio at room temperature should be very close to unity: $N(5^1)/N(1^1 4^1) = 1.013$. In the presence of $10 \sim 100$ torr of N_2 , the 3207.0 \AA (5^1) and the 3215.1 \AA ($1^1 4^1$) excitations give an identical "equilibrated" spectrum consisting of the emission from the two SVL's as shown in figure 1 (middle). Considering the lifetimes ($\sim 15 \text{ nsec}$) and the pressures used, the collision induced vibrational relaxations to other vibronic levels are negligible and that the $5^1 \rightarrow 1^1 4^1$ relaxation is considerably more efficient as in rotational relaxation. The intensity ratios, $I_F(5^1)/I_F(1^1 4^1)$, obtained from the two excitation wavelengths as a function of N_2 pressure gives a limiting value of ~ 1.8 at high pressures. Therefore, $k_R(5^1)$ is 1.8 times greater than $k_R(1^1 4^1)$. Using the value of $k_R(5^1) = 1.3 \times 10^6 \text{ sec}^{-1}$ obtained previously [1] we calculate $k_R(1^1 4^1)$ to be $\sim 0.7 \times 10^6 \text{ sec}^{-1}$. This value is greater than $k_R(4^1) = 0.5 \times 10^6 \text{ sec}^{-1}$ obtained previously [1].

In conclusion, the present data clearly indicate that the radiative transitions (even from the 5^1 level) show insignificant involvement of the ν_5 mode for the Herzberg-Teller type vibronic coupling but yet the overall radiative rate from the 5^1 level is 1.8 times greater than that from the $1^1 4^1$ level. Also, it appears that $k_R(1^1 4^1)$ is also 1.4 times as great as $k_R(4^1)$. We believe that further theoretical advance should shed more light on the significance of the "frozen" mode in enhancing the radiative transition rates.

References

- [1] Miller, R. G., and Lee, E. K. C., *Chem. Phys. Lett.*, **33**, 104 (1975).
- [2] Tang, K. Y., and Lee, E. K. C., submitted for publication to *Chem. Phys. Lett.*

LASER EXCITED NO₂ FLUORESCENCE LIFETIME STUDIES IN THE 600 NM REGION

V. M. Donnelly and F. Kaufman

Department of Chemistry
University of Pittsburgh
Pittsburgh, PA 15260

A partial analysis of the absorption and fluorescence spectra of NO₂ indicates that the ²B₁ state is responsible for much of the absorption above 23,000 cm⁻¹ [1]¹, while below 19,000 cm⁻¹ the ²B₂ state carries virtually all the oscillator strength [2,3]. The visible absorption spectrum is extremely complex due mainly to extensive perturbations of the excited states by high vibrational levels of the ground state. This factor also accounts, at least in part, for the fact that both excited states exhibit fluorescence lifetimes much longer than the 0.3 μsec order of magnitude value calculated from the integrated absorption coefficient. Broad band modulated excitation studies [4] have reported fluorescence lifetimes of 50 to 90 μsec in the 400-600 nm region. Narrow bandwidth pulsed laser experiments have shown that in the 451-461 nm region [5], decays are slightly non-exponential with average lifetimes of about 80 μsec, while at 593 nm, decays are very non-exponential due to at least two components with lifetimes of 30 and 115 μsec [3]. We report here the results of laser excited fluorescence lifetime experiments in the 578-612 nm region. At pressures as low as 10⁻⁵ torr decays are highly non-exponential for some excitation wavelengths, and nearly exponential for others. These results can be explained in terms of a single electronic state (²B₂) vibronically coupled to high vibrational levels of the ground state.

Fluorescence was excited by a Nd-YAG pumped tunable dye laser with a bandwidth of either 1.5 or 0.15 cm⁻¹. The fluorescence was detected through cutoff or interference filters by a photomultiplier tube which observed the central portion of a 72λ spherical fluorescence cell. Fluorescence decays were summed over 10⁴ to 10⁵ laser pulses on a multi-channel analyzer with 10 μsec per channel time resolution. Nonexponential decays were fit to the expression

$$I(t) = Re^{-t/\tau_S} + e^{-t/\tau_L} \quad (1)$$

Very good fits were obtained in all cases. However this does not prove that decays are simple biexponentials, so the parameters τ_S , τ_L and R should be interpreted with caution. Decays were recorded as a function of excitation energy and pressure ($P < 25$ mtorr). For excitation coincident with the strong ²B₂ + ²A₁ absorption at 585, 593, and 612 nm, the decays are highly non-exponential. Plots of τ_S^{-1} and τ_L^{-1} vs. P extrapolated to zero pressure give "lifetimes" in the 22-75 μsec range for τ_S and 170-260 μsec for τ_L . The slopes of the τ_S^{-1} vs. P and τ_L^{-1} vs. P plots are typically 5×10^{-10} and 0.75×10^{-10} cm³ sec⁻¹, respectively. When the laser wavelength does not correspond to strong ²B₂ features (578, 594, 603 nm) the decays are nearly exponential at all pressures. The slopes and intercepts of the τ^{-1} vs. P plots at these wavelengths are in the same range as the τ_L^{-1} vs. P plot slopes and intercepts at 585, 593, and 612 nm. R in eq. (1) varies from ~0 to 3 over the 578-612 nm region. Other experiments show that τ_S and especially R vary strongly for small changes (0.15 cm⁻¹) in the excitation energy. The largest R and the shortest τ_S correspond to strong features in the fluorescence excitation spectrum.

¹Figures in brackets indicate the literature references at the end of this paper.

The overwhelming spectroscopic evidence [2,3] against the existence of more than one strongly absorbing electronic state in this wavelength region leads us to believe that these results are due to variable vibronic coupling between the 2B_2 state and upper vibrational levels of the ground state as suggested by Douglas [6]. Excitation at 578, 594, and 603 nm is due to high levels of the ground state which lie close enough to levels of the 2B_2 state so that they can borrow oscillator strength and make transitions possible. Absorption to and fluorescence from such levels are weak since they are mostly 2A_1 in character and the transition is forbidden; hence the fluorescence lifetime will be much longer than that calculated from the integrated absorption coefficient. At 585, 593, and 612 nm the upper state has more 2B_2 character due to the coincidence of these wavelengths with positions of zero-order 2B_2 levels. Even so, the state populated is still mostly 2A_1 because of vibronic coupling. So at these latter wavelengths the average lifetime would be expected to be shorter than at 578, 594, and 603 nm, but still much longer than the integrated absorption coefficient value. Previous attempts to explain the lifetime anomaly by electronic state mixing were not successful because the ratio of the density of ground state to excited state vibrational levels is only about a factor of ten (at ~600 nm) leaving an unexplained factor of about 30. However, this calculation was based on a single excited state, whereas it has been demonstrated that over the entire absorption region, two electronic states are excited. In order to get a more reasonable estimate we have assumed, first, that the 2B_1 state is responsible for all absorption at energies above 25,000 cm^{-1} ; second, that all absorption at energies less than 18,000 cm^{-1} is due to the 2B_2 state; and third, that absorption by the 2B_2 state is symmetric about a maximum at 20,000 cm^{-1} where it is responsible for 70% of the total absorption. We thereby calculate a lifetime of roughly 3 μsec for the 2B_2 state. When this is multiplied by a level density ratio of 10 the lifetime anomaly for the 2B_2 state is essentially removed. If this argument is valid, then our data are qualitatively consistent with the theory of Bixon and Jortner [7]. This theory predicts that the type of vibronic coupling described above results in many additional vibronic states, each with a different lifetime, the magnitude of which is inversely related to the amount of excited electronic state character the state possesses. Due to the thermal distribution of rotational energy in the ground state, these states are seen as overlapping vibronic bands in the room temperature absorption spectrum. The rotational structure is very dense, so that even a narrow band width laser excites more than one vibronic state, resulting in non-exponential fluorescence decays. The strongest absorbing states near 585, 593 and 612 nm possess the shortest lifetimes, so exciting here one finds the most highly non-exponential decays. At wavelengths which do not correspond to these states (at 578, 594 and 603 nm) decays are more nearly exponential. This explanation should help in an understanding of that part of NO_2 absorption due to the perturbed 2B_2 electronic state.

References

- [1] Douglas, A. E., and Huber, K. P., *Can. J. Phys.* 43, 74 (1965); Hardwick, J. L., and Brand, J. C. D., *Chem. Phys. Lett.* 21, 458 (1973); Senum, G. I., and Schwartz, S. E., *Chem. Phys. Lett.* 32, 569 (1974).
- [2] Abe, K., Myers, F., McCubbin, T. K., Jr., and Polo, S. R., *J. Mol. Spectrosc.* 50, 413 (1974); Brand, J. C. D., Hardwick, J. L., Pirkle, R. J., and Seliskar, C. J., *Can. J. Phys.* 51, 2184 (1973); Smalley, R. E., Wharton, K., and Levy, D. H., *J. Chem. Phys.* 63, 4977 (1975).
- [3] Stevens, C. G., Swagel, M. W., Wallace, R., and Zare, R. N., *Chem. Phys. Lett.* 18, 465 (1973).
- [4] Keyser, L. F., Kaufman, F., and Zipf, E. C., *Chem. Phys. Lett.* 2, 523 (1968); Schwartz, S. E., and Johnston, H. S., *J. Chem. Phys.* 51, 1286 (1969); Keyser, L. F., Levine, S. Z., and Kaufman, F., *J. Chem. Phys.* 54, 355 (1971).
- [5] Sackett, P. B., and Yardley, Y. T., *J. Chem. Phys.* 57, 152 (1972).
- [6] Douglas, A. E., *J. Chem. Phys.* 45, 1007 (1966).
- [7] Bixon, M., and Jortner, J., *J. Chem. Phys.* 50, 3284 (1969).

LASER FLUORESCENCE STUDIES, INCLUDING THE $B^3\Pi(0^+)$ STATES OF BrF, IF AND ICl

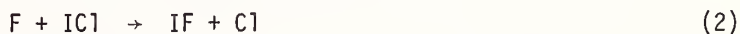
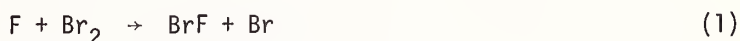
Michael A. A. Clyne, Alan H. Curran and I Stuart McDermid

Department of Chemistry
Queen Mary College
Mile End Road, London E1 4NS, England

A number of new laser excitation spectra, mostly of transient molecules, are reported. These include: (a) the $B^3\Pi(0^+) - X^1\Sigma^+$ transitions of BrF, IF and ICl (440-630 nm); and (b) the $A^3\Pi - X^1\Sigma^+$ transition of SO (259-261 nm). We also report that laser excitation of ClO radicals is unobservably weak in the most favourable (263-280 nm) region of its $A^2\Pi - X^2\Pi$ system; fluorescence is therefore unlikely to be useful as a monitor for stratospheric ClO.

In this paper, we emphasize results of spectroscopic studies of the $B^3\Pi(0^+) - X^1\Sigma^+$ visible transitions of BrF, IF and ICl, using laser fluorescence. Rotational constants for the excited B state of BrF ($8 > v' > 3$) have been measured for the first time (in collaboration with J. A. Coxon). An interesting predissociation at $v' = 8$, $J' \approx 29$ of BrF $B^3\Pi(0^+)$ has been identified. Results on this predissociation, and hopefully also on the lifetimes of the excited state, will be presented.

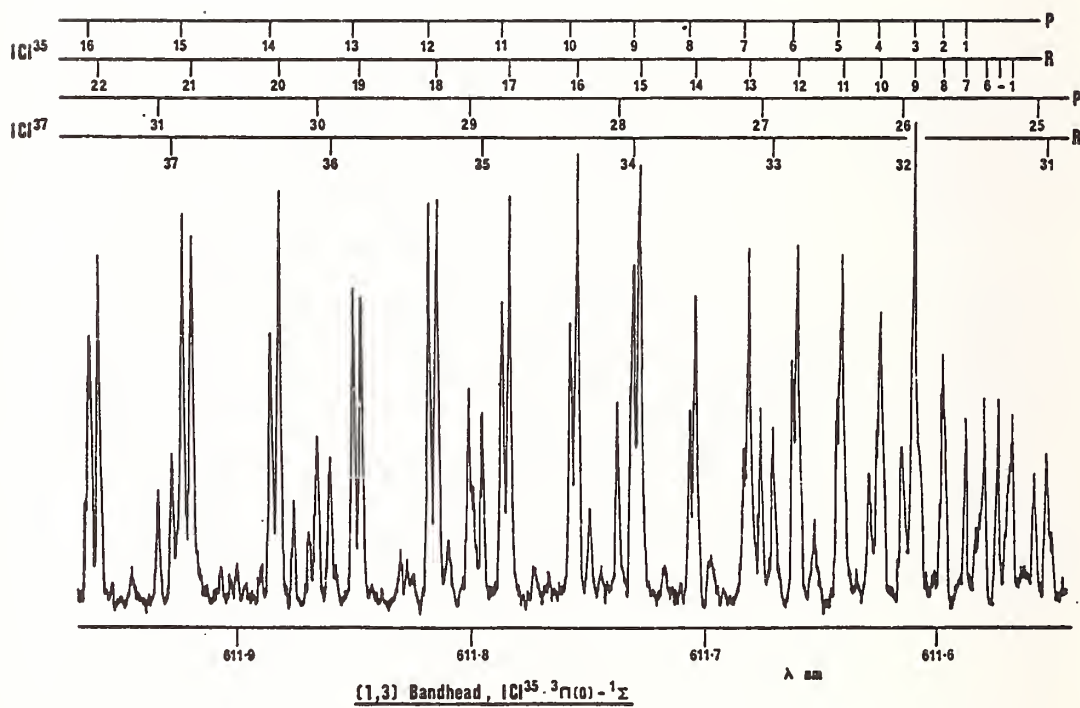
Strong fluorescence by the transient molecule IF also was observed over a wide range of excited B state vibrational levels, up to $v' = 11$, $J' = 45$, where the onset of predissociation is confirmed. The source of the transient BrF and IF molecules were the rapid reactions (1) and (2) carried out in a discharge-flow system [E. H. Appelman and M. A. A. Clyne, JCS Faraday I, 1975, 71, 2072]:



Observation of fluorescence from the B state of ICl, which is very weakly bound, was surprising. Because of the unexpectedly short lifetime of the $B^3\Pi(0^+)$ state, fluorescence to the ground state from the normally dominant, but long-lived (~ 100 μ sec) $A^3\Pi(1)$ state of ICl, could be quenched out almost entirely by using ICl pressures near 5 Torr. In this way, the overlapping strong A-X fluorescence could be virtually completely suppressed. Energy levels up to $v' = 2$, $J' \approx 70$, of $I^{35}Cl$ $B^3\Pi(0^+)$ were observed in fluorescence in the B-X transition. The dominant transition at 300 K were the 2,3; 1,3; 2,4 and 1,4 bands. Absence of fluorescence from $v' = 3$, which is sharp in absorption, indicates that the B state of ICl is completely predissociated above $v' = 2$.

RKGC potential energy curves and Franck-Condon factors for the B and X states of IF, ICl and IBr will be presented. The absence of detectable fluorescence from the $B^3\Pi(0^+)$ state of IBr will be discussed in the light of these results.

The non-collisional lifetimes of the $B^3\Pi(0^+)$ states of the halogens and interhalogens will be discussed, in relation to the corresponding B-X absorption spectra.



LASER-INDUCED FLUORESCENCE OF CN RADICALS PRODUCED BY PHOTODISSOCIATION OF RCN

Regina J. Cody and Michael J. Sabety-Dzvonik¹

Astrochemistry Branch
NASA/Goddard Space Flight Center
Greenbelt, MD 20771

Laser-induced fluorescence spectroscopy has become a useful tool in probing free radical processes in photodissociation, flames, electric discharges, etc. With this technique measurements have been made of radical properties and formation processes and of the internal energy content of product radicals. In addition to laboratory dissociative processes, radical emissions are also widely observed in astronomical spectra, including those originating from comets. Generally, the first radical emission observed as a comet comes toward the sun is the Violet Band system of CN. The source mechanisms for many of these cometary radicals are unknown. It has been postulated that photodissociation of appropriate parent molecules by solar radiation could be a source for these radicals. In this work we will report our observations on the CN radicals formed by the VUV photodissociation of cyanoacetylene (C_2HCN), which has been seen in interstellar space, and of methylcyanide (CH_3CN) and HCN, both of which were observed in the atmosphere of Comet Kohoutek.

The flash photolysis-laser induced fluorescence apparatus has been described previously in detail [1-3]². Two flashlamps with different spectral outputs are coupled with various UV filters to dissociate the parent compounds in different absorption regions above 135 nm. One flashlamp is a commercial xenon lamp with a spectral output above 190 nm, while the other is an argon lamp ($\sim 0.6 \mu s$ FWHM, 0.8 - 1.0 joule, 50 pps, pressure ≥ 1 atm) with a spectral output above 135 nm (short wavelength cut-off of SrF_2). The spectral outputs of both lamps were measured with a 1 m normal incidence spectrometer using a sodium salicylate coated photomultiplier tube. The time delay between the firing of the flashlamp and the triggering of the N_2 laser pumped dye laser can be varied from 2 μs to 20 ms. The $CN(X^2\Sigma^+)$ fragments produced by the photolysis are excited by the dye laser output to the $B^2\Sigma^+$ state via the Violet Band system, $\Delta v = 0$ sequence. The fluorescence radiated by these $CN(B)$ radicals is detected by a photomultiplier tube after passage through an holographic grating monochromator which acts essentially as a broad band interference filter (FWHM ~ 10 nm). The number of collisions which the radicals undergo between formation and detection is controlled by the time delay and the total gas pressure. Both pure parent gas samples and mixtures of RCN in N_2 or an inert gas are photolyzed.

Pure samples of C_2HCN were photolyzed at pressures of 0.02 - 0.04 mm Hg and time delays of 2-3 μs , which correspond to a collision number of < 2 for a kinetic temperature of 300 °K. The argon lamp coupled with either a SrF_2 window ($\lambda > 135$ nm) or a sapphire window ($\lambda > 145$ nm) was used for these photolysis experiments. As shown in fig. 1, the spectrum of the CN radicals showed predominantly the 0-0, 1-1, and 2-2 bands with strong bandheads for the 0-0 and 1-1 bands. After correction for the variation in laser intensity with wavelength, the intensities of the rotational lines in the R branches of the 0-0 and 1-1 bands were computer fitted to the Maxwell-Boltzmann equation to yield rotational temperatures. The areas under the rotational distribution curves were

¹ NAS/NRC Research Associate.

² Figures in brackets indicate the literature references at the end of this paper.

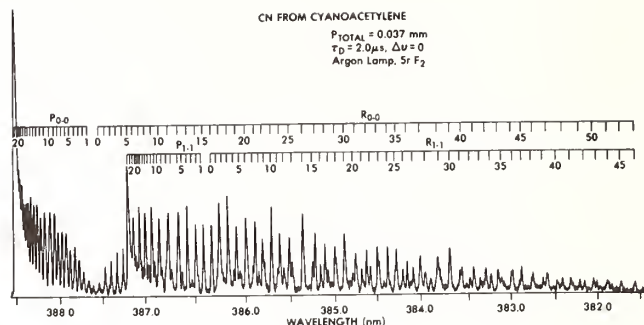


Figure 1. Laser-Induced Fluorescence Spectrum of $\text{CN}(\text{X}^2\Sigma^+)$ Radicals.

integrated and ratioed to give the relative vibrational population distributions. Since only a small number of the rotational lines in the 2-2 band could be measured due to the low signal intensity, Boltzmann graphs for this band were not made. To obtain the vibrational population ratio for the $v'' = 2$ level, individual line intensities were ratioed to the appropriate 0-0 lines, and these ratios were averaged. The results for the low collision number experiments are summarized in Table I.

Table I. Summary of $\text{CN}(\text{X})$ from cyanoacetylene

EXCITATION WAVELENGTH (nm)	VIBRATIONAL LEVEL	ROTATIONAL TEMPERATURE (K)	VIBRATIONAL POPULATION RATIO	VIBRATIONAL TEMPERATURE (K)
> 135 (SrF_2)	0	1822 ± 166	1.0	----
	1	1667 ± 198	0.50 ± 0.05	4300
	2	-----	0.32 ± 0.07	5100
> 145 (Sapphire)	0	1368 ± 123	1.0	----
	1	1130 ± 236	0.40 ± 0.06	3200
	2	-----	0.18 ± 0.05	3400

Previous work [2-4] has shown that CN formed in the $\text{A}(^2\Pi_1)$ state, $v = 0$ level, can be collisionally induced to transfer energy into the X state, $v'' = 4$ level, through near energy resonances between certain rotational states in the A and X states. This energy transfer results in an enhancement of the intensity of the 4-4 band at high collision number. The vibrational population distributions resulting from the photolysis of high pressure ($P = 50$ mm) mixtures of $\sim 0.2\%$ C_2HCN in N_2 or He are shown in figure 2. For photolysis at $\lambda > 145$ nm (sapphire) the vibrational curve shows that very little, if any, CN is formed in the A state. However, for $\lambda > 135$ nm (SrF_2) the vibrational distribution indicates that a small amount of CN is formed in the A state. It is not possible to form $\text{CN}(\text{B})$ in the photolysis, since the threshold wavelength for the production of B state is ≤ 131.8 nm [5], and a SrF_2 window was the shortest wavelength cut-off ($\lambda \sim 135$ nm) used.

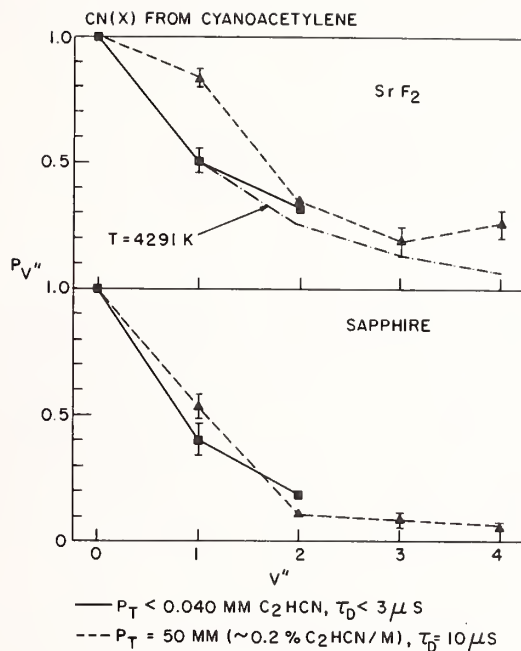


Figure 2. Vibrational population distributions of $\text{CN}(X^2\Sigma^+)$ radicals.

Photolysis of HCN and CH_3CN samples confirm that the CN radicals are formed predominantly in the A state. Photolysis at $\lambda > 135$ nm of high pressure ($P = 50$ mm) mixture of $\sim 1\%$ CH_3CN in Ar (delay time = $3 \mu\text{s}$) yielded a vibrational population distribution of $N_0:N_1:N_2:N_3:N_4:N_5 = 1.00:0.78:1.21:4.63:5.80:1.47$.

References

- [1] Jackson, W. M., *J. Chem. Phys.* **61**, 4177 (1974).
- [2] Jackson, W. M., and Cody, R. J., *Ibid.*, 4183 (1974).
- [3] Cody, R. J., Sabety-Dzvonik, M. J., and Jackson, W. M., submitted to *J. Chem. Phys.* (1976).
- [4] Savety-Dzvonik, M. J., Cody, R. J., and Jackson, W. M., submitted to *Chem. Phys. Lett.* (1976).
- [5] Okabe, H., and Dibeler, V. H., *J. Chem. Phys.* **59**, 2430 (1973).

PHOTOFRAGMENT SPECTROSCOPY OF THE $A \leftrightarrow X$ TRANSITION IN CN USING TWO PULSED LASERS

Andrew Baronavski¹ and J. R. McDonald

Chemistry Division
Naval Research Laboratory
Washington, DC 20375

1. Introduction

The CN radical has been studied extensively for many decades [1-4]²; still little is known of the dynamics of its formation and decay. Ling and Wilson [5] studied the photofragment spectroscopy of ICN with a high power (70 mJoule) laser photolysis source and mass spectrometric detection to determine the translational energy and angular dependence of the CN radicals. Ling and Wilson inferred from their results that 60% of the CN is formed in the first excited electronic state ($A^2\Pi_{1/2,3/2}$) and 40% is formed in the ground state with a vibrational energy inversion as high as $v''=3$ and a rotational temperature of a few thousand degrees Kelvin. More recent work by Savety-Dzvonik and Cody [6] uses flashlamp photolysis of ICN and fluorescence detection following excitation to the $B^2\Sigma^+$ state of CN. This work indicates that for photolysis at $\lambda > 220$ nm, the vibrational distribution of the CN fragments maximizes at $v''=0$ with very little $v''=1$. They also report rotational temperatures as high as 2700°K. In their work they were limited to detection at times ~ 3 μ sec after the photolysis pulse and to pressures at which several gas kinetic collisions take place before detection. These workers report no detectible yield of CN A state under these conditions. Clearly a severe conflict exists between the observations of the two groups of workers.

2. Experimental

We have designed a photofragment spectrometer based upon fluorescence excitation detection of the fragment species. In our experimental system, (see fig. 1) a moderate power Nd³⁺ YAG laser is frequency quadrupled to 266 nm providing pulses with typically 80 joules energy at 35 nsec FWHM. This laser is used as the photolysis source; excitation of the fragments is accomplished by synchronizing this laser with a tunable flashlamp pumped dye laser (Chromatix Model CMX-4). The probe laser is characterized by 0.06-2.6 mJoule pulse energies depending upon wavelength and ~ 1 μ sec FWHM pulses. Briefly, the internal trigger circuitry of the CMX-4 laser is defeated; the sync out pulse from the CMX-4 triggers a double pulse generator which sends one pulse to trigger the YAG laser. Since there is a 250 μ sec delay between the YAG lamp trigger and the internally generated Q-switch the second trigger pulse from the pulse generator must be delayed by a corresponding or greater amount. The second pulse from the pulse generator then goes back to trigger the sparkgap of the CMX-4 laser. The result is a photolysis pulse which can be followed from 0 to approximately 250 μ sec. laser by the probe pulse. The temporal jitter between pulses is ± 0.5 nsec. The repetition rate is up to 30 Hz. In the experiment to be described a $\overline{30}$ cm diameter cell with windows one meter apart and with internal baffles to reduce scattered laser light is used. Fluorescence is detected at 90° with either an RCA 31000A or a cooled RCA 7102 photomultiplier tube. The input gate of a PAR 160 Boxcar Integrator is matched to the

¹NRC Postdoctoral Fellow.

²Figures in brackets indicate the literature references at the end of this paper.

fluorescence signal and the output sent to a strip chart recorder or a Nicolet Model 1070 signal averager. The signal averager digitizes at such a rate that each channel on a single scan accumulates the fluorescence signal from several laser pulses. When it is desired to measure fluorescence lifetimes, the fluorescence signal from the photomultiplier goes to a Biomation Model 8100 transient digitizer (10 nsec/point) and then to the Nicolet Model 1070 signal averager.

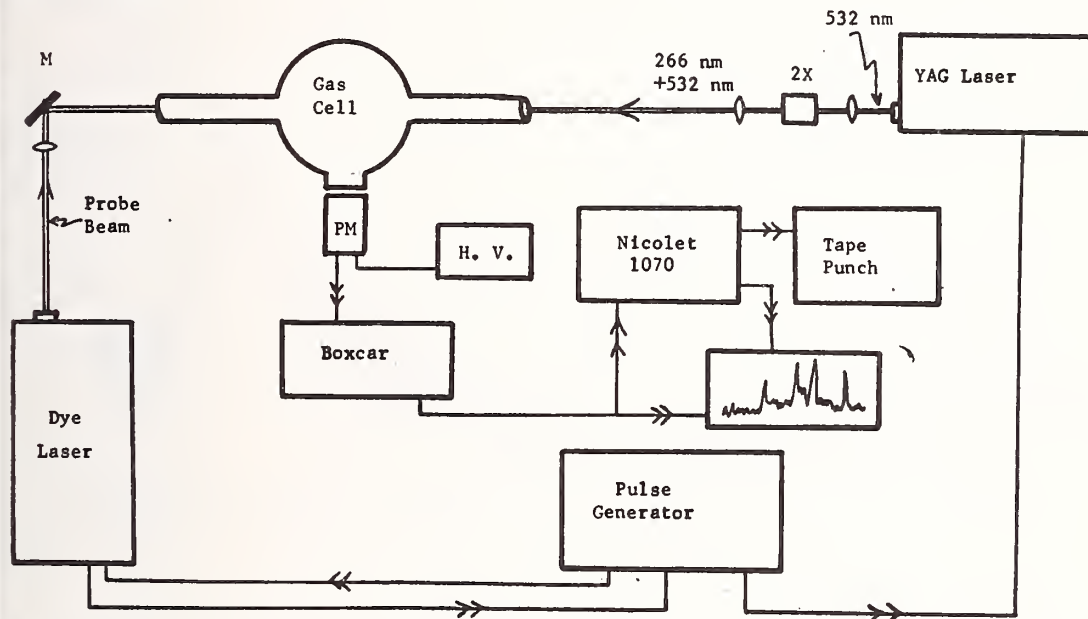


Figure 1. Block diagram of the photofragment experimental apparatus.

3. Results

Excitation spectra were recorded for ICN pressures in the range of 8-35 mtorr and for CN + He mixtures with He pressures of 0.200-100 torr. Figure 2 shows a typical spectrum obtained for 18 mtorr ICN in 2.4 torr of He buffer gas. This excitation spectrum encompasses the $v''=0 \rightarrow v'=4$ and $v''=1 \rightarrow v'=5$ vibronic bands of the $A \leftarrow X$ CN transition and is uncorrected for laser power. Analysis of this and other spectra indicates a vibrational temperature of 700°K. We find a vibrational distribution of $\sim 99\%$ in $v''=0$, $\sim 1\%$ in $v''=1$ and $<0.1\%$ in $v''=2$. These values are for the collision free initial vibrational population distributions. In spectra of ICN without buffer gas rotational structure is evident out to $J \sim 50$ which indicates that the rotational temperature in the $v''=0$ level is several thousand degrees Kelvin. Spectra such as that in Figure 2 show that helium is very effective in equilibrating the rotational distribution.

The number density of CN for the ICN pressures employed in our experiments was in the range of 10^9 - 10^{11} molecules/cm³. A signal to noise of approximately one is observed for excitation in the 0-3 band of CN at an ICN total pressure of 1 mtorr, which indicates the sensitivity of the experiment; i.e. we can routinely make experimental measurements on CN samples at the equivalent of 1 μ torr pressure.

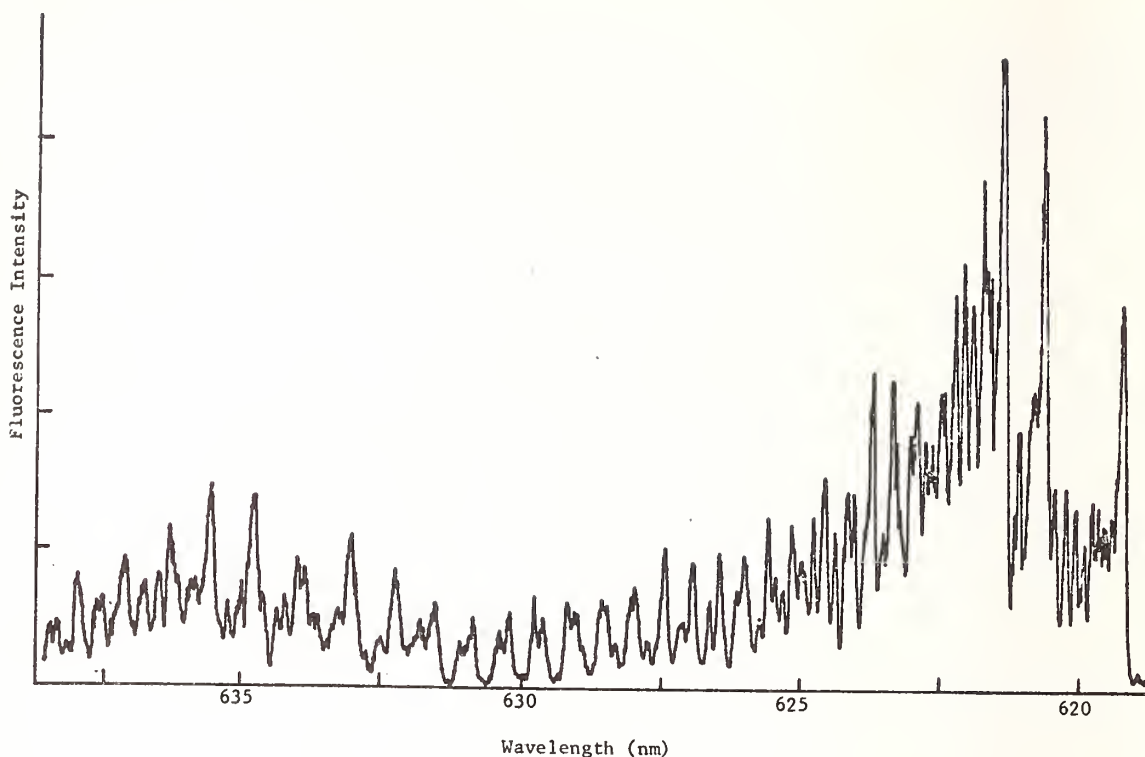


Figure 2. Fluorescence excitation spectrum of 18 mtorr ICN and 2.4 torr He. The Q_1 , R_1 , and R_2 band heads of the 0-4 transition are evident at 619.2 nm, 620.5 nm, and 621.4 nm. The Q_1 band head of the 1-5 transition appears at 635.5 nm. This spectrum has not been corrected for laser power.

An attempt was made to observe fluorescence from the CN ($A^2\Pi$) state which is reportedly formed [5] by photolysis of ICN at 266 nm. A cooled RCA 7102 P.M. was used for detection at several mtorr pressure. A fluorescence signal from excitation of the 0-3 band by the probe laser was easily observable, however, when the probe laser is blocked no 0-0 band fluorescence is observable. Based upon these and other observations we estimate that an upper limit of 0.1% of the CN formed by photolysis is created in the A state.

Lifetimes of various $A^2\Pi$ single vibronic levels will be reported as will the electronic bimolecular quenching rates of A state CN by ICN.

4. Conclusions

Our results essentially agree with the conclusions of Savety-Dzvonik and Cody even though their photolysis was carried out at higher energies. We find that CN is formed primarily in $v''=0$ in the $X^2\Sigma^+$ state with a rotational temperature of several thousand degrees and find no direct formation of CN $A^2\Pi$ state; both of these results are in contrast to Ling and Wilson's observations. We have shown that photofragment spectroscopy utilizing two pulsed lasers can be a very sensitive and general technique for probing the dynamics of photodissociation processes. Number densities of 10^{10} molecules/cm³ can be routinely probed with sufficient resolution and at low enough total pressures to determine the initial electronic, vibrational and rotational distributions in the absence of collisions.

References

- [1] Jenkins, F. A., Roots, Y. K., and Mulliken, R. S., *Phys. Rev.*, 39, 16 (1932).
- [2] Herzberg, G., and Phillips, J. G., *Astrophysical J.*, 108, 163 (1948).
- [3] Davis, S. P., and Phillips, J. T., The Red System ($A^2\Pi-X^2\Sigma^+$) of the CN Molecule, University of California Press, Berkeley and Los Angeles (1963).
- [4] Coxon, J. A., Setser, D. W., and Duewer, W. H., *J. Chem. Phys.*, 58, 2244 (1973).
- [5] Ling, J. H., and Wilson, K. R., *J. Chem. Phys.*, 63, 101 (1975).
- [6] Savety-Dzvonik, M. J., and Cody, R., to be submitted to *J. Chem. Phys.*

SPECTROSCOPIC AND PHOTOCHEMICAL STUDIES OF GASEOUS IONS USING TUNABLE DYE LASERS

John R. Eyler

Department of Chemistry
University of Florida
Gainesville, FL 32611

In recent years tunable laser sources have been used in ever-increasing numbers for both spectroscopic and photochemical studies of neutral species. However, there have been few applications of these powerful, essentially monochromatic light sources to the study of ionic species. Our work involves a wide ranging study of the irradiation of gaseous ions by tunable organic dye lasers, with the belief that results of importance to both ionic spectroscopy and ionic photochemistry will be forthcoming. Investigations to date have been carried out in the areas of photodetachment of negative ions ($A^- + h\nu \rightarrow A\cdot + e^-$) and photodissociation of positive ions ($A^+ + h\nu \rightarrow B + C$).

These studies use a pulsed ion cyclotron resonance (icr) mass spectrometer [1,2]¹ to generate either positive or negative ions by several mechanisms and to trap them for periods as long as several seconds in duration. During this time the ions are subjected to tunable irradiation from a flashlamp-pumped dye laser. The effect of this irradiation upon the trapped ions is greatly enhanced by use of an intracavity technique [3] which places the icr cell inside the laser cavity. Such a technique gives improved sensitivity when examining processes of low cross-section and threshold behavior.

Recent experimental work in the area of negative ion photodetachment has been carried out by Brauman and co-workers using an icr spectrometer and a conventional arc lamp-monochromator illumination source [4]. Species such as NH_2^- , PH_2^- , AsH_2^- , SeH^- , $C_5H_5^-$, $C_4H_4N^-$, $C_6H_5O^-$, and $C_6H_5S^-$ have been investigated and improved values of electron affinities and related thermochemical quantities for these species and associated neutrals have been obtained. A value for the spin-orbit coupling constant of $SeH\cdot$ was determined from an analysis of the relative cross-section vs. wavelength curve for SeH^- photodetachment. Tunable laser irradiation has been used to photodetach negative ions in a beam experiment [5] by Lineberger and co-workers. Use of laser irradiation allows much higher precision in electron affinity determinations, and makes possible observation of two-photon effects.

Our initial research using the laser-icr technique involved the photodetachment of SH^- ions [6] ($SH^- + h\nu \rightarrow SH\cdot + e^-$). This work demonstrated that fine structure unobserved in previous SH^- photodetachment studies could be obtained when using this technique which combines production of ions with relatively low rotational "temperatures" with the inherently high resolution of the tunable dye laser. Current work involves study of photodetachment of species such as SD^- , Cl_2^- , and C_2H^- .

A majority of the ionic photodissociation studies reported in the past several years have been carried out by Dunbar and co-workers [7] using an icr spectrometer and arc lamp illumination. These have produced much valuable information about the thermochemistry, energy levels, and structures of various gaseous ions such as NO^+ , $C_4H_8^+$, $C_{10}H_{14}^+$, and CH_3Cl^+ . In addition, these workers have studied the chemistry of photo-produced ions in selected systems. Recently, other groups have also reported photodissociation results [8,9].

¹Figures in brackets indicate the literature references at the end of this paper.

Our first experiments in the area of dye laser-induced photodissociation involved $C_7H_8^+$ (parent) ions in gaseous toluene ($C_7H_8 + h\nu \rightarrow C_7H_7 + H\cdot$) [10]. The observed onset and general shape of the dissociation spectrum were in quite good agreement with an earlier study [11] of much lower resolution. The ease of studying both negative ion photodetachment and positive ion photodissociation with the laser-icr technique allowed a comparison of the cross-section for $C_7H_8^+$ photodissociation versus that for SH^- photodetachment under quite similar experimental conditions. This resulted in a value of $\sigma(490\text{ nm}) = 1.01 \pm 0.24 \times 10^{-18}\text{ cm}^2$ for the absolute cross-section for $C_7H_8^+$ photodissociation at 490 nm.

No significant fine structure was seen in the photodissociation spectrum of $C_7H_8^+$ in spite of the high energy resolution of dye laser irradiation. We are currently investigating a number of positive ions of simpler structure, in hopes that fine structure related to vibrational energy levels in the pertinent electronic states of the ions involved will be observed. Two of the species being studied are $C_2H_5Cl^+$ and $CHOCHO^+$.

References

- [1] Baldeschwieler, J. D., and Woodgate, S. S., *Accounts Chem. Res.* 4, 114 (1971); Beauchamp, J. L., *Ann. Rev. Phys. Chem.* 22, 527 (1971); and Henis, J. M. S., in *Ion-Molecule Reactions*, Volume 2, Ed. by J. L. Franklin (Plenum Press, New York, 1972), Ch. 9.
- [2] McIver, R. T., Jr., and Dunbar, R. C., *Int. J. Mass. Spectrom. Ion Phys.* 7, 471 (1974).
- [3] Eyler, J. R., *Rev. Sci. Instrum.* 45, 1154 (1974).
- [4] Richardson, J. H., Stephenson, L. M., and Brauman, J. I., *J. Amer. Chem. Soc.* 97, 296 (1975), and references contained therein.
- [5] Lineberger, W. C., in *Chemical and Biochemical Applications of Lasers*, Volume 1, Ed. by C. B. Moore (Academic Press, New York, 1974), Ch. 3.
- [6] Eyler, J. R., and Atkinson, G. H., *Chem. Phys. Lett.* 28(2), 217 (1974).
- [7] Dunbar, R. C., in *Interactions Between Ions and Molecules*, Ed. by Pierre Ausloos (Plenum Press, New York, 1975), p. 579.
- [8] Freiser, B. S., and Beauchamp, J. L., *J. Amer. Chem. Soc.* 96, 6260 (1975).
- [9] Vestal, M. L., and Futrell, J. H., *Chem. Phys. Lett.* 28, (4), 559 (1974).
- [10] Eyler, J. R., *J. Amer. Chem. Soc.*, in press.
- [11] Dunbar, R. C., *Ibid.*, 95, 472 (1973).

PHOTODISSOCIATION SPECTRA OF POSITIVE IONS WITH TIME-OF-FLIGHT ANALYSIS

Timothy F. Thomas and John F. Paulson
Air Force Geophysics Laboratory (LKB)
Hanscom AFB
Bedford, MA 01731

One of the many new opportunities provided photochemists by the development of tunable lasers in the visible and UV regions is the study of very dilute systems such as well-defined ion beams. Recent applications include measurement of photodetachment spectra of numerous negative ions [1]¹, photo-destruction spectra of polyatomic negative ions such as CO_3^- and O_3^- [2], and determination of kinetic energy spectra upon photodissociation of H_2^+ and D_2^+ [3,4]. We have assembled an apparatus capable of determining both absolute photodissociation cross-sections of ions as a function of wavelength (the photodissociation spectrum) and the kinetic energy spectrum of product ions by time-of-flight analysis.

Figure 1 shows the apparatus used. A pulsed laser beam, $\sim 2\frac{1}{2}$ mm in diameter, crosses a mass-selected ion beam whose energy can be varied from 10 to 200 eV by the decelerating plates shown. The quadrupole mass analyzer is set to pass only the product ion formed during a photolysis, or to monitor the primary beam intensity intermittently. A photo-diode triggers the time-of-flight logic at the start of each laser pulse so that the time between the pulse and arrival of a product ion at the electron multiplier can be measured to an accuracy of 10 nanoseconds, if desired. The polarization rotator shown in the laser beam permits determination of the direction of the electronic transition moment, as well as checking whether product ions ejected at large angles to the flight axis are accepted by the quadrupole mass analyzer.

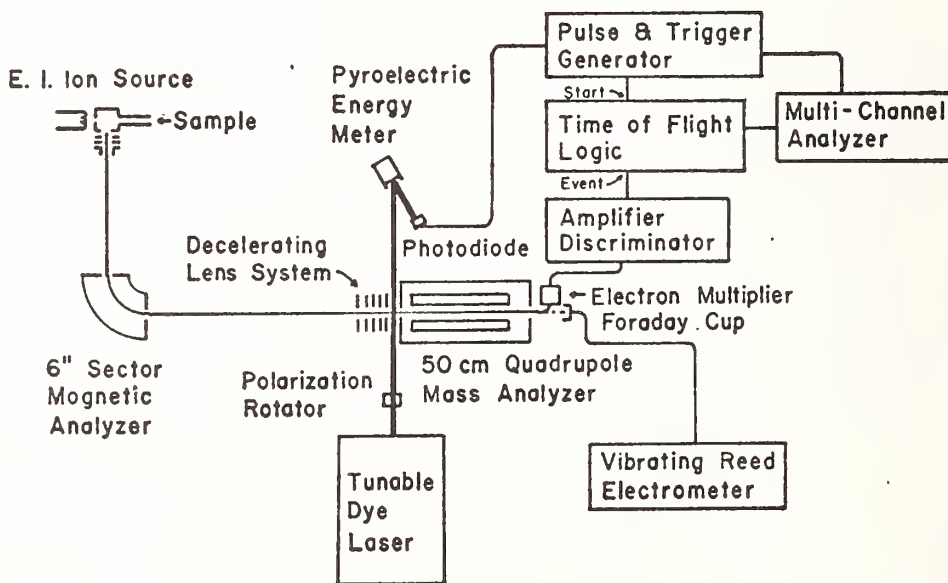


Figure 1. Apparatus for photo-dissociation of ions with time-of-flight analysis of product ions.

¹Figures in brackets indicate the literature references at the end of this paper.

Partial results obtained for three reactant ions are given below.

D_2^+ . The only transition accessible at the available wavelengths is $1s\sigma_g \rightarrow 2p\sigma_u$. Figure 2 confirms that the dipole moment of the transition lies along the internuclear axis. Figure 3 shows the time-of-flight spectrum obtained at primary ion energies so low that only D^+ ions ejected in the forward direction are accepted by the quadrupole mass analyzer. Product ions produced from different vibrational levels of the $1s\sigma_g$ state possess different kinetic energies and thus show different flight times as indicated on the figure.

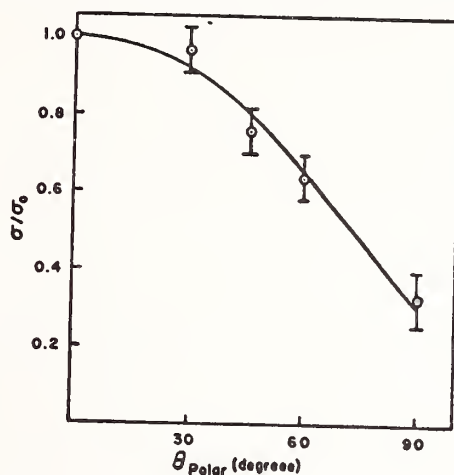


Figure 2. Effect of direction of laser beam polarization on cross section for photo-dissociation. $\theta_{\text{polar}} = 0$ corresponds to horizontal polarization. Primary ion energy: 23 V.

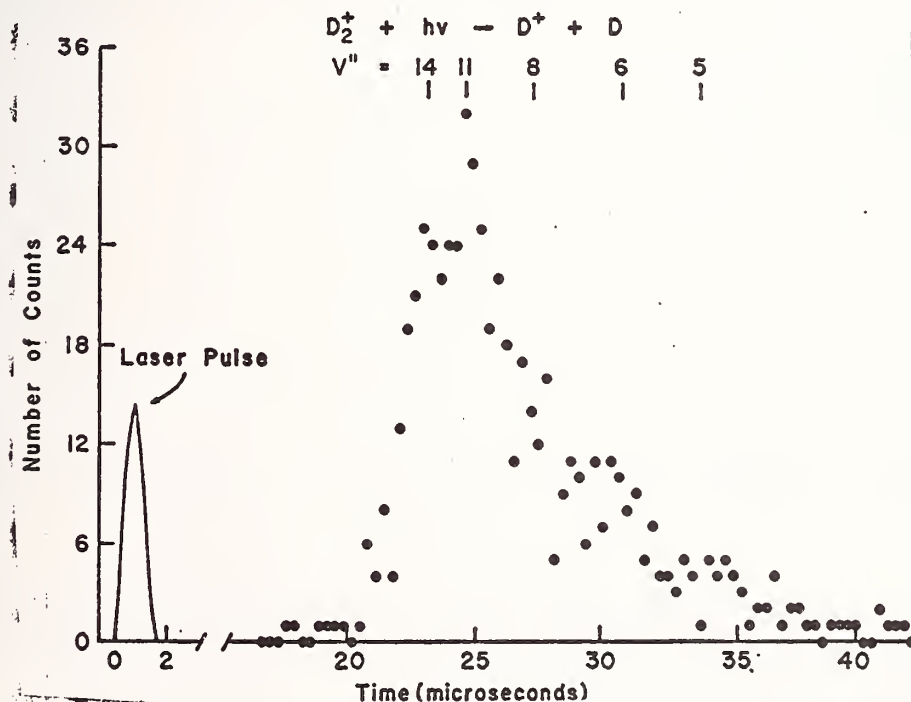


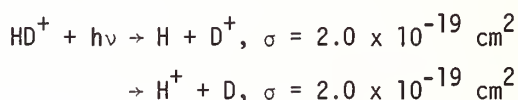
Figure 3. Time-of-flight spectrum for D_2^+ . $\lambda_{\text{irr}} = 580.0$ nm, primary ion energy = 17.5 V, source pressure = 0.64 Torr, ionizing voltage = 200 V. Quadrupole rods were biased at $\sim +8.5$ V.

To obtain absolute cross sections the primary ion energy was increased to 173 V so that all product ions were accepted by the quadrupole analyzer. Average values obtained are shown in Table I, along with the photodestruction results of von Busch and Dunn [5] who used a band width of 200 Å versus ≤ 1 Å used here.

Table I. Cross Sections for $D_2^+ + h\nu \rightarrow D^+ + D$

λ (nm)	=	445	585	590	595	600
$\sigma \times 10^{19}(\text{cm}^2)$	=	9.5 ± 0.7	5.3 ± 0.3	5.1 ± 0.2	5.7 ± 0.3	5.2 ± 0.3
von Busch & Dunn: (interpolated)	+	9.9	5.8	5.7	5.6	5.5

HD^+ . Following the same electronic transition as in D_2^+ , two dissociative processes are possible:



The cross sections shown are average of several results at 590 nm, using a source pressure of 0.62 Torr, ionizing voltage of 200 V, and primary ion energy of 173 eV.

N_2O . Table II shows a few features of the highly-structured photo dissociation spectrum that has been obtained for the processes:

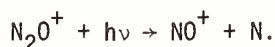
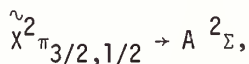


Table II. Photodissociation Cross Sections for N_2O^{+a}

$\lambda(\text{nm})$	=	340.1	338.5	324.9	323.6	311.0	308.5
$\sigma \times 10^{19}(\text{cm}^2)$	=	15.2	25.7	3.5	7.9	1.1	1.2
(V_1', V_1'')	=	(1,0)	(1,0)	(2,0)	(2,0)	(3,0)	(3,0)

^aSource pressure = 0.82 Torr, ionizing voltage = 70.4, primary ion energy = 173 eV.

Analysis of the emission spectrum of N_2O^+ , at high resolution [6], indicates that the transition involved here must be



with the pairs of peaks in Table II representing a progression in the symmetric stretching mode ($\tilde{\nu}_1 = 1345.5 \text{ cm}^{-1}$) of the upper electronic state. The splitting between members of each pair corresponds reasonably well to the reported spin-orbit coupling constant of $132. \text{ cm}^{-1}$ [6] in the 2π state.

Photo-dissociation cross sections have also been measured at 445 ($5 \times 10^{-21} \text{ cm}^2$) and 640 ($1.3 \times 10^{-21} \text{ cm}^2$) nm. These low values, and the failure to observe a significant change in $\sigma_{321.8}$ upon addition of N_2 to increase the source pressure to 1.9 Torr, indicate that most of the N_2O^+ ions enter the photolysis region in their ground vibrational states. However, several peaks in the photo-dissociation spectrum, e.g. at 336.5 and 321.8 nm, may be due to the Renner effect operating in 2π state ions possessing one or more quanta in the bending mode.

Recent photoelectron-photoion coincidence spectroscopy of N_2O indicates the onset of predissociation in the \tilde{A} state lies at the $v_1' = 1$ level, where $\sim 40\%$ of the ions dissociate and the remainder presumably fluoresce [7]. Our preliminary analysis of the TOF spectra at low primary ion energies (17.4 eV) clearly shows that a significant fraction of the NO^+ are produced with kinetic energies in excess of 1 eV, requiring that the nitrogen atom be produced in its ground electronic state (4S). This can only occur if predissociation proceeds via a state of higher multiplicity, such as $^4\Sigma^-$ [8].

References

- [1] Lineberger, W. C., et al., *J. Chem. Phys.* 61, 1300 (1974), and references therein.
- [2] Peterson, J. R., et al., *J. Chem. Phys.* 62, 4826; 63, 1612 (1975).
- [3] van Asselt, N. P. F. B., Maas, J. G., and Los, J., *Chemical Physics* 5, 429 (1974).
- [4] Ozenne, J. B., Pham, D., and Durup, J., *Chem. Phys. Lett.* 17, 422 (1972).
- [5] Busch, F. v., and Dunn, G. H., *Phys. Rev.* A5, 1726 (1972).
- [6] Callomon, J. H., *Proc. Chem. Soc.* 13 (1959); Callomon, J. H., and Creutzberg, F., *Int. Conf. on Spectroscopy*, Bombay, 1967, p. 143.
- [7] Eland, J. H. D., *J. Mass Spectrom. Ion Phys.* 12, 389 (1973); 13, 251 (1974).
- [8] Lorquet, J. C., and Cadet, C., *Int. J. Mass Spectry. Ion Phys.* 7, 245 (1971).

VIBRATIONAL STATES OF MOLECULES IN THE VISIBLE REGION BY THERMO-OPTICAL SPECTROSCOPY AND THE LOCAL MODE MODEL^{1,2}

A. C. Albrecht

Department of Chemistry
Cornell University
Ithaca, NY 14853

When a very small fraction of an incident laser beam is absorbed by a liquid, a steady state temperature gradient on the order of millidegrees can appear transverse to the propagation direction of the incident light. This produces an index of refraction gradient causing the transitting beam to diverge. When a tunable laser is used for the heating beam, this thermal lens effect provides a basis for an extremely sensitive new spectroscopy [1]³. We have explored the absorption characteristics in the red (Rhodamine 6-G) region of the visible spectrum of several characteristic organic molecules. These include several aromatic hydrocarbons, methanol, acetone, methylenedichloride, and several alkanes. Isotope studies show that absorption by these molecules is derived from stretching excitations of bonds containing the hydrogen atom. The excitation energy is more than fifty percent of that needed for bond dissociation. Thus this spectroscopy offers an opportunity to explore molecular potential energy surfaces along reaction coordinates and at energies approaching those required for breaking bonds.

The spectroscopy itself has been developed both in a single beam transient mode as well as in a dual beam, automatic scanning mode. In the latter case a fixed wavelength laser is used to probe the lens which is formed by a chopped, tunable, heating beam. Synchronous detection is used. In the single beam mode the time course of the developing lens is followed from the first moment the sample is illuminated to the point where the stationary temperature gradient has appeared. An absolute measure of the extinction coefficient can be made in this case. Extinction coefficients nine orders of magnitude weaker than those of typical allowed electronic transitions can easily be measured. Samples having optical thicknesses of kilometers give easily detected thermal lensing effects in centimeter path lengths. Singlet-triplet transitions are candidates for such spectroscopy. One such transition has been identified in anthracene.

The theoretical understanding of vibrational molecular states responsive to light in the visible region appears to be greatly facilitated by the local-mode model (LM). Here the zeroth order description of an excited state is not given by the usual overtone or combination (normal mode) approach but rather by expressing the occupation number of local mode anharmonic vibrators. Thus in benzene for example [2], the LM model pictures the C-H stretching states to be built up of six identical, uncoupled, anharmonic C-H oscillators. The LM model can incorporate any degree of anharmonicity in its zeroth order framework. Since it is an uncoupled system model, and since the perturbation due to the light wave is also separable, the LM model predicts that multiple quantal excitation can be one-photon allowed only when they take place within one bond. The model predicts the very simple spectroscopy of a one dimensional anharmonic oscillator for all degrees of excitation even though the state density rises abruptly. The number of states for j identical oscillators

¹ Supported in part by a grant from the National Science Foundation and the Materials Science Center of Cornell University.

² This paper includes work found in references 1 and 2 as well as more recent studies carried out in our laboratory by Dr. R. Swofford and Mr. M. Burberry.

³ Figures in brackets indicate the literature references at the end of this paper.

containing altogether v quanta is just the binomial coefficient $((j + v - 1)/(j - 1))$. Thus for the six dimensional C-H stretching space in benzene ($j=6$) there are 462 states at $v=6$. The observed line however is that of a single state - that (of E_{1u} symmetry) which carries all six quanta in one bond. This is by far the most anharmonic of the 462 states. The LM model can enumerate all levels appearing at any v once a two parameter fit is made to the observed 'overtone' spectrum. The corresponding energy level diagram for the deuterium isotope is automatically determined by the mass effect. Although only two parameters are needed for the energy fit, an effort to predict intensities requires an expansion of the potential energy function at least to the fifth power in displacement. Thus the attempt to match intensities of these very weak transitions provides considerable analytical insight into the potential energy surface. As even higher transitions are observed it is expected that a serious challenge to theory may emerge, for now, as dissociation is approached, the zeroth order Born-Oppenheimer approximation must be questioned.

The LM model predicts that in a polyatomic molecule having several equivalent oscillators there is a remarkable harmonic multi-photon channel that can provide a rapid route for the deposit of intense monochromatic infrared laser radiation in a manner having photochemical significance. The fact that pulsed infrared light can bring about very energetic molecular excitation, as seen by visible luminescences as well as by photo-decomposition, has been the subject of intense interest. The basic question concerns the mechanism of how a large number of photons of a single frequency can build up in a single molecule, especially when its vibrational levels are known to be anharmonic. We will show how in benzene, for example, the LM model predicts a highly allowed six photon, sequential, transition among vibrational states which are harmonic. (At $v = 6$ this harmonic state is the one where one excitation appears in each of the six uncoupled C-H oscillators). The implications of this to examples in the literature will be touched upon.

References

- [1] Long, M. E., Swofford, R. L., and Albrecht, A. C., *Science* 191, 183 (1976).
- [2] Long, M. E., Swofford, R. L., and Albrecht, A. C., *J. Chem. Phys.* 65, 000 (1976).

MECHANISM OF HIGH INTENSITY I.R. PHOTODECOMPOSITION OF MOLECULES

W. Braun and W. Tsang

National Bureau of Standards
Washington, DC 20234

There has been considerable recent interest in the photodecomposition of polyatomic molecules using resonant infrared radiation from TEA lasers [1]¹. Most of the emphasis has been on the separation of isotopes, with the smaller polyatomic molecules as the absorbent [2]. Except for empirical observations for use in optimizing isotope separations very little has been done to describe the nature of the decomposition process. A greater understanding may well provide essential inputs for the selection of molecules to be used for isotope separations as well as dictate the conditions for optimizing such processes. Furthermore, this is a new and unique means of molecular excitation and the possibility that it can be used to probe fundamental properties of molecules is certainly worthy of investigation. This, in turn, can lead to solutions for a wide range of problems in gas kinetics, combustion and analytical chemistry.

In the present investigation we will deal specifically with describing the nature of the photodecomposition process and we will look in detail at the products derived from the photodecomposition of somewhat larger polyatomic organic molecules. We focus specifically on the i.r. high intensity photolysis of isobutyl and ethyl chlorides, bromides and iodides.

The experimental arrangement is shown in fig. 1. laser radiation, P(36) level, 10.6 band, from a CO₂-TEA laser (approximately 0.300 joules/pulse) is focused by means of a spherical mirror and a 10 cm NaCl lens (effective focal length 5 cm) into the 1.0 cc reaction cell. From 10 to 100 pulses are used for each experiment. With a pulse rate of 1 to 2 pulses/sec, mixing of the products in the cell after each pulse is assured. Pressures in the reaction cell ranged up to 50 torr He and 0.5 to 2-torr of the organic compound of interest. In this pressure and concentration range the extent of alkyl halide decomposition per flash is invariant. Gas chromatography with flame ionization detection is used for analysis. The columns used are 8 ft. Porosil "C" (1/8"), and 6 ft. Poropak Q (1/8"). The former makes excellent separation but appears to be somewhat reactive. The latter is a boiling point column and was used initially in order to get a rough idea of the product distribution. Except for isobutyl iodide the compounds were pumped and degassed in the usual manner. No other attempts at further purification were made.

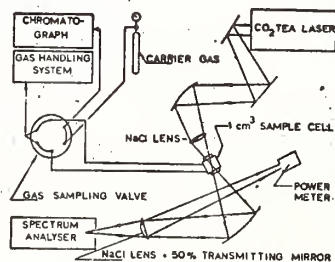


Figure 1. Experimental setup.

¹Figures in brackets indicate the literature references at the end of this paper.

Chromatographic results of laser pyrolysis on the three isobutyl halides as well as those of isobutene and propylene are presented in Figure II. With respect to the halides a cursory examination reveals striking similarities. This is particularly the case with respect to isobutyl chloride and bromide and suggests that the photolysis of a common precursor may be responsible. The most logical precursor candidate is isobutene. It is a product, and the compounds formed from its laser photolysis must in any case be accounted for. This hypothesis is supported by the results on the laser photolysis of isobutene.

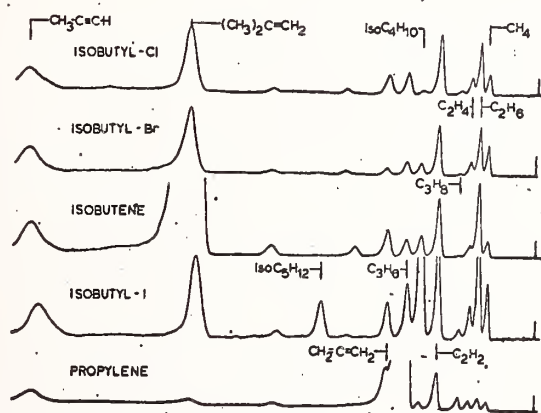


Figure 2. Gas Chromatograms for the photolysis of isobutyl chloride, isobutyl bromide, isobutane, isobutyl iodide, and propylene, 10.6μ (34) CO_2 laser line. Isobutyl chloride - 2.5 torr $\text{C}_4\text{H}_9\text{Cl}$, 47.5 torr He, 120 pulses; sensitivity x 2. Isobutyl bromide - 2.5 torr $\text{C}_4\text{H}_9\text{Br}$, 47.5 torr He, 180 pulses; sensitivity x 1. Isobutane - 1.25 torr C_4H_8 , 48.75 torr He, 20 pulses; sensitivity x 1. Isobutyl iodide - 2.5 torr $\text{C}_4\text{H}_9\text{I}$, 47.5 torr He, 210 pulses; sensitivity x 2.5. Propylene - .625 torr C_3H_6 , 49.37 torr He, 20 pulses; sensitivity x 1.

Figure II shows clearly that there is a definite correspondence (from the C_4 peaks down) between the "cracking" pattern for isobutene and isobutyl chloride and bromide. More quantitatively, the important products from isobutyl chloride and bromide photolysis (in order of relative concentration) are isobutene, methyl acetylene, acetylene, ethane and allene, while for isobutene photolysis the order of important products is also methyl acetylene, acetylene, ethane and allene. The carbon/hydrogen ratio for the products are 1.9 for isobutyl chloride, 1.9 for isobutyl bromide and 2.0 for isobutene. With respect to isobutyl iodide, comparison with the bromide and chloride spectra indicate that for the former there is a relatively larger amount of ethane, isobutane (most prominent), isopentane and propylene (less prominent) superimposed upon the basic bromide or chloride "cracking" pattern.

The chromatograms (not shown) from the ethyl halide photolysis are cleaner and thus less striking. For the bromide and chloride the main products are ethylene and acetylene. The product ethylene, is however also partially photolyzed by the laser light, with acetylene, the dominant product. Thus, as in the isobutyl system, it is not unreasonable to assume that photolysis of the initial product will account for a significant if not all of the other compounds formed.

For isobutyl chloride and bromide photolysis the observed "primary" products are consistent with a photolytic mechanism as given in Figure III. After the laser pulse, assuming high extent of reaction, there will be significant quantities of radicals in the reactive zone (cone) and one can assume that a large amount of combination and addition

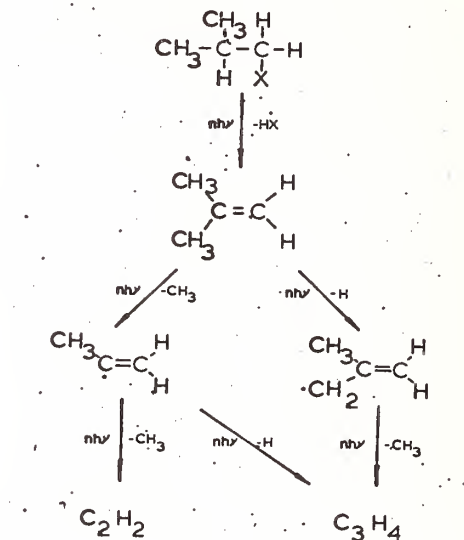
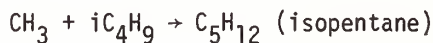


Figure 3. Mechanism of isobutyl chloride and bromide decomposition.

will occur. These processes are summarized in Figure IV and account for all of the observed "secondary" products. Such a mechanism shows why there is quantitative agreement between isobutyl chloride and isobutyl bromide "cracking" patterns. The isobutyl iodide "cracking" pattern shows some differences which lead us inevitably to the conclusion that some C-I fission occurs. The newly formed isobutyl radical can then isobutane and isopentane via the reactions



and



These products are minor or absent in isobutyl chloride and isobutyl bromide photolysis.

The mechanism for ethyl halide decomposition can be considered to be similar to that for the isobutyl halides. That is direct formation of ethylene and the hydrogen halide, the photolysis of ethylene, and in the case of the iodide some contributions due to C-I bond splitting.

chloride is vastly more labile than propylene over all temperature conditions. Thus the failure of propylene to induce any isobutyl chloride decomposition provides extraordinarily strong evidence for the specific, non-thermal, nature of the laser excitation.

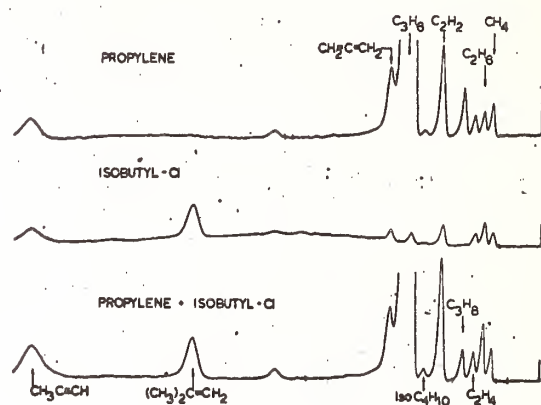


Figure 6. Gas chromatogram from the photolysis of isobutyl chloride, propylene and in combination. 10.6 μ P(34) CO₂ laser line. Propylene - .31 torr C₃H₆; 49.69 torr He, 60 pulses. Isobutyl chloride - .94 torr C₄H₉Cl; 49.1 torr He, 60 pulses. Propylene + Isobutyl chloride - 31 torr C₃H₆; .94 torr C₄H₉Cl; 48.75 torr He, 60 pulses.

The overall picture that can be derived from these data and analysis is that there is a rapid vibrational excitation of an absorbing molecule to a level at which it is unstable (within the time frame of the laser pulse). Inasmuch as the specific rate constant for the decomposition of (an unstable very highly vibrationally excited) molecule is almost exponentially dependent on the energy above any reaction threshold [5], it is easy to see that, in general, a molecule will seek to escape from the laser excitation by decomposing through its lowest energy dissociation channel. Indeed such a dependence on lifetime or energy suggests that rather large increments in energy must be added into the system if one wishes to activate higher decomposition channels. All of these observations fit well within the framework of our present day understanding about thermal stability of molecules.

References

- [1] Freeman, M. P., and Travis, D. N., *J. Chem. Phys.*, **60**, 231 (1974).
- [2] Lyman, J. L., and Rockwood, S. D., *J. Appl. Phys.*, **47**, 595 (1976).
- [3] Benson, S. W., and O'Neal, H. E., *Kinetic Data on Unimolecular Reaction*, NSRDS-NBS-21, U.S. Government Printing Office, 1970.
- [4] O'Neal, H. E., and Benson, S. W., in *Free Radicals*, Ed., J. K. Kochi, Vol. II, Wiley Interscience, NY, 1973, pp. 275.
- [5] Robinson, P. J., and Holbrook, K. A., *Unimolecular Reaction*, Wiley Interscience, NY, 1972.

THE IN-SITU MEASUREMENT OF ATOMS AND RADICALS IN THE UPPER ATMOSPHERE

James G. Anderson

Department of Atmospheric and Oceanic Science
Space Physics Research Laboratory
University of Michigan
Ann Arbor, MI 48109

Although upper atmospheric photochemistry has become rapidly more complicated in the past five years as our appreciation for the multitude of gases present in the stratosphere has grown, the basic reaction pattern displayed by each of the chemical cycles involving oxygen, hydrogen, nitrogen and chlorine remains simple. Figure 1 generalizes this pattern into three common parts:

- (1) Chemical source terms, which represent the upward flow of stable polyatomic molecules from the earth's surface and troposphere;
- (2) Linking radicals or molecular fragments which are formed from the chemical source terms either by photolysis or by chemical reaction;
- (3) Reservoir or sink terms which are formed by the recombination of the radicals and are recycled into the radical system by photolysis and chemical reaction and removed by downward and meridional transport.

The source and sink terms are relatively stable chemically, having chemical lifetimes on the order of weeks to months so that their global distribution is, in general, governed by transport processes rather than by details of the local chemical environment. In contrast, the radicals have chemical lifetimes on the order of minutes and they thus reflect, with considerable alacrity, the chemical conditions in their vicinity. A composite of the hydrogen, nitrogen and chlorine systems, including only the major reaction paths, is shown in Figure 2 which can be subdivided by inspection into three cycles similar in form to Figure 1.

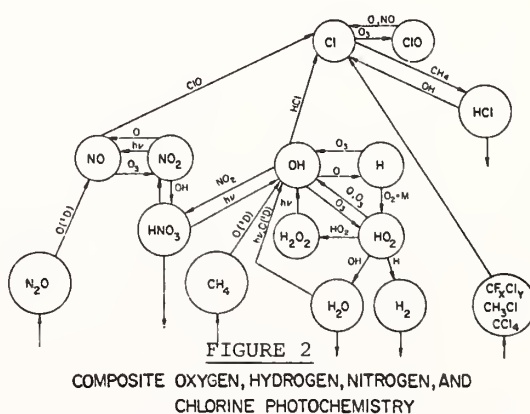
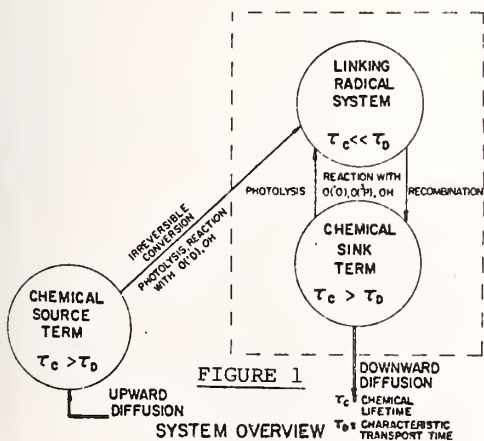


Figure 1. System overview.

Figure 2. Composite oxygen, hydrogen, nitrogen, and chlorine photochemistry.

Significant progress has been made over the past five years in the measurement of stratospheric source and sink terms most notably by infrared absorption and emission techniques, whole air samples and filter trapment. These techniques have proven to be powerful for the determination of absolute concentrations in the part per million to part per billion range where extended regions of spatial integration were acceptable. Because of the long chemical lifetime of these species, details of their local structure were not relevant and there developed a very direct and beneficial exchange between field measurements and theoretical calculations.

In order to hope for such a exchange in the case of radicals, an experiment must (a) have a detection sensitivity in the part per trillion range in a defined volume element in which other interacting radicals are simultaneously measured, (b) possess a means for accurate absolute calibration and (c) be capable of measuring the diurnal behavior of several species.

A technique which quite naturally satisfies these requirements is atomic and molecular resonance fluorescence in combination with a high velocity sample flow which eliminates heterogeneous interaction between the atmospheric sample and the instrument. This geometry is familiar to laboratory gas phase kinetics studies and its adaptation for this work is shown in Figure 3. A beam of photons, resonant with a preselected electronic transition of an atom or molecule is passed across the flowing gas sample confined to the interior of a pod or "nacelle" which establishes laminar flow around and through the device as it is lowered through the atmosphere on a stabilized parachute platform. Photons scattered out of the lamp beam are collected and counted by a photomultiplier with associated optics which observes in a direction perpendicular to both the incident photon beam and the gas flow direction.

Absolute calibration is accomplished using a laboratory system shown in Figure 4 which provides a known quantity of the atom or radical in a flow at the appropriate total pressure, temperature and flow velocity. As Figure 4 shows, the flight instrument occupies the central portion of the reaction zone so that a known concentration of the atom or radical, formed either by discharge alone or by chemical reaction in the upstream portion of the reaction zone, flows through the instrument's interior. After calibration, the instrument is removed from the system, fitted with airfoil sections and flown optically unaltered from its configuration during calibration.

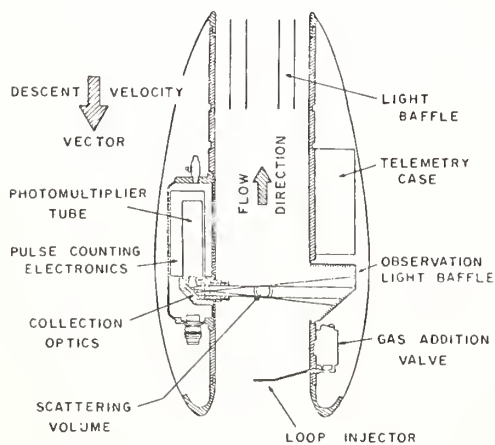


FIGURE 3

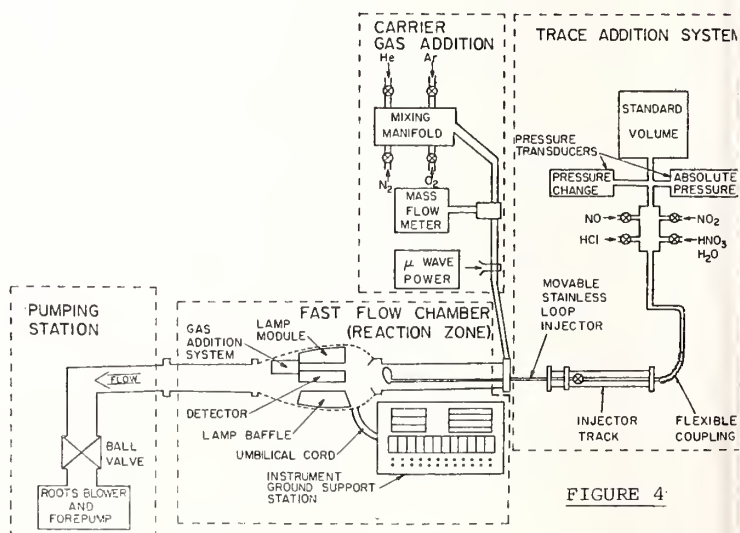


FIGURE 4

Figure 3

Figure 4

Helium filled research balloons capable of lofting the instrument package to 45 kilometers from where the measurement commences upon deployment onto the stabilized parachute platform have thus far been used exclusively although rocket or aircraft deployment is equally possible. Results of two flights for the measurement of ground state atomic oxygen $O(^3P)$ are shown in Figure 5 and two flights investigating the vertical profile of the OH radical are shown in Figure 6. These results will be discussed as well as the development of instruments for the measurement of Cl , ClO , NO , NO_2 and H_2O .

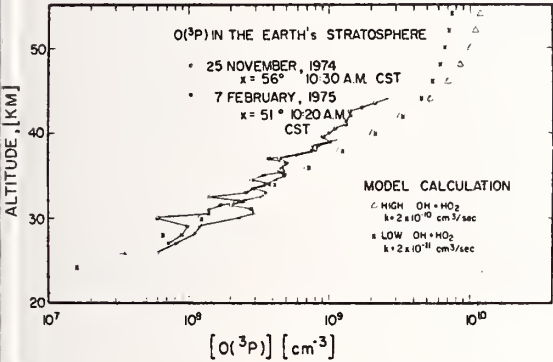


Figure 5

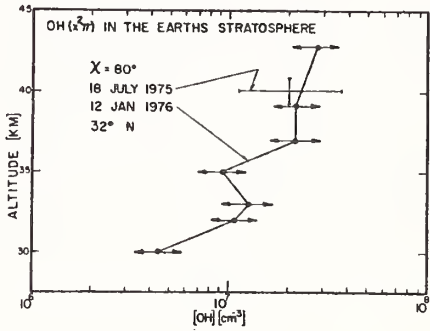


Figure 6

THE O(¹S) AIRGLOW - NEW LABORATORY RESULTS

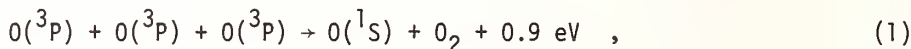
Tom Slanger and Graham Black

Stanford Research Institute

Menlo Park, CA 94025

Ever since it was postulated [1]¹ by Sidney Chapman forty-five years ago that the energy source for the production of O(¹S) in the lower thermosphere (~100 km) was the recombination of ground state oxygen atoms, it has been realized that the intensity of the 5577 Å O(¹S) → O(¹D) transition in the airglow is a measure of the O(³P) density. Not until relatively recently has any kinetic data become available to make it possible to transform the 5577 Å intensities, which have now been measured from the ground [2], from rockets [3], and from satellites [4], into oxygen atom concentrations.

In order to perform this transformation, one needs to know the production and loss rate coefficients of O(¹S) in the atmosphere at a temperature of ~200°K. There are two alternate production schemes, the one linked with Chapman's name, involving a single three-body interaction,



and the one proposed by Barth and Hildebrandt [5], in which there is an intermediate O₂* state,



No laboratory measurements have been able to choose between these alternatives. The only significant O(¹S) losses in the atmosphere are radiation and quenching by O(³P) and O₂; is now generally believed that O(³P) quenching is dominant in the region of peak O(³P) densities.

In the present work, we have measured the O(¹S) production rate coefficient in a flowing afterglow, and the O(¹S)-O(³P) interaction rate coefficient in a combination photolysis-afterglow system, in both cases as a function of temperature. In the production rate measurements, O(¹S) is generated through recombination in an O(³P) stream, from a conventional NO-titrated N₂ afterglow. The absolute O(¹S) intensity is determined by O(³P) + NO photometry, while the O(³P) concentration is determined by NO₂ titration. The O(¹S) is then quenched with N₂O, to observe the competition between the O(¹S) reaction with N₂O and the other loss processes. Accurate measurements of the temperature-dependent rate coefficient for the O(¹S)-N₂O interaction were needed and carried out [6]. From these data, it is possible to extract a value for the overall production rate coefficient, but not to state whether it refers to reaction (1) or the more complex reaction scheme embodied in

¹Figures in brackets indicate the literature references at the end of this paper.

reactions (2), (3), and (4). The reason for this ambiguity is that it was not possible to work at total pressures low enough for the $[M]$ -dependence of the complex mechanism to become apparent. The resultant overall rate coefficient [7] is $1.4 \times 10^{-30} \exp(-1300/RT) \text{ cm}^6 \text{ molec}^{-2} \text{ sec}^{-1}$, a figure considerably larger than that used until now. The positive activation energy suggests that the mechanism is not the same for the usual 3-body reaction.

The $O(^1S)-O(^3P)$ quenching was studied by generating $O(^1S)$ from N_2O photolysis at 1300 Å in a pulsed mode, and observing its decay time as a function of added $O(^3P)$, from a partially titrated nitrogen discharge. We were able to show that the observed increase in $O(^1S)$ loss rate was due only to $O(^3P)$, and a quenching rate coefficient of $5.0 \times 10^{-11} \exp(-610/RT) \text{ cm}^3 \text{ molec}^{-1} \text{ sec}^{-1}$ was established [8]. This is slightly more than a factor of two larger at 300°K than the value determined by Felder and Young [9], but orders of magnitude larger than the recent theoretical prediction of Krauss and Neumann [10]. An Arrhenius plot is shown in figure 1.

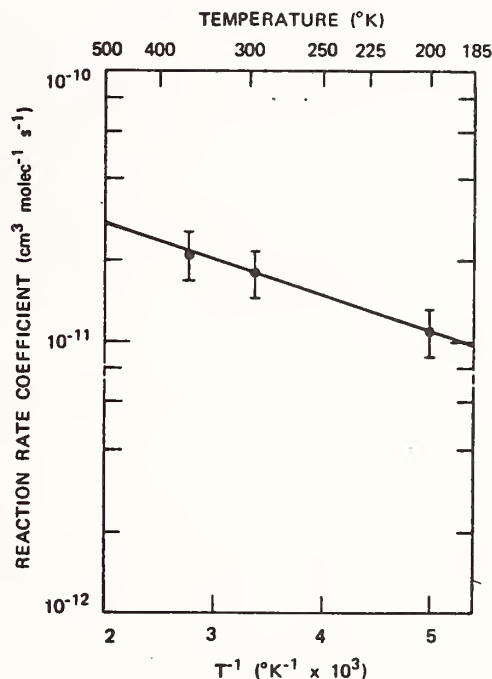


Figure 1. Reaction rate coefficient vs T^{-1} for $O(^1S) + O(^3P) \rightarrow 2O$.

Application of these new rate coefficients to the atmosphere leads to some interesting results. If we ask whether the atmospheric observations correlate better with the laboratory results through reaction (1) or through reactions (2)-(4), the answer is quite clear. Based on current $O(^3P)$ profiles, the assumption that our laboratory rate coefficient pertains to the simple mechanism, reaction (1), results in calculated 5577 Å intensities that are far too high. To utilize the complex scheme, we need to make assumptions about the efficiencies of reactions (2) and (3) in giving the necessary electronic states, but with this flexibility [which involves identifying O_2^* as $O_2(A^3\Sigma_u^-)$], a very good correlation can in fact be made [11], which indicates that typical mid-latitude peak $O(^3P)$ densities are in the neighborhood of $6 \times 10^{11} \text{ cm}^{-3}$. The work that remains is to test these assumptions, which involves making kinetic measurements on $O_2(A^3\Sigma_u^-)$ and also, if possible, on the other electronic states of O_2 in the same energy region. These states are difficult to produce and detect because of their metastable nature.

References

- [1] Chapman, S., *Proc. Roy. Soc. (London)* A132, 353 (1931).
- [2] Hernandez, G., *Planet. Space. Sci.* 19, 467 (1971).
- [3] Greer, R. G. H., and Best, G. T., *Planet. Space Sci.* 15, 1857 (1967).
- [4] Donahue, T. M., Guenther, B., and Thomas, R. J., *J. Geophys. Res.* 78, 6662 (1973).
- [5] Barth, C. A., and Hildebrandt, A. F., *J. Geophys. Res.* 66, 985 (1961).
- [6] Slanger, T. G., and Black, G., Temperature dependence for quenching of $O(^1S)$ by N_2O , to be published in *J. Chem. Phys.*, Sept. 1, 1976.
- [7] Slanger, T. G., and Black, G., *J. Chem. Phys.* 64, 3767 (1976).
- [8] Slanger, T. G., and Black, G., *J. Chem. Phys.* 64, 3763 (1976).
- [9] Felder, W., and Young, R. A., *J. Chem. Phys.* 56, 6028 (1972).
- [10] Krauss, M., and Neumann, D., *Chem. Phys. Lett.* 36, 372 (1975).
- [11] Slanger, T. G., and Black, G., $O(^1S)$ in the lower thermosphere - Chapman vs Barth, to be published in *Planet. Space Sci.* (1976).

A QUANTUM YIELD DETERMINATION FOR $O(^1D)$ PRODUCTION FROM OZONE VIA LASER FLASH PHOTOLYSIS

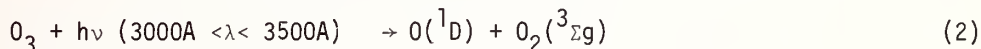
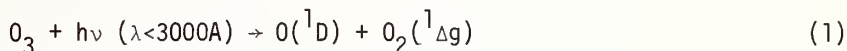
Dan L. Philen, Robert T. Watson¹ and Douglas D. Davis

Department of Chemistry
University of Maryland
College Park, MD

1. Introduction

It is now generally accepted that the OH free radical is one of the single most important species which controls the chemistry of numerous trace gases in both the troposphere and stratosphere. The principal source of OH is also now believed to be the result of the reaction of $O(^1D)$ with atmospheric water vapor ($O(^1D) + H_2O \rightarrow 2OH$).

The source of $O(^1D)$ in turn is the photolysis of ozone in the Hartley continuum ($<3000\text{\AA}$) and possibly in the Huggins bands between 3000\AA and 3500\AA .

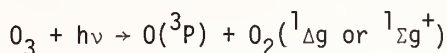


Thus, it is very important to know the production rate of $O(^1D)$ from the photolysis of ozone in the region 3000\AA to 3400\AA in order to better understand both tropospheric and stratospheric chemistry.

2. Previous Work

The absorption cross section has been measured for the wavelength region of tropospheric interest by Wanatabe [1]², Inn and Tanaka [2] and Vigroux [3]. These data have been compiled by Ackerman [4] and in addition, the absorption coefficients of ozone in the UV and visible region have been compiled by Griggs [5].

On thermochemical grounds, one would expect reaction (1) to occur at wavelengths shorter than 3100\AA and extensive studies [6] of ozone photolysis have established that reaction (1) is indeed the dominant process at wavelengths shorter than 3000\AA . The reaction



has also been shown to be the only process occurring at wavelengths equal to or greater than 3400\AA . Unfortunately, conflicting results have been obtained in the 3000 - 3200\AA region, which is the fall off region for $O(^1D)$ production.

¹Jet Propulsion Laboratory, Pasadena, CA.

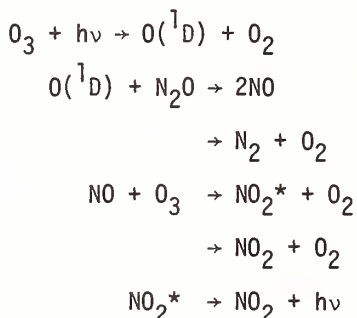
²Figures in brackets indicate the literature references at the end of this paper.

The gas phase photolysis of ozone has been studied by several groups in the region of 3130Å. Jones and Wayne [7] measured the variation of O_3 disappearance, $\phi[O_3]$, with O_3 pressure and determined a value of $O(^1D)$ production of 0.1. However, Castellano and Schumacher [8] report a value of 1.0 based on results of similar experiments. Simonaitis et al. [9] studied the reaction of $O(^1D)$ with N_2O and concluded that the quantum yield of $O(^1D)$ was 0.5, from the amount of N_2 formed; and recently Kajimoto and Cvetanovic [10] have studied the temperature dependence of $O(^1D)$ production in the region of 3130Å using the same techniques.

Lin and DeMore [11] measured the yield of isobutanol from the photolysis of O_3 with isobutane and reported a value of less than 0.1 for $\phi[O_3]$ relative to the values below 3000Å which is assumed to be unity. Thus it is evident that a careful study is needed to determine the quantum yield of $O(^1D)$ from the photolysis of ozone.

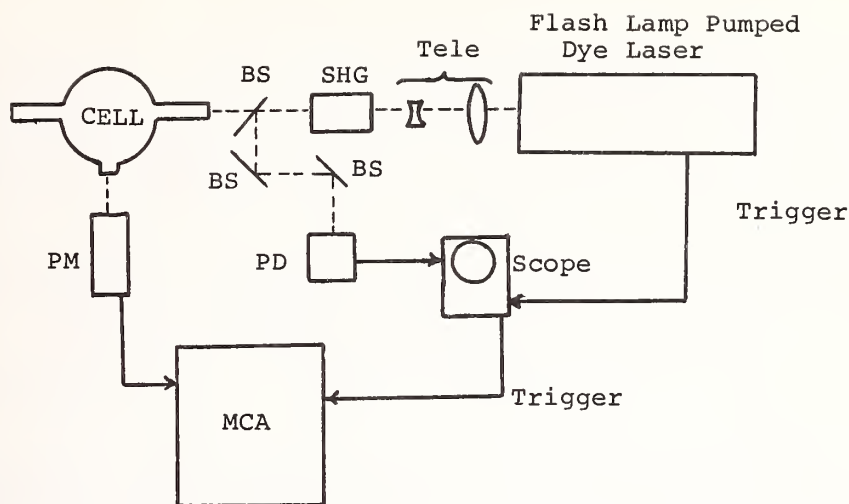
3. Experimental

Moorgat [12] and Martin [13] have both studied the photolysis of ozone with CW arc lamps using the reaction of $O(^1D)$ with N_2O to subsequently produce excited state NO_2^* . This technique is used in the present investigation and involves the reaction of $O(^1D)$ with N_2O according to the following scheme:



Thus, the amount of NO_2^* formed is directly related to the amount of $O(^1D)$ produced. The quantum yield of $O(^1D)$ can now be determined by measuring the fluorescence of NO_2^* as a function of wavelength for the photodissociation of ozone. N_2O does not absorb in the photodissociation region of approximately 3000Å, and the NO_2 fluorescence occurs at wavelengths greater than 6000Å so that conditions exist for an inherently clean experiment. The experimental arrangement consists of a flashlamp pumped dye laser which is frequency doubled to provide the photodissociation energy in the region of 2900Å to 3200Å (see figure 1). The use of a tunable dye laser allows a high photon flux and a high spectral resolution to give better definition to the nature of the quantum yield. Doubling is accomplished by the use of an ADA and an RDP temperature tuned crystal and the NO_2 fluorescence is monitored by standard photon counting techniques.

Results of this investigation will be discussed in light of previous experiments and newly acquired data.



SHG Second Harmonic Generation
 BS Beam Splitter
 PD Photodiode
 PM Photo Multiplier
 MCA Multi-Channel Analyzer
 Tele Beam Reducing Telescope

Figure 1.

References

- [1] Wanatabe, K., Inn, E. C. V., and Zelikoff, M., *J. Chem. Phys.*, 21, 1026 (1953).
- [2] Inn, E. C. Y., and Tanaka, Y., *J. Opt. Soc. Am.*, 43, 870 (1953).
- [3] Vigroix, M., Contribution a l'etude experimentals de l'ozone, *Marson et cie, Paris* (1953).
- [4] Ackerman, M., in *Mesospheric Models and Related Experiments*, D. Reidel, Ed., Dordrecht (1971), p. 149.
- [5] Griggs, M., *J. Chem. Phys.*, 49, 857 (1968).
- [6] Hampson, R. F., ed., *J. Phys. Chem. Ref. Data*, 3 (1973).
- [7] Jones, I. T. N., and Wayne, R. P., *Proc. Roy. Soc. A.*, 319, 273 (1970).
- [8] Castellano, E., and Schumacher, H. J., *Z. Physik. Chem.*, 65, 62 (1969).
- [9] Simonaitis, R., Braslonsky, S., Heicklen, J., and Nicolet, M., *Chem. Phys. Lett.*, 19, 601 (1973).
- [10] Kajimoto, O., and Cvetanovic, R. J., *Chem. Phys. Lett.*, 37, 533 (1976).
- [11] Lin, C. L., and DeMore, W. B., *J. Photochem.*, 2, 161 (1973-74).
- [12] Moorgat, G. K., and Warneck, P., *Z. Naturforsch.*, 30A, 835 (1975).
- [13] Martin, D., Girnan, J., and Johnston, H. S., 167 ACS National Meeting, March 31 - April 5, Los Angeles, 1974.

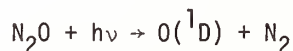
ABSENCE OF N₂O PHOTOLYSIS IN THE TROPOSPHERE

D. H. Stedman, R. J. Cicerone, W. L. Chameides and R. B. Harvey

Department of Atmospheric and Oceanic Science
University of Michigan
Ann Arbor, MI 48109

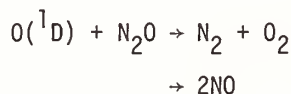
Since the early studies of Bates and Hays (1967) it has been accepted that N₂O photolyzes in the troposphere. Thus, it was thought that not all of the N₂O released at ground level (by whatever natural source) could be transported intact to the stratosphere. Once in the stratosphere a small fraction of the N₂O is attacked by O(¹D) to yield NO molecules, and this process furnishes the NO to counterbalance much of the natural production of O₃ [Crutzen, 1970; McElroy and McConnell, 1971]. From theoretical numerical models (e.g., Crutzen, 1974; McElroy et al., 1974), an N₂O source of about 3.5 x 10⁷ metric tons per year was needed to balance the altitude-integrated photochemical loss of N₂O, almost half of which loss was tropospheric.

Using the photodissociation cross section shown by Bates and Hays, the photodissociation rate, $j(\text{N}_2\text{O})$



when Rayleigh scattering is included, is calculated to be about 3 x 10⁻¹⁰sec⁻¹ in the lower troposphere. Recently, however, Johnston and Selwyn (1975) have shown that the absorption cross section is negligible in the $\lambda > 260$ nm spectral region important for tropospheric photochemistry. Their work would imply a zero value for $j(\text{N}_2\text{O})$ in the troposphere.

While their work was in progress we decided to use an actinometer, previously used to measure $j(\text{NO}_2)$ (Jackson et al., 1975), to directly measure $j(\text{N}_2\text{O})$ at ground level. In the experiment for $j(\text{N}_2\text{O})$, pure N₂O at 1 atm was used as the flowing gas in the quartz tube [Jackson et al., 1975] with a flow just enough for the downstream NO detector (~30 cm³min⁻¹). The residence time in the tube was about 100 sec. If the N₂O were photolyzed then the product O(¹D) reacts according to:



at equal rates [see data survey edited by Hampson and Garvin, 1975]. Thus a quantum yield of one NO per N₂O photolyzed is expected. If $j(\text{N}_2\text{O}) \sim 3 \times 10^{-10}\text{sec}^{-1}$ then the yield of NO would be 3 x 10⁻¹⁰ x 100 = 3 x 10⁻⁸ atm. Since the NO detector has a noise level ~10⁻⁹ atm. then quantitative detection of $j(\text{N}_2\text{O})$ was possible if Bates and Hays' cross sections applied.

When the experiment was first performed, exposure of the N₂O-containing tube to sunlight generated significant quantities of NO. At this point, the calibrated NO detector was switched to the NO_x (NO + NO₂) mode, and an impurity ~0.2 ppm NO₂ in the N₂O was determined. The photolysis of this impurity was generating the NO, and when the impurity was removed with an ascarite trap the NO generated by sunlight on N₂O became undetectable. Figure 1 shows the trace from such an experiment, performed at a time when $j(\text{NO}_2)$ was also being measured.

Results of twenty-seven measurements around solar noon gave an upper limit for (N_2O) determined experimentally as $<1 \times 10^{-11} \text{ sec}^{-1}$. Thus, tropospheric photolysis of N_2O as been shown to be negligible by direct experiment, as predicted by the concurrent spectroscopic study of Johnston and Selwyn. With the Bates and Hays (1967) cross sections a $(N_2O) = 10^{-11} \text{ sec}^{-1}$ could only be observed with an O_3 column of $>3 \times 10^{-19} \text{ cm}^{-2}$, three or four times larger than the normal ozone content.

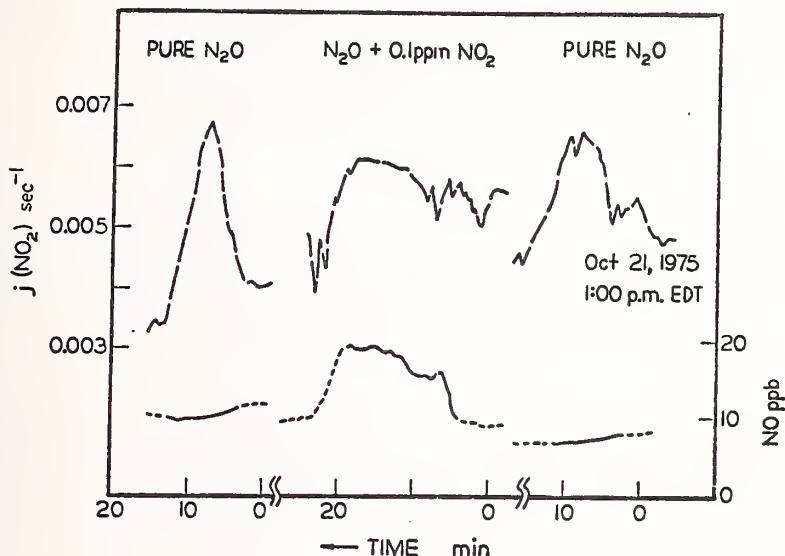


Figure 1. The lower trace and right hand axis shows a record of NO formation in the solar photolysis of N_2O , with and without a small impurity of NO_2 . Three traces are shown with sunlight intercepted by a black cloth at the beginning and end of each trace (dotted lines). The upper trace shows the concurrent measured value of the solar photolysis rate of NO_2 , $j(NO_2)$, on the left hand axis. NO production in the absence of impurities is not distinguishable from the background.

References

- Bates, D. R., and Hays, P. B., Atmospheric nitrous oxide, *Planet. Space Sci.* **15**, 189-197 (1967).
- Crutzen, P. J., The influence of nitrogen oxides on the atmospheric ozone content, *Quart. J. Roy. Met. Soc.* **96**, 320-327 (1970).
- Crutzen, P. J., A review of upper atmospheric photochemistry, *Can. J. Chem.* **52**, 1659-1581 (1974).
- Hampson, R. F., and Garvin, D., (editors), Chemical kinetic and photochemical data for modelling atmospheric chemistry, *NBS Technical Note 866* National Bureau of Standards, Washington, DC, 113 p., 1975.
- Hunten, D. M., Residence time of aerosols and gases in the stratosphere, *Geophys. Res. Lett.* **2**, 26-28 (1975).
- Jackson, J. O., Stedman, D. H., Smith, R. G., Hecker, L. H., and Warner, P.O., Direct NO_2 photolysis rate monitor, *Rev. Sci. Instrum.* **46**, (4) 376-378 (1975).
- Johnston, H. S., and Selwyn, G., New cross sections for the absorption of near ultra-violet radiation by nitrous oxide (N_2O), submitted to *Geophys. Res. Lett.*, 1975.

McElroy, M. B., and McConnell, J. C., Nitrous oxide: a natural source of stratospheric NO, *J. Atmos. Sci.* 28, 1095-1098 (1971).

McElroy, M. B., Wofsy, S. C., Penner, J. E., and McConnell, J. C., Atmospheric ozone: possible impact of stratospheric aviation, *J. Atmos. Sci.* 31, 287-303 (1974).

TEMPERATURE DEPENDENCE OF $O(^1D)$ REACTIONS OF ATMOSPHERIC IMPORTANCE

J. A. Davidson and H. I. Schiff
York University, Toronto, Ontario, Canada

and

G. E. Streit, A. L. Schmeltekopf and Carleton J. Howard
Aeronomy Laboratory
NOAA Environmental Research Laboratories
Boulder, CO 80302

The reactions of $O(^1D)$ with N_2O , H_2O , H_2 , and CH_4 are now well established as the principal sources of the radical species (NO , OH) responsible for the natural destruction of stratospheric ozone. Because of the importance of these reactions, there have been many determinations of the relative rates of the reactions of $O(^1D)$ with these and other species [1,2]¹. On the other hand, systematic investigations of absolute reaction rates have been limited to those conducted in Husain's [3-6] lab and our own [7].

In order to assess the relative importance of $O(^1D)$ deactivation and reaction to produce radical species under stratospheric conditions we have undertaken an investigation of the temperature dependence of the reactions of $O(^1D)$ of stratospheric importance.

The apparatus used in these studies has been described in detail previously [7] and hence will only be discussed briefly here. A frequency quadrupled Nd-YAG laser, yielding 1-4 mJ at 266 nm in a 10 nsec pulse, was employed to photolyze O_3 to produce $O(^1D)$ in a temperature regulated cell. The time evolution of the $O(^1D)$ concentration was then followed by means of the emission at 630 nm. Because $O(^1D)$ has a long radiative lifetime ($\tau = 100$ sec) and reacts at near collision frequency with most gases, signal averaging techniques were required to obtain a statistically meaningful decay trace. Our treatment of this data in order to extract rate constants has been previously reported [7].

In Table I our room temperature rate constants are compared with the results from other laboratories. With the exception of O_3 , the results obtained in Husain's lab using time resolved attenuation of resonance absorption are significantly higher than our results. We have previously suggested that this discrepancy may be due to the use of a rather large correction to Beer's law employed by Husain. Subsequently, Phillips [13] has calculated that in the case of the O_3 rate determination this correction was appropriate, while in all other cases the correction should have been much smaller, hence leading to a reduction of the reported rates by about a factor of 2.

¹Figures in brackets indicate the literature references at the end of this paper.

Table 1. Summary of $O(^1D)$ absolute rate constant measurements ($298 \pm 2^\circ K$)

O_3	O_2	N_2	CO_2	N_2O	H_2O	CH_4	H_2	D_2	HCl	NH_3	Reference
(10 ⁻¹⁰ cm ³ /molecule-sec)											
5.3 \pm 2.6	0.74 \pm .15	0.54 \pm .15	1.8 \pm .4	2.2 \pm .4	3.5 \pm .6	4.0 \pm .9	2.9 \pm .5				1,2
3.3 \pm	0.003	0.22 \pm .1			0.3 \pm .13						8,9,10
	0.63 \pm .3										11
2.5 \pm 1.0											12
2.7 \pm .2	0.70 \pm .05	0.69 \pm .06	2.1 \pm .2	2.2 \pm .2	3.0 \pm .3	3.1 \pm .4	2.7 \pm .3	1.8 \pm .2			3,4,5,6
2.4 \pm .1	0.41 \pm .05	0.30 \pm .01	1.2 \pm .09	1.4 \pm .1	2.1 \pm 1.0	1.3 \pm .3	1.3 \pm .05	1.3 \pm .05	1.4 \pm .3	3.4 \pm .3	This Work*

* Error limits imply precision only. Accuracy estimated to be $\pm 15\%$.

The results of our temperature dependence studies are summarized in Table II. Those molecules which deactivate $O(^1D)$ primarily through a reactive channel (N_2O , H_2O , CH_4 , H_2 , NH_3 , HCl and O_3) exhibit rate constants which are invariant with temperature. The rate constants for those molecules which deactivate $O(^1D)$ through an energy exchange process (N_2 , O_2 , and CO_2) increase with decreasing temperature. In the case of CO_2 this increase extends only to about 200K below which rate constant remains independent of temperature.

Table 2. Arrhenius parameters for the deactivation of $O(^1D)$ ($k = Ae^{-E/RT}$)

Molecule	A(cm ³ /molecule sec)	E(cal/mole)	Range($^\circ K$)
N_2O	1.1×10^{-10}		204 - 359
H_2O	2.3×10^{-10}		253 - 353
CH_4	1.4×10^{-10}		198 - 357
H_2	9.9×10^{-11}		204 - 352
NH_3	2.5×10^{-10}		204 - 354
HCl	1.4×10^{-10}		199 - 379
O_3	2.4×10^{-10}		103 - 393
N_2	2.0×10^{-11}	$-214 \pm 15^*$	104 - 354
O_2	2.9×10^{-11}	$-134 \pm 20^*$	104 - 354
CO_2	6.8×10^{-11}	$-233 \pm 47^*$	200 - 354
and	1.2×10^{-10}		139 - 200

* One standard deviation

Accuracy is estimated to be $\pm 20\%$

This research was conducted in the NOAA Aeronomy Laboratory and was supported in part by NASA contract NGR 52-134-005.

References

- [1] Cvetanovic, R. J., *Can. J. Chem.* 53, 1452 (1974).
- [2] Garvin, D., and Hampson, R. F., editors, *NBSIR 74-430* (1974).
- [3] Heidner, R. F., III, Husain, D., and Wiesenfeld, J. R., *Chem. Phys. Lett.* 16, 530 (1972).
- [4] Heidner, R. F., III and Husain, D., *Nature Phys. Sci.* 241, 10 (1973).
- [5] Heidner, R. F., III and Husain, D., *Int. J. Chem. Kinet.* 5, 819 (1973).
- [6] Heidner, R. F., III and Husain, D., *Int. J. Chem. Kinet.* 6, 77 (1974).
- [7] Davidson, J. A., Sadowski, C. M., Schiff, H. I., Streit, G. E., Howard, C. J., Jennings, D. A., and Schmeltekopf, A. I., *J. Chem. Phys.* 64, 57 (1976).
- [8] Biedenkapp, D., Hartshorn, L. G., and Bair, E. J., *Chem. Phys. Lett.* 5, 379 (1970).
- [9] Snelling, D. R., and Bair, E. J., *J. Chem. Phys.* 47, 228 (1967).
- [10] Snelling, D. R., and Bair, E. J., *J. Chem. Phys.* 48, 5737 (1968).
- [11] Noxon, J. F., *J. Chem. Phys.* 52, 1852 (1970).
- [12] Gilpin, R., Schiff, H. I., and Welge, K. H., *J. Chem. Phys.* 55, 1087 (1971).
- [13] Phillips, L. F., *Chem. Phys. Lett.* 37, 421 (1976).

MODELING STRATOSPHERIC PHOTOCHEMISTRY AND KINETICS

John McAfee and Paul J. Crutzen
National Center for Atmospheric Research
Upper Atmospheric Research Branch
Boulder, CO 80303

An analysis will be presented of our present understanding of stratospheric photochemistry. The effect of uncertainties in rate coefficients will be discussed with emphasis on the impact of human activity on the ozone layer.

THE RATE CONSTANT FOR $O + NO + M$ FROM 217-500 K IN FIVE HEAT BATH GASES

J. V. Michael¹, W. A. Payne and D. A. Whytock²

Astrochemistry Branch
Laboratory for Extraterrestrial Physics
NASA/Goddard Space Flight Center
Greenbelt, MD

The absolute rate constant for $O + NO + M$ has been measured previously by a variety of techniques [3]³ and is of interest in atmospheric modelling [4]. Most workers have used the discharge flow method with chemiluminescent detection of $[O]$; however mass spectrometric and e.s.r. detection have also been employed. Values relative to a known reaction have also been reported from steady state photochemical experiments. There are six real time studies. Three utilize phase sensitive detection and two make direct measurements from chemiluminescence [3,4]. There has been only one direct measurement with the O atom resonance fluorescence technique, at room temperature in Ar [5]. The currently accepted value for the temperature dependent rate constant is based primarily on the work of Klein and Herron and Clyne and Thrush and is given from 200-500 K in Arrhenius form as $k_t = 3.0 \times 10^{-33} \exp(940/T) \text{ cm}^6 \text{ molecule}^{-2} \text{ sec}^{-1}$ ($M = O_2, Ar$) [3,4].

The apparatus used in the present study has been described previously [6]. Binary mixtures of NO in heat bath ($2.5 \times 10^{-4} \leq X_{NO} \leq 10^{-2}$) were repetitively flash dissociated ($\lambda > 142 \text{ nm}$, $\tau = 2.5 \text{ } \mu\text{sec}$) in a flowing system yielding $N(^4S)$ and $O(^3P)$ after the method of Stuhl and Niki [7]. Further $O(^3P)$ is produced by the fast reaction, $N(^4S) + NO \rightarrow N_2 + O(^3P)$. This reaction is effectively complete before the first data are collected (delay time $\geq 300 \text{ } \mu\text{sec}$). Flash energies, and therefore concentrations, are sufficiently low so that the secondary reaction, $O + NO_2 \rightarrow O_2 + NO$, is totally negligible.

Fluorescent photons are repetitively counted and stored with a multichannel analyzer under a given set of experimental conditions. The resulting decay constant can be expressed as,

$$k_{\text{observed}} = k_t[NO][M] + k_d \quad , \quad (1)$$

where k_t is the termolecular rate constant for $O + NO + M$, and k_d is the diffusional loss rate constant out of the viewing zone. At a given pressure and temperature, at least three decay constants are obtained as a function of $[NO]$. Plots of k_{obs} against $[NO]$ yield $k_{bi} = k_t[M]$ as the linear least squares slope, and the intercept gives k_d . Plots of k_{bi} against $[M]$ then yield k_t as the linear least squares slope for a given temperature. In nearly all cases the least squares standard deviation in the intercept is within one standard deviation of zero. Determinations at six temperatures (217 K, 252 K, 298 K, 355 K, 418 K, and 500 K) are then carried out for any given heat bath gas. The heat bath gases used are N_2 , He, Ne, Ar, and Kr.

¹ NAS/NRC Senior Resident Research Associate.

² Catholic University, on leave from the Chemistry Department, The University of Essex, Colchester, England.

³ Figures in brackets indicate the literature references at the end of this paper.

The results for $M = N_2$ are shown in Table I and can be expressed in Arrhenius form as $k_t = (15.5 \pm 2.0) \times 10^{-33} \exp(582 \pm 37)/T \text{ cm}^6 \text{ molecule}^{-2} \text{ sec}^{-1}$. This result can be directly compared to that of Klein and Herron [8] who give $(3.97 \pm 0.55) \times 10^{-33} \exp((971 \pm 50)/T) \text{ cm}^6 \text{ molecule}^{-2} \text{ sec}^{-1}$ ($M = N_2$). The room temperature values are in good agreement, but discrepancies occur for all other temperatures above room temperature, the largest being at 500°K where the present results are 1.8 times larger. The temperature dependence of k_t with the other heat bath gases appears to be similar.

Table I. Rate data for $O + NO + N_2 \rightarrow NO_2 + N_2$

T/K	$k_t/10^{-32} \text{ cm}^6 \text{ molecule}^{-2} \text{ sec}^{-1}$
217	20.8 ± 1.2^a
252	17.2 ± 2.3
298	11.5 ± 0.9
355	7.40 ± 0.68
418	6.24 ± 0.23
500	4.92 ± 0.25

^aQuoted error limits are the standard deviation.

References

- [1] NAS/NRC Senior Resident Research Associate.
- [2] Catholic University, on leave from the Chemistry Department, The University of Essex, Colchester, England.
- [3] Reviewed by D. L. Baulch, D. D. Drysdale, D. G. Horne, and A. C. Lloyd, Evaluated kinetic data for high temperature reactions, Vol. 4, Butterworths, London, 1972.
- [4] Hampson, R. F., Jr., and Garvin, D., editors, Chemical kinetic and photochemical data for modelling atmospheric chemistry, *NBS Technical Note 866*, U.S. Government Printing Office, Washington, DC, 1975.
- [5] Slanger, T. G., and Black, G., *J. Chem. Phys.* **53**, 3717 (1970).
- [6] Klemm, R. B., and Stief, L. J., *J. Chem. Phys.* **61**, 4900 (1974).
- [7] Stuhl, F., and Niki, H., *J. Chem. Phys.* **55**, 3943 (1971).
- [8] Klein, F. S., and Herron, J. T., *J. Chem. Phys.* **41**, 1285 (1964).

DETERMINATION BY THE PHASE SHIFT TECHNIQUE OF THE TEMPERATURE DEPENDENCE OF THE REACTIONS
OF $O(^3P)$ WITH HCl , HBr , AND HI

D. L. Singleton and R. J. Cvetanovic

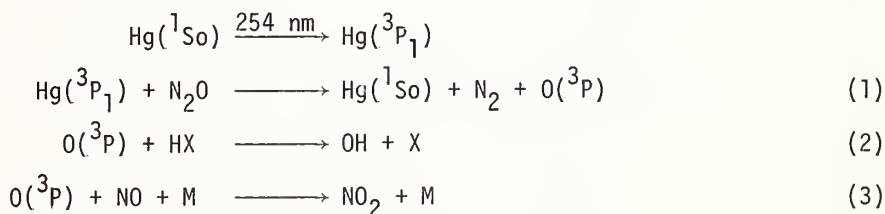
Division of Chemistry
National Research Council of Canada
Ottawa, Canada

A few studies have been reported recently on some specific aspects of the reaction of ground state oxygen atoms with hydrogen halides, $O + HX \rightarrow OH + X$, namely, the effect of HX vibrational energy on the reaction rate [1]¹ and the relative yields of excited products [2], $OH(v=0,1)$ and $X(^2P^{3/2}, ^1/2)$. The temperature dependence of the bulk rate constants has received little attention, and, in the case of HCl , where more than one determination has been reported, the results are in poor agreement.

We have used a phase shift technique to determine the rate constants for the reactions of $O(^3P)$ with HCl , HBr , and HI between 298-554 K. Also, as an incidental part of this work, the rate constant of the reaction $O(^3P) + NO + M \rightarrow NO_2 + M$ ($M = HCl$) has been determined between 298-398 K.

2. Experimental

As described previously [3] ground state oxygen atoms are formed by modulated photo-sensitized decomposition of nitrous oxide in a flowing mixture of N_2O , NO , HX , and Hg according to the simple reaction scheme:



The expression for the phase shift, ϕ , between the incident 254 nm light, modulated at frequency ν , and the chemiluminescence from reaction (3) is

$$\frac{2\pi\nu}{\tan\phi} = k_2[HCl] + k_3[NO][M] \quad .$$

The phase angles are measured with appropriate filter - photomultiplier combinations and a lock-in amplifier.

¹Figures in brackets indicate the literature references at the end of this paper.

Two methods of modulation were used. The first, for the HCl reaction below 500 K where frequencies of 30-90 Hz were required, involved mechanically chopping the light from a rf powered low pressure mercury lamp. In the second method, for all the other reactions, which required frequencies of 1.3-6 kHz, the amplitude of the rf that powered the lamp was modulated.

Total pressures were between 30-70 Torr and were varied by a factor of two at each temperature except for HCl at 298 K where the total pressure was 16-18 Torr. Approximate relative concentrations $[N_2O]:[NO]:[HX]$ were: HCl ($T < 500$ K), 1:0.001-0.01:0.1-1; HCl ($T > 500$ K), 1:0.1:0.1; HBr, 1:0.1:0.01-0.1; HI, 1:0.1:0.001-0.01. The residence time of the gases in the reaction cell was < 0.4 sec for the HI experiments; < 2.5 sec for HBr and HCl ($T > 500$ K); and < 0.2 sec for HCl ($T < 500$ K). The total flow rates were between 10^{-4} to 10^{-3} mole sec^{-1} . The rate of production of O-atoms was about 1×10^{12} atoms $\text{cm}^{-3}\text{sec}^{-1}$ as determined by gas chromatographic analysis of the products of the O + 1-butene reaction.

3. Results

For the reactions with HCl ($T > 500$ K), HBr, and HI, the rate constants k_2 and k_3 were determined from intercepts and slopes of plots of $2\pi\nu/[HX]\tan\phi$ vs. $[NO][M]/[HX]$. The values of k_3 ($M = N_2O$) were within about 10% of the previously determined values. The standard deviation of each value of k_2 was 7-9% for HCl and 2-5% for HBr and HI. The values of k_2 are shown in figure 1.

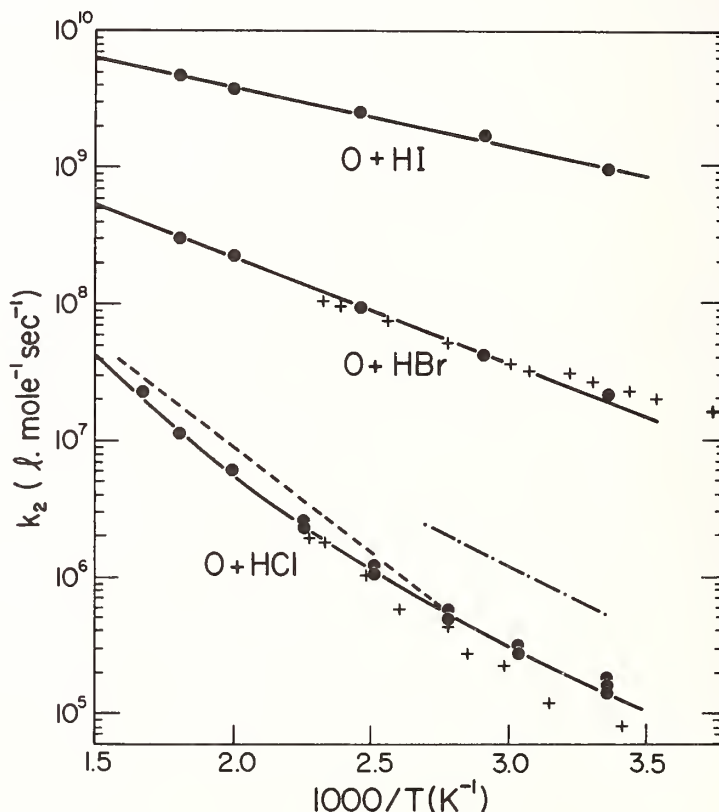


Figure 1. Arrhenius plots of k_2 ; \bullet this work; $+$ Ref. 4; ---- Ref. 5; —·— Ref. 6.

The rate constants plotted in figure 1 cover a range of reactivity of four to five orders of magnitude. The reactions of oxygen atoms with HCl ($T > 500$ K) and with HBr and HI are sufficiently fast to be measured by the procedure described previously [3]. The reaction with HCl at temperatures smaller than about 500 K is much slower and required a modified procedure.

The reaction with HCl ($T < 500$ K) required lower frequencies, but at these longer time scales, diffusional loss of $O(^3P)$ occurred from the viewing zone of the photomultiplier that detected the chemiluminescence. In this case, eq. (1) becomes $2\pi\nu/\tan\phi = k_3[NO][M] + k_D/[M]$ in the absence of HCl and assuming a first order diffusional loss of oxygen atoms. The first order diffusion rate constant, k_D , was obtained in experiments without HCl present from the intercept of plots of $2\pi\nu[M]/\tan\phi$ vs. $[NO]$. $[M]^2$ at each temperature below 500 K. The slopes gave values for k_3 ($M = N_2O$) which were in good agreement with previously determined values. An additional complication arises because the higher HCl concentrations (which were even as high as the N_2O concentrations at 298 K and 330 K) meant that HCl was a significant third body in reaction 3. Incorporating k_D and α , (the third body efficiency for HCl), into the simple mechanism, we obtain, in place of eq. (1), $2\pi\nu/\tan\phi = k_2[HCl] + k_3[NO]([N_2O] + \alpha[HCl]) + k_D/[M]$. Plots of $2\pi\nu/\tan\phi - k_D/[M]$ vs. $[NO]$, in experiments where $[NO]$ was varied while all other concentrations were held constant, gave $k_2[HCl]$ as the intercept. From the slope, the value of α was obtained at each temperature (298-443 K) using the known concentrations of N_2O and HCl, and the previously determined value of k_3 ($M = N_2O$).

The results are given in figure 1. The Arrhenius expression for the $O + HBr$ reaction is $(8.09 \pm 0.86) \times 10^9 \exp(-3.59 \pm 0.08 \text{ kcal mole}^{-1}/RT) \text{ l. mole}^{-1}\text{sec}^{-1}$. The plot of $\ln k_2$ vs. $1/T$ for $O + HCl$ is not linear. A one parameter empirical expression for the results over the temperature interval of these experiments is $k_2 = (3.7 \pm 2.1) \times 10^{-13} T^{(7.11 \pm 0.09)} \text{ l. mole}^{-1}\text{sec}^{-1}$, which was obtained from a least squares treatment of $\ln k_2$ vs. $\ln T$. All the indicated uncertainties are one standard deviation.

At room temperature, HCl is 1.7 times as efficient as N_2O as a third body in reaction 3. The Arrhenius expression for reaction 3, with $M = HCl$, is $(3.3 \pm 1.0) \times 10^{10} \exp(0.6 \pm 0.2 \text{ kcal mole}^{-1}/RT)$ between 298-398 K, which compares with the previously determined expression for $M = N_2O$, $6.12 \times 10^9 \exp(1.23 \text{ kcal mole}^{-1}/RT) \text{ l.}^2\text{mole}^{-2}\text{sec}^{-1}$.

A comparison is made with some literature values for k_2 in figure 1. The results for HBr are in good agreement with Smith's values [4] and with Glass's room temperature value [2], $2.7 \times 10^7 \text{ l. mole}^{-1}\text{sec}^{-1}$. For HI, the only available comparison is with the approximate room temperature value reported by Glass [2] ($\sim 1 \times 10^9 \text{ l. mole}^{-1}\text{sec}^{-1}$), which is in close agreement. For HCl, the present values agree well at higher temperatures with Smith's values but are somewhat larger at lower temperatures.

Some recent experiments in which HCl was replaced by argon indicate that the rate constants for the $O + HCl$ reaction below 500 K may have to be revised downward. However, further experiments are required on this part of the present work.

References

- [1] Karny, Z., Katz, B., and Szoke, A., *Chem. Phys. Lett.* **35**, 100 (1975); Arnoldi, D., and Wolfrum, J., *Chem. Phys. Lett.* **24**, 234 (1974); Quigley, G. P., and Wolga, G. J., *J. Chem. Phys.* **63**, 5263 (1975).
- [2] Takacs, G. A., Glass, G. P., *J. Phys. Chem.* **77**, 1182 (1973).
- [3] Singleton, D. L., Furuyama, S., Cvetanovic, R. J., and Irwin, R. S., *J. Chem. Phys.* **63**, 1003 (1975).
- [4] Brown, R. D. H., and Smith, I. W. M., *Int. J. Chem. Kinet.* **7**, 301 (1975).
- [5] Wong, E. L., and Belles, F. E., *NASA Technical Note D-6495* (1971).
- [6] Balakhnin, V. P., Egorov, V. I., and Intezarova, E. I., *Kinetics and Catalysis* **12**, 258 (1971).

HIGH ENERGY PULSED LASER PHOTOLYSIS OF SOME CHROMIUM (III) AND COBALT (III) COMPLEXES

Arthur W. Adamson, A. R. Gutierrez, R. E. Wright and R. T. Walters

Department of Chemistry
University of Southern California
Los Angeles, CA 90007

A current interest of this Laboratory is in the study of excited state processes through the use of a high energy pulsed laser system. Results of three types of experiments will be reported. Figure 1 allows illustration of the first two. The photochemical literature for Cr(III) complexes so far consists just of quantum yield measurements [1]¹. The yield for photochemistry from the first thermally equilibrated excited (thexi) quartet state ($^4L_1^0$) is given by $\phi_1 = \phi k_c \tau$, where ϕ is the yield for producing $^4T_1^0$, k_c is its chemical rate constant, and $1/\tau = k_{cg} + k_{nrg} + k_{eq}$, k_{cg} and k_{eq} being the nonradiative and radiative deactivation rate constants respectively. Alternatively, photochemistry may derive from reaction of the first doublet thexi state (2D in O_h), with $\phi_2 = \phi_d k_{cd} \tau_d$, where k_{cd} is the chemical rate constant and $1/\tau_d = (k_{cd} + k_{nrd} + k_{ed})$. In addition, it has been postulated that the 2D and $^4L_1^0$ states may thermally interconvert [2].

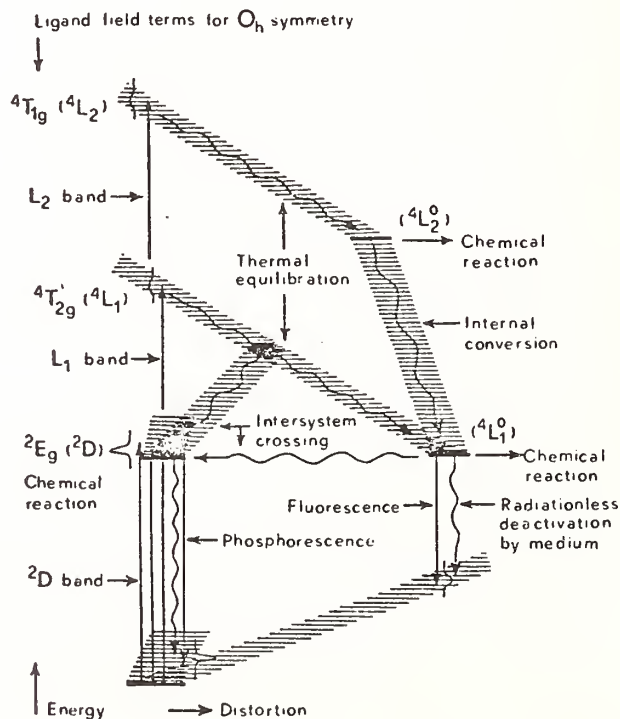


Figure 1

¹ Figures in brackets indicate the literature references at the end of this paper.

Clearly, a full elucidation of such systems requires determination of the separate rate constants. It is certainly insufficient to find $\phi_1 + \phi_2$ or even the separate yields. These last have been inferred from quenching experiments [1,2].

The first type of laser study is that of the determination of ligand and solvent effects on k_{nr} through studies of emission lifetimes. Weak room temperature emission has been reported for several Cr(III) complexes [3,4] and additional results are included in Table 1. These demonstrate that emission lifetimes of various complexes vary greatly with the type of ligation. We attribute these variations more to changes in k_{nr} (the rate constant for non-radiative decay of the first doublet excited state) than to changes in k_e (the emission rate constant). Thus, at 77 °C, the lifetimes for $\text{Cr}(\text{NH}_3)_6^{3+}$ and $\text{Cr}(\text{NH}_3)_5(\text{H}_2\text{O})^{3+}$ are 56 and 70 μsec , respectively, presumably approximating the $1/k_e$ values [5]. At room temperature, τ for the first complex has dropped to 1.8 μsec or 31 fold, while that for the aquopentaamine has dropped to less than 20 nsec, or more than 3500 fold. We infer that coordinated water enhances the non-radiative deactivation rates and speculate that this is due to hydrogen bonding into the solvation shell which establishes good vibrational communication with the medium.

Table 1. Emission lifetimes for Cr(III) complexes at 25 °C

Complex	τ , ns (in water)	Complex	τ , ns (in water)
$\text{Cr}(\text{bipy})_3^{3+}$	45,000	$\text{Cr}(\text{NH}_3)_5\text{NCS}^{2+}$	140 (148 in 60% AN)
$\text{Cr}(\text{NH}_3)_6^{3+}$	1,800	$\text{t-Cr}(\text{NH}_3)_2(\text{NCS})_4^-$	7 (120 in AN)
$\text{t-Cr}(\text{en})_2(\text{NCS})_2^+$	1,490	$\text{Cr}(\text{NCS})_6^{3-}$	< 20 (30 in AN)
$\text{t-Cr}(\text{en})_2\text{F}_2^+$	1,360	$\text{Cr}(\text{acac})_3$	1.5 (Windsor)
$\text{Cr}(\text{en})_3^{3+}$	1,300		

AN = acetonitrile. $\text{Cr}(\text{en})_2(\text{H}_2\text{O})\text{F}_2^{2+}$, $\text{Cr}(\text{NH}_2)_5(\text{H}_2\text{O})^{3+}$, $\text{cis-Cr}(2,3,2\text{-tet})\text{Cl}_2^+$, $\text{cis-}\alpha\text{-Cr}(\text{trien})\text{Cl}_2$: $\tau < 20$ ns. $\text{Cr}(\text{urea})_6^{23+}$: no observable emission

Figure 2 shows a point by point emission spectrum for $\text{Cr}(\text{NH}_3)_6^{3+}$. The long wavelength peak is shifted by 160 cm^{-1} on deuteration, in essentially mirror image behavior to that found for the doublet adsorption band. Clearly, it would be better to have more detailed emission spectra, but the general effect seems clear. We are, however, very interested in obtaining such spectra for other complexes, and in other solvent media.

Table 2 shows the marked solvent dependence that we have found for the emission lifetimes of $\text{trans-Cr}(\text{NH}_3)_2(\text{NCS})_4^-$ (reinecke salt). Note that water and hydrogen bonding solvents materially shorten the lifetime relative to that in less polar and non-hydrogen bonding media. Figure 3 shows the data for water-acetonitrile mixtures plotted vs. mole fraction and according to solvation sphere composition as estimated by Langford [6]. This plot is linear, obeying Stern-Volmer kinetics. Thus, k_{nr} behaves as a bimolecular rate constant, first order in complex and first order in solvent. The yields for thiocyanate release reported by Langford increase with water content, contrary to expectation were reaction occurring from the doublet or emitting state. This is an acceptable finding, however, since it is generally recognized that most of the reaction occurs from the first quartet excited state. This interpretation does imply, however, that the doublet and quartet states are not in rapid thermal equilibrium.

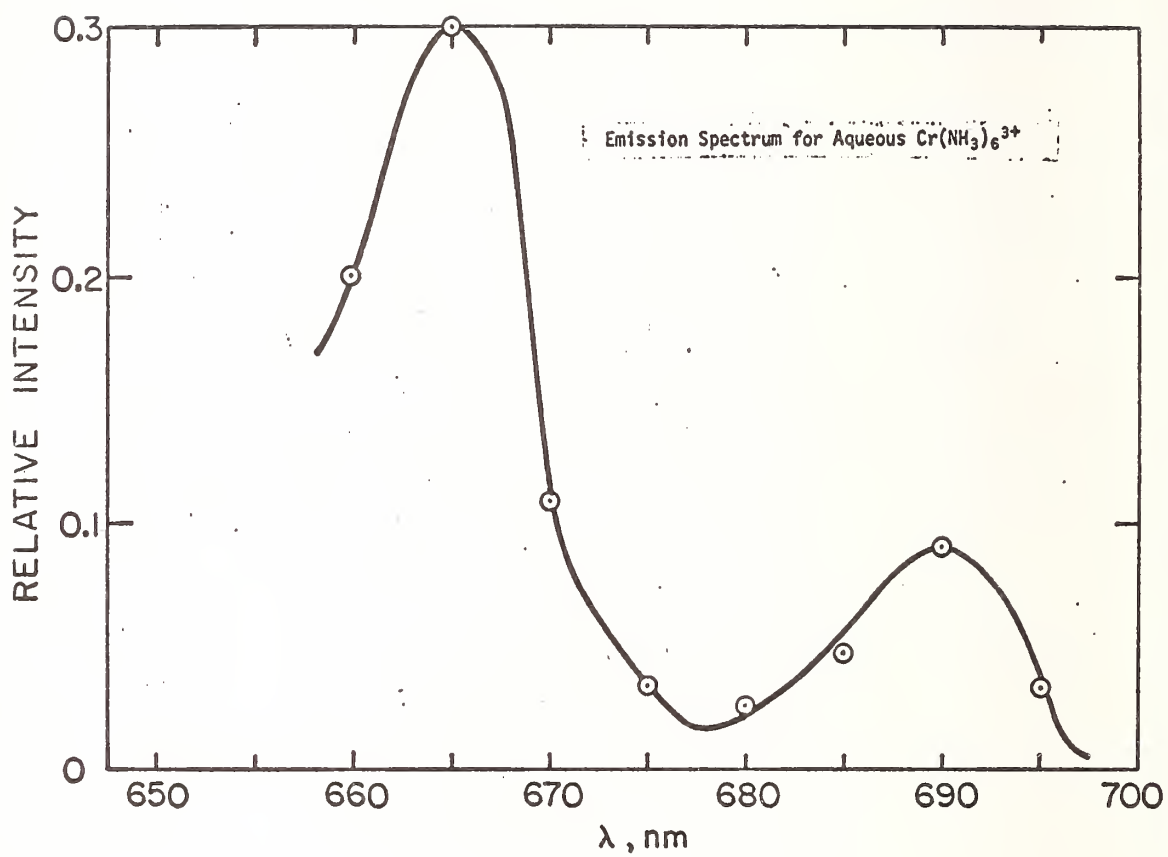


Figure 2. Emission spectrum for aqueous $\text{Cr}(\text{NH}_3)_6^{3+}$

Table 2. Emission lifetimes of $\text{trans-Cr(NH}_3)_2(\text{NCS})_4^-$, $\sim 20^\circ\text{C}$

Solvent	τ , ns	Solvent	τ , ns	Solvent	τ , ns
$\text{CH}_3\text{CN}^*(\text{AN})$	177	CH_3NO_2	105	glycerol	28
$\text{CH}_2\text{Cl}_2^{**}$	175	DMSP	89	acetic acid	26
acetone	158	pyridine	87	$(\text{C}_2\text{H}_5)_2\text{NH}$	25
40% AN + ϕ	153	DMF	78	CH_3OH	23
40% AN + CHCl_3	135	THF	39	$(\text{CH}_2\text{OH})_2$	22
AN	120	$\text{C}_2\text{H}_5\text{OH}$	31	H_2O	7

* deaerated

** solubilization by 18-6 crown ether

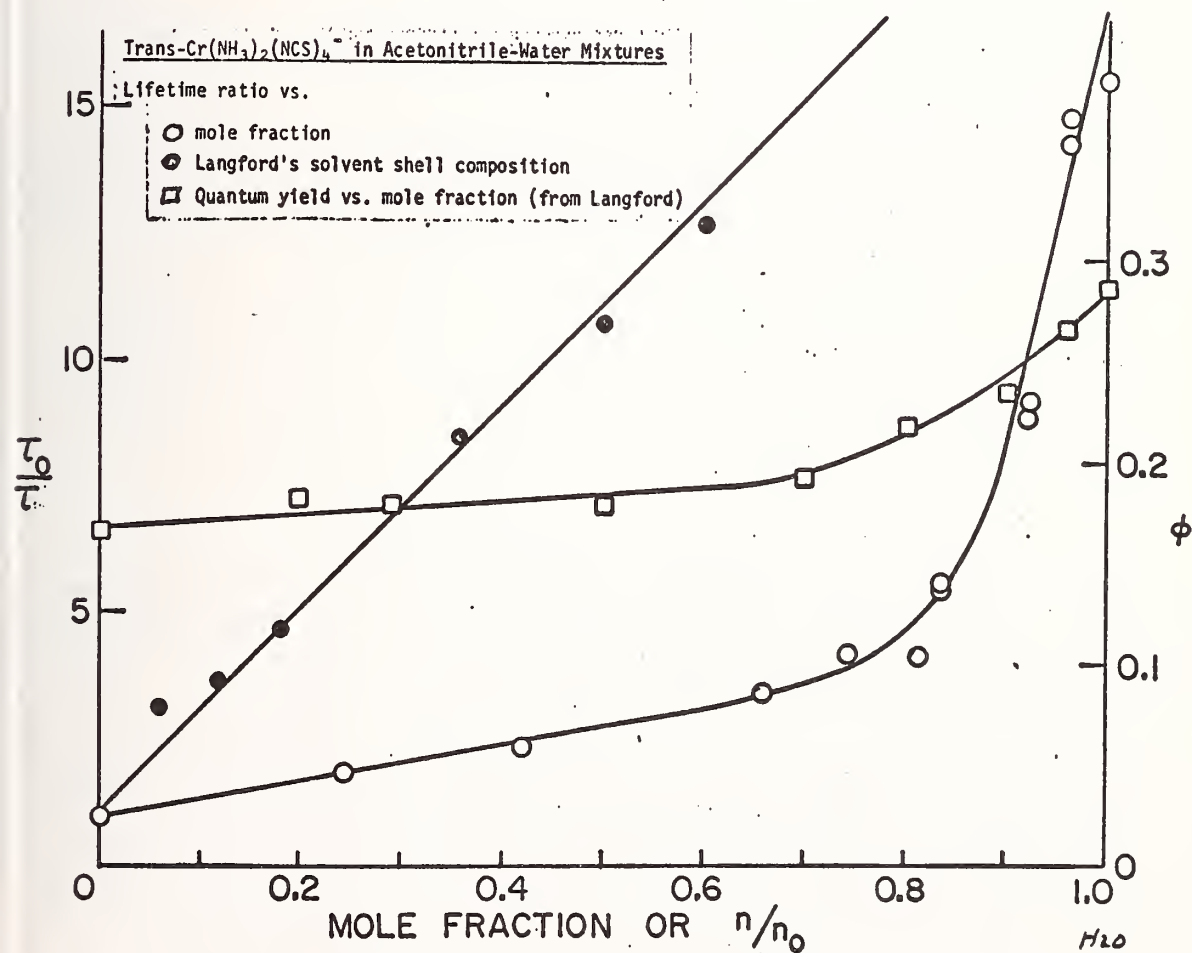


Figure 3. $\text{Trans-Cr(NH}_3)_2(\text{NCS})_4^-$ in acetonitrile-water mixtures.

Several of the systems have been studied over a range of temperatures; some data are shown in tables 3 and 4. Fairly high activation energies are found. The values are in general agreement with those obtained from phosphorescence yields by Kane-Maguire and Langford. We also have I_0 values, that is, emission intensities immediately following the stimulating flash. Preliminary results indicate that these also show a temperature dependence, contrary to simple expectation. We need, however, to make sure that the emission spectra are not changing with temperature, perhaps an unlikely effect, but one which could account for the I_0 changes.

Table 3. Emission parameters for Cr(III) amines

<u>Complex</u>	<u>Solvent</u>	<u>E*, kcal/mole</u>	
		<u>Emission</u>	<u>Relative I_0</u>
Cr(en)_3^{3+}	H_2O	10.2	6.8
	D_2O	12.0	---
Cr(bipy)_3^{3+}	H_2O	7.5	---

Table 4. Emission parameters for $\text{trans-Cr(NH}_3)_2(\text{NCS})_4^-$

<u>Solvent</u>	<u>E*, kcal/mole</u>		
	<u>Emission</u>	<u>Relative I_0</u>	<u>Viscosity</u>
CH_3OH	12.5	-1.0	2.6
CH_3CN	11.4	-7.3	1.6
$(\text{C}_2\text{H}_5)_2\text{NH}$	9.7	-4.6	
Acetone	12.7	-3.1	1.5

The second and third types of study are ones for which the laser system was designed. The system comprises a Q-switched, gated, amplified, and frequency doubled Nd oscillator; maximum output is 1 to 1.5 J at 530 nm with 20 nsec halftime. If the beam is collimated to 3 mm diameter, the nominally absorbed number of photons (i.e. assuming no ground state bleaching) can be made greatly to exceed the number of molecules of compound.

This capability makes possible the investigation of (a) two (successive) photon processes and (b) single pulse photolyses in which primary product formation is monitored. As an example of (a), we obtain τ_d for $\text{trans-Cr(NH}_3)_2(\text{NCS})_4^-$ in acetonitrile both from emission decay and from excited state absorption (for which the spectrum has been reported [7]). For several systems excited state absorption has also been observed as an excess attenuation of the transmitted pulse, the pulse shape being skewed if the lifetime of the absorbing excited state is greater than that of the pulse. A third experiment of type (a) is that of two-photon processes involving Co(III) amines. As illustrated in figure 4, adsorption of a second 530 nm pulse should populate a charge transfer excited state, the evidence being the appearance of Co(II) as photolysis product. The effect has been reported for $\text{Co(NH}_3)_6^{3+}$ using a highly focussed, multiply pulsed N_2 laser (337 nm) [8]. We find it for $\text{Co(NH}_3)_5\text{Br}^{2+}$ after a few unfocussed pulses at 530 nm.

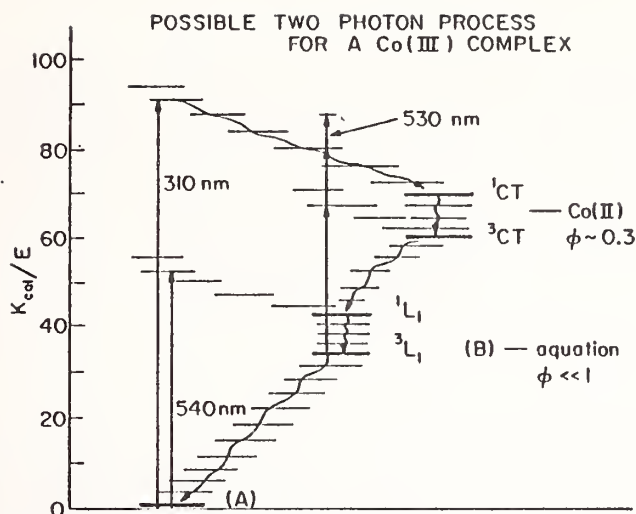


Figure 4. Possible two photon process for a Co(III) complex.

Type (b) experiments are in progress with various Cr(III) amines and acidoamines. We observe the rise time of primary photo-product formation by means of a suitably monochromated monitoring beam. The ϕ_2 process should lead to product with an appearance time τ_d , which typically is in the short microsecond range. The ϕ_1 process may produce product much more quickly; the rise time in this case should yield the so far inaccessible τ_q .

References

- [1] Zinato, E., *Concepts of Inorganic Photochemistry*, A. W. Adamson and P. F. Fleischauer, Wiley, 1975.
- [2] Ballardine, R., Varani, G., Wasgestian, H. F., Morri, L., and Balzani, V., *J. Phys. Chem.* **77**, 2947 (1973).
- [3] Kane-Maguire, N. A. P., and Langford, C. H., *Chem. Commun.* 895 (1971).
- [4] Adamson, A. W., Geosling, C., Pribush, R., and Wright, R., *Inorg. Chim. Acta* **16**, L5 (1976).
- [5] Chatterjee, K. K., and Forster, L. S., *Spectrochim. Acta* **20**, 1603 (1964).
- [6] Sastri, V. S., Henwood, R. W., Behrendt, S., and Langford, C. H., *J. Amer. Chem. Soc.* **94**, 753 (1972).
- [7] Ohno, T., and Kato, S., *Bull. Chem. Soc. Japan*, **43**, 8 (1970).
- [8] Cunningham, K. M., and Endicott, J. F., *Chem. Comm.*, 1024 (1974).

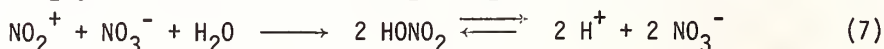
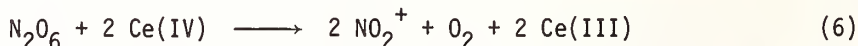
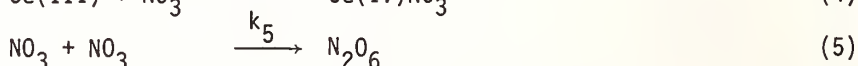
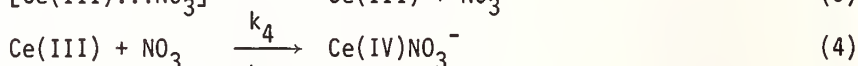
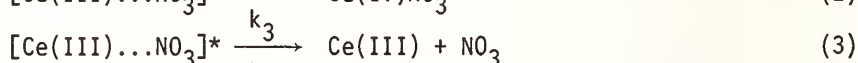
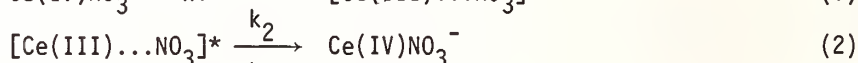
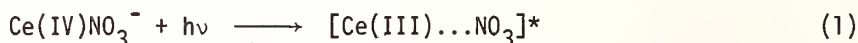
STUDIES USING A COMBINATION OF FLASH PHOTOLYSIS AND PULSED MAGNETIC INDUCTION:
APPLICATION TO THE NO₃ RADICAL IN AQUEOUS ACID SOLUTION AT 25 °C

T. W. Martin and M. V. Stevens¹

Department of Chemistry
Vanderbilt University
Nashville, TN 37235

1. Introduction

The photolysis of (NH₄)₂Ce(NO₃)₆ in acid solution is a convenient means of studying the chemistry of the NO₃ radical, one of the strongest oxidants known. Over the years we have learned a few things about its absorption spectrum [1]², decay kinetics [2], and competitive electron transfer with various Ce(III) species [3]. More recently, by using a pulsed laser and kinetic spectroscopy, we have obtained deeper insight into the comprehensive mechanism of the generation and decay of the NO₃ radical in nitric and perchloric acid solutions at room temperature [4]. It was found that the 20 ns pulse from a 4-joule frequency-doubled ruby laser was virtually instantaneous in comparison to the thermal rate processes involved. Hence, it was possible to make a kinetic analysis over the complete lifetime of NO₃ in these solvents. These studies revealed that an excited-state metastable complex, [Ce(III)...NO₃]*, is a precursor to the NO₃ radical. Thus, the earlier published mechanism [5] must be enlarged as follows to account for this complex:



The measured rate constants and quantum yields derived from our analyses, together with a new value of the extinction coefficient for NO₃ are summarized in table 1. From these data, with regard to the generation of NO₃, we infer that k₂ increases on dilution of HONO₂ because of increased coordination of H₂O with Ce(IV); whereas the opposite is true for k₃ which increases with increased coordination by NO₃. From these trends and since $\phi_{\text{NO}_3} = k_3/(k_2 + k_3)$, it is not surprising that ϕ_{NO_3} becomes constant and equal to unity when [HONO₂] ≥ 6M. As to the decay modes, k₄ follows similar trends to k₃, but k₅ is essentially constant and independent of [HONO₂].

¹ Duckworth Pathology Laboratory, Methodist Hospital, 1265 Union Avenue, Memphis, TN 38104.

² Figures in brackets indicate the literature references at the end of this paper.

Table 1. Summary of rate constants and quantum yields for the photolysis of $(\text{NH}_4)_2\text{Ce}(\text{NO}_3)_6$ in aqueous acid solutions at $25 \pm 1^\circ\text{C}$

Solvent ^a	$(k_2 \pm \sigma)$ $\times 10^{-4} \text{s}^{-1}$	$(k_3 \pm \sigma)$ $\times 10^{-4} \text{s}^{-1}$	$(k_4 \pm \sigma)$ $\times 10^{-6} \text{M}^{-1} \text{s}^{-1}$	$(k_5 \pm \sigma)^b$ $\times 10^{-6} \text{M}^{-1} \text{s}^{-1}$	$(\phi_{\text{NO}_3})^c$
1.00 M HONO_2	$5.12 \pm .37$	$4.36 \pm .37$	$.600 \pm .089$	d	$.46 \pm .04$
2.00 M HONO_2	$2.14 \pm .34$	$6.41 \pm .34$	$.743 \pm .059$	d	$.75 \pm .04$
3.00 M HONO_2	$.63 \pm .05$	$6.76 \pm .21$	$1.08 \pm .04$	$.91 \pm .11$	$.92 \pm .02$
5.00 M HONO_2	~ 0	$7.74 \pm .20$	$1.78 \pm .10$	$.93 \pm .09$	$1.00 \pm .01$
12.00 M HONO_2	~ 0	$8.75 \pm .22$	$4.08 \pm .16$	$.92 \pm .08$	$.99 \pm .01$
3.00 M HOCIO_3	$6.04 \pm .62$	$2.01 \pm .62$	$.372 \pm .050$	d	$.25 \pm .02$
1.00 M HOCIO_3	d	d	$.352 \pm .070$	d	$.11 \pm .02$

^aInitial samples also contained about 1.00 mM Ce(IV) and 3.00 to 10.00 mM Ce(III).

^bCalculated assuming $\epsilon(\text{NO}_3)_{635 \text{ nm}} = 4.80 \pm 48 \text{ M}^{-1} \text{cm}^{-1}$ and an effective pathlength, $l_E = .55 \text{ cm}$.

^cBased on $\phi_{\text{NO}_3} = k_3/(k_2 + k_3)$ and assuming ϕ_{NO_3} is maximum as well as equal to 1.00 in 6 M HONO_2 .

^dDatum not measured.

2. Magnetic Studies

Concurrent with our NO_3 work, we developed an apparatus which can combine either conventional flash photolysis or pulsed laser techniques with the simultaneous use of a high field pulsed magnet capable of generating inductions to 200 kilogauss (kG). The purpose was to test if magnetic inductions could in any way truly influence either the excited or the ground states of species in solution at 25°C . So far, we have measured two *bona fide* magnetic effects. One had to do with the classic photoisomerization of stilbene [6] where the inductions stimulated the $S \rightarrow T$ intersystem crossing mode in the excited state as efficiently as benzophenone*; the other is the reverse effect of stimulating the $T \rightarrow S$ rate determining step monitored by k_4 in the above mechanism.

Because of the novelty and lack of theory for this experimental approach, we have hesitated to publish our results. But this second effect involving NO_3 has convinced us of the possible general applicability of this method for probing mechanism in both the ground and excited state or organic as well as inorganic systems.

In table 2, where the $[\text{HONO}_2]$ is relatively high, we note that the size of k_4^B is only slightly enhanced, about 6 percent, which is probably due only to a small magnetstriction effect on the concentration of paramagnetic species in the ground state. However, in perchloric acid (table 3), where the coordination sphere of Ce(III) is richer in H_2O than NO_3^- , we observe a large specific rate enhancement that is quite non-linear particularly at $B > 75 \text{ kG}$. We suspect this enhancement at $B > 150 \text{ kG}$ will approach an upper limit of 3, because we believe k_4 normally monitors the electron transfer process involving only one of the levels of the ground triplet recombination complex,

Table 2. Effect of a magnetic induction of 150 kilogauss on the decay of NO_3 in aqueous nitric acid at $25 \pm 1^\circ\text{C}$

[HONO ₂]	$(k_4^B \pm \sigma) \times 10^{-6} \text{M}^{-1} \text{s}^{-1}$ at B = 150 kG	$(k_4 \pm \sigma)^a \times 10^{-6} \text{M}^{-1} \text{s}^{-1}$ at B = 0 kG	k_4^B/k_4
1.00 M	.630 \pm 0.75	.599 \pm .089	1.06 \pm .18
3.00 M	1.08 \pm .039	.996 \pm .036	1.09 \pm .05
6.00 M	1.86 \pm .14	1.78 \pm .10	1.06 \pm .10
12.00 M	4.08 \pm .16	3.96 \pm .26	1.03 \pm .08

^aControl samples run under identical conditions except B = 0 kG.

Table 3. Effect of magnetic induction on the decay of NO_3 in 3M aqueous perchloric acid at $25 \pm 1^\circ\text{C}$

Magnetic Induction B(kG)	$(k_4^B \pm \sigma) \times 10^{-6} \text{M}^{-1} \text{s}^{-1}$	$(k_4 \pm \sigma)^a \times 10^{-6} \text{M}^{-1} \text{s}^{-1}$ at B = 0 kG	k_4^B/k_4
150	.896 \pm .150	.372 \pm .052	2.31 \pm .52
150	.771 \pm .055	.352 \pm .071	2.18 \pm .47
75	.425 \pm .052	.356 \pm .022	1.20 \pm .16
75	.428 \pm .078	.356 \pm .022	1.21 \pm .20

^aControl samples run under identical conditions except B = 0 kG.

$[\text{Ce(III)} \dots \text{NO}_3]^{\text{T}_0}$, which is active in converting to the ground singlet state, $[\text{Ce(IV)NO}_3]^{\text{S}_0}$. We postulate that this non-linear magnetic effect either tends to make all three levels of the triplet complex kinetically active in undergoing $\text{T}_0 \rightarrow \text{S}_0$ crossing or it acts to mix those levels in such a way as to enhance the population of the one active level so as to increase k_4^B with respect to the unperturbed specific rate k_4 . If either interpretation is correct, this technique represents a new way, independent of magnetic resonance, for demonstrating and studying CIDEP effects by monitoring short-lived intermediates in both organic and inorganic systems. Its sensitivity to the structure of the ligand coordination sphere is also remarkable.

We are grateful to the National Science Foundation, the U.S. Atomic Energy Commission and Vanderbilt University for sponsoring these studies.

References

- 1] Martin, T. W., et al., *J. Am. Chem. Soc.* 85, 113 (1963).
- 2] *ibid.*, 86, 2595 (1964).
- 3] *ibid.*, 92, 5075 (1970).
- 4] Manuscript in preparation.
- 5] *J. Am. Chem. Soc.*, 5084 (1970).
- 6] Manuscript in preparation.

LUMINESCENCE OF SOME METAL TRISDITHIOACETYLACETONATE COMPLEXES

M. K. DeArmond and J. T. Merrill

Department of Chemistry
North Carolina State University
North Carolina

1. Introduction

Luminescence of metal complexes can, within the limit of small mixing of ligand and metal d-orbitals, be classified as "d-d" emission (localized orbital), charge transfer (delocalized orbital) or ligand localized orbital (delocalized orbital) [1]¹. Since emission typically occurs only from the lowest manifold of excited states, only localized "d-d" orbital emission is observed for first transition series complexes while either localized and delocalized orbital emission can be observed for heavy d⁶ transition metal complexes dependent upon the ligand. Emission of d⁶ Rh(III) and Ir(III) complexes can be categorized as "metal localized orbital" (*i.e.*, Rh(dtc)₃)² or "delocalized orbital," ([Rh(bpy)₃]³), [Ir(bpy)₂Cl₂]⁴ where bpy = 2,2'-bipyridyl). The former type of emission is broad, structureless and exhibits a large Stokes Shift while the latter emission exhibits vibrational structure and a relatively smaller Stokes Shift.

The β -diketone complexes of Rh(III) and Ir(III) have been reported [4] to exhibit d-d emission at 11.8 and 11.3 kK, although the spectra was so weak that no lifetime could be measured. Such an emission is unique since no d-d absorption can be identified at energies lower than the intense delocalized orbital transitions. However, large Stokes Shifts of emission are characteristic of d⁶, localized orbital emitters [2,3,52]. Therefore the d-d absorption may be covered by the intense low energy bands.

In the limit of small mixing of ligand and metal orbitals, the low lying d-d absorption although hidden by the more intense delocalized orbital transitions, may still permit typical d-d emission to be observed. But, in the limit of substantial mixing of metal and ligand orbital, the emission should be of the characteristic "delocalized orbital" type for these weak field ligands.

To better understand the interaction between d orbitals and high energy ligand π -orbitals and the resultant energy transfer processes, neutral tris dithio β -diketonate complexes, M(SacSac)₃ and M(SSSBB)₃ of Cr(III), Rh(III) and Ir(III), were synthesized, absorption, emission and photoselection determined and lifetimes measured.

2. Experimental

All SacSac complexes (Cr(III), Rh(III), and Ir(III)), figure 1 were synthesized according to literature methods [6], purified by recrystallization and preparative thin layer chromatography. All compounds were analyzed for C, H, and S by Atlantic Microlab, Inc., Atlanta, Georgia, and have proper stoichiometry. The Rh(SSSBB)₃ and Ir(SSBB)₃ were synthesized by a method developed in this laboratory and the stoichiometry verified by analysis.

¹ Figures in brackets indicate the literature references at the end of this paper.

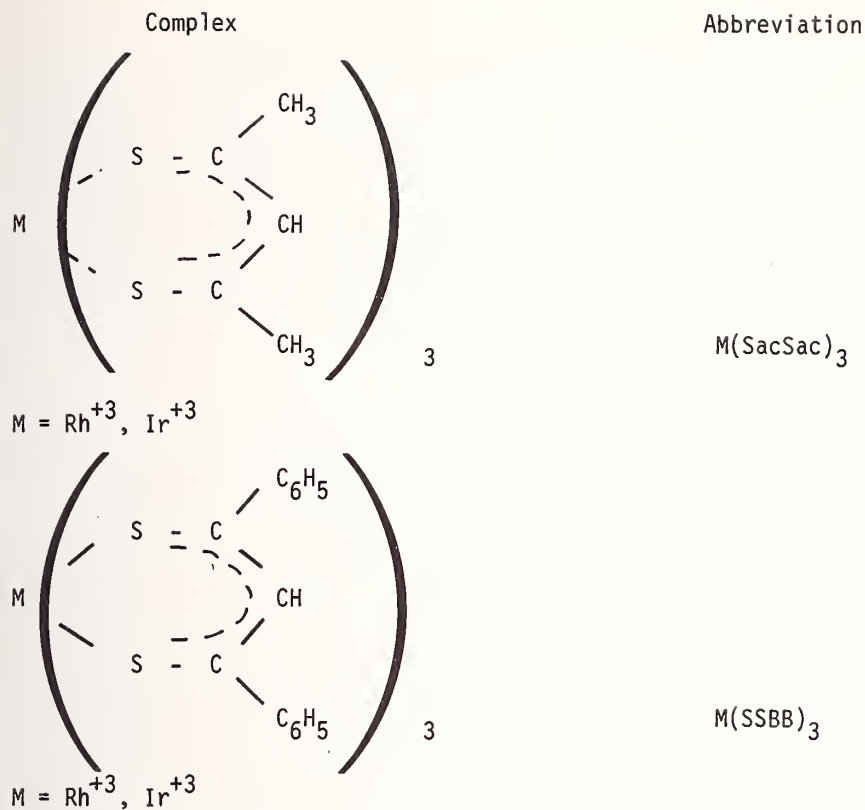


Figure 1. Formulas and abbreviations of chelates studied.

Absorption spectra were determined at room and liquid nitrogen temperature using a Cary 14 spectrophotometer. Emission and excitation spectra were determined with an Aminco-man Spectrophotofluorometer (SPF) at 77 °K in solvents of EPA, cyclohexane, and a toluene, ethanol mixture (30-60 volume percent toluene) with both a Hamamatsu R-136 and RCA 9312 red sensitive tube. The photoselection method described by Albrecht [7] and utilized by various workers to relate the relative orientation of emitting and absorbing oscillators in frozen randomly oriented samples was done at 77 K in glassy alcohol solvents. The Aminco SPF equipped with Glan-Thompson prisms for excitation and emission was calibrated with phenanthrene [8] and tested with $C_{29}d^6$ metal chelate complexes [9]. (A maximum depolarization value of ~ 0.4 was obtained).

Emission decay was determined using a Laser Energy Incorporated (LEI) 20 K watt pulsed N_2 laser ($\lambda \sim 337$ nm, pulse width = 5 ns) both with the single shot technique and photomultiplier detection and using pulse averaging technique with a Princeton Applied Research (PAR) Boxcar Averager Model 160 with an X-Y recorder. Lifetime values were determined from decay curves using a least squared program.

3. Results

The $Cr(\text{SacSac})_3$ complex gave no emission out to $1.0 \mu\text{m}$. The $Rh(\text{SacSac})_3$, $Ir(\text{SacSac})_3$, $Cr(\text{SSBB})_3$ and $Ir(\text{SSBB})_3$ gave broad emission bands with maxima in the near IR (table 1). Lifetime values determined from experimental decay curves are tabulated in table 1.

The emission and absorption spectra overlap substantially in the case of the SSBB complexes of Rh^{III} and Ir^{III} . The $Rh(\text{SacSac})_3$ complex exhibits a weak ($\epsilon \sim 1$) absorption band at 14.5 kK on the tail of the intense absorption band. The $Ir(\text{SacSac})_3$ likewise exhibits a weak band ($\epsilon \sim 75$) on the tail of the intense structured absorption at 16.1 kK.

Table 1. Absorption and emission data for sulfur chelates.

Complex	Absorption		Emission (77 K)		
	$\bar{\nu}_{\max}$ (kK) (83 K)	ϵ_{\max} (298 K)	$\bar{\nu}_{\max}$ (kK)	τ_p (μsec)	$\tilde{\nu}_{1/2}$ (cm ⁻¹)
Rh(SacSac) ₃	14.5	< 3			
	19.6	7750			
	22.3		12.8	23.8	1840
Ir(SacSac) ₃	16.1	76			
	19.5				
	20.1		12.3	1.1	2090
	21.4	7000			
Rh(SSBB) ₃	17.6				
	20.2	8220	12.3	30.3	2100
Ir(SSBB) ₃	17.4				
	19.7		12.5	2.5	2600
	21.6	7850			

Polarization (P) values obtained at 77 K from excitation and emission spectra for the lowest energy absorption bands were small and slightly negative (-0.02 to -0.060), much greater than the theoretical limit (-0.33) for a planar emitter-linear absorber and much smaller than the 0.14 limit of a planar emitter-planar absorber combination.

4. Discussion and Conclusions

On the basis of the energy, band shape and lifetime, the orbital and spin character of the emitting state for the four d⁶ complexes are the same and within the ligand field model best assigned as "d-d" localized orbital emission with the corresponding absorption transitions overlapped by an intense charge transfer transition. The small magnitude polarization (P) values could result from a small trigonal splitting of the parent T₁(O_h) state such that both the A₂ and the E state are populated at 77 K.

An anomaly is noted if the weak low energy absorption bands for the Rh(SacSac)₃ (14.5 kK) and Ir(SacSac)₃ (16.1 kK) are associated with the respective emission bands. Then, the experimental Stokes Shift of the emission is much smaller than that for typical d⁶ emitters (as for the S coordinated complexes Rh(dtc)₃ and Ir(dtc)₃²). Such data may suggest that: (1) the ligand field is not appropriate, *i.e.*, significant mixing of d and π orbitals is occurring, or (2) that the weak absorption bands are *not* associated with the emission bands. Additional photoselection spectra at low temperature (4 K) and high resolution may clarify these points.

The overlap of the absorption and emission spectra for the SSBB chelates of Rh^{III} and Ir^{III} implies that emission is occurring from a state other than the lowest excited state. Such phenomena are unique but not unknown. Organic emitters such as azulene do exhibit fluorescence from an upper singlet while some mixed ligand d^6 metal complexes do exhibit multiple emission [10,11] from energetically close lying states localized in different portions of the molecule.

The character of the lowest excited states for $\text{Cr}(\text{SacSac})_3$ cannot be determined since no emission could be observed. The absence of emission may result from either a very low quantum efficiency and/or it may be beyond $1\ \mu\text{m}$.

References

- [1] DeArmond, M. K., *Accounts Chem. Res.* 7, 309 (1974).
- [2] Hillis, J. E., and DeArmond, M. K., *Chem. Phys. Letts.* 10, 325 (1971).
- [3] Hillis, J. E., and DeArmond, M. K., *J. Chem. Phys.* 54, 2247 (1971).
- [4] Crosby, G. A., Watts, R. J., and Westlake, S. J., *J. Chem. Phys.* 55, 4663 (1971).
- [5] Thomas, T. R., and Crosby, G. A., *J. Mol. Spectrosc.* 38, 118 (1971).
- [6] Heath, G. A., Martin, R. L., and Masters, A. F., *Aus. J. Chem.* 25, 2547 (1972).
- [7] Albrecht, A. C., *J. Mol. Spectrosc.* 6, 84 (1961).
- [8] Azumi, T., and McGlynn, S. P., *J. Chem. Phys.* 37, 2413 (1962).
- [9] Carlin, C., Merrill, J. T., and DeArmond, M. D., to be published.
- [10] Halper, W., and DeArmond, M. K., *J. Lumin.* 5, 225 (1972).
- [11] Watts, R. J., Brown, M. J., Griffith, B. G., and Harrington, J. S., *J. Amer. Chem. Soc.* 97, 6029 (1975).

LUMINESCENT TRANSITION METAL COMPLEX PHOTSENSITIZERS

J. N. Demas, J. W. Addington, R. P. McBride, W. E. Harris and S. Peterson

Chemistry Department
University of Virginia
Charlottesville, VA 22901

Ruthenium(II), osmium(II) and iridium(III) complexes with diimine ligands possess nearly ideal properties as photosensitizers. They absorb intensely, emit strongly in fluid solution, have long lives, are generally highly photostable and exhibit wavelength independent efficiencies of population of the emitting state.

Table 1 shows properties of thirteen complexes which have been studied as photosensitizers. The zero point energies of the excited state, E_0 's, the mean lifetimes, τ_0 's, the bimolecular quenching constants for oxygen deactivation, k_2 's and the limiting quantum yields, ϕ_0 's, for photooxygenation of tetramethylethylene (TME) at infinite concentrations of O_2 and TME for each complex are indicated; all values are for methanol at $\sim 21^\circ C$.

Table 1. Properties of transition metal complexes photosensitizers^{a,b} in methanol at $\sim 21^\circ C$

Complex	E_0 (kK)	τ_0 (μsec)	$k_2 \times 10^{-9}$ ($M^{-1}s^{-1}$)	ϕ_0 (TME)
$[Ru(bipy)_3]^{2+}$	18.0	0.765	1.8	0.86
$[Ru(phen)_3]^{2+}$	18.4	0.313	3.3	0.75
$[Ru(Clphen)(phen)_2]^{2+}$		0.947	2.3	0.81
$[Ru(Brphen)(phen)_2]^{2+}$		0.989	2.3	0.80
$Ru[(SO_3\phi_2)phen](phen)_2$	17.9	3.98	1.8	0.82
$Ru(bipy)_2(CN)_2$	18.3	0.40	2.8	0.79
$Ru(phen)_2(CN)]$	18.3	1.58	5.0	0.68
$[Os(bipy)_3]^{2+}$	14.9	0.049	4.5	----
$[Os(phen)_3]^{2+}$	15.3	0.183	5.7	0.76
$[Os(\phi_2phen)(phen)_2]^{2+}$	15.0	0.212	4.6	0.78
$Os[(SO_3\phi)_2phen](phen)_2$	14.8	0.093	6.8	0.74

Table 1. Properties of transition metal complexes photosensitizers^{a,b} in methanol at ~ 21 °C (continued)

Complex	E ₀ (kK)	τ ₀ (μsec)	k ₂ × 10 ⁻⁹ (M ⁻¹ s ⁻¹)	φ ₀ (TME)
[Ir(bipy) ₃] ³⁺	22.7	2.4	0.34	----
[Ir(phen) ₃] ³⁺	22.5	2.6	0.28	----
Rose Bengal	----	---	----	0.80

^abipy = 2,2'-bipyridine, phen = 1,10-phenanthroline, Xphen = 5-halo,1,10-phenanthroline, Ø₂phen = 4,7-diphenyl-1,10-phenanthroline, (SO₃Ø)₂phen = disulphonated-4,7-diphenyl-1,10-phenanthroline.

^bData taken in part from references [1-3].

The φ₀'s are all less than unity. The Rose Bengal yield of 0.80 equals its intersystem crossing yield of 0.84 within experimental error. Thus, the subunity yields for the complexes do not arise from inefficient reaction of ¹O₂ with TME. Since the intersystem crossing/internal conversion efficiencies for complexes of this type has been shown to be unity, the inefficiencies of photo-oxygenations are caused by an inefficient energy transfer step. We attribute this inefficiency to formation of an exciplex which undergoes radiationless deactivation before dissociation to form ¹O₂.

From a combination of intensity and decay time quenching data, it has been found that Cu²⁺, CO₂²⁺ and Ni²⁺ quench Ru(phen)₂(CN)₂ and Ru(bipy)₂(CN)₂ by both static and dynamic processes. The association constant estimated from these data are given in table 2. Since other neutral complexes without CN groups do not give static quenching, and since CN can be a bridging ligand, the association appears to arise from the RuL₂(CN)₂ complex acting as a ligand for the metal ion to yield a Ru-CN-M species.

Table 2. Association constants for metal ions with ruthenium(II)-cyanide complexes in water at ~ 22 °C

	K _{eq} (M ⁻¹)	
	Ru(bipy) ₂ (CN) ₂	Ru(phen) ₂ (CN) ₂
Cu ²⁺	220	270
Ni ²⁺	10	20
Co ²⁺	11	17

Ru(bipy)₂(CN)₂ and Ru(phen)₂(CN)₂ are also protonated, presumably at the CN. In the case of Ru(bipy)₂(CN)₂, we find evidence for reversible acid-base equilibrium in the excited state. Details will be presented.

References

- [1] Demas, J. N., and Addington, J. W., *J. Amer. Chem. Soc.*, in press.
- [2] Demas, J. N., Harris, E. W., Flynn, C. M., Jr., and Diemente, D., *J. Amer. Chem. Soc.* 97, 3838 (1975).

PICOSECOND STUDIES OF TRANSITION METAL COMPLEXES

Patrick E. Hoggard, Alexander D. Kirk¹, Gerald B. Porter², Mark G. Rockley³,
and Maurice W. Windsor⁴

Department of Chemistry
Polytechnic Institute of New York
New York, NY

Lifetimes of excited electronic states of a number of transition metal complexes have been measured in solution at room temperature with picosecond time resolution [1]⁵. Two experimentally distinct lifetimes can be retrieved with this technique. The ground state bleaching (GSB) lifetime is that for the total repopulation of the ground state, measured by the regrowth in intensity of absorption bands, initially bleached because of depopulation by the pumping pulse. The excited state absorption (ESA) lifetime is that for depopulation of a particular excited state, measured by the decay of the electronic absorption spectrum from that state.

Both of these processes are observed only under somewhat special conditions, and in addition we have thus far been limited by the necessity that the sample absorb significantly at 530 nm, the double frequency of a Nd³⁺ laser. To observe GSB, the molar extinction coefficient at 530 nm must be higher than about 5000. A similar requirement applies to ESA - the extinction coefficient must be high, somewhere within the range of the instrumentation and the continuum pulse used for analysis. Additionally, observation is impossible if the excited state absorption is masked by the ground state absorption.

In spite of these restrictions, a number of transition metal complexes have been found for which we can observe GSB and/or ESA. A summary of some of these results is shown in the table.

In the case of the Fe(II) complexes, there are two absorption bands in the visible region, an intense band above 500 nm, representing a CTTL transition, and another much weaker band below 900 nm, assigned to a $^3T_{1g} \leftarrow ^1A_{1g}$ ligand field transition. In addition, transitions from 3CT and $^1T_{1g}$ states are probably masked by the spin allowed charge transfer band. An estimate of the radiative lifetime of the 1CT state from the absorption spectrum plus the absence of observable luminescence allows us to rule out this state as too short-lived to contribute to the observed GSB lifetime. The 830 ps lifetime is consistent with estimates for the $^3T_{1g}$ lifetime, but could represent decay into the ground state from any of $^3T_{1g}$, $^1T_{1g}$, or 3CT .

Department of Chemistry, University of Victoria, B.C., Canada.

Department of Chemistry, University of British Columbia.

Department of Chemistry, Oklahoma State University.

Department of Chemistry, Washington State University.

Figures in brackets indicate the literature references at the end of this paper.

Chromium (III) complexes exhibit small extinction coefficients in general, so that GSB is not expected to be observed. Excited state absorption from the lowest ligand field states, ${}^4T_{2g}$ and 2E_g would also be expected to exhibit small extinction coefficients within the manifold of ligand field states. Observation of ESA in the visible range is thus to be expected only with ligands which induce charge transfer states in the region of 30-40 kK above the ground state. Thiocyanate and acetylacetonate complexes exhibit the required CT bands, and ESA was observed for these complexes.

Table

Complex	Ground state bleaching	Excited state absorption	Type of transition
$[\text{Fe}(\text{bipy})_3]^{2+}$	$\tau = 830 \text{ ps}$		
$[\text{Fe}(\text{phen})_3]^{2+}$	Observed		
$[\text{Ru}(\text{bipy})_2(\text{CH}_3\text{OH})_2]^{2+}$	$\tau = 620 \text{ ps}$	$\lambda_{\text{max}} < 425 \text{ nm}$	probably intraligand
$[\text{Cr}(\text{NH}_3)_2(\text{NCS}_4)]^-$		$\lambda_{\text{max}} \text{ ca } 520 \text{ nm}$ $\tau = 5 \text{ ns}$	Charge transfer M \rightarrow L
$[\text{Cr}(\text{acac})_3]$		$\lambda_{\text{max}} \text{ ca } 500 \text{ nm}$ $\tau = 1.5 \text{ ns}$	Charge transfer M \rightarrow L
$[\text{Cr}(\text{NCS})_6]^{3-}$		$\lambda_{\text{max}} \text{ ca } 540 \text{ nm}$ $\tau = 5 \text{ ns}$	Charge transfer M \rightarrow L

Although the ${}^4T_{2g}$ state is reached by absorption, the ESA spectra of all 3 complexes match the ESA of the 2E_g state measured at 77 K by Ohno and Kato [2]. Unless the ESA spectra of ${}^4T_{2g}$ and 2E_g states are fortuitously the same, it appears that the ${}^4T_{2g}$ state undergoes intersystem crossing to the 2E_g state in a time less than the duration of the pump pulse (ca. 5 ps).

References

- [1] Kirk, A. D., Hoggard, P. E., Porter, G. B., Rockley, M. G., and Windsor, M. W., *Chem. Phys. Lett.* **37**, 199 (1976).
- [2] Ohno, T., and Kato, S., *Bull. Chem. Soc. Japan*, **43**, 8 (1970).

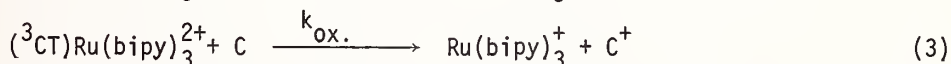
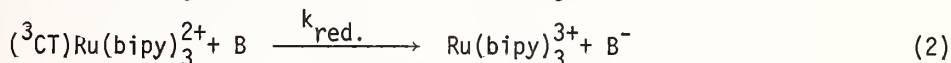
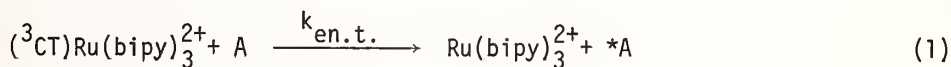
ELECTRON TRANSFER PROPERTIES OF EXCITED STATES OF TRANSITION METAL COMPLEXES

V. Balzani, F. Bolletta, M. Maestri, A. Juris, and N. Serpone¹

Istituto Chimico "G. Ciamician" dell'Università
Bologna, Italy

Until a few years ago, the attention of inorganic photochemists was entirely focussed on the intramolecular photoreactions and on the photosolvation reactions of transition metal complexes [2,3]. In the last few years, however, there has been an increasing interest in the intramolecular redox properties of transition metal complexes.

The protagonist of this new trend in inorganic photochemistry is the $\text{Ru}(\text{bipy})_3^{2+}$ complex, whose lowest excited state, commonly indicated by $(^3\text{CT})\text{Ru}(\text{bipy})_3^{2+}$ since it has triplet multiplicity [4] and metal-to-ligand charge transfer character is able to act as an energy donor [6], electron donor [7-10], and electron acceptor [11,12] depending on the specific nature of the reaction partner:



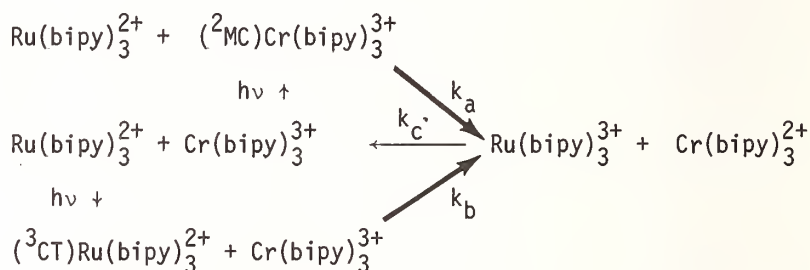
The $(^3\text{CT})\text{Ru}(\text{bipy})_3^{2+}$ excited state is luminescent in fluid solution at room temperature, a very precious property because it provides a simple means of monitoring the interactions between the excited state and the quencher. The lifetime of $(^3\text{CT})\text{Ru}(\text{bipy})_3^{2+}$ is 80 ns in deaerated aqueous solution. The absorption spectrum of this excited state has recently been obtained by means of laser flash spectroscopy and shows a maximum at about 60 nm [13]. The quantum yield of triplet formation, which has been measured with different techniques, is certainly higher than 0.5 [13] and probably near unity [6,14,15]. It should also be recalled that the $\text{Ru}(\text{bipy})_3^{2+}$ complex absorbs strongly in the visible, with a maximum at 450 nm ($\epsilon = 15,000$).

The "thermodynamic" barriers for reactions 1, 2, and 3 may be evaluated knowing that the energy difference between $(^3\text{CT})\text{Ru}(\text{bipy})_3^{2+}$ and ground state $\text{Ru}(\text{bipy})_3^{2+}$ is 17.1 kK (2.12 eV), and that the reduction potentials of the $(^3\text{CT})\text{Ru}(\text{bipy})_3^{2+}/\text{Ru}(\text{bipy})_3^{2+}$ and $\text{Ru}(\text{bipy})_3^{3+}/(^3\text{CT})\text{Ru}(\text{bipy})_3^{2+}$ couples are +0.84 V [11] and -0.83 V [11,16], respectively, vs. the NHE. Kinetic barriers have also been found to play an important role in both energy [6] and electron [9,11] transfer reactions; unfortunately, systematic studies are still lacking. It is interesting to note that reactions 2 and 3 provide for the conversion of light energy into chemical energy. The products of these reactions, however, are difficult to separate and generally undergo a fast back electron transfer reaction which dissipates the converted light energy as heat in the reaction medium. Indeed, when the two products of reaction 2 (or 3) have opposite electric charge the back electron transfer reaction is too fast to be seen with conventional flash techniques [16,17]. However, relatively high stationary concentrations of the products can be obtained in more favorable cases, and this can be used to produce a photogalvanic effect [18].

¹Figures in brackets indicate literature references at the end of this paper.

Another very interesting complex from the point of view of electron transfer reactions is $\text{Cr}(\text{bipy})_3^{3+}$. Its lowest excited state, which has doublet multiplicity and metal-centered character, is relatively long lived (about 50 μsec) and emits luminescence in fluid solution. As the $\text{Cr}(\text{bipy})_3^{3+}$ - $\text{Cr}(\text{bipy})_3^{2+}$ reduction potential is -0.25 V and the spectroscopic excitation energy of $(^2\text{MC})\text{Cr}(\text{bipy})_3^{3+}$ is 13.8 kK (1.72 eV), the reduction potential of the $(^2\text{MC})\text{Cr}(\text{bipy})_3^{3+}$ - $\text{Cr}(\text{bipy})_3^{2+}$ couple is expected to be about +1.45 V [19]. Thus, the $(^2\text{MC})\text{Cr}(\text{bipy})_3^{3+}$ excited state is expected to act as a very strong oxidant. This expectation seems to be verified since $(^2\text{MC})\text{Cr}(\text{bipy})_3^{3+}$ is quenched at nearly diffusion controlled rates by a number of species which do not possess excited states lower than 13.8 kK but have $E^\circ(\text{Q-Q}^-)$ lower than 1.45 V [20]. The quenching of $(^2\text{MC})\text{Cr}(\text{bipy})_3^{3+}$ by electron transfer to the quencher is presently under investigation in our laboratory.

One of the most interesting systems we have examined thus far is that given by a solution containing $\text{Ru}(\text{bipy})_3^{2+}$ and $\text{Cr}(\text{bipy})_3^{3+}$ [17,19]. The excited Ru complex is able to reduce the ground state Cr complex, and the excited Cr complex is able to oxidize the ground state Ru complex. In both cases, one obtains the $\text{Ru}(\text{bipy})_3^{3+}$ and $\text{Cr}(\text{bipy})_3^{2+}$ complexes which then undergo a back electron transfer reaction to reach their equilibrium situation:



We have here a system in which light absorption leads to the same products, regardless of the absorbing species. The rate constants for the two excited state reactions are $k_a = 3.3 \times 10^3 \text{ mol}^{-1}\text{s}^{-1}$ and $k_b = 4.0 \times 10^8 \text{ mol}^{-1}\text{s}^{-1}$. The reason for $k_a > k_b$ is probably due to kinetic factors which are related to the different electronic distribution in the two excited states.

The redox properties of the excited states of the Ru(II) and Cr(III) complexes as well as of other transition metal complexes are currently under investigation.

Financial support from the Italian National Research Council is gratefully acknowledged.

References

- [1] On leave from the Department of Chemistry, Sir George Williams Campus, Concordia University, Montreal, Canada.
- [2] Balzani, V., and Carassiti, V., *Photochemistry of Coordination Compounds* (Academic Press, London, 1970).
- [3] Adamson, A. W., and Fleischauer, P. D., eds., *Concepts in Inorganic Photochemistry* (Wiley, New York, 1975).
- [4] Strictly speaking, the spin label is meaningless because of the dominant role played by spin-orbit coupling [5].
- [5] Crosby, G. A., Hipps, K. w., and Elfring, Jr., W. H., *J. Am. Chem. Soc.* **96**, 629 (1974).

- 6] Balzani, V., Moggi, L., Manfrin, M. F., Bolletta, F., and Laurence, G. S., *Coordination Chem. Rev.* 15, 321 (1975).
- 7] Gafney, H. D., and Adamson, A. W., *J. Am. Chem. Soc.* 94, 8238 (1972).
- 8] Bock, C. R., Meyer, T. J., and Whitten, D. G., *J. Am. Chem. soc.* 96, 4710 (1974).
- 9] Navon, G., and Sutin, N., *Inorg. Chem.* 13, 2159 (1974).
- 10] Laurence, G. S., and Balzani, V., *Inorg. Chem.* 13, 2976 (1974).
- 1] Creutz, C., and Sutin, N., *Inorg. Chem.* 15, 496 (1976).
- 2] Juris, A., Gandolfi, M. T., Manfrin, M. F., and Balzani, V., *J. Am. Chem. Soc.* 98, 1047 (1976).
- 3] Bensasson, R., Salet, C., and Balzani, V., *J. Am. Chem. Soc.* 98, 3722 (1976).
- 4] Demas, J. N., and Crosby, G. A., *J. Am. Chem. Soc.* 93, 2841 (1971).
- 5] Bolletta, F., Maestri, M., and Balzani, V., submitted for publication.
- 6] Bock, C. R., Meyer, T. J., and Whitten, D. G., *J. Am. Chem. Soc.* 97, 2909 (1975).
- 7] Ballardini, R., Varani, G., and Scandola, F., to be published.
- 8] Lin, C. T., and Sutin, N., *J. Phys. Chem.* 80, 97 (1976).
- 9] Bolletta, F., Maestri, M., Moggi, L., and Balzani, V., *J.C.S. Chem. Commun.*, 901 (1975).
- 10] Maestri, M., Serpone, N., Bolletta, F., Moggi, L., and Balzani, V., manuscript in preparation.

A COMPARISON OF THE EXCITED-STATE ELECTRON-TRANSFER REACTIONS OF

$\text{Ru}(\text{bipy})_3^{2+}$ AND $\text{Os}(\text{bipy})_3^{2+}$

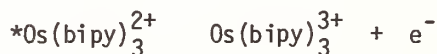
Peter Fisher, Edward Finkenberg and Harry D. Gafney

City University of New York
Department of Chemistry
Queens College
Flushing, NY 11367

The mechanism of quenching of $\text{Ru}(\text{bipy})_3^{2+}$ (bipy denotes bipyridine) luminescence is an area of active investigation [1]¹. Recent studies with organic and inorganic substrates have established that quenching can occur by an electron transfer or energy transfer mechanism. For the quenching of the luminescent charge transfer state, LCT, of $\text{*Ru}(\text{bipy})_3^{2+}$ by the acidopentaamminecobalt(III) complexes, $\text{Co}(\text{NH}_3)_5\text{x}^{\text{n}+}$, the evidence, at present, supports an electron-transfer mechanism.

A detailed study of the reduction of 13 $\text{Co}(\text{NH}_3)_5\text{x}^{\text{n}+}$ complexes by $\text{*Ru}(\text{bipy})_3^{2+}$ offers further support for an excited-state electron-transfer reaction [2]. The reduction potential of $\text{*Ru}(\text{bipy})_3^{2+}$, 0.8v [1], and small values, $2.0 \frac{\text{kcal}}{\text{mole}}$, of the energies of activation suggest the reactions are not thermodynamically controlled. As indicated by the data in table 1, some degree of correlation exists between $\phi_{\text{Co(II)}}$ and the thermal rates of reduction of the cobalt(III) complexes. This correlation suggests the reactions are kinetically controlled, that is, the rate of electron transfer must be competitive with the rate of relaxation of the excited state of the electron donor. The correlation is not perfect, indicating other factors are also important. Since $\text{*Ru}(\text{bipy})_3^{2+}$, a strong reductant, is converted on electron transfer to a strong oxidant, $\text{Ru}(\text{bipy})_3^{3+}$, a necessary criteria for a net electron transfer to occur is that the oxidant undergo an irreversible reduction. For these cobalt(III) complexes, an irreversible reduction is accompanied by dissociation of the coordinated ligands. The differences in reactivities of $\text{Co}(\text{NH}_3)_5\text{H}_2\text{O}^{3+}$, $\text{Co}(\text{NH}_3)_5\text{NCS}^{2+}$, $\text{Co}(\text{NH}_3)_5\text{N}_3^{2+}$, and $\text{Co}(\text{NH}_3)_5\text{SO}_4$, only the latter two show a measurable $\phi_{\text{Co(II)}}$, is attributed to differences in the rate of ligand dissociation and/or intersystems crossing within the reduced cobalt substrate. The latter rate must be competitive with the rate of reverse electron transfer from the reduced cobalt substrate to $\text{Ru}(\text{bipy})_3^{3+}$ in order for a net reaction to occur.

To further test these conclusions, a study of the reduction of the same cobalt(III) complexes by $\text{*Os}(\text{bipy})_3^{2+}$ under identical conditions has been undertaken. Like $\text{*Ru}(\text{bipy})_3^{2+}$, $\text{*Os}(\text{bipy})_3^{2+}$ is of sufficient potential to reduce all cobalt(III) complexes studied. The potential of the reaction



has recently been calculated to be 0.96v [1]; consequently $\text{*Os}(\text{bipy})_3^{2+}$ is a better reducing agent than $\text{*Ru}(\text{bipy})_3^{2+}$, $E^0 = .84\text{v}$ [1]. Although a stronger reducing agent, the lifetime of $\text{*Os}(\text{bipy})_3^{2+}$, 19.2 ns [1], is considerably shorter than that of $\text{*Ru}(\text{bipy})_3^{2+}$, 600 ns. *A priori*, it was expected that $\text{*Os}(\text{bipy})_3^{2+}$ would reduce only those cobalt(III) complexes which had thermal rates of reduction $\geq 10^7\text{M}^{-1}$, i.e., $\text{Co}(\text{NH}_3)_5\text{Cl}^{2+}$,

¹Figures in brackets indicate the literature references at the end of this paper.

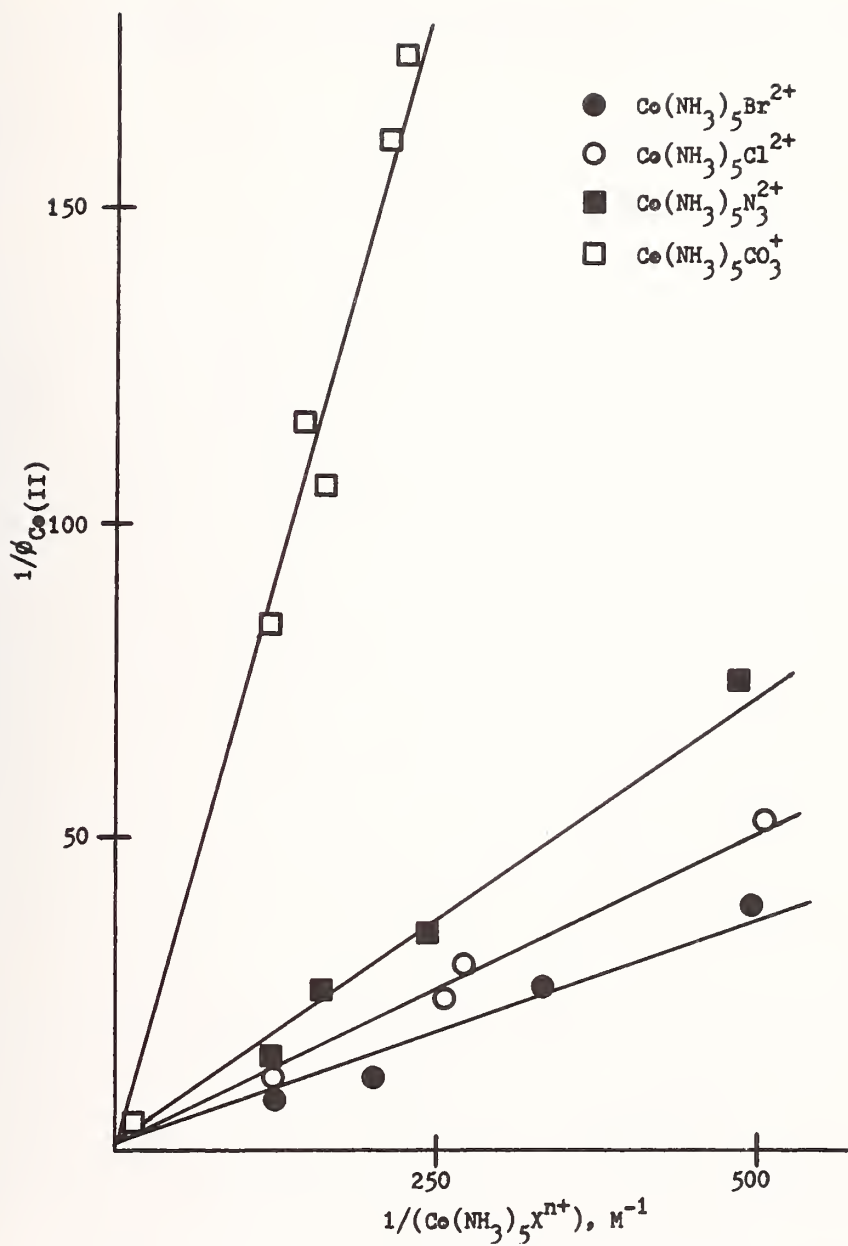


Figure 1. Dependence of $\phi_{\text{Co(II)}}$ on the concentration of $\text{Co}(\text{NH}_3)_5\text{X}^{n+}$

Table 1. Comparison of the quantum yields of reduction of various $\text{Co}(\text{NH}_3)_5\text{X}$ complexes by $^*\text{Ru}(\text{bipy})_3^{2+}$ with the thermal rates of reduction by $\text{Cr}(\text{bipy})_3^{2+}$.

Complex ^a	$\phi_{\text{Co(II)}}$	$\phi_{\text{Co(II)}}^\infty$	$k(\text{M}^{-1}\text{sec}^{-1})^b$
RNH_3^{3+}	<.001	-	6.9×10^2
RCN^{2+}	<.001	-	-
RH_2O^{3+}	<.001	-	5.0×10^4
RF^{2+}	<.0003	-	1.8×10^3
ROOCH_3^{2+}	<.001	-	1.2×10^3
RNCS^{2+}	<.0001	-	1.0×10^4
RCO_3^+	0.014	-	-
RN_3^{2+}	0.051	0.1	4.1×10^4
RSO_4^+	0.043	0.1	4.5×10^4
RCI^{2+}	0.063	0.6	8.0×10^5
RBr^{2+}	0.104	0.7	5.0×10^6
RI^{2+}	0.141	1.0	-
$\text{R}'\text{C}_2\text{O}_4^+$	0.097	-	-

R = $\text{Co}(\text{NH}_3)_5$, R' = $\text{Co}(\text{NH}_3)_4$

$\text{Co}(\text{NH}_3)_5\text{Br}^{2+}$, and $\text{Co}(\text{NH}_3)_5\text{I}^{2+}$. As indicated by figure 1, the available data indicates $^*\text{Os}(\text{bipy})_3^{2+}$ reacts with cobalt(III) complexes which have thermal rates of reduction $<10^7 \text{M}^{-1}\text{sec}^{-1}$. This suggests that the rate of electron transfer is much faster than the rate of relaxation. Furthermore, the limiting yields of $\phi_{\text{Co(II)}}$ obtained with $^*\text{Os}(\text{bipy})_3^{2+}$, figure 1, are essentially unity and much larger than those obtained with $^*\text{Ru}(\text{bipy})_3^{2+}$, table 1. The increased limiting efficiency of $^*\text{Os}(\text{bipy})_3^{2+}$ is thought to reflect a decrease in the rate of reverse electron transfer due to the lower oxidation potential of $\text{Os}(\text{bipy})_3^{2+}$ [1].

References

- [1] Lin, C. T., and Sutin, N., *J. Phys. Chem.* **80**, 97 (1976); and references therein.
- [2] Lam, P. K., Adamson, A. W., and Gafney, H. D., submitted to *J. Amer. Chem. Soc.*

PHOTODISSOCIATION OF SIMPLE POLYATOMIC MOLECULES

J. P. Simons

Chemistry Department
The University
Birmingham B15 2TT, England

Ten years ago, the majority of photochemists were satisfied if they were able to identify the primary products of a molecular photodissociation. Now, with the advent of the new heavy artillery of techniques for studying energy disposal and angular distribution [1]¹, they are much more demanding, and as the new results have flowed in, the theoretical models have burgeoned [2] to codify and rationalize the new data. Until recently, all the dynamical models for treating the problem of vibrational energy disposal adopted the quasi-diatomic approximation, an artificial device that resolves the full intramolecular potential into two components but has the virtue of allowing the analysis of a complex process in a relatively simple way. Each of the publications follows the format -- introduction to the physical model, mathematical analysis, comparison with current experimental data. The last section is essential, not only because it is the experimental horse that pulls the theoretical cart, but also because none of the models is predictive. This has often led to a "Comedy of Errors" because the current data chosen for comparison (commonly the near u.-v. photodissociation of ICN or the quenching of $\text{Hg}(6^3\text{P}_0)$ by CO or NO), proved to be inaccurate. The most recent dynamical models [2a-2d] have chosen the vacuum u.-v. photolysis of the halogen cyanides [3] for comparison, but here, too, experimental re-appraisal of the data suggests that some of the results may have been in error [4]. Nevertheless, there is now a general consensus on the importance of geometry and force constant changes in the transfer from the bound to the repulsive electronic surface during photodissociation and the utility of a Franck-Condon description for "predicting" vibrational energy distributions in the separating fragments. The new data for vibrational energy disposal in the vacuum u.-v. photodissociation of BrCN at 123.6 nm will be presented and compared with alternative theoretical models. The data indicate that vibrational populations calculated from observations of the fluorescence of CN in the $\text{B}^2\Sigma^+$ state are relaxed at pressures as low as 30 mtorr, either by collisionally induced transfer from fragments in the $\text{a}^4\Sigma^+$ state or by very efficient vibrational energy transfer from translationally excited $\text{CN}(\text{B}^2\Sigma^+)$ radicals. Collisional interchange between the A and B states of CN, previously suggested by Luk and Bersohn [5] to account for the pressure dependence of the fluorescence decay of $\text{CN}(\text{B})$, may also contribute, since rotational perturbations can be observed in the (0,0) band of the fluorescence spectrum at the lower pressures.

Results obtained using a new variation of the photofluorescence technique, polarized photofluorescence excitation spectroscopy [6], will be presented. The technique depends on the formation of rotationally excited fluorescent fragments which retain their memory of the orientation of the photo-selected parent molecule: the requirement is not restrictive since rotational excitation following photodissociation in the vacuum u.-v. appears to be the rule rather than the exception. Measurement of the polarization of the fluorescence as a function of the absorbed photon energy provides information relating to the symmetry of the vibronic state initially populated and its lifetime prior to dissociation. The technique is a member of the family of anisotropic photodissociation experiments developed by Zare, Bersohn, Wilson and their co-workers [1a,6]. Polarized spectra obtained from the halogen cyanides, HCN, H_2O and D_2O will be discussed [6,8].

¹Figures in brackets indicate the literature references at the end of this paper.

The rotational excitation in the $\text{CN}(\text{B}^2\Sigma^+)$ produced from the photodissociation of BrCN at 147 nm follows a Boltzmann distribution having a temperature of (1100 ± 250) K [4]. A simple Franck-Condon model will be presented which shows the observed rotational energy disposal to be consistent with predissociation from a very near linear, photo-excited state (bond angle 175°). The model also accounts for the rotational energy disposal in the photodissociation of cyanoacetylene, reported at this meeting [9].

References

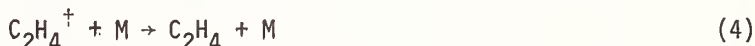
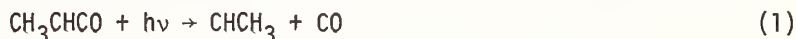
- [1] See, for example,
 (a) anisotropic photodissociation: Bersohn, R., and Yang, S.-C., *J. Chem. Phys.*, 61, 4400 (1974); Bersohn, R., Dzvonik, M., and Yang, S.-C., *J. Chem. Phys.*, 61, 4408 (1974).
- [2] (b) photofragment spectroscopy: Busch, G. E., and Wilson, K. R., *J. Chem. Phys.*, 56, 3626, 3638, 3655 (1972).
 (c) photodissociation laser spectroscopy: West, G. A., and Berry, M. J., *J. Chem. Phys.*, 61, 4700 (1974); Berry, M. J., *J. Chem. Phys.*, 61, 3114 (1974).
- [2] For leading references, see
 (a) Band, Y. B., and Freed, K. F., *J. Chem. Phys.*, 63, 3382, 4479 (1975).
 (b) Mukamel, S., and Jortner, J., *J. Chem. Phys.*, 60, 4760 (1974).
 (c) Berry, M. J., *Chem. Phys. Letters*, 29, 323, 329 (1974): also ref. 1(c).
 (d) Simons, J. P., and Tasker, P. W., *Mol. Phys.*, 26, 1267 (1973) 27, 1691 (1974).
 (e) Quack, M., and Troe, J., *Ber. Bunsenges.*, 79, 469 (1975).
- [3] Mele A., and Okabe, H., *J. Chem. Phys.*, 51, 4798 (1969).
- [4] Ashfold, M. R. N., and Simons, J. P., unpublished work.
- [5] Luk, C. K., and Bersohn, R., *J. Chem. Phys.*, 58, 2153 (1973).
- [6] Chamberlain, G. A., and Simons, J. P., *J. Chem. Soc. Faraday Trans. II*, 71, 2043 (1975).
- [7] Van Brunt, R. J., and Zare, R. N., *J. Chem. Phys.*, 48, 4304 (1968).
- [8] Macpherson, M. T., and Simons, J. P., unpublished work.
- [9] Cody, R. J., and Savety-Dzvonik, M. J., *12th Informal Conference on Photochemistry*, NBS, 1976.

ENERGY DISTRIBUTION IN THE PHOTODISSOCIATION OF METHYLKETENE AT 215 NM

M. E. Umstead, R. G. Shortridge, and M. C. Lin

Physical Chemistry Branch
Chemistry Division
Naval Research Laboratory
Washington, DC 20375

The photolysis of methylketene has been studied by Kistiakowsky and co-workers [1,2]¹. They concluded that the reaction proceeded principally by means of the following paths:



a mechanism which is consistent with that proposed by Frey for the photodissociation of diazoethane [3].

We have investigated the photodissociation of methylketene ($\text{CH}_3\text{CH}=\text{C}=\text{O}$) in a quartz flash system ($\lambda \geq 200$ nm) at 300 °K. The products of the photodecomposition were analyzed by gas chromatograph, and the initial vibrational excitation of the CO formed was measured by means of a laser resonance absorption method [4]. The results of the product analysis indicated the presence of CO, C_2H_2 , and C_2H_4 , with lesser amounts of CH_4 , C_2H_6 , C_3H_6 , C_3H_4 (propadiene and propyne) and various C_4 hydrocarbons, and are generally in agreement with those of Chong and Kistiakowsky [2].

In order to measure the initial vibrational population distribution of the CO, a stabilized cw CO laser preset at the various vibrational-rotational CO lines was directed along the axis of a quartz flash tube. Mixtures of methylketene in He were flash photolyzed, and the population distribution determined from time-resolved absorption curves measured for all vibrational levels populated by the photodissociation.

The CO laser resonance absorption measurements showed that the CO formed in the photodissociation of methylketene in the 200-230 nm region was vibrationally excited to $v=9$ and had a Boltzmann vibrational temperature of 3800 ± 500 °K. The results of two sets of $\text{C}_3\text{H}_4\text{O}$ data are plotted in figure 1. One set was obtained from a 1% mixture of $\text{C}_3\text{H}_4\text{O}$ in He, flashed at an energy of 0.5 kJ, and the other from a 1.5% mixture flashed at 1.0 kJ. The fact that the two sets of data led to the same population distribution, even though the $\text{C}_3\text{H}_4\text{O}$ concentrations and the flash energies differend considerably, provides evidence that the excited CO is indeed produced in the primary step, and not be secondary reactions.

This is also supported by an experiment in which O_2 was added as a free radical scavenger. A mixture containing 1% $\text{C}_3\text{H}_4\text{O}$ and 2% O_2 in He was flashed at an energy of 1.0 kJ. The results of the CO excitation measurements were the same as those from the O_2 -free mixtures, within experimental error.

¹ Figures in brackets indicate the literature references at the end of this paper.

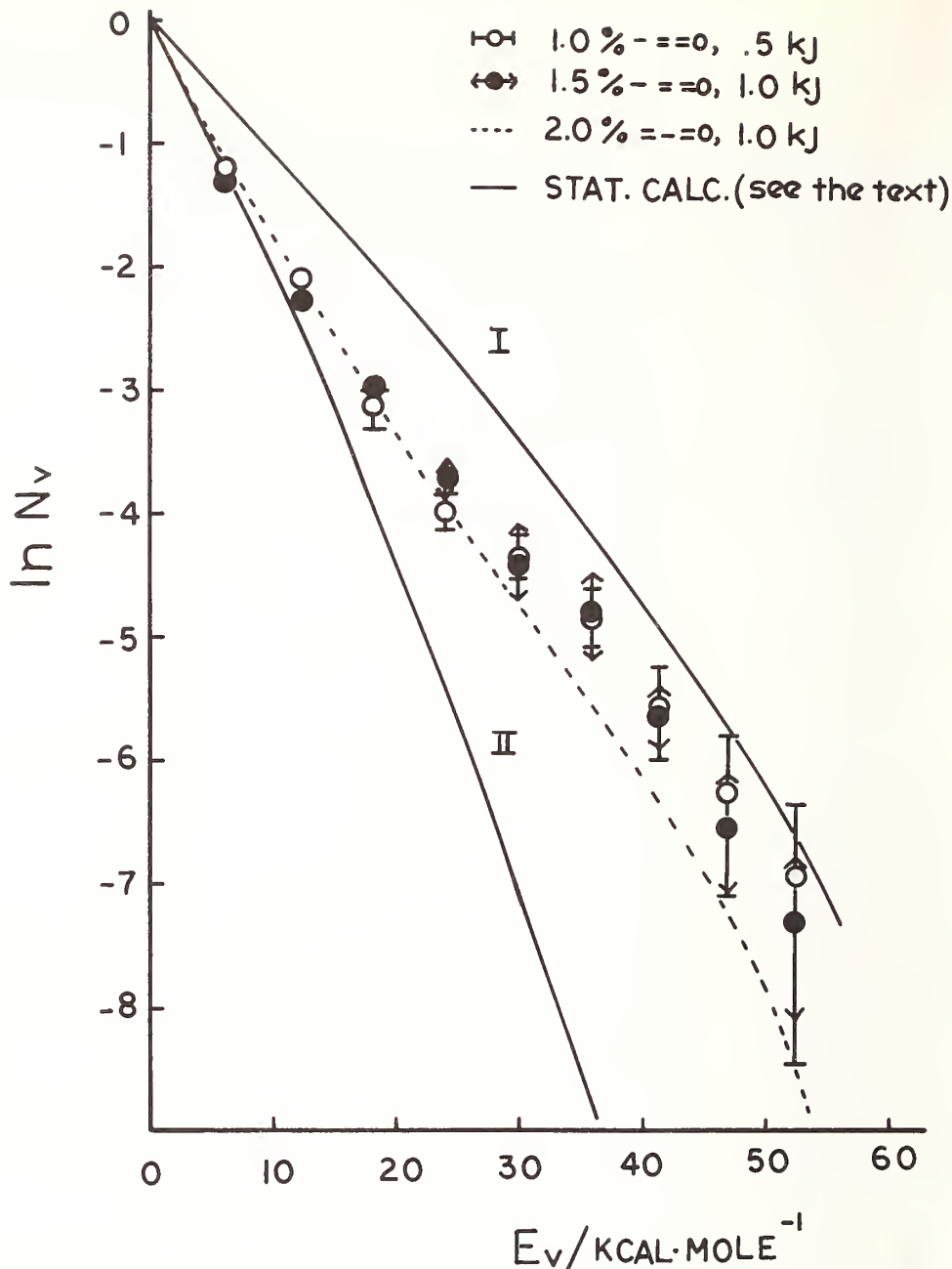


Figure 1. Vibrational energy distributions of the CO formed in the photodissociation of methylketene and acrolein.

The amount of vibrational energy channelled into CO was calculated from the expression

$$\langle E_v \rangle = \sum_{v \geq 0} f_v E_v$$

where $f_v = N_v / \sum_{v \geq 0} N_v$ is the normalized vibrational population distribution and E_v is the vibrational energy of CO at the v th level with the zero-point energy excluded. The data presented in figure 1 give rise to $E_v = 3.7 \pm 0.34$ kcal/mole, which indicates that only about 3% of the total available energy, $E_{\text{tot}} = h\nu - \Delta H_0^\circ + RT \approx 126$ kcal/mole, is carried the CO as vibrational energy.

The results obtained for methylketene are listed in the table and are compared with those obtained for the isomeric compound, acrolein [5], and the chemically activated systems, $O(^3P) + \text{propadiene}$ and propyne. In the propadiene and propyne reactions, it has been shown, based upon calculations in terms of simple statistical models, that the reaction energies have been randomized in the activated complexes before dissociation takes place [6]. Randomization of E_{tot} from the propadiene reaction in an activated cyclopropanone complex followed by its direct dissociation into CO and ethylene provided good agreement between the calculated and the experimental values of $\langle E_V \rangle$. In the case of propyne, however, an excited methylketene complex was assumed, along with its dissociation into CO and CH_3CH which subsequently isomerized to C_2H_4 . Thus the heat of isomerization of CH_3CH , $\Delta H_{\text{iso}}^\circ$ among the modes of the complex provided a calculated value for $\langle E_V \rangle$ which agreed with the experimental.

Table. Average Vibrational Energy of CO Formed in the Decomposition of Various $\text{C}_3\text{H}_4\text{O}$ Molecules#

Reaction	$\text{C}_3\text{H}_4\text{O}$	E_{tot}	$\langle E_V \rangle$
$==0$	$==0^*$	~ 126	3.7 ± 0.3
$=-0$	$=-0^*$	~ 131	$3.3 \pm .2$
$0+==$	0^+	123	$6.8 \pm .6$
	Δ		
$0+-$	$==0^+$	122	$2.3 \pm .3$

All energies in kcal/mole.

Also shown in figure 1 are the experimental CO population distribution from the photodissociation of acrolein, and calculated curves for methylketene, Curves I and II. Curve I is the distribution obtained by randomizing the full E_{tot} in the statistical model and clearly predicts too hot a CO vibrational distribution. Curve II assumes dissociation of the complex into CH_3CH and CO^+ , and thus is based upon randomization of $E_{\text{tot}} - \Delta H_{\text{iso}}^\circ$. It provides better agreement with the experimental values, but indicates that energy randomization is not complete before dissociation takes place. The results obtained from methylketene and acrolein are very similar to each other. At this time, it is not known with certainty whether this indicates that the photodissociation of both compounds proceeds *via* similar complexes, or is merely fortuitous.

References

- [1] Kistiakowsky, G. B., and Mahan, B. H., *J. Am. Chem. Soc.*, **79**, 2412 (1957).
- [2] Chong, D. P., and Kistiakowsky, G. B., *J. Phys. Chem.*, **68**, 1793 (1964).
- [3] Frey, H. M., *J. Chem. Soc.*, **1962**, 2293.
- [4] Lin, M. C., and Shortridge, R. G., *Chem. Phys. Lett.*, **29**, 42 (1974).
- [5] Shortridge, R. G., Umstead, M. E., and Lin, M. C., presented at *VIII International Conference on Photochemistry*, August 1975.
- [6] Lin, M. C., Shortridge, R. G., and Umstead, M. E., *Chem. Phys. Lett.*, **37**, 279 (1976).

THE PRODUCTION AND REACTIONS OF VIBRATIONALLY EXCITED 1,1,2,2-TETRACHLOROETHANE

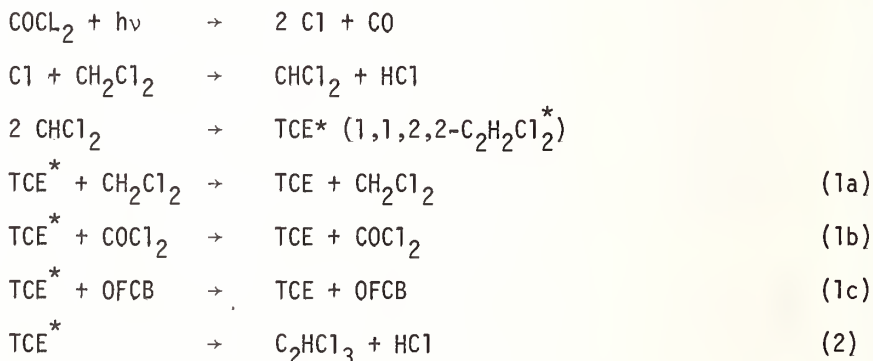
M. H. J. Wijnen

Chemistry Department, Hunter College of the
City University of New York
695 Park Avenue
New York, NY 10021

Decomposition reactions of vibrationally excited haloethanes have been investigated extensively by Setser and co-workers [1]¹ and by Pritchard [2] and co-workers. In the past vibrationally excited chloroethanes were produced by the photolysis of ketene in the presence of chlorinated methanes or by photochemical reactions of mixtures of chlorinated methanes. Both techniques yield two different radicals and thus three vibrationally excited ethanes (the direct combination and the cross-combination products of the radicals involved).

It would, of course, be advantageous to study a system in which only one type of excited molecule is produced. Such a system is provided by the photolysis of phosgene in the presence of chlorinated methanes. To illustrate this method we have studied the photolysis of phosgene in the presence of CH_2Cl_2 at various pressures and in the presence of octafluorocyclobutane (OFCB) as an inert deactivator.

The important reactions occurring in this system are given by:



As clearly shown in the mechanism only one type of vibrationally excited molecule is produced, thus simplifying the analysis and the interpretation of the results. We have carefully looked for decomposition products other than HCl elimination products. We have not observed any evidence for the occurrence of H_2 or Cl_2 eliminations from 1,1,2,2-tetrachloroethane.

¹ Figures in brackets indicate the literature references at the end of this paper.

The following experiments were carried out:

- A) COCl_2 was photolysed in the presence of CH_2Cl_2 (ratio $\text{COCl}_2/\text{CH}_2\text{Cl}_2 = 1$) at total pressure between 0.3 and 5.1 torr.
- B) COCl_2 was photolysed at a constant pressure of 0.85 torr, the pressure of CH_2Cl_2 was varied from 0.85 to 4.6 torr.
- C) COCl_2 (part. press. 0.85 torr) was photolysed in the presence of CH_2Cl_2 (0.85 torr), while the pressure of OFCB was varied from zero to 6.2 torr.

The data were plotted according to the following equations:

$$R_{\text{TCE}}/R_{\text{C}_2\text{HCl}_3} = (k_{1a} + k_{1b})/k_2 P_{\text{part.}} \quad (\text{A})$$

$$R_{\text{TCE}}/R_{\text{C}_2\text{HCl}_3} = k_{1b}(\text{COCl}_2)/k_2 + k_{1a}/k_2 \text{CH}_2\text{Cl}_2 \quad (\text{B})$$

$$R_{\text{TCE}}/R_{\text{C}_2\text{HCl}_3} = k_{1a} + k_{1b}/k_2 P_{\text{part.}} + k_{1c}/k_2 (\text{OFCB}) \quad (\text{C})$$

The plot of $R_{\text{TCE}}/R_{\text{C}_2\text{HCl}_3}$ versus the partial pressures of COCl_2 ($= \text{CH}_2\text{Cl}_2$) should give a straight line without intercept. The ratio $R_{\text{TCE}}/R_{\text{C}_2\text{HCl}_3}$ varies linearly with pressure but a small intercept is observed, indicating that perhaps some other minor reactions may play a part in the mechanism. The following quantitative data were obtained:

$$(k_{1a} + k_{1b})/k_2 = 3.8 \text{ torr}^{-1} \quad (\text{Eq. A})$$

$$k_{1a}/k_2 = .15 \text{ torr}^{-1} \quad (\text{Eq. B})$$

$$k_{1b}/k_2 = 4.1 \text{ torr}^{-1} \quad (\text{Eq. B})$$

$$(k_{1a} + k_{1b})/k_2 = 5.9 \text{ torr}^{-1} \quad (\text{Eq. C})$$

$$k_{1c}/k_2 = 2.2 \text{ torr}^{-1} \quad (\text{Eq. C})$$

It is clear that the data are quite consistent since three different plots (obtained from different series of experiments) yield a value of 3.8; 5.6 and 5.9 torr^{-1} for the sum of the deactivation steps 1a and 1b over the decomposition step 2 thus confirming the simplicity and reliability of our method. A comparison of our data with those available in the literature will be made.

References

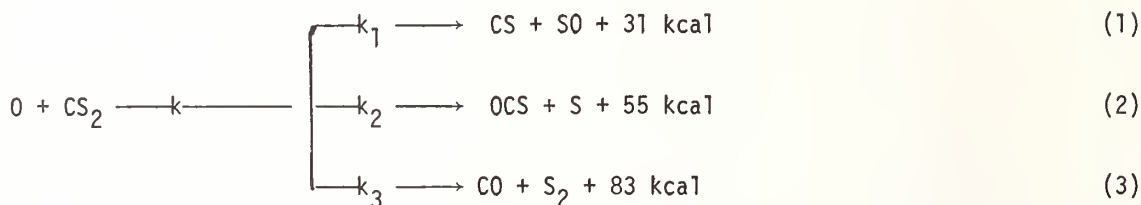
- [1] Setser, D. W., and co-workers, *J. Chem. Phys.*, 76, 283 (1972) and earlier publications.
- [2] Pritchard, G. O., et al., *J. Am. Chem. Soc.*, 90, 4782 (1968) and earlier publications.

MEASUREMENT OF BRANCHING RATIOS FOR THE $O + CS_2 \rightarrow OCS + S$ Reaction¹

Ronald E. Graham and David Gutman

Department of Chemistry
Illinois Institute of Technology
Chicago, IL 60616

The reaction between oxygen atoms and carbon disulfide has been shown to proceed by all three possible exothermic channels [1,2]²,



Highly vibrationally excited CO is also produced in this system by a rapid secondary reaction involving the CS produced in Route (1),



This vibrationally excited CO is capable of producing either pulsed and continuous laser emission in a variety of experimental arrangements. The kinetics of this system has been studied to better understand the performance of this chemical laser [3,4]. It has been shown that the products of Routes (2) and (3) can significantly effect the laser output. The OCS produced by Route (2) selectively relaxes the lower excited vibrational states of CO enhancing the laser output from higher levels and decreasing it from lower levels. The CO produced in Route (3) is itself vibrationally excited and is produced with a different vibrational population distribution than that produced in Reaction (4) [5].

Quantitative information on all three routes is still needed to better understand the factors which govern the performance of the chemical laser driven by this reaction. We report here measurements of the branching ratio for Route (2), $R_2 = k_2/k$, as a function of temperature. Slagle, Gilbert, and Gutman have measured R_2 at 302°K and found it to be 0.093 [2]. Nielsen and Bauer have used this value in their modeling study of the $CS_2 + O_2$ chemical laser and report that the OCS produced by Route (2) has a significant effect on laser output and is in fact the most important relaxer of CO^* near $v = 5$ [3]. This room temperature value of R_2 was used since there have been no determinations of this branching ratio near the laser temperatures, 400-600°K, and there is no knowledge of its temperature dependence. Because of the demonstrated importance of Route (2) in this chemical laser, we have measured R_2 at seven temperatures between 249 and 500°K.

¹The authors gratefully acknowledge support for this research from the National Science Foundation.

²Figures in brackets indicate the literature references at the end of this paper.

Oxygen atoms (produced by the $N + NO \rightarrow N_2 + O$) reaction and CS_2 were mixed in a fast flow reactor. The rate of CS_2 loss and OCS production were simultaneously monitored by mass spectrometric analyses of gas sampled through a 0.033 cm diam hole in the end of the reactor. The experimental procedure and data analysis were the same as described before. The branching ratio for Route (2) was obtained from the relation [2],

$$R_2 = k_2/k = \Delta[OCS]_t / \Delta[CS_2]_t \quad , \quad (I)$$

where $\Delta[OCS]_t$ is the concentration of OCS at time t, and $\Delta[CS_2]_t = [CS_2]_0 - [CS_2]_t$, is the decrease in $[CS_2]$ from its initial value. At each of the seven temperatures between 249 and 500°K, R_2 was measured in 6-9 experiments and found to be independent of $[O]_0$, $[CS_2]_0$, $[M]$, flow velocity, and extent of reaction. In experiments in which $[O]$ was in great excess, $[CS_2]$ vs. t profiles were used to also obtain k, the overall rate constant for the $O + CS_2$ reaction [2]. The results of these experiments are given in Table 1.

Table 1. Results of experiments to measure $O + CS_2$ rate constants and branching ratios

Temperature (°K)	$R_2 \times 10^2$ (k_2/k)	$k \times 10^{12}$ ($cm^3 molec^{-1} sec^{-1}$)
249	9.8 (± 0.4)*	2.9 (± 0.2)*
273	9.8 (± 0.5)	3.6 (± 0.3)
295	9.6 (± 0.6)	4.1 (± 0.2)
335	9.4 (± 0.5)	5.1 (± 0.6)
376	8.7 (± 0.5)	6.6 (± 0.3)
431	8.2 (± 0.1)	8.5 (± 0.6)
500	8.1 (± 0.7)	11.2 (± 0.8)

* Average of at least 6 experiments, with one standard deviation given in parenthesis. Estimated accuracy $\pm 20\%$.

The branching ratio for route (2) decreases only slightly in importance between 249 and 500°K dropping from 0.098 ± 0.004 to 0.081 ± 0.007 . The small monotonic decrease in R_2 , although statistically evident, cannot be used for lengthy extrapolations to other temperatures due to the large uncertainty of each determination (about $\pm 20\%$). We would suggest a value of $R_2 = 0.085$ as probably being most appropriate in the 400-600°K range.

The overall rate constants measured between 249 and 500°K are consistent with other determinations obtained from flow reactor studies in which $[O]$ was in excess, but lie somewhat above those from studies in which $[CS_2]$ was in excess and in which a stoichiometric factor had to be determined and used.

Calculations of "Prior" branching ratios predict lower values with virtually no temperature dependence.

References

- [1] Smith, I. W. M., *Trans. Faraday Soc.*, 64, 378 (1968).
- [2] Slagle, I. R., Gilbert, J. R., and Gutman, D., *J. Chem. Phys.*, 61, 704 (1974).
- [3] Nielsen, N., "Development of a Computer Model for the ($\text{CS}_2 + \text{O}_2$) Chemical Laser," Department of Chemistry, Cornell University, 1974.
- [4] Lilenfeld, H. V., Webbink, R. F., Jeffers, W. Q., and Kelly, J. D., "Modeling of the CW CO Chemical Laser," *I.E.E.E., J. Quantum Electr.*, in press.
- [5] Hudgens, J. W., Gleaves, J. T., and McDonald, J. D., *J. Chem. Phys.*, 64, 2528 (1976).

PHOTODISSOCIATION OF MOLECULAR BEAMS OF METALLIC IODIDES¹

M. Kawasaki, H. Litvak, S.-J. Lee and R. Bersohn

Department of Chemistry
Columbia University
New York, NY 10027

Photodissociation processes are among the most important in photochemistry, but are difficult to study by conventional absorption methods; molecular beam photofragment spectroscopy, on the other hand, has proven to be a very effective technique for elucidating photodissociation dynamics. We report here photofragment spectroscopy studies of the elementary photodissociation processes of TlI and CdI₂ at wavelengths ~300 nm. The photochemical and reaction dynamics of metallic halides have long been subjects of interest, while photodissociation of iodo-compounds is particularly relevant to the development of new laser systems.

Our apparatus has been largely described elsewhere [1]² and consists basically of mutually perpendicular molecular beam, intersecting polarized photon beam, and ultrahigh vacuum (~10⁻⁹ torr) mass spectrometer photofragment detector. The molecular beam effuses from a high temperature (~600 K) oven in a separate vacuum chamber (~10⁻⁷ torr background pressure); the photon beam is from either a Chromatix CMX-4 frequency-doubled tunable dye laser or a 1000W Hg-Xe lamp with appropriate polarizer and filters (laser polarization is controlled by means of a Fresnel rhomb 1/2 wave plate). With this apparatus, we are able to observe (1) the photofragment mass spectrum, (2) the angular distribution of recoiling fragments with respect to the electric vector of the polarized light, (3) the time-of-flight (TOF) distribution of photofragments arriving at the detector following a laser pulse, and (4) the variation of the above quantities with photon energy. From the angular distribution $f(\theta)$ one can obtain the symmetry of the dissociative transition by use of the relation

$$f(\theta) = \frac{3}{4\pi} \left\{ 1 + \beta \left[\frac{3}{2} \cos^2(\theta - \theta_0) - \frac{1}{2} \right] \right\},$$

where θ is the angle between the photon electric vector and the fragment recoil direction (which is necessarily into the mass spectrometer for detected fragments!), θ_0 is an angular offset produced by the transformation from center-of-mass (c.m.) to laboratory (lab) coordinates, and β is the anisotropy parameter (in the lab system; the anisotropy in the c.m. system is usually nearly the same [2]); for purely parallel transitions, $\beta = 2$ and $f(\theta)$ peaks at $(\theta - \theta_0) = 0^\circ$, while for purely perpendicular transitions, $\beta = -1$ and $f(\theta)$ peaks at $(\theta - \theta_0) = 90^\circ$. (This is true for *direct* dissociations, which seem to be the case in the present study; for indirect transitions, one needs to take into account the lifetime of the predissociative state [3].) From the TOF distribution, (also processed via a lab \rightarrow c.m. transformation), one can obtain the translational energy of the recoiling fragments and thus, through energy conservation, their internal excitation as well.

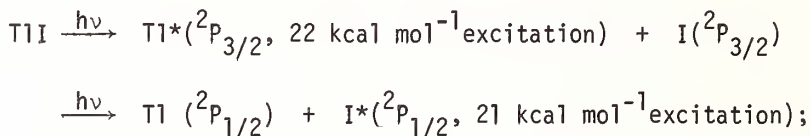
¹This work is supported by NSF grant MPS-74-22100.

²Figures in brackets indicate the literature references at the end of this paper.

Results and Discussion

1. TII

The TOF distribution of I fragments from laser dissociation at 300 nm shows that either or both of the following processes must occur:



the energy difference between these two processes is too small to resolve in our experiments. (The first process has been observed previously using Tl atomic resonance absorption [4]). There is no evidence for dissociation into two ground state atoms. The angular distribution of I fragments at ~ 310 nm obtained with the Hg-Xe lamp is nearly isotropic ($\beta = 0.07 \pm 0.02$, $\theta_0 = -6^\circ \pm 10^\circ$) and is consistent with photodissociation via two separate transitions of opposite symmetry or via a single transition of mixed (parallel plus perpendicular) symmetry, as would be the case if either (or both) the ground or excited states contains even a slight ($\sim 5\%$) mixing of ionic and covalent character [5,6].

2. CdI₂

The TOF distribution of I fragments (and to a much lesser extent of CdI fragments) from laser dissociation at 300 nm shows two partially resolved peaks having different angular distributions. The angular distribution of the slower peak has a maximum at $(\theta - \theta_0) = 0^\circ$, corresponding to a parallel transition, while the translational energy of this peak corresponds to 33 kcal mol^{-1} ($\sim 80\%$ of the total available energy) internal excitation of the fragments. The parallel symmetry of the transition suggests that the photodissociation process is $\text{CdI}_2 \xrightarrow{h\nu} \text{CdI}(X^2\Sigma) + \text{I}^*(^2\text{P}_{1/2}, 21 \text{ kcal mol}^{-1} \text{ excitation})$, the remaining 12 kcal mol^{-1} going into CdI vibration and rotation. The angular distribution of the fast peak has a maximum at $(\theta - \theta_0) = 90^\circ$, corresponding to a perpendicular transition, while only $\sim 44\%$ of the total available energy (18 kcal mol^{-1}) appears as fragment internal excitation. This is too little energy for production of I^* , and the perpendicular symmetry of the transition suggest the production of ground state I and vibrationally/rotationally excited (the full 18 kcal mol^{-1}) CdI($X^1\Sigma$). The existence of two transitions of opposite symmetry (and of unequal probabilities) is consistent with the relatively low anisotropy ($\beta = 0.46 \pm 0.08$, $\theta_0 = 30^\circ \pm 3^\circ$) observed in the I fragment angular distribution at ~ 310 nm obtained with the Hg-Xe lamp (but without TOF discrimination). Additional experiments at different photon energies are in progress.

References

- [1] Dzvonik, M. J., and Yang, S. C., *Rev. Sci. Instrum.*, **45**, 750 (1974).
- [2] Busch, G. E., and Wilson, K. R., *J. Chem. Phys.*, **56**, 3638 (1972).
- [3] Dzvonik, M., Yang, S., and Bersohn, R., *J. Chem. Phys.*, **61**, 4408 (1974).
- [4] Davidovits, P., and Bellisio, J. A., *J. Chem. Phys.*, **50**, 3560 (1969).
- [5] Ormerod, R. C., Powers, T. R., and Rose, T. L., *J. Chem. Phys.*, **60**, 5109 (1974).
- [6] Zare, R. N., and Herschbach, D. R., *J. Mole. Spectrosc.*, **15**, 462 (1965).

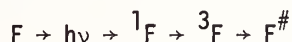
THE PHOTOCHEMISTRY OF 2-FURALDEHYDE IN THE GAS PHASE

A. Gandini, P. A. Hackett, J. M. Parsons and R. A. Back

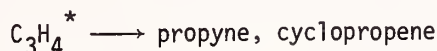
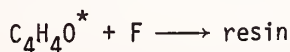
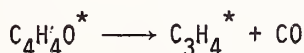
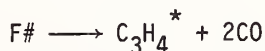
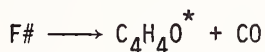
Division of Chemistry
National Research Council of Canada
Ottawa, Canada

The photochemistry and photophysics of 2-furaldehyde vapor following excitation in its first two absorption bands have been studied. Excitation in the $\pi^* \leftarrow \pi$ transition (220-275 nm) led to photodecomposition but yielded no detectable emission of light. Photolysis at 253.7 nm at 65° and furaldehyde pressures between 0.2 and 7 Torr gave CO, furan, propyne, allene and cyclopropene as major products, with acetylene and CO₂ in much smaller yields. A study of the variation in product quantum yields with furaldehyde pressure showed that ϕ_{CO} approaches 2 at low pressure and decreases towards 0 at high pressure or with added CO₂. The yields of the other major products follow a similar trend but with more complex pressure dependence, particularly in the case of furan, as shown in the figure. The mercury-photosensitized decomposition at 253.7 nm gave essentially the same results as the direct photolysis.

The mechanism invoked to explain these observations at 253.7 nm postulates the rapid initial sequence,



where 1F and 3F are the $\pi^* \leftarrow \pi$ excited singlet and triplet states, and $F^\#$ is the vibrationally excited ground state of furaldehyde, from which decomposition occurs. The reactions following this fast double intersystem crossing involve $F^\#$ and excited furan and C₃H₄ intermediates which can decompose, isomerize, polymerize, or be deactivated by collision:



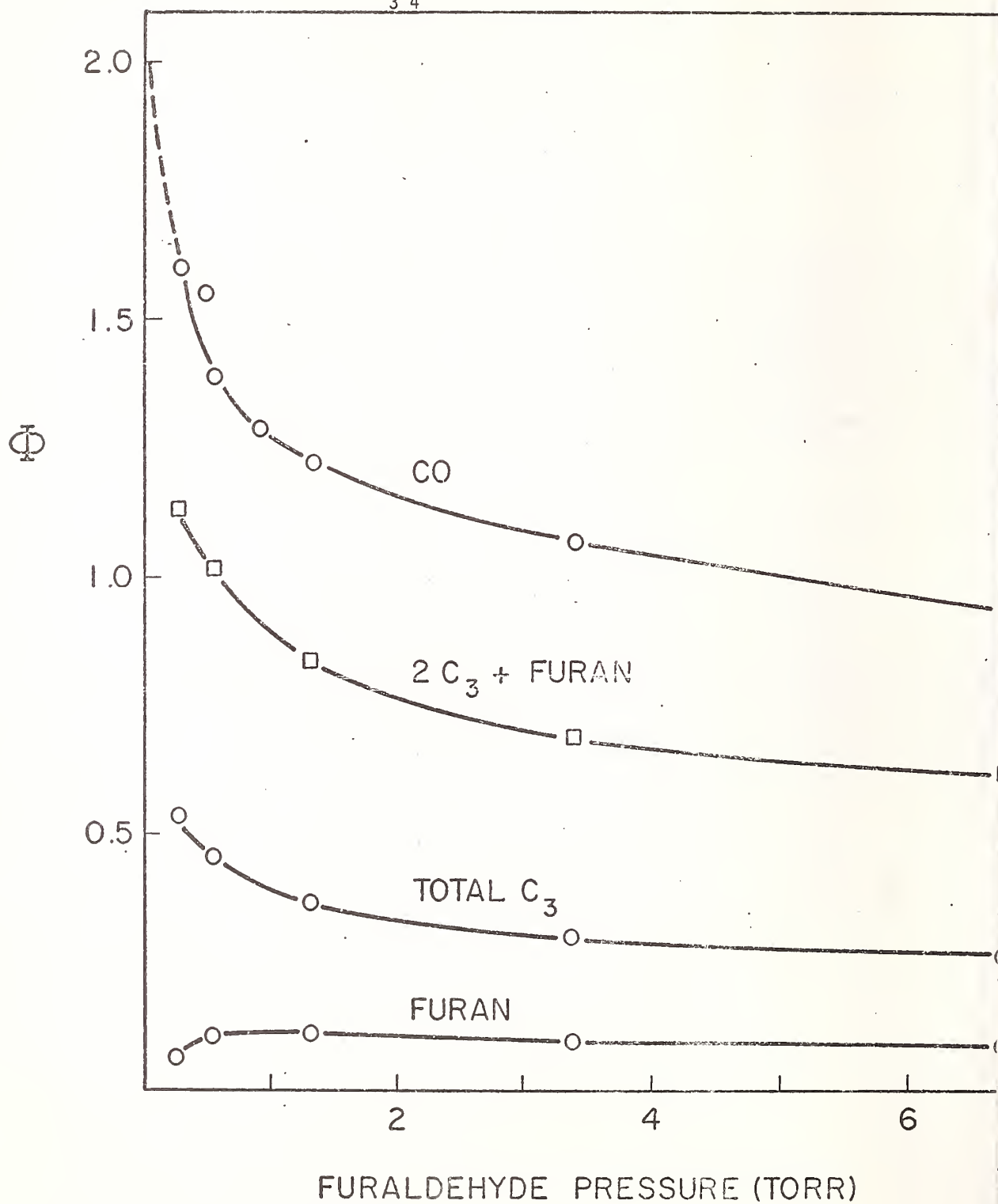
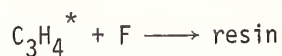
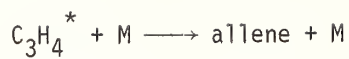
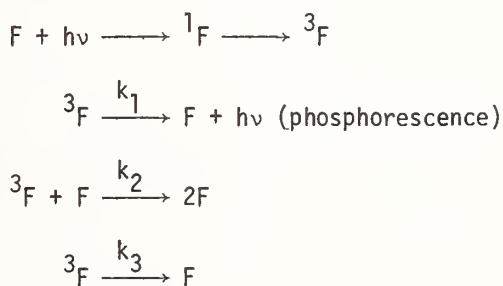


Fig. Furaldehyde pressure (torr).

It is suggested that the mercury photosensitized reaction directly populates the 3F state, which then undergoes the same reactions as in the direct photolysis. Evidence for the proposed mechanism is discussed, in particular the lack of light emission and the lack of efficient quenching by oxygen, both of which point to very short lifetimes for 1F and 3F . A comparison of the present results [1]¹ with the earlier ones obtained by Hiraoka and Srinivasan [2] show some significant differences which are tentatively explained.

The behaviour of 2-furaldehyde excited in the $\pi^* \leftarrow n$ transition (290-370 nm) is quite different. Although the products of the photolysis at 313 and 336 nm were the same as the major ones found at 253.7 nm, quantum yields were much smaller, falling in the range 10^{-2} - 10^{-3} . Resinification on the cell walls was more important, with a quantum yield of about 0.05, which made quantitative studies of the photolysis virtually impossible, particularly at the lower pressures. The large difference in the yields of decomposition from the two excited states may probably be attributed to the difference in their energies.

Photophysical experiments showed that excitation in the $\pi^* \leftarrow n$ band of furaldehyde gave no detectable fluorescence, but modest phosphorescence was observed. The dependence on pressure, temperature and excitation wavelength of both the lifetime and the quantum yield of this emission from the $\pi^* \leftarrow n$ triplet state were investigated, having established that the quantum yield of intersystem crossing is close to unity at pressures above about 0.3 Torr. The results have been interpreted in terms of the following mechanism:



where 3F and 1F are now the $\pi^* \leftarrow n$ triplet and singlet states of furaldehyde. Values of $k_1 = 1.1 \text{ s}^{-1}$, $k_2 = 6.3 \times 10^7 \text{ M}^{-1}\text{s}^{-1}$ and $k_3 = 1.2 \times 10^2 \text{ s}^{-1}$ were obtained at room temperature, and k_2 showed a negative temperature dependence. A long-lived emission from a quenching impurity present in trace amounts in all samples of furaldehyde tested was also observed. This was minimized by rigorous purification and was taken into account in the treatment of the phosphorescence results.

References

- [1] Gandini, A., Hackett, P. A., Parsons, J. M., and Back, R. A., *Can. J. Chem.*, in press.
- [2] Hiraoka, H., and Srinivasan, R., *J. Chem. Phys.*, 48, 2185 (1968).

¹Figures in brackets indicate the literature references at the end of this paper.

PHOTOINITIATED DECOMPOSITION OF MONOSILANE

E. R. Austin and F. W. Lampe
The Pennsylvania State University
University Park, PA 16802

A mass-spectrometric study of the hydrogen-atom initiated decomposition of monosilane has been carried out. Silyl radicals were generated by mercury photosensitization of hydrogen-monosilane mixtures which consisted of about 95% hydrogen. Under these conditions more than 94% of the $\text{Hg}(^3\text{P}_1)$ atoms that are quenched by collision react with hydrogen to form hydrogen atoms and all the hydrogen atoms formed react with monosilane via (1) to form silyl radicals [1,2]¹. Our attention is centered on the further reactions of the silyl radicals.



The reactions were carried out in a photolysis cell containing a pin-hole leak leading into the ionization region of a time-of-flight mass spectrometer. In the photolysis of such a flow system the concentrations of all substances will approach steady-states that are reached when the rates of introduction into the cell become equal to rates of loss from the cell.

Illumination of the photolysis cell containing the H_2 - SiH_4 mixture with 2537 Å radiation results mainly in the formation of Si_2H_6 and depletion of SiH_4 . Small amounts of Si_3H_8 and Si_4H_{10} appear after long illumination times. In addition to the volatile products a solid film is deposited on the walls and quartz window of the cell.

In figure 1 is shown the time dependence of the concentrations of SiH_4 and Si_2H_6 (both relative to the initial concentration of SiH_4) for two cells, one with a pyrex wall and one with a stainless steel wall. For irradiation times greater than 50 seconds the behavior in the two cells is different. However, the initial slopes of both the depletion of SiH_4 and the formation of Si_2H_6 are independent of the cell wall. When the stainless steel cell was packed with quartz wool, identical results for the initial slopes were obtained. A fourth cell prepared by presilanation of the pyrex wall with $(\text{CH}_3)_2\text{SiCl}_2$ gave completely different results; the depletion rate of SiH_4 was reduced by a factor of 2, while the formation rate of Si_2H_6 was decreased by a factor of 7.

These data indicate that in a clean cell, with walls which do not contain adsorbed silanes, the *initial* rates of depletion of SiH_4 and formation of Si_2H_6 are independent of the nature and area of the surface. The ratio of the initial rate of depletion of SiH_4 to the initial rate of formation of Si_2H_6 is 2 as the simple stoichiometry of (2) requires.



When the cell walls are silanated, most of the SiH_4 consumed does not produce Si_2H_6 or any other volatile produce but results in an increased formation of film on the walls of the cell

¹ Figures in brackets indicate the literature references at the end of this paper.

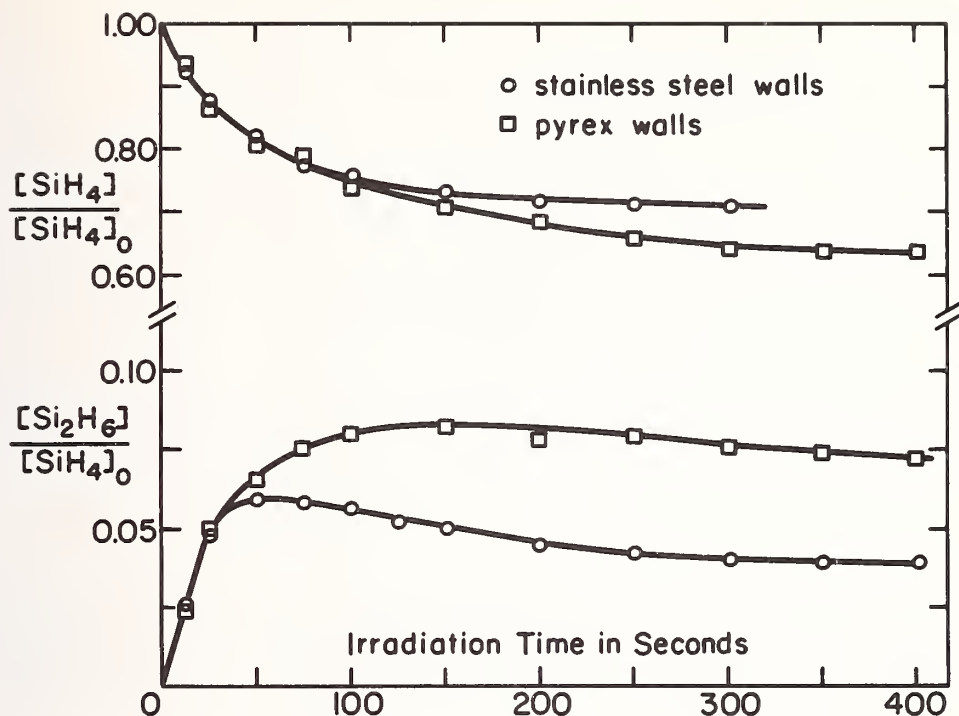


Figure 1. Depletion of SiH_4 and formation of Si_2H_6 during photolysis.

The protium-deuterium isotopic composition of the disilane formed by the $\text{Hg}(^3\text{P}_1)$ photosensitized reaction in a (96:2:2) H_2 - SiH_4 - SiD_4 mixture has been studied. The method used was to determine the mass spectra of the 56-68 region at a series of ionizing electron energies near the ionization potential of Si_2H_6 . Ion-currents of all parent ions and of m/e 60 relative to the ion current at m/e 68 were plotted as a function of nominal electron energy. A linear extrapolation of the i_{60}/i_{68} ratio yields a nominal electron energy of 11.0 eV for the disappearance of all fragment ions from the spectrum. The relative amounts of the various deuterated disilanes are given by extrapolating each of the plots in figure 2 to 11.0 eV and making isotope corrections. These results are shown below.

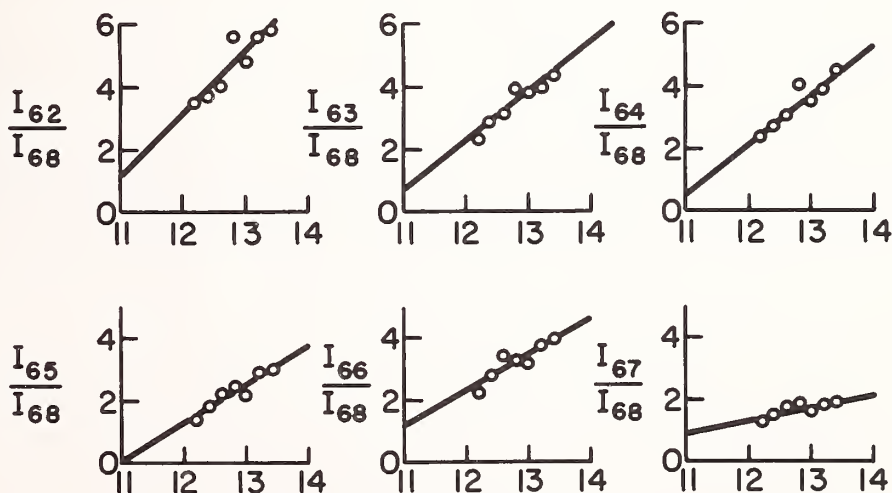


Figure 2. Ion current ratios versus nominal electron energy.

²⁸Si-Mass Spectrum of Disilane Products at 11 eV

m/e	Ion	Relative Abundance
62	Si ₂ H ₆ ⁺	90 ± 26
63	Si ₂ H ₅ D ⁺	43 ± 11
64	Si ₂ H ₄ D ₂ ⁺	37 ± 15
65	Si ₂ H ₃ D ₃ ⁺	3 ± 13
66	Si ₂ H ₂ D ₄ ⁺	100 ± 16
67	Si ₂ HD ₅ ⁺	66 ± 11
68	Si ₂ D ₆ ⁺	74 ± 16

It is clear that Si₂H₃D₃ is virtually absent. This is in agreement with the proposal of Strausz et al [3] that association of silyl radicals does not occur and that the formation of disilane occurs by the sequence (3) and (4). The distribution of disilanes suggests that the H-atom



attacks SiH₄ to form SiH₃ radicals about twice as fast as it attacks SiD₄ to form SiD₄ to form SiD₃ radicals. This is in accord with the corresponding rate constant ratio of 2-2.5 as reported by Potzinger et al [4].

References

- [1] Potzinger, P., Glasgow, L. C., and Reimann, B., *Z. Naturforsch.*, **29a**, 493 (1974).
- [2] Mihelcic, D., Potzinger, P., and Schindler, R. N., *Ber. Bunsenges. Phys. Chem.*, **78**, 82 (1974).
- [3] Pollack, T. L., Sandhu, H. S., Jodhan, A., and Strausz, O. P., *J. Am. Chem. Soc.*, **95**, 1017 (1973).
- [4] Laupert, R., Potzinger, P., Mihelcic, D., and Schubert, V., to be published in *J. Phys. Chem.*

EXCITATION OF HNO BY $O_2(^1\Delta_g)$

T. Ishiwata, H. Akimoto¹ and I. Tanaka

Department of Chemistry
Tokyo Institute of Technology
Ohokayama, Meguroku, Tokyo, Japan

In the discharge flow experiment, the chemiluminescence of HNO (fig. 1) was observed when NO and C_2H_4 were introduced successively to active oxygen containing O atoms and $O_2(^1\Delta_g)$. A further experiment indicated that an addition of $O_2(^1\Delta_g)$ to the reaction

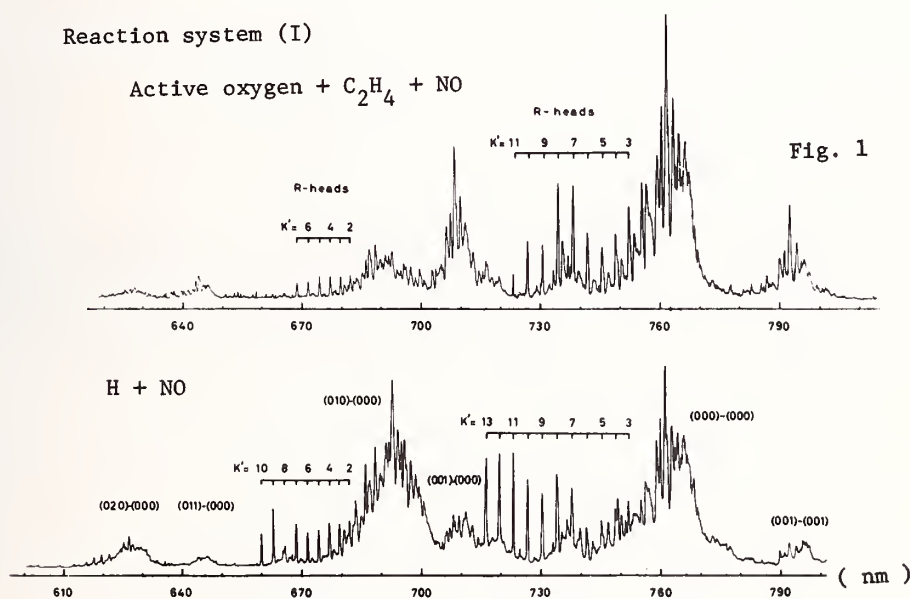


Figure 1.

of $H + NO$ resulted in a remarkable increase of the HNO emission intensity and a change of the spectral profile (fig. 2). The emission spectra of HNO obtained from the reaction systems of (I) $O + C_2H_4 + NO + O_2(^1\Delta_g)/O_2$ and (II) $H + NO + O_2(^1\Delta_g)/O_2$ showed a similar spectral profile, but, had quite different vibrational and rotational distribution features in the upper state from that observed in the reaction system of $H + NO$.

¹ National Institute for Environmental Studies.

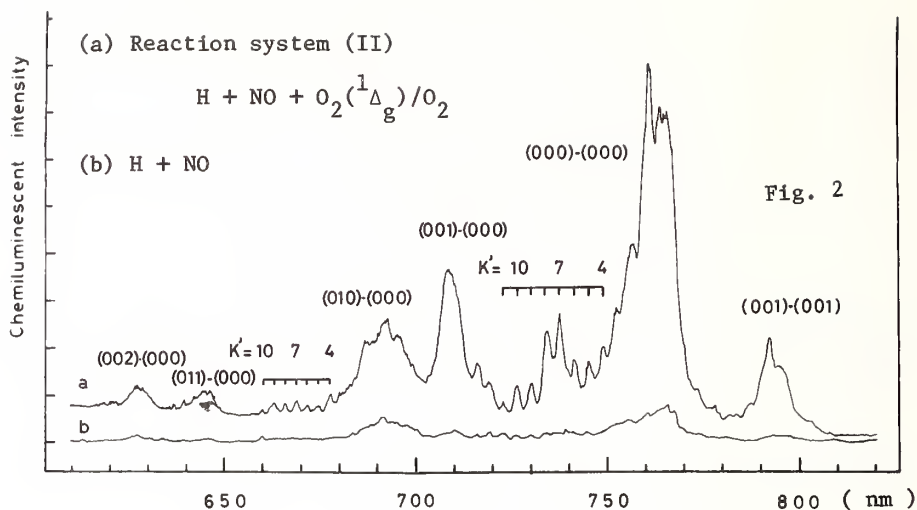


Figure 2

The spectra in the reaction systems of (I) and (II) denoted that the sudden intensity decrease of the chemiluminescence intensity at 42 kcal mol^{-1} on the rotational levels of $K' = 9$ at (000)-(000) and the lower K' levels of (010)-(000) bands (fig. 3). In the reaction system (I) the R-head of the $K' = 8$ of (010)-(000) band corresponding the energy of 45 kcal mol^{-1} was hardly discernible. However, for the same band of HNO a series of band heads was observed up to the R-head of the $K' = 10$ subband in the reaction system (II).

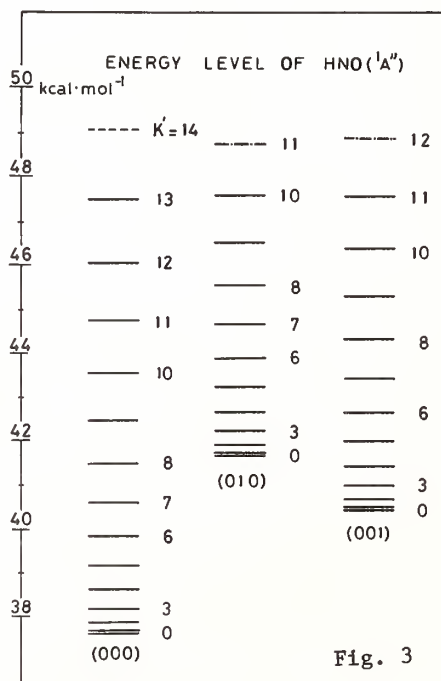


Figure 3

It can be noted that $O_2(^1\Delta_g)$ played a predominant role in producing the HNO in the upper state and the chemiluminescent intensity dependence on the $O_2(^1\Delta_g)$ flow rate was proportional to the power of $1.7 \sim 2.0$ and $0.8 \sim 1.3$ on the $O_2(^1\Delta_g)$ flow rate in the reaction systems (I) and (II), respectively (figs. 4 and 5).

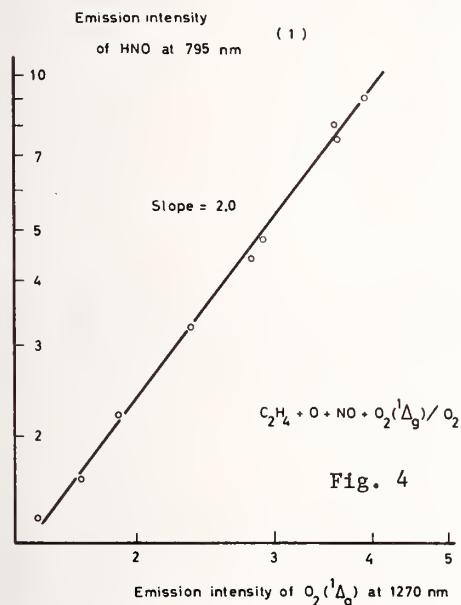


Figure 4

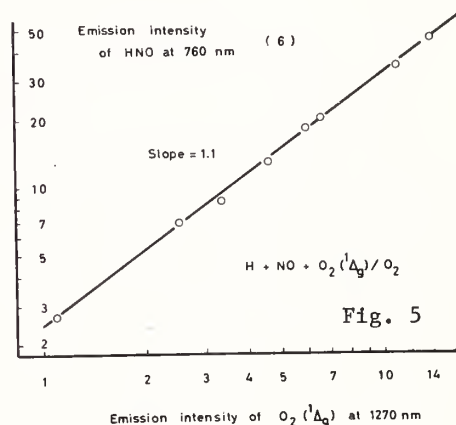
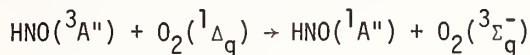
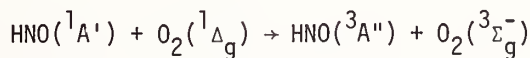


Figure 5

Thus the excitation mechanism of HNO in the reaction system (I) was proposed to be



The internal relaxation in the triplet state of HNO would be responsible to the intensity alternation at 42 kcal mol^{-1} in the chemiluminescent spectra. In the reaction system (I) the formation of the highest rotational level with $K' = 7$ of (010) would due to the two step energy transfer processes without relaxation in the triplet state, since two $O_2(^1\Delta_g)$ molecules possess the energy of 45 kcal mol^{-1} .

In the reaction system (II), the spectral information and the nearly first order dependency of $O_2(^1\Delta_g)$ differed from the reaction system (I) probably indicates the direct formation of HNO in the triplet state from the reaction of $H + NO$ and the followed excitation step by $O_2(^1\Delta_g)$.

This stepwise mechanism suggests the triplet state energy of HNO at 0.8 eV above the ground state. Recent theoretical values are presented in table together with our value.

Table

State	calc. (eV)			exptl. (eV)	
	a	b	c	d	e
$1A'$	0.0	0.0	0.0	0.0	0.0
$3A''$	0.73	0.68	0.71	0.8	---
$1A''$	1.45	2.04	1.61	---	1.63

References

- [1] Salloto, A. W., et al., *J. Chem. Phys.*, 52, 2936 (1970).
- [2] Williams, G. R., *Chem. Phys. Lett.*, 30, 495 (1975).
- [3] Wu, A. A., et al., *Chem. Phys. Lett.*, 35, 316 (1975).
- [4] Our value, *Chem. Phys. Lett.*, 27, 260 (1974).
- [5] Clement, M. J. Y., et al., *Can. J. Phys.*, 39, 205 (1961).

SOLAR PHOTODISSOCIATION RATES FOR ClONO_2 ; AN ESTIMATE OF CURRENT LEVELS OF ClONO_2 IN THE STRATOSPHERE

J. P. Jesson, L. C. Glasgow and P. Meakin
Central Research and Development Department
E. I. du Pont de Nemours and Company
Experimental Station
Wilmington, DE 19898

Rowland et al [1]¹ have suggested that chlorine nitrate may act as a temporary chlorine sink in the mid-stratosphere in addition to the well established temporary sink hydrochloric acid. Chlorine nitrate is formed in the three body reaction (1)



so that both odd chlorine (ClO) and odd nitrogen (NO_2) are converted into a less reactive form. The rate of (1) has been measured by several workers and is ca. $1.5 \times 10^{-31} \text{cm}^6 \text{molecule}^{-2} \text{sec}^{-1}$ at 300 °K [2,3,4,5], Birks [2] gives the temperature expression as $k_5 = 4.0 \times 10^{-33} \exp(1066/T)$. ClONO_2 could be decomposed by photolysis or by chemical reaction. Preliminary investigations [6,7] of the rates of reaction of ClONO_2 with O, OH, O_3 , NO, NO_2 , HCl and H_2O indicate that these are too slow to compete with photolysis. We report here our measurements of the ClONO_2 absorption cross-section and calculated solar photodissociation rates assuming a quantum yield of one. A vertical profile for ClONO_2 is calculated using a one-dimensional model of atmospheric chemistry and transport.

Experimental

ClONO_2 was prepared by the low temperature reaction of Cl_2O with N_2O_5 in an atmosphere of ozonized oxygen [8]. Excess N_2O_5 was used to insure complete reaction of Cl_2O . Undesired side products Cl_2 and NO_2 were removed by distillations at -119° (ethyl bromide slush) and -78°C, respectively.

Cl_2O was prepared by passing Cl_2 through a column packed with HgO on glass beads [9].

N_2O_5 was made by dehydration of nitric acid with P_2O_5 ¹⁰.

Samples were transferred into 10 cm quartz cells on a greaseless vacuum system and spectra recorded on a Cary 14 spectrophotometer.

Absorption Spectrum of ClONO_2

Figure 1 shows the absorption cross-section of chlorine nitrate as a function of wavelength. Each point is the average of at least three determinations at various pressures. At wavelengths longer than 350 nm, a correction for traces of NO_2 in the sample was applied. The residual NO_2 was calculated from the absorbance at 500 nm using the data of Blacet and Hall [11]. No samples completely free of NO_2 were produced although levels of less than 0.1% NO_2 could be achieved by repetitive distillations at -65° (chloroform slush). Even

¹Figures in brackets indicate the literature references at the end of this paper.

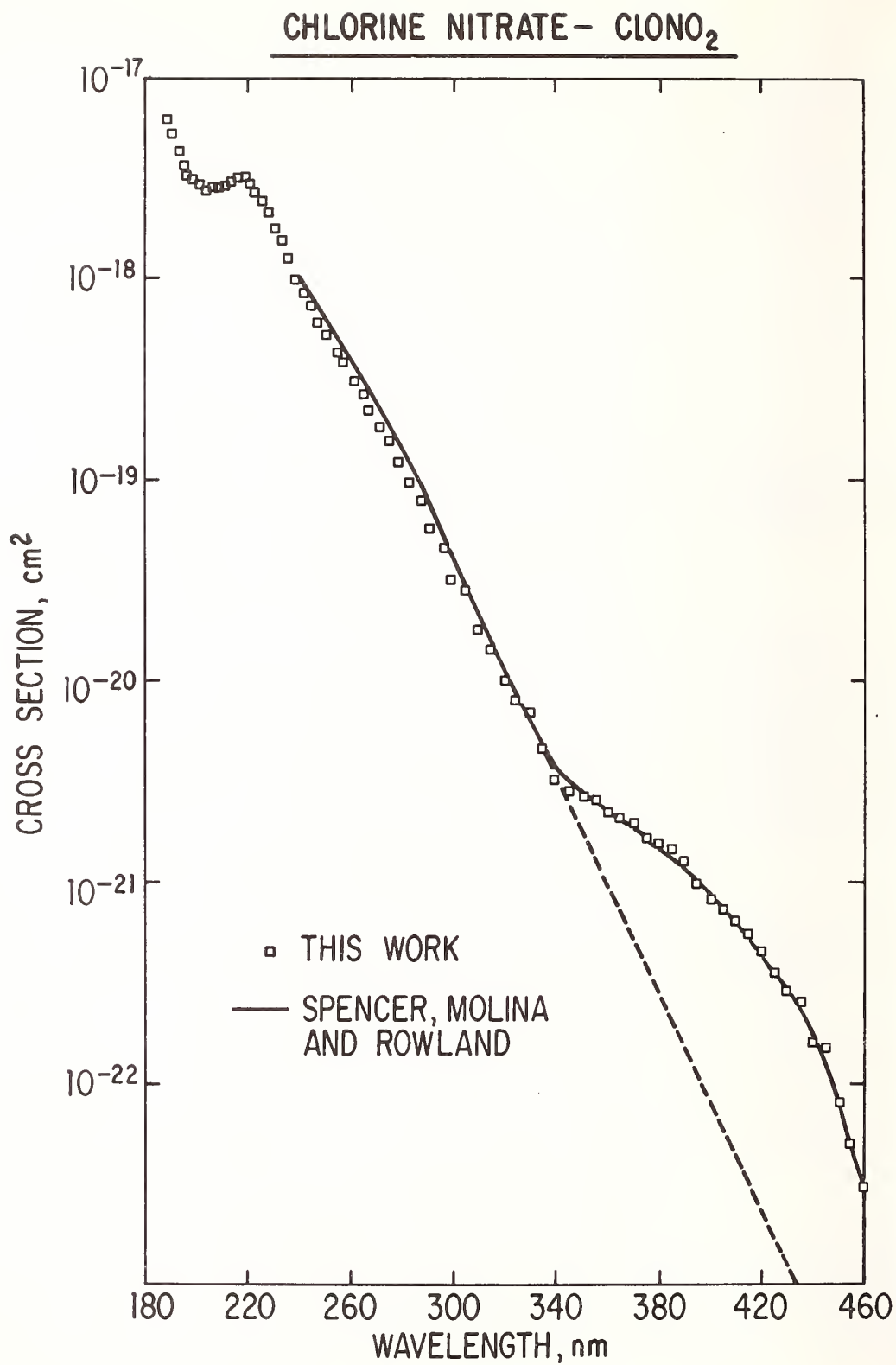


Figure 1

with repetitive distillations and correcting for residual NO₂, there is an apparent absorption tail in the 250-450 nm region. Pressures of 0.2-1.0 atm of ClONO₂ were required to make measurements in this spectral region. The possibility that the tail is due to absorption by a species other than ClONO₂ cannot be excluded.

The absorption cross-section data are in excellent agreement with the revised data of Rowland et al [12].

Solar Photodissociation Rates

Table 1 shows solar photodissociation rates as a function of altitude (J_z) calculated assuming a quantum yield of 1.0 for reaction (2)



The tables of Gelinass were used to calculate the penetration of solar radiation at each altitude considering absorption by O₂ and O₃ only. The O₂ profile was obtained from U.S. Standard Atmosphere 1962 assuming a mixing ratio of 0.2095. The O₃ profile was obtained from an experimental mid-latitude model (Report of Task Group V U.S. Committee on Extension to the Standard Atmosphere). These rates are globally averaged according to the equation:

$$J(z) = \frac{\int_0^{\pi/2} J(\theta,z) \sin \theta \, d\theta}{2 \int_0^{\pi/2} \sin \theta \, d\theta} \tag{7}$$

The inclusion of the tail absorption increases J_z by 16-50% in the critical 35-20 km region. For comparison, J_z calculated using the data of Spencer et al [12] is also included.

Table 1. Calculated photodissociation cross sections for ClONO₂

Comparison of calculated global ave photodissociation rates (x10⁵ sec) for ClONO₂

Altitude	Original Rowland	Revised Rowland	This Work	This work without long λ absorption
10.5	1.62	2.92	2.91	1.77
15.5	1.70	3.00	2.99	1.85
20.5	1.91	3.22	3.20	2.05
25.5	2.45	3.78	3.69	2.55
30.5	3.83	5.26	4.91	3.76
35.5	7.32	8.84	7.89	6.75
40.5	15.6	16.6	14.6	13.4
45.5	30.0	29.3	25.5	24.3
50.5	44.3	41.7	36.2	35.0

Table 2 shows the variation in photodissociation rate with solar zenith angle and altitude. Note that ClONO₂ is strongly photodissociated above 30 km and cannot account for the decreasing mixing ratio of HCl with increasing altitude [13].

Table 2. Calculated photodissociation cross sections for ClONO₂
ClONO₂ Photodissociation Rates (x10⁵ sec)

Altitude, kms	Zenith Angle						Global Ave.
	0	15	30	45	60	75	
10.5	7.09	7.03	6.85	6.54	6.05	5.26	2.92
15.5	7.32	7.26	7.07	6.74	6.23	5.41	3.00
20.0	7.99	7.91	7.66	7.26	6.68	5.76	3.22
25.5	10.2	10.1	9.50	8.67	7.68	6.50	3.78
30.5	16.5	16.1	14.8	12.9	10.4	7.78	5.26
35.5	29.7	28.9	26.9	23.2	17.9	11.3	8.84
40.5	53.9	52.9	49.8	44.3	35.6	22.3	16.6
45.5	83.8	83.0	80.4	75.1	65.3	46.1	29.3
50.5	102.5	102.0	100.1	98.1	92.4	77.6	41.7

Estimation of the Present Day Concentration Profile for Chlorine Nitrate in the Atmosphere

Atmospheric concentrations have been estimated for ClONO₂ between 0 and 60 km using a one-dimensional model of atmospheric transport and photochemistry. The reaction set and reaction rate coefficients defining the H, C, O, N chemistry were taken from Wuebbles and Chang [14] and were supplemented by the appropriate "chlorine" reactions. For the reaction



the rate expression of Anastasi et al [15]

$$2.3 \times 10^{-13} e^{880/T} \left(\frac{[\text{M}]}{2.6 \times 10^{18} + [\text{M}]} \right) \text{ cm}^3 \text{ molecule}^{-1} \text{ sec}^{-1}$$

was assumed. The rate constant for reaction (5)



was taken as $2 \times 10^{-11} \text{ cm}^3 \text{ molecule}^{-1} \text{ sec}^{-1}$ as recommended by Kaufmann [16].

The tables of Gelinas [17] were used to calculate most of the photodissociation rates as a function of altitude. The rate of photolysis of ClONO_2 was calculated including the tail absorption between 350 and 450 nm, assuming a quantum yield of 1.

The eddy diffusion model of Hunten [18] multiplied by 1.5 at all altitudes was used to simulate vertical transport in the model. Additional details concerning the model will be published at a future date [19].

CALCULATED PRESENT DAY ODD CHLORINE
MIXING RATIO PROFILES (WITH ClONO_2)

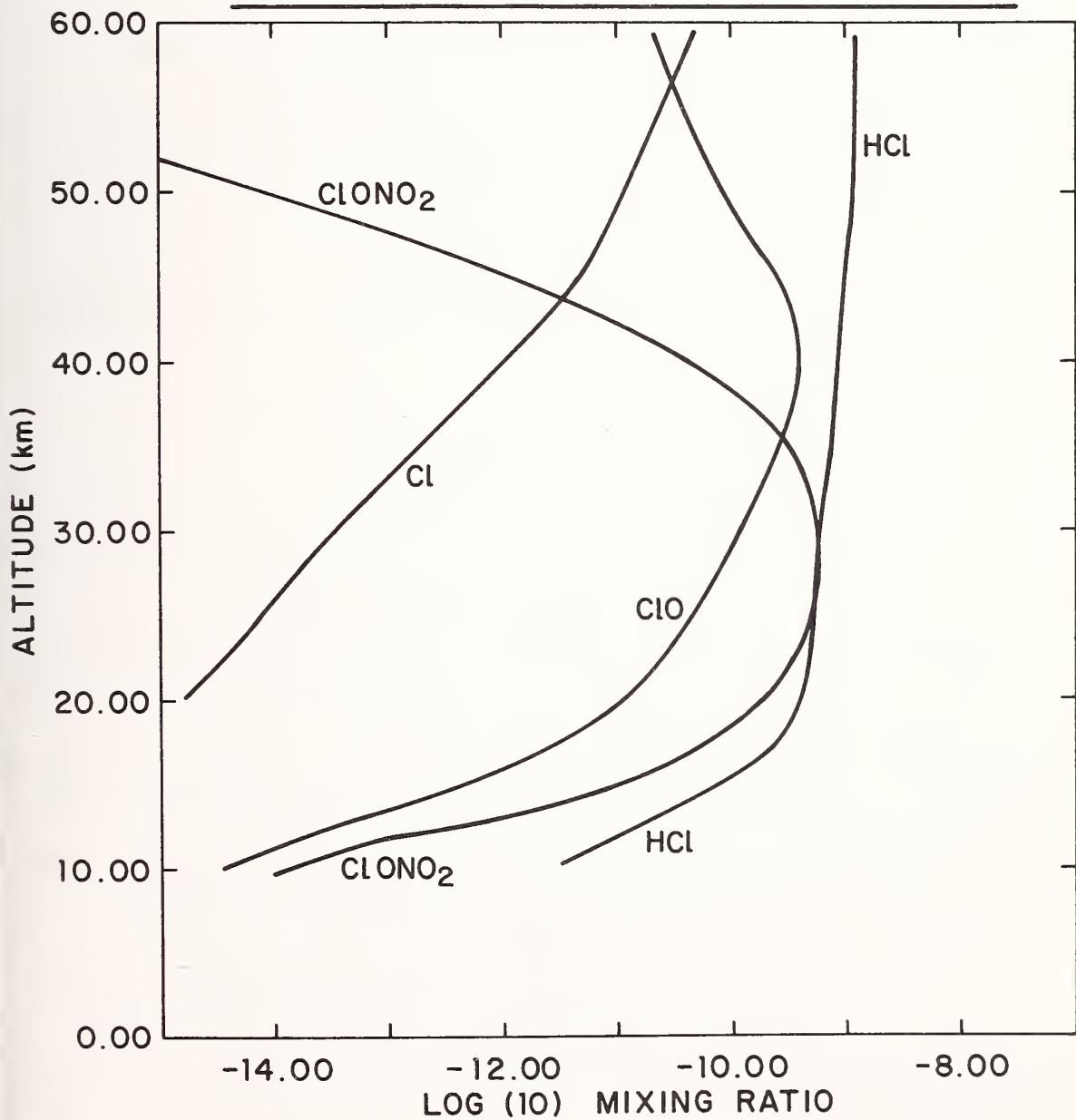


Figure 2.

The calculated present day mixing ratio profiles for the members of the odd chlorine family are shown in figure 2. This calculation includes only the contributions from CF_2Cl_2 , CFCl_3 , CCl_4 , CH_3Cl and CH_3CCl_3 . Accurate time dependent fluxes calculated from release data [20] were used as the lower boundary conditions for CFCl_3 and CF_2Cl_2 . For CH_3CCl_3 the lower boundary flux was calculated from an estimate of total world release based on U.S. production data [21]. Both CCl_4 and CH_3Cl were assumed to be at steady state with constant mixing ratios of 100 ppt and 750 ppt, respectively, at the lower boundary [22,23].

A maximum ClONO_2 concentration of $\sim 4 - 5 \times 10^8$ molecules cm^{-3} is calculated near 25 km with a total vertical column density of $5 - 6 \times 10^{14}$ molecules cm^{-2} . Globally averaged photodissociation rates were used in this calculation. Since the photochemical lifetime of ClONO_2 is of the order of a few hours, it is clear that diurnal calculations will be required if meaningful comparisons are to be made between observed and calculated ClONO_2 concentrations at a particular time and place. However, we do not expect that the results of a diurnal calculation will vary substantially from those given above.

References

- [1] Rowland, F. S., Spencer, J. E., and Molina, M. J., presented at *Meeting of NASA Advisory Committee on Stratospheric Research*, JPL, Pasadena, March 1976.
- [2] Birks, J., presented at *12th Informal Conf. on Photochemistry*, Gaithersburg, MD, 1976.
- [3] Kaufman, presented at *12th Informal Conf. on Photochemistry*, Gaithersburg, MD, 1976.
- [4] Leu, M., and DeMore, W. B., personal communication, 1976.
- [5] Young, R. A., and Glasgow, L. C., unpublished results, 1976.
- [6] Ravishankara, A. R., Smith, G., Tesi, G., and Davis, D. D., presented at *12 Informal Conference on Photochemistry*, Gaithersburg, MD, 1976.
- [7] Birks, J., personal communication.
- [8] Schmeisser, M., *Inorganic Synthesis*, Volume IX, p. 127 (1967).
- [9] Cady, G. H., *Inorganic Synthesis*, Vol. V, p. 156 (1957).
- [10] Gruenhut, N. S., Goldfrank, M., Cushing, M. L., and Caesar, G. V., *Inorganic Synthesis*, Vol. III, p. 78 (1950).
- [11] Hall, T. C., and Blacet, F. E., *J. Chem. Phys.*, 20, 1745 (1952).
- [12] Spencer, J. E., Molina, M. J., and Rowland, F. S., presented at *12th Informal Conf. on Photochemistry*, Gaithersburg, MD, 1976.
- [13] Lazrus, A. L., Gandrud, B. W., Woodward, R. N., and Sedlacek, W. A., presented at *NASA Advisory Committee Meeting*, JPL, Pasadena, 1976.
- [14] Wuebbles, D. J., and Chang, J. S., Lawrence Livermore Laboratory Preprint UCRL-75602 (Rev. 1).
- [15] Anastasi, C., Bemand, P. P., and Smith, I. W. M., *Chem. Phys. Lett.*, 37, 370 (1976).
- [16] Kaufman, F., in "Atmospheres of the Earth and the Planets," B. M. McCormac, ed., p. 219-232, D. Reidel Publishing Co., Dordrecht, 1975.
- [17] Gelinas, R. J., Lawrence Livermore Laboratory Preprint, UCRL-74944 (Change 4), 1974.
- [18] Johnston, H. S., Kattenhom, D., and Whitten, G., *J. Geophys. Res.*, 81, 368 (1976).
- [19] Meakin, P. Z., Franks, R. G. E., Hirsch, R. G., Glasgow, L. C., and Jesson, J. P., to be published.

- [20] Bower, F. A., McCarthy, R. L., and Jesson, J. P., preprint, submitted to *Atmos. Env.*, (1976).
- [21] McCarthy, R. L., presented by F. A. Bower at the *Fall Annual AGU Meeting*, San Francisco, 1974.
- [22] Cox, R. A., Derwent, R. G., Eggleton, A. E. J., and Lovelock, J. E., *Atmos. Env.*, 10, 305 (1976).
- [23] Lovelock, J. E., *Nature*, 252, 292 (1974).

THE TROPOSPHERIC LIFETIME OF CFC1_3

J. P. Jesson, P. Meakin and L. C. Glasgow

Central Research and Development Department
E. I. du Pont de Nemours and Company
Experimental Station
Wilmington, DE 19898

Current models used to predict the effects of CFC1_3 and CF_2Cl_2 on stratospheric ozone assume an infinite lifetime for these compounds in the troposphere [1,2]¹. However, an empirical comparison of the known [3] production and release of CFC1_3 with expected atmospheric concentrations calculated for a range of assumed tropospheric lifetimes indicates that the most probable lifetime for slow eddy diffusion models is 15-20 years.

Most CFC1_3 is produced and released in the northern mid-latitudes. Hence, a critical step in converting measured atmospheric concentrations into true global averages involves correcting for the fact that the troposphere is not "well mixed" with respect to CFC1_3 . Lovelock [4] has made an extensive set of CFC1_3 measurements on a cruise from 65°N to 60°S latitude and back in 1971-1972. These data can be used to derive a set of scaling factors for converting a measurement made at a particular latitude into a global average. The scale factor is simply the ratio of Lovelock's measured CFC1_3 concentration at a given latitude to the calculated global average (49.8 ppt, obtained by taking the $\cos \theta$ weighted average of Lovelock's data, where θ is the latitude). It should be noted that over 50 data sets are involved and that, since the correction involves a ratio, it is not sensitive to detector calibration.

Figure 1 shows the time dependence of the tropospheric concentration of CFC1_3 as a function of tropospheric lifetime calculated using a one-dimensional model [5] for transport and removal processes, assuming Hunten's [6] eddy diffusion model. The Points (Δ) in figure 4 represent the latitude corrected results of continuous CCl_3F monitoring at Bowerchalk and Adgrigole for a period of five years [7]. The round circles (o) are southern hemisphere data [7] scaled with the appropriate factor. The two lines of experimental data are in remarkable agreement and indicate a tropospheric lifetime of 15-20 years. All of the data analyzed were obtained with the same electron capture GC detector and are considered to be both consistent and free from systematic error [7]. The possibility of an absolute calibration error will be easy to assess at a later date its absolute standards are established. It would then be a simple matter to revise the overall conclusions reached in the present paper. However, since the data obtained by other groups (Washington State University and Stanford Research Institute) leads to similar conclusions, significant revision due to calibration changes are unlikely.

Faster diffusion profiles would lead to longer calculated tropospheric lifetimes. Thus, the Crutzen II profile [8] gives a tropospheric lifetime of about 50 years.

If values of CF_2Cl_2 concentrations of 207 ppt for Washington in the fall of 1975 are correct [9], the lifetime for CF_2Cl_2 must be similar to that of CFC1_3 .

This analysis does not attempt to distinguish specific sink mechanisms for halo-carbons. Possibilities for such removal mechanisms include: trapping at the poles, photolysis at wavelengths longer than 290 nm, heterogeneous processes, ion molecule reactions and destruction by atmospheric discharges.

¹ Figures in brackets indicate the literature references at the end of this paper.

F-11 1966-1975 EDDY 3 (HUNTEN) 85% RELEASE

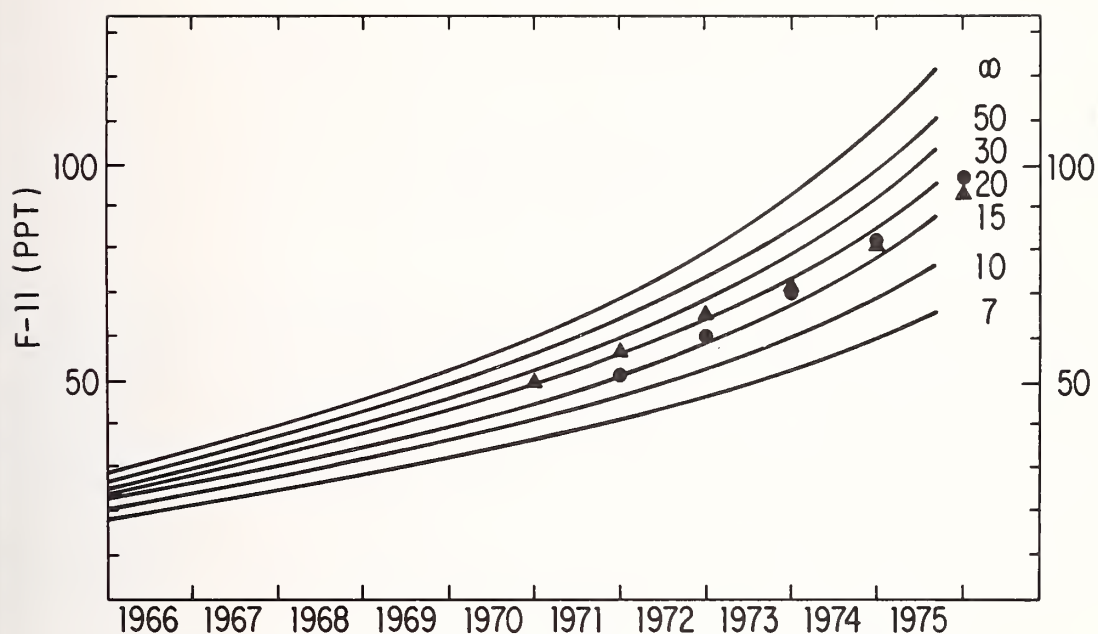


Figure 1. A comparison of CCl_3 mixing ratios in the troposphere calculated for tropospheric lifetimes of ∞ , 50, 30, 20, 15, 10, and 7 years with the measurements of Lovelock.
 Δ Data from exponential least squares fit to all Bowerchalke and Adrigole data (51°N) adjusted for latitude. \circ Southern hemisphere data adjusted for latitude.

References

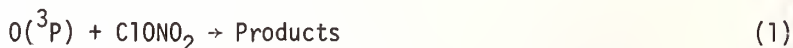
- [1] Molina, M. J., and Rowland, F. S., *Nature*, 249, 810 (1974).
- [2] Wofsy, S. C., McElroy, M. B., and Sze, N. D., *Science*, 187, 535 (1975).
- [3] McCarthy, R. L., Bower, F. A., and Jesson, J. P., to be published.
- [4] Lovelock, J. E., Maggs, R. J., and Wade, R. J., *Nature*, 241, 194 (1973).
- [5] Jesson, J. P., Gumerman, P. S., Glasgow, L. C., and Meakin, P., to be published.
- [6] Johnston, H. S., Kattenhorn, D., and Whitten, G., *J. Geophys. Res.*, 81, 368 (1976).
- [7] Pack, D. H., Lovelock, J. E., Cotton, G., and Curthoys, C., to be published.
- [8] Crutzen, P. J., *Geophys. Res. Letters*, 1, 205 (1974).
- [9] Grimsrud, E. P., and Rasmussen, R. A., *Atmospheric Environment*, 9, 1010 (1975).

THE GAS KINETIC AND PHOTOCHEMICAL DEGRADATION OF CHLORINE NITRATE

A. R. Ravishankara, G. Smith, G. Tesi¹, and D. D. Davis

University of Maryland
Department of Chemistry
College Park, MD 20742

Rowland and co-workers have recently suggested that chlorine nitrate (ClONO_2) is of possible significance as a temporary sink for both chlorine and nitrogen oxides in the mid-stratosphere. If this hypothesis is borne out to be true, the projected ozone depletion rate will have to be scaled down significantly. The effectiveness of this new sink in altering the ozone depletion rate would depend on the rates of both formation and depletion of ClONO_2 in the stratosphere. There are two possible modes of destruction of ClONO_2 ; viz, photolysis by sunlight and removal by chemical reactions. Most likely, such a reaction would be with $\text{O}(^3\text{P})$, the most abundant radical in the stratosphere. Hence, we measured the rate constant for the reaction



at 245 K using the technique of flash photolysis resonance-fluorescence. The bimolecular rate constant at 245 K for reaction 1 is $(2.1 \pm .2) \times 10^{-13} \text{ cc molecular}^{-1}\text{sec}^{-1}$. This result indicates that the extent of ClONO_2 destruction through photolysis is ~ 10 times more than through reaction 1.

In the light of the above results, it is important to identify the photodissociation products of ClONO_2 . Based on bond energy data, it is generally assumed that ClONO_2 gives ClO and NO_2 upon photolysis. However, we found that at least below 1900 Å and above 1050 Å (LiF cut off), the photolysis products include O and Cl atoms.

The technique of flash photolysis - resonance fluorescence was employed for this investigation. $\text{O}(^3\text{P})$ atoms were formed by a N_2 -flash lamp photolysis of O_2 in Ar atmosphere. The $\text{O}(^3\text{P})$ atoms were detected using a discharge flow resonance lamp and photon counting of the O -atom fluorescence using an EMR vacuum UV photomultiplier tube. The pseudo-first order rate constant $k^1([\text{ClONO}_2] \gg [\text{O}(^3\text{P})])$ for the disappearance of $\text{O}(^3\text{P})$ was measured as a function of ClONO_2 concentration to obtain the bimolecular rate constant for reaction 1.

The above mentioned O -atom detection technique was used to detect the formation of $\text{O}(^3\text{P})$ from ClONO_2 upon photolysis with light of wavelength between 1900 and 1050 Å. A similar technique of using a chlorine atom discharge-flow resonance lamp was employed in detecting Cl atoms. Our results show that Cl and O atoms are amongst the photodissociation products of ClONO_2 when the wavelength of photolysing light is less than 1900 Å. Under the same conditions, our attempts to detect ClO through the indirect method of titration of ClO with NO to get Cl was unsuccessful; however, this result is not conclusive.

¹ On Sabbatical from NSF.

PHOTOGALVANIC CELLS

M. D. Archer and M. I. C. Ferreira

The Royal Institution
21 Albemarle Street
London W1X 4BS United Kingdom

and

W. J. Albery and W. R. Bowen
Physical Chemistry Laboratory
South Parks Road
Oxford OX1 3QZ United Kingdom

We consider the performance of photogalvanic cells of the type shown in figure 1 and scheme 1, with particular reference to the much studied iron - thionine cell [1]¹. The electrodes are identical, and the device is a concentration cell, working by virtue of the different chemical compositions of the dark and photostationary states. Cell performance is characterized by three parameters: open circuit potential, short circuit current and maximum power.

Scheme 1

In dark solution: $A + Z \rightleftharpoons B + Y$

Photochemistry : $A + Z \rightarrow B + Y$

At electrodes : $A + e \rightarrow B$

$Y + e \rightarrow Z$

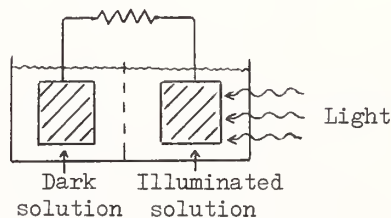


Figure 1. The photogalvanic cell.

The open circuit potential change on illumination, from a thermodynamic dark potential to a mixed potential, depends upon the electrode kinetics of A, B and Y, Z [2]. If both couples are highly reversible, then the electrode restores thermodynamic equilibrium at its surface, and there is no potential change on illumination, and now power can be obtained from such a cell. If one couple is more reversible than the other, then the electrode potential does change on illumination, to an extent which depends on the balance between the electrode kinetics, and the rates of back reaction in solution and of transport to the electrode. Maximum potential shifts are obtained if one couple (A, B say) is completely reversible and the other (Y, Z) completely irreversible. In this case, the electrode potential follows the Nernst expression for the A, B couple.

In the iron-thionine cell, although both couples, thionine/leucothionine (T/L) and Fe^{3+}/Fe^{2+} are separately reversible at clean metallic electrodes, the iron couple is rather strongly repressed by the presence of thionine in solution, as illustrated by figures 2 and 3, and so the potential shift on illumination is negative. Full Nernstian behaviour with respect to the T, L couple is not observed on platinum, as shown in figure 4. Chronocoulometric measurements can reveal the extent to which thionine is adsorbed on the electrode surface.

Figures in brackets indicate the literature references at the end of this paper.

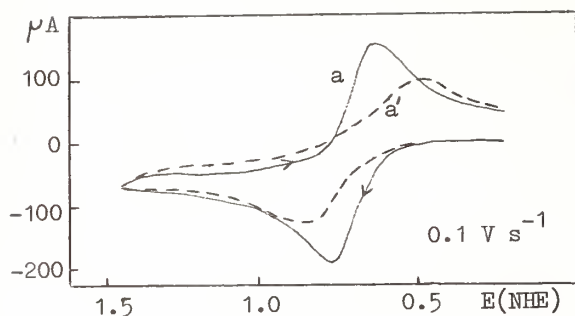


Figure 2. Cyclic voltammograms on Pt spherical microelectrode. (a) 10^{-2}M FeSO_4 in 0.5M H_2SO_4 . (a') Same + $3 \times 10^{-5}\text{M}$ thionine.

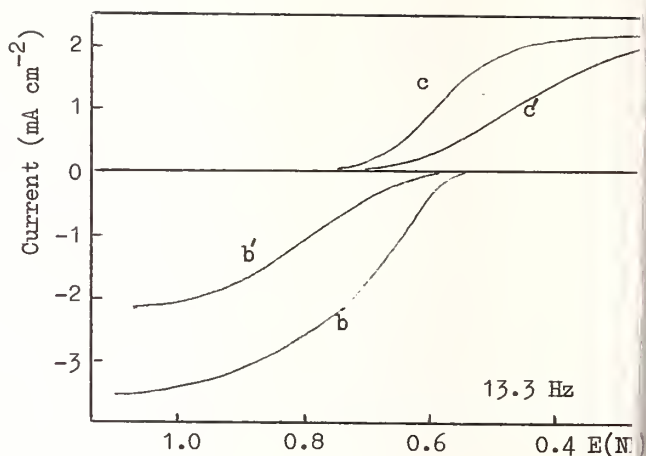
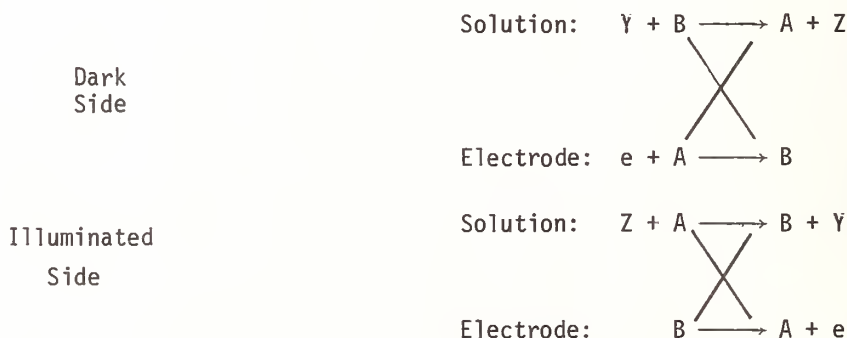


Figure 3. DC voltammograms on platinum rotating disc electrode. (b) 10^{-2}M FeSO_4 in 0.1M K_2SO_4 . (b') Same + $3 \times 10^{-5}\text{M}$ thionine. (c) $3.5 \times 10^{-3}\text{M}$ $\text{Fe}_2(\text{SO}_4)_3$ in 0.1M K_2SO_4 . (c') Same + $3 \times 10^{-5}\text{M}$ thionine.

When the photogalvanic cell is short circuited, then the current obtained is a maximum if one couple is completely reversible at the electrode and the other completely irreversible [3]. (The iron-thionine system on platinum is therefore not ideal.) In this case, the electrode processes are the reduction of A at the dark electrode, and the oxidation of B at the illuminated electrode. If the kinetic lengths of A and B (the distances over which they diffuse before they react with Z and Y respectively) are shorter than the diffusion layer thickness at the electrode surface, then there may be an important catalytic contribution to the short circuit current from the following sequence of reactions:



The homogeneous reactions regenerate the species that is reacting at the electrode. Thus by appropriate manipulation of the thermal and photochemical reaction rates in bulk solution, it may be possible to increase the present low efficiencies of photogalvanic cells considerably.

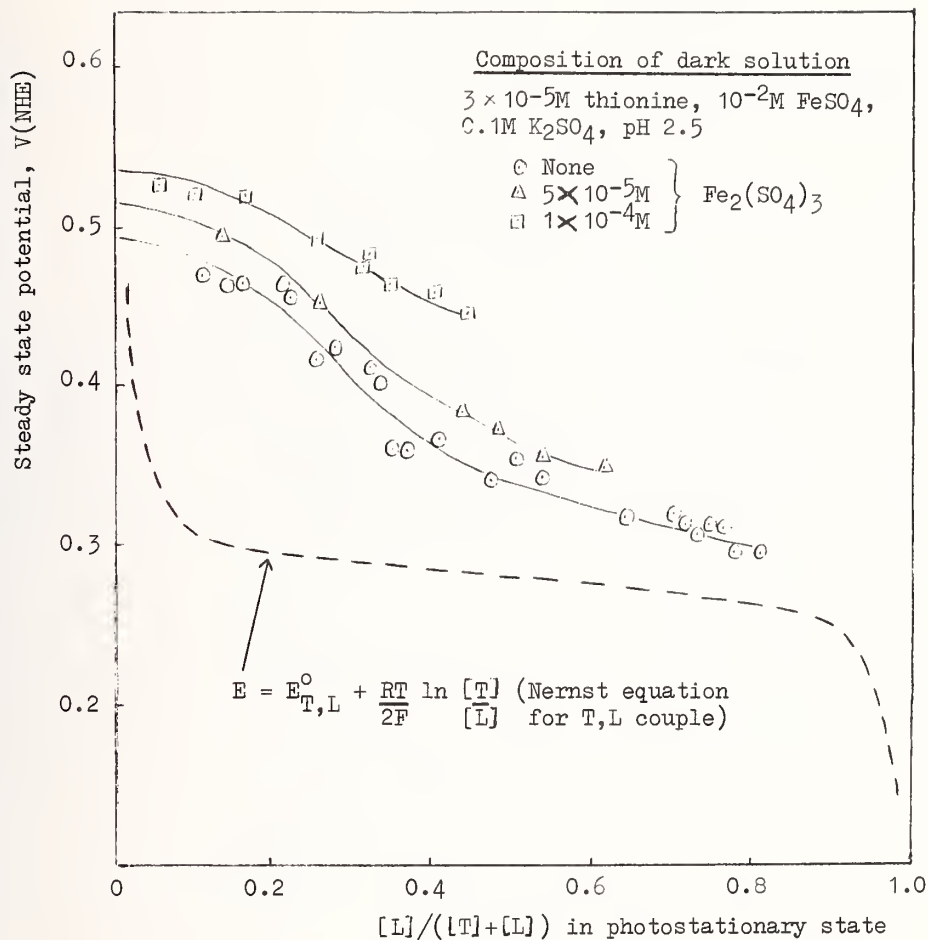


Figure 4. Steady state potential of illuminated electrode as a function of the composition of the photostationary state.

References

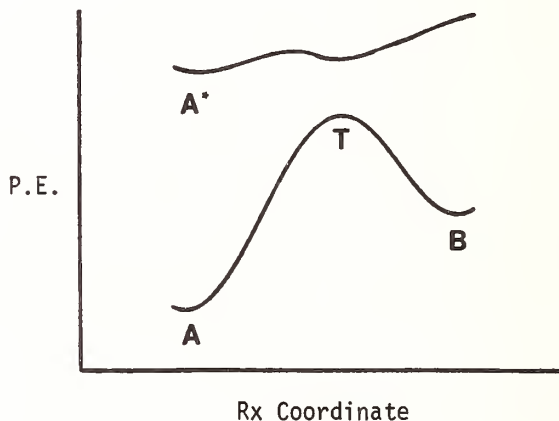
- 1] Archer, M. D., *J. Appl. Electrochem.* 5, 1975, 17 gives pre-1975 references. See also R. Gomer, *Electrochim. Acta* 20, 13 (1975) and W. D. K. Clark and J. A. Eckert *Solar Energy* 17, 147 (1975).
- 2] Alberty, W. J., and Archer, M. D., *Electrochim. Acta*, in press.
- 3] Alberty, W. J., and Archer, M. D., submitted to *J. Electrochem. Soc.*

THE IMPORTANCE OF INTERMEDIATE PARTITIONING IN ENERGY STORING PHOTOREACTIONS

G. Jones, II, W. R. Bergmark and M. Santhanam

Department of Chemistry
Boston University
Boston, MA 02215

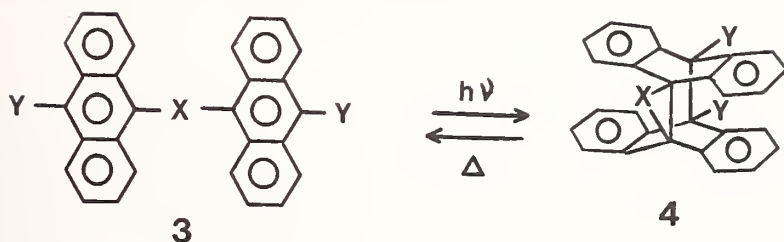
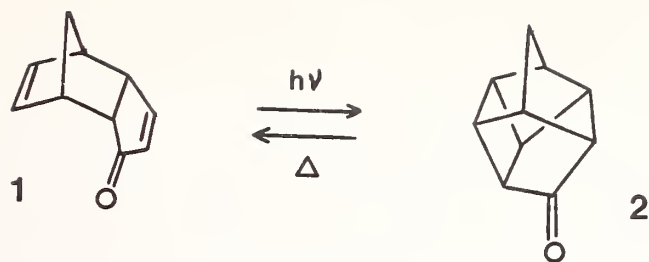
The problem which is central to the observation of significant photoreactivity using low energy (single) photons (practically speaking, the visible portion of solar radiation) is illustrated in the figure below. The objective of one energy conversion scheme is to drive a starting material A to photoproduct B, which is energy-rich, reasonably kinetically stable, and revertible to A. Quantum efficiency will depend largely on the extent to which A^* avoids a sizeable ground state potential energy barrier. In selecting materials which absorb increasingly toward the red, a point is reached at which A^* has insufficient energy to mount the thermal surface, and photoreactivity will cease unless special mechanisms are employed (*e.g.*, significant thermal activation of A^* , tunneling). We have examined



several model systems for which the excitation energy ($A - A^*$) exceeds the thermal barrier ($A - T$) by no more than 20 kcal/mol. The data permit the generalizations that kinetically identifiable intermediates are important for endoergic photoisomerizations to stable products, and that it is the partitioning of these intermediates (and not competitive decays of the initial excited species) which determine quantum efficiencies.

The case for intermediate partitioning is illustrated for dienone λ . Quenching studies show that the lifetime of reactive triplet λ is extremely short and temperature dependent ($k_{\text{decay}} = 1.1 - 3.5 \times 10^{10} \text{sec}^{-1}$, 4 - 51°C) [1]¹. Normal (unreactive) radiationless decay for cyclic enones is no faster than 10^8sec^{-1} . A fast reactive decay channel for triplet λ appears responsible for the short lifetime, but direct formation of λ without competition is ruled out by the observed quantum efficiency ($\phi = 0.36$, 320 - 380 nm). The required mechanism involves one or more intermediates, formation of which from triplet λ is lifetime limiting and partitioning of which (to λ and to λ') determines the quantum yield.

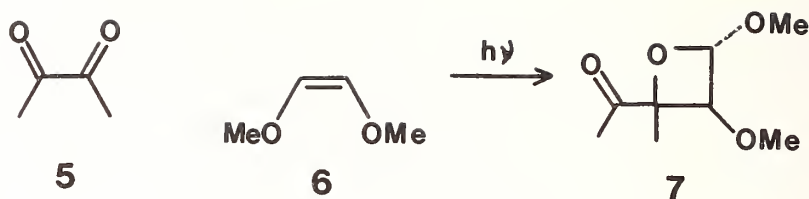
¹Figures in brackets indicate the literature references at the end of this paper.



X	Y	ϕ_{cyc}	ϕ_{flr}	$\tau_{\text{flr}}(\text{nsec})$
CH ₂ CH ₂	H	0.26	0.16	1.7
CH ₂ CH ₂	CH ₃	0.05	0.14	2.8
CH ₂	H	0.15	0.06	<0.5
CHOH	H	0.29	0.02	<0.5
CH ₂ CH ₂	CH ₂ CH ₂	0.36	<0.001	(~0.01)

A similar pattern of kinetics and quantum yields is found for linked anthracenes **3** (see table). The linking of anthracenes leads to enhanced quantum efficiencies for photocycloaddition (**3** \rightarrow **4**). (The concentration dependent quantum yield for 9-methylanthracene photodimerization reaches a maximum of 0.14 [2]). Fluorescence quantum yields are low and fluorescence lifetimes short in a way highly dependent on structure (note table divisions) and not related to quantum efficiency for photoisomerization. Neither emission nor radiationless deactivation expected for anthracenes (normally, intersystem crossing, $k \sim 10^8 \text{sec}^{-1}$, followed by triplet decay) account significantly for the rapid decay of excited singlets **3**. The results are consistent with efficient formation of an intermediate which partitions to **3** and **4**.

The photocycloaddition of biacetyl (**5**) and olefins has been investigated. The interaction of excited biacetyl and cis-1,2-dimethoxyethene (**6**) in benzene leads to quenching; $k(\text{flr}) = 2.5 \times 10^9 \text{M}^{-1}\text{sec}^{-1}$. The quantum yield for photocycloaddition (**5** + **6** \rightarrow **7**) is 0.05 ± 0.01 at 0.001 - 0.01 M **6** (a concentration range in which virtually all biacetyl triplets, but negligible singlets, are quenched). This limiting value of the quantum yield indicates that triplet quenching encounters not only lead to product (**7**) but also provide a path for decay back to **5** and **6**. A clue to the nature of an intermediate species which would account for the results (but not exclusively) is found in the reaction stereochemistry (*i.e.*, **5** + **6** \rightarrow trans oxetane as shown).



Should this pattern of intermediate partitioning be even more general? Current theory regarding reactive radiationless decay affirms the trend [3]. The systems selected, for which kinetic stability and thermodynamic instability in photoproduct are compatible, exhibit weakly avoided surface crossings (normally S_0 and S_2). At some near mid-point along the reaction coordinate, excited and ground surfaces will be close lying for facile radiationless transition and minima in S_1 and T_1 will be provided. From this diradical or biradicaloid geometry (corresponding, in the cycloadditions presented, to structures with one bond made and the other left incomplete) excited molecules funnel to product and back to reactant. Anticipation of electronic factors which control partitioning should be valuable in designing energy storing systems which can be driven with high quantum efficiency.

— This work was supported by the Office of Naval Research, the Advanced Research Projects Agency, and the National Science Foundation (through a fellowship to W.R.B.)

References

- [1] Jones, G., II and Ramachandran, B. R., *J. Photochem.*, in press.
- [2] Vember, T. M., Veselova, T. V., Obyknoennaya, I. E., Cherkasov, A. S., and Shirokov, V. I., *Izvestiya Akademii Nauk SSR. Seriya Fizicheskaya* 37, 837 (1973).
- [3] Michl, J., *Fortschritte der Chem. Forschung* 46, 1 (1974).

OPTIMIZATION OF THE IRON-THIONINE PHOTO GALVANIC CELL; PHOTOCHEMICAL ASPECTS

P. D. Wildes, N. N. Lichtin and M. Z. Hoffman

Department of Chemistry
Boston University
Boston, MA 02159

The iron-thionine photogalvanic cell was first investigated by E. Rabinowitch [1]¹ and has since been the subject of a number of investigations [2-6]. Studies of this cell can be regarded as prototypical efforts directed towards ultimate realization of a photogalvanic device which is a practical and economically significant means of converting the solar flux to electrical power. One requirement which must be met to achieve this goal is conversion of incident solar power ($\sim 100 \text{ mW cm}^{-2}$ at ground level) to electrical power with an efficiency of $\sim 5\%$ (*i.e.*, a 5% engineering efficiency). If the quantum efficiency of the iron-thionine photogalvanic cell for conversion of absorbed photons to electrons delivered to an external circuit were 100%, its engineering efficiency could be at best only $\sim 3\%$. This follows because no more than 15% of solar power falls within the absorption band of thionine and the potential of the cell is no more than 20% of the potential of the incident photons. Sensitization to the blue with a quantum efficiency of 100% would afford the possibility of increasing maximum engineering efficiency to $\sim 9\%$. Optimization of photochemical and photophysical processes is thus a necessary (but not sufficient) condition for achievement of a practical sunlight engineering efficiency. Photochemical aspects with which we have been concerned include efficiency of photooxidation of Fe(II) by triplet thionine ($^3\text{TH}_2^{2+}$) [7], sensitization to the blue and composition as well as kinetics of decay of the photochemical steady state at high concentrations of thionine.

Table 1 summarizes information on the dependence of rate constants upon solvent and anions for thionine and methylene blue.

The rate constant for the first order decay of $^3\text{TH}_2^{2+}$ and $^3\text{MBH}^{2+}$ is not significantly affected by a change in anion from CF_3SO_3^- to $\text{HSO}_4^-/\text{SO}_4^{2-}$ or by a change in solvent from water to 50 v/v per cent aqueous acetonitrile. The rate of reaction of $^3\text{TH}_2^{2+}$ and $^3\text{MBH}^{2+}$ with Fe(II) is, however, strongly affected by changes in the anion present and in some cases by changes in solvent. The faster rate of reaction of the triplet excited dyes in the presence of sulfate anions compared to solutions with CF_3SO_3^- anions may result from reduction in electrostatic repulsion by ion pairing. In any case, the efficiency of photooxidation of Fe(II) by $^3\text{TH}_2^{2+}$ is higher in the presence of sulfate anions than with F_3SO_3^- anions.

¹Figures in brackets indicate the literature references at the end of this paper.

Table 1. Kinetics of excited states of thionine and methylene blue first order decay, k_1 , and reduction by Fe(II), k_2 , of triplet states^a

DYE	SOLVENT	pH ^b	ANION	IONIC STRENGTH M	$10^5 k_1 \text{sec}^{-1}$	$10^5 M^{-1} k_2 \text{sec}^{-1}$
TH+	H ₂ O	2.0	HSO ₄ ⁻ /SO ₄ ⁼	---	1.3	600
TH+	H ₂ O	1.7	F ₃ CSO ₃ ⁻	---	1.5	65
TH+	50 v/v % aq. MeCN	"2.0"	HSO ₄ ⁻ /SO ₄ ⁼	---	1.2	5,000
TH+	50 v/v % aq. MeCN	"1.7"	F ₃ CSO ₃ ⁻	---	1.2	55
MB+	H ₂ O	1	HSO ₄ ⁻ /SO ₄ ⁼	---	2.4	38
MB+	H ₂ O	1	F ₃ CSO ₃ ⁻	---	2.2	9
MB+	H ₂ O	2.0	HSO ₄ ⁻ /SO ₄ ⁼	0.2	2.2	55
MB+	H ₂ O	2.1	HSO ₄ ⁻ /SO ₄ ⁼	1.0	2.2	80
MB+	H ₂ O	3.1	HSO ₄ ⁻ /SO ₄ ⁼	1.0	2.2	80
MB+	50 v/v % aq. MeCN	"2"	HSO ₄ ⁻ /SO ₄ ⁼	0.2	2.0	700
MB+	50 v/v % aq. MeCN	"2"	F ₃ CSO ₃ ⁻	0.2	2.1	10

^aAt the pH of these measurements, triplet TH₂²⁺ and MBH²⁺.

^bValues in quotation marks are pH values of solutions of identical composition in H₂O.

We are also studying factors which affect the rates of other reactions occurring in the cell solutions. The maximum current obtained from the cell is related to the concentration of reduced thionine present at the anode when the cell is irradiated with sunlight. Under constant illumination, the cell solution attains a photostationary state composition in which some of the dye has been reduced. The photostationary state composition of the solution depends on several parameters including the initial concentrations of dye, Fe(II) and Fe(III), the intensity of light and the length of the light path through the cell solution. Table 2 summarizes some data showing the dependence of photostationary state solution composition on reactant concentrations and cell thickness. The details of the solution dynamics which result in the photostationary state compositions shown and the implications of these values in maximizing the cell engineering efficiency are currently being investigated.

Table 2. Photoreduction^a of thionine in 50 v/v% aqueous acetonitrile solution containing 0.01N H₂SO₄

[Thionine] ^b <u>M</u> x 10 ⁻⁴	[Fe(II)] ^b <u>M</u>	[Fe(III)] ^b <u>M</u> x 10 ⁻⁴	Cell Thickness cm x 10 ⁻⁴	% Reduction of Thionine at Photostationary State ^c
7.5	0.01	0.9	80	40
7.5	0.025	2.25	80	41
7.5	0.05	4.5	80	25
7.5	0.01	0.9	25	51
7.5	0.025	2.25	25	56
7.5	0.05	4.5	25	45
3.75	0.01	0.9	80	59
3.75	0.025	2.25	80	74
3.75	0.05	4.5	80	42
3.75	0.01	0.9	25	73
3.75	0.025	2.25	25	66
3.75	0.05	4.5	25	47

^aUnder illumination with ~50mW/cm² of light from a Xenon lamp.

^bInitial dark concentrations.

^cProbable errors are ±10%.

This work was supported by NSF RANN Grant SE/AER/72-03597. We wish to acknowledge valuable conversations with Dr. E. Berman (Boston University), J. A. Eckert (Exxon Research and Engineering Co.) and Professor H. Linschitz (Brandeis University) and the use of laser flash equipment in the laboratories of Professor Linschitz and Dr. E. Hayon (U.S. Army Natick Laboratories).

References

- [1] Rabinowitch, E., *J. Chem. Phys.* 8, 560 (1940).
- [2] Miller, L. J., U.S. Dept. Commerce, Off. tech. Serv., Report AD 282, 878 (1962).
- [3] Potter, A. E., and Thaler, L. H., *Sol. Energy* 3, 1 (1957).
- [4] Mathai, K. G., and Rabinowitch, E., *J. Phys. Chem.* 66, 663 (1962).
- [5] Kamiya, N., and Okawara, M., *Denki Kagaku* 38, 273 (1970).
- [6] Clark, W. D. K., and Eckert, J. A., *Sol. Energy* 17, 147 (1975).
- [7] Faure, J., Bonneau, R., and Jousset-Dubien, J., *Photochem. Photobiol.* 6, 331 (1967).

A BIOMIMETIC APPROACH TO SOLAR ENERGY CONVERSION¹

Thomas R. Janson and Joseph J. Katz

Chemistry Division
Argonne National Laboratory
Argonne, IL 60439

A generation ago, R. Emerson and W. Arnold developed the concept of the photosynthetic unit as the basic device used by green plants in photosynthesis for light energy conversion. Chlorophyll (chlorophylls a and b in green plants, bacterio-chlorophyll in photosynthetic bacteria) acts as the primary photoacceptor in this photosynthetic unit.

A large number of chlorophyll molecules (300 hundred or more) act cooperatively in this light conversion process with the great majority of the chlorophyll molecules in the photosynthetic unit passive and acting as antennas to collect light quanta. This light energy is then funneled to a few special chlorophyll molecules in a photo-reaction center where energy conversion occurs. Antenna and photo-reactive chlorophyll, together with electron transfer proteins that serve as conduits, constitute the photosynthetic unit in which light energy is made available for chemical purposes.

It has long been known that the visible absorption spectra of both antenna and photoreaction center chlorophyll are red-shifted relative to a solution of chlorophyll in, for example, ether or acetone solution prepared in the laboratory. It has also long been established that a characteristic free radical signal is produced in photo-reaction center chlorophyll in the process of light conversion. Laboratory investigations, mainly by infrared and magnetic resonance spectroscopy, now make it possible to provide plausible interpretations on the molecular level for the anomalous visible absorption spectra of in vivo chlorophyll, and for the unusual features of the free radical signal. Thus, new models for both antenna and reaction center chlorophyll have emerged and these have become the basis for a serious effort to produce new devices for solar energy conversion.

The information so far developed on plant photosynthesis can be used in a biomimetic approach to solar energy conversion. Essentially, solar energy conversion in a biomimetic context is an attempt to mimic those aspects of photosynthesis whereby plants convert absorbed solar energy into useful chemical energy with a high degree of efficiency.

First steps have been taken in the direction of such a device. The device studied consists of a cell composed of two glass compartments, each with its own platinum electrode. External leads are gold soldered to each platinum electrode and connected to an electrometer to monitor current, emf, and resistance changes.

¹ Work performed under the auspices of USERDA.

When assembled the cell compartments are separated by a membrane (a plastic film or metal foil) carrying a photoactive chlorophyll-water adduct. In the case of metal foils the photo-active chlorophyll species is deposited on one side (generally the side facing the electron donor) by evaporation of an octane suspension of a chlorophyll-water adduct. This chlorophyll-water adduct is used because of its similar photoactive behavior as compared to reaction-center chlorophyll. One compartment is then filled (under nitrogen) with 1-2 ml of a suitable degassed aqueous solution of an electron donor such as sodium ascorbate. The other compartment is filled with a similar solution of an electron acceptor such as potassium ferricyanide, dichlorophenol indophenol (DCPIP) or the sodium salt of anthraquinone sulfonic acid. After thermal equilibration in the dark the supported photo-active chlorophyll film is irradiated with visible (or red) light and the electrical consequences observed.

A change in potential (emf) across the separating membrane upon irradiation with visible light was the most commonly measured electrical parameter. Under our experimental conditions, we observed increases in emf, decreases in resistance, increases in conductivity, and increases in current flow. In our best cell to date, using an aluminum support film, a potential difference of 422 mV was recorded associated with a current flow of 2.36×10^{-5} amp. A typical photo-response in the cell is illustrated in figure 1. A rough estimate of the efficiency of the photo-activity of this cell is 0.0024%, comparable to the best organic photo-voltaic devices in the literature. The magnitude of the photo-induced effects has been shown to depend on the type of film support used, the nature of the donor and acceptor, and on the light flux. The dependence on metal film support is seen in table 1 where results can be correlated with the photo-electric work functions of the particular metal involved.

Table 1. Dependence on metal foil support

<u>Metal</u>	Work Function (eV)	Emf (mV)
Ag	3.67	181
Pt	4.09	125
Au	4.82	94.5

Finally, although white light was generally used in these experiments, it should be noted that red light (~ 740 nm, which corresponds to the absorption maximum of the chlorophyll-water adduct film) is equally as effective in producing photo-responses in the cell. Action spectra confirm this result indicating that the chlorophyll-water adduct is indeed the primary photo-active species in the cell and initiates the observed photo-responses.

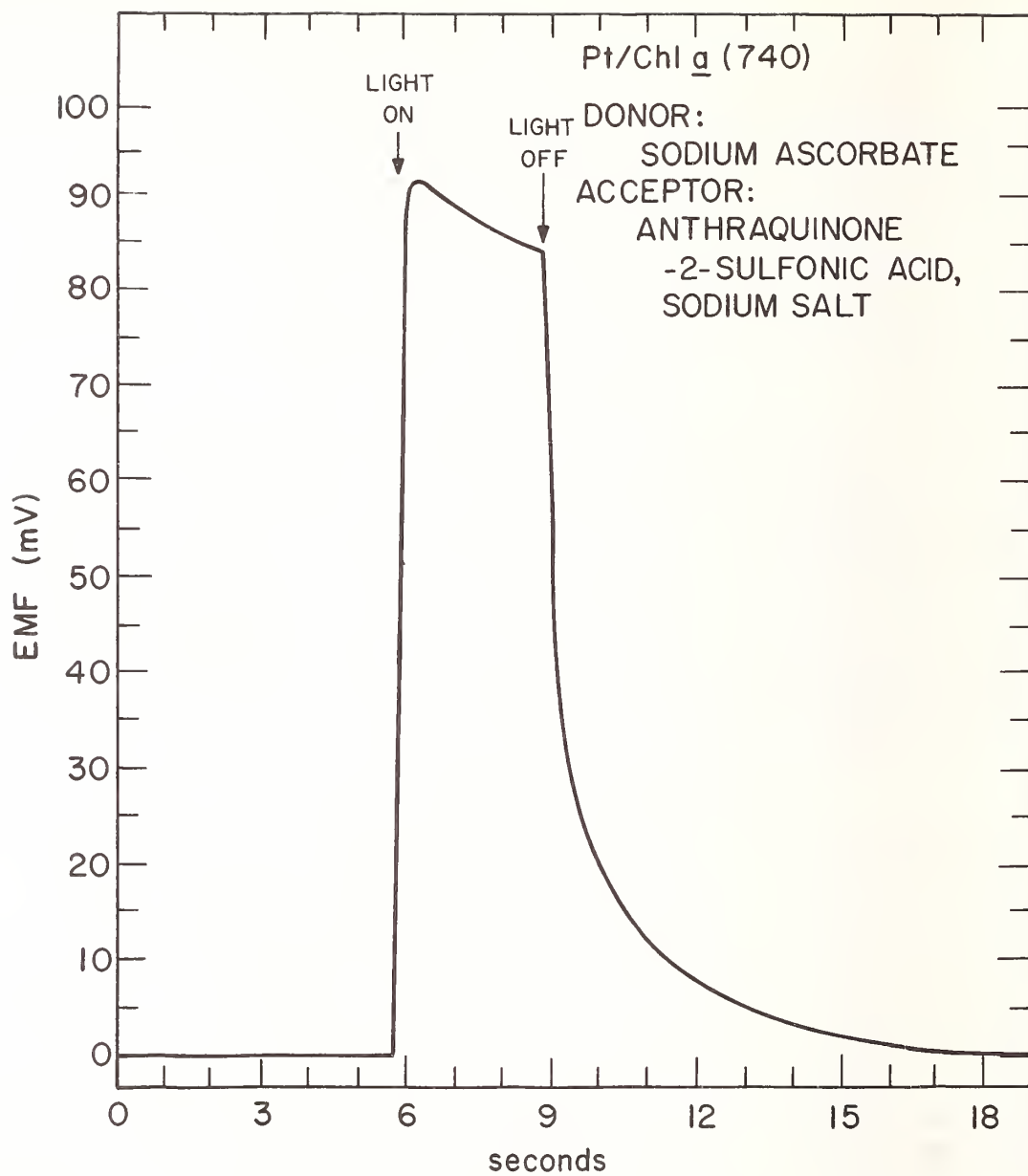


Figure 1.

LIGHT ENERGY CONVERSION VIA PHOTOREDOX PROCESSES IN MICELLAR SYSTEMS

Michael Grätzel

Hahn-Meitner-Institut für Kernforschung
Berlin GmbH Bereich Strahlenchemie
D 1000 Berlin 39

This paper describes electron transfer reactions involving excited states of organic molecules by which exploitation of solar light energy may be achieved. Three different types of processes are discussed:

- 1) Photoejection of electrons from a photoactive probe P into a polar liquid such as alcohol or water:

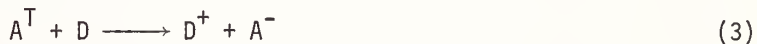


where P^+ stands for a cation radical and e_{solv}^- for the solvated electron

- 2) Electron transfer from the triplet state of the molecule (P^T) to various acceptors:



- 3) Electron transfer from various donors to an acceptor triplet A^T



These reactions are examined by conventional photolysis and pulsed laser techniques. A frequency doubled, Q-switched ruby laser (pulse-width 15 ns, 347.1 nm) is used to excite the photoactive species. Transitory species are identified and their kinetics monitored by fast kinetic spectroscopy or conductivity technique.

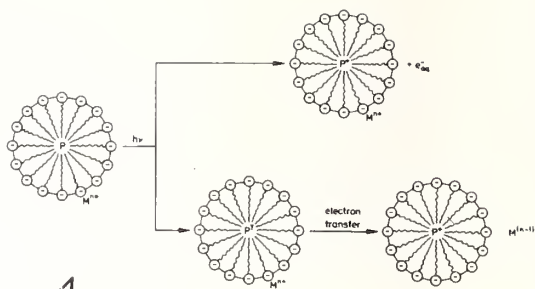
A prominent feature of this work is the comparison of the nature of photoreactions 1-3 and subsequent dark reactions in homogeneous polar media such as alcohol or water and aqueous micellar solutions. It is attempted to illustrate the important role surfactant micelles could play in the search for photochemical systems suitable for conversion of light energy into chemical or electrical energy.

Reaction (1) has attracted attention as a possible pathway for photochemical production of hydrogen from water since hydrated electrons produced in the photoionisation event are known to undergo the diffusion controlled reaction



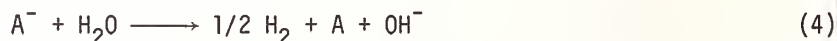
The two major problems which heretofore have prevented successful application of such a system are: (a) The majority of organic sensitizers with ionization potentials low enough to permit electron ejection by visible or near u.v. light are sparsely soluble or insoluble in water; (b) Rapid recombination of e_{aq}^-/P^+ ion pairs leads to annihilation of electrons before hydrogen can be formed. These obstacles may be overcome by usage of anionic micellar solutions. A schematic illustration of a photoionization event in such a system is given in figure 1.

Figure 1. Schematic presentation of photoionization and electron transfer processes in solutions of surfactant micelles containing a solubilized photoactive probe P. The electron acceptor M^{n+} is located in the Stern layer of the micelle.



The sensitizer P is solubilized in the hydrophobic interior of the micellar aggregate whose negative surface charge prevents reentry of the hydrated electron and recombination with the parent ion P^+ . These phenomena are illustrated by laser photolysis results obtained from solutions of N, N, N',N'-tetramethylbenzidine (TMB) in sodiumlaurylsulfate micelles. Comparison of photoionization cross sections in alcoholic and micellar solution also reveals the favourable result that the micelles enhance strongly the yield of electrons. This effect is discussed in terms of an electron tunneling.

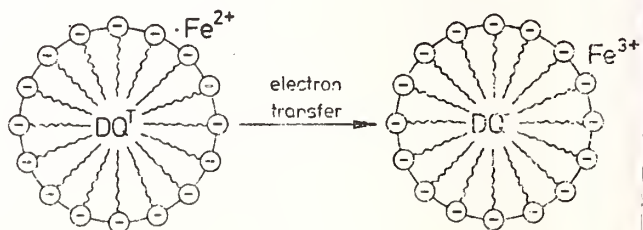
The triplet states of phenothiazine (PTH^T) and TMB were found to have strongly reducing properties and readily transfer electrons to acceptors such as methyl viologen, duroquinone, europium(III) and chromium(III) ions. Some of these reactions have particular importance for the photo reduction of water as the reduced form of the acceptor is capable of evolving hydrogen from water according to



This reaction has to compete with back transfer of electrons from A^- to P^+ which in homogeneous solution occurs at a diffusion controlled rate. Included in figure 1 is an illustration of a forward electron transfer process in a micellar system. These intramicellar processes occur at a very fast rate. The back reaction, however, may be strongly inhibited by the micellar systems.

The last type of photo redox processes discussed in this paper are electron abstraction reactions of triplet duroquinone (DQ^T). In mixtures of water/ethanol DQ^T abstracts electrons from a variety of substrates such as Fe^{2+} , $Fe(CN)_6^{4-}$, CO_3^{2-} , diphenylamin and trimethoxy benzene. The rate constants for these redox processes are close to the diffusion controlled limit (10^9 - $10^{10} M^{-1} s^{-1}$) except for CO_3^{2-} where k equals $7 \times 10^7 M^{-1} s^{-1}$. Anionic micelles were found to have a pronounced catalytic effect on the reaction of Fe^{2+} with DQ^T . A schematic illustration of such an intramicellar electron transfer process is given in figure 2. Conversely cationic micelles drastically enhance the rate of electron transfer

Figure 2. Schematic illustration of an intramicellar electron transfer process from Fe^{2+} to DQ^T solubilized in anionic micelles.



from CO_3^{2-} to DQ . The latter process is of particular interest as CO_3^{2-} is known to form oxygen in its subsequent reactions. Hence O_2 evolution from water by visible light becomes feasible via excited quinone redox reactions.

PHOTOELECTROLYSIS OF WATER BY SOLAR ENERGY¹

D. I. Tchernev

Lincoln Laboratory
Massachusetts Institute of Technology
Lexington, MA 02173

Although the free energy required for the decomposition of water into gaseous H_2 and O_2 is only 1.23 eV, while the peak of the solar spectrum occurs at a photon energy of about 2.4 eV, solar energy cannot be utilized for the production of H_2 fuel by the direct photodecomposition of water, because the threshold energy for this direct reaction is about 6.5 eV. Fujishima and Honda have recently shown, however, that this threshold can be greatly reduced if decomposition is accomplished by means of photoelectrolysis, a process in which a semiconductor is used as a catalyst. This is a promising process for the large-scale utilization of solar energy to produce H_2 fuel. We have been investigating the physics and electrochemistry of photoelectrolysis by experiments on cells with polycrystalline as well as single-crystal TiO_2 anodes. This work has led to studies with $SrTiO_3$ anodes, and we report some of these results as well.

The basic photoelectrolysis cell consists of an n-type semiconducting working electrode, an electrolyte, and a Pt counterelectrode. Because of the difference in work functions between the semiconductor and the electrolyte, the energy bands of the semiconductor are bent at the surface, so that the analog of a Schottky barrier exists at the semiconductor-electrolyte interface. The semiconductor surface is irradiated by photons of energy at least equal to its energy gap. The photon-generated hole-electron pairs do not recombine but are separated by the electric field of the barrier; the electrons move away from the surface into the bulk of the semiconductor and then through the external circuit to the Pt cathode, where they discharge $H_2(2e^- + 2H^+ \rightarrow H_2)$, while the holes remain at the surface of the semiconductor anode, where they can interact with the electrolyte to produce $O_2(2p^+ + H_2O \rightarrow 1/2 O_2 + 2H^+)$. The overall chemical reaction is



provided the semiconductor is chemically inert, serving only to absorb the light and to produce the holes and electrons that make the reaction possible. Two conditions are necessary for efficient photoelectrolysis: (1) The energy bands at the semiconductor-electrolyte interface must be bent in order to separate the holes and electrons excited by the light and (2) the relevant electronic levels must line up, *i.e.*, the hole states of the anode with $\epsilon(H_2O/O_2)$ and the Fermi level of the cathode with $\epsilon(H^+/H_2)$.

The anode material used in most of our experiments was the rutile form of TiO_2 . Some TiO_2 anodes were fabricated from single crystals, but most were polycrystalline disks prepared by hot-pressing powdered rutile at 750°C under a pressure of 10,000 psi. To make the disks conducting ($\rho \sim 10^3 \Omega\text{-cm}$), they were heated in vacuum for three hours at $\sim 600^\circ\text{C}$.

¹This work was sponsored by the Department of the Air Force.

In initial experiments the external quantum efficiency, η , defined as the ratio of the number of electrons flowing in the external circuit (N_e) to the number of photons incident on the cell (N_p), was measured as a function of photon energy $h\nu$. The maximum values of η , 82% for the single crystal and 60% for the polycrystalline disk, occur at $h\nu \sim 4$ eV. Quantum efficiency measurements were also made with TiO_2 films on Ti foil that had been thermally oxidized. The efficiencies were comparable to those obtained with single crystal anodes.

When the maximum measured η values are corrected by taking account of estimated reflection and absorption losses, we find that the internal quantum efficiency was close to 100% for both single-crystal and polycrystalline TiO_2 anodes. This high quantum efficiency shows that the band bending in TiO_2 was sufficient to separate the electron-hole pairs generated by photon absorption and in addition that the hole states of the anodes lined up with the ($\text{H}_2\text{O}/\text{O}_2$) level of the electrolyte. As stated above, however, for efficient photoelectrolysis it is also necessary for the Fermi level of the cathode, ϵ_F , to line up with the electrochemical potential of the H^+/H_2 level in the solution, $\epsilon(\text{H}^+/\text{H}_2)$.

The quantum efficiency experiments just described were performed with the photoelectrolysis cell open to air, so that the electrolyte contained dissolved oxygen. In this case the energetically favorable process at the cathode is the transfer of electrons from the cathode (at ϵ_F) to the $\text{H}_2\text{O}/\text{O}_2$ causing the reduction of oxygen:



The cell now functions in the galvanic mode, and no H_2 gas is evolved. Under these conditions, we have observed that the O_2 bubbles formed at the anode migrate to the cathode, where they disappear.

This obstacle to the production of H_2 gas can be eliminated by removing the dissolved oxygen from the cathode compartment of the cell. However, the cell current then decreases considerably, so that η becomes only 1-2%, even for the best TiO_2 anodes. This occurs because the band bending under photoelectrolysis conditions is very small for TiO_2 . However, better results are obtained for SrTiO_3 , for which the band bending is ~ 0.2 V larger because of its lower electron affinity. This increase in band bending results in a quantum efficiency for photoelectrolysis of 10% at $h\nu = 3.8$ eV, about one order of magnitude larger than that for TiO_2 . The SrTiO_3 experiments were performed with single-crystal and polycrystalline anodes. When dissolved O_2 was removed from the solution, the amounts of H_2 evolved at the cathode and O_2 evolved at the anode were in good agreement with the predictions of eq. (1), showing that photoelectrolysis was the only reaction occurring.

Ultimately, the efficiency with which solar energy can be used to generate H_2 by photoelectrolysis will depend on the semiconductors that are used as electrode materials. Only about 10% of the solar energy reaching the earth is supplied by photons with energies higher than 3.0 eV, the energy gap of TiO_2 or SrTiO_3 . Therefore the efficiency of solar utilization will be limited to a few percent unless it is possible to find a suitable electrode material with a significantly lower energy gap.

Desmond V. O'Connor and William R. Ware

Photochemistry Unit
Department of Chemistry
University of Western Ontario
London, Ontario, Canada

While there have been numerous studies reported in the literature aimed at revealing the photophysical and photochemical properties of exciplexes, there have been relatively few that attempted to obtain simultaneously (a) a test of mechanism (b) all the pertinent rate constants (c) the temperature coefficients of these rate constants and thus the activation parameters as well as the thermodynamic properties of the exciplex equilibrium. In fact, what is needed are such studies carried out with a number of donor-acceptor pairs of different properties in a number of solvents ranging from non-polar to polar. The results of such studies cannot fail to enhance our knowledge of the exciplex. Such a program is currently underway and this paper constitutes a preliminary report.

Exciplex photophysics have been investigated by observing the fluorescence decay of both the monomer and exciplex, by observing the relative yields of monomer and exciplex emission as a function of quencher concentration and by measuring the steady-state monomer quenching. The fluorescence decay measurements were done with the single photon technique and deconvolution accomplished by iterative convolution.

The principal system to be discussed is α -cyanonaphthalene quenched by dimethylcyclopentene. This has been investigated in hexane and diethyl ether (DEE) over a wide temperature range.

$$\begin{array}{c}
 A \xrightarrow{I_a(t)} A^* \\
 \begin{array}{c}
 \swarrow k_1 \quad \searrow k_2 \\
 A + h\nu_F \quad A
 \end{array} \\
 A^* + Q \rightleftharpoons (AQ)^* \xrightarrow{k_6} \text{prod.} \\
 \downarrow k_5 \\
 A + Q + h\nu_F
 \end{array}$$

The appropriate equations are

$$I_M(t) = C_1 e^{-\lambda_1 t} + C_2 e^{-\lambda_2 t} \quad (1)$$

$$I_E(t) = C_3 (e^{-\lambda_1 t} - e^{-\lambda_2 t}) \quad (2)$$

$$\lambda_{1,2} = 1/2[k_1 + k_2 + k_3[Q] + k_4 + k_p \pm \{(k_1 + k_2 + k_3[Q] - k_4 - k_p)^2 + 4k_3k_4[Q]\}^{1/2}] \quad (3)$$

$$k_p = k_5 + k_6 \quad (4)$$

One also has

$$\lambda_1 + \lambda_2 = k_1 + k_2 + k_3[Q] + k_4 + k_p \quad (5)$$

$$\lambda_1 \lambda_2 = (k_1 + k_2)(k_4 + k_p) + k_3k_p[Q] \quad (6)$$

Another useful equation is the indicial equation used to derive eq. (1) and (2). This is

$$\lambda^2 - [k_1 + k_2 + k_3[Q] + (k_4 + k_p)]\lambda + (k_1 + k_2)(k_4 + k_p) + k_3k_p[Q] = 0 \quad (7)$$

Finally, the two steady-state equations are

$$K_{SV} = \frac{k_3 k_p}{(k_1 + k_2)(k_4 + k_p)} = \left\{ \frac{I_M^0}{I_M} - 1 \right\} \frac{1}{[Q]} \quad (8)$$

$$\frac{\Phi_E}{\Phi_M} = \left\{ \frac{k_5}{k_1} \right\} \left\{ \frac{k_3}{k_4 + k_p} \right\} [Q] \quad (9)$$

These equations were utilized to calculate individual rate constants on the assumption that the mechanism is valid. It will be shown that quantitative aspects of the experimental results are consistent with this model.

The results are summarized in the table. The following conclusions appear consistent with the data.

- (a) The forward rate of quenching is diffusion controlled.
- (b) The low-temperature results in hexane are consistent with the high-temperature results in hexane where the rapid equilibrium approximation is valid (see J. Am. Chem. Soc. 96, 7853 (1974)). Thus the kinetics are now resolved over a range of 85°.
- (c) The quenching is inefficient and this appears entirely due to the feedback step (k_4).
- (d) The thermodynamic parameters and activation parameters are similar to those obtained for other exciplexes and the exciplex binding energy is consistent with electrochemical data.

(e) The steady-state studies confirm the fluorescence decay measurement.

(f) Changing from hexane to DEE has a profound effect on k_4 but leaves ΔE_4^\ddagger and ΔH_c unchanged. While k_4 and k_p decrease as one goes to DEE, K_{SV} increases!

(g) In hexane $k_5 \neq f(T)$.

T°K	Hexane					Diethyl ether			
	273	262	251	242	233	303	293	283	273
$k_3 \times 10^{-10}$ $M^{-1} \text{sec}^{-1}$	0.98	0.88	0.78	0.67	0.60	1.23	1.21	1.08	0.93
$k_4 \times 10^{-8}$ sec^{-1}	1.14	0.49	0.20	0.10	0.040	0.55	0.25	0.17	0.054
$k_p \times 10^{-8}$ sec^{-1}	0.98	0.77	0.62	0.52	0.46	0.79	0.65	0.54	0.44
$\log k_3/k_4$	1.94	2.25	2.58	2.82	3.18	2.35	2.69	2.81	3.24
ΔS_3^\ddagger	-4.78	-4.68	-4.58	-4.53	-4.44	-4.42	-4.18	-4.11	-4.10
ΔS_4^\ddagger	18.97	18.94	19.00	19.25	19.18	14.27	13.97	14.56	13.75
ΔS°	-23.15	-23.62	-23.58	-23.83	-23.62	-18.68	-18.15	-18.67	-17.85
ΔG°	-2.42	-2.70	-2.97	-3.13	-3.39	-3.26	-3.60	-3.64	-4.05
ΔG_3^\ddagger	2.36	2.31	2.25	2.23	2.17	2.56	2.46	2.42	2.42
ΔG_4^\ddagger	4.78	5.02	5.23	5.36	5.55	5.81	6.06	6.06	6.44

CHARGE TRANSFER AND HYDROGEN ATOM TRANSFER REACTIONS OF EXCITED

AROMATIC HYDROCARBON - AMINE SYSTEMS

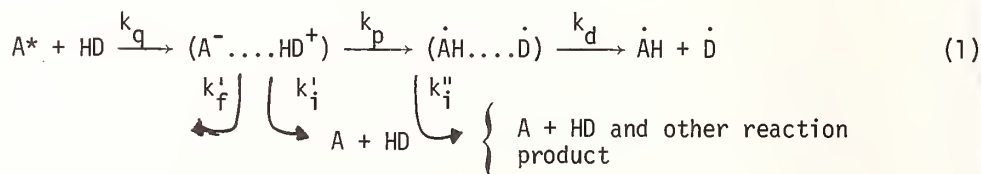
N. Mataga, T. Okada and T. Mori

Department of Chemistry
 Faculty of Engineering Science
 Osaka University
 Toyonaka, Osaka 560, Japan

It is well known that excited aromatic hydrocarbon forms exciplexes with N,N-dimethylaniline (DMA) or N,N-diethylaniline (DEA). Contrary to this, when amines with free N-H groups such as aniline and N-methylaniline are used as electron donors for the exciplex formation with excited aromatic hydrocarbons in solution, no exciplex fluorescence can be observed although the fluorescence of aromatic hydrocarbon is quenched [1]¹. On the basis of preliminary studies upon pyrene-aniline system by means of laser photolysis as well as the measurements of the effects of solvent polarity upon the fluorescence quenching rate, hydrogen atom transfer assisted by charge transfer interaction in the encounter complex has been proposed as a mechanism of the quenching of exciplex fluorescence [2]. Since this is an important problem in the exciplex chemistry, we have made a more detailed and extensive studies by means of fluorescence and transient absorption measurements with laser photolysis as well as conventional flash photolysis methods.

The bimolecular rate constants (k_q) of the quenching of pyrene fluorescence in n-hexane by various primary and secondary amines were measured. The k_q values in the case of aliphatic amines are considerably smaller than those of the aromatic amines, which seems to indicate that an additional activation energy over that for the aromatic amine system appears necessary for the quenching by aliphatic amines. The difference of the quenching rate constant between aromatic and aliphatic amines was also observed in the case of the fluorescent exciplex formation of pyrene-DMA and pyrene-tributylamine (TBA) systems [3]. It may be possible to assume similar structural change in case of the present systems.

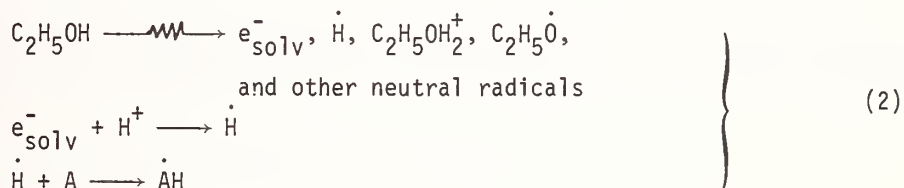
It has been confirmed that the k_q values increase remarkably with decrease of the ionization potential (I_p) of the amines. This result suggests the fluorescence quenching mechanism of the charge transfer in the encounter complex. Although the values of k_q as well as i , for N-methylaniline (NMA) or N-ethylaniline (NEA) are rather close to those of DMA or DEA, respectively, no exciplex fluorescence can be observed in the case of the formers. This result suggests the following mechanism of the quenching.



Assuming that the rate constants of the radiative and radiationless transitions (k_f' and k_i') of $(A^{\cdot-} \cdots HD^{\cdot+})$ are equal to those of pyrene-DMA or pyrene-DEA exciplex in hexane, respectively, $(k_p + k_i') \sim k_p$ has been estimated to be larger than $2 \times 10^{10} \text{ s}^{-1}$.

¹Figures in brackets indicate the literature references at the end of this paper.

If AH and \dot{D} radicals are formed by the process k_d , their absorption spectra may be observed by means of flash photolysis. Transient absorption bands were observed in the 380 ~ 430 nm region for many pyrene-primary and secondary amine systems in hexane. The observed spectra can be explained as a superposition of absorption bands of pyrene triplet state and those of some other transient species. At the delay time of 50 μ s, the T-T absorption band becomes much weaker while the absorption band of the other transient remains fairly strong. In order to identify the long lived transient, 1,2-dihydropyrene (AH_2) in methylcyclohexane-isopentane (3:1) mixture at 77K was irradiated with a low pressure mercury lamp, and absorption spectra of photoproduct were measured. It seems probable that the radical AH is formed by irradiation. The obtained spectrum of the photoproduct is rather close to that of the long lived transient species observed by the flash photolysis method. Furthermore, the spectrum of AH was measured by means of pulse radiolysis of solutions of pyrene in ethanol containing 1 vol.% sulfuric acid, where AH may be produced by the following reactions



The spectrum shows peaks at 405 nm and 395 nm and is essentially identical with the spectrum obtained by subtracting the T-T absorption band of pyrene from the observed transient spectra in pyrene-primary amine and secondary amine systems.

The confirmation of the formation of \dot{D} by means of the transient spectrum measurement is rather difficult since the absorption spectra of anilino radicals are observed in the wavelength region of about 400 nm and their intensities are rather weak. However, since the absorption spectrum of diphenyl amino radical shows maximum at ca. 770 nm, we have examined pyrene-diphenyl amine (DPA) system in hexane solution and have observed clearly the absorption band of diphenyl amino radical in addition to the absorption band of AH. Thus, the formation of both AH and \dot{D} has been confirmed.

Although it is assumed in eq. (1) that the radicals are formed from the singlet excited state, it might be possible that they are formed by the reaction in the triplet state. We have examined this problem by using a dilute solution of anthracene-DPA system in hexane, and confirmed that no reaction occurs in the triplet state since the decay process of anthracene triplet state is not affected by the addition of DPA.

If the charge transfer mechanism of the fluorescence quenching is valid, k_q will depend upon the solvent polarity. Actually, we have confirmed in several cases where the additional activation energy over that for the diffusional motion is necessary for the charge transfer, that the k_q value decreases with increase of the solvent polarity. This result indicates that not only the I_0 value but also the solvent polarity affects the additional activation energy and it is decreased with increasing solvent polarity. For example, in the case of pyrene-aniline system, k_q is $5.7 \times 10^8 M^{-1} s^{-1}$ in hexane, $2.6 \times 10^9 M^{-1} s^{-1}$ in isopropanol, and $5.3 \times 10^9 M^{-1} s^{-1}$ in acetonitrile, and for the pyrene-dibutylamine system, it is $3.0 \times 10^7 M^{-1} s^{-1}$ in hexane, $2.0 \times 10^8 M^{-1} s^{-1}$ in ethylether, $8.4 \times 10^8 M^{-1} s^{-1}$ in acetone, and $8.7 \times 10^8 M^{-1} s^{-1}$ in acetonitrile.

Roughly speaking, approximately linear relation can be observed between $\log k_q$ and the reciprocal of the solvent dielectric constant ϵ . This result can be explained satisfactorily on the basis of the reasoning given elsewhere [2]. Namely, we assume that the activation energy for the charge transfer is determined by the Horiuchi-Polanyi's relation. The free energy of the final state of the charge transfer (the solvated ion pairs) may be written as,

$$F_i = (A/\epsilon) + B \quad (3)$$

where A and B are constants irrelevant of ϵ .

The change of F_i with ϵ (from ϵ° to ϵ) is,

$$\Delta F_i = A(1/\epsilon^\circ - 1/\epsilon) \quad (4)$$

Then, the change of activation energy ΔE is given by,

$$\Delta E = \alpha \Delta F_i, \quad \alpha : \text{constant} \quad (5)$$

according to Horiuchi-Polanyi's relation. The ratio of k_q 's in solvents with dielectric constant ϵ and ϵ° can be written as,

$$k_q(\epsilon)/k_q(\epsilon^\circ) = \exp(\alpha \Delta F_i/RT) \quad (6)$$

Thus, $\log k_q(\epsilon)$ is inversely proportional to ϵ . Of course, in sufficiently polar solvents such as acetone and acetonitrile, ionic dissociation into solvated radical ions, A^- and HD^+ , will complete with the proton transfer in the encounter complex. Actually, transient spectra observed by the laser photolysis of pyrene-aniline system in acetonitrile show strong absorption bands of solvated radical ions.

References

- [1] Mataga, N., Okada, T., and Oohari, H., *Bull. Chem. Soc. Japan* 39, 2563 (1966).
- [2] Mataga, N., in "*Exciplex*," ed. by M. Gordon and W. R. Ware, Academic Press, New York, 1975, p. 113.
- [3] Nakashima, N., Mataga, N., and Yamanaka, C., *Int. J. Chem. Kinetics* 5, 833 (1973).

PROTOLYSIS EQUILIBRIA OF LUMICHROME (6,7-DIMETHYL-ALLOXAZINE) IN THE LOWEST EXCITED SINGLET STATE

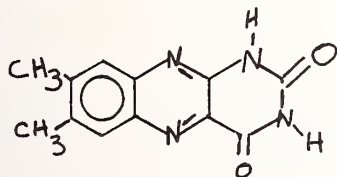
Bertil Holmström

Sture Bergström and Hans-Bertil Larson

Department of Physical Chemistry

Chalmers Univ. of Technology and the Univ. of Gothenburg
Gothenburg, Sweden

Fluorescence is a standard method of assay for riboflavin (Vitamin B₂). The substance is very unstable to light, two major decomposition products being lumiflavin (6,7,9-trimethyl-iso-alloxazine) and lumichrome (6,7-dimethyl-alloxazine). A thorough study of the fluorescence properties of these compounds may, therefore, be of some practical importance. Lumiflavin has a fluorescence spectrum very similar to that of the parent compound (an emission peak at 520 nm); the emission disappears in acid medium (pH = 1.5) and in basic medium (pH = 10).



lumichrome \equiv H₂Lc

In contrast to this, the pH variation of lumichrome fluorescence presents a very complicated picture containing several features of more general interest. In the acidity/basicity range of this study, from concentrated sulphuric acid to strong sodium hydroxide solution, at least three different protolysis forms are evident in emission and four in absorption (cf Fig. 1 and 2). The various pK^* values were estimated by two principally different methods: (i) direct observation of the change in fluorescence spectrum with pH, and (ii) from observed absorption and emission spectra of the "pure" protolytic forms using the Förster cycle. Additional information on the dynamics of the system in weakly acid and weakly basic media was obtained by studying the change in emission spectrum with buffer concentration, and also by measuring fluorescence lifetimes (following pulse excitation).

1. CHANGES IN EMISSION SPECTRA WITH PH

In the acid region, the change in emission spectrum occurs at a slightly lower pH than the change in absorption spectrum, indicating that the exciting form of the neutral dye is slightly stronger as a base than the ground state molecule ($pK_1 = -1$, $pK_1^* = 0$). In strong sulphuric acid medium, there is another change in absorption spectrum ($pK_0 = -8$) without any corresponding change in the emission spectrum. Both absorption and emission spectra exhibit marked red shifts when going to stronger acid. In basic medium, there is a change in the absorption spectrum corresponding to $pK_2 = 12$.

2. THE FÖRSTER CYCLE

If the entropy change on protonation is assumed to be the same in the excited state as in the ground state (i.e. $\Delta S^{o*} = \Delta S^o$), the difference between the two states in standard free energy change on protonation ($\Delta G^{o*} - \Delta G^o$) will be the same as the difference between the two states in the enthalpy change on protonation ($\Delta H^{o*} - \Delta H^o$). If the latter can be determined

from the observed absorption and emission spectra, it is possible to estimate the difference in pK between the two protolysis forms (cf Fig. 3):

$$pK^* - pK = \frac{hc}{kT} \ln 10 (\tilde{\nu}'' - \tilde{\nu}') = 21.0 (\tilde{\nu}'' - \tilde{\nu}')/\mu m^{-1}$$

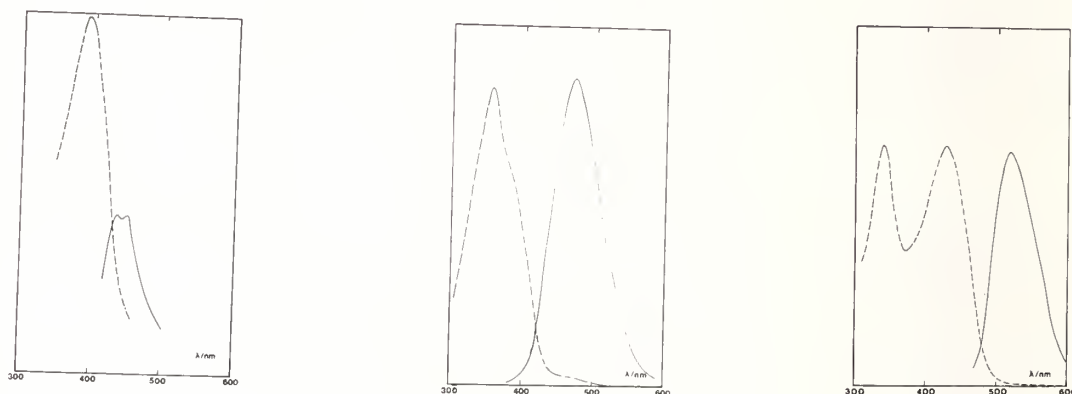


Figure 1. Absorption spectra (broken lines; Bausch & Lomb Spectronic 505) and emission spectra (full lines; Aminco Bowman, uncorrected). (1) Strong sulphuric acid; (2) Weakly acid solution; (3) Basic solution.

where $\frac{hc}{kT} \tilde{\nu}'$ and $\frac{hc}{kT} \tilde{\nu}''$ represent the energy differences between the first excited singlet state and the ground state (the energy of the 0-0 band) in the two protolysis forms. In the ideal case of mirror image symmetry between absorption and emission spectra, the energy of the 0-0 transition is quite well defined. The best thing that can be done in the lumichrome case is to take the mean of the wave number of the absorption maximum, $\tilde{\nu}_a$, and the emission maximum, $\tilde{\nu}_e$. This leads to the prediction $pK_1^* = pK \pm 0.0$ and $pK_2^* = pK_2 - 6.7 \approx 5$, in rather good agreement with the values obtained by the previous method.

3. CHANGES IN EMISSION SPECTRA WITH BUFFER CONCENTRATION

In "neutral" solutions ($5 \leq pH \leq 9$), the shape of the emission spectrum (cf Fig. 4) is strongly dependent on the buffer concentration $[B]$. At low $[B]$, the emission peak is at 470 nm (as in more strongly acid solution); at high $[B]$, the peak is at 520 nm (as in alkaline solution). The peak ratio, $\mu \equiv F(520)/F(470)$, varies from $\mu_{min} = 0.43$ to $\mu_{max} = 5.5$.

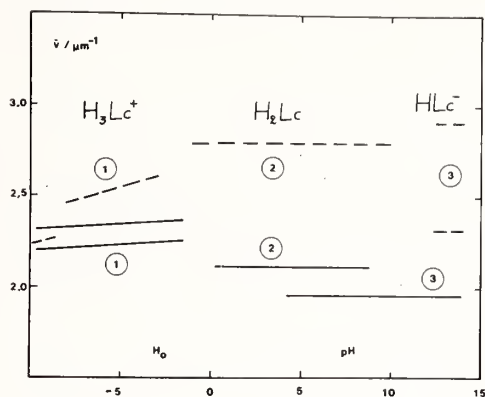


Figure 2. Summary of absorption and fluorescence data for lumichrome, taken from curves like those shown in Fig. 1. The ordinate gives the absorption for (uncorrected) emission maxima. Abscissa vlaues below 0 refer to the Hammet function.

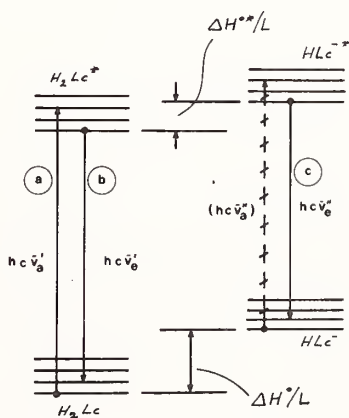


Figure 3. The Förster cycle. L = Avogadro's constant.

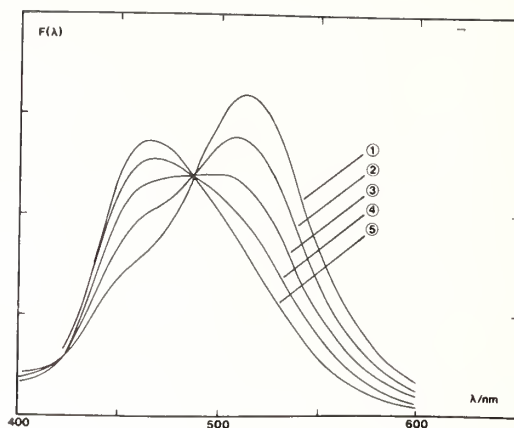
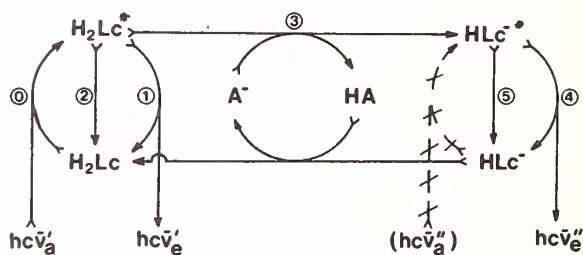


Figure 4. Fluorescence spectra of weakly acidic lumichrome solutions pH = 5.5, with different concentrations of acetate: 1: 4.50M, 2: 2.25M, 3: 1.12M, 4: 0.56M, 5: 0.02M.

This is interpreted as a competition between the direct fluorescence from H_2Lc^* and the establishment of a new protolytic equilibrium, according to "Scheme I":



In the region in question, $[OH^-]$ is low and reaction (3) is dependent on a diffusional encounter between H_2Lc^* and B (the base component of the buffer system).

One would then expect proportionality between the buffer concentration $[B]$ and the ratio of transformed fluorescence to direct fluorescence, r_4/r_1 , which in turn can be shown to be proportional to the experimental quantity

$$\Lambda \equiv (\mu - \mu_{\min}) (\mu_{\max} - \mu)^{-1}$$

This prediction is in excellent agreement with experiment, as shown in Fig. 5. From the slope \underline{k} of the line in Fig. 5, together with proper absorption and emission parameters for the two protolytic forms, it is possible to evaluate $\tau'k_3$. At $\text{pH} \approx 8$, \underline{k}_3 appears to be slightly lower than $\underline{k}_{\text{diff}}$, at $\text{pH} \approx 6$ still a factor of 2 lower.

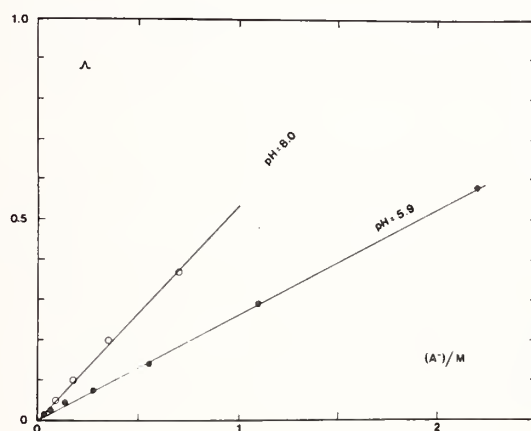


Figure 5. The parameter Λ (see text) vs. concentration of basic component of buffer system. ● acetate, $\text{pH} = 5.9$; ○ phosphate, $\text{pH} = 8.0$.

PHOTOCHEMISTRY OF PHEOPHYTINS AND PORPHYRINS¹

D. C. Brune, J. Fajer and S. P. Van

Division of Molecular Sciences
Department of Applied Science
Brookhaven National Laboratory
Upton, NY 11973

Recent pulsed laser spectroscopic results have revealed two short lived intermediates involved in the primary photochemistry of photosynthetic bacteria. The first of these, which appears in less than ten picoseconds is postulated to consist of a dimeric bacteriochlorophyll cation radical and of an anion radical of a demetallated chlorophyll, bacteriopheophytin. When further chemistry is blocked, this primary charge separation is annihilated (in nanoseconds) by recombination of the radicals to yield fluorescence and a triplet state [1-5]². We describe here the *in vitro* photochemical generation as well as the optical and magnetic characterization of the anion radicals of bacteriopheophytins a and b, the pigments found in *Rhodospseudomonas spheroides* and *viridis*, respectively. The radicals undergo isotopic substitution at the proton positions which carry high unpaired spin densities.

The occurrence of chlorophyll-derived anion and cation radicals in photosynthesis has logically led to attempts at mimicking the natural act with artificial porphyrin systems. One of these is a heterogeneous system consisting of multiple monolayers of porphyrins deposited on an aluminum electrode which is immersed in a ferro-ferricyanide aqueous solution. This photoelectrochemical cell, originally described by Wang [6] was reported to generate ~1 V versus a platinum electrode (open circuit) on illumination of the porphyrin-coated electrode. Attempts to reproduce this cell using a number of porphyrins which exhibit a range of oxidation potentials have been unsuccessful, the photovoltages actually observed are an order of magnitude less than previously reported, notwithstanding efforts to remove or introduce impurities or charge carriers.

A. Chlorophyll radicals

Photolysis of bacteriopheophytin (BPh) a and b in pyridine containing 10M Na₂S and 1 M H₂O yields radicals which, on the basis of their optical (Fig. 1) and electron spin resonance spectra (Fig. 2) are similar to the one electron reduction products obtained by electrolysis in aprotic solvents [5]. The reduction can be induced by irradiation in each of the absorption bands of the pheophytins. For BPh a (5×10^{-5} M, room temperature) the quantum yield at 750 nm is 5×10^{-2} .

Analysis of the esr spectra is facilitated by electron-nuclear double resonance which reveals some of the photon interactions predicted [5] by self-consistent field molecular orbital calculations and by selective deuteration experiments. Examples of the latter are provided in Figs. 3-5 which display the esr spectra of deuterated BPh^{•-} a in deuterated pyridine and water, and computer simulations of the experimental spectra using the hyperfine splitting constants shown. If photolysis is performed in the presence of H₂O instead of D₂O, exchange of hydrogen for deuterium occurs first at the α , β , δ methine positions (Fig. 4), and eventually the methyl groups 1 and/or 5 undergo exchange (Fig. 5). The assignments have been verified by nuclear magnetic resonance. BPh b^{•-} reacts similarly (Fig. 6).

¹This work was performed under the auspices of the U.S. Energy Research and Development Administration.

²Figures in brackets indicate literature references at the end of this paper.

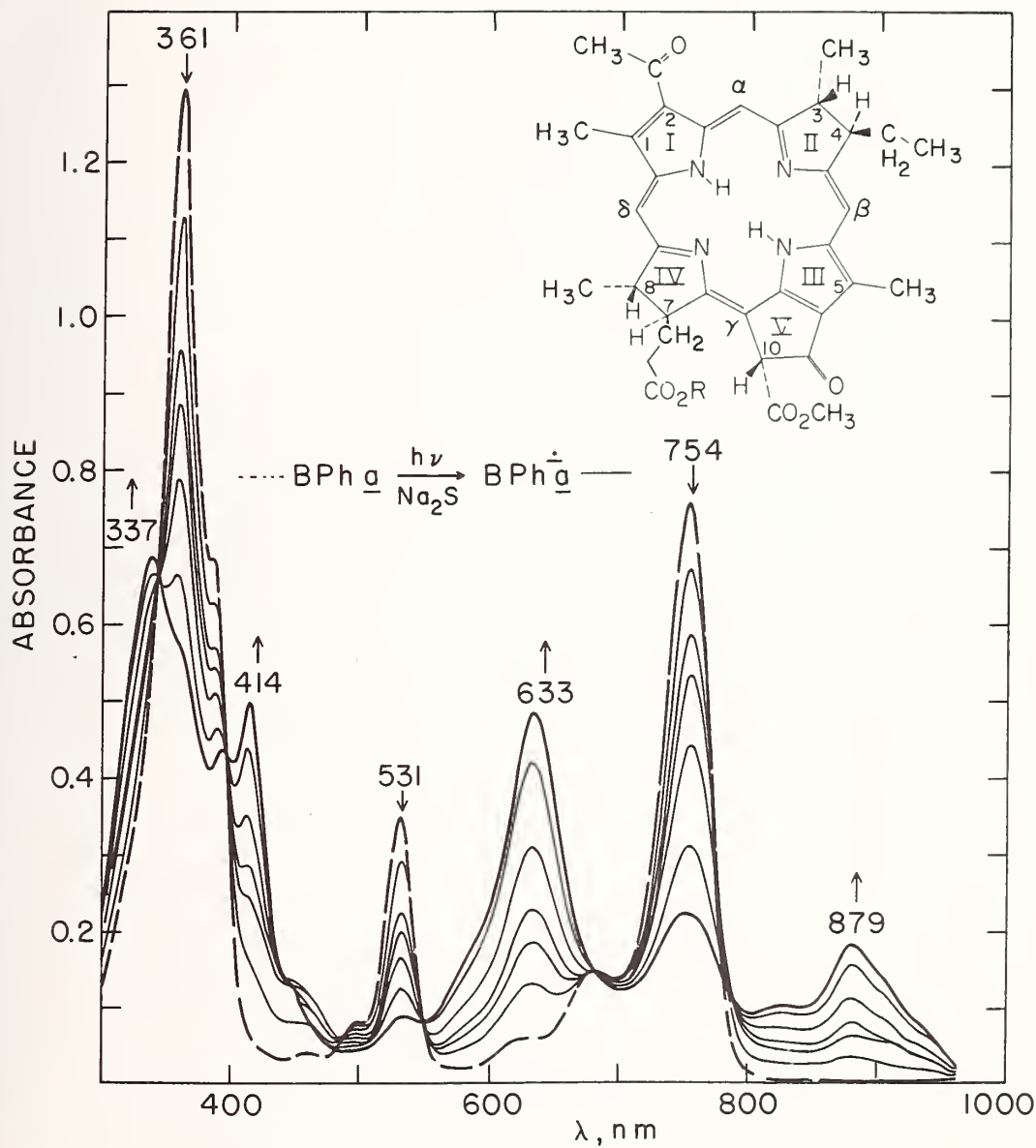


Figure 1. Optical changes, in $\text{C}_5\text{H}_5\text{N}/\text{H}_2\text{O}$ observed on photoreduction of BPh a to its anion radical. (Deviations from the isobestic points are due to traces of a "phase test" impurity [5].)

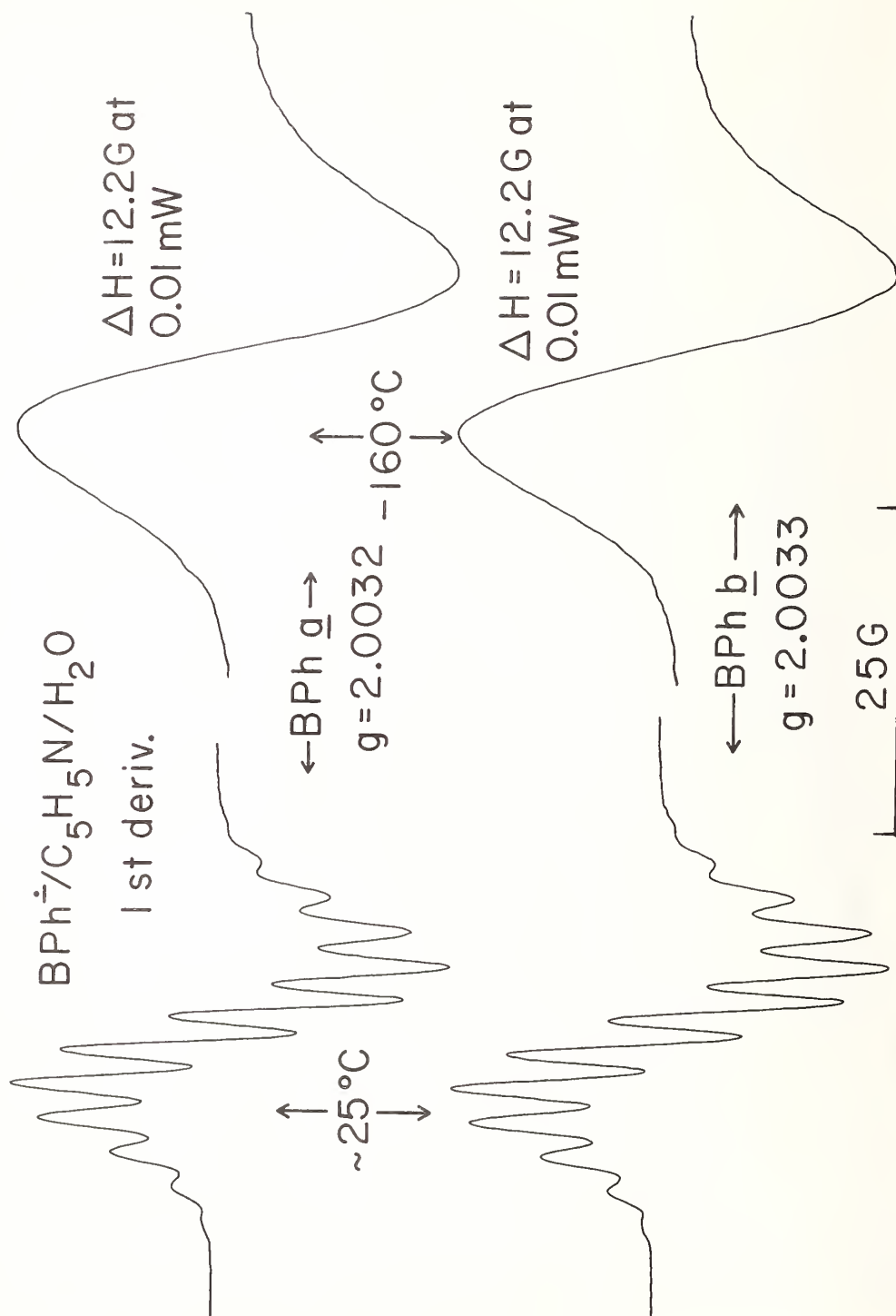


Figure 2. First derivative esr spectra, in $\text{C}_5\text{H}_5\text{N}/\text{H}_2\text{O}$, of the anion radicals of BPh a and b at 25 and -160°C . ΔH is the peak linewidth obtained at 0.01 mW.

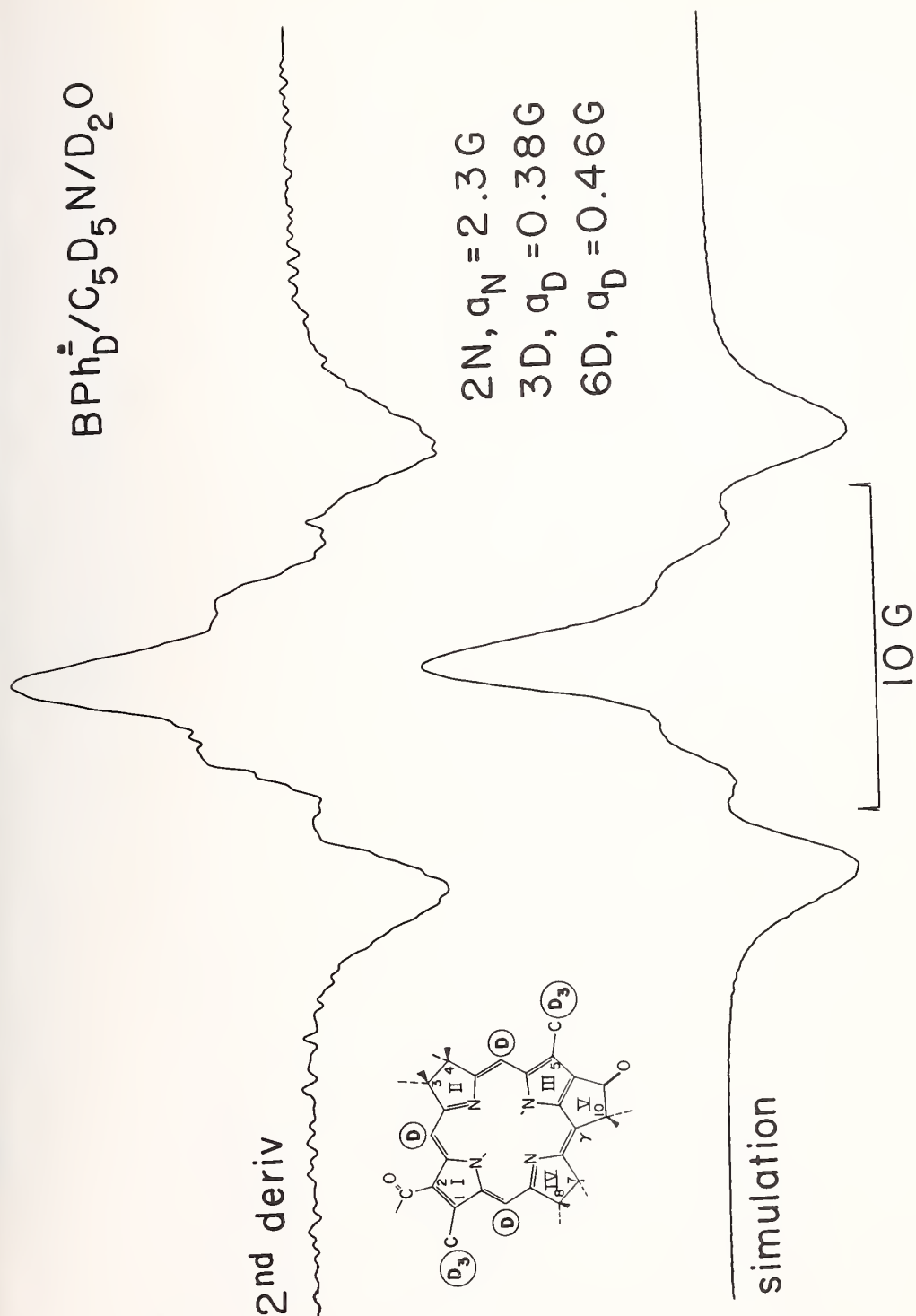


Figure 3. Second derivative esr spectrum of the perdeuterated BPh a anion generated photolytically in $\text{C}_5\text{D}_5\text{N}/\text{D}_2\text{O}$ and a computer simulation which assumes the splitting constants shown.

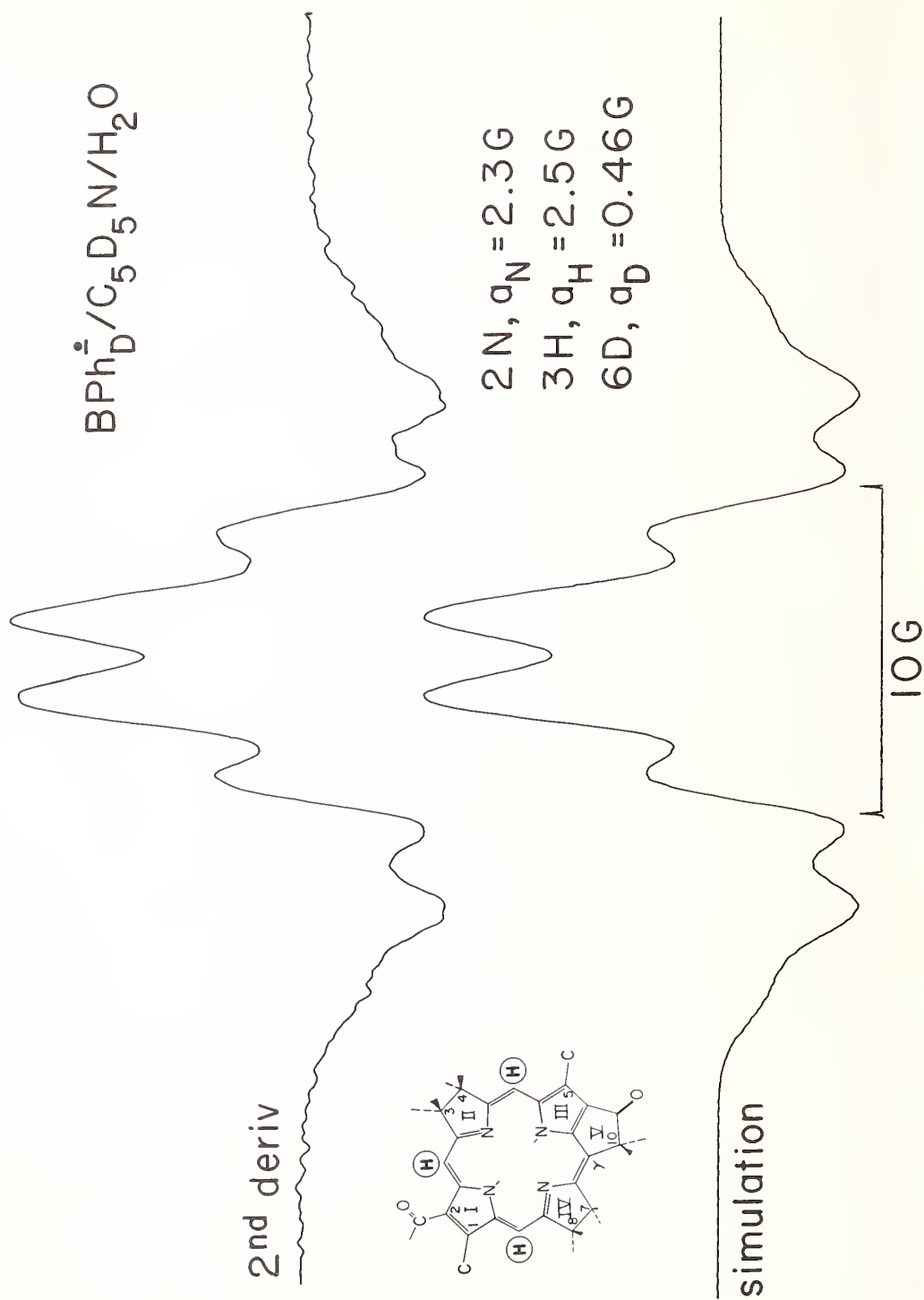


Figure 4. BPh^{\bullet} generated in $\text{C}_5\text{D}_5\text{N} / \text{H}_2\text{O}$, in which the methine deuterons have exchanged.

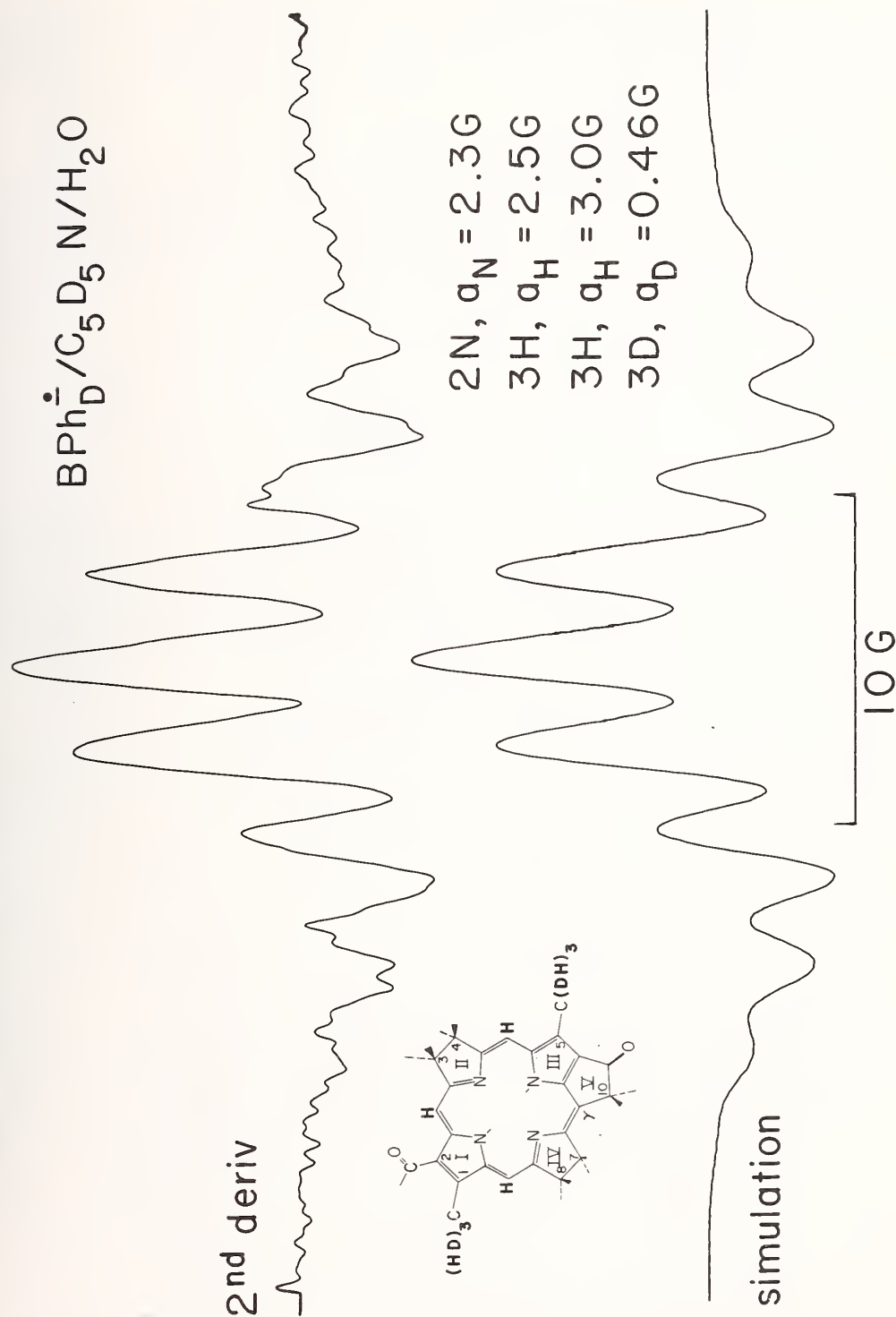


Figure 5. BPh a^{· -} in C₅D₅N/H₂O, in which the methine and ~50% of the 1 and 5 methyl deuterons (or 100% of either 1 or 5) have exchanged.

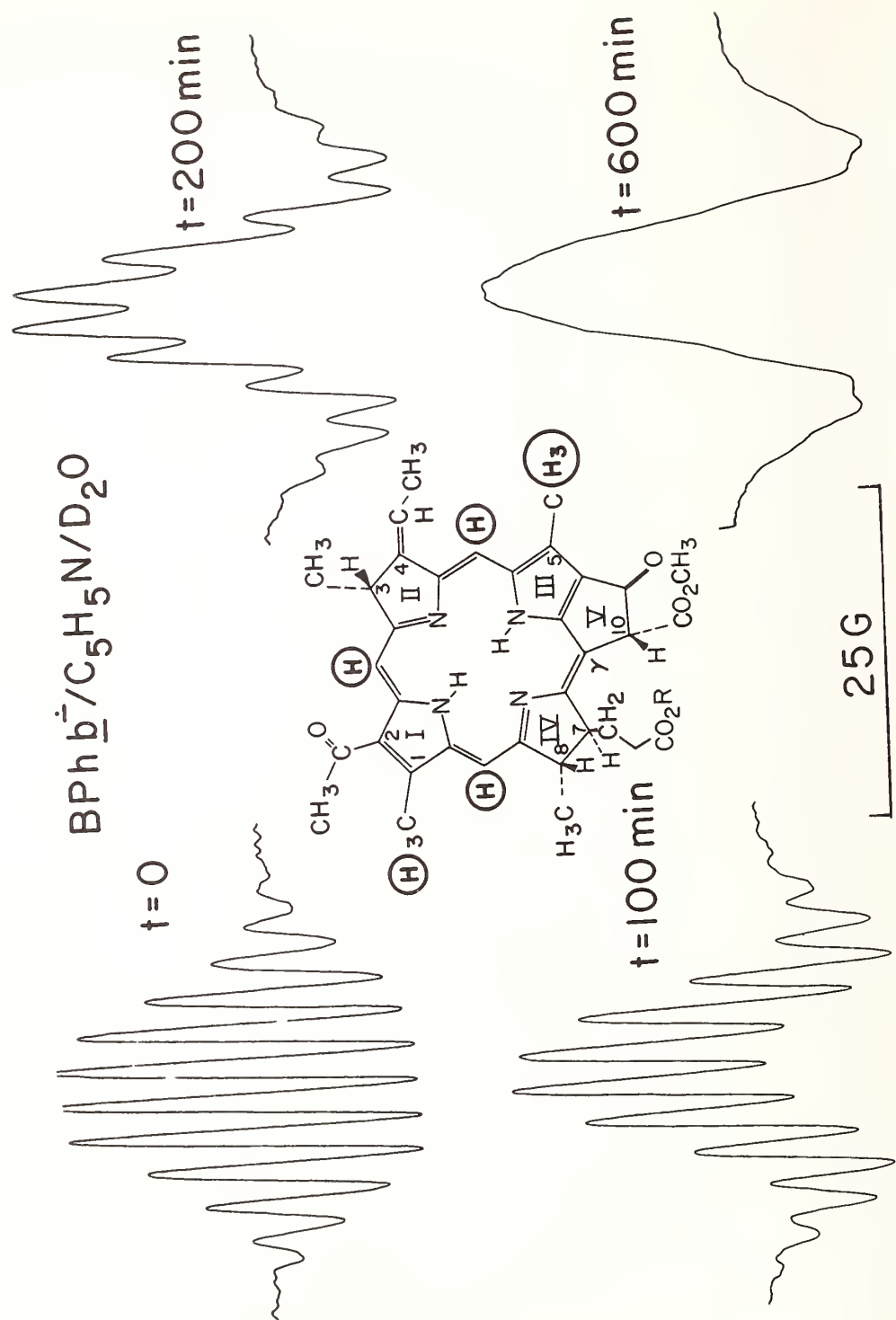
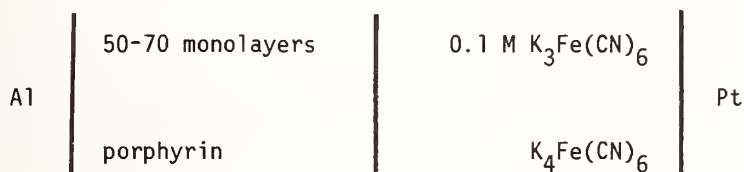


Figure 6. Changes in the esr spectra of BPh b^- , in $\text{C}_5\text{H}_5\text{N}/\text{D}_2\text{O}$, due to gradual replacement of protons by deuterons.

The exchange sites are those which carry high unpaired spin densities and a significant isotope kinetic effect is observed as well. Protonated BPh⁺ will substitute deuterium approximately an order of magnitude faster than the deuterated BPh⁺ will exchange with hydrogen.

B. Photoelectrochemical cells

Cells patterned on the Wang design shown were tested for photo-effects using copper, zinc, the μ -oxo-iron (III) dimer of meso tetraphenyl-porphyrins, zinc-porphine and-phthalocyanine. The cell consisted of 50-70 layers of porphyrin, deposited on a clean aluminum surface in a Langmuir trough, and immersed in an aqueous solution of potassium ferri-ferrocyanide.



Photovoltages (open circuit) of approximately 100 mv can be induced using white light with ultraviolet and infrared cut offs or by direct excitation of the porphyrin bands (~ 400 or 500 nm). Attempts to improve the photovoltages by changing the electrode surface, or by including free base porphyrins, or a porphyrin cation radical as possible impurities into the porphyrin coated electrode yielded no significant effects.

References

- [1] Rockley, M. G., Windsor, M. W., Cogdell, R. J. and Parson, W. W. (1975), Proc. Nat. Acad. Sci. USA 72, 2251.
- [2] Kaufman, K. J., Dutton, P. L., Netzel, T. L., Leigh, J. S. and Rentzepis, P. M. (1975), Science 188, 1301.
- [3] Dutton, P. L., Kaufmann, K. J., Chance, B. and Rentzepis, P. M., (1975) FEBS Lett. 60, 275.
- [4] Thurnauer, M. C., Katz, J. and Norris, J. R. (1975), Proc. Nat. Acad. Sci. USA 72, 3270.
- [5] Fajer, J., Brune, D. C., Davis, M. S., Forman, A. and Spaulding, L. D. (1975), Proc. Nat. Sci. USA 72, 4956; (1976) Brookhaven Symp. Biol. 28, in press.
- [6] Wang, J. H. (1969), Proc. Nat. Acad. Sci. USA 62, 653.

A KINETIC STUDY OF CH_3O_2 AND $(\text{CH}_3)_3\text{CO}_2$ RADICAL REACTIONS BY
KINETIC FLASH SPECTROSCOPY

Michael R. Whitbeck, Jan W. Bottenheim, Stuart Z. Levine, and
Jack G. Calvert

Department of Chemistry
The Ohio State University
Columbus, Ohio

The reactions of the hydroperoxy (HO_2), alkyl peroxy (RO_2), and the acylperoxy (RCOO_2) radicals are believed to be essential components of the reaction mechanism which describes photochemical smog generation. For example, these radicals are believed to be largely responsible for the oxidation of NO to NO_2 in the NO_x -hydrocarbon-polluted atmospheres:



It is postulated that HO , RO , and RCO_2 radical products of these reactions react in the atmosphere with O_2 , hydrocarbons, aldehydes, CO , etc., to regenerate other HO_2 , RO_2 and RCOO_2 radicals. In theory the $\text{NO} \rightarrow \text{NO}_2$ conversion continues to occur by way of these chain reactions, and the increasing ratio of $[\text{NO}_2]/[\text{NO}]$ causes the ozone to rise through the rapid chemical interactions of the sequence (4-6):



In view of the great significance attached to the reactions (1-3) by atmospheric scientists today [1]¹, it is disappointing to observe that the rate constant for reaction (1) has been determined only in indirect experiments [2], while those for reactions (2) and (3) have not been determined experimentally by any method to our knowledge; present estimates were derived from computer simulations of very complex smog chamber experiments and are of very limited accuracy.

In theory the alkyl peroxy radicals may also be important reactants in the atmospheric oxidation of SO_2 :



¹ Figures in brackets indicate literature references at the end of this paper.

Davis and coworkers [2a] have studied reaction (8) for which they estimated $k_8 = (5.2 \pm 1.1) \times 10^5 \text{ l} \cdot \text{mole}^{-1} \text{sec}^{-1}$. This rate constant coupled with the computer simulation of the complex chemistry of the polluted atmosphere suggest that reaction (8) is a major removal path for SO_2 in the polluted atmosphere [1b]. In view of the fact that reaction (7) is about 8 kcal/mole more exothermic than reaction (8), the rate constant for reaction (7) could in theory be somewhat larger than k_8 . If this is the case, then the significance of reaction (7) in the atmospheric conversion of SO_2 is probable.

In this work we attempted to study the reactions of several alkyl peroxy radicals using kinetic flash spectroscopy. We generated CH_3O_2 and $(\text{CH}_3)_3\text{CO}_2$ radicals by flash photolysis of $(\text{CH}_3)_2\text{N}_2\text{-O}_2$ and $[(\text{CH}_3)_3\text{C}]_2\text{N}_2\text{-O}_2$ mixtures, respectively. Previous work of Bjellqvist and Reitberger [3], Parkes and co-workers [4], and Burggraf and Firestone [5], have shown that the alkylperoxy radicals exhibit an ultraviolet absorption band (2400-3000 Å) of moderate intensity which is convenient for kinetic studies of these radicals.

The xenon flash lamp employed in these experiments operated at 20 kJ per flash with a half-width at half-maximum intensity of about 50 μsec . The Vycor tube of the flash lamp paralleled the quartz reaction cell (220 cm in length, 6.3 cm in internal diameter) but was separated from it by a Pyrex plate filter (0.5 cm thickness) which transmitted only light of $\lambda > 2900 \text{ Å}$. A white surfaced reflector surrounded the flash lamp and cell. The cell housed a multiple reflection White optical system which was set for a path length of 800 cm in most of this work. Actinometric estimates of the extent of azoalkane photolysis, and hence the number of alkyl (and RO_2) radicals formed per flash, were made by two independent methods: (1) measurements of the pressure increase which resulted in the flash photolysis of the pure azoalkane (1-5 Torr); (2) measurements of the amount of nitrogen product formed following the flash photolysis using mass spectrometric analysis. Both methods gave essentially the same results. Since very small amounts of decomposition of the azoalkane occurred in these experiments (less than 0.48 percent of the initial amount), and the pressure of added oxygen was high (about 50 Torr), the temperature rise during an experiment was no more than a few degrees. The ultraviolet and visible spectrum of the flash products was recorded photographically using a 0.65 m Hilger spectrograph and a small argon flash lamp which was fired with delay times varied from 0.6 to 2.0 msec following the flash. In kinetic runs a continuous 150 w point source xenon arc was employed together with a 0.5 m Jarrell Ash monochrometer equipped with an RCA 1P-28 photomultiplier-oscilloscope combination. Both sets of data define an absorption band with a maximum near 2550 Å which we believe results from the RO_2 radicals. In most kinetic runs absorbance at 2650 Å was followed to obtain the rate data.

The kinetics of the CH_3O_2 and $(\text{CH}_3)_3\text{CO}_2$ radical disappearance was found to be second order when the appropriate azoalkane was photolyzed in mixtures with pure O_2 . The rate constants for the radical decay are in reasonable accord with those of Parkes and co-workers [4] who used a modulated beam photolysis experiment. However, this agreement may be somewhat fortuitous in that the absorption spectrum observed by these workers and attributed to the CH_3O_2 radical is somewhat different in band position and extinction than we observe. Perhaps interferences from the HO_2 radical absorption may have been important in the previous modulated beam photolysis studies. The build-up of CH_2O product and its time dependence observed in the previous study would insure a major source of HO_2 species.

Experiments with flash photolyzed mixtures of azoalkane, O_2 , and SO_2 were made in an attempt to derive the constant for reaction of CH_3O_2 with SO_2 . The addition of SO_2 to this system at pressures in excess of 0.5 Torr resulted in aerosol formation following the flash, and so the useful range of SO_2 pressure was very limited. The present data suggest that $k_7 \leq 2 \times 10^6 \text{ l} \cdot \text{mole}^{-1} \text{sec}^{-1}$. We are continuing further work with the flash system and with a steady state photochemical system with FTS infrared analysis in an attempt to further define estimates of k_2 and k_7 .

References

- [1] For a general review of the very extensive literature and a more detailed discussion of the current ideas concerning the mechanism of photochemical smog formation, see: a) Demerjian, K. L., Kerr, J. A. and Calvert, J. G., *Adv. Environ. Sci. Technol.*, 4, 1 (1974); b) Calvert, J. G. and McQuigg, R. D., *Int. J. Chem. Kinet.*, Symp. No. 1, 113 (1975); c) Niki, H., Daby, E. E. and Weinstock, B., Chapter 2, in "Photochemical Smog and Ozone Reactions," Gould, F. F., Editor, *Advances in Chemistry Series 113*, Amer. Chem. Soc., Washington, D. C., 1972, p. 16; d) Altshuller, A. P. and Bufalini, J. J., *Environ. Sci. Technol.*, 5, 39 (1971).
- [2] a) Payne, W. A., Stief, L. J. and Davis, D. D., *J. Amer. Chem. Soc.*, 95, 7614 (1973); b) Simonaitis, R. and Heicklen, J., *J. Phys. Chem.*, 77, 1096 (1973).
- [3] Bjellqvist, B. and Reitberger, T., *INIS*, 1104 (1971).
- [4] Parkes, D. A., Paul, D. M., Quinn, C. P., and Robson, R. C., *Chem. Phys. Letters*, 23, 425 (1973).
- [5] Burggraf, L. W. and Firestone, R. F., *J. Phys. Chem.*, 78, 508 (1974).

THE REACTION OF OH RADICALS WITH C_3H_6 AND C_2H_4 ¹

Ralph Overend and George Paraskevopoulos

Division of Chemistry
National Research Council of Canada
Ottawa, Canada K1A 0R9

1. Introduction

There is considerable interest in the mechanism and the rates of reaction of olefins with radicals of atmospheric interest. In the case of hydroxyl radicals with ethylene and propylene there are few absolute rate data at atmospheric pressure; the majority of the data [1]² having been obtained at low pressures. The reported rates vary by a factor of 3-5 and in the case of ethylene a systematic effect of pressure has been identified [1a]. In the present paper we report measurements of hydroxyl radical reactions over the pressure range 20-400 torr and with various third bodies, as measured by the technique of flash photolysis resonance absorption.

The results for ethylene show an effect due to pressure and nature of the third body while those of propylene are pressure independent in the range of our measurements.

2. Experimental

The apparatus and technique have been described in detail elsewhere [2]. Hydroxyl radicals were created by the Vacuum U.V. ($\lambda > 160$ nm) photolysis of water in the presence of the other reactant; their concentration was monitored by following the time resolved attenuation of the OH resonance radiation (Q_1^3 or Q_1^4 rotational lines of the (o,o) band of the $A^2\Sigma^+ \rightarrow X^2\Pi$ transition) produced by a microwave discharge in a low pressure Ar/H₂O mixture. Signal averaging was used to improve the signal to noise ratio. The concentration of the olefin was such that the measured pseudo-first order rates were between 4×10^3 and 3×10^4 s⁻¹.

To minimize the photolysis of the olefin while still permitting the generation of sufficient hydroxyl radicals from the water vapor, a filter 8 mm deep of NH₃ at 10 torr was used to reduce photolysis at wavelengths longer than 190 nm.

3. Results and Discussion

A. Propylene

Initial experiments with the propylene/OH system showed that the apparent rate decreased with repeated flashes on the same mixture and that the decrease was larger with high (≈ 600 J) flash energy and high absorption by OH, (i.e., high hydroxyl concentration). Gas chromatographic analyses of C₃H₆/He mixtures corresponding to our experimental range showed that the direct photolysis of C₃H₆ at 600 J was approximately 5 - 10 percent per flash, while with water present $\sim 30 - 40$ percent of C₃H₆ was consumed per flash. All experimental values reported were obtained in experiments of a single flash < 100 J and

¹Issued as N.R.C.C. No. 15482

²Figures in brackets indicate the literature references at the end of this paper.

low H_2O pressure (i.e., absorption by OH of <5 percent). Under these conditions, we calculate that photolysis of C_3H_6 is insignificant and that even at low C_3H_6 pressures the ratio $\text{C}_3\text{H}_6/\text{OH}$ is larger than 20 and consumption of olefins should not significantly affect our measurement. The second order rate constant k_{II} obtained for C_3H_6 is, $k_{\text{II}} = 2.5 \pm 0.5 \times 10^{13} \text{ cm}^3 \text{ mol}^{-1} \text{ s}^{-1}$ and was not affected by the pressure or the nature of the third body ($M = \text{He}$, 50 torr to $M = \text{SF}_6$, 400 torr.) A twenty fold variation of the ratio $\text{C}_3\text{H}_6/\text{OH}$ did not produce a change in the measured rate within the experimental error; this, in accordance with a numerical simulation [2] would indicate no influence of secondary radical reactions on the rate constant.

B. Ethylene

The conditions for minimum OH concentration described above were also used in the experiments with C_2H_4 . The reaction was studied over a range of pressures and with He, SF_6 , CF_4 and H_2O as third bodies. The rate was found to depend slightly on the pressure and the nature of the third body; the value of k_{II} was found to be $5.4 \pm 0.5 \times 10^{12}$ and $6.5 \pm 0.5 \times 10^{12} \text{ cm}^3 \text{ mol}^{-1} \text{ s}^{-1}$, for 50 torr of He and 400 torr of SF_6 or CF_4 respectively. These values are higher than those found in previous studies at low pressures of He and with low levels of H_2O cf. reference [1a]. In a series of experiments the k_{II} was measured at 50 torr of He, constant C_2H_4 concentration, and decreasing pressure of H_2O . The results are shown in figure 1. Although the precision of our measurement decreases with

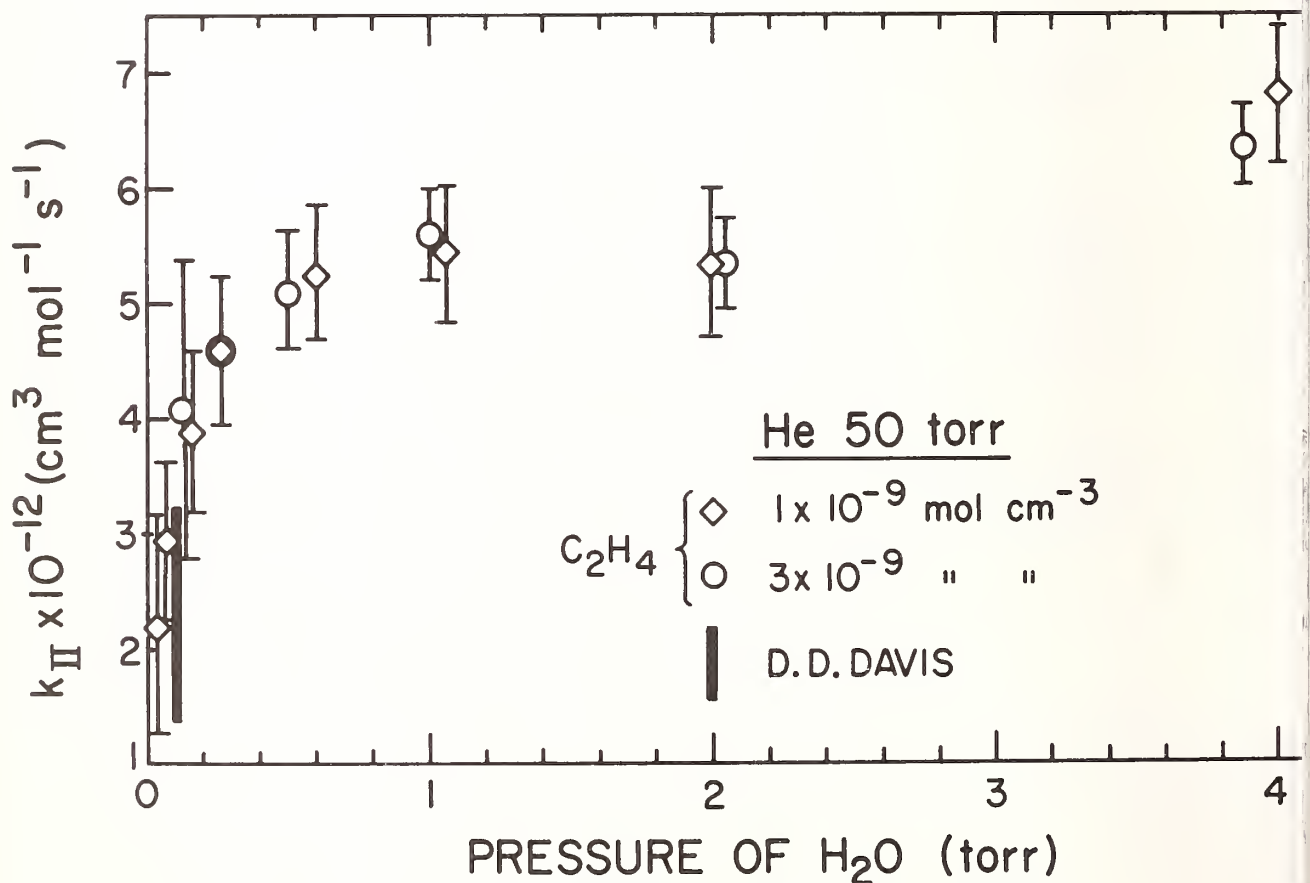
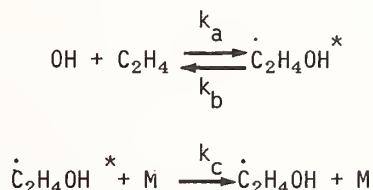


Figure 1. Pressure of H_2O (torr)

decreasing OH concentration, the values of k_{II} obtained approach those of Davis et al. [1a] with decreasing water pressure as may be seen in the figure. This could be attributed to the high efficiency of H_2O as a third body as was found to be the case in the $OH + NO$ combination [3]. It could also be attributed to secondary reaction of OH. It was not possible to change the ratio C_2H_4/OH over a very large range, because the pressure of H_2O had to be kept constant. Nevertheless a variation of the ratio C_2H_4/OH by a factor of 4 at several pressures of H_2O did not produce a change in the measured rate within the experimental error. If we assume then, as is indicated by the above tests, that our results are free from interference from secondary reactions, the rate must depend on the pressure and nature of the third body and not on the OH concentration, according to the following scheme:



in which H_2O , SF_6 and CF_4 are very efficient third bodies while He is inefficient.

Assuming this interpretation to be correct a steady state treatment with respect to the concentration of the adduct \dot{C}_2H_4OH gives,

$$\frac{1}{k_{II}} = \frac{1}{k_a} + \frac{k_b}{k_a k_c [M]}$$

and a plot of k_{II}^{-1} against $[M]^{-1}$ for H_2O gives

$$k_{II\infty} = 6.3 \pm 0.5 \times 10^{12} \text{ cm}^3 \text{ mol}^{-1} \text{ s}^{-1}$$

This value is in good agreement with the measured value of $6.5 \pm 0.5 \times 10^{12} \text{ cm}^3 \text{ mol}^{-1} \text{ s}^{-1}$ at 400 torr of SF_6 and with the value of $5.2 \pm 1 \times 10^{12} \text{ cm}^3 \text{ mol}^{-1} \text{ s}^{-1}$ determined at atmospheric pressure of air by a relative method [4]; on the other hand it is double the value by Palmer [5] ($\sim 3 \times 10^{12} \text{ cm}^3 \text{ mol}^{-1} \text{ s}^{-1}$) from a similar treatment of the results of Davis et al. [1a].

Work on the reactions of OH with olefins is continuing with emphasis on tests for secondary reactions.

References

- 1a] Davis, D. D., Fischer, S., Schiff, R., Watson, R. T., and Bolinger, W., J. Chem. Phys. 63, 1707 (1975).
- 1b] Atkinson, R. and Pitts, J. N., *ibid.* 63, 3591 (1975).
- 1c] Pastrana, A. V. and Carr, R. W., Jr., J. Phys. Chem. 79, 765 (1975) and references therein.

- [2] Overend, R. P., Paraskevopoulos, G., and Cvetanovic, R. J., Can. J. Chem. 53, 3374 (1975).
- [3] Overend, R. P., Paraskevopoulos, G., and Black, C., J. Chem. Phys. 64, 4149 (1976).
- [4] Lloyd, A. C., Darnall, K. R., Winer, A. M., and Pitts, J. N., Jr., J. Phys. Chem. 80, 789 (1976).
- [5] Palmer, H. B., J. Chem. Phys. 64, 2699 (1976).

ON THE TRIPLET STATE(s) OF SULPHUR DIOXIDE

Jan W. Bottenheim, Fu Su, David L. Thorsell, Jack G. Calvert and Edward Damon

The Ohio State University
Columbus, Ohio 43210

1. Introduction

Theoretical work [1]¹ indicates that the first three triplet-states of SO_2 ($^3\text{B}_2$, $^3\text{A}_2$, $^3\text{B}_1$) are very close in energy and can be expected in the wavelength range of 400-3900 Å. High resolution spectroscopic work has shown perturbations in $^3\text{B}_1$ bands which give indirect evidence of the proximity of the $^3\text{A}_2$ and $^3\text{B}_2$ states in this region, although the major features of the optical spectrum are undoubtedly due to the $^3\text{B}_1$ -state [2].

Phosphorescence-sensitization studies with SO_2 -biacetyl mixtures form other evidence for the presence of at least one other triplet state besides the $^3\text{B}_1$ -state in this region [3]. Moreover, photochemical reaction studies seem to imply the participation of more than the two optically accessible singlet states ($^1\text{A}_2$ and $^1\text{B}_1$) and the $^3\text{B}_1$ -state only [4]. Direct evidence for the presence of the other triplet states is missing as of today, however.

The theoretically calculated zero-pressure lifetime of the emitting $^3\text{B}_1$ -state of SO_2 , based on measurements of the integrated absorption spectrum indicates a reciprocal lifetime of $79 \pm 5 \text{ sec}^{-1}$ [5]. The reported experimental values of this lifetime, based on phosphorescence of lifetime studies, are rather dramatically at odds with this number, ranging from 75 to 2000 sec^{-1} [6]. If these data are correct a large part of the $^3\text{B}_1$ -state molecules should decay in a unimolecular non-radiative fashion, which is not expected within the present theories of radiationless transitions, and a modification of this theory might be necessary.

We have initiated research to establish more clarity into these matters and will report some of the results here. Two different approaches were followed. The direct singlet-triplet absorption spectrum was probed with a much longer pressure-path than before in an attempt to identify new absorption-bands that might be described to the other triplet-states. The major part of this work concerns phosphorescence lifetime studies, in which we used several different lasers to excite SO_2 -molecules at a range of important wavelengths.

2. Experimental

The direct singlet-triplet absorption study was performed with a 2 m long multiple-pass White-cell. With SO_2 pressures of 400 to 600 Torr a pressure-pathlength of 28,800 to 43,200 Torr-meter was obtained. The absorption-spectrum was probed with a 150 Watt e-high-pressure lamp with a soft-glass filter in front to minimize output below 3200 Å, and monitored with a 0.5 m Jarrel-Ash monochromator.

In the phosphorescence experiments the reaction cell was of the 22 l variety (diameter 5 cm) to allow the measurement of long-living emitting species to low pressure regions

Figures in brackets indicate the literature references at the end of this paper.

without having major wall-deactivation effects to correct for [7]. The cell has two side-arms with fused-on Brewster angle windows (Suprasil) for entrance and exit of the laser-beam, and a third side-arm at 90° with a 2 inch diameter Suprasil-window to which as close as possible was positioned an RCA 7265 photomultiplier. Between the window and the PM-tube a Kodak Wrattan 2B filter and an Optics Industries cutoff filter nr. WG-395 were inserted to minimize scattered laserlight and fluorescence of singlet-excited SO₂-molecules.

All lasers used in this study were KDP-doubled dye-lasers of moderately high power in the uv (3 to 10 Kwatt). An echelle grating in the 100 percent mirror in the dye-laser cavity narrowed all laserlight to a 2.5 Å bandwidth. For excitation at 3631 Å a Ruby laser pumped solution of dye nr 16 (Candela) was employed, resulting in an approximate 1 Mwatt 25 nsec laserpulse at 7262 Å. All other wavelengths were obtained by flashlamp-excitation of appropriate dye-solutions in a coaxial flashlamp-dyeflow cell (Candela, model CL-66), resulting in approximately 0.150 Mwatt, 150 nsec laser pulses.

The lasers could not be rapidly pulsed, so essentially single-shot experiments were done. The phosphorescence signals were monitored via a Tektronix 7704 oscilloscope, and digitized with a Biomation 610 transient digitizer for storage on paper tape. The traces of several shots at a particular SO₂ pressure were computer averaged and then displayed in a semi-log form on the CRT-screen of a PDP-7 computer, after which appropriate least-square treatment was performed to establish the decay-parameters.

3. Results and Discussion

A. Direct singlet-triplet absorption study

Several new bands were observed in the absorption spectrum between 3800 and 4100 Å. A close analysis shows that all these bands are hot bands of the $\tilde{a}^3B_1-X^1A_1$ spectrum, however. Table 1 shows the identification of these bands, whereas Table 2 compares some relative integrated absorption-intensities with calculated relative number densities of ground state SO₂, assuming a Boltzmann distribution only. A conclusive test was next performed, where the cell was cooled to -15 °C. A dramatic decrease of intensity of all new bands was observed.

Table 1

Band-nr	$\nu_{cm^{-1}}$	Identification	$\tilde{\Delta\nu}_{exp}^a$	$\tilde{\Delta\nu}_{calc}^a$
1	24631	(0,0,0)←(1,0,0)	1145	1151
2	24732	(0,0,0)←(0,2,0)	1042	1035.4
3	24989	(0,1,0)←(1,0,0)	1149	1151
1st hot band	25258	(0,0,0)←(0,1,0)	518	518
4	25466	(0,2,0)←(0,2,0)	1029	1035.4
0-0 band	25776	(0,0,0)←(0,0,0)	(b)	(b)
5	25991	(0,2,0)←(0,1,0)	503	518
		(1,1,0)←(0,2,0)	1043	1035.4

^a $\tilde{\Delta\nu}$ indicate the experimental and calculated distance to the indicated triplet band.

^bThis band was used as reference. All other bands are determined from their distance to this band.

Table 2

	$(0,0,0) \leftarrow (0,1,0)$	$(0,0,0) \leftarrow (0,2,0)$	$(0,0,0) \leftarrow (1,0,0)$
Calc	1	0.084	0.048
Exp.	1	0.101	0.056

From these experiments it follows that the integrated extinction coefficient of transitions to other triplet-states, if present in the studied wavelength-area should be at least a factor 50 less than to the 3B_1 -state. It seems therefore unlikely that such other states will be identifiable at all in absorption.

B. Phosphorescence studies

Our data-analysis was initially directed to detect similar non-exponential decay-curves as seen in fluorescence-studies by Brus and McDonald [8]. Only single-exponential decay was observed to pressures as low as 2 m Torr. Some curvature below this pressure becomes noticeable, but this is readily shown to be due to residual fluorescence under these conditions. (Only with excitation in the singlet manifold was it possible to study the phosphorescence down to these low pressures.)

Figure 1 shows a Stern-Volmer plot of the measured decay-rates of the phosphorescence signal as function of pressure for some different wavelengths of excitation. Since all

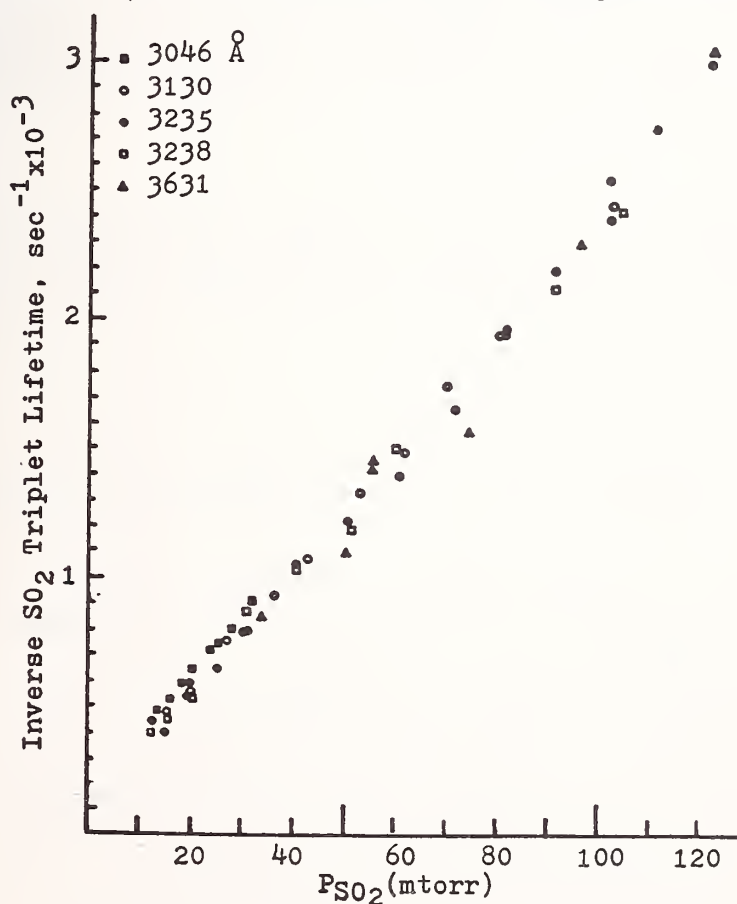


Figure 1. Stern-Volmer plot for the phosphorescence of SO₂

data points fall very well within the error limits of the least squares line, we conclude that no matter how SO_2 is excited, the same phosphorescing state is monitored. This applies equally well for excitation at 3631 Å, at which wavelength strong perturbations are observed in the absorption-spectrum, tentatively ascribed to the influence of other triplet-states, and for excitation at 3130 Å at which wavelength two singlet states are populated ($^1\text{A}_2$ and $^1\text{B}_1$) as possible precursors for the triplet-state.

The latter observation is of interest, since it indicates that the very efficient collisional deactivation of the $^1\text{A}_2$ -state should lead at least in part to triplet-population. In fact, simple spin-orbit coupling should favor the $^1\text{A}_2$ -state as the precursor to the $^3\text{B}_1$ -state; and for excitations at 3235 Å and 3251 Å, where we estimate that the $^1\text{A}_2$ -state is initially populated to the extent of 24 and 58 percent at 3235 Å and 3251 Å respectively.

All these results point to the same conclusion that only one triple state is seen in phosphorescence. Although cascading from another triplet-state has been suggested [10] is not excluded, it is unlikely in view of the fact that our conclusion holds to pressures down to at least 10 m Torr, where even complete vibrational relaxation within the $^3\text{B}_1$ -state is not complete [11].

Our phosphorescence data permit a new estimate of the zero-pressure lifetime of the $^3\text{B}_1$ -state. It has been suggested that the much higher experimentally determined reciprocal zero pressure lifetimes are in error due to too long extrapolation to zero pressure [6]. Our data based on several excitation-wavelengths in the pressure-region of 10 to 100 m Torr, see figure 1, all tend to indicate a value of 130 to 150 sec^{-1} . Taking the inherent experimental errors in our experiments and in the determination of the integrated absorption-coefficient into account, we feel this value is the same order of magnitude and therefore suggest with some caution that the true zero pressure quantum yield of phosphorescence of the $^3\text{B}_1$ -state may be near unity in agreement with the existing theory.

Many stimulating discussions with Professor J. D. Meadors during the construction of the different lasers is gratefully acknowledged. Professor C. Weldon Mathews, Dr. K. J. Chung, Mrs. R. Damon and B. Hessler made valuable contributions to parts of this work, and computer time was contributed by the ElectroScience Laboratory of The Ohio State University.

References

- [1] Hayes, T. F. and Pfeiffer, G. V., J. Am. Chem. Soc., 90, 4773 (1968); Hillier, I. H. and Saunders, V. R., Molec. Phys. 22, 193 (1971); Chung, K. J., Ph.D Thesis, Ohio State University, 1974.
- [2] Brand, J. C. D., Jones, V. T., and diLauro, C., J. Mol. Spectr., 45, 404 (1973).
- [3] Fatta, A. M., Mathias, E., Heicklen, J., Stockburger, III, L., and Braslavski, S., J. Photochem., 2, 119 (1973/74).
- [4] cf. ref. 3; also Chung, K. J., Calvert, J. G., and Bottenheim, J. W., Int. J. Chem. Kinet., 7, 161 (1975).
- [5] Strickler, S. J., Vikesland, J. P., and Bier, H. D., J. Chem. Phys., 60, 664 (1974).
- [6] Briggs, J. P., Caton, R. B., and Smith, M. J., Can. J. Chem., 53, 2133 (1975).

- 7] Sackett, P. B. and Yardley, J. T., J. Chem. Phys., 57, 152 (1972).
- 8] Brus, L. E. and McDonalds, J. R., J. Chem. Phys., 61, 97 (1974).
- 9] Mettee, H. D., J. Chem. Phys., 49, 1784 (1968).
- 10] James, F. C., Kerr, J. A., and Simons, J. P., Chem. Phys. Lett., 25, 431 (1974).
- 11] Canton, R. B. and Gangadharan, A. R., Can. J. Chem., 52, 2389 (1974).

THE $\text{SO}_2(^3\text{B}_1)$ PHOTSENSITIZED ISOMERIZATION OF CIS AND
TRANS-1,2-DICHLOROETHYLENE

Fred B. Wampler

University of California
Los Alamos Scientific Laboratory
Los Alamos, NM 87545

Jan W. Böttenheim

Chemistry Department
Ohio State University
Columbus, Ohio

Recently, several investigations of irradiated sulfur dioxide and 2-butene systems have been reported by Cox [1]¹, Penzhorn and Güsten [2], Penzhorn and Filby [3], Demerjian, Calvert, and Thorsell [4], and Demerjian and Calvert [5]. These studies indicate that the chemistry is consistent with the SO_2 photosensitized isomerization of one isomer of 2-butene to the other isomer. Demerjian, Calvert, and Thorsell [4] populated the $\text{SO}_2(^3\text{B}_1)$ state directly from the $\text{SO}_2(\text{X}, ^1\text{A}_1)$ ground state using broad band 3500-4100 Å excitation radiation and their results indicated that the $\text{SO}_2(^3\text{B}_1)$ state can photosensitize the isomerization of the 2-butenes. The other studies, references [1-3,5], were consistent with the role of $\text{SO}_2(^3\text{B}_1)$ molecules having the capability to cause isomerization, but their initial excitation routes did involve population of excited electronic states other than $\text{SO}_2(^3\text{B}_1)$ and consequently their results regarding the role of $\text{SO}_2(^3\text{B}_1)$ molecules cannot be as unequivocal as those of Demerjian, Calvert, and Thorsell [4].

The study of SO_2 -olefinic systems other than 2-butene certainly seemed worthwhile to try to better characterize the reactions of excited SO_2 molecules with olefins. It seemed desirable to restrict the excited populated state to $\text{SO}_2(^3\text{B}_1)$ and to investigate its photochemistry with cis and trans-1,2-dichloroethylene. These isomers do permit the olefinic collision partner to be quite chemically different from 2-butene and thus allow one to see if the Demerjian, Calvert, and Thorsell mechanism can be extended to other olefins.

Lifetime measurements of $\text{SO}_2(^3\text{B}_1)$ molecules in the presence of cis and trans-1,2-dichloroethylene were made using time resolved laser induced phosphorescence. A modified Candella flashlamp pumped dye laser (Rhodamine B) was tuned to 6260 Å, passed through a KDP crystal to double the frequency to yield 3130 ± 1 Å, and the filtered 3130 Å laser pulse (10 kwatt peak power, 15 nsec full width at half intensity) entered at the Brewster angle to the 23 l. reaction vessel which had been designed to allow for proper viewing of emitted light at right angles to the laser beam. The sweep time base on the oscilloscope was adjusted to allow for the rapid decay of the fluorescence from excited singlet sulfur dioxide molecules, and the phosphorescence decay could be distinctly separated with confidence from the fluorescence. These decay curves permitted a direct evaluation of the quenching constants at 22 °C for the removal of $\text{SO}_2(^3\text{B}_1)$ molecules by the cis and trans isomers.

Quantum yields for the SO_2 photosensitized isomerization of cis and trans-1,2-dichloroethylene were measured. The light source was a 1000 watt Hg-Xe lamp properly positioned in an Oriel Model 6140 housing. An Oriel Model 6128 Universal Lamp Power Supply was used in conjunction with the lamp. A focusing sleeve, to provide proper illumination, was positioned between the lamp and the entrance slit of a Schoeffel 1/4 meter grating

¹ Figures in brackets indicate literature references at the end of this paper.

monochromator. A grating blazed at 3000 Å and having a reciprocal linear dispersion of 3 Å/mm slit width was employed. The monochromator's output was centered at 3712 Å and had a full width at half intensity of 150 Å. Relative light intensity measurements were made with a 7020 Oriel Radiometer Unit utilizing a photodiode which had a spectral sensitivity maximum near 3400 Å. Absolute intensity measurements were made using either potassium ferrioxalate actinometry or by using a Scientech Model 36-001 disc calorimeter in conjunction with a Scientech Model 362 power energy meter. Agreement between the two methods was found to be ± 2 percent, and because of its simplicity of use most absolute intensity measurements were made using the disc calorimeter. Product analysis was by gas chromatography.

A kinetic treatment of the initial quantum yield data was consistent with the formation of a polarized charge-transfer intermediate whenever $\text{SO}_2(^3\text{B}_1)$ molecules and one of the 1,2-dichloroethylene isomers collide which ultimately decays unimolecularly to the cis isomer with a probability of 0.70 ± 0.26 and to the trans isomer with a 0.37 ± 0.16 probability. Quenching rate constants for removal of $\text{SO}_2(^3\text{B}_1)$ molecules by cis and trans-1,2-dichloroethylene have been estimated from quantum yield data and from laser excited phosphorescence lifetimes. Estimates of the quenching rate constant (units of $\ell. \text{mole}^{-1}\text{sec}^{-1}$) for the cis isomer are: $(1.63 \pm 0.71) \times 10^{10}$, quantum yield data, and $(2.44 \pm 0.11) \times 10^{10}$, lifetime data; and for the trans isomer: $(2.59 \pm 0.09) \times 10^{10}$, lifetime data, and $(2.35 \pm 0.89) \times 10^{10}$, quantum yield data. An experimentally determined photostationary composition, $[\text{cis-C}_2\text{Cl}_2\text{H}_2]/[\text{trans-C}_2\text{Cl}_2\text{H}_2] = 1.8 \pm 0.1$, was in good agreement with a value of 2.00 ± 1.15 which was predicted from rate constants derived in this study.

The mechanism choice, to be discussed, required that $1/\phi$ be a linear function in the $[\text{O}_2]/[\text{C}_2\text{Cl}_2\text{H}_2]$ ratio and figure 1 depicts a plot to test this relationship. Representative

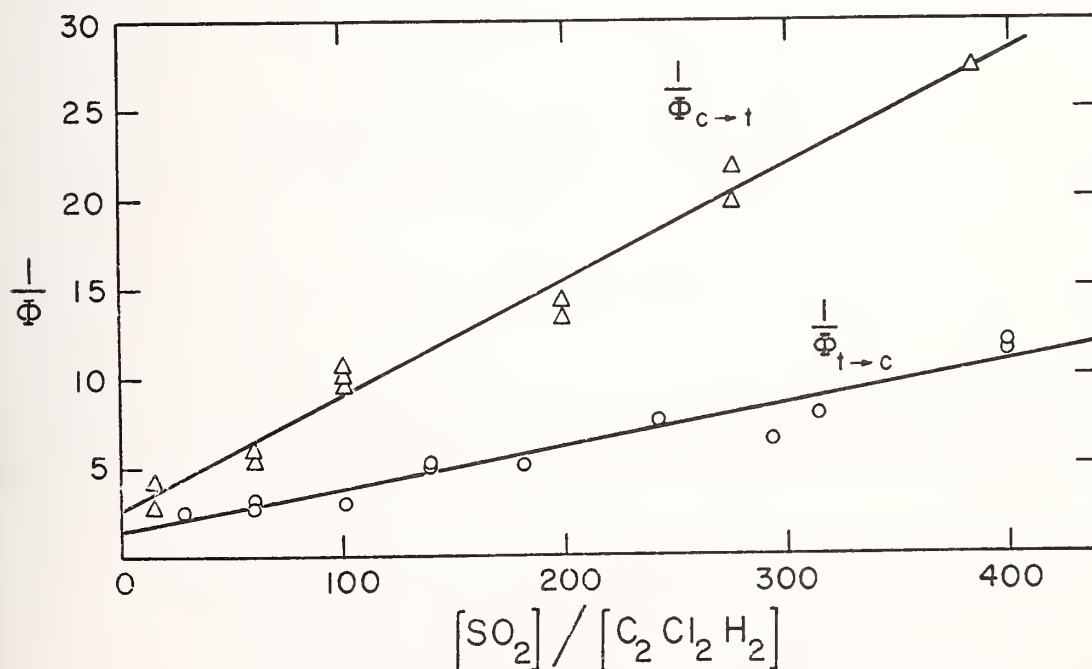


Figure 1. Plot of $1/\phi$ versus the $[\text{SO}_2]/[\text{C}_2\text{Cl}_2\text{H}_2]$ ratio at 22 °C and 3712 Å.

data from the time resolved phosphorescence experiments are depicted in figure 2.

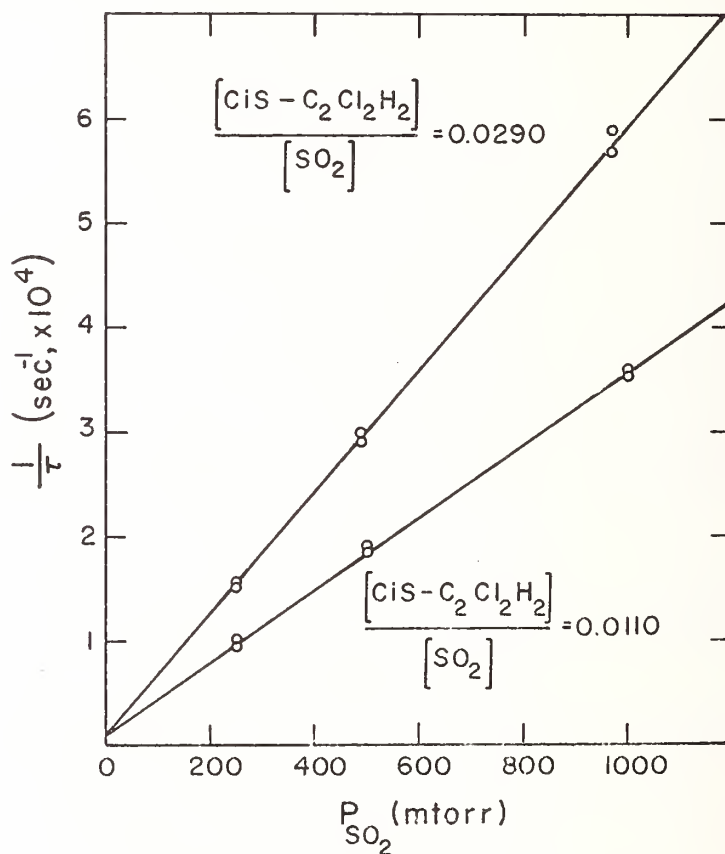


Figure 2. Plot of the reciprocal lifetimes of $\text{SO}_2(^3\text{B}_1)$ molecules at 22 °C and in the presence of $\text{cis-C}_2\text{Cl}_2\text{H}_2$ versus P_{SO_2} .

References

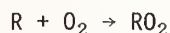
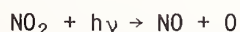
- [1] Cox, R. A., J. Photochem., 2, 1 (1973-4).
- [2] Penzhorn, R. D. and Gusten, H., Z. Naturforsch., 27a, 1401 (1972).
- [3] Penzhorn, R. D. and Filby, W. G., J. Photochem., 4, 91 (1975).
- [4] Demerjian, K. L., Calvert, J. G., and Thorsell, D. L., Int. J. Chem. Kinet., 6, 829 (1974).
- [5] Demerjian, K. L. and Calvert, J. G., Int. J. Chem. Kinet., 7, 45 (1974).

GAS PHASE PHOTOCHEMICAL SYNTHESIS OF PEROXYACYL NITRATES VIA CHLORINE-ALDEHYDE REACTION

Bruce W. Gay, Jr., Richard C. Noonan,
Joseph J. Bufalini, Philip L. Hanst

Environmental Protection Agency
Environmental Sciences Research Laboratory
Research Triangle Park, North Carolina 27711

Reaction mechanisms of photochemical smog involve the radicals HO, HO₂, R, RO, RO₂. These radicals are primarily responsible for hydrocarbon disappearance and serve as chain initiators for propagating reactions. The reaction steps in a system containing oxides of nitrogen and hydrocarbons include:



A chain terminating step involves the formation of stable compounds. Peroxyacetyl nitrate (PAN) is one such compound formed from the reaction of nitrogen dioxide with peroxyacetyl radical.

PAN, a strong oxidizing compound, is one of the principal nitrogen-containing products of photochemical smog; it and its homologs have been shown to be strong eye irritants and cause severe plant damage.

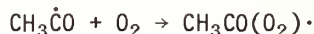
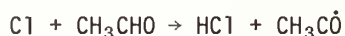
The infrared absorption bands of PAN were first observed in laboratory irradiations of auto exhaust by Stephens et al. in 1956 [1]¹, and shown present in the Los Angeles atmosphere in 1957 [2]. It was first called "Compound X" because of the unidentified IR absorption band in the spectra of irradiated auto exhaust. In 1961 the formula of "Compound X" was established as that of peroxyacetyl nitrate.

A simple preparation of PAN-type compounds that produce high yields in a short time was developed to prepare samples for research, testing and calibration of PAN detection instruments. Several methods have been employed to prepare PAN-type compounds. These are:

1. Photolysis of nitrogen dioxide in the presence of an olefin.
2. Photolysis of di-acyl compounds and nitrogen dioxide.
3. Photolysis of low concentrations of alkyl nitrite in oxygen.
4. The dark reaction of an aldehyde with nitrogen dioxide and ozone.

Figures in brackets indicate the literature references at the end of this paper.

A new PAN synthesis suggested itself during a study of reactions of chlorine atoms with organic material. Chlorine atoms are highly selective in the abstraction of hydrogen atoms. The weakest bonded hydrogen is preferentially abstracted to form HCl. The chlorine atom abstraction of an aldehydic hydrogen from an aldehyde yields the acyl-type free radicals that are precursors of PAN-type compounds. In the presence of oxygen and nitrogen dioxide PAN-type compounds are formed. Any of the PAN homologs can be produced from its parent aldehyde cleanly and at very high yields. In the case of acetaldehyde the reactions are:



The reactions were carried out in a 690 liter glass photochemical reaction cell surrounded by forty-eight 40 watt black lamps in which molecular chlorine photodissociated with a half-life of about 2 minutes. A rapid scan Fourier Transform Infrared Spectrometer was used to analyze reactants and products with an absorption path length of 500 meters.

The formation of PAN is shown in figure 1. The conversion of aldehyde is essentially complete after twenty minutes. Only traces of such side products as CO, HCOOH, HNO₃ and CH₂O were observed.

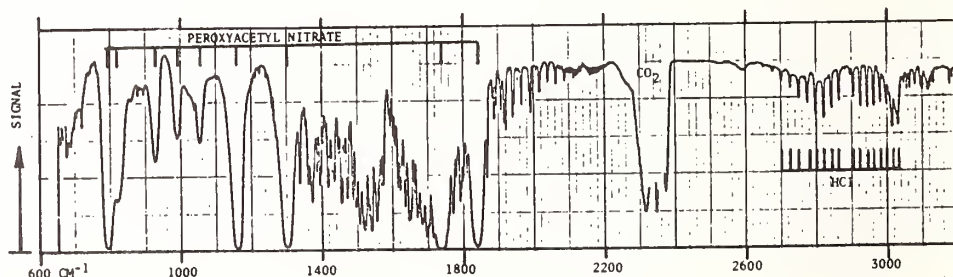


Figure 1. Spectrum at 500-M path length of peroxyacetyl nitrate formed from the irradiation of 4 ppm acetaldehyde, 2 ppm NO₂, 2 ppm Cl₂ in 760 torr air.

When 4 ppm acetaldehyde, and 1.6 ppm NO₂ were photolyzed in the absence of chlorine, PAN formed very slowly, only 0.15 ppm PAN formed after 120 minutes of irradiation. With the addition of 0.8 ppm chlorine to the system, PAN increased from 0.15 to 1.55 ppm after four minutes of irradiation.

Figure 2 shows the peroxypropionyl nitrate formed from propionaldehyde, and figure 3 shows the peroxybenzoyl nitrate formed from benzaldehyde.

Peroxyformyl nitrate, the simplest homolog of the series, is apparently formed in the irradiation of formaldehyde, NO₂ and chlorine but is very unstable.

The chlorine-aldehyde-NO₂ method of PAN preparation appears to be general in its application. High yields of PAN are produced relatively free of organic side products and gives further confirmation to the generally accepted molecular structure of peroxyacyl nitrates.

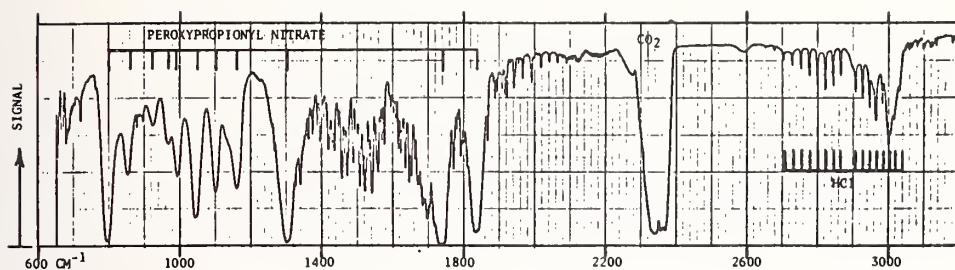


Figure 2. Spectrum at 500-M path length of peroxypropionyl nitrate formed from the irradiation of 3 ppm propionaldehyde, 3.1 ppm NO_2 , 1.6 ppm Cl_2 in 760 torr air.

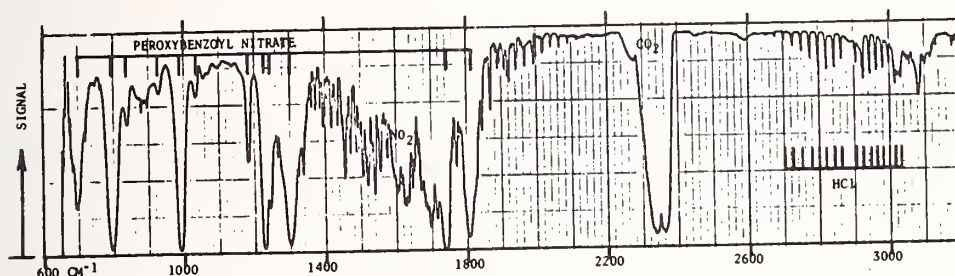


Figure 3. Spectrum at 500-M path length of peroxybenzoyl nitrate formed from the irradiation of 3 ppm benzaldehyde, 3.4 ppm NO_2 , 1.8 ppm Cl_2 in 760 torr air.

References

- [1] Stephens, E. R., Hanst, P. L., Doerr, R. C., and Scott, W. E., *Ind. Eng. Chem.*, **48**, 1998 (1956).
- [2] Scott, W. E., Stephens, E. R., Hanst, P. L., and Doerr, R. C., *Proc. Am. Petrol. Inst. (III)* 171 (1957).

CHEMICAL CONTROL OF PHOTOCHEMICAL SMOG

Julian Heicklen

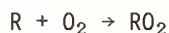
Department of Chemistry and Center for Air Environment Studies
The Pennsylvania State University
University Park, PA 16802

We are testing diethylhydroxylamine (DEHA) as a possible additive to urban atmospheres for the purpose of preventing photochemical smog. Photochemical smog is generally associated with the atmospheric condition resulting from the chemical reactions of hydrocarbons and the oxides of nitrogen in the atmosphere under the influence of sunlight. A principal source of the hydrocarbons and oxides of nitrogen is from automobile exhausts.

The automobile exhaust contains unburned and partially oxidized hydrocarbons, as well as nitric oxide, NO. Relatively little nitrogen dioxide, NO₂, is emitted directly from automobiles. It, as well as O₃ and other oxidants, are produced in the atmosphere and are secondary pollutants.

The initially emitted gases are non-toxic at their concentrations in the atmosphere. On the other hand, O₃ and other oxidants are a danger in the atmosphere.

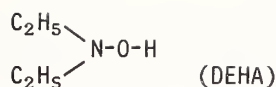
The photochemical cycle which causes the conversion of NO to NO₂ is now generally accepted to be of a free radical nature involving the HO radical and can be summarized as



where HC represents the hydrocarbons and R represents the free radical. The HO radical, which must be produced initially as the result of photolysis of some compound in the atmosphere (presumably aldehydes) is regenerated in the chain and can catalyze the oxidation of many NO molecules.

If the conversion of NO to NO₂ is effected through a long chain mechanism involving HO radicals, then this conversion could be inhibited by molecules which remove HO radicals in such a manner that the chain is not regenerated. Such molecules would most likely contain an easily abstractable hydrogen atom. However, the radical that is produced (either initially or ultimately) when this hydrogen atom is removed must not retain a hydrogen atom on the α -carbon atom, so that the chain will not be regenerated.

In our laboratory several such free radical scavengers have been tested, and they all inhibit the conversion of NO to NO₂ in irradiated synthetic HC-NO-O₂ mixtures. As an inhibitor for possible use in urban atmospheres, we have chosen diethylhydroxylamine (DEHA):



for two reasons:

1. It is one of the most effective inhibitors found, only surpassed by N-methylaniline, of the inhibitors tested.
2. It is a simple non-aromatic molecule composed only of C, N, H, and O atoms, and thus it and its reaction products are more likely to be non-toxic than more complex molecules at the required atmospheric concentrations.

Studies in our laboratory have shown that with C_2H_4 as the hydrocarbon and DEHA present at 25 percent of the C_2H_4 levels, the removal rate of C_2H_4 is reduced by a factor of 5 and the rate of conversion of NO to NO_2 is reduced by a factor of 20. There are two effects operating. One of these is the scavenging of free radicals by DEHA to inhibit the photochemical oxidation processes. The second effect is that only O_3 produced reacts rapidly with DEHA (as shown in separate experiments) to produce CH_3CHO , $\text{C}_2\text{H}_5\text{OH}$, and $\text{C}_2\text{H}_5\text{NO}_2$. Therefore any NO_2 that is produced photodissociates to convert it back to NO, and the oxygen atom produced adds O_2 to produce O_3 which is removed by DEHA. As a result photochemical smog formation not only is delayed but is eliminated as long as DEHA is present.

The $\text{C}_2\text{H}_5\text{NO}_2$ and $\text{C}_2\text{H}_5\text{ONO}_2$ are not produced in the initial inhibiting reaction but are formed only when the DEHA is nearly exhausted from our reaction mixtures and NO_2 and O_3 are produced. The $\text{C}_2\text{H}_5\text{ONO}_2$ and $\text{C}_2\text{H}_5\text{NO}_2$ come from the oxidation of DEHA in the presence of NO_2 and O_3 , respectively. Under conditions that would prevail in the atmosphere with DEHA present, no NO_2 or O_3 would be produced and consequently little $\text{C}_2\text{H}_5\text{ONO}_2$ or $\text{C}_2\text{H}_5\text{NO}_2$ should be formed. The overall effect of adding DEHA to the atmosphere would be to retard hydrocarbon oxidation and to convert some of the NO to N_2O . N_2O is already present at 0.25 ppm in the air. It diffuses to the stratosphere where 98 percent of it becomes N_2 .

The results appear to be the same in the presence or absence of H_2O vapor. Changing the initial concentrations of reactants by a factor of 15 also appears to have little if any effect, though all of our mixtures were of the same relative composition, i.e. $[\text{olefin}]/[\text{NO}]/[\text{DEHA}] = 4/2/1$. If these results can be extrapolated to urban atmospheres then we can expect that 30-50 ppb of DEHA will have a sufficient retarding effect on the oxidation of NO to NO_2 (i.e. about a factor of 3 or more) to effectively prevent photochemical smog formation (i.e. keep oxidant levels below 0.08 ppm). Presumably DEHA would be needed for 6-8 hours a day for 100-200 days/year in Los Angeles and 50-100 days/year in another 10 U. S. cities.

The advantages of adding DEHA, or another free radical scavenger, to urban atmospheres rather than using automobile control devices are numerous:

1. The chemical control method controls stationary as well as mobile source emissions.
2. The chemical control method is projected to cost about \$200 million annually, which is about a factor of 100 cheaper than automobile control devices.
3. The chemical control method can provide the immediate elimination of photochemical smog, whereas it will take at least 10 years to equip all cars with emission control devices.
4. No government regulation of the individual is involved with chemical control, thus minimizing government interference into the lives of the individual citizen.

5. The chemical control method will not introduce H_2SO_4 into the air, unlike the projected catalytic control devices which will introduce significant and harmful amounts of H_2SO_4 into the atmosphere.
6. In fact not only does chemical control not introduce H_2SO_4 into the air, but it should reduce H_2SO_4 concentrations because it will inhibit and free radical oxidation of SO_2 . Furthermore DEHA is a mild base and has the potential for neutralizing H_2SO_4 .

One obvious problem that must be faced is how DEHA is to be dispersed into the air. Since the reaction times in the air are of the order of several hours, mixing does not have to be rapid. DEHA could be introduced by evaporation (vapor pressure is 3-4 Torr at 25°C) or spraying from moving or stationery sources on the freeways.

DEHA is a colorless liquid and its vapor does not absorb radiation above 2700\AA , so that it is not photochemically reactive (no radiation $< 2900\text{\AA}$ reaches the troposphere).

The odor threshold of DEHA is 0.5 ppm, > 10 times the level that would be used. Thus it will cause no annoyance to the general population. It has a faint odor at 1.4 ppm and a moderate odor at 7.5 ppm, so that the odor is a built-in safety device in case high concentrations develop in some region.

Detailed toxicological studies on rats have been conducted in our laboratory. The animals were exposed for over 1700 hours to 9 ± 1 ppm DEHA, 10 ± 1 ppm $\text{C}_2\text{H}_5\text{NO}_2$, and the vapor of $(\text{C}_2\text{H}_5)_2\text{NOS} \begin{smallmatrix} \text{O} \\ \diagup \quad \diagdown \\ \text{H} \end{smallmatrix}$ (the adduct of DEHA and SO_2). Animals have been periodically sacrificed and subjected to hematological and blood chemistry evaluation and complete post mortem examinations. Only four deviations have occurred between the control and test animals.

1. After 855 hours of exposure one male rat was found to have a malignant tumor in the skin on a rear leg. No other tumors have appeared.
2. After 1227 hours exposure to the two exposed and one of two control females that were sacrificed had fluid in the uterus. Subsequent matings of 9 other exposed females with 3 exposed males (3 females per male) resulted in normal births with normal offspring.
3. Animals sacrificed after 1227 hours of exposure showed chronic tracheitis and degenerative thyroid lesions. The degenerative thyroid lesions were not present in the animals sacrificed after 1688 hours of exposure.
4. Mutagenic tests are in progress. Some activity has been indicated in the urine of exposed animals. At the present time this problem appears serious.

PHOTOCHEMICALLY INDUCED FREE RADICAL REACTIONS
IN NITROGEN DIOXIDE-ACETALDEHYDE MIXTURES¹

E. R. Allen

Atmospheric Sciences Research Center
State University of New York at Albany
Albany, New York 12222

Abstract

Photochemical studies have been made of the room temperature rates of formation of products and decay of reactants during irradiation at 366 nm of binary mixtures of nitrogen dioxide and acetaldehyde. Preliminary results from computerized numerical modelling, incorporating currently accepted kinetic parameters of the elementary processes occurring in these systems, has enabled a viable overall mechanism to be established. In addition, this work provides reliable information on less well known rate constants for hydrocarbon radical-nitrogen oxide reactions. Knowledge of the latter is of importance in chemical models describing the propagation of photochemical air pollution and in estimating urban concentrations of potentially reactive or environmentally hazardous nitrogenous products.

1. Introduction

Static photolysis studies of nitrogen oxide-hydrocarbon mixtures were undertaken at the NCAR laboratories to complement and augment parallel investigations of related atomic oxygen-hydrocarbon reactions utilizing dynamic discharge flow techniques [1]². The latter studies provided kinetic data on the initial (primary thermal process) O-atom attack on hydrocarbons, whereas the former investigations were employed to indicate the mode of O-atom attack on the hydrocarbons and allowed us to follow the subsequent reactions (secondary thermal processes) involving product free radicals and the various molecular species present. In addition, the static photochemical experiments were designed to provide information concerning relative and absolute rate coefficients for the simultaneous and consecutive secondary processes which, due to their competitive nature, are not easily isolated for study by other techniques. The basic system employed, which consists of a photochemical reactor used in conjunction with periodic sampling and gas chromatographic analysis of irradiated mixtures, has been described elsewhere [1-4]. Since these early reports the system has been substantially upgraded and refined to the extent that additional details, concerning modifications and improvements incorporated more recently, warrant inclusion here.

Early work consisted mainly of preliminary investigations designed to: a) test the feasibility of using gas chromatographic analysis to follow the course of reaction during photolysis, b) isolate and identify the products of reaction, c) calibrate the analytical system for known products and reactants, and d) obtain relative rate coefficients of elementary processes from initial rates of product formation. The latter studies assumed that the steady state approximation method applied for the experimental conditions selected and that initial production curves were linear. A similar experimental approach has been used by

Work performed at the National Center for Atmospheric Research (NCAR), Boulder, Colorado. NCAR is sponsored by the National Science Foundation.

Figures in brackets indicate literature references at the end of this paper.

other investigators [5-7] to study reactions in the nitrogen oxide-acetaldehyde system. However, these investigators examined different aspects of initial O-atom attack and end-product formation and obtained different results to those presented here due to dissimilar experimental procedures and priorities. Here we are mainly concerned with defining the overall mechanism of reaction and assigning rate constants to the elementary processes involved.

These studies were part of a laboratory program to quantitatively identify selected chemical transformations occurring in polluted air and to provide kinetic data on elementary processes suitable for incorporation into atmospheric chemical models, which are being used to describe the urban and industrial atmospheric environment.

2. Experimental

Experiments were conducted in a conventional high vacuum, mercury-free static photolysis system. All glass stopcocks were lubricated with Dow Corning silicone grease, which proved to be more stable to attack by nitrogen oxides and organic vapors than other commercially available lubricants. Radiation at 366 nm was obtained from the filtered (Corning CS-7-83) emission of a PEK110 high pressure mercury arc lamp. Intensities incident on the photochemical reactor were measured using a potassium ferrioxalate actinometer [8] and transmitted radiation monitored by recording the output of an RCA935 phototube coupled to a Pacific Photometric Photometer. Periodically small aliquots (0.1 cm^3) of the reaction mixture in the cell (300 cm^3) were extracted using a leak-free rotary valve developed from a design reported by Alperstein and Bradow [9]. These samples were immediately injected either on to parallel Poropak Q columns at room temperature and -78°C for separation and detection of CH_4 , CO_2 , N_2O and N_2 , O_2 , NO , respectively, using helium ionization detection; or on to a 100' capillary column at 50°C coated with β , β' oxydipropionitrile for the separation and detection of organic compounds using flame ionization. Gas pressures were monitored using a modified Wallace and Tiernan absolute gauge and a Satham PA707 TC-5-350 transducer.

Eastman Organic Chemicals acetaldehyde and calibration samples of organic products were purified by trap to trap distillation at reduced temperatures. Matheson nitrogen dioxide (99.5 percent min.) was oxidized by bubbling oxygen through the liquid at 0°C , dried with P_2O_5 and distilled into a blackened storage reservoir. Permanent gases of high purity were obtained directly from Matheson cylinders.

3. Results and Discussion

The thirteen step mechanism outlined below is proposed to account for all of the products observed under the experimental conditions selected. The irradiated system to be analyzed both theoretically and experimentally was a 10:1 mixture of acetaldehyde ($2.7 \times 10^{-4} \text{ mole l}^{-1}$) and nitrogen dioxide ($2.7 \times 10^{-4} \text{ mole l}^{-1}$) at 23°C and at a total pressure of 55 torr. Although a variety of other mixtures have been studied, they will not be reported here. Measured products of reaction over a two hour photolysis period for this particular mixture of reactants were nitric oxide, oxygen, carbon dioxide, methyl nitrate and methyl nitrite. Water, nitric and nitrous acid vapors, nitromethane and nitrosomethane were predicted products also; however, the first three were not measured and the last two were detectable but were not observed in this study. On the basis of material balance the proposed mechanism accounts for at least 95 percent of the measured products. For example, the balance in nitrogenous materials at 80 minutes into the photolysis (reaction) is given by the relationship:

$$-\Delta[\text{NO}_2] = \Delta[\text{NO}] + \Delta[\text{CH}_3\text{ONO}_2] + \Delta[\text{CH}_3\text{ONO}] + \Delta[\text{CH}_3\text{NO}_2] + \Delta[\text{CH}_3\text{NO}]$$

where

$$-\Delta[\text{NO}_2] = (2.54 - 1.59) \times 10^{-4} \text{ mole } \ell^{-1} = 9.5 \times 10^{-5} \text{ mole } \ell^{-1} .$$

$$\Delta[\text{NO}] = 7.17 \times 10^{-5} \text{ mole } \ell^{-1}$$

$$\Delta[\text{CH}_3\text{ONO}_2] = 1.04 \times 10^{-5} \text{ mole } \ell^{-1}$$

$$\Delta[\text{CH}_3\text{ONO}] = 0.54 \times 10^{-5} \text{ mole } \ell^{-1}$$

$$\Delta[\text{CH}_3\text{NO}_2] = 0.28 \times 10^{-5} \text{ mole } \ell^{-1} \text{ (estimated)}$$

Thus, the balance in nitrogenous materials formed accounts for 95 percent of the nitrogen dioxide consumed. The small inconsistency is for the most part due to the inaccuracies involved in measuring nitric oxide in the system.

Proposed Reaction Mechanism

Initially Selected Rate Coefficients at 296 °K

$\text{NO}_2 + h\nu \rightarrow \text{NO} + \text{O}$	(1)	$I_0 = 3.0 \times 10^{-9} \text{ einstein sec}^{-1}$
$\text{O} + \text{NO}_2 \rightarrow \text{O}_2 + \text{NO}$	(2)	$k_2 = 1.2 \times 10^9 \ell \text{ mole}^{-1} \text{ sec}^{-1}$
$\text{O} + \text{CH}_3\text{CHO} \rightarrow \text{OH} + \text{CH}_3\text{CO}$	(3)	$k_3 = 2.0 \times 10^8 \ell \text{ mole}^{-1} \text{ sec}^{-1}$
$\text{OH} + \text{CH}_3\text{CHO} \rightarrow \text{H}_2\text{O} + \text{CH}_3\text{CO}$	(4)	$k_4 = 9.6 \times 10^9 \ell \text{ mole}^{-1} \text{ sec}^{-1}$
$\text{OH} + \text{NO}_2 \xrightarrow{\text{M}} \text{HNO}_3$	(5)	$k_5 = 2.5 \times 10^9 \ell \text{ mole}^{-1} \text{ sec}^{-1}$
$\text{OH} + \text{NO} \xrightarrow{\text{M}} \text{HNO}_2$	(6)	$k_6 = 8.4 \times 10^8 \ell \text{ mole}^{-1} \text{ sec}^{-1}$
$\text{CH}_3\text{CO} + \text{NO}_2 \rightarrow \text{CH}_3 + \text{CO}_2 + \text{NO}$	(7)	$k_7 = 1.2 \times 10^{10} \ell \text{ mole}^{-1} \text{ sec}^{-1}$
$\text{CH}_3\text{CO} \rightarrow \text{CH}_3 + \text{CO}$	(8)	$k_8 = 1.0 \times 10^5 \text{ sec}^{-1}$
$\text{CH}_3 + \text{NO}_2 \rightarrow \text{CH}_3\text{NO}_2$	(9)	$k_9 = 4.8 \times 10^9 \text{ mole}^{-1} \text{ sec}^{-1}$
$\text{CH}_3 + \text{NO}_2 \rightarrow \text{CH}_3\text{O} + \text{NO}$	(10)	$k_{10} = 7.8 \times 10^9 \ell \text{ mole}^{-1} \text{ sec}^{-1}$
$\text{CH}_3\text{O} + \text{NO}_2 \rightarrow \text{CH}_3\text{ONO}_2$	(11)	$k_{11} = 1.2 \times 10^9 \ell \text{ mole}^{-1} \text{ sec}^{-1}$
$\text{CH}_3\text{O} + \text{NO} \rightarrow \text{CH}_3\text{ONO}$	(12)	$k_{12} = 4.0 \times 10^8 \ell \text{ mole}^{-1} \text{ sec}^{-1}$
$\text{CH}_3 + \text{NO} \xrightarrow{\text{M}} \text{CH}_3\text{NO}$	(13)	$k_{13} = 2.4 \times 10^9 \ell \text{ mole}^{-1} \text{ sec}^{-1}$

The "initially selected" rate coefficients, as displayed above with the proposed mechanism, for the twelve thermal reactions, (2) through (13) were either taken from the literature as being the best available, or were estimated from previous reported relative rate measurements, or were arbitrarily chosen to be representative of the elementary process described. This chemical model was then used to simulate the formation of products and removal of reactants over a two hour continuous photolysis period. A computer program was developed to numerically solve the sets of differential equations describing product formation and reactant removal using the Runge-Kutta technique at sequential 5 second intervals over the two hour reaction period. The program additionally provided for plotting the instantaneous concentrations of reactants and products at 1 minute reaction intervals on a linear concentration versus reaction time graph. The initially produced "theoretical" plots, shown as dashed lines in the figures were then compared with experimental data obtained under identical conditions. A successive iteration procedure was used to match the computed curves with the experimental data as follows. Each time a rate coefficient or some other parameter was adjusted to obtain the best fit to a set of data points the complete program was rerun and a new set of concentration-time profiles was generated. It should be noted

that the solid lines in the figures are the result of making necessary adjustments to the kinetic parameters for all reactions and are the final plots rather than plots at intermediate stages in the development of the quantitative model.

The following sequence of operations was adhered to because of the close interdependence of the consecutive and competitive processes occurring in the proposed mechanism. The incident light intensity at 366 nm, I_0 , was determined by external actinometry using potassium ferrioxalate solution and was confirmed by internal actinometry using the photolysis of nitrogen dioxide alone. In the initial computation the starting reactant concentrations were $[NO_2] = 2.7 \times 10^{-4}$ mole ℓ^{-1} and $[CH_3CHO] = 2.7 \times 10^{-3}$ mole ℓ^{-1} . In practice, however, the initial concentration of nitrogen dioxide was 2.54×10^{-4} mole ℓ^{-1} (4.7 torr). To correct for this discrepancy the program was rerun with the actual concentration of NO_2 used. As a result the computed nitrogen dioxide concentration-time profile shifted from the dashed line shown in Figure 1 to the solid line running through the NO_2 data points (open circles in Figure 1). Also, according to the theoretical program the rate of formation of oxygen (dashed line in Figure 1) was approximately half that found by experiment (closed circles in Figure 1). Consequently, the rate coefficient k_2 was adjusted to obtain the best fit to the $[O_2]$ data points. A value for $k_2 = 2.7 \times 10^9$ ℓ mole $^{-1}$ sec $^{-1}$ was found to produce the computed $[O_2]$ concentration-time profile, the solid line running through the oxygen data points (closed circles in Figure 1). This revised value corresponds closely to reported values by Ford and Endow [10] (2.1×10^9 ℓ mole $^{-1}$ sec $^{-1}$), Stuhl and Niki [11] (2.6×10^9 ℓ mole $^{-1}$ sec $^{-1}$) and Hampson and Garvin [12] (2.6 – 5.7×10^9 ℓ mole $^{-1}$ sec $^{-1}$). After the two previous adjustments to the computational program it was found that the nitric oxide data points, shown as crosses in Figure 1, coincided quite closely with the computed profile for NO (dashed line in Figure 1) during the early stages of reaction, but diverged markedly at longer photolysis times. However, this product is quite sensitive to the free radicals produced and, thus, the validity of the NO data cannot be checked until all of the necessary adjustments to the rate coefficients of subsequent reactions have been made. Ultimately, when the quantitative model was finalized the computed nitric oxide concentration-time profile obtained was the solid line running through the NO data points (crosses in Figure 1).

The value, $k_3 = 2.0 \times 10^8$ ℓ mole $^{-1}$ sec $^{-1}$, was arbitrarily selected in view of the large variation in reported rate coefficients for this reaction by Cvetanovic [13] (1.2×10^8 ℓ mole $^{-1}$ sec $^{-1}$), Cadle and Powers [14] (2.7×10^8 ℓ mole $^{-1}$ sec $^{-1}$), Cadle and Allen [1] (2.2×10^8 ℓ mole $^{-1}$ sec $^{-1}$) and Singleton and Cvetanovic [15] (2.6×10^8 ℓ mole $^{-1}$ sec $^{-1}$). The rate coefficient, $k_4 = 9.6 \times 10^9$ ℓ mole $^{-1}$ sec $^{-1}$ was selected on the basis of measurements reported by Morris, Stedman and Niki [16]. The computed production of water vapor by reaction (4) is shown as a dashed line in Figure 2, but no measurements were made of this product. Production of nitric and nitrous acids in this system are represented by reactions (5) and (6), respectively in the mechanism. The rate coefficient, $k_5 = 2.5 \times 10^9$ ℓ mole $^{-1}$ sec $^{-1}$ is that reported by Niki, Daby and Weinstock [17] and subsequently confirmed by Howard and Evenson [18]; Anderson, Margitan and Kaufman [19]; and Chapman, Harris and Wayne [20] to fall in the range $(2.5$ – $3.1) \times 10^9$ ℓ mole $^{-1}$ sec $^{-1}$. Similarly, the rate coefficient, $k_6 = 8.4 \times 10^8$ ℓ mole $^{-1}$ sec $^{-1}$ was reported by Niki, Daby and Weinstock [17] and subsequently confirmed by other investigators [18–20]. The computed production profiles for nitric and nitrous acids in this system are shown as dashed lines in Figures 3. It should be noted that for most of the reaction nitric acid concentrations exceed nitrous acid concentrations by at least an order of magnitude, but $[HNO_3]$ is about one to two orders of magnitude less than the concentrations of carbonaceous products. Thus, reactions (5) and (6) account for a very small fraction of the nitrogen oxides present and they have a negligible effect (<1 percent) on the overall material balances.

Reaction (7) is assumed to be the only one capable of producing carbon dioxide in the system. Initially an arbitrary value of 1.2×10^{10} ℓ mole $^{-1}$ sec $^{-1}$ was assigned to k_7 . However, a comparison of the computed carbon dioxide production (dashed line in Figure 2) with experimental carbon dioxide data points (open circles in Figure 2), clearly showed that the value for k_7 was too large. As a result, a value for $k_7 = 8.4 \times 10^9$ ℓ mole $^{-1}$ sec $^{-1}$ was adopted in order to obtain the best fit (solid line in Figure 2) to the experimental values for $[CO_2]$. This adjustment, together with other adjustments to rate coefficients for reactions of free radicals with nitrogen oxides had the effect of reducing $[NO]$ during the later stages of reaction but did not markedly affect the $[NO_2]$ reaction profile. Reaction (8), unimolecular first order decomposition of acetyl radicals, is the only reaction producing carbon monoxide in the system. However, this reaction accounts for less than 5 percent of the total acetyl radicals produced and under the experimental conditions carbon monoxide production is negligible, even after a two hour photolysis period.

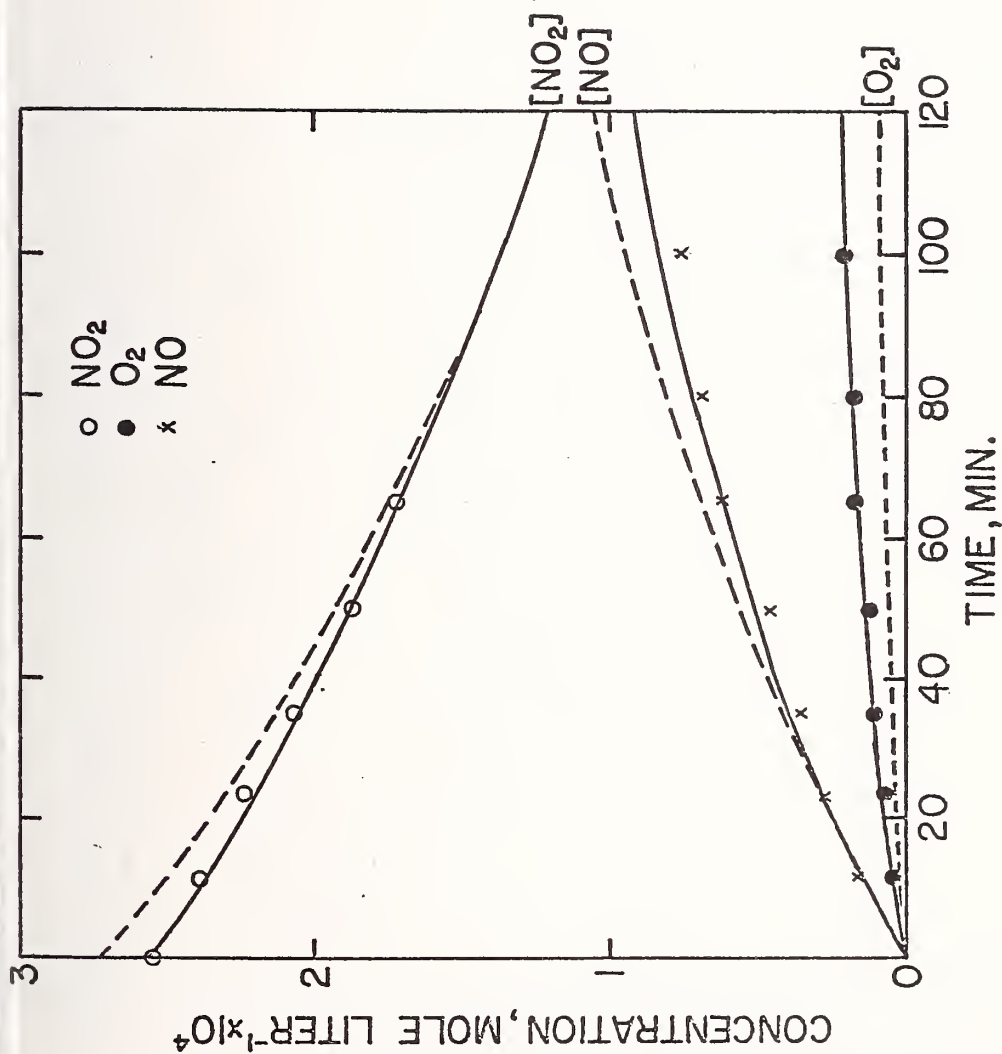


Figure 1. Computed concentration-time profiles and experimental data points for NO_2 , NO and O_2 . Dashed lines are "initial" computations, solid lines are "final" computations.

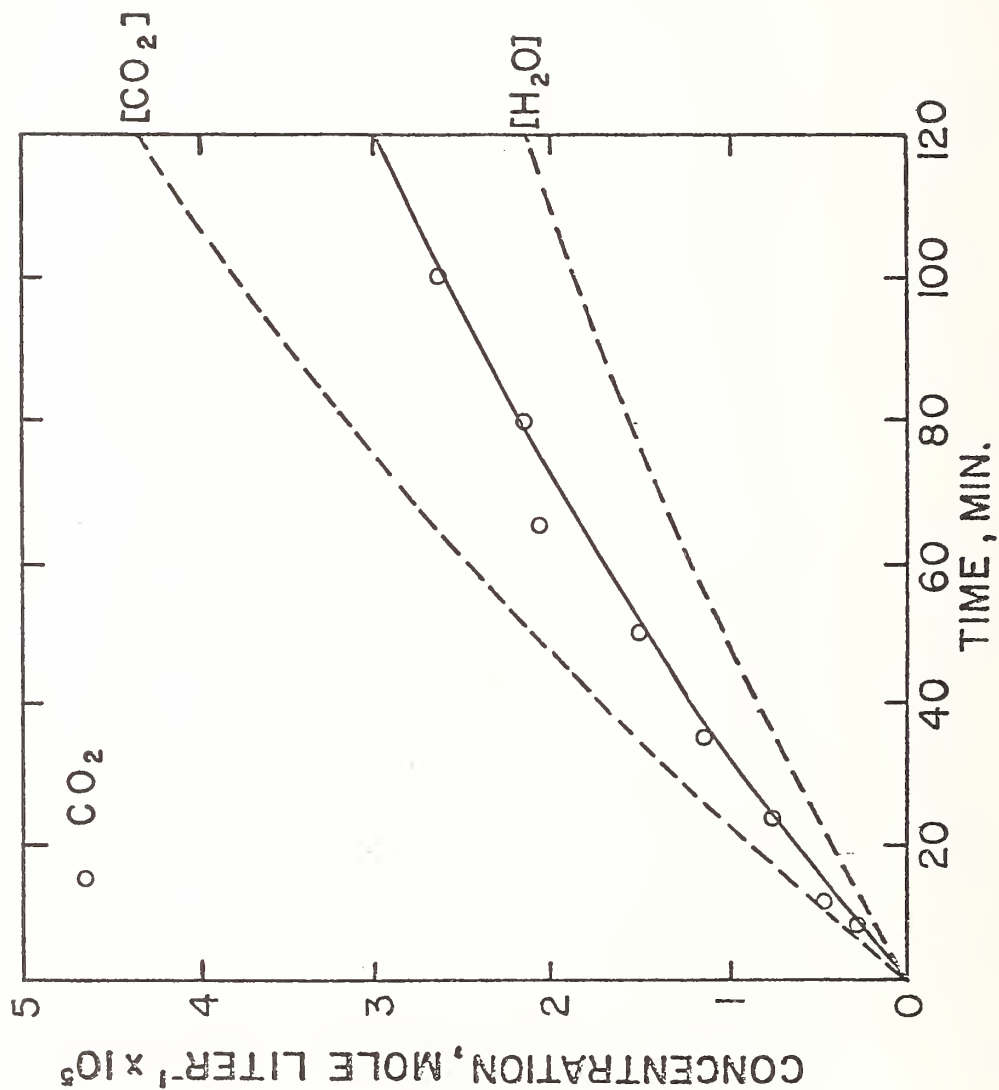


Figure 2. Computed concentration-time profiles and experimental data points for CO_2 and H_2O . Dashed lines are "initial" computations, solid line is "final" computation.

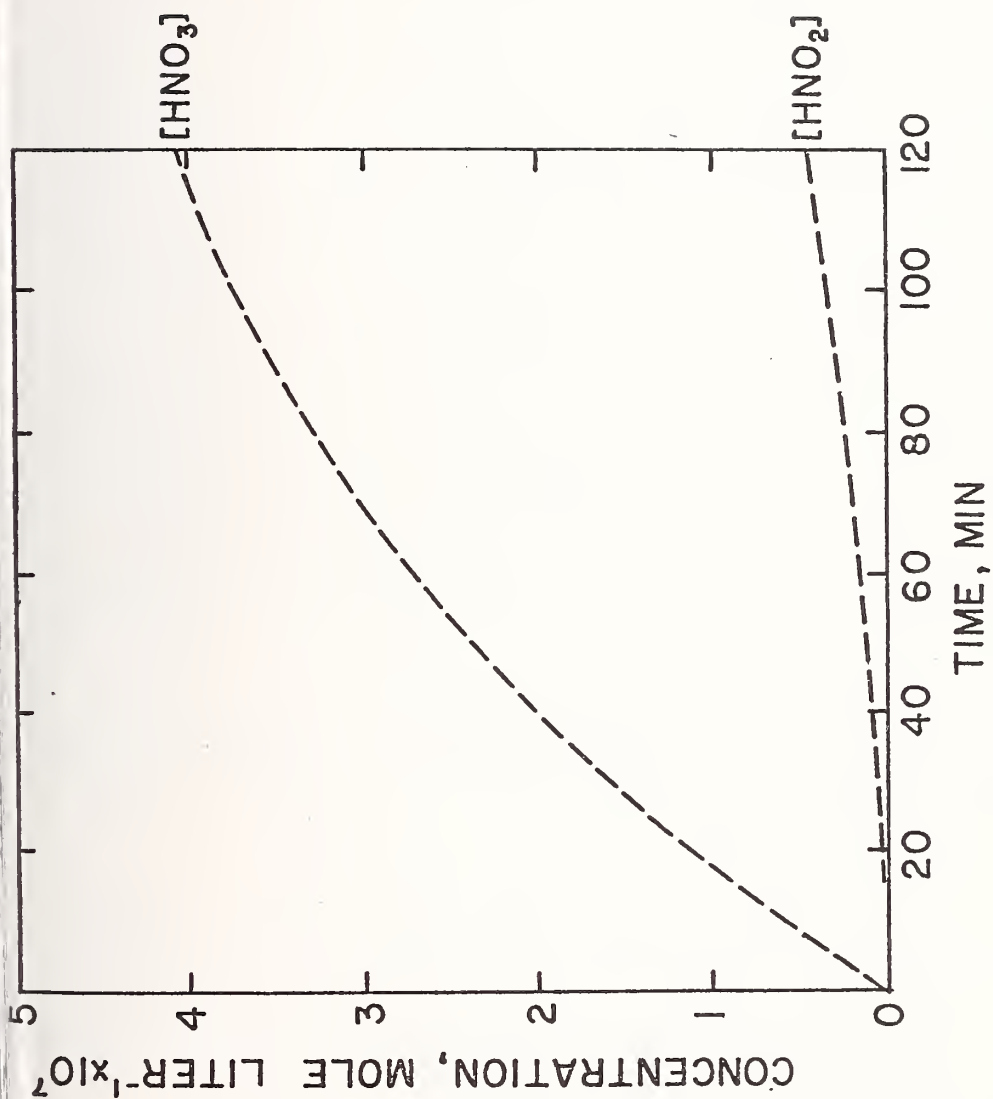


Figure 3. Computed concentration-time profiles for HNO_3 and HNO_2 . Dashed lines are "initial" computations.

Nitromethane is produced by reaction (9), the rate of coefficient $k_9 = 4.8 \times 10^9 \text{ l mole}^{-1} \text{ sec}^{-1}$ was arbitrarily selected and gave the computed $[\text{CH}_3\text{NO}_2]$ profile shown as a dashed line in Figure 4. In practice, however, nitromethane was undetectable after two hours of irradiation, because of the low sensitivity to detection of this compound. Consequently, a value for $k_9 \leq 1.3 \times 10^9 \text{ l mole}^{-1} \text{ sec}^{-1}$ was estimated. It should be noted that this upper limit is at least an order of magnitude lower than that suggested by Glanzer and Troe [21] ($1.7 \times 10^{10} \text{ l mole}^{-1} \text{ sec}^{-1}$). Methyl nitrate is produced by the sequence of reactions (10) and (11). The rate coefficient, $k_{10} = 7.8 \times 10^9 \text{ l mole}^{-1} \text{ sec}^{-1}$ was chosen so that $k_9/k_{10} = 0.61$, determined from previous investigations [1,3]. Thus, k_{10} was adjusted to be $\leq 2.1 \times 10^9 \text{ l mole}^{-1} \text{ sec}^{-1}$ as a result of the change in k_9 . It is apparent in this case also that the value for k_{10} reported here is substantially less than that proposed for the same elementary process by Glanzer and Troe [21] ($2.0 \times 10^{10} \text{ l mole}^{-1} \text{ sec}^{-1}$). The rate coefficient, $k_{11} = 1.2 \times 10^9 \text{ l mole}^{-1} \text{ sec}^{-1}$, was selected on an arbitrary basis. When used in conjunction with the "adjusted" rate coefficients reported earlier, the theoretical curve for methyl nitrates production was generated (shown as dashed line in Figure 4). However, the experimental data for $[\text{CH}_3\text{ONO}_2]$ (open circles in Figure 4) lie considerably below the "theoretical" concentration profile. As a result of this discrepancy, the rate coefficient was adjusted to $k_{11} = 6.6 \times 10^8 \text{ l mole}^{-1} \text{ sec}^{-1}$ to obtain the best fit to the experimental data (shown as solid line in Figure 4). This "adjusted" rate coefficient is at least three times larger than the value estimated by Demerjian, Kerr and Calvert [22] ($2.0 \times 10^8 \text{ l mole}^{-1} \text{ sec}^{-1}$). Methyl nitrite is produced by reaction (12), the initially selected value, $k_{12} = 4.0 \times 10^8 \text{ l mole}^{-1} \text{ sec}^{-1}$ was responsible for the theoretical methyl nitrite production curve (dashed line) in Figure 4. Experimental data points for methyl nitrite filled circles in Figure 4) lie considerably above the theoretically computed curve, consequently the rate coefficient was adjusted to $k_{12} = 1.5 \times 10^9 \text{ l mole}^{-1} \text{ sec}^{-1}$ to obtain the best fit curve (solid line in Figure 4) to the $[\text{CH}_3\text{ONO}]$ experimental data. The adjusted value for k_{12} reported here is an order of magnitude larger than that estimated by Demerjian, Kerr and Calvert [22] ($1.0 \times 10^8 \text{ l mole}^{-1} \text{ sec}^{-1}$) for reaction (12). Finally, nitrosomethane is produced by reaction (13). The second order rate coefficient for this reaction, $k_{13} = 2.4 \times 10^9 \text{ l mole}^{-1} \text{ sec}^{-1}$, is that measured by Basco, et al. [23] and confirmed later by Laufer and Bass [24]. Although nitrosomethane was detectable it did not reach the minimum level of detectability ($10^{-6} \text{ mole l}^{-1}$) during the two hour photolysis period of this particular nitrogen dioxide-acetaldehyde mixture.

Assuming that the rate coefficients for reactions (3), (4), (5), (6), (8) and (13) are representative of the reactions taking place in the system under investigation, then the following rate coefficients of 296 °K are recommended for use in future chemical modelling applications; with a 20 percent maximum deviation estimated from the sensitivity of curve fitting and the accuracy of experimental data.

$$k_2 = 2.7 (\pm 0.5) \times 10^9 \text{ l mole}^{-1} \text{ sec}^{-1}$$

$$k_7 = 8.4 (\pm 1.7) \times 10^9 \text{ l mole}^{-1} \text{ sec}^{-1}$$

$$k_9 \leq 1.3 (\pm 0.3) \times 10^9 \text{ l mole}^{-1} \text{ sec}^{-1}$$

$$k_{10} \leq 2.1 (\pm 0.4) \times 10^9 \text{ l mole}^{-1} \text{ sec}^{-1}$$

$$k_{11} = 6.6 (\pm 1.3) \times 10^8 \text{ l mole}^{-1} \text{ sec}^{-1}$$

$$k_{12} = 1.5 (\pm 0.3) \times 10^9 \text{ l mole}^{-1} \text{ sec}^{-1}$$

These values will be checked and refined further in the near future by performing similar analyses of different nitrogen dioxide-acetaldehyde mixtures.

Acknowledgement

The author is greatly indebted to T. R. Englert who performed the large number of necessary experiments, and M. Sutterlin, who developed and ran the computer program.

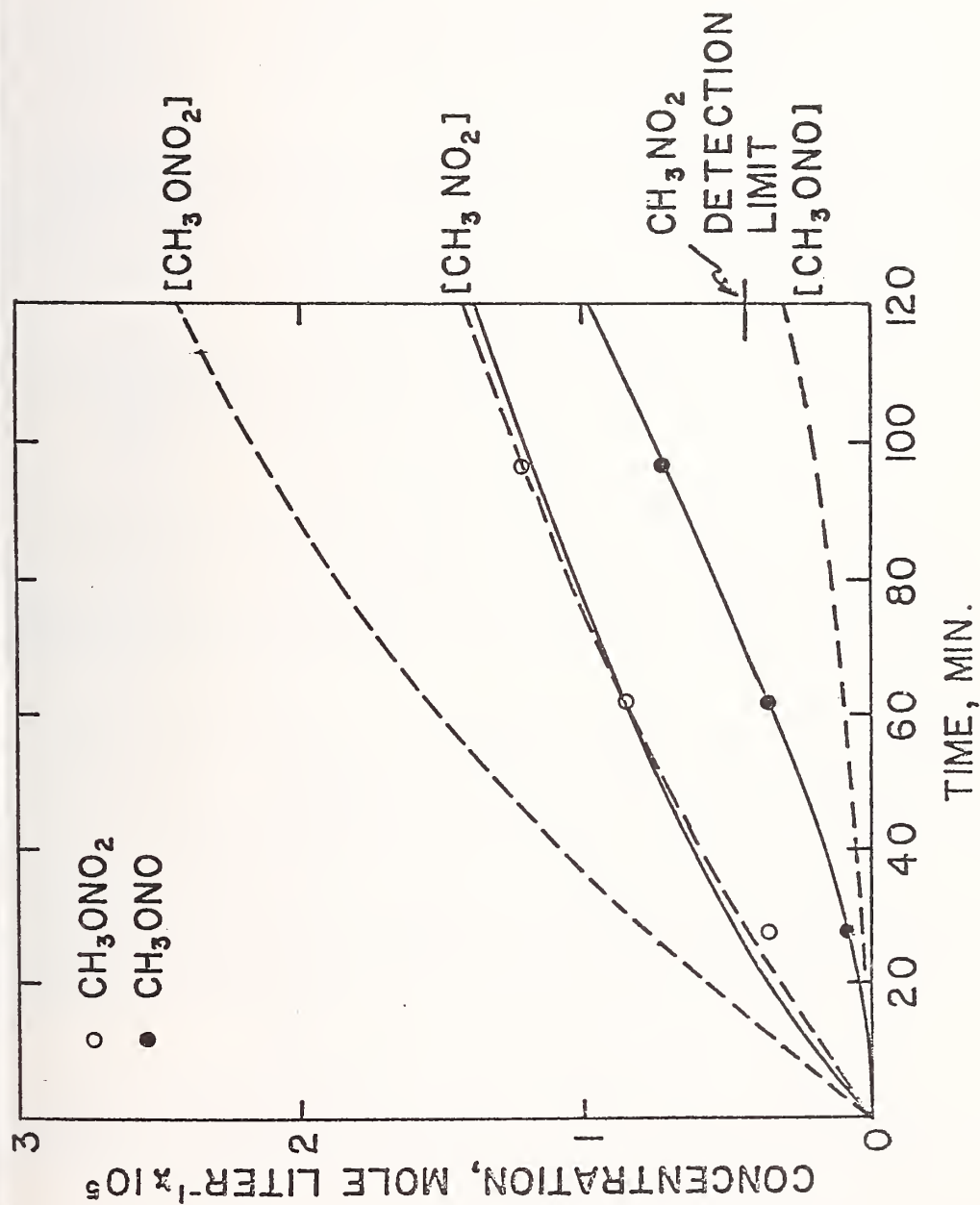


Figure 4. Computed concentration-time profiles and experimental data points for CH_3ONO_2 , CH_3NO_2 and CH_3ONO . Dashed lines are "initial" computations, solid lines are "final" computations.

References

- [1] Cadle, R. D. and Allen, E. R., "Reactions of O(³P) Atoms with Aldehydes in Photochemical Smog." In "Chemical Reactions in Urban Atmospheres," C. S. Tuesday (ed.), Elsevier Publishing Co., pp. 63-87 (1971).
- [2] Allen, E. R. and Bagley, K. W., *Berichte Bunsenges. Physik. Chemie.*, 72, 227 (1968).
- [3] Allen, E. R., "Recent Studies of the Reaction of Radicals with the Oxides of Nitrogen." Paper presented at 8th Conference on Photochemistry, Ottawa, Ontario, Canada, June 1968.
- [4] Watkins, K. W., Ogren, P. J. and Allen, E. R., "The Effects of Collisional Moderator Gases on Photochemically-Induced Reactions in Nitrogen Oxide-Propylene Mixtures." Paper presented at 8th International Conference on Photochemistry, Edmonton, Alberta, Canada, August 1975.
- [5] Avery, H. E. and Cvetanovic, R. J., *J. Chem. Phys.*, 43, 3727 (1965).
- [6] Collins, B. M. and Christie, M. I., *Nature*, 218, 1245 (1968).
- [7] Avery, H. E., Hayes, D. M. and Phillips, L., *J. Phys. Chem.*, 73, 3498 (1969).
- [8] Hatchard, C. G. and Parker, D. A., *Proc. Roy. Soc. (London)*, A235, 518 (1956).
- [9] Alperstein, M. and Bradow, R. L., *Anal. Chem.*, 38, 366 (1966).
- [10] Ford, H. W. and Endow, N., *J. Chem. Phys.*, 27, 1156, 1277 (1957).
- [11] Stuhl, F. and Niki, H., *Chem. Phys. Lett.*, 7, 197 (1970).
- [12] Hampson, R. F. Jr. and Garvin, D., "Chemical Kinetic and Photochemical Data for Modeling Atmospheric Chemistry," NBS Tech. Note 866, U. S. Dept. of Commerce, Washington, D. C., June 1975, p. 13-14.
- [13] Cvetanovic, R. J., *Can. J. Chem.*, 34, 775 (1956).
- [14] Cadle, R. D. and Powers, J. W., *J. Phys. Chem.*, 71, 1702 (1967).
- [15] Singleton, D. L. and Cvetanovic, R. J., Private Communication, July, 1976.
- [16] Morris, E. D. Jr., Stedman, D. H. and Niki, H., *J. Amer. Chem. Soc.*, 93, 3570 (1971).
- [17] Niki, H., Daby, E. E. and Weinstock, B., "Mechanisms of Smog Reactions." Paper presented at the Symposium on Photochemical Smog, Division of Physical Chemistry, 161st National Meeting of the American Chemical Society, Los Angeles, California, March 1971.
- [18] Howard, C. J. and Evenson, K. M., *J. Chem. Phys.*, 61, 1943 (1974).
- [19] Anderson, J. G., Margitan, J. J. and Kaufman, F., *J. Chem. Phys.*, 60, 3310 (1974).
- [20] Chapman, C. J., Harris, G. W. and Wayne, R. P., *J. Chem. Soc. Faraday I*, 71, 610 (1975).
- [21] Glanzer, K. and Troe, J., in Reference 12, p. 44.
- [22] Demerjian, K. L., Kerr, J. A. and Calvert, J. G., *Advances Environ. Sci. Technol.*, 4, 1 (1974).
- [23] Basco, N., James, D. G. L. and Suart, R. D., *Int. J. Chem. Kinet.*, 2, 215 (1970).
- [24] Laufer, A. H. and Bass, A. M., in Reference 12, p. 39.

PHOTO-OXIDATION OF TOLUENE-NO₂-O₂-N₂ SYSTEM IN GAS PHASE

H. Akimoto, M. Hoshino, G. Inoue, M. Okuda and N. Washida

Division of Atmospheric Environment
National Institute for Environmental Studies
P. O. Yatabe, Ibaraki 300-21, Japan

1. Introduction

Although a few studies [1-3]¹ on the photo-oxidation of aromatic hydrocarbon-NO₂-air system have been made as a model reaction of photochemical air pollution in urban atmosphere, most of the studies are concerned with the so called "photochemical reactivity," and studies on the reaction products characteristic of aromatic hydrocarbons have rarely been carried out.

The purpose of this study is the elucidation of the reaction mechanism of photo-oxidation of the toluene-NO₂-O₂-N₂ system in the concentration range of 34 ppm of toluene, 0 - 200 ppm of NO₂ in N₂ and/or O₂ at 1 atm.

2. Experimental

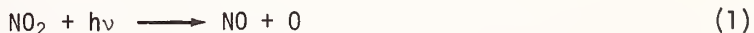
The reaction chamber was a Pyrex cylinder with the dimensions of 240 mm i.d., 1660 mm long and 67 l volume, and was evacuable to less than 1×10^{-6} torr. Each end of the reaction chamber was sealed with a Pyrex window of 20 mm thick, through which photolyzing light beam was transmitted into the gas sample. Light source was a 500 W xenon short arc lamp and a parallel light beam of 200 mm ϕ was obtained with an elliptic mirror, a lens and an off-axis parabolic mirror.

The reaction mixture was first sampled into a constant volume glass sampling bulb (about 700 cc) and then concentrated in a GC sampling tube. The sampling tube was a Pyrex spiral with a 2 mm i.d. and about 4 m extended length. The concentration of the reaction mixture was achieved by evacuating the air and NO₂ while cooling the tube with ethanol - liquid N₂ at -60 ~ -80 °C to 200 °C. After the concentration, the sampling tube was heated with hot water and the sample was fed into a gas chromatograph directly. This procedure was found to minimize thermal reaction of NO₂ with toluene and cresols in the sampling tube.

Product identification was performed with a gas chromatograph mass spectrometer (JEOL, MS-D100) using a 3 m GC column of Se-30 on Shimalite W. The GC oven temperature was raised from 80 °C to 200 °C at a rate of 4 °C/min. Quantitative GC analysis was carried out using the same column as above.

3. Results and Discussion

In the present study, the wavelength of the irradiation light is limited to about 350 nm and longer. In this spectral region, the photo-oxidation of toluene-NO₂-O₂-N₂ system is initiated by the photo-dissociation of NO₂.

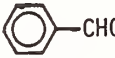
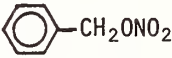
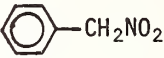
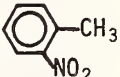


¹Figures in brackets indicate literature references at the end of this paper.

The radiation intensity gave a photo-dissociation rate coefficient for NO_2 of $1.1 \times 10^{-3} \text{ sec}^{-1}$.

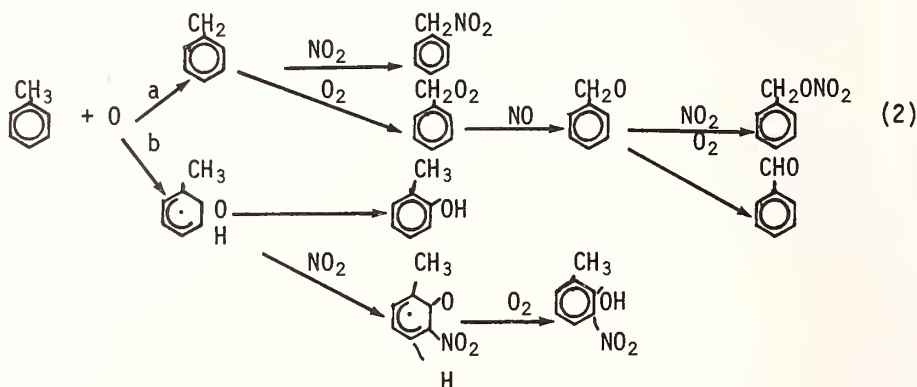
In the reaction system of toluene (34 ppm) - NO_2 (50 ~ 310 ppm) - N_2 (1 atm), oxygen atoms produced in reaction (1) react with toluene competing mainly with the reaction with NO_2 . Products observed in the above mentioned O_2 free system are o-cresol (other isomers are less than a few percent of o-cresol), α -nitrotoluene and m-nitrotoluene. The relative product yields are shown in table 1. The relative yield of α -nitrotoluene to cresol increased with the increase of the initial concentration of NO_2 , whereas that of m-nitrotoluene decreased. The production of α -nitrotoluene strongly suggests the presence of benzyl radical and would imply that the hydrogen abstraction from the methyl group of toluene by oxygen atom does occur, although Jones and Cvetanovic [4], Grovenstein and Mosher [5] and Gaffney et al., [6] did not detect a product originated from primary hydrogen abstraction under their experimental conditions.

Table 1. Relative product yields in the photo-oxidation of toluene- NO_2 - O_2 - N_2 system as normalized to cresol plus nitrocresol.

NO_2 (ppm)	HNO_2 (ppm)	Atmos- phere (1atm.)				
180	-	air	0.18	0.057	-	0.025
180	-	N_2	-	-	0.14	0.029
50	-	air	0.17	0.044	-	0.056
50	-	N_2	-	-	0.081	0.039
10	-	air	0.19	0.019	-	0.071
2	6	air	0.65	-	-	0.30

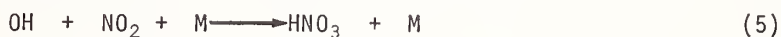
In the presence of initial O_2 , for example toluene (34 ppm) - NO_2 (11 ~ 207 ppm) -air system, benzaldehyde, benzylnitrate and nitrocresols are formed in addition to cresols and m-nitrotoluene. The production of α -nitrotoluene is completely suppressed. The relative yield of benzylnitrate and nitrocresols increased with the increase of the initial concentration of NO_2 , whereas that of m-nitrotoluene decreased as in the case of O_2 free system.

The reaction mechanism of toluene- NO_2 - O_2 / N_2 system under our experimental condition is most likely,



Formation of m-nitrotoluene both in the O_2 free and O_2 present system would be explained by the reaction initiated by OH radical as follows:

the competition between the reaction (3) and reactions



According to the above reaction scheme the formation ratio of (α -nitrotoluene + benzyl nitrate + benzaldehyde) to (cresols + nitrocresols) should be constant in the toluene- O_2-O_2/N_2 system and give the rate constant ratio k_{2a}/k_{ab} . Figure 1 shows the ratio in the experiment under various initial concentrations. Thus, the branching ratio of abstraction to addition of the reaction of oxygen atom with toluene is determined to be 0.22 ± 0.02 . This value should be taken as the upper limit since the contribution of OH radical reaction may not be negligible.

- [] Altshuller, A. P. and Leach, P. W., Int. J. Air Water Poll., 8, 37 (1964).
- [] Heuss, J. M. and Glasson, W. A., Environ. Sci. Tech., 2, 1109 (1968).
- [] Kopczynsky, S. L., Int. J. Air Water Poll., 8, 107 (1964).
- [] Jones, G. R. H. and Cvetanovic, R. J., Can. J. Chem. 39, 2444 (1961).
- [] Grovenstein, E., Jr. and Mosher, A. J., J. Amer. Chem. Soc., 92, 3810 (1970).
- [] Gaffney, J. S., Atkinson, R., and Pitts, J. N., J. Amer. Chem. Soc., 98, 1828 (1976).

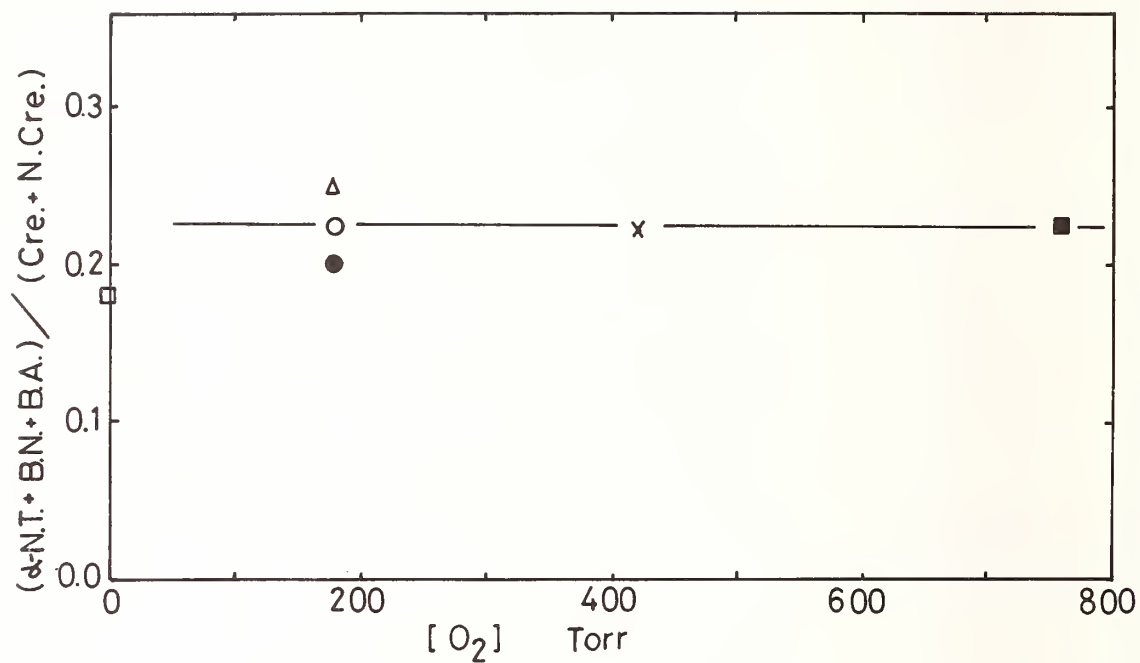


Fig. 1. The formation ratio of α -nitrotoluene (α -N.T.) + benzylnitrate (B.N.) + bezaldehyde (B.A.) to cresol (Cre.) + nitrocresol (N. Cre.). $\text{NO}_2/\text{O}_2 = 2.2 \times 10^{-5}$ (x,), 2.4×10^{-5} (o), 3.3×10^{-5} (o), 30.6×10^{-5} (Δ) and ∞ ().

EFFECTS OF SOLAR ENERGY DISTRIBUTION ON PHOTOCHEMICAL SMOG FORMATION

Gary Z. Whitten, James P. Killus and Henry Hogo

Systems Applications, Incorporated
San Rafael, California

Marcia C. Dodge

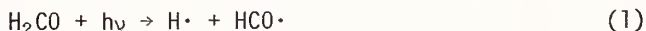
Environmental Protection Agency
Research Triangle Park, North Carolina

1. Introduction

The most documented photochemical reaction leading to ozone formation is NO_2 photolysis by ultraviolet light. Thus, the intensity of ultraviolet light as monitored in urban areas is often related to or even quantified by the rate of NO_2 photolysis (Holmes et al., 1973) [3]¹. Similarly, the light source in smog chambers is often calibrated by measuring NO_2 photolysis (Wu and Niki, 1975) [7,8]. The time to the NO_2 peak, i.e., the time to highest NO_2 concentration produced by an irradiated mixture of hydrocarbons and nitrogen oxides, is widely used to indicate the reactivity of the mixture (Altshuller and Cohen, 1963) [1].

Even though NO_2 photolysis is central to photochemical oxidant formation, more information regarding the UV spectrum of the light source may be necessary to properly estimate the oxidant severity. Indeed, Jaffe et al., (1974) [4] observed significant differences in oxidant formation from light sources that caused similar NO_2 photolysis rates but had different UV spectra. Aldehyde photolysis has recently been shown to be important in smog chemistry (Hecht et al., 1973) [2], and the ultraviolet wavelengths that photolyze aldehydes to form radicals are different from those that photolyze NO_2 . This paper discusses the implications of this wavelength difference on the chemistry of smog formation.

The quantum yield for NO_2 photolysis is unity at wavelengths below 400 nm, and rapidly decreases to zero at longer wavelengths. NO_2 photolysis in smog formation occurs mainly by absorption of UV light between 300 and 400 nm (Jones and Bayes, 1973) [5]. Formaldehyde is a major fraction of the total aldehyde found in photochemical smog, but its photolysis reactions are not as well understood as NO_2 photolysis. Of its two photolysis reactions,



the former is much more important in smog chemistry because it produces two radicals. The quantum yields for reactions (1) and (2) are known to vary with wavelength. The quantum yield is nearly unity at short UV wavelengths for reaction (1) and at long UV wavelengths for reaction (2). The quantum yields equal 0.5 for both reactions at about 312 nm. Thus, the aldehyde photolysis reaction important in smog photochemistry occurs by absorption of UV light near the short-wavelength edge of the solar spectrum.

¹ Figures in brackets indicate literature references at the end of this paper.

2. Results

Personnel at the University of California at Riverside Statewide Air Pollution Research Center (SAPRC) performed two smog chamber experiments with very similar initial concentrations and the same light source 4-1/2 months apart (Table 1). During the time between these two experiments the light source was found to have deteriorated by about 8.5 percent as measured by the NO_2 photolysis rate. However, spectral distribution measurements were not obtained for these two experiments.

Table 1. Initial conditions of smog chamber experiments.

	Experiment 1	Experiment 2*
Propylene (ppm)	1.036	1.040
NO (ppm)	1.12	1.11
NO_2 (ppm)	0.16	0.15
HCHO (ppb)	16.0	0.0
CH_3CHO (ppb)	7.0	2.0

* Experiment 2 was carried out in the same smog chamber with the same light source 4-1/2 months after Experiment 1.

The time to the NO_2 peak differed by a factor of two between these two experiments. In current mechanistic schemes, an 8.5 percent decrease in NO_2 photolysis cannot explain such a drastic difference in time to the NO_2 peak. We were interested to see whether a decrease in the intensity of short UV emitted by the light source could account for this decrease in reactivity.

Using a chemical kinetic mechanism for propylene/ NO_x systems developed with SAPRC data by Systems Applications, Incorporated, we performed computer simulations in which aldehyde photolysis rate constants were varied to obtain best fits to the experimental data for Experiments 1 and 2. We have recently modified our mechanism to include the formation of stable ozonides from the ozone-propylene reaction. We found that about thirty percent ozonide and the remainder to radical formation gave improved fits to observed data and seemed consistent with the findings of Niki et al. (1976) [8]. Moreover, by cutting back on one source of radicals (the ozone-olefin reactions) the dependence on aldehyde photolysis for radicals to sustain the formation of smog has increased markedly from that reported by Hecht et al. (1974) [2]. The values of these rate constants that produced the best fits are shown in Table 2.

Thus, large differences in aldehyde photolysis rates can explain the major difference in reactivity between these two experiments, assuming that our chemical kinetic mechanism for propylene is basically correct.

Some corroboration for the changes in aldehyde rate constants shown in Table 2 is provided by recent measurements of spectra during the replacement of the light source in the SAPRC chamber. It was found that the used light source emitted less UV light at wavelengths than the new source, and that the difference in intensity was largest at the short wavelengths.

Table 2. Rate constants for best fits of computer simulations to experimental results.

	<u>Experiment 1</u>	<u>Experiment 2</u>
NO ₂ photolysis rate		
constant (min ⁻¹)	0.223	0.204
HCHO photolysis rate		
constant* (min ⁻¹)	4.5 x 10 ⁻⁴	1.4 x 10 ⁻⁴
CH ₃ CHO photolysis rate		
rate constant† (min ⁻¹)	3.5 x 10 ⁻⁴	0.8 x 10 ⁻⁴
Time to NO ₂ peak		
Observed	105	210
Calculated	110	210

* By Reaction (1), $\text{HCHO} + h\nu \rightarrow \text{H}\cdot + \text{HCO}\cdot$.

† By the reaction $\text{CH}_3\text{CHO} + h\nu \rightarrow \text{CH}_3\cdot + \text{HCO}\cdot$.

3. Conclusions

Two smog chamber experiments at SAPRC with similar initial conditions showed a difference of a factor of two in reactivity, as measured by the time to the NO₂ peak. To determine whether this difference could be explained by a deterioration of the chamber light source, we simulated these experiments with a computer model. Our results indicate that a decrease in the intensity of short UV emitted by the light source could have caused the observed difference in reactivity.

Calculations and measurements of UV in the real atmosphere show changes in intensity, as measured by NO₂ photolysis, and in spectral distribution. Recent measurements of erythral radiation have been made and the erythral radiation spectrum resembles the absorption spectra of aldehydes (Machta et al., 1975) [6]. Hence the technology apparently exists to easily determine the ratio of light flux in the aldehyde-absorbing region to the flux for NO₂ absorption in the atmosphere. The combination of this measurement with the flux for NO₂ absorption should provide more reliable data for relating the concentration of photochemical oxidant to the light intensity.

References

- [1] Altshullter, A. P. and Cohen, I. R., Int. J. Air Water Pollut., Vol. 7, p. 787, (1963).
- [2] Hecht, T. A., Liu, M. K., and Whitney, D. C., Mathematical Simulations of Smog Chamber Photochemical Experiments, EPA-650/4-74-040, U.S. Environmental Protection Agency, Research Triangle Park, North Carolina, (1974).

- [3] Holmes, J. R., O'Brien, R. J., Crabtree, J. H., Hecht, T. A., and Seinfeld, J. H., Measurement of Ultraviolet Radiation Intensity in Photochemical Smog Studies, Environ. Sci. Tech., Vol. 7, p. 519, (1973).
- [4] Jaffe, R. J., Smith, F. C., Jr., and Last, K. W., Study of Factors Affecting Reactions in Environmental Chambers, EPA-640/3-74-004a, U.S. Environmental Protection Agency, Research Triangle Park, North Carolina, (1974).
- [5] Jones, I. T. N. and Bayes, K. D., Photolysis of Nitrogen Dioxide, J. Chem. Phys., Vol. 59, p. 4836, (1973).
- [6] Machta, L., Cotton, G., Hass, W., and Komhyr, W., Erythemat Ultraviolet Solar Radiation and Environmental Factors, CIAP Report (February 28, 1975).
- [7] Wu, C. H. and Niki, M., Methods for Measuring NO_2 Photodissociation Rate, Environ. Sci. Tech., Vol. 9, p. 46, (1975).
- [8] Niki, H., Maker, P., Savage, C., and Breitenbach, L., Fourier Transform Spectroscopic Studies of Gas Phase Ozone-Olefin Reactions, 171st American Chemical Society National Meeting, (1976).

PHOTOPHYSICS OF BOUND AND DISSOCIATIVE STATES OF SMALL MOLECULES IN CONDENSED PHASES

L. E. Brus and V. E. Bondybey

Bell Laboratories
Murray Hill, NJ 07974

The cage effect on dissociating small molecules in rare gas solids has been investigated via the techniques of time, wavelength, and polarization resolved fluorescence. Strongly predissociated molecules, such as ICl, and directly dissociating molecules, such as Cl₂ and CH₃I, have been studied. In the solid the host prevents permanent dissociation, and the fragments recombine within a few vibrational periods into the various bound electronic states. In the solid there is no quantized vibrational structure at excitation energies corresponding to gas phase dissociation. This strong cage effect occurs in the impulsive limit with respect to the bulk compressibility relaxation time of the rare gas host. However, bound-bound spectra, involving zero phonon lines of levels very close to the dissociation limit, imply only a weak van der Waals cage influence on the molecular potential. This result implies only minor cage effect for processes occurring in the adiabatic limit with respect to host compression. Polarized excitation ("photo-selection") studies allow one to unravel the various radiationless transition pathways in the common case where the absorption spectrum contains several overlapping continua. The predissociated B 0 state of ICl has an effective double minimum shape in the solid. Excitation below the dissociation barrier produces B (v=0) fluorescence with near unity quantum yield, while excitation above the barrier produces principally A ³Π(v=0) emission via radiationless relaxation through the outer minimum of B. In CH₃I, it is observed that the "repulsive" 0 excited state, which is employed in gas phase photodissociation I* ²P_{1/2} → ²P_{3/2} lasers, is actually slightly (< 2000 cm⁻¹) chemically bound. In Cl₂, the observed emitting bound state is tentatively assigned as the "forbidden" lowest multiplet component ³Π₂.

Vibrational relaxation rates of high frequency (> 1000 cm⁻¹) modes in small molecules are slow because a large number of 50 cm⁻¹ lattice phonons must be simultaneously produced. An energy gap law has been predicted, such that the rate should decrease exponentially with the quantum size. This prediction is observed to be violated in the vibrational relaxation of OH (A ²Σ) and NH (A ³Π), where the hydrides actually relax faster than the deuterides. The electronic spectra show these molecules to be undergoing slightly perturbed free rotation at 4.2°K; and the relaxation data are thought to reflect the involvement of this localized motion. When energy relaxation is slow, long range energy transfer processes have time to develop, and may dominate the excited state population evolution. Three near resonant vibrational energy transfer processes from ND (A ³Π) to ¹²CO and ¹³CO have been studied. The transfer quantum yield, and the non-exponential time resolved donor population, both follow Forster (dipole-dipole) kinetics as a function of the acceptor concentration. A strong energy gap (transfer exothermicity) law is found of the form $k \propto \exp [-\Delta E / (28 \text{ cm}^{-1})]$ where $\Delta E = \hbar(\omega_d - \omega_a)$. Transfer from NH (A ³Π) to CO is anomalously fast in view of the size of ΔE, again indicating the hydride dissipates energy into the matrix especially efficiently.

A number of spin and symmetry forbidden internal radiationless transitions have been observed in the first row diatomics C₂ and C₂⁻. For example, vibrational relaxation in C₂ (B ²Σ_u⁺) occurs by sequential intersystem crossing, to and from, the nearby ⁴Σ_u⁺ state.

Similarly in C_2 excitation into $A\ ^1\Pi_u$ produces with high quantum yield the lowest triplet a $^3\Pi_u$. Population in $v=0-3$ of a $^3\Pi_u$ subsequently undergoes the spin and symmetry forbidden intersystem crossing into $X\ ^1\Sigma_g^+$ on a 10^{-5} sec time scale. An extremely strong energy gap law prevails over the low intramolecular matrix elements in these processes.

The photodissociation cage effect allows one to study transient species that have very weakly bound ground electronic states. For example, several bound-free and bound-bound fluorescences have recently been observed in the diatomics XeO and XeF . The polarized excitation spectra in solid Ar allow one to unravel the symmetries and energies of the various excited states. In XeO , both the $^1\Sigma$ and $^1\Pi$ states correlating with $O(^1D) + Xe$ have been observed in fluorescence from the $^1\Sigma$ state which correlates with $O(^1S) + Xe$. The ground $X^1\Sigma$ state of XeF isolated in solid Ne exhibits $\omega_e = 247\text{ cm}^{-1}$ and $\omega_e x_e = 10.7\text{ cm}^{-1}$, yielding an extrapolated Morse oscillator $D_e \cong 1500\text{ cm}^{-1}$.

SPECTROSCOPY AND PHOTOCHEMISTRY OF MATRIX ISOLATED METAL HEXAFLUORIDES

William F. Coleman and Robert T. Paine

Department of Chemistry
University of New Mexico
Albuquerque, NM 87131

and

R. Burton Lewis, Robin S. McDowell,
Lewellyn H. Jones and Larned B. Asprey

Los Alamos Scientific Laboratory
University of California
Los Alamos, NM 87544

Although the uranium hexafluoride (UF_6) molecule has been of great interest to chemists and physicists for more than 35 years, it is only recently that reliable spectroscopic data have been available. The photochemistry of UF_6 , an area of great potential applicability in an isotope separation program, has not been reported prior to this work. We survey here recent work from our laboratories on the vibrational, electronic absorption, emission and excitation spectra and the ultraviolet photochemistry of low temperature thin film and matrix isolated UF_6 .

1. Vibrational Spectra

The six fundamental frequencies of UF_6 have been recently determined in dilute Ar matrices at 14 °K [1]. In addition to the IR and Raman active modes sufficient combination bands were observed to allow assignment of all fundamentals. Shifts of up to 6 cm^{-1} from the most reliable gas phase data [2] were obtained in the solid and some evidence exists for the formation of low concentrations of UF_6 aggregates in the matrices. Strong perturbations are observed in different matrix hosts, the general trend being that stretching frequencies are more susceptible to the matrix than bending frequencies. Table 1 gives the values of $\nu_1 \rightarrow \nu_6$ in the Ar matrix.

Table 1

Fundamental Frequencies of Matrix-Isolated UF_6 (cm^{-1})

ν_1 (A_{1g} stretch)	666
ν_2 (E_g stretch)	530
ν_3 (F_{1u} stretch)	619.3
ν_4 (F_{1u} bend)	183.5
ν_5 (F_{2g} bend)	200
ν_6 (F_{2u} bend)	143.2

Figures in brackets indicate literature references at the end of this paper.

2. Electronic Spectra

The general features of the UF_6 ultraviolet spectrum have been known for sometime [3]. The spectrum consists of two major regions of absorption a) a weak absorptio envelope from 340-410 nm (the A band) and b) a strong manifold from 330 nm to higher energies (the B band). The weak band has previously been reported to exhibit some structur A recent study has revealed a significant amount of structure in both the A and B bands for low temperatures matrices [4]. The A band has been assigned as arising from a forbidde charge transfer transition to two excited electronic states, one predominately singlet in character and the second (the lower energy state) predominately triplet in character. The vibronic transitions have been assigned with (singlet, electronic) = $25,270\text{ cm}^{-1}$, (triple electronic) = $24,510\text{ cm}^{-1}$, $\nu_1 = 580\text{ cm}^{-1}$, $\nu_3 = 480\text{ cm}^{-1}$ and $\nu_4 = 185\text{ cm}^{-1}$. The B band region has been assigned as arising from both allowed charge-transfer transitions and a weak forbidden transition. Comparison of the observed spectra with several recent calculations [5,6] on the electronic structure lead to the conclusion that the spin-orbit coupling in UF_6 is intermediate and the best fit is obtained by applying spin-orbit couplin to the $X\alpha$ calculations [5].

3. Emission Spectra

The luminescence of solid UF_6 was first discussed in detail by Sheremetèv in 1957 [7] and has been observed several times since then. Our matrix luminescence spectra represents the first instance in which significant vibronic structure is present. At 14 °K in 200/1 Ar/ UF_6 matrix more than 200 lines are observed in the emission spectrum. Progressions in ν_6 , $\nu_6 = n\nu_5$ ($n = 1-16$) and several other combinations are observed. Phonons, apparently arising from the matrix gas, are observed with differing frequencies in the different matrices. The quantum efficiency is quite temperature and concentration dependent and the position of the 0-0 band is strongly concentration dependent. The 0-0 band is much more intense in a UF_6 thin film supporting a structure change from matrix to thin film. The excitation spectrum verifies the presence of two electronic states in the A band region, the second having an internal conversion efficiency to the emitting stste of less than unity. The internal conversion from the B band to the emitting state is a very inefficient process and is compatible with the observed photochemistry (vide infra).

4. Photochemistry

Photolysis of matrix isolated UF_6 in dilute Ar matrices leads to significant and reversible changes in the vibrational and emission spectra. New bands attributed to isolated UF_5 appear in the IR [1] and a weak near IR luminescence is detected. These spectral features disappear rapidly following exclusion of the UV radiation and the spectra of UF_6 are regenerated. In more concentrated matrices (20/1 Ar/ UF_6) the emission intensity does not return to the initial value indicative of irreversible formation of polymeric UF_5 . In CO matrices, which should be efficient fluorine-atom scavengers, the process is irreversible and IR bands appear which can be assigned to FCO , $(\text{FCO})_2$ and F_2CO .

The photolysis is much more efficient for irradiation in the B band than for the A band and a wavelength dependence of the photolysis quantum yield is observed within the A band.

The discussion will focus primarily on recent results in the emission and photochemical studies.

References

- [1] Paine, R. T., McDowell, R. S., Asprey, L. B., and Jones, L. H., J. Chem. Phys. (Communication), 64,0000 (1976).
- [2] McDowell, R. S., Asprey, L. B., and Paine, R. T., J. Chem. Phys., 61, 3571 (1974).
- [3] Lipkin, D., and Weissman, S. I., "Photochemistry of Systems Containing Uranium Compounds," University of California, Radiation Laboratory Report A-520, 1942.

- 4] Lewis, W. B., Asprey, L. B., Jones, L. H., McDowell, R. S., Rabideau, S. W., Zeltmann, A. H., and Paine, R. T., J. Chem. Phys., 64, 0000 (1976).
- 5] Boring, M., J. Chem. Phys., (to be published).
- 6] Ellis, D. E., and Koelling, D. D., unpublished calculations.
- 7] Sheremetèv, Optica i Spektroskopiya, 2, 99 (1957).

MERCURY PHOTOSENSITIZED PRODUCTION OF TRAPPED RADICALS IN ORGANIC GLASSES AT <77 K¹

N. Bremer, B. J. Brown, G. H. Morine, and J. E. Willard

Department of Chemistry, University of Wisconsin
Madison, Wisconsin 53706

1. Introduction

Solutions of mercury in liquid hydrocarbons ($\sim 5 \times 10^{-6}M$ at $25^\circ C$)[2] may be stabilized in the glassy state by quench cooling in liquid nitrogen at 77 K (fig. 1)[3]. When a glassy solution in 3-methylpentane (3MP) is exposed to 254 nm radiation absorbed by the Hg, the intensity of the Hg absorption band diminishes while a broad absorption from 200 nm to 300 nm (fig. 2) attributable, in part, to 3-methylpentyl radicals appears in parallel

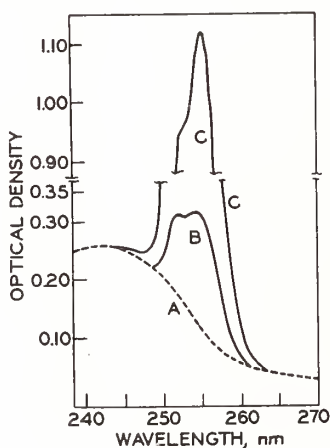


Fig. 1. Spectra of Hg in 3MP glass at 77 K (5-cm pathlength in two 2.5-cm^2 quartz cells): (A) spectrum of cell walls, 3MP is transparent in this region; (B) 3MP saturated with Hg at $25^\circ C$ and quenched to 77 K; (C) 3MP saturated with Hg at $\sim 55^\circ C$ and quenched to 77 K.

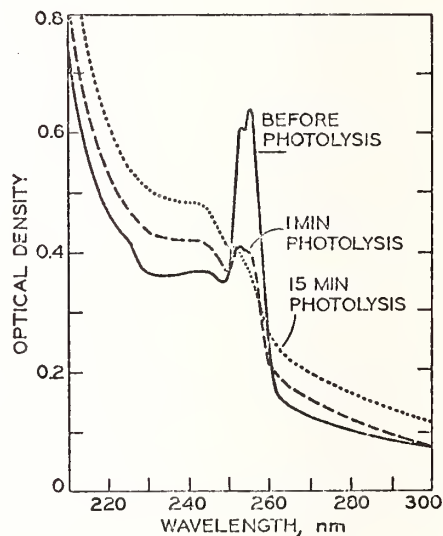


Fig. 2. Spectra of 3MP-Hg glass at 77 K at different times of illumination with 200 nm- 300 nm medium pressure Hg lamp.

with growth in the known ESR signal of the radicals. The rate of growth of the radical concentration approaches zero with continued monochromatic 254 nm illumination (fig. 3), but increases upon exposure to broad band 200 nm- 300 nm light. Exposure of a fresh 3MP-Hg glass sample to the broad band light at 77 K causes continuous growth in the radical concentration with no plateau, many radicals being produced for each Hg atom present (fig. 4). These observations indicate that a species formed in a primary or secondary act

¹Figures in brackets indicate literature references at the end of this paper.

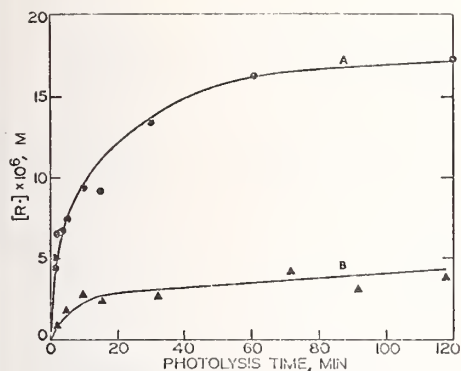


Fig. 3 Concentration of trapped radicals, measured by ESR, as a function of time of illumination of 3MP-Hg glass at 77 K with 254 nm light from Vycor low pressure Hg lamp. Curve A, $4.1 \times 10^5 \text{ ergs cm}^{-2} \text{ sec}^{-1}$; Curve B, $1.7 \times 10^4 \text{ ergs cm}^{-2} \text{ sec}^{-1}$.

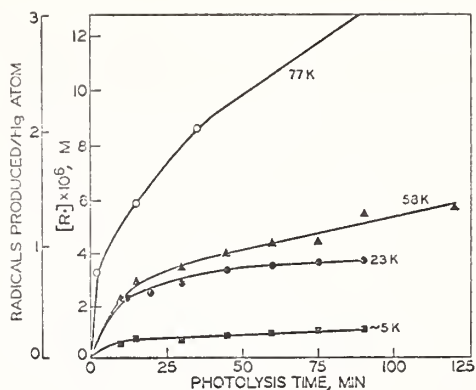


Fig. 4. Concentration of trapped radicals, as a function of time of illumination of 3MP-Hg glass at 77 K, 58 K, 23 K and 5 K with 200 nm-300 nm light from medium pressure Hg lamp.

Following photoactivation of the Hg by 254 nm light (e.g. HgH , HgR or HHgR) absorbs in the broad band region and is decomposed, liberating Hg which again absorbs 254 nm photons and produces more radicals. No ESR signal from the intermediate has been found, indicating that it is not paramagnetic or that the spectrum is too broad to detect.

The initial rate of radical production by illumination of a fresh 3MP-Hg sample is directly proportional to the light intensity. At plateaus of the type of figure 3, the ratio of radicals to Hg atoms which have disappeared may be greater than unity and it increases with the light intensity, but to a power less than first order. This seems to imply that the initially formed intermediate absorbs 254 nm to regenerate Hg (e.g. $\text{HgH} \xrightarrow{h\nu} \text{Hg} + \text{H}$) in competition with a reaction which forms a species with relatively low extinction coefficient for 254 nm (e.g., $\text{HgH} + \text{R} \cdot \rightarrow \text{HHgR}$), which is decomposed at other wavelengths of the broad band light (e.g. $\text{HHgR} \xrightarrow{h\nu} \text{Hg} + \text{RH}$).

Illuminations with the broad band light at 5 K do not produce continuing radical growth as at 77 K, but rather lead to a steady state concentration at ~ 0.2 radicals per Hg atom (fig. 4). This may be attributed to concerted formation within the low temperature parent cage of a compound with the properties attributed above to HHgR , coupled with an inability of the low temperature matrix to deactivate the HHgR without decomposition when it is activated by a photon from the broad band source. At 23 K the plateau is higher than at 5 K, while at 58 K continued growth occurs, though at a lower rate than at 77 K. Thermal decay of the radicals produced by the photosensitization is only a few percent per hour at 77 K and is undetectable over hours at the lower temperatures studied.

These studies indicate: 1) energy transfer from $\text{Hg}(6^3\text{P}_1)$ atoms to molecules in a hard organic glass inducing bond rupture as in the gas [4] and liquid phases [4]; 2) a new method of producing trapped radicals for study in glassy matrices; 3) a means of trapping intermediates from Hg photosensitization reactions which may in further investigations assist in identifying them and their reactions; 4) a potential source of information on the kinetics of radical-radical reactions in radical clusters in solids; 5) the possibility of false interpretation of photochemical results in condensed systems containing unsuspected gas as a contaminant.

All experiments were made with purified degassed reagents; optical measurements used 5 cm light path; radical concentrations were determined from the double integral of the first derivative ESR spectrum.

References

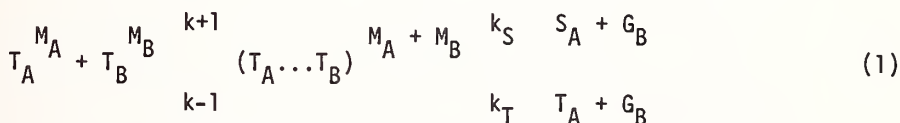
- [1] This work has been supported in part by the U.S. Energy Research and Development Administration under Contract No. AT(11-1)-1715 and by the W. F. Vilas Trust of the University of Wisconsin.
- [2] (a) Spencer, J. N. and Voigt, A. F., *J. Phys. Chem.*, 72, 464 (1968); (b) Kuntz, R. R. and Mains, G. J., *ibid.*, 68, 408 (1964).
- [3] Bremer, N., Brown, B. J., Morine, G. H., and Willard, J. E., *J. Phys. Chem.*, 79, 2187 (1975).
- [4] For reviews of Hg-photosensitization reactions and references, refer to (a) J. G. Calvert and J. N. Pitts, "Photochemistry," Wiley, New York, N.Y., 1966; (b) R. J. Cvetanovic, *Prog. React. Kinet.*, 2, 39 (1964); (c) A. B. Callear and P. M. Wood, *J. Chem. Soc., Faraday Trans. 2*, 68, 302 (1972); (d) A. C. Vikis and D. J. LeRoy, *Can. J. Chem.*, 51, 1207 (1973).

MAGNETIC FIELD EFFECTS ON TRIPLET-TRIPLET ANNIHILATION IN CRYSTALS¹

S. H. Tedder and S. E. Webber

Department of Chemistry
University of Texas at Austin
Austin, Texas 78712

It has been known since 1967 [1]² that external magnetic fields influenced the intensity of delayed fluorescence in molecular crystals. The theory of this effect was first presented by Merrifield [2], and has been refined by Merrifield [3] and others. Excellent reviews are available [4]. The essential idea of the original explanation of Merrifield may be represented by the "reaction"



where T^M is a triplet exciton in sublevel M , $(T_A \dots T_B)^{M_A+M_B}$ is an "intermediate" with total M quantum number of M_A+M_B (spin relaxation is ignored), and S_A and G_B are excited and ground state singlets, respectively. The S_A state is responsible for the delayed fluorescence. At high fields triplet exciton pair states $(|M_A, M_B\rangle)$ will not be degenerate in general because of zero-field coupling terms in the total Hamiltonian. For certain orientations of the magnetic field with respect to the crystallographic axis the levels will become degenerate and the states involved in reaction (1) are mixed with a concomitant change in the rate of singlet formation (usually a decrease). Hence the level crossing resonance is observed as a change in the intensity of delayed fluorescence. An example of this type of data for anthracene doped phenanthrene crystals for different orientations of the crystal in the plane of the magnetic field is given in figure 1(a). For this case the annihilation is heterogeneous, i.e., between a phenanthrene triplet exciton and an anthracene trapped triplet molecule. To a good approximation the minimum of the delayed fluorescence corresponds to the angle at which the high field states $|\pm 1_A, \mp 1_P\rangle$, $|0_A, 0_P\rangle$ (A = anthracene, P = phenanthrene) become degenerate. Similar results have been observed for the delayed fluorescence of pure naphthalene or naphthalene crystals lightly doped with anthracene. Heavier doping with anthracene (but still less than 10^{-6} M/M) totally changes the pattern of resonances for naphthalene crystals in a way that is not presently understood.

As can be seen from figure 1(a) the character of the level crossing resonance changes rather drastically with the orientation of the crystal. Simple application of previous theory does not account for this effect and we have been led to postulate that the triplet exciton-trapped triplet interact with each other during this annihilation via the intermolecular spin-spin interaction. H_{SS} depends on the orientation of the crystallographic axis with respect to the magnetic field, if the spin states are expressed in the high field representation. If the spin states are mixed by the H_{SS} , and the quantum yield of singlet formation is calculated using a kinetic scheme like (1) and (2), we obtain results which have a qualitative resemblance to our experimental data, see figure 1(b) [5]. It is our intention to extend these calculations to the naphthalene system.

¹ Supported by the Robert A. Welch Foundation.

² Figures in brackets indicate literature references at the end of this paper.

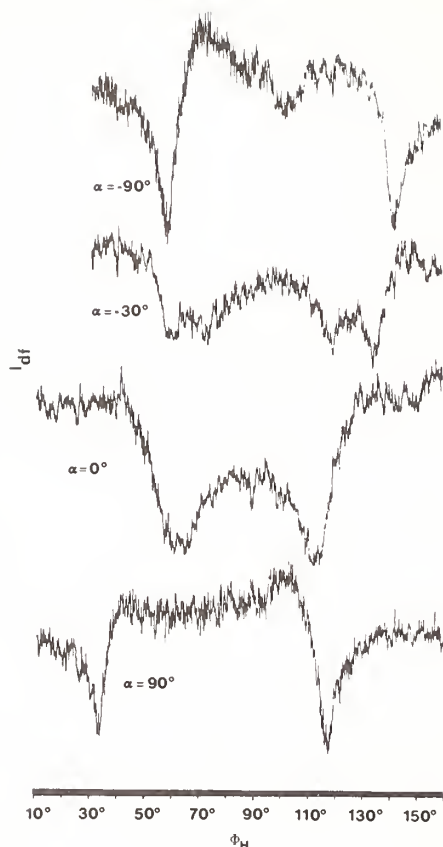


Fig. 1(a). The intensity of anthracene delayed fluorescence as a function of the angle ϕ_H of the applied 8 kG magnetic field. The values of α are -90° (H//ac*, b up); 30° (H//bc*, a down), and 90° (H//ac*, b down). The traces are not all to the same scale.

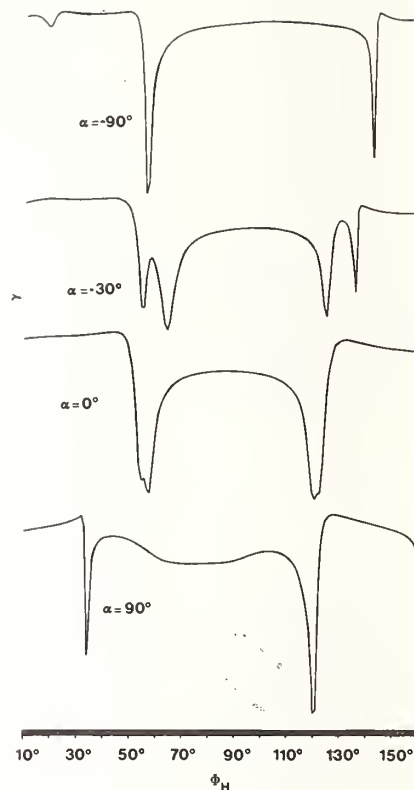


Fig. 1(b). A model calculation of γ using eq. (2) and considering interexcitation spin-spin interaction. For these calculations $k_{-1} = 0.05$, $k_s = 1.0$ and $k_T = 0.5$ (k_{+1} does not affect the relative changes of γ and only the relative values of the other constants are important).

A second theoretical model that has been studied is the use of level avoided crossing (LAC) theory, which has previously been applied to magnetic field effects on prompt fluorescence of small molecules in the gas phase [6]. This model is also similar, but not identical to, an approach given by Johnson and Merrifield [3]. In this model it is assumed that each quantum mechanical pair state evolves in time coherently, and interference effects between states play a significant role in the observed line shape. This theoretical model is much more difficult to apply than the kinetic model, but preliminary calculations have demonstrated qualitative agreement with experimental results. Our current goals are: (1) to establish if one or the other (or either) of these models is to be preferred, and (2) to establish if these experiments elucidate the nature of the interaction between the triplet state molecules during annihilation.

References

- [1] Johnson, R. C., Merrifield, R. E., Avakian, P. and Flippen, R. B., Phys. Rev. Lett. 19, 285 (1967).
- [2] Merrifield, R. E., J. Chem. Phys. 48, 4318 (1968).
- [3] Johnson, R. C. and Merrifield, R. E., Phys. Rev. B 1, 896 (1970).
- [4] Swenberg, C. E. and Geacintov, N. E., Organic Molecular Photophysics Volume 1 (ed. Birks, J. E., John Wiley and Sons, New York, 1973), Chapter 10; *ibid*, Volume 2, p. 395.
- [5] Tedder, S. H. and Webber, S. E., Chem. Phys. 12, 253 (1976).
- [6] Levy, D., Adv. Magn. Resonance 6, 1 (1973).

THE CONTRIBUTION OF THE PHYSICAL AND CHEMICAL DEFECTS TO THE PHOTOCHEMISTRY OF CRYSTALLINE DURENE AT VERY LOW TEMPERATURES

A. Despres, V. Lejeune, and E. Migirdicyan

Laboratoire de Photophysique Moléculaire du C.N.R.S.
Université de Paris-Sud
91405 Orsay, France

1. Introduction

It has been known [1]¹ for some time that line defects (dislocations) and point defects (impurities) may play an important role in photochemical reactions developed in single crystals. The disposition of the molecules at crystalline defects is generally different from that of molecules in the regular lattice. These structural imperfections can affect the migration of excitons through the crystal and/or may facilitate the formation of a transition complex leading to a chemical reaction.

The aim of the present work is to study the contribution of the physical and chemical defects to the photochemistry at very low temperatures (10-20 K) of durene single crystals doped with aldehydic guests in substitutional position.

The solid state photolysis of durene doped with orthomethyl substituted benzaldehydes like 2,4,5-trimethylbenzaldehyde (TMB), 2,4- and 2,5-dimethylbenzaldehydes (2,4-DMB and 2,5-DMB) gives rise, between 200 and 300 K, to a photoenolization reaction [2] (hydrogen transfer from the methyl to the carbonyl group in ortho position) as well as to the production of duryl (2,4,5-trimethylbenzyl) radicals [3]. These radicals are formed by the detachment of a hydrogen from a durene methyl group and are identified by their characteristic green fluorescence [4]. Neither photoenolization reaction nor duryl radical production are however detected between 200 and 300 K, under similar photolysis conditions, in durene doped with 3,4-dimethylbenzaldehyde (3,4-DMB) or with 3,4-dimethylacetophenone (3,4-DMA), both guests having no methyl substituent in ortho position with respect to the carbonyl group. These results suggest that in durene mixed crystals, the guest intramolecular and the guest-host intermolecular hydrogen abstraction reactions are in some way related to each other in this temperature range, since duryl radicals are produced only with ortho-methylated benzaldehyde guests where a photoenolization reaction is also generated. Consequently, the intermolecular hydrogen abstraction leading to duryl radical production in the solid state photolysis of TMB, 2,4-DMB and 2,5-DMB in durene between 200 and 300 K is not a primary photochemical process as this is the case for the ketyl radical production during the liquid state photolysis of benzophenone in hydrogen donor solvents.

In contrast, when the UV photolysis is carried out at 10-20 K, duryl radicals are always produced in durene doped with aromatic carbonyl compounds which are substituted (TMB, 2,4-DMB and 2,5-DMB) or not (3,4-DMB and 3,4-DMA) in ortho position with methyl groups.

At these very low temperatures, the photoenolization reaction was found to be negligible, in agreement with our previous results [2] which indicate that this process requires an activation energy. These observations suggest that the mechanism of duryl radical formation is different in the high (200-300 K) and in the low (10-20 K) temperature range.

Furthermore, in highly purified durene single crystals where no impurity emission is detected at these very low temperatures, duryl radicals are not produced during a massive UV irradiation at 10-20 K. This indicates that the presence of the aldehydic guest is necessary.

¹Figures in brackets indicate literature references at the end of this paper.

to induce photochemical activity and consequently, the dissociation of the host molecules is photosensitized by the aldehydic guest.

The information concerning the photochemistry of durene mixed crystals at very low temperatures are based on the following spectroscopic observations.

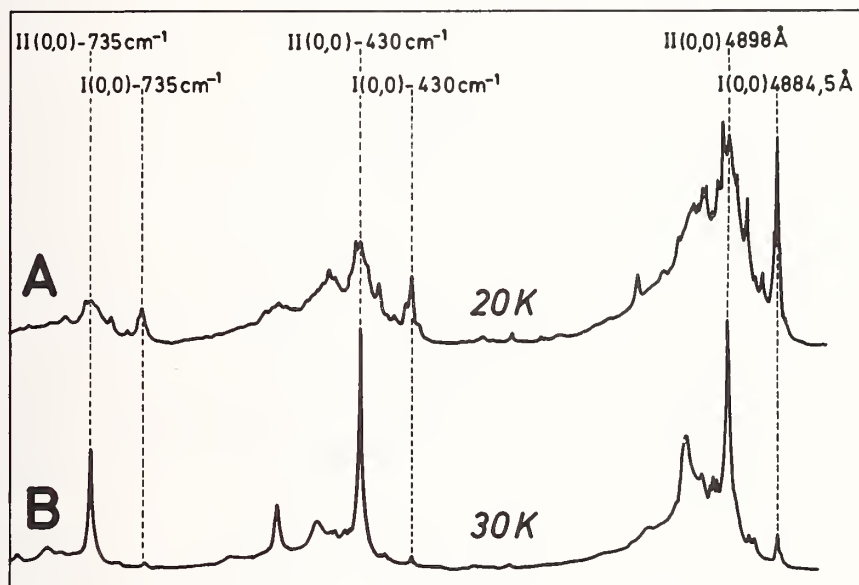
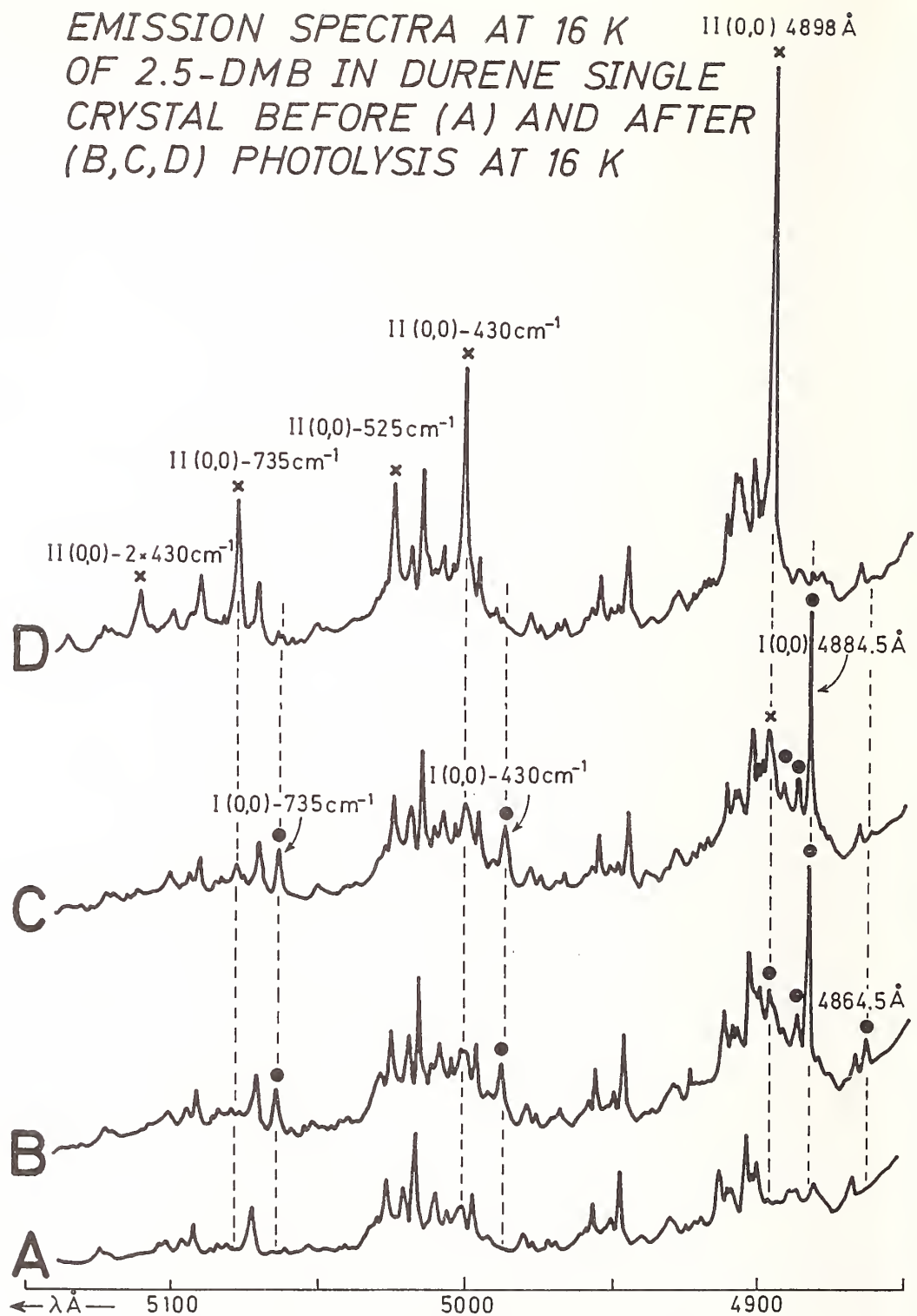


Figure 1.

In the figure are presented the emission spectra of durene single crystals doped with 2,5-DMB at 16 K before (A) and after (B,C,D) photolysis with the full UV emission of a high pressure mercury lamp (Osram HBO 200) where the visible light was filtered by means of a Schott UG11 glass. The bands present on curve A are the weak phosphorescence bands of the aldehydic guest in this wavelength range. The photolysis of the sample at 16 K reveals new emission bands shown in spectrum B: a weak band at 4864,5 Å and a predominant band at 4884,5 Å followed by two relatively strong bands at respectively, 430 and 735 cm^{-1} from the latter. When the sample is annealed in the dark by a warming up to 60 K and a freezing down to 16 K cycle, no great changes are observed on the spectrum C except for the disappearance of the weak band at 4864,5 Å and the slight increase in intensity of the band at 4898 Å. However, when the sample is annealed up to 70 K, the entire structure of the emission subsequently recorded at 16 K is dramatically changed: the band at 4884,5 Å as well as its two companion bands at 430 and 735 cm^{-1} have completely disappeared and are replaced by a shifted spectrum starting at 4898 Å with two intense bands again at 430 and 735 cm^{-1} from the origin. This new spectrum is identical to that recorded in this very low temperature range for duryl radicals prepared at room temperature either by photolysis of durene mixed crystals or by radiolysis of purified durene. Consequently, the spectrum starting at 4884,5 Å with a similar vibrational structure as that starting at 4898 Å, can reasonably be attributed to duryl radicals which are trapped in a different crystalline environment when prepared at 10-20 K. Similar results are obtained when samples of durene doped with 2,4-DMB, TMB, 3,4-DMB or 3,4-MA are photolyzed at 10-20 K.

All these observations can therefore be rationalized in the following way: the bands at 4864,5 Å and at 4884,5 Å are the fluorescence origins of duryl radicals produced photochemically in transient defects created because of the stress experienced by durene single crystals during the cooling at 10-20 K. These transient species first formed in crystalline defects are then reoriented for temperatures higher than 60 K, so as to give more stable duryl radicals whose fluorescence origin is shifted to 4898 Å.



(C)=(B) Warmed up to 60K and refrozen at 16 K
(D)=(C) Warmed up to 70K and refrozen at 16 K

Figure 2

In a recent paper published while this work was in progress, Udagawa and Hanson [5] have also observed that the duryl radicals produced photochemically in a durene host either at 2-15 K or at temperatures higher than 80 K have different fluorescence origins respectively located at 4885 Å and 4898 Å, in good agreement with our spectroscopic data. From their study of the Stark effect on the lowest excited state of these species, they have concluded that the radicals prepared in the low or higher temperature range have different orientations which result from the recoil of the duryl radical in the photodissociation process.

2. The Dependence on Photolyzing Light Intensity of Duryl Radical Production at 16 K

In order to get information on the mechanism responsible for duryl radical production in transient defects at very low temperatures, the dependence on photolyzing light intensity of this reaction rate was studied at 16 K.

The relative rates of radical production were measured by monitoring the intensity I of the fluorescence band at 4884,5 Å during the UV irradiation. The plot of I versus time of irradiation with constant light intensity presents an initial linear region starting at the coordinates origin. This indicates that the reaction takes place either without any photochemical precursor or through a precursor having a lifetime of the order of the minute or less. The relative rates were determined from the initial linear regions. However, the intensity changes level off at high radiation doses because of secondary reactions and a possible inner filter effect of the radical produced.

The relative light intensity was modified by introducing wire screens between the light source and the sample. The screens were placed at sufficient distance from the sample to insure uniform illumination. The use of wire screens which reduce the photolyzing light intensity by factors of 3,6 or of 7,7 decreases the rate of radical production by factors of 3,5 and 7,6, respectively. This indicates that the duryl radical production at 16 K depends linearly on photolyzing light intensity. According to the overall kinetic scheme established for similar processes [6], such a result suggests that the reaction is either monophotonic or biphotonic with the guest triplet state as intermediate. In particular, when the decay process from the guest triplet state is negligible compared with absorption of the second photon from that state, then the reaction rate can depend linearly on photolyzing light intensity even for a biphotonic reaction. From our previous investigations, the triplet lifetime of 2,5-DMB in durene single crystal at 16 K is known to be 15 m sec. This short lifetime together with an approximate evaluation, for our experimental device, of the incident light intensity for second photon absorption, indicates that, in our conditions, the decay from the guest triplet state is not negligible compared with absorption of the second photon from that state. Consequently, the duryl radical production at 16 K is indeed a monophotonic process.

A consideration of the singlet and triplet electronic state energies of the aldehydic guests and the durene host allow us to discard the dissociation of the host via guest-host energy transfer in a monophotonic process.

One remaining possibility is the direct hydrogen abstraction of the aldehydic guest excited in the triplet state from the durene molecule in the ground state. This reaction was discarded in the high temperature range (200-300 K) on the basis of our experimental results. However, it is very well possible that, in the crystalline defects created in durene single crystals at very low temperatures, the steric conditions required by this reaction are achieved and lead to the duryl radical production.

References

- [1] Thomas, J. M., and Williams, J. O., Progr. Solid State Chem. 6, 119 (1971) and references therein.
- [2] Migirdicyan, E., Despres, A., Lejeune, V., and Leach, S., J. Photochem., 3, 383 (1974/75).

- [3] Migirdicyan, E., J. Chem. Phys. 55, 1861 (1971).
- [4] Leach, S and Migirdicyan, E., Chem. Phys. Lett. 1, 21 (1967).
- [5] Udagawa, Y., and Hanson, D. M., J. Chem. Phys. 64, 3753 (1976).
- [6] Stevens, B., and Walker, M. S., Chem. Commun. 1, 8 (1965).
- [7] Despres, A., Migirdicyan, E., and Blanco, L., Chem. Phys. 14, 229 (1976).

PHOTOCHEMISTRY OF ELECTRONS TRAPPED IN ORGANIC GLASSES [1]¹

G. C. Dismukes, S. L. Hager, D. P. Lin, G. H. Morine and J. E. Willard

Department of Chemistry
University of Wisconsin
Madison, Wisconsin 53706

It has been known for some time that mobile electrons generated in organic glasses by γ radiolysis or photoionization of solutes at <77 K become physically trapped with significant yields [2]. These e_t^- give broad absorption spectra (>3 eV) with maxima in the visible or near infrared. The spectra have bandwidths at half-height ranging from ~ 0.5 eV to >1 eV, long tails on the higher energy side of λ_{\max} , shorter tails on the low energy side, and extinction coefficients at λ_{\max} of 10^3 - 10^4 . Trapped electrons can be removed from their traps by photons and migrate to encounter solutes with which they can react in competition with retrapping. Products may include molecular anions produced by reaction with molecules with a positive electron affinity (e.g., biphenyl), carbanions (by reaction with trapped radicals) free radicals (by dissociative electron capture), and neutral molecules (by reaction with cations). This paper reviews some of the photochemistry of such trapped electrons observed in recent and continuing work in our laboratory.

Until relatively recently it was not known whether the broad spectra of e_t^- , such as illustrated in figure 1, are representative of electrons bound in uniform traps or are envelopes of the spectra of electrons in trapping sites with a continuum of energies. Data such as those of figures 2 and 3 give strong support to the conclusion that the spectra represent continua of trapping energies [2]. Figure 2 [3] indicates that exposure to light in the 700 nm-1000 nm region of the spectrum of e_t^- in 3-methylpentane ($\lambda_{\max} = 1600$ nm) increases the absorption above 1900 nm and decreases it below, the process being reversed in the dark. This can be explained if the detrapped electrons are retrapped in weaker traps which they cause to deepen by coulombic interaction with bond of dipoles of the surrounding molecules. Figure 3 [4] illustrates energy-selective detrapping of e_t^- in methyltetrahydrofuran (MTHF) at 25 K by 1338 nm light, and relatively uniform bleaching by 1064 light. Figure 4 is a formalized model to suggest the type of continuum of e_t^- spectra which might be responsible for the effects observed. Evidence that the detrapping of e_t^- is monophotonic, rather than occurring by a biphotonic mechanism involving promotion to an excited state of the trap followed by absorption of a second photon, is given by the first order dependence of photoconductivity (fig. 5) and photobleaching on the intensity of monochromatic light used for the detrapping [5]. When the trapped electrons are produced by γ -irradiation of the organic glass, the matrix also contains trapped radicals which compete with the trapped cations for capture of detrapped electrons. The photoionization thresholds of the carbanions formed lie in the region of 600 nm (2 eV) [6]. When a γ -irradiated hydrocarbon glass is exposed alternately to infrared and ultraviolet light, electrons may be repeatedly converted from the trapped state to the carbanion state and back with 5 percent still remaining after 7 cycles [7]. The heat released by electrons on reaction with cations plus radicals in γ -irradiated glasses following photodetrapping has been measured by differential thermal analysis at 77 K [8]. It decreases with dose, consistent with an increasing ratio of radicals to cations (fig. 6). The extrapolated value at zero dose sets a limit on the heat of solvation of the cation in 3MP. Current work in our laboratory is using bleaching with monochromatic light to further resolve the contributions of varying trap depths to the broad e_t^- spectra.

Figures in brackets indicate literature references at the end of this paper.

References

- [1] This work has been supported in part by the U.S. Energy Research and Development Administration under Contract No. AT(11-1)-1715 and by the W. F. Vilas Trust of the University of Wisconsin.
- [2] For a review and references see Willard, J. E., J. Phys. Chem., 79, 2966 (1975).
- [3] Hager, S. L. and Willard, J. E., Chem. Phys. Lett., 24, 102 (1974).
- [4] Hager, S. L. and Willard, J. E., J. Chem. Phys. 61, 3244 (1974).
- [5] Dismukes, G. C., Hager, S. L., Morine, G. H., and Willard, J. E., J. Chem. Phys., 61, 426 (1974).
- [6] Dismukes, G. C., Ph.D. Thesis, University of Wisconsin-Madison, 1975.
- [7] Lin, D. P. and Willard, J. E., J. Phys. Chem., 78, 1135 (1974).
- [8] Hager, S. L. and Willard, J. E., J. Chem. Phys., 63, 942 (1975).

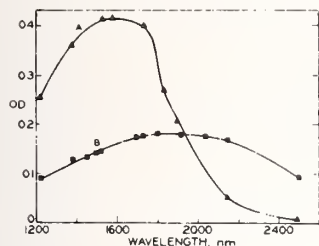


Fig. 1. Spectra of trapped electrons in MP-d₁₄ at 23 K: (A) electrons produced by photoionization of TMPD at 72 K and cooled to 23 K; (B) after partial photobleaching of A at 23 K with 700-1000 nm light.

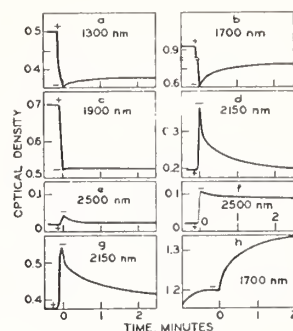


Fig. 2. Optical density changes resulting from illumination of trapped electron populations and of TMPD in 3MP glass. Onset of illumination indicated by (+) and termination by (-). Analyzing wavelength shown on each plot. (a-e), 700-1000 nm illumination at 72 °K of electrons generated in 3MP-d₁₄ by UV photoionization of TMPD at 27 °K. (f), same as (a-e) except illumination at 23 °K after TMPD ionization at 72 °K. (g), 700-1000 nm illumination of electrons generated by γ -irradiation, T = 72 °K. (h), optical density at 1700 nm during and after generation of trapped electrons by UV photoionization of TMPD in 3MP-d₁₄; (-) mark signifies end of 2 min. UV illumination.

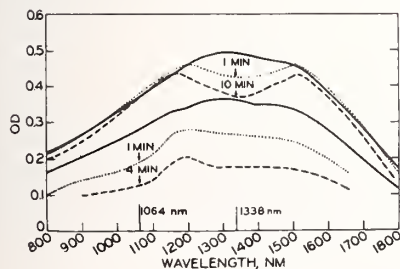


Fig. 3. Effect of bleaching with 1338 and 1064 nm light on the spectrum of e_t^- in MTHF. Solid lines, before bleaching. Upper three lines, 1338 nm experiment, e_t^- produced and bleached at 20 K. Lower three lines, 1064 nm experiment, 25 K. Intensities $\sim 30 \text{ mW cm}^{-2}$.

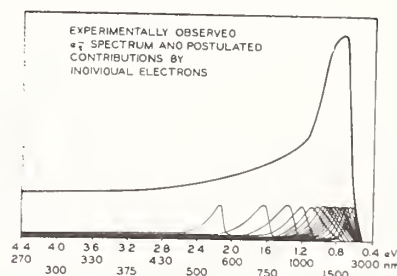


Fig. 4. Schematic representation of hypothetical spectra of individual electrons in different trap depths (lower lines), the summation of which gives the envelope (upper line) typical of the observed absorption by e_t^- in alkanes at 77 K.

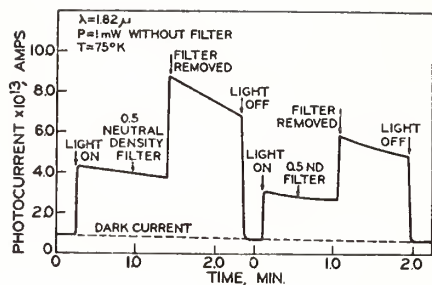


Fig. 5. Effect of intensity of 1820 nm laser light on photoconductivity of 3-methylhexane glass at 77 K. γ -Dose $2.6 \times 10^{19} \text{ eV g}^{-1}$; maximum light intensity of 1.0 mW cm^{-2} .

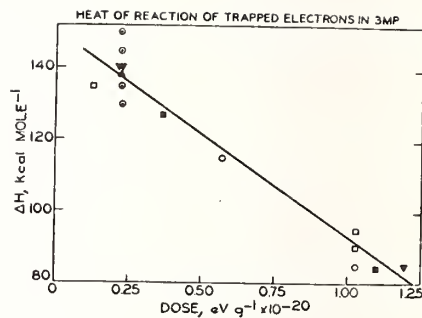


Fig. 6. Heat of reaction of photodetraped electrons in γ -irradiated 3MP as a function of γ -dose.

SPIN LABELS AND THE MECHANISM OF THE $S_1 \rightarrow T_1$ NONRADIATIVE PROCESS
IN DURALDEHYDE; POSSIBLE MANIFESTATION OF PSEUDO JAHN-TELLER
FORCES ON NONRADIATIVE PROCESSES

Alan Campion and M. A. El-Sayed

Department of Chemistry
University of California
Los Angeles, California 90024

Recently, the new technique of Zeeman PMDR [1-4]¹ has been successfully applied to the elucidation of the mechanism by which molecules initially excited to the lowest singlet state (S_1) intersystem cross (ISC) to the lowest triplet (T_1). The experiments use phosphorescence-microwave double resonance [5] (PMDR) techniques to monitor changes in the steady-state populations of the three magnetic sublevels of the T_1 state, as they are mixed by a weak (< 1 kG) external magnetic field. The results of the experiments to date have confirmed the importance of a selection rule [6] which predicts that ISC between states arising from different types of electronic promotion (e.g., $n, \pi^* \leftrightarrow \pi, \pi^*$) should be at least an order of magnitude more important than ISC between states of the same type of electronic promotion (e.g., $n, \pi^* \leftrightarrow n, \pi^*$ or $\pi, \pi^* \leftrightarrow \pi, \pi^*$). This has been convincingly demonstrated for the nitrogen heterocyclics where it was shown [3,4] that intermediate triplet states play an important role in the ISC process if they are of different orbital configuration than S_1 . In benzophenone, however, the mechanism is found [2] to involve the singlet and triplet n, π^* states. This was accounted for by a proposed efficient ISC between these states, in molecules where the carbonyl and aromatic moieties are not planar [7].

In order to examine the $n, \pi^* \leftrightarrow \pi, \pi^*$ selection rules in planar carbonyls, we have selected duraldehyde (2,4,5-trimethylbenzaldehyde). The lowest singlet state [8] is n, π^* , T_1 is $^3\pi, \pi^*$ and T_2 , which lies [9] ca. 400 cm^{-1} higher in energy than T_1 , is an n, π^* state. In addition, the principal axes of the zero-field tensor of the T_1 state have been found [10] for this molecule in a durene host single crystal and the dynamic parameters that characterize the T_1 state in this host at 1.5 K have been reported [11].

In the Zeeman-PMDR experiment, a weak, external magnetic field mixes the zero-field states to give

$$\tau_i^H = \sum_j C_{ij} \tau_j^0 \quad (1)$$

where the subscripts label principal axes of the zero-field tensor and the mixing coefficients C_{ij} depend upon the projection of the field on these axes as well as the zero-field energy splitting ΔE . The populating (K) and decay (k) rates in the field are then given by

$$K_i^H(k_i^H) = \sum_j |C_{ij}|^2 K_j^0(k_j^0) \quad (2)$$

the ISC is direct $S_1 \rightarrow T_1$. By calculating the field-dependent rates from this equation, we may predict both the magnitude and sign of the PMDR signal as a function of field in these low fields for a direct ISC process. Then, by comparison of the experimental results

Figures in brackets indicate literature references at the end of this paper.

with these calculations, it is possible to immediately determine whether the ISC is direct or not. If the experiments show that it is not direct, then K_1^H is modified to

$$K_i^H = \sum_{j,m} \left| \sum_k C_{ik}^* C_{jk}' \right|^2 \left| C_{jm}' \right|^2 K_m^0 \quad (3)$$

where the primed coefficients refer to the mixing in a second triplet state and the sum over k expresses the projection of the net spin polarization from the higher triplet to T_1 . The expression for K_1^H remains as that given in eq. (2). These equations, along with the experimental data, may be used to arrive at a model for the zero-field energies and populating rates of the higher triplet.

We have followed the change of the 9.0 and 11.4 GHz PMDR signals in duraldehyde with fields up to 1 kG directed along the duraldehyde \underline{a} or \underline{c}' crystal axes. With the field parallel to \underline{a} , there occurred a rapid diminution of the 9.0 GHz signal until the external field was ~ 400 G, where the signal changed from negative to positive. The calculations, based upon a direct mechanism, showed that the signal should remain negative while gradually decreasing as the field increases to 1 kG. Similar, though less dramatic, deviations from the calculated behavior occurred for both the $|D - E|$ and $|D + E|$ transitions with field along \underline{a} or \underline{c}' .

These four experiments have led us to conclude that the ISC in duraldehyde is not completely direct. By adopting a model for the second triplet state that is similar to the formaldehyde n, π^* triplet, we are able to fit all our observations by setting the $\tau_2 / T_2 / T_1$ relative ISC rates to 0.2. Thus, most of the ISC in duraldehyde appears to be direct, but a non-negligible fraction involves the T_2 state.

These observations may be interpreted to give a measure of the degree of vibronic mixing of pure n, π^* and π, π^* triplets. If we use a pure n, π^* state and pure π, π^* state as zero-order descriptions for T_2 and T_1 respectively, and assume zero probability for the ISC between T_2 and T_1 respectively, and assume zero probability for the ISC between the S_0, π^* and the zero order T_0, π^* states, then the Zeeman experiments yield the vibronic mixing coefficient directly; T_2 contains ca. 20 percent π, π^* character and vice versa. This number is quite reasonable, considering the close proximity ($\Delta E_{T_1-T_2} \approx 400 \text{ cm}^{-1}$) of the lowest two triplet states in this molecule.

The authors wish to acknowledge the financial support of the Energy Research and Development Administration. AC would like to acknowledge IBM for a predoctoral research fellowship. Computing time was made available by the UCLA Campus Computing Network, to whom we are grateful.

References

- [1] Leyerle, R. W., Ph.D. Dissertation, University of California, Los Angeles, CA, 1974.
- [2] El-Sayed, M. A. and Leyerle, R. W., J. Chem. Phys. 62, 1579 (1975).
- [3] Zinsli, P. E. and El-Sayed, M. A., Chem. Phys. Lett. 34, 304 (1975).
- [4] Zinsli, P. E. and El-Sayed, M. A., Chem. Phys. Lett. 36, 290 (1975).
- [5] El-Sayed, M. A., Ann. Rev. Phys. Chem. 26, 235 (1975).
- [6] El-Sayed, M. A., J. Chem. Phys. 38, 2834 (1963).
- [7] El-Sayed, M. A. and Zinsli, P., J. of Luminescence, in press.

- [8] Fischer, G., Mol. Cryst. and Liq. Cryst. 11, 85 (1970).
- [9] Migirdicyan, E., Chem. Phys. Lett. 12, 473 (1972).
- [10] Sharnoff, M., Mol. Cryst. 5, 297 (1969).
- [11] Cheng, T. H. and Hirota, N., Mol. Phys. 27, 281 (1974).

PHOTODESORPTION FROM METALS: MEASURED DESORPTION RATES IN COMPARISON WITH A MO-TREATMENT

N. Trappen

Inst. f. phys. Chemie, Universität
des Saarlandes, Saarbrücken

Carbon monoxide adsorbed on clean metal surfaces can be desorbed by irradiation with ultraviolet light [1]¹. Simultaneously, the formation of carbon dioxide has been observed. This can be explained by excitation of the adsorbed CO due to irradiation followed by desorption or dissociation with reaction to CO₂. The photo-reaction was measured by application of a quadrupole mass analyzer in an ultra high vacuum system, the metal surfaces being ultra pure MARZ-grade polycrystalline foils. The different metals were tantalum, tungsten, rhenium and molybdenum.

From the experiment follows, that the quantity of the desorbed material depends strongly both from the wavelength of the inserted light and from the nature of the used metal. The desorption rate decreases rapidly in the range between 200 to 300 nm being the most effective using tantalum as adsorbent and decreasing via tungsten and rhenium to molybdenum.

A quantum chemical treatment was executed in order to correlate calculated values with the experimental data. Starting the calculation of a statement of Tompkins [2] was used. Following these arguments the properties of adsorption complexes are influenced mainly by the atomic properties of the adsorbing material. Consequently, it should be possible to compare a system like Me-CO with the adsorption complexes within this experiment.

A modified closed-shell SCF-LCAO-MO program with configuration interaction according to Bloor and Gilson [3] was used to calculate bonding strengths and excitation energies of CO adsorbed on the different metals. Hereby the parameters for d-orbitals were taken according to Hartree-Fock calculations by Maly and Hussenot [4].

It can be shown, that the bonding strength of C=O in the Me-CO complex decreases from Mo over Rh and W to Ta. The excitation energy of the first electronic excited state decreases in the same way. The shape of the calculated values is consistent with the experimental results.

The dependency of the excitation energy from the kind of metal in the adsorption complex explains the corresponding energy acceptance of the CO molecule with either the possibility to desorb or to dissociate.

The decreasing bonding strength explains the higher probability of the dissociation of CO on the metal surface resulting in formation of CO₂.

So it seems to be possible to predict the behavior of CO on other metals with the aid of these calculations. The experimental part of this work was sponsored by the Deutsche Forschungsgemeinschaft.

References

- [1] Moesta, H. and Trappen, N., Naturw. 57, 38 (1970).

¹Figures in brackets indicate literature references at the end of this paper.

- Culver, R., Pritchard, J. and Tomphins, F. C., Zeitschr. f. Elektrochem. 63, 741 (1959).
- QCPE Program No. 71 by Bloor, J. E. and Gilson, B. R.
- Maly, J. and Hussenais, M., Theoret. Chim. Acta (Berl.) 31, 137 (1973).

MATRIX ISOLATION SPECTROSCOPIC STUDIES OF FREE RADICALS AND
MOLECULAR IONS PRODUCED BY COLLISIONS OF
MOLECULES WITH EXCITED ARGON ATOMS

Marilyn E. Jacox

National Bureau of Standards
Washington, DC 20234

In early 1974, a series of experiments was initiated in this laboratory in which the products of the interaction of simple molecules with the periphery of a microwave discharge excited in a beam of pure argon were rapidly frozen onto a substrate maintained at 14 °K, permitting the trapping of free radical and ion products in concentration sufficient for direct infrared and and ultraviolet spectroscopic detection. The discharge configuration used for these experiments is shown in Fig. 1, which illustrates the relative orientation

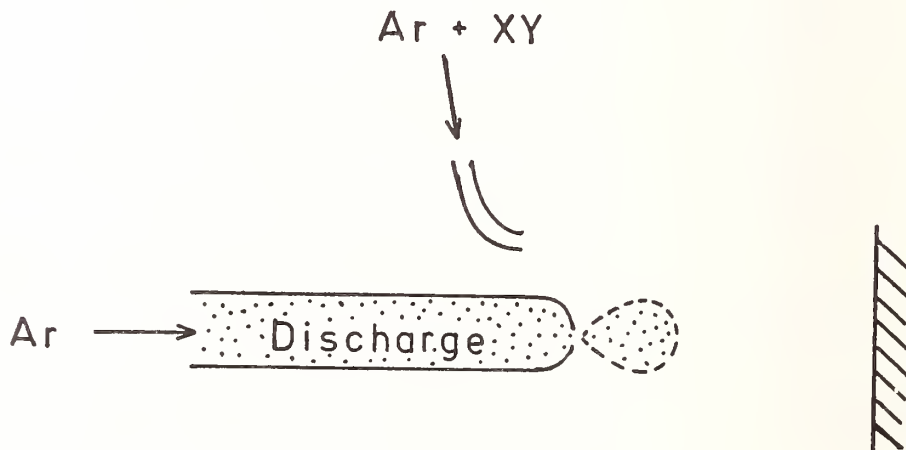


Figure 1

of the discharge tube, the sample inlet, and the cryogenically cooled surface inside the temperature cell. The discharge is adjusted so that it extrudes slightly beyond the pinhole in the Pyrex discharge tube. The molecule XY, mixed with at least a hundredfold excess of argon, can collide with excited argon atoms in the discharge region between the pinhole and the cooled surface, which are separated by approximately 3 cm. The pinhole, which has an area of 1 to 2 mm², retards backstreaming of molecules into the body of the discharge and filters most of the vacuum ultraviolet radiation produced in the discharge from the sample deposit.

In the first experiments using this discharge configuration [1]¹, the intensity of the 1848 cm⁻¹ infrared absorption of HC₂, produced by the interaction of C₂H₂ with the periphery of the discharge, compared favorably with that obtained in the best photolysis experiments utilizing 121.6 nm radiation [2]. The discharge study also led to the assignment of the C-H stretching fundamental of HC₂ at 3612 cm⁻¹, suggesting that the C-H bond of this species is unusually strong. In a study of the visible-ultraviolet spectrum of a similar sample, shown in Fig. 2, the Mulliken band of C₂, which appears in an argon matrix at 238 nm, was

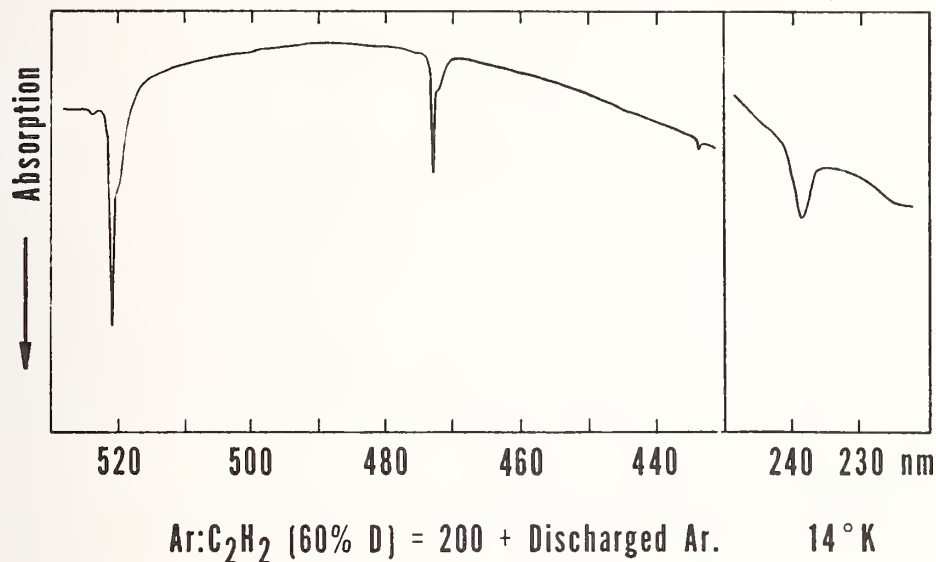


Figure 2

only moderately intense, whereas a prominent progression assigned to C₂⁻ [3] was observed between 521 and 430 nm. These results may be contrasted with those typical of 121.6 nm photolysis of matrix-isolated C₂H₂, in which the Mulliken band was extremely prominent and the C₂⁻ bands were somewhat less intense.

The emission spectrum of the discharge showed prominent lines between 470 and 415 nm, 11 of which are readily assigned to argon atom emissions between upper-state levels 14.4-14.6 eV above the ground state and lower-state levels 11.5-11.8 eV above the ground state. Two of these lower-state levels involve metastable argon atoms in the ³P₀ and ³P₂ states, recently reported [4] to have collisional lifetimes on the order of 1 sec. This observation suggested a series of studies of the interaction of HCCl₃ with the discharge; previous studies [5] had established that the principal primary product of the photodecomposition of matrix-isolated HCCl₃ by 121.6 nm radiation was CCl₃, whereas prominent HCCl₂⁺ absorptions and very little CCl₃ resulted when 106.7 nm (11.6 eV) photolyzing radiation was used. Typical spectra obtained for HCCl₃ and DCCl₃ samples are shown in Figs. 3 and 4, respectively. Although some CCl₃ and CCl₂ were present in the discharge experiments, the yields of HCCl₂⁺ and DCCl₂⁺, which have an appearance potential of 11.49 eV in gas-phase studies of the photoionization of chloroform [6], were several times as great as in the best 106.7 nm photolysis experiments. Only a small concentration of HCCl₂ or of DCCl₂ was observed. There was very little evidence for secondary decomposition products such as CCl, HCCl, or CCl₂. These experiments suggest that collisions of HCCl₃ with metastable argon atoms play an important role in the observed product formation, leading to direct production of the cation. The HCCl₂⁺ and DCCl₂⁺ anions, which provide the requisite overall charge neutrality of the matrix deposit, have been demonstrated to result from associative electron capture by chloroform. Studies of the photodecomposition of the ion

¹Figures in brackets indicate literature references at the end of this paper.

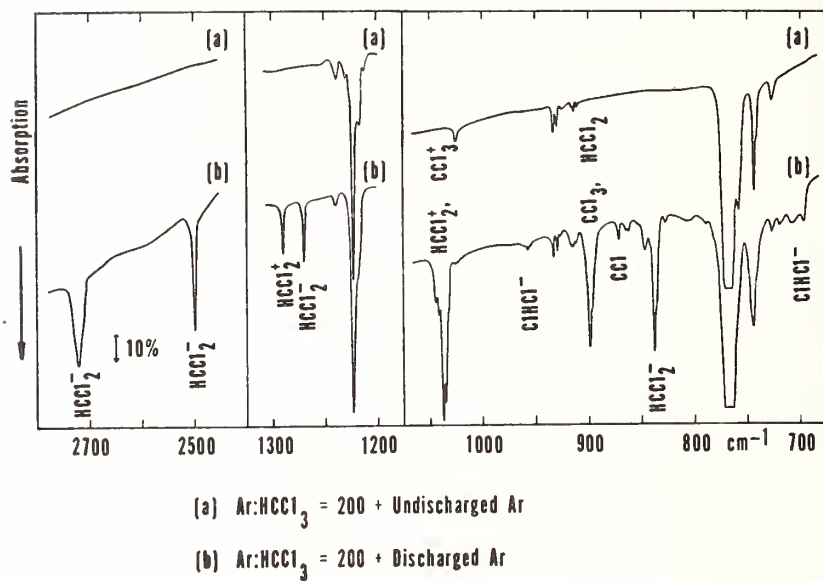


Figure 3

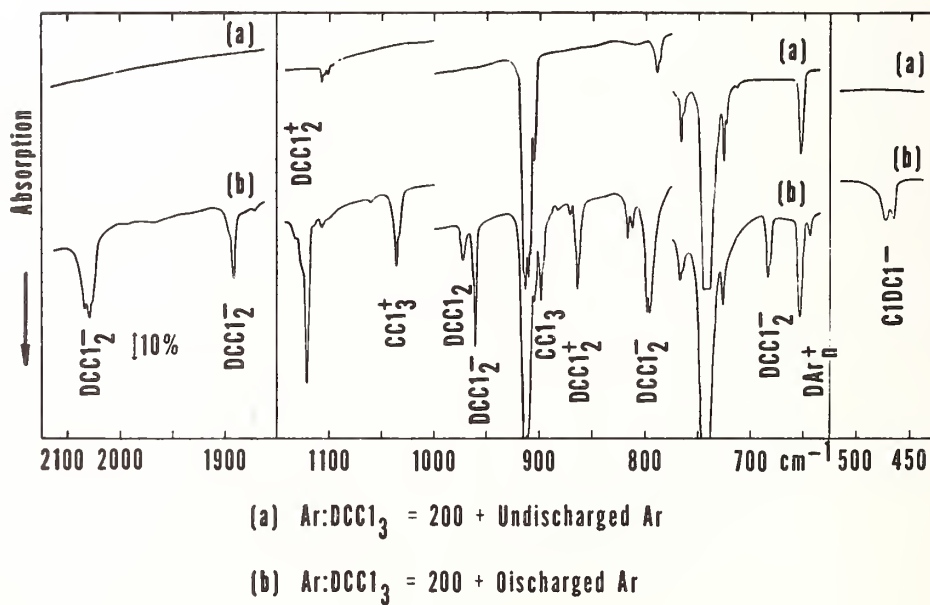


Figure 4

products upon subsequent filtered mercury-arc irradiation of the matrix deposit have yielded evidence for a photoinduced proton transfer from HCCl_2^+ to the argon lattice [7].

The corresponding discharge experiments on HCCl_2F have led to the stabilization of the Cl_2CF free radical and of the HCClF^- and $\text{Cl}_2\text{C}\cdots\text{HF}^-$ molecular anions in sufficient concentration for direct infrared observation. Several relatively weak absorptions may be contributed by a hydrogen-containing cation. Although a value of 12.4 ± 0.2 eV has been reported for the ionization potential of HCCl_2F [8], Sieck [9] has detected a weak ion signal due to HCCl_2F^+ on exposure of gas-phase HCCl_2F to 11.6 and 11.8 eV argon resonance radiation.

Although the reported ionization potential of HCClF_2 , 12.59 ± 0.15 eV [8], is somewhat higher than that of HCCl_2F and although no ion signal was detected in the gas-phase study using argon resonance radiation [9], very prominent anion absorptions, assigned to HCF_2^- and to $(\text{ClCF})\cdots\text{HF}^-$, were observed in the discharge experiments on HCClF_2 , with little evidence for infrared absorptions attributable to the cations which must be present to preserve overall charge neutrality of the sample. Processes which may account for ion production in this system include chemiionization on collision of argon atoms excited above the first Rydberg state with HCClF_2 and charge transfer between electronically excited argon atoms and HCClF_2 , resulting in the formation of molecular anions and Ar^+ , which in turn may form cluster ions in the argon matrix. The yield of ion products may be enhanced above that possible for gas-phase collision processes alone by energy transfer between excited argon atoms and the surface of the matrix; the diffusion length for the "free" $n = 1$ exciton state in solid argon has been estimated [10] to be on the order of 100 Å.

Discharge experiments on CCl_4 , CFCl_3 , CF_2Cl_2 , and CF_3Cl have also yielded evidence for the stabilization of ionic species in the matrix. Of especial interest are the studies on CF_3Cl , recently found to have an ionization potential of 12.5 eV [11]. No ions were detected in gas-phase observations using argon resonance radiation [9]. Processes similar to those postulated for the discharge experiments on HCClF_2 may account for the observed ion production in the CF_3Cl studies.

References

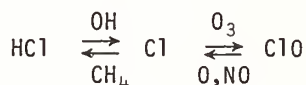
- 1] Jacox, M. E., Chem. Phys., 7, 424 (1975).
- 2] Milligan, D. E., Jacox, M. E. and Abouaf-Marguin, L., J. Chem. Phys., 46, 4562 (1967).
- 3] Milligan, D. E. and Jacox, M. E., J. Chem. Phys., 51, 1952 (1969).
- 4] Van Dyke, R. S. Jr., Johnson, C. E. and Shugart, H. A., Phys. Rev., A5, 991 (1972).
- 5] Jacox, M. E. and Milligan, D. E., J. Chem. Phys., 54, 3935 (1971).
- 6] Werner, A. S., Tsai, B. P. and Baer, T. J., Chem. Phys., 60, 3650 (1974).
- 7] Jacox, M. E., Chem. Phys., 12, 51 (1976).
- 8] Hobrock, D. L. and Kiser, R. W., J. Phys. Chem., 68, 575 (1964).
- 9] Sieck, L. W., private communication.
- 10] Ophir, Z., Schwentner, N., Raz, B., Skibowski, M. and Jortner, J., J. Chem. Phys., 63, 1072 (1975).
- 11] Ajello, J. M., Huntress, W. T. and Rayermann, P., private communication.

ATMOSPHERIC CHEMISTRY OF CHLOROFLUOROCARBONS

Mario J. Molina

Department of Chemistry
University of California
Irvine, California 92717

The chlorofluorocarbon-ozone depletion theory has been the subject of close examination by several research groups. Many facets of the fluorocarbon problem are currently under investigation; we are concerned here with its chemical and photochemical aspects. The theory assumes a lack of reactivity for the chlorofluorocarbons in the lower atmosphere, and an appreciable reactivity in the upper stratosphere for their photodecomposition products, which include chlorine atoms. This chemical reactivity--described in detail elsewhere [1]¹--consists mainly of the following reactions:



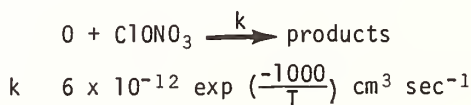
The various assumptions on tropospheric and stratospheric chemistry may be tested by two different procedures. First, additional chemical and photochemical reactions can be studied in the laboratory and evaluated for their possible significance. Second, measurements of atmospheric concentrations of the various species may be compared to the values predicted by theory.

We have recently carried out some laboratory studies on the species ClONO_2 (chlorine nitrate) [2]. Our current results indicate that an appreciable fraction of the chlorine atoms in the mid-stratosphere may be present as ClONO_2 .

The formation of this compound involves the following three-body process:



The rate of this reaction has now been measured in the laboratory by at least three research groups; the reaction is about 15 times slower than the similar reaction between NO_2 and OH radicals. In the stratosphere, chlorine nitrate will be destroyed mainly by photolysis. We have measured the optical absorption cross sections in the UV of purified samples of gaseous ClONO_2 [2]. These cross sections, when combined with values of solar intensities, provide estimates for the photodissociation rates at various altitudes: the photochemical lifetime is about 3 hours at 30 km and about 1 hour at 40 km (for overhead sun). We have also studied the reaction between ground state oxygen atoms and chlorine nitrate [3]:



¹ Figures in brackets indicate literature references at the end of this paper.

This rate constant value is small enough to make this reaction unimportant compared to photolysis in the stratosphere.

The possible importance of ClONO_2 for stratospheric chemistry can be assessed by calculating the distribution of chlorine among the species ClONO_2 , HCl , ClO , and Cl , that is, by considering the formation and destruction of ClONO_2 in addition to the reactions discussed earlier [1]. The amount of ClONO_2 present at mid-stratospheric altitudes might be large enough for actual in situ detection to be feasible, perhaps by infrared spectroscopy. Furthermore, due to the nature of the photodissociation process, diurnal variability in ClONO_2 concentrations is to be expected.

However, due to the relatively large photodissociation rates, our calculations--which incorporate this diurnal effect--indicate that the amount of ClONO_2 should be smaller than the amount of HCl at all altitudes, and the ozone depletion predictions are diminished only by about 30 percent as compared to earlier calculations.

As mentioned above, another aspect of the theory--namely, the stability of chlorofluorocarbons in the lower atmosphere--can also be tested by two separate procedures. First, we can evaluate the various proposed mechanisms or "sinks" which lead to chlorofluorocarbon removal (e.g., reaction with ions, dissolution in the ocean, trapping in Antarctic snow, etc.). To date, no such specific sinks have been found to be of importance when compared to stratospheric photolysis. Second, the amount of chlorofluoromethanes now found in the atmosphere can be compared with the cumulative amount already manufactured and released to the environment, taking into account that some stratospheric photolysis has already occurred. We have conducted a careful evaluation of this comparison for CCl_3F (fluorocarbon 11) [4]. We conclude that a tropospheric residence time of less than 30 years is not compatible with experimental observations. The results are certainly consistent with the assumption that stratospheric photolysis is the only sink, but the existence of an additional tropospheric sink of similar magnitude cannot be ruled out on the basis of these comparisons.

One of the largest uncertainties in this evaluation results from difficulties in the absolute calibration of the analytic instrument used to measure CCl_3F levels in ambient air. We have carried out absolute calibrations in our laboratories by successive expansions and dilutions of a known initial amount of CCl_3F . Our results are in good agreement with those of several other research groups employing similar methods.

References

- [1] Rowland, F. S. and Molina, M. J., *Rev. Geophys. Space Phys.*, **13**, 1 (1975).
- [2] Rowland, F. S., Spencer, J. E. and Molina, M. J., *The Stratospheric Formation and Photolysis of Chlorine Nitrate, ClONO_2* , (to be published).
- [3] Molina, L. T., Spencer, J. E. and Molina, M. J., *Rate Constant for the Reaction $\text{O} + \text{ClNO}_3$* , (to be published).
- [4] Rowland, F. S. and Molina, M. J., *An Experimental Estimate of the Importance of Tropospheric Sinks for CCl_3F (Fluorocarbon-11)*, to be published in *J. Chem. Phys.*

ULTRAVIOLET PHOTOABSORPTION CROSS-SECTIONS OF CF_2Cl_2
AND CFCl_3 AS A FUNCTION OF TEMPERATURE

Arnold M. Bass and Albert E. Ledford, Jr.

National Bureau of Standards
Washington, DC 20234

Because of recent interest [1a,b]¹ in the effect of commonly used halocarbons upon the stability of the earth's stratospheric ozone layer, we have undertaken a remeasurement of the photoabsorption cross-sections of fluorocarbons 11 and 12 (CFCl_3 and CF_2Cl_2). Although some measurements of this absorption have been reported previously [1b,2a,b], the recent report of a temperature dependence of the absorption [3] motivated us to measure this property of these substances in greater detail.

Measurements were made over the wavelength region 185-230 nm, the wavelength region over which photodissociation occurs in the stratosphere. In order to determine the effect of the reported temperature dependence upon the estimated dissociation rates of these substances in the stratosphere, absorption measurements were made at two temperatures, 296 K and 223 K.

The measurements were made with a 0.75 m Fastie-Ebert monochromator equipped with a 2400 groove mm grating. Absorption measurements were made at intervals of 0.2 nm with a spectral resolution of 0.05 nm. The absorption cell in which the gas samples were placed was made of stainless steel. It was 50 cm long, and by using the multiple pass design of White [4] and Bernstein and Herzberg [5] path lengths up to a maximum of 10 meters could be used. Temperature control of the gas sample was obtained by circulation of a refrigerated fluid, usually methanol, through the outer jacket of the cell. The gas temperature was measured by means of calibrated chromel-constantan thermocouples inside the cell. At a cell temperature of 220 K the temperature variation of the sample over the length of the cell was approximately 1 °C.

The absorption cell was placed in the exit beam of the monochromator. Immediately in front of the cell a sapphire plate was used to split the light beam and a portion of the signal illuminated a photomultiplier tube and served to monitor the variation of the light source. A broad band interference filter which passed radiation of wavelength between 175 and 250 nm was inserted between the hydrogen continuum source and the entrance slit. This filter effectively removed all radiation outside of this range, and eliminated all scattered radiation. Data acquisition was automated by photon counting in conjunction with a stepping motor control for the monochromator wavelength drive, as described previously [6].

Dichlorodifluoromethane (CF_2Cl_2) was purified by trapping with liquid nitrogen the exit stream from a gas chromatograph equipped with a squalane column and a thermal conductivity detector. The major impurity, which was CF_2ClH , could be removed entirely by this method. After purification the CF_2Cl_2 was better than 99.99 mole percent pure with respect to detectable organic impurities. The fluorotrichloromethane (CFCl_3) was better than 99.99 mole percent pure with respect to detectable organic impurities, as received. Both components were used after low-temperature degassing.

¹Figures in brackets indicate literature references at the end of this paper.

The results of these measurements are shown in Figure 1, and in Table I (a complete table of measured cross-section is available upon request). The measurements at room temperature are essentially in agreement with those reported by Rowland and Molina [1b], but are approximately 15-20 percent lower than the values reported by Huebner, et al. [2b]. The only measurements reported at low temperature are those by Rebbert and Ausloos [3] at the wavelength of the zinc resonance line, 213.9 nm. The temperature effect on the absorption cross-section that we have observed between 296 K and 223 K is not as large as they reported, being approximately a factor of two reduction for CF₂Cl₂, but only 30 percent in the case of CFC1₃.

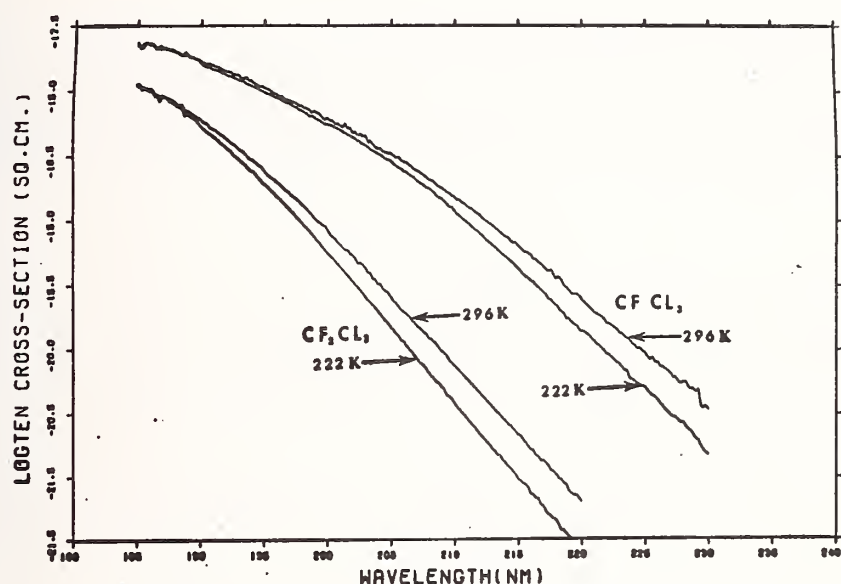


Figure 1

Table I. Absorption Cross-Sections for CF₂Cl₂ and CFC1₃

Wavelength/nm	Cross-Section x 10 ⁺²⁰ cm ² molec ⁻¹			
	CF ₂ Cl ₂		CFC1 ₃	
	296 K	223 K	296 K	223 K
230.0	--	--	0.34	0.15
225.0	--	--	0.94	0.51
220.0	0.063	0.026	2.45	1.38
215.0	0.22	0.095	6.48	4.26
210.0	0.74	0.38	15.3	12.1
205.0	2.60	1.50	33.4	29.3
200.0	8.56	5.70	62.6	55.6
195.0	25.2	19.5	106.2	98.4
190.0	61.3	55.0	169.9	163.9
185.0	110.7	111.9	221.9	236.7

$$\text{Cross-section } (\sigma) = \frac{1}{n_o \ell} \cdot \frac{I}{P} \cdot \frac{760}{273} \cdot \ell n \frac{I_o}{I}$$

Photodissociation rate constants for CFCl_3 and CF_2Cl_2 have been calculated for two altitudes using the absorption coefficients applicable at 296 K and 222 K. These are summarized in Table II. The ratio of the two rates for each condition (same altitude and zenith angle) provides a measure of the systematic error that can be introduced into a model by ignoring the change in absorption coefficient with temperature. For CFCl_3 the error is about 15 percent and for CF_2Cl_2 it is about 25 percent. These systematic errors probably are maximum estimates because, when the lower temperature absorption cross sections are used, higher concentrations will be estimated for higher altitudes where the photodissociation rate constant is greater.

The calculations were made using the absorption cross sections averaged over one nanometer wavelength intervals and direct solar fluxes applicable at 30 and 35 km. Photoabsorption rate constants were calculated for each one nanometer interval from 185 to 230 nm and summed to give the results in Table X. We are indebted to Dr. John DeLuise, Environmental Research Laboratories, NOAA, Boulder Colorado for the solar flux tables used. These are for a moderately active sun [7], compositions from the U.S. Standard atmosphere for mid latitude [8], and an average mid latitude ozone model [9]. Absorption by both oxygen [10] and ozone [11] are included.

REFERENCES

- [1] a) M. J. Molina and F. S. Rowland, *Nature* 249, 810 (1974).
 b) F. S. Rowland and M. J. Molina, *Rev. Geophys. Space Phys.* 13, 1 (1975).
- [2] a) J. Doucet, P. Sauvageau, and C. Sandorfy, *J. Chem. Phys.* 58, 3708 (1973).
 b) R. H. Huebner, D. L. Bushnell, Jr., R. H. Celotta, S. R. Mielczarek, and C. E. Kuyatt, *Nature* 257, 376 (1975).
- [3] R. E. Rebertus and P. J. Ausloos, *J. Photochem.* 4, 419 (1975).
- [4] J. U. White, *J. Opt. Soc. Am.* 32, 285 (1942).
- [5] H. J. Bernstein and G. Herzberg, *J. Chem. Phys.* 16, 30 (1948).
- [6] A. M. Bass and A. H. Laufer, *J. Photochem.* 2, 465 (1974).
- [7] Donnelly and Pope, NOAA-TR-ERL 276-SEL 25.
- [8] U.S. Committee on Extension to the Standard Atmosphere, U.S. Standard Atmosphere Supplements, 1966 (Government Printing Office, Washington, D.C. 1967).
- [9] Krueger, NASA-TR-X-912-74-291.
- [10] Craig, R. et al. in "The Natural Stratosphere of 1974", Reiter, E., (ed.) (Climatic Impact Assessment Program Monograph 1, DOT-TST-75-51 (1975)). Chapter 4, Table 4.2 which quotes from the following source: Ackerman, M. in "Mesospheric Models and Related Experiments," Fiocco, G., (ed.), (D. Reidel Publishing Co., Dordrecht, Netherlands (1971)), pp. 149-159.
- [11] Ackerman, M., Loc. Cit. Vigroux, E., *Ann. Phys.* 8, 709-62 (1953).

PHOTODISSOCIATION OF CCl_4

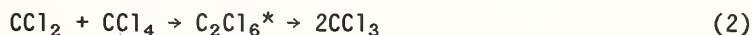
R. E. Rebbert and P. Ausloos

National Bureau of Standards
Washington, DC 20234

In several recent investigations [1-3]¹ of the photolysis of CCl_4 it was suggested that the elimination of a chlorine molecule from an excited state of CCl_4 may occur under certain conditions.



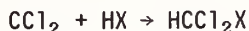
The CCl_2 formed in this process was thought [2,3] to insert readily into CCl_4 to form two CCl_3 radicals



In order to assess the importance of process 1 relative to that of the Cl-atom producing fragmentation steps



CCl_4 was photolyzed at 300 °K in the presence of various selective reagent gases such as Br_2 , HBr , HCl , C_2H_6 and O_2 . Ethane served mainly as an efficient Cl-atom interceptor, while HCl and HBr were found to scavenge CCl_2 species via the insertion reaction



(where $\text{X} = \text{Cl}$ or Br). No evidence could be found for the insertion of reaction 2. In the photolysis of CCl_4 - C_2H_6 mixtures, CCl_2 radicals react by the recombination reaction $\text{CCl}_2 + \text{CH}_3\text{CH}_2 \rightarrow \text{CH}_3\text{CH}_2\text{CCl}_2^* \rightarrow \text{CH}_3 + \text{CH}_2\text{CCl}_2$. A detailed analysis of the experimental findings leads to the following quantum yields

¹Figures in brackets indicate literature references at the end of this paper.

Table I

Quantum Yields of Primary Radicals Formed in the Photolysis of
CCl₄ and 213.9 and 163.3 nm

	<u>213.9 nm</u>	<u>143.3 nm</u>
$\phi(\text{Cl})$	0.9 \pm 0.15	1.9 \pm 0.2
$\phi(\text{CCl}_3)$	0.9 \pm 0.15	0.2 \pm 0.05
$\phi(\text{CCl}_2)$	<0.05	0.8 \pm 0.1

The primary fragmentation processes 3 and 4 can account for these derived quantum yields.

In contrast with a previous report [3], no evidence could be found for the occurrence of process 1 at 213.9 nm independent of pressure.

References

- [1] Currie, J., Sidebottom, H., and Tedder, J., Int. J. Chem. Kin. 6, 481 (1974).
- [2] Davis, D. D., Schmidt, J. F., Neeley, C. M., and Hanrahan, R. J., J. Phys. Chem. 79, 11 (1975).
- [3] Jayanty, R. K. M., Simonaitis, R., and Heicklen, J., J. Photochem. 4, 203 (1975).

THE PHOTOLYSIS OF ClO_2

S. Jaffe

California State College
Los Angeles, California

and

W. B. DeMore

Jet Propulsion Laboratory
Pasadena, California

1. Introduction

In a previous study of the photolysis of $\text{Cl}_2 - \text{O}_3$ mixtures, (C. L. Lin, S. Jaffe, and W. B. DeMore, presented at Philadelphia ACS meeting, 1975), a mechanism was proposed to account for catalytic destruction of O_3 which involved the reaction

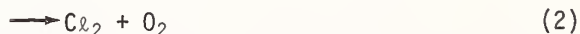
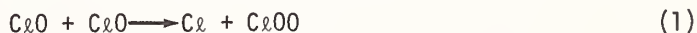
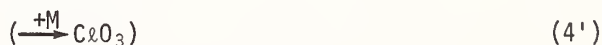
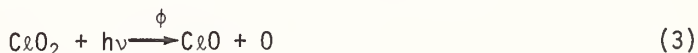


According to this mechanism, the quantum yields of O_3 destruction depended mainly on the rate of reaction (1) relative to the competing process,



However, the observed quantum yields at room temperature and 1 atm pressure required a ratio k_1/k_2 of approximately unity, this being in disagreement with previous work which indicated that reaction (2) is the dominant path at pressures higher than about 75 torr. (For a review of earlier work, see R. T. Watson, "Rate Constants of ClO_x of Atmospheric Interest," NBSIR 74-516, June, 1974.)

It was therefore considered desirable to obtain independent evidence on the question of Cl atom regeneration in the ClO disproportionation at high pressures. For this purpose the photolysis of ClO_2 was chosen, because the quantum yields of ClO_2 destruction should be dependent on the ratio k_1/k_2 , as can be seen from the following mechanism:



Thus, for $k_2 \gg k_1$, and assuming $\phi = 1$, the maximum quantum yield for ClO_2 photolysis would be two. However, for $k_2 \sim k_1$ as suggested by the $\text{Cl}_2 - \text{O}_3$ experiments, very high quantum yields would result because each Cl atom produced can lead to the formation of two ClO radicals by reaction (6). It was therefore considered that quantum yield measurements in the ClO_2 photolysis would be a good test for the occurrence of reaction (1) at high pressures.

The photolysis was studied as a function of several variables, including pressure, temperature, and surface.

2. Experimental Methods

Most of the photolyses were carried out at wavelengths near the maximum ClO_2 absorption (3515Å), using light from an Oriel medium pressure Hg lamp which was passed through a Bausch and Lomb monochromator (Cat. No. 33-86-45). Light intensities were measured by means of an Epply gauge, and the fraction of light absorbed was measured by comparison of Epply readings with the empty cell and the filled cell. Concentrations of ClO_2 were determined by means of a Cary spectrophotometer, using molar absorption coefficient (decadic) of $3000 \text{ M}^{-1}\text{cm}^{-1}$ at 3515Å. The experiments were carried out for the most part in standard cylindrical quartz cells.

3. Results

A. Quantum Yields

The apparent quantum yields were quite high, 30 being a typical value. As discussed in following sections, the exact quantum yields vary considerably and are dependent on a number of experimental variables, including the surface.

B. Effect of Pressure

As shown in Figure 1, pressurization with N_2 or O_2 decreased the rate of photolysis. Initial rates were faster in the presence of O_2 than in the presence of N_2 . However, in experiments with high light intensity the rate with added N_2 increased as the photolysis proceeded, ultimately exceeding the rate with added O_2 . No acceleration of rate was observed with added O_2 .

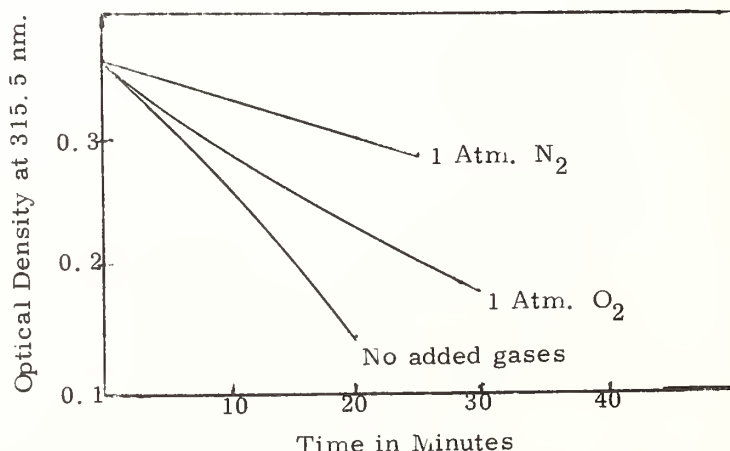


Figure 1. Relative Rates of ClO_2 Decomposition.

C. Effect of Surface

The effect of increased surface area was tested by addition of 0.002 inch diameter Superbrite glass beads to the bottom of the photolysis cells. Figure 2 shows how the photolytic decomposition rate varied with added surface, with and without added N_2 . It can be seen that the presence of added surface slowed the reaction considerably. This result is consistent with removal of chain carriers at the surface.

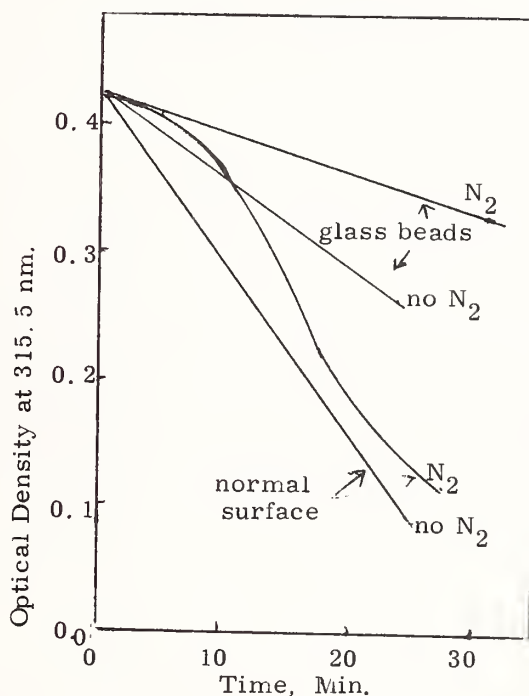


Figure 2. Effect of Surface.

D. Effect of Temperature

The photolysis rate increased by more than an order of magnitude when the temperature was increased from 25 °C to 45 °C.

4. Discussion

The major conclusions of this work are as follows:

1. The quantum yields of CxO_2 photolysis at 1 atm total pressure are high, consistent with $k_1 \sim k_2$.
2. Surface effects are important in determining the actual value of the quantum yield. It can be shown that this is not unexpected.
3. The rate of photolysis decreases upon pressurization with N_2 or O_2 . This may be due to slight enhancement of reaction (2) relative to (1) by added third body.
4. Increasing temperature increases the quantum yield, consistent with the suggestion that reaction (1) is enhanced at higher temperature.
5. The relative effects of added O_2 and N_2 are complex. However, there is some evidence that O_2 inhibits reaction (1) relative to (2), based on the observation that acceleration of the photolysis rate was observed with added N_2 but not O_2 . It is not known why the initial rate was always faster with O_2 compared to N_2 , although surface effects may be involved.

STRATOSPHERIC REACTIONS OF CHLOROFLUOROMETHANES

R. J. Donovan and H. M. Gillespie

Department of Chemistry
University of Edinburgh

and

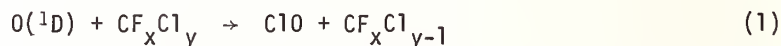
J. Wolfrum and K. Kaufmann

Max-Planck-Institut für
Strömungsforschung, 34 Göttingen

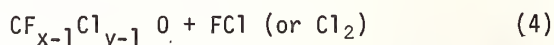
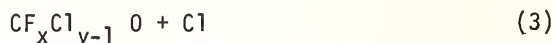
1. Introduction

Upper atmosphere reactions involving chlorofluoromethanes (freons) are of considerable current interest [1-5]¹. It has been suggested that the diffusion of freons, from the troposphere into the stratosphere, where photochemical and reaction processes produce free chlorine atoms, could lead eventually to a depletion of ozone in the upper atmosphere [1,2], via the ClO_x cycle [2,3].

The reaction of O(²D₂) with freons 11-13 (CFCl₃, CF₂Cl₂ and CF₃Cl) is known to give rise to ClO radicals [5],



and thus provides a means of direct entry into the ClO_x cycle. However, a number of other channels may contribute to the overall rate of removal^x of O(¹D), viz:



Little is known about the importance of these other channels, or of the subsequent radical reactions which can in some cases give rise to further release of Cl atoms.

The work to be presented was directed towards obtaining a more detailed understanding of the primary and secondary processes which take place in the photochemically initiated reaction between O(¹D) and the chlorofluoromethanes.

2. Experimental

Two experimental techniques were employed: firstly, nozzle-beam mass spectrometric sampling from a fast flow system, coupled with flash photolysis (see fig. 1) and secondly, time resolved optical spectroscopy [5]. O(¹D) atoms were produced by photolysis of O₃ in

¹ Figures in brackets indicate literature references at the end of this paper.

the Hartley Continuum (200-300 nm) and by photolysis of N_2O ($\lambda < 200$ nm). In the fast flow system, reagents were mixed just prior to entry into the flow tube (flow rates of typically 10 m s^{-1} , with total pressures in the range $300\text{--}400 \text{ N m}^{-2}$ and O_3 :halocarbon:He = 1:10:40, were used). Products of the primary and secondary radical reactions were monitored as a function of time with the mass spectrometer (Extranuclear quadrupole) set to sample a pre-selected mass number. The analogue output from the mass spectrometer was then digitized and stored in a 200 channel signal averager (Datalab, DL102A); in most cases it was necessary to average the results of sixteen experiments before adequate signal/noise ratios were observed. Little electronic interference from the flash was observed, however some variation in the interference with mass number was found and was thus checked for all experimental runs. The experimental conditions used for the time resolved optical studies were similar to those given in reference [5].

3. Nozzle-Beam Mass Spectrometric Sampling Results

Formation of ClO was observed ($m/e=51$) following the photolysis of O_3 in the presence of freons 11-13 and CCl_4 , supporting previous observations using ultraviolet absorption spectroscopy [5]. No signal at $m/e=51$ was observed when O_3 was excluded from the flow mixtures under otherwise identical conditions. The yield of ClO was found to increase with increasing partial pressure of O_3 (over the accessible range, $5\text{--}13 \text{ N m}^{-2}$), as expected from the increase in $O(^1D)$ production.

Other products observed immediately following photolysis of mixtures containing O_3 , were FCl, CFCIO (both from $CFCl_3$) and CF_2O from CF_2Cl_2 . Small yields of CCl_2 and CFCI were also observed from direct photolysis of $CFCl_3$ and CF_2Cl_2 , respectively. As these transient species have the same charge/mass ratio as CFCIO and CF_2O , a small correction to yields of the latter species was made.

The formation of FCl provides direct evidence for the primary process,

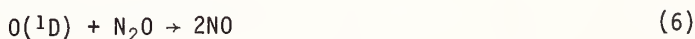


(atomic recombination processes would be too slow to account for our observations on FCl).

4. Optical Spectroscopy Results

Previous work on reaction (1) has been extended using N_2O as the source of $O(^1D)$. It was shown that the reaction of chlorine atoms with N_2O , to yield ClO, is negligibly slow under the conditions employed and thus any Cl atoms formed in reaction (3) do not contribute to ClO formation, (i.e., the ClO observed in the N_2O + freon system must result entirely from reaction (1)).

In the absence of added freons photolysis of N_2O leads to the formation of NO via the reaction,



which provides a convenient means of establishing the initial concentration of $O(^1D)$ produced by photolysis. The absolute concentration of ClO produced when $O(^1D)$ reacts with a freon can then be measured as the extinction coefficient of ClO in the ultraviolet is known [5]. A small correction to the observed ClO concentration is necessary due to removal via



By this method the branching ratio into channel (1) was determined as $k_1 \geq 0.4(k_1 + k_2 + k_3 + k_4)$.

Secondary reactions involving $\text{CF}_x\text{Cl}_{y-1}$ radicals and related studies involving bromomethanes will also be discussed.

References

- [1] Molina, M. J. and Rowland, F. S., *Nature*, 249, 810 (1974).
- [2] Rowland, F. S. and Molina, M. J., *Rev. Geophys. Space Phys.*, 13, 1 (1975).
- [3] Stolarski, R. S. and Cicerone, R. J., *Can. J. Chem.*, 52, 1610 (1974).
- [4] Pitts, J. N., Sandoval, H. L. and Atkinson, R., *Chem. Phys. Lett.*, 29, 31 (1974).
- [5] Gillespie, H. M. and Donovan, R. J., *Chem. Phys. Lett.*, 37, 468 (1976).

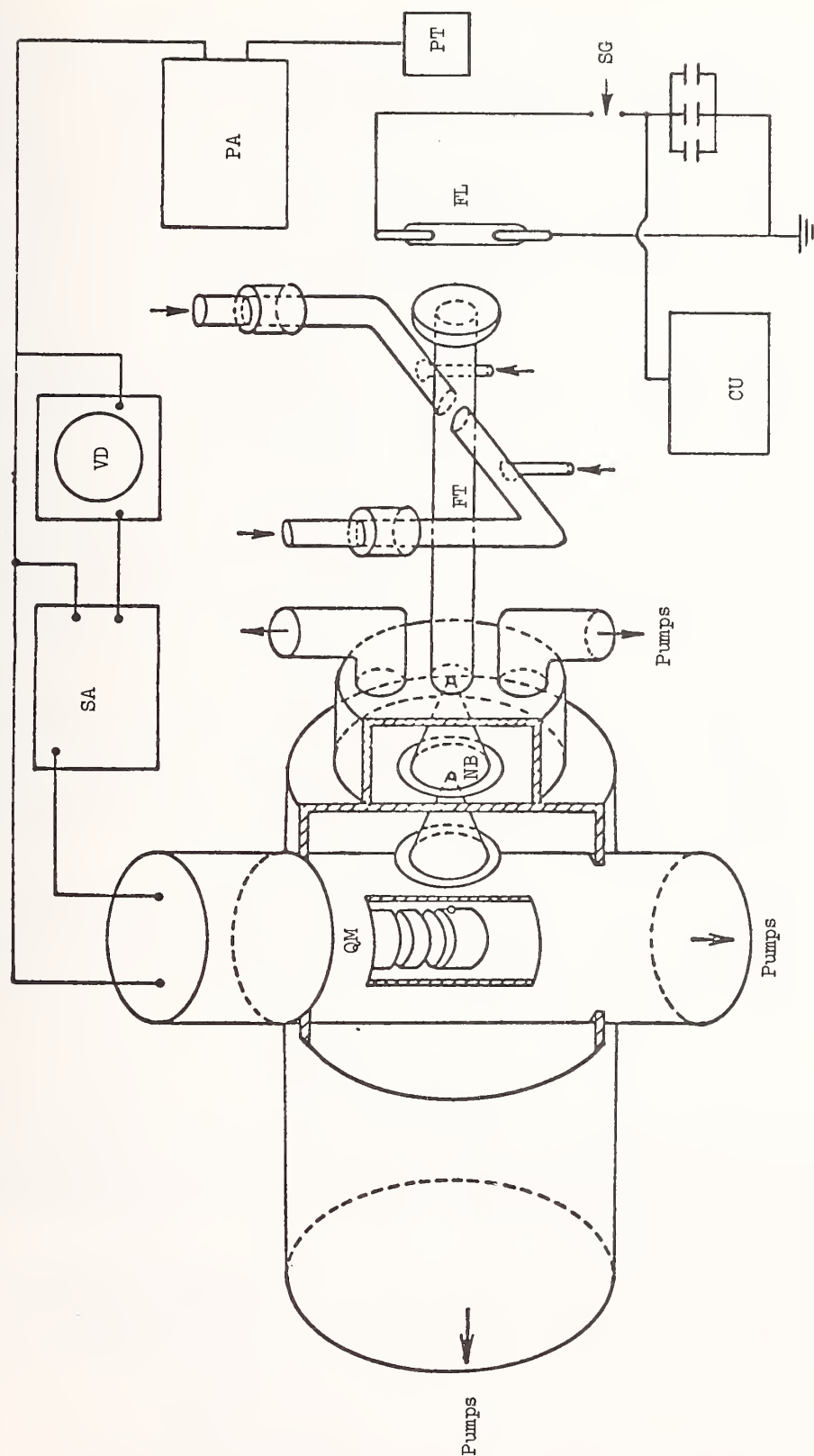


Fig. 1. Schematic representation of the flow tube, flash unit and nozzle-beam mass spectrometric sampling system; NB, nozzle-beam sampling system; QM, quadrupole mass spectrometer; FL, flash lamp; FT, flash unit; SG, spark gap; PT, photo-trippler; PA, pulse averager; VD, visual display; SA, signal amplifier.

SOME FUNDAMENTAL AND APPLIED ASPECTS OF THE ATMOSPHERIC REACTIVITY OF ORGANIC MOLECULES

James N. Pitts, Jr., Roger Atkinson, Arthur M. Winer, Karen R. Darnall
Alan C. Lloyd and Robert A. Perry

Statewide Air Pollution Research Center
University of California
Riverside, CA 92502

In the last several years, there has been a gratifying increase in the use of fundamental photochemical and kinetic information to obtain a better understanding of atmospheric chemistry; this has tended to break down somewhat arbitrary distinctions between "basic" and "applied" research. Thus, for example, it is now widely recognized that the hydroxyl radical is the major chain carrier in the chemistry of both the natural and polluted troposphere and stratosphere [1]¹.

A second example involves the current national debate over the degree of control of photochemically reactive emissions from a variety of industrial and domestic sources. The significance of this issue has grown with the improvement in the efficiency of control of emissions from motor vehicles which, of course, increases the relative importance of stationary source emissions.

An important approach to this problem, developed over the last decade, has been the utilization of photochemical hydrocarbon reactivity scales as the basis for controlling the formulations of commercial solvents. Such phenomena as rates of NO to NO₂ conversion, maximum levels, or loss of hydrocarbon have been employed to date to generate such reactivity scales. The vast majority of such data have been obtained by irradiation of NO_x-HC-air mixtures in smog chambers of a variety of types. However, this use of secondary smog manifestations, while of great utility, nevertheless has led to some significant inconsistencies when comparisons of various reactivity scales are made.

In this presentation, data will be given for OH radical rate constants determined in our laboratories, together with their use in the development and interpretation of such hydrocarbon reactivity scales. Also, mention will be made of recent experiments concerning the effects of UV spectral distribution on the rates of product formation in smog chamber experiments with simulated polluted atmospheres.

1. OH RADICALS REACTION RATES

Rate constants for the reaction of OH radicals with a variety of organic molecules have been determined in our laboratory by two very different techniques. The first is a flash photolysis-resonance fluorescence technique in which OH radicals are produced by the pulsed vacuum ultraviolet photolysis ($\lambda > 105$ nm) of H₂O and monitored by resonance fluorescence [2]. With this method, absolute rate constants can be determined over a wide range of pressure (~ 15 -650 torr) and temperature (~ 295 -475 °K).

In the second technique, relative rate constants are obtained from the initial rates of disappearance of organics as measured during irradiation of NO_x-hydrocarbon-air mixtures in a 6400 liter, all glass (Pyrex) chamber at 1 atmosphere total pressure and at ~ 305 °K [3-5]. These relative rate constants can be placed on an absolute basis using the literature rate

¹Figures in brackets indicate literature references at the end of this paper.

constants for the reaction of OH radicals with either n-butane or isobutene, one or both of which are included in the NO_x-hydrocarbon-air mixture studied. Computer modeling [3,4,6,7] has shown that in the early stages of such an irradiation the major loss of the hydrocarbon is by reaction with the hydroxyl radical. For alkanes and aromatics, this is almost the exclusive reaction loss process, while for alkenes, reaction with O₃ can become important at later stages of the irradiation when O₃ is formed. Small corrections for this effect have been applied wherever necessary.

Tables I and II compare the room temperature rate constants obtained by the flash photolysis-resonance fluorescence (FP-RF) and all-glass chamber (AGC) techniques with selected literature values. It can be seen that in general the agreement between the two techniques is excellent and there is also generally good agreement with literature values, especially those of Davis and co-workers [8,9] and of Niki and co-workers [10,11]. The lower value obtained for propene by Morris and Niki [10] using the discharge flow technique may be due to the reaction being in the fall-off region between second and third order kinetics as has been noted for OH + ethene by Davis and co-workers [9,12] at pressures below 300 torr.

Table 1. Comparison of room temperature rate constants, k, for the reaction of OH radicals with aromatic hydrocarbons from the present work with literature values.

Aromatic Hydrocarbon	k X 10 ¹² cm ³ molecule ⁻¹ sec ⁻¹			
	This Work FP-RF ¹⁷ (a)	AGC ³ (b)	Davis, Bollinger & Fischer ⁸ (c)	Morris & Niki ¹⁰ (d)
Benzene	1.24 ± 0.12	≤3.8	1.59 ± 0.12	
Toluene	5.78 ± 0.58	4.2 ± 1.5	6.11 ± 0.40	
o-Xylene	15.3 ± 0.58	12.8 ± 3.8		
m-Xylene	23.6 ± 2.4	23.2 ± 1.7		18.7
p-Xylene	12.2 ± 1.2	12.3 ± 2.5		
1,2,3-Trimethylbenzene	26.4 ± 2.6	23 ± 5		
1,2,4-Trimethylbenzene	33.5 ± 3.4	33 ± 5		
1,3,5-Trimethylbenzene	47.2 ± 4.8	51.5 ± 6.5		

a) Total pressure >50 torr (Ar).

b) Total pressure 1 atmosphere air; rates relative to OH + n-butane placed on an absolute basis using the rate constant for OH + n-butane = 3.0 x 10⁻¹² cm³ molecule⁻¹ sec⁻¹.

c) Total pressure 100 torr (He).

d) Total pressure ~1 torr (He), mixture of isomers.

Table 2. Comparison of the present room temperature rate constants, k , for the reaction of OH radicals with propene and the butenes with selected literature values.

Olefin	$10^{11} \times k \text{ cm}^3 \text{ molecule}^{-1} \text{ sec}^{-1}$				
	This Work		Fischer et al. ⁹	Morris & Niki ¹⁰	Wu, Japar & Niki ¹¹ b)
	AGC ⁴ a)	FP-RP ^{18,19}			
Propene	2.9 ± 0.6	2.51 ± 0.25	$1.59 \pm 0.06^c)$	1.7	2.15
1-Butene		3.53 ± 0.36	2.95 ± 0.28	4.1	2.79
Isobutene		5.07 ± 0.51		6.5	4.94
<u>cis</u> -2-Butene	6.5 ± 1.3	5.37 ± 0.54	4.26 ± 0.25	6.1	(5.37)
<u>trans</u> -2-Butene		6.99 ± 0.70		7.1	6.98
2-Methyl-2-butene		7.8 ± 0.9		11.9	

a) Relative to n-butane, placed on an absolute basis using $\text{OH} + \text{n-butane} = 3.0 \times 10^{-12} \text{ cm}^3 \text{ molecule}^{-1} \text{ sec}^{-1}$.

b) Relative to $\text{OH} + \text{cis-2-butene}$, placed on an absolute basis using $\text{OH} + \text{cis-2-butene} = 5.37 \times 10^{-11} \text{ cm}^3 \text{ molecule}^{-1} \text{ sec}^{-1}$.

c) Davis (private communication, 1976) has obtained a rate constant of $2.6 \times 10^{-11} \text{ cm}^3 \text{ molecule}^{-1} \text{ sec}^{-1}$ for propene.

2. APPLICATION OF OH RATE DATA TO DEVELOPMENT OF A HYDROCARBON REACTIVITY SCALE

Using the OH rate data, we have proposed [13,14] a hydrocarbon reactivity scale based on the rate of disappearance of hydrocarbons due to reaction with OH, i.e. based on OH rate constants. Previous workers [6,10] have noted correlations between OH reaction rates and relative rates of NO to NO_2 conversion observed in HC-NO_x photooxidation studies. We have derived a five-class scale relative to methane in which the classes differ by factors of 10. The half-lives and reactivity (relative to methane) corresponding to each class in our proposed scale are summarized in Table III.

Table 3. Reactivity scale for hydrocarbons based on rate of disappearance of the hydrocarbon due to reaction with the hydroxyl radical^{13,14}.

Class	Half-Life ^{a)}	Reactivity Relative to Methane (= 1)
I	>10 days	<10
II	1 - 10 days	10 - 100
III	0.1 - 1 day	100 - 1000
IV	0.01 - 0.1 day	1000 - 10,000
V	0.01 day	>10,000

a) $t_{1/2} = 0.693/k_{\text{OH}}[\text{OH}]$.

Selected examples of compounds appearing in the various classes are given in Table IV. Our scale re-emphasizes the fact that consideration has to be given to some of the slower reacting species such as alkanes in order to reduce hydrocarbons to sufficient levels to achieve the Federal air quality standard for photochemical oxidant during episodes of prolonged irradiation (>10-12 hours) [15].

Table 4. Proposed reactivity classification of hydrocarbons based on reaction with the hydroxyl radical¹³.

Class I	Class II	Class III	Class IV*	Class V*
Methane	Methanol	n-Butane	n-Octane	2-Methyl-2-Butene
	Acetylene	n-Hexane	Xylenes	Carvomenthene
	Ethane	Ethene	Ethyltoluenes	
		Benzene	Propene	d-Limonene
		Toluene	1-Hexene	
		Ethyl Acetate	Trimethyl Benzenes	
		Ethanol	α - & β -Pinene	
		Isopropyl Alcohol	1,3-Butadiene	
		Methylethylketone		
		Diethyl Ketone		

*Selected Examples

3. EFFECT OF UV SPECTRAL DISTRIBUTION ON PHOTOCHEMICAL SMOG MANIFESTATIONS

We have recently observed enhanced photochemical smog manifestations in environmental chamber irradiations of HC-NO_x-air systems under simulated atmospheric conditions, upon incrementally increasing the short wavelength component of the UV photolyzing radiation [16]. For example, as shown in Figure 1, a decrease by 15 nm in the short wavelength cut-off (50% transmission point) of filters on the solar simulator caused the ozone maximum in a propene-n-butane-NO_x photolysis in the SAPRC evacuable chamber-solar simulator facility to increase from 0.57 to 0.70 ppm and to occur at 2.5 hours instead of 5 to 6.5 hours of irradiation. Similar results were observed for other products such as NO₂, PAN and formaldehyde. These observations can be shown to be consistent with current chemical mechanisms of photochemical smog formation. The implications of these results for effects upon urban and rural smog problems are treated in detail in a forthcoming paper [16].

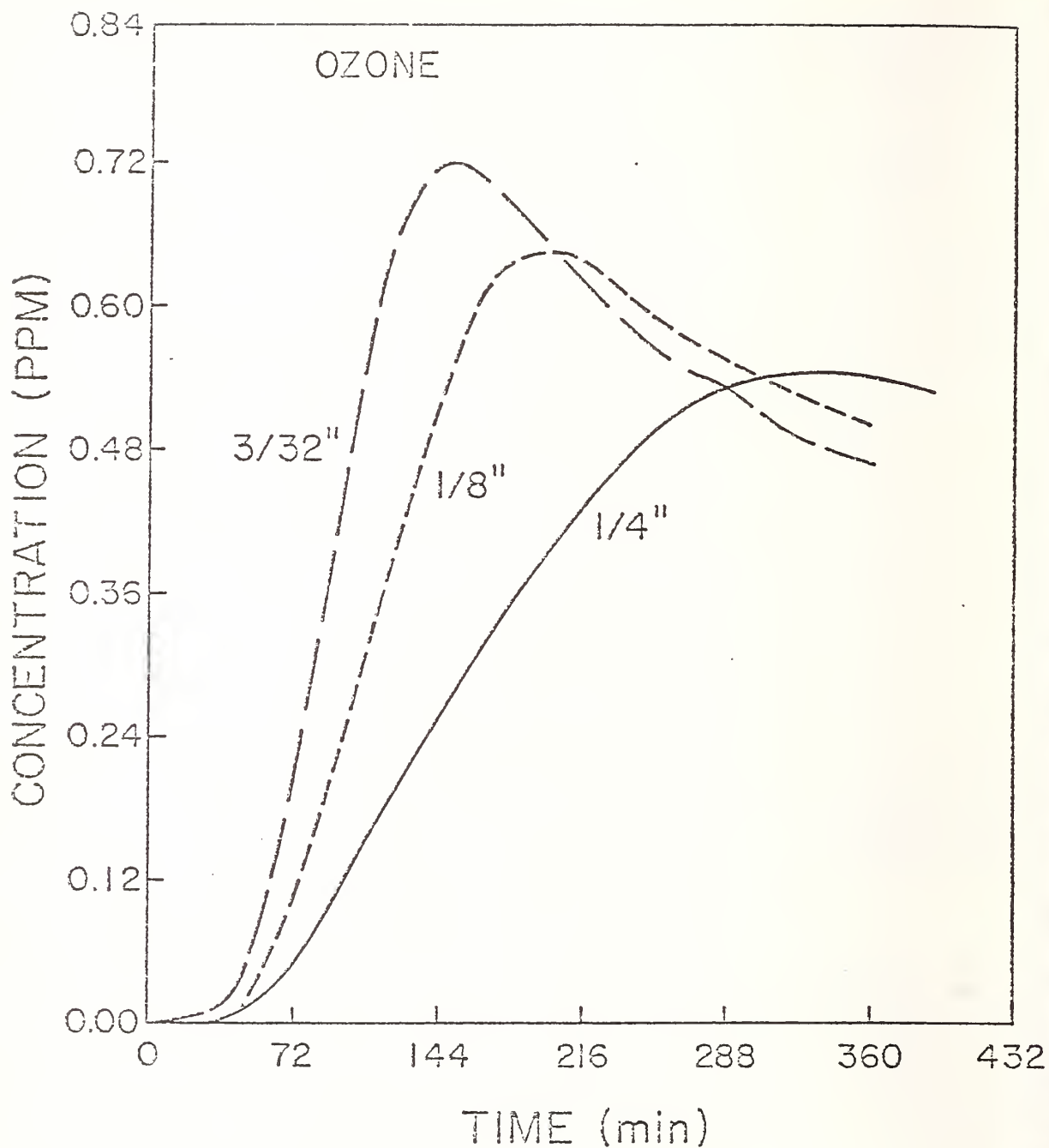


Figure 1. Ozone concentration profiles resulting from irradiations of 0.4 ppm propene, 2.0 ppm n-butane and 0.5 ppm NO_x with three different Pyrex filters for solar simulator beam (from reference 16).

4. ACKNOWLEDGEMENTS

This work was supported in part by the National Science Foundation (Grants GP-38053X and MPS73-08638A02), the National Science Foundation-RANN (Grant No. AEN73-02904-A02) and the California Air Resources Board (Grant No. 5-067-1 and Contract No. 5-385).

REFERENCES

- [1] Pitts, J. N. Jr. and Finlayson, B. J., *Angew. Chem., Int. Ed.*, 14, 1 (1975); Finlayson, B. J. and Pitts, J. N. Jr., *Science*, 192, 111 (1976).
- [2] Atkinson, R., Hansen, D. A. and Pitts, J. N. Jr., *J. Chem. Phys.*, 62, 3284 (1975); *ibid*, 63, 1703 (1975).
- [3] Doyle, G. J., Lloyd, A. C., Darnall, K. R., Winer, A. M. and Pitts, J. N. Jr., *Environ. Sci. Technol.*, 9, 237 (1975).
- [4] Lloyd, A. C., Darnall, K. R., Winer, A. M. and Pitts, J. N. Jr., *J. Phys. Chem.*, 80, 789 (1976).
- [5] Winer, A. M., Lloyd, A. C., Darnall, K. R. and Pitts, J. N. Jr., *J. Phys. Chem.*, 80, 1635 (1976).
- [6] Niki, H., Daby, E. E. and Weinstock, B., *Adv. Chem. Ser. No. 113*, 16 (1972).
- [7] Demerjian, K. L., Kerr, J. A. and Calvert, J. G., *Adv. Environ. Sci. Technol.*, 4, 1 (1974).
- [8] Davis, D. D., Bollinger, W. and Fischer, S., *J. Phys. Chem.*, 79, 293 (1975).
- [9] Fischer, S., Schiff, R., Machado, E., Bollinger, W. and Davis, D. D., "A Kinetic Study of Several Reactions of the Hydroxyl Radical with Olefinic and Aromatic Compounds," 169th National ACS Meeting, Philadelphia, PA, April 6-11, 1975.
- [10] Morris, E. D. Jr. and Niki, H., *J. Phys. Chem.*, 75, 3640 (1971).
- [11] Wu, C. H., Japar, S. M. and Niki, H., *J. Environ. Sci. and Health-Environ. Sci. Eng.*, A11, 191 (1976).
- [12] Davis, D. D., Fischer, S., Schiff, R., Watson, R. T. and Bollinger, W., *J. Chem. Phys.*, 63, 1707 (1975).
- [13] Darnall, K. R., Lloyd, A. C., Winer, A. M. and Pitts, J. N. Jr., *Environ. Sci. Technol.*, 10, 692 (1976).
- [14] Pitts, J. N. Jr., Lloyd, A. C., Winer, A. M., Darnall, K. R. and Doyle, G. J., "Development and Application of a Hydrocarbon Reactivity Scale Based on Reaction with the Hydroxyl Radical," Presented at the 69th Air Pollution Control Association Annual Meeting, Portland, OR, June 27-July 1, 1976.
- [15] Altschuller, A. P., in "Proceedings of the Solvent Reactivity Conference," U.S. Environmental Protection Agency, Research Triangle, Park, NC, EPA-650/3-74-010, November, 1974, pp. 2-5.
- [16] Winer, A. M., Breuer, G. M., Carter, W. P. L., Darnall, K. R., Lloyd, A. C. and Pitts, J. N. Jr., "Effects of UV Spectral Distribution on the Photochemistry of Simulated Polluted Atmospheres," to be submitted to *Atmospheric Environment*, 1976.
- [17] Hansen, D. A., Atkinson, R., Pitts, J. N. Jr., *J. Phys. Chem.*, 79, 1763 (1975).
- [18] Atkinson, R. and Pitts, J. N. Jr., *J. Chem. Phys.*, 63, 3591 (1975).
- [19] Atkinson, R., Perry, R. A. and Pitts, J. N. Jr., *Chem. Phys. Lett.*, 38, 607 (1976).

IR FOURIER-TRANSFORM SPECTROSCOPIC STUDIES OF ATMOSPHERIC REACTIONS

H. Niki, P. Maker, C. Savage and L. Breitenbach

Research Staff
Ford Motor Company
Dearborn, MI 48121

Current knowledge of atmospheric reactions involving polyatomic radicals is severely limited due primarily to the lack of adequate analytical methods for monitoring reactants and product. Fourier-transform IR spectroscopy offers a highly sensitive in situ detection method. In order to maximize system performance in signal detection and in computer-aided data processing and analysis, we have assembled a rapid scan, high resolution IR Fourier-transform facility based on an EOCOM Model 7001 interferometer, a PDP 11/40 on-line computer, and in-house software.

The interferometer is equipped with a liq. N₂ cooled HgCdTe detector and is capable of monitoring IR signals in the 600 ~ 4000 cm⁻¹ range with $\Delta\nu \geq 1/16$ cm⁻¹ and scanning speed <10 sec. Spectra of products are derived from interferograms, ratioed against background, converted to absorbance, and analyzed using linear desynthesis with reference spectra. The two photochemical reactor-IR absorption cells used in this study are a 1-l Pyrex cylinder (50-cm long, double pass) and a 70-l Pyrex cylinder (1-m long, 40 pass). The standard spectra of reactants and products were recorded typically at 0.1 Torr and/or 1 ppm (=2.5 x 10¹³ molecule cm⁻³) in the respective cells. The noise level of the product spectra was comparable to 0.5 percent of the reference spectra.

To illustrate this technique, results obtained on the oxidation of HCO will be presented. The HCO was produced by Cl-atom sensitized reaction of HCHO at ppm level in 1 atm. air. In this system, CO produced by $\text{HCO} + \text{O}_2 \rightarrow \text{CO} + \text{HO}_2$ accounts for up to 80 percent of the HCHO reacted. Hydrogen peroxide is a major hydrogen-containing product as expected. In addition, CO₂ and HCOOH were observed as products with a combined yield of about 20 percent. Thus, the addition reaction producing HC(O)OO appears to occur to a small but significant degree under these conditions. Weak IR signal probably arising from HC(O)OOH was detected. This compound is known to decay to HCOOH rapidly. As an attempt to chemically trap the peroxy radicals, i.e., HO₂ and HC(O)OO, NO₂ was added to the Cl₂-HCHO system to produce the corresponding nitrates. These results are shown in Figs. 1 and 2.

Time-resolved product spectra of Cl₂-HCHO-NO₂ mixture at 20 ppm each (Fig. 1) show the formation of a "new product." The spectrum of this compound is shown in Fig. 2(B), which was obtained by desynthesizing the difference spectrum (Fig. 2(A)), i.e., difference between 4 and 0 min. spectra in Fig. 1. This spectrum has well-resolved "nitrate-type" bands plus an OH band at 3540.0 cm⁻¹ (not shown here). Notably, the "PAN" (peroxyacetyl nitrate)-type C = O band at 1840 cm⁻¹ is not present. Thus this new product is likely to be peroxy nitric acid (PNA) rather than peroxyformyl nitrate. Further evidence for PNA was obtained from the photolysis of Cl₂-H₂-NO₂ mixture in air. The residual spectrum observed in this system is identical to that shown in Fig. 2(B). This compound is unstable and has a lifetime of less than 5 min. in the dark. Attempts to characterize the kinetics of PNA formation are under way.

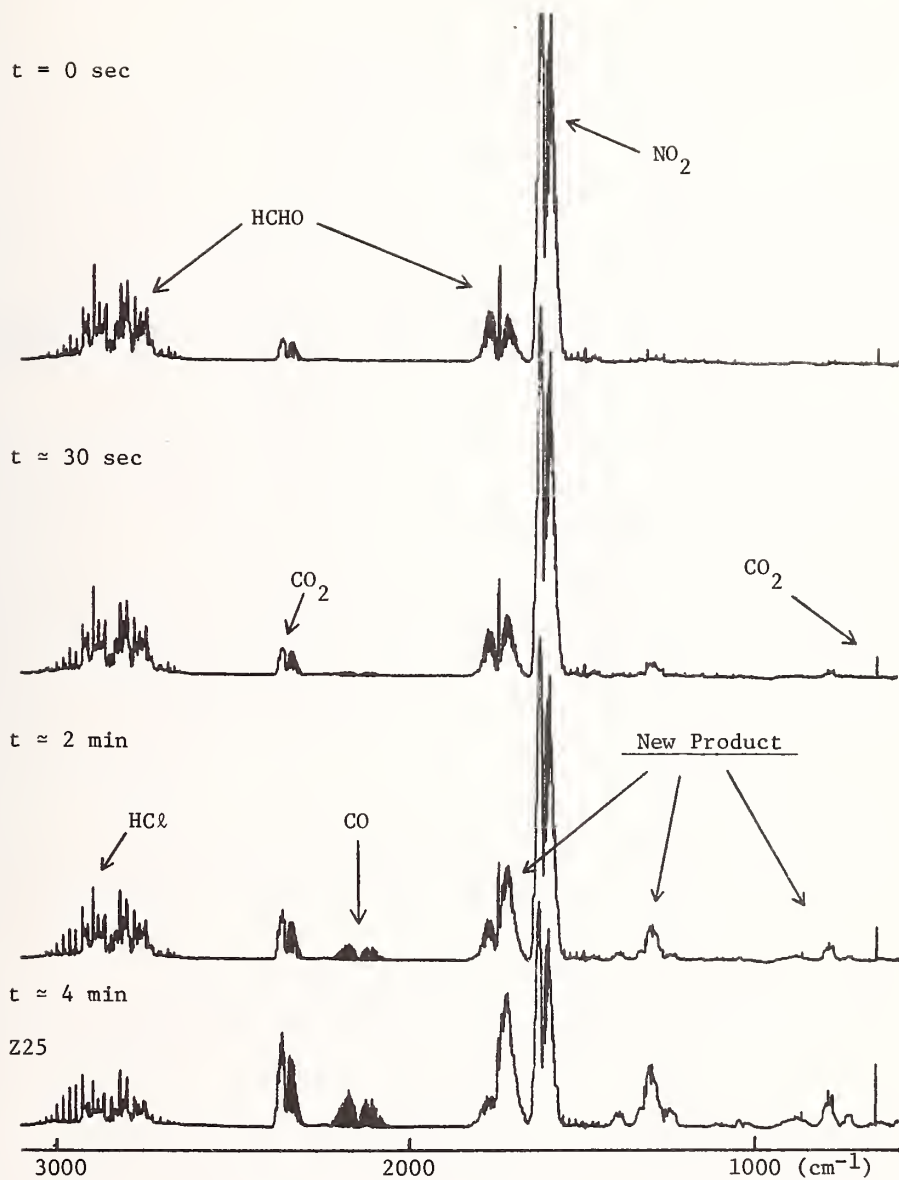
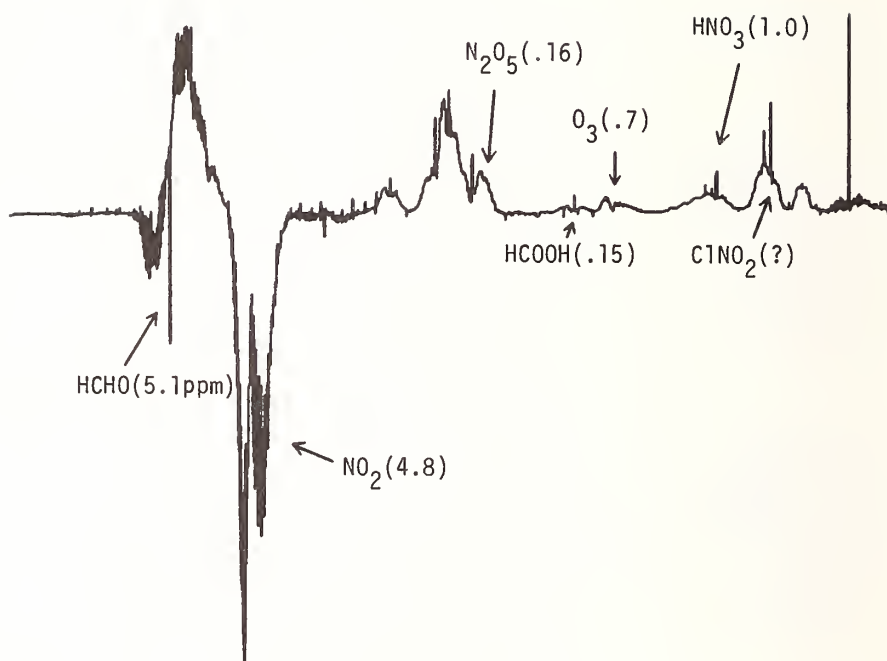


Figure 1. Photolysis of $\text{HCHO-NO}_2\text{-Cl}_2$ System, 10 ppm Each

(A) Difference Spectrum ($\Delta t = 4$ min)



(B) Spectrum of PNA (HOONO_2)(x2)

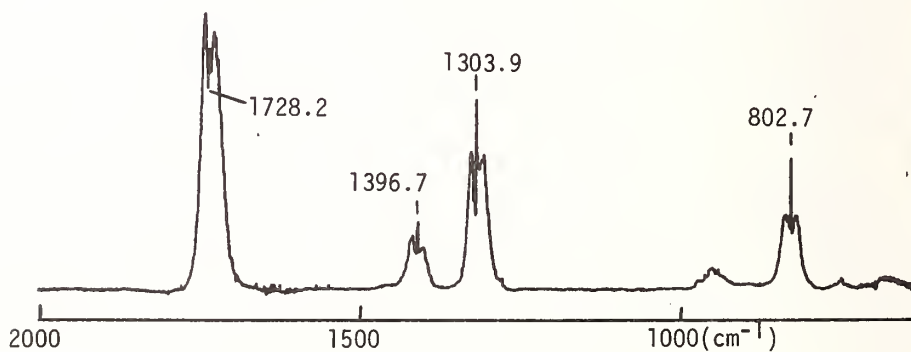


Figure 2. Product Spectra of $\text{HCHO}-\text{NO}_2-\text{Cl}_2$ System, 10 ppm Each

PHOTOCHEMICALLY GENERATED OZONE FROM ISOLATED STRONG POINT SOURCES

D. D. Davis and W. Keifer

Chemistry Department
University of Maryland
College Park, Maryland

In spite of increasingly tight controls on a wide range of emission sources, cities up and down the east coast of the United States continue to experience very high levels of air pollution. Of particular concern has been the high level of ozone observed both in urban as well as non-urban areas of this part of the country. In the Nation's Capital, the summer of 1975 delivered yet another bumper crop of days having air pollution index readings of 100 and over.

In probing the question as to where this pollution is coming from, various answers can be had from various authorities in the field. These answers range from the city automobile being the major source to that of the lush natural summer vegetation of the east coast being the cause. In general, however, there have been far more predictions made based on desk calculator experiments than on actual field studies.

To be reported in this talk will be the results of an aircraft field sampling program carried out in the vicinity of Washington, D. C. to determine if the air quality of the Nation's Capital is being controlled from inner city sources, from outlying non-urban sources, or from both. The aircraft employed in the study was an Essna 205 equipped with an overhead air sampling duct and sampling instrumentation which included: a Monitor Labs NO/NO₂/NO_x detector; a Monitor Labs Ozone detector; a Meloy SO₂, H₂S, CS₂ (Total Sulfur) Analyzer; and Environmental Labs Condensation Nuclei Counter; an Ecolyzer CO Analyzer, and a Beckman Total Hydrocarbon Analyzer.

The principal geographical region of investigation in this study was an approximate 12,000 square mile corridor south-southwest of Washington, D.C. One of the major reasons for the selection of this region was an earlier observation that summer winds from the south-southwest have resulted in the highest air pollution index readings recorded in the Washington, D.C. area.

A total of 45 to 50 flights have been made in this corridor over the period of October 1973 to June 1976. Much of this flying has been concentrated on detailed studies of power plants in the area and has taken place during late spring, summer, and early fall, periods during which Washington, D. C., like other cities, has experienced its highest air pollution index readings.

As indicated earlier in the text, one of the major questions which we hoped to explore in this study was that of why SW or southerly winds typically result in the highest air pollution index readings in D.C. The correlation between the air quality index and wind direction is most definitely not a simple one since a very large number of meteorological factors can be involved (i.e., wind variability in speed and direction, surface winds vs. winds at one to two thousand feet, humidity, cloud cover, and temperature).

The results of the study to date have shown that the high index readings recorded with SW or southerly winds do not, in general, reflect strong sources being present in the immediate southern part of the greater Metropolitan Washington, D.C. area. In fact, what was observed was that typically under conditions of high temperature, high humidity, and high solar flux, ozone levels 1.5 to 3 times that of ambient air were found blowing toward or into the Washington, D.C. area from distances going out to anywhere from 50 to 100 miles.

During one of the worst air pollution periods in D.C., with SW winds, levels of ozone in Washington, D.C.-Richmond corridor reached into the 200 to 300 ppb range.

The above information is not to be interpreted, we believe, as a direct indication that all air pollution problems in D.C. originate from out-of-town air masses. The air quality of any large city is most definitely the result of multidimensional sources. In the case of the greater Washington, D.C. area, the high density of automobiles is clearly a major contributing factor. Our new findings, however, would also indicate that the air mass moving into the city from far out into the countryside also appears to be a major contributor of photochemical oxidant.

One of the important questions to be answered concerning the observed high ozone levels to the southwest and south of D.C., is that of the source. Thus far, our studies have shown that at least four sources are involved, (1) automobile traffic on Interstate 95 between Washington and Richmond, (2) two large power plants located at Possum Point, Virginia, on the Potomac River and Morgantown, Maryland, on the Potomac River, (3) a cellophane factory located at Fredericksburg, Virginia, and, (4) the urban plume from Richmond, Virginia, which itself is a complex mixture of point sources. A final source which should be mentioned but cannot be well-defined is the diffuse source still upwind of the corridor which we generally refer to as ambient air. Significant variations in the level of ozone in this upwind ambient air obviously also reflect multidimensional sources consisting of highly diluted urban plumes diluted strong point source plumes, regional photochemistry involving natural constituents from forest, and to some extent stratospheric injected ozone. Details on each of the sources mentioned in conjunction with the Washington, D.C.-Richmond corridor will be discussed. Suffice it to say at this point that a quantitative assessment of the contribution of ozone from each of these sources will require much further investigation.

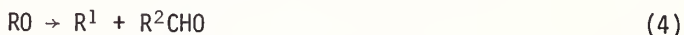
A final comment that should be made to maintain some perspective on the problem being discussed is the following. Although Washington, D.C. has been placed as the focal point of a site being affected by external pollution sources, this in no way implies that D.C. itself is not a major air pollution source for other cities downwind from it. Data, in fact, will also be presented which shows this phenomenon.

EVIDENCE FOR ALKOXY RADICAL ISOMERIZATION IN C₄-C₆ ALKANES IN NO_x-AIR SYSTEMS

William P. L. Carter, Karen R. Darnall, Alan C. Lloyd,
Arthur M. Winer, and James N. Pitts, Jr.

Statewide Air Pollution Research Center
University of California
Riverside, California 92502

Most photochemical smog models, whether detailed or lumped, predict that the following are the most important reactions in the photooxidation of alkanes in the presence of oxides of nitrogen under ambient conditions:



To obtain insight concerning the adequacy of this simple mechanism, data concerning other possible reactions of the major radical intermediates is required. In view of the paucity of data obtained under ambient conditions concerning the mechanism and products of alkane oxidations, we have examined the extensive gas phase studies of free radical reactions and hydrocarbon oxidation carried out at temperatures of ~250 °C and above. A type of reaction commonly encountered at these temperatures is the isomerization of alkyl, alkoxy, and alkylperoxy radicals via internal hydrogen (H) abstractions. Similar intramolecular reactions have been postulated and observed in liquid phase studies at temperatures close to ambient. However, to the best of our knowledge, these processes have not been incorporated in mechanisms proposed for the hydrocarbon oxidations occurring in photochemical air pollution.

We have estimated Arrhenius parameters in order to permit calculation of approximate rate constants (at 300 K) for intramolecular hydrogen shift reactions for alkyl, alkoxy, and alkylperoxy radicals which are expected to be involved in the photooxidation of C₄-C₆ alkanes. To evaluate the potential significance of the radical isomerizations under ambient conditions, we have compared their rates as calculated to the expected rates for the competing processes with O₂ or NO which are believed to be important in the atmosphere. While isomerizations of alkyl, and probably most alkylperoxy radicals, do not appear to be important, we find that the possibility of 1,5 hydrogen shifts in alkoxy radicals with δ hydrogens must be considered.

Figure 1 shows the reaction sequence and products predicted in the photooxidation of n-pentane with and without the proposed alkoxy radical 1,5 H shift isomerization. If the OH radical abstracts a hydrogen from the 3 position in n-pentane, no rapid isomerization is possible while rapid isomerization is predicted following abstraction from the 1 or 2 position.

In order to test these predictions and to ascertain the importance of intramolecular alkoxy radical isomerization in photochemical air pollution, we have performed a series of experiments under simulated atmospheric conditions in two environmental chambers.

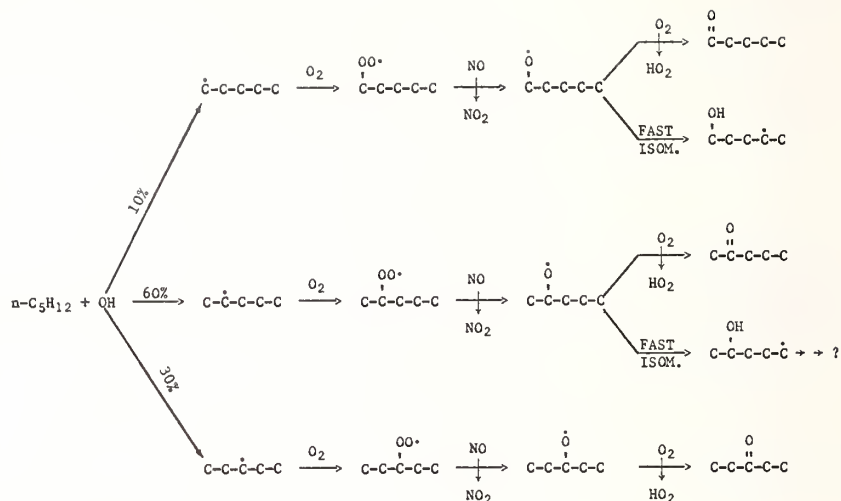


Figure 1. Suggested sequence of major reactions following abstraction from n -pentane by hydroxyl radicals in $n\text{-C}_5\text{H}_{12}\text{-NO}_x$ -air mixtures. The relative percentages for the OH reactions are derived from the data of Greiner (1970).

Irradiations of alkane (n -butane, n -pentane or n -hexane)- NO_x systems in air were carried out in a 5800 liter evacuable, Teflon-coated environmental chamber using a 25,000 watt solar simulator. Analogous studies were carried out in a 6400 liter all-glass environmental chamber equipped with fluorescent black lights. Detailed results from the experiments in both chambers will be presented.

Computer kinetic model calculations with and without the 1,5 H shift reaction of alkoxy radicals were carried out simulating the experimental systems studied. Results of calculations of the yields of the pentanone isomers for a selected n -pentane experiment (Run 164) are shown in table 1. The pentanone yields predicted when alkoxy radical isomerization is not included reflect the relative rates of OH abstraction shown in figure 1. On the other hand, the calculated yields of 1- and 2-pentanone are significantly lower when isomerization of their precursors is assumed.

The experimental results for four n -pentane- NO_x -air irradiations are also shown in table 1. It is clear from the results of Run 164 (glass chamber) that both the relative and absolute yields of the pentanone isomers are consistent with the predicted importance of 1,5 hydrogen shift isomerization of the pentoxy radicals. Results from the evacuable (Teflon-lined) chamber for the same initial n -pentane concentration are in excellent agreement. Data for both higher and lower n -pentane concentrations give the same relative yields of the pentanone isomers, although the absolute amounts vary as expected. Additional support for the occurrence of intramolecular alkoxy radical isomerization is found in the yields of acetaldehyde and propionaldehyde, both of which are expected decomposition products of the 2- and 3-pentoxy radicals under the experimental conditions employed.

Similar results will be presented for studies of the n -butane and n -hexane photo-oxidation systems.

Table 1. Calculated and observed absolute yields and percentages of pentanone isomers from the n-pentane-NO_x-air photooxidation under a variety of conditions.

				Product Yields in ppb (% of total pentanones)		
				1-Pentanone	2-Pentanone	3-Pentanone
MODEL CALCULATIONS ^{a)}						
No isomerization				31 ppb (20%)	83 ppb (54%)	40 ppb (26%)
With isomerization				0.2 (1%)	9 (23%)	30 (77%)
EXPERIMENTAL DATA						
Run	Chamber	Initial HC (ppm)	Initial NO _x			
164	Glass	4	0.9	b)	8 (21%)	30 (79%)
135	Evacuatable (Teflon-lined)	4	0.1	b)	8 (16%)	42 (84%)
165	Glass	35	9	b)	32 (17%)	160 (83%)
166	Glass	0.4	0.1	b)	<1 (0-17%)	6 (100-83%)

^{a)} Using initial conditions of Run 164. Similar % yields were obtained using initial conditions of other runs and are omitted for clarity.

b) None observed; detection limit 0.5 ppb.

Table 1. Calculated and observed absolute yields and percentages of pentanone isomers from the n-pentane-NO_x-air photooxidation under a variety of conditions.

				Product Yields in ppb (% of total pentanones)		
				1-Pentanone	2-Pentanone	3-Pentanone
MODEL CALCULATIONS ^{a)}						
No Isomerization				31 ppb (20%)	83 ppb (54%)	40 ppb (26%)
With Isomerization				0.2 (1%)	9 (23%)	30 (77%)
EXPERIMENTAL DATA						
Run	Chamber	Initial HC (ppm) NO _x				
164	Glass	4	0.9	b)	8 (21%)	30 (79%)
135	Evacuatable (Teflon-lined)	4	0.1	b)	8 (16%)	42 (84%)
165	Glass	35	9	b)	32 (17%)	160 (83%)
166	Glass	0.4	0.1	b)	<1 (0-17%)	6 (100-83%)

a) Using initial conditions of Run 164. Similar percent yields were obtained using initial conditions of other runs and are omitted for clarity.

b) None observed; detection limit 0.5 ppb.

On the basis of our work, it appears that alkoxy radical isomerizations, which are well known from elevated temperature free radical and oxidation studies as well as in certain liquid phase systems around room temperature do, in fact, occur under photochemical smog conditions at ambient temperatures. The implications of these results for alkane oxidation under ambient conditions, including the formulation of photochemical smog models which incorporate higher alkanes ($\geq C_4$), will be discussed.

This work was supported in part by the National Science Foundation-RANN (Grant No. AEN73-02904-A02). The contents do not necessarily reflect the views and policies of the National Science Foundation-RANN, nor does mention of trade names or commercial products constitute endorsement or recommendation for use. The authors also gratefully acknowledge support of the California Air Resources Board (Grant No. 5-067-1 and Contract No. 2-377) for the construction of the chamber facility employed in this study.

COLLISIONAL DESTRUCTION OF ROVIBRONIC LEVELS IN S_1 GLYOXAL: ELECTRONIC,
VIBRATIONAL AND ROTATIONAL STATE CHANGES

L. G. Anderson, A. E. W. Knight, and C. S. Parmenter

Department of Chemistry
Indiana University
Bloomington, IN 47401

At pressures above 100 mtorr, the decay of S_1 glyoxal (CHOCHO) is dominated by collisions. In addition to collision-induced vibrational and rotational relaxation within the S_1 state, every collision partner so far tried is effective in destroying the S_1 electronic state itself. The competition between these channels and some fine details of collisional state changes can be worked out with unusual clarity because of the open structure in both S_1 - S_0 fluorescence and absorption spectra.

Early studies identified the collisional destruction of the electronic state as collision-induced intersystem crossing [1]¹. Subsequent investigation of fluorescence lifetimes and quenching from low S_1 vibrational levels ($\epsilon_{\text{vib}} \leq 2000 \text{ cm}^{-1}$) characterized this crossing as "small molecule" S_1 -T mixing [2-4]. This transforms to intermediate mixing as increasingly higher levels are pumped by the exciting light, and finally, statistical decay is observed from very high S_1 levels [5].

Quenching cross sections σ for destruction of the $S_1 0^0$ level by collision-induced triplet formation are known for over twenty collision partners [2-4]. Several correlations of these cross sections have been given [6,7]. We find another and particularly simple relationship, namely $\ln \sigma \propto (\epsilon_{\text{QQ}})^{1/2}$, where ϵ_{QQ} is the potential well depth between pairs of quenching molecules (He-He, CO-CO, etc.). This is effective not only for correlation of cross sections for S_1 glyoxal quenching, but also for correlation of cross sections in numerous other studies spanning vibrational and rotational relaxation as well as collision-induced predissociation. When considering cross sections of a series of quenchers Q acting on a single excited species S, the parameter $(\epsilon_{\text{QQ}})^{1/2}$ is proportional to the well depth ϵ_{SQ} . Thus the correlation is indicative of interactions using primarily the attractive part of the potential, and consistent with this view, we observe that the correlation is a poor representation of relative cross sections in cases where collisions are inefficient in bringing about state changes.

We have deduced the absolute cross sections for rotational, vibrational and electronic state changes after pumping narrow rotational distributions in the 0^0 or the 7^1 levels of the S_1 state (ν_7 is the lowest frequency fundamental, 235 cm^{-1}). We observe that the cross sections are all large and competitive with each other. They are given specifically in Table 1 for the collision partners S_0 glyoxal and Ar. They are in the form of the second order rate constants in units of $10^6 \text{ torr}^{-1} \text{ s}^{-1}$. A hard sphere collision has in these units a rate constant of about 10.

¹Figures in brackets indicate literature references at the end of this paper.

Table I. Rate constants (in $10^6 \text{ torr}^{-1} \text{ s}^{-1}$) for destruction of 1A_u levels in glyoxal-Hard sphere ≈ 10

State change	from level 0^0		from level 7^1	
	G	Ar	G	Ar
el	2	0.7	2	0.7
vib	3	0.7	13	3
rot	21	12	10	11

The analysis of rotational structure in 12 S_1 - S_0 absorption bands by Ramsay and co-workers has allowed us to detect a selection rule for rotational relaxation in experiments which observe fluorescence at ca. 0.5 cm^{-1} resolution after excitation of small groups of rotational levels with an $\Delta\nu = 0.33 \text{ cm}^{-1}$ Ar⁺ laser line. We observe in glyoxal-glyoxal collisions that cross sections for $\Delta K = \pm 2$ collisions far exceed those of other rotational state changes.

A curious selection rule appears in vibrational relaxation effected by glyoxal-glyoxal collisions after pumping the level 7^2 . Fluorescence structure shows that the cross section for $\Delta\nu_7 = -2$ is large whereas that for the vibrational change $\Delta\nu_7 = -1$ is relatively small. The fluorescence spectra display this in two ways. First, we observe at pressures where collisional effects are first introduced that the 0^0 band is substantially brighter in fluorescence than the 7^1 band (these relative intensities represent the respective 0^0 and 7^1 level populations). Second, we observe that the "spiky" rotational structure in the 7^2_2 fluorescence band at these low pressures is mirrored by spiky structure in the developing 0^0 band, whereas the rotational structure in the 7^1 band is substantially without these "non-Boltzmann" features. Apparently the cross section for 0^0 population after 7^2 excitation is competitive with that for rotational relaxation within the 7^2 level itself. As a result, the rotational disequilibrium produced in 7^2 upon excitation is largely retained during the initial stages of 0^0 population. On the other hand, the cross section for 7^1 population is sufficiently small so that appreciable progress towards rotational equilibration in the 7^2 level occurs before collisions populate 7^1 . Thus a near Boltzmann rotational distribution is transferred to the level 7^1 during its initial stages of growth.

REFERENCES

- [1] L. G. Anderson, C. S. Parmenter, H. M. Poland, J. D. Rau, Chem. Phys. Lett. **8**, 232 (1971).
- [2] J. T. Yardley, G. W. Holleman, and J. L. Steinfeld, Chem. Phys. Lett. **10**, 266 (1971).
- [3] L. G. Anderson, C. S. Parmenter, and H. M. Poland, Chem. Phys. **1**, 401 (1973).
- [4] R. A. Beyer, P. F. Zittel, and W. C. Lineberger, J. Chem. Phys. **62**, 4016, 4024 (1975).
- [5] R. van der Werf, E. Schutten, J. Kommandeur, Chem. Phys. **11**, 281 (1975).
- [6] J. E. Selwin and J. I. Steinfeld, Chem. Phys. Lett. **4**, 217 (1969).
- [7] C. A. Thayer and J. T. Yardley, J. Chem. Phys. **57**, 3992 (1972).

THE VIBRONIC DEPENDENCE OF GLYOXAL PHOTODISSOCIATION [1]¹

George H. Atkinson and C. G. Venkatesh

Department of Chemistry
Syracuse University
Syracuse, New York 13210

The selective excitation of single vibronic levels (SVL) in polyatomic molecules has been established as a very useful method for examining state-to-state relaxation. The relaxation mechanism is usually monitored through the detection of radiative decay channels (mostly fluorescence). As a consequence, only the net effect of all nonradiative channels is usually measured even though several processes may be simultaneously contributing to the mechanism (e.g., internal conversion, intersystem crossing, vibrational relaxation and photochemistry). A significantly more detailed view of the relaxation mechanism can be obtained by monitoring only one of these nonradiative channels in conjunction with SVL excitation.

We report in this paper a study of the photodissociation mechanism of glyoxal based on the direct observation of a dissociation product following the selective excitation of single vibronic levels in the parent molecule. The study was carried out in a low pressure regime where the collisional perturbations on excited-state processes can be controlled. It is intended to establish the relationship between the vibronic character of the initially populated 1A_u level and the net efficiency for dissociation into a specific product, CO. Selective excitation was obtained from a tuned dye laser and the concentrations of CO are measured by resonance fluorescence. To our knowledge, this is the first reported study combining these two experimental techniques for measurements of SVL photodissociation.

Single vibronic levels in glyoxal vapor were selectively populated by a tuned (0.1 Å bandwidth) nitrogen laser pumped dye laser. The absolute wavelength of the dye laser radiation was set by means of a one meter spectrometer working in the second order of an 800 g/mm grating (resolution > 0.08 Å). The pulsed laser radiation was detected by a photomultiplier and the signal analyzed with a box car integrator.

Carbon monoxide was detected by resonance emission from the fourth positive system of CO in the vacuum ultraviolet. [2] A xenon lamp, powered by a microwave discharge (2450 Hz), initiated the resonance emission from CO which was detected by a solar blind photomultiplier (10^6 gain) with a CsI photocathode. The photomultiplier signal was amplified and the total signal offset in order to suppress contributions from dark current and scattered resonance lamp emission. The resulting signal was measured on a voltmeter. The signal was calibrated by using known pressures of high purity CO measured by a capacitance manometer. The error in the linearity of the entire detection technique was less than 1%.

The relationships between the ϕ_{CO} and the SVL initially populated are shown in figure 1 as a function of glyoxal pressure. Four distinct phenomena are observed: for a specific SVL, (1) the ϕ_{CO} increased with pressure below approximately 1 torr and (2) decreases with pressure above approximately 1 torr, (3) the value ϕ_{CO} at a given pressure depends on the vibronic level initially populated, and (4) the rate of decrease of ϕ_{CO} with pressure above 1 torr is a function of the SVL initially populated.

¹Figures in brackets indicate literature references at the end of this paper.

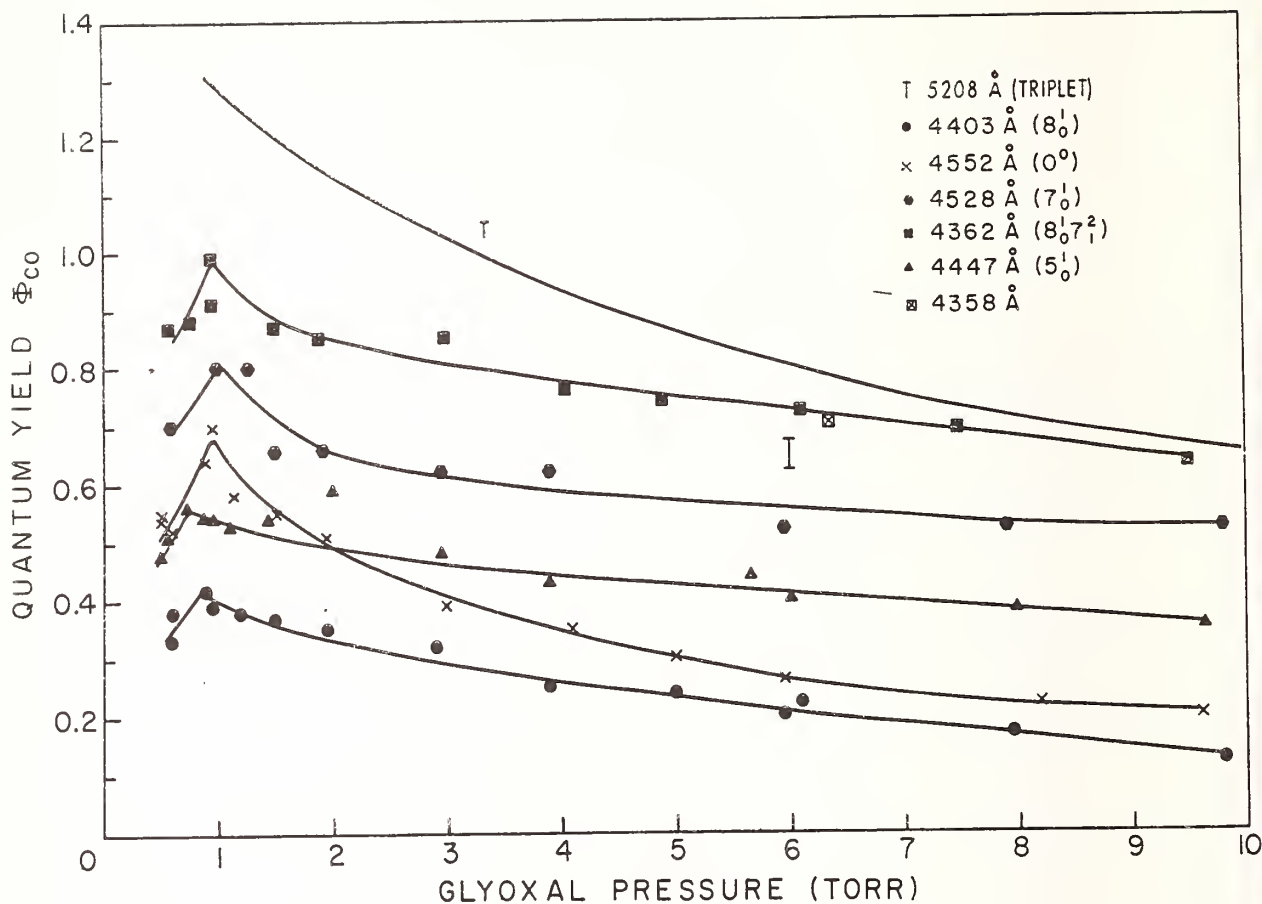


Figure 1. Quantum yield of CO following excitation to SVL in glyoxal versus glyoxal pressure

The change in pressure dependence near 1 torr reflects the presence of two competing decay channels. Below 1 torr, collisionally-induced intersystem crossing 1A_u to 3A_u levels appears to control the net efficiency for CO production by virtue of observation 1.^u Above 1 torr, control of the mechanism shifts to the competitive decay of the intermediate designated as H. The intermediate H was first proposed by Yardley [3] in an analysis of data obtained by Parmenter. [4] It is formed subsequent to the population of 3A_u glyoxal and undergoes first order decay to yield CO. Collisional quenching of H occurs in competition with CO formation and accounts for the inverse pressure dependence of ϕ_{CO} at higher pressures. Plots of ϕ_{CO}^{-1} versus the pressure of glyoxal for this pressure region are linear for all SVL studied.

The dependence of ϕ_{CO} on the initial SVL populated obtains from the presence of a non-Boltzmann distribution of energy among the vibrational levels in the 1A_u state in this pressure region. Fluorescence and collisionally-induced vibrational relaxation (VR) and intersystem crossing (ISC) to 3A_u all compete to relax the initially pumped SVL. ISC leads to CO production via the decay of 3A_u levels and the specie H. VR redistributes energy within the 1A_u state among a variety of vibrational levels. This distribution remains non-Boltzmann up to pressure of approximately 10 torr. SVL fluorescence spectra have been obtained which establish the existence of these unique vibronic distributions in this pressure regime. At a given pressure and for a specific SVL excitation, this unique non-Boltzmann distribution determines the total amount of ISC occurring from 1A_u to 3A_u and

thereby controls the ϕ_{CO} . Thus, it is from these distributions that the vibronic dependence of ϕ_{CO} at a given pressure arises. In a completely analogous way, the rate of decrease of ϕ_{CO} with glyoxal pressure for excitation of specific SVL also derives from these non-equilibrated vibrational distributions within 1A_u .

REFERENCES

- [1] Supported by the U.S. Army Office of Research - Durham under Grant DAHCO4-75-G-0104.
- [2] T. G. Slanger and G. Black, J. Chem. Phys., 55, 2164 (1971) and references therein.
- [3] J. T. Yardley, J. Chem. Phys., 56, 6192 (1972).
- [4] C. S. Parmenter, J. Chem. Phys., 41, 658 (1964).

BEHAVIOUR OF BENZENE IN LOW VIBRATIONAL LEVELS

S. A. Lee, J. M. White and W. A. Noyes, Jr.

Department of Chemistry
University of Texas
Austin, Texas 78712

Fluorescence, triplet state, and isomerization yields from benzene vapor have been determined at several wavelengths but principally at 266.8 nm where $^1B_{2u}$ molecules are formed in the zeroth vibrational level. Fluorescent yields were determined using 0.18 for benzene vapor at 20 torr and 253 nm as a standard. Triplet yields were determined by two methods: 1) The sensitized triplet emission of biacetyl and 2) The sensitized isomerization of the 2-butenes. The former has the advantage of using much smaller amounts of foreign gas and hence collisional vibrational equilibration is also smaller. When used under comparable conditions the two methods give comparable results.

It is well known that there are many isomers of benzene, but benzvalene seems to be the only one which should concern us here. It absorbs strongly from 210 to 230 nm. The production and destruction of benzvalene was studied using a conventional photolysis system. In these experiments cis-2-butene was mixed with the benzene prior to irradiation as a means of removing triplet benzene. Differential absorption spectra were measured after the photolysis with a Cary-14 spectrometer using a benzene blank. The relative amount of benzvalene produced was estimated semiquantitatively by measuring the area under the absorption curve in the region 210-230 nm. In some experiments, a benzvalene-benzene mixture, produced by photolysis at one wavelength were rephotolyzed at a second wavelength. From the resulting data we are able to draw some conclusions about the wavelength dependence of the probability of benzvalene formation and destruction.

The $^1B_{2u}$ molecules in their zeroth vibrational level show no variation of fluorescent yield Q_f with pressure until pressures of 20 torr are reached. At high pressure Q_f decreases to a value near 0.18, the same value reached at 253 nm and at 20 torr. This might be interpreted to be the yield from $^1B_{2u}$ molecules with vibrational energy equilibrated with the surroundings. Thus at low vibrational levels Q_f appears not to increase with increases in vibrational energy. Below about 20 torr and at 266.8 nm, Q_f is constant at 0.22. This result implies that the variation in Q_f with pressure at 253 nm or 259 nm originates with the occupation of different vibronic levels. Presumably equilibration of vibrational energy in the $^1B_{2u}$ state does not give the yield of 0.22 because increasing the pressure of inert gases causes the yield to be lowered. The acquisition of vibrational energy at the zero-point energy level is apparently much slower than the loss of vibrational energy from high levels. To explain the difference between these two yields, it is suggested that the thermal equilibration of vibrational energy following absorption at 253 or 259 nm leads to appreciable population of the 237 cm^{-1} vibrational level (this is the same mode as the 398 cm^{-1} vibrational level in the ground state and is an out-of-plane motion). Emission from this level to the ground state would not be symmetry forbidden but should have a very low transition probability due to the Franck-Condon principle. Population of 237 cm^{-1} vibrational level as the result of collisions would make this level important after excitation at shorter wavelength but it would not be so important in the processes occurring after excitation at 266.8 nm.

In the isomerization study, it was found there was no benzvalene formation observed at 266.8 nm, but as shorter wavelengths benzvalene is formed and the steady state concentration is higher at shorter wavelengths. Illumination at 253 nm up to the steady state followed by irradiation at 266.8 nm caused benzvalene to disappear. Even though benzvalene is not formed at 266.8 nm, it is destroyed by a benzene sensitized reaction, since benzvalene quenches $^1B_{2u}$ ($v=0$) molecules presumably energy transfer can occur from benzvalene to $^1B_{2u}$ molecules and results in such electronic relaxation. Illumination at 253 nm followed by irradiation at 247.2 nm caused the benzvalene to increase. This suggests that the photostationary state depends on the excitation wavelength.

It has been assumed that photons absorbed by benzene caused fluorescence, triplet state formation, and isomerization. A fourth possibility, a radiationless transition from the $^1B_{2u}$ state (or possibly the $^3B_{1u}$ state) to the ground state, has been neglected. At 266.8 nm the isomerization yield seems to be zero at low pressures and the sum of Q_f and triplet yield is about 0.97 and thus nearly all the input photons can be accounted for. The energy balance is not found at any shorter wavelength, and is partly due to benzvalene formation, but since the primary isomerization yields are not known, it is difficult to have complete accountability of the absorbed photons. Benzvalene appears to quench the $^1B_{2u}$ state of benzene so that fluorescent yields tend to decrease with increase in exposure.

The authors wish to thank the Robert A. Welch Foundation for financial support of the work described in this abstract.

DUAL LIFETIME FLUORESCENCE FROM PYRIMIDINE

Kenneth G. Spears and Mahmoud El-Manguch

Department of Chemistry
Northwestern University
Evanston, Illinois 60201

The 1,3 diazabenzene (pyrimidine) 1B_1 ($n \rightarrow \pi^*$) electronic state has a nonradiative relaxation characterized by a dual lifetime in low pressure gas phase emission. The molecule is especially interesting as a system with non-bonded electrons, substantial spin-orbit coupling, and a small S-T energy gap (1800 cm^{-1}). A primary goal is to understand the nature of the S-T coupling with respect to the low triplet state density and non-bonding electrons.

Early work on the molecule has been substantial and a partial list of references include a critical review of the electronic state spectroscopy of all azabenzenes [1]¹, the detailed spectroscopy of pyrimidine 1B_1 [2] and condensed phase analysis of fluorescence and phosphorescence yields [3]. The recent work of Parmenter and associates [4] has analyzed the fluorescence emission spectroscopy (SVL) and re-assigned some bands in the absorption spectrum. Recent work by Parmenter and Knight has shown that the molecule is very sensitive to collisions with self quenching rates higher than expectations based on hard sphere collision diameters. We have reported our early measurements on pyrimidine excited to several higher vibrational levels above the 0-0 band ($\sim 200 \text{ cm}^{-1}$) [5]. We found a dual emission lifetime for these states with lifetimes near 1 nsec and 100-200 nsec at 0.1 Torr. Very recent work of Uchida, Yamazaki and Baba [6] has also reported dual emission but no precise measurements of longer lifetimes were possible.

We have extended our results to many absorption bands, including the 0-0 band. We find that the lower bands fit the model of Lahmani, Tramer and Tric [7] for a reversible intersystem crossing. The data fit the case of a forward crossing rate k_i , a reverse crossing rate k_r , a singlet fluorescence decay rate k_f , and a singlet internal conversion rate k_{ic} . For the case of observed dual lifetime emission (k_s is the fast decay) in the form $I(t) = C_s e^{-k_s t} + C_L e^{-k_L t}$ we can derive the individual parameters k_i , k_r , k_f , k_{ic} , the number of effective states, N , coupling to the singlet state, the average triplet density of states ρ .

Our experiments measure C_s , k_s , C_L , k_L as well as relative quantum yields for various bands. We have used a recent absolute fluorescence yield measurement of Parmenter in our calculated results using the case 1 simplifications of the model [1] as well as computer fits to the equations. Our initial experimental results on the 0-0, $6a^1$, and 12^1 vibronic bands show that the ratio C_s/C_L is a constant from 0.01 to 0.05 torr. The quenching of the long lifetime is very efficient with cross-sections of $1.0 \times 10^8 \text{ torr}^{-1} \text{ sec}^{-1}$ corresponding to a collision diameter of $\sim 16 \text{ \AA}$ (~ 3 times hard sphere). The respective

¹Figures in brackets indicate literature references at the end of this paper.

zero pressure long lifetimes and short lifetimes of the 0-0, 6a¹, and 12¹ bands are (1100, 1.8), (932, 1.6), (643, 1.5) nanoseconds. The following table contains some of the results of the model.

state	E(cm ⁻¹)	ρ(cm)	N	K _{ic} x 10 ⁻⁷ (sec ⁻¹)	K _f x 10 ⁻⁶ (sec ⁻¹)
0-0	0	41	6	0.44	2.4
6a ¹	613	1100	34	3.5	2.7
12 ¹	1012	2500	73	11.0	3.0

The constancy of radiative lifetime is a good check on the quality of the data but an explanation is needed for the rapidly changing internal conversion rate constant. The number of coupled energy levels in the triplet, N, are too large to be vibronic levels with an energy gap of 1800 cm⁻¹. The density, ρ, must be interpreted as rotational level densities. The results indicate that the initially populated singlet state evolves to a triplet and later in time there is some probability to find molecules back in the singlet where they can either emit or internally convert to the ground state. Rotational relaxation by collision is sufficient to remove the molecule from those rotational states that are coupled to the singlet thereby giving an effective quenching of emission.

The experimental apparatus used in these time-resolved measurements is capable of very high accuracy for dual lifetimes, especially in the case of very different intensities and lifetimes. We have developed an argon-ion laser pumped dye laser in which the dye cavity is acousto-optically mode-locked and synchronously cavity dumped. For high resolution studies with etalon line narrowing the cavity dumper will give 20 nsec duration pulses with frequencies of up to 5 MHz. The mode locked and dumped cavity yields sub-nanosecond pulses with selected rates as high as 5 MHz. The output of this laser has reasonable peak power pulses for creation of tunable ultraviolet. The temperature tuned SHG of 5 MHz mode-locked pulse trains depends on laser mode quality and the crystal quality but 0.5 - 3.0 mW average power is typical with 25 - 200 mW average visible input. The lifetime measurement is by time-correlated photon counting. In this method the time difference between an excitation pulse and detected photon is stored in a multichannel analyzer to yield number of counts as a function of time. By running an inverted time-to-amplitude converter (TAC) we can count every emitted photon and assign its time of emission with very low background. In case of time separated spectra we either run complete time spectra at each wavelength or separate time regions using a discriminators on the TAC output. The high resolution studies use the latter method with simultaneous absorption spectra and interferometer measurement of wavelength.

REFERENCES

- [1] K. K. Innes, J. P. Byrne and I. G. Ross, J. Mole. Spectr., 22, 125 (1967).
- [2] K. K. Innes, H. D. McSwiney, Jr., J. D. Simmons, and S. G. Tilford, J. Mole. Spectr., 31, 76 (1969).
- [3] B. J. Cohen and L. Goodman, J. Chem. Phys., 46, 713 (1967).
- [4] A. E. W. Knight, C. M. Lawburgh and C. S. Parmenter, J. Chem. Phys., 63, 4334 (1975).
- [5] K. G. Spears and M. El-Manguch, Paper at Molecular Spectroscopy Symposium, Columbus, Ohio, June 1975. Paper at VIII International Conference on Photochemistry, Edmonton, Canada, Aug. 1975.
- [6] K. Uchida, I. Yamazaki and H. Baba, Chem. Phys. Letters, 38, 133 (1976).
- [7] F. Lahmani, A. Tramer and C. Tric, J. Chem. Phys., 60, 4431 (1974).
- [8] C. Parmenter, private communication.

TIME RESOLVED EMISSION SPECTRA OF LOW PRESSURE AROMATIC MOLECULES

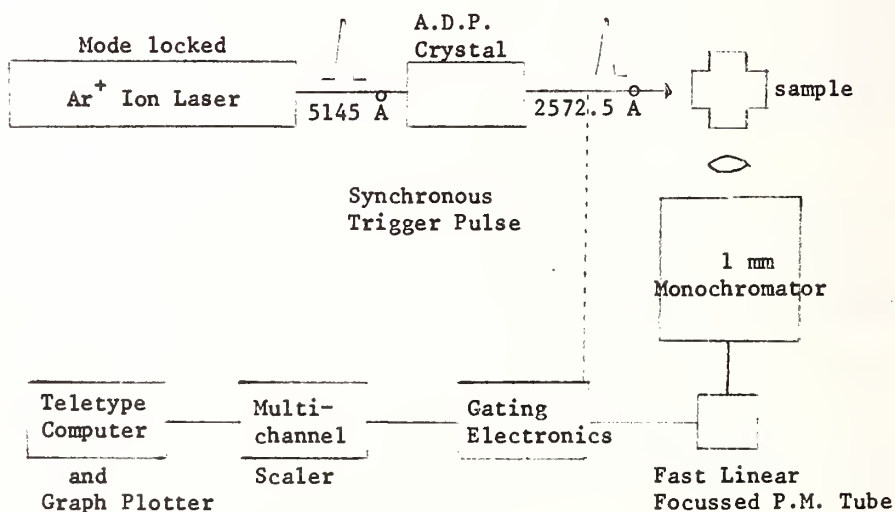
M. D. Swords, A. W. Sloman, and D. P. Phillips

Department of Chemistry
The University
Southampton SO9 5NH, U.K.

An apparatus has been constructed which has enable us to obtain medium resolution time resolved fluorescence spectra of low pressure gases. The principal experimental features are:

- (i) Mode-locked Ar^+ ion laser with A.D.P. frequency doubling crystal.
- (ii) 1 metre monochromator (8 Å/mm dispersion) and fast linear focussed photomultiplier detection.
- (iii) Nanosecond time resolution gating electronics.
- (iv) Multichannel scaler

A schematic diagram of the experimental assembly is illustrated below.



¹Figures in brackets indicate literature references at the end of this paper.

The principal features to note are:

- (i) The laser is a Spectra Physics 166/366 fitted with a combination mode-locker and cavity dump. This enables pulse repetition rates from single shot to 100 MHz to be generated. The integrated average power for the 5145 Å line is typically 7-800 mW at 5 MHz for the 10 ns (f.w.h.m.) gaussian cavity dumped pulses. This decreases to 50 mW average of 500 ps mode-locked pulses at the same repetition rate. Frequency doubling is 2-3% efficient and reduces the pulse width by a factor of $\sqrt{1/2}$ in the normal manner.
- (ii) The gating system, based on Emitter Coupled Logic circuitry is of novel design and has been reported elsewhere [1]¹. Information can be processed at the rate of 5 MHz with a minimum operating gate width of the order of 1 ns. Output is digital and is stored in a multichannel scaler (Northern NS600) but a D.A.C. and chart recorder can also be used.
- (iii) Frequency doubling is by a 5 cm temperature tuned A.D.P. crystal; the monochromator is a Rank Precision Monospek 1000 and detection is with an E.M.I. 9594 fast linear focussed photomultiplier.

Intra and intermolecular processes in polyatomic molecules, particularly aromatic molecules, has been an active and fruitful field of research in recent years. Theoretical work (Freed [2], Jortner [3], Rice [4], and many others) has developed a framework which experiment [5-7] has tested and amplified. This is particularly true for the case of single vibronic level (SVL) excitation of low pressure gases.

A logical step from this situation is to the pressure region where collisions perturb the prepared state, especially the intermediate pressure region where vibrational relaxation is on the same time scale as fluorescence.

Freed [8], following an earlier technique of Montrall and Shuler [9], developed a model describing the relaxing polyatomic molecule which reduced the molecule to one effective oscillator. Assuming the processes occurring on collision were $n = 0 \pm 1$ "vibrational quantum" change, he derived a generating function which allowed, from output data on fluorescence lifetime versus ΔE , pressure and collision cross-section, best fit to an energy loss per collision.

This model gives good fit for experimental data [10]. However, allowing for the gross nature of the approximations involved, the results are of limited analytical value. A more detailed picture of the time dependence in both absorption [11] and emission [12] has been developed from this model.

We report experimental data on the time resolved fluorescence of benzene and substituted benzenes. Using this data a more detailed analysis of the collisional deactivation of a prepared level can be obtained.

REFERENCES

- [1] A. W. Sloman and M. D. Swords, J. Phys. (E), submitted.
- [2] K. F. Freed, J. Chem. Phys., 52, 1345 (1970).
- [3] J. Jortner, S. A. Rice and R. M. Hochstrasser, Adv. Photochem., 7, 149 (1969).
- [4] W. M. Gelbart, S. A. Rice and K. F. Freed, J. Chem. Phys., 52, 5718 (1970).
- [5] K. G. Spears and S. A. Rice, J. Chem. Phys., 55, 5561 (1971).
- [6] M. G. Rockley and D. Phillips, J. Phys. Chem., 78, 7 (1974).

- [7] A. S. Abramson, K. G. Spears and S. A. Rice, J. Chem. Phys., 56, 2291 (1972).
- [8] K. F. Freed and D. F. Heller, J. Chem. Phys., 61, 3942 (1974).
- [9] E. W. Montroll and K. E. Shuler, J. Chem. Phys., 26, 454 (1957).
- [10] G. S. Beddard, G. R. Fleming, O. L. Gijzeman and G. Porter, Proc. Roy. Soc. (A), 340 519 (1974).
- [11] G. R. Fleming, O. L. Gijzeman and S. H. Lin, J. C. S. Faraday II, 70, 1074 (1974).
- [12] G. R. Fleming, O. L. Gijzeman, K. F. Freed and S. H. Lin, J. C. S. Faraday II, 71, 773 (1974).

STUDIES IN THE MECHANISM OF RADIATIONLESS CONVERSION OF ELECTRONIC ENERGY*

T. A. Gregory and Sanford Lipsky

Department of Chemistry
University of Minnesota
Minneapolis MN 55455

For most polyatomic molecules in condensed phases, excitation to an upper singlet state S_n results ultimately in the production of the lowest excited singlet state S_1 by some non-radiative or succession of non-radiative processes. The $S_n \rightarrow S_1$ conversion must be extremely rapid, at least as compared to S_n emission, since it is usually observed that the major emission originates from S_1 even when there is much larger $S_n \rightarrow S_0$ oscillator strength [1]¹. In the absence of high concentrations of fluorescence quenchers, the $S_1 \rightarrow S_0$ fluorescence spectrum in solution is invariant to excitation wavelength. On the other hand, under the same conditions, the $S_1 \rightarrow S_0$ fluorescence quantum yield may exhibit important variations [2]. These are conveniently expressed by the ratio of the quantum yield when excitation is at some wavelength λ to the yield when excitation is into the first absorption system. This ratio, after suitable correction [2], is usually interpreted to be a measure of the overall efficiency, $\beta(\lambda)$, with which the λ excitation to some state S_n converts to the emitting vibronic levels of the state S_1 , and, as expected from this interpretation, is always observed to be less than or equal to unity.

For dilute solutions of benzene or toluene in some suitable transparent saturated hydrogen solvent (e.g., isooctane), β generally declines as the excitation wavelength decreases and then at a wavelength close to the maximum of the third absorption system (~ 185 - 190 nm) reverses direction and begins to rise [3-6]. For p-xylene and generally more complex molecules, β remains about equal to unity over this entire spectral range [1,2].

The origin of these variations has never really been satisfactorily explained. Clearly there exists for benzene and toluene an inefficiency in the $S_n \rightarrow S_1$ conversion process but its source is unknown. More importantly still, the overall mechanism of the conversion process has never been elucidated. It has generally been conjectured that $S_n \rightarrow S_1$ conversion proceeds via a cascade involving successive $S_n \rightarrow S_{n-1}$ internal conversions but there is, in fact, no experimental proof of this for any polyatomic molecule. Also to be considered is that ionization thresholds in condensed phases [7] may be lowered sufficiently from their gas phase values that for many aromatic molecules, at relatively low excitation energies, the non-radiative conversion to S_1 could importantly involve electron-ion pairs as intermediates in the process. Indeed, Laor and Reinreb, [8] have reported for excitation wavelengths within the third absorption systems of benzene and toluene, a decrease in β in the presence of electron-scavenging additives. Also Fuchs, Heisel and Voltz [9] have conjectured that the upswing in β of benzene and toluene at ~ 180 nm is somehow due to the onset there of an autoionization.

*Figures in brackets indicate literature references at the end of this paper.

In two recent publications we reported observation of a very weak $S_3 \rightarrow S_0$ and $S_2 \rightarrow S_0$ fluorescence from a number of aromatic molecules when excited into their third absorption systems at 184.9 nm [10, 11]. With the capability now of monitoring the emission from the three electronic states S_3 , S_2 and S_1 rather than just the terminal state S_1 , we have begun a series of studies directed towards the elucidation of the mechanism of $S_0 \rightarrow S_1$ radiationless conversion. Our first results for p-xylene are presented below.

The fluorescence quantum yields of p-xylene in isooctane excited at 184.9 nm have been determined for the transitions $S_3 \rightarrow S_0$ (Φ_3), $S_2 \rightarrow S_0$ (Φ_2) and $S_1 \rightarrow S_0$ (Φ_1) as functions of the concentration of p-xylene (c_x) and of the concentration of added quenchers (CCl_4 , $CHCl_3$, $c - C_7F_{14}$) and compared with the $S_1 \rightarrow S_0$ fluorescence quantum yield (Φ_1) for excitation at 253.7 nm in the same solutions. Also vapor fluorescence quantum yields have been re-determined for the $S_3 \rightarrow S_0$ and $S_2 \rightarrow S_0$ transitions. It has been found that the total non-radiative decay rate constants of S_3 ($2.5 \times 10^{14} \text{ sec}^{-1}$) and of S_2 ($1.0 \times 10^{13} \text{ sec}^{-1}$) are essentially the same for dilute solution and vapor phases. Also it is found that in dilute solution, Φ_3 is independent of concentration of quencher whereas Φ_2 is strongly quenched and to about the same extent as is the ratio $\beta = \Phi_1/\Phi_3$. In more concentrated solutions ($c_x \gtrsim 3 \text{ M}$), Φ_3 rapidly declines to unobservable levels whereas Φ_2 and β appear to increase-but only slightly. On the basis of these results the following is concluded for a dilute solution of p-xylene in isooctane excited into S_3 (at 184.9 nm); i) the S_3 state either radiates ($k_r = 3.0 \times 10^9 \text{ sec}^{-1}$) or makes internal conversion to S_2 ($k = 2.5 \times 10^{14} \text{ sec}^{-1}$). No autoionization occurs nor do any other decay channels such as $S_3 \rightarrow S_1$ or $S_3 \rightarrow S_0$ have appreciable probability; ii) The S_2 state either radiates ($k_r = 1.3 \times 10^8 \text{ sec}^{-1}$), makes internal conversion to S_1 ($k = 1.0 \times 10^{13} \text{ sec}^{-1}$) or autoionizes ($k \gtrsim 10^{14} \text{ sec}^{-1}$). All other decay channels are of negligible importance; iii) In the absence of quencher, the ejected electron returns to the parent positive ion to regenerate S_2 and not a lower state. In the presence of quencher the electron is scavenged and no longer can contribute to any emission. Possible mechanisms for the disappearance of Φ_3 at high c_x are considered. Preliminary results for benzene and toluene will also be presented.

* This work was supported by the U. S. Energy Research and Development Administration, Document No. C00-913-61.

REFERENCES

- [1] J. B. Birks, Photophysics of Aromatic Molecules (Wiley-Interscience, London, 1970) and references cited therein.
- [2] C. W. Lawson, F. Hirayama and S. Lipsky, J. Chem. Phys. 51, 1590 (1969).
- [3] C. L. Braun, S. Kato and S. Lipsky, J. Chem. Phys. 39, 1645 (1963).
- [4] S. Feinleib, Ph.D. Dissertation, University of Minnesota, 1965.
- [5] U. Laor and A. Weinreb, J. Chem. Phys. 43, 1565 (1965).
- [6] J. B. Birks, J. C. Conte, and G. Walker, J. Phys. B (Proc. Phys. Soc.) Ser. 2,
- [7] R. C. Jarnagin, Accts. Chem. Res. 4, 420 (1971) and references cited therein.
- [8] U. Laor and A. Weinreb, J. Chem. Phys. 50, 94 (1969).
- [9] C. Fuchs, F. Heisel and R. Voltz, J. Phys. Chem. 75, 3867 (1972).
- [10] F. Hirayama, T. A. Gregory and S. Lipsky, J. Chem. Phys. 58, 4696 (1973).
- [11] T. A. Gregory, F. Hirayama and S. Lipsky, J. Chem. Phys. 58, 4697 (1973).

PHOTOSENSITIZATION OF THE 2-BUTENES BY BENZALDEHYDE IN THE GAS PHASE

A. J. Yarwood

Department of Chemistry
McMaster University
Hamilton, Ontario, Canada

G. R. De Mare and M. Termonia

Laboratoire de Chimie Physique Moleculaire
Faculte des Sciences
Universite Libre de Bruxelles
50 av. F.-D. Roosevelt
B-1050 Brussels, Belgium

The sum of the quantum yields of the benzaldehyde photosensitized ($\lambda = 366$ nm) *cis*-*trans* and *trans*-*cis* isomerizations for both the 1,3-pentadienes (independent of pressure over the range studied: 10 - 400 Torr) and the 1,2-dichloroethylenes (for substrate pressures ≥ 100 Torr) is near unity, indicating that the quantum yield for intersystem crossing in benzaldehyde irradiated at 366 nm is also near unity [1, 2]¹. Supporting evidence for this high intersystem crossing yield for benzaldehyde in the gas phase was given by Berger, Goldblatt and Steel [3] who found $\phi(C_5) \approx 0.85$ for the benzaldehyde sensitized decomposition of 2,3-diazabicyclo (2.2.1) hept-2-ene.

The fall-out in the quantum yields of isomerization of 1,2-dichloroethylene with increasing pressure below 100 Torr was interpreted as being the consequence of the competition of unimolecular deactivation steps of triplet benzaldehyde with the bimolecular energy transfer [1]. That benzaldehyde phosphorescence actually competes with the energy transfer to 1,2-dichloroethylene has now been confirmed with laser and flash excitation sources.

Preliminary competition experiments have shown that energy transfer from triplet benzaldehyde to *cis*-1,2-dichloroethylene, requiring an average of 10^4 collisions [1], proceeds at about 1/40 the rate of energy transfer to *trans*-1,3-pentadiene. This was not expected because the energy transfer to 1,2-dichloroethylene is either slightly endothermic or thermoneutral while the transfer to 1,3-pentadiene is exothermic by over 10 kcal/mole. For the 2-butenes the energy transfer from triplet benzaldehyde should be endothermic by about 4 to 6 kcal/mole. Surprisingly, competition experiments showed that energy transfer to both *cis*- and *trans*-2-butene proceeds at about 1/35 the rate of energy transfer to *trans*-1,3-pentadiene (it is thus slightly faster than the energy transfer to 1,2-dichloroethylene). We have therefore undertaken a detailed study of the benzaldehyde sensitized isomerization of the 2-butenes in the gas phase.

¹ Figures in brackets indicate literature references at the end of this paper.

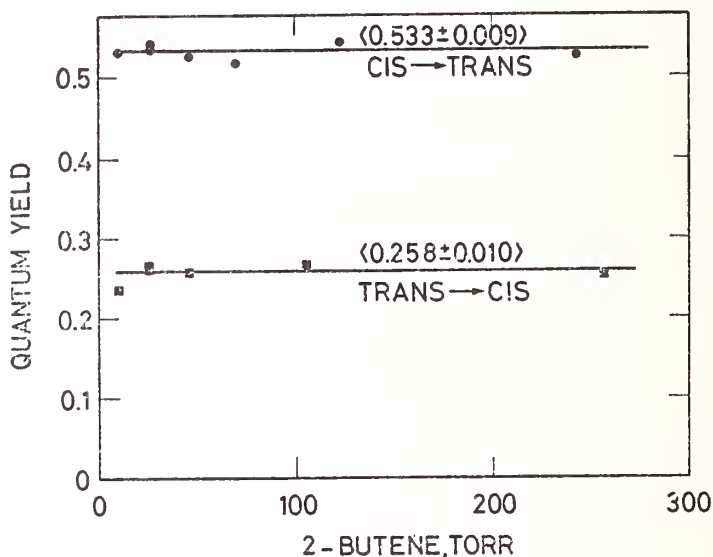
Experimental

The experiments were performed using a cylindrical Pyrex cell (11.9 cm long; 3.8 cm diameter) which was enclosed in a box fitted with glass windows. The temperature was regulated at 60.00 ± 0.05 °C. The light source, a Philips Philora HPK 125 watt "Wood" lamp, supplied an incident intensity of $0.46 \pm 0.02 \times 10^{-9}$ Einstein $\text{cm}^{-2} \text{s}^{-1}$ at $\lambda = 366$ nm (the mercury lines, 365.0 - 366.3 nm). The absorption coefficient of benzaldehyde vapour for this light is $\epsilon(\text{decimal}) = 4.4 \text{ cm}^{-1} \text{l mole}^{-1}$ [4].

Results and discussion

Benzaldehyde sensitization of the 2-butenes at 366 nm and 60.0 °C leads only to geometric *cis* \rightarrow *trans* isomerization. No extraneous peaks were observed when the reaction mixture was analyzed by gas chromatography with a flame ionization detector. Also, prolonged irradiation causes no observable (~ 0.1 Torr) pressure change in the reaction cell.

The quantum yields of the *cis* \rightarrow *trans*, ($\phi(\text{C} \rightarrow \text{t})$), and *trans* \rightarrow *cis* ($\phi(\text{t} \rightarrow \text{c})$), isomerizations were determined under initial conditions (less than 2% isomerization) for 2-butene pressures ranging from 9.9 to 250 Torr and benzaldehyde pressures ranging from 3.3 to 8.2 Torr. $\phi(\text{c} \rightarrow \text{t}) = 0.533 \pm 0.009$ and $\phi(\text{t} \rightarrow \text{c}) = 0.258 \pm 0.010$, independent of the 2-butene pressure (see Figure). Thus $\phi(\text{c} \rightarrow \text{t})/\phi(\text{t} \rightarrow \text{c}) = 2.07 \pm 0.11$.



The ratios of the quantum yields or of the initial rates for 2-butene isomerization are given for a few sensitizers. The increase in the ratio *c* \rightarrow *t*/*t* \rightarrow *c* indicates that the branching ratio for triplet 2-butene is different for sensitizers with triplet energy below 80 kcal/mole or that the sensitization mechanism has changed.

Sensitizer	E_T , Kcal/mole	Ratio $c \rightarrow t / t \rightarrow c$	Ref.
Benzaldehyde	71.9	2.07	This work.
Sulfur dioxide	73.4	2	5
Pyrazine (313 nm)	76	1.60	6
Benzene	84.4	1.02	7
Cadmium	87.7	1.00	8, 10
Mercury	112.7	1.00	9, 10

Financial aid from the N.R.C. (Canada), the F.N.R.S. (Belgium) and N.A.T.O. is gratefully acknowledged.

REFERENCES

- [1] De Mare, Fontaine, Huybrechts and Termonia, J. Photochem. 1 (1972/73) 289.
- [2] Termonia, D. Sc. Thesis, U.L.B. 1976, in preparation.
- [3] Berger, Goldblatt and Steel, J.A.C.S., 95 (1973) 1717.
- [4] De Mare, Fontaine and Huybrechts, Bull. Soc. Chim. Belges, 81 (1972) 171.
- [5] Penzhorn and Gusten, Z. Naturforsch., 27a (1972) 1401; Demerjian and Calvert, Int. J. Chem. Kinetics, VII (1975) 45.
- [6] Jones and Brewer, J.A.C.S., 94 (1972) 6310; Ivanoff, Lahmani, Delouis and Le Gouill, J. Photochem., 2 (1973) 199.
- [7] Lee, Denschlag and Haninger, J. Chem. Phys., 48 (1968) 4547.
- [8] Hunziker, J. Chem. Phys., 50 (1969) 1294.
- [9] Cundall, Prog. Reaction Kinetics, 2 (1964) 165; Cundall and Palmer, Trans. Faraday Soc., 56 (1960) 1211; Termonia and De Mare, Chem. Phys. Letters, 25 (1974) 402.
- [10] Tsunashima and Sato, Bull. Chem. Soc. Japan, 41 (1968) 284.

NEAR INFRARED DETECTION OF PEROXYL RADICALS IN
MERCURY PHOTSENSITIZED REACTIONS

Heinrich E. Hunziker

IBM Research Laboratory
5600 Cottle Road
San Jose, California 95193

While peroxy radicals play a pervasive role in low temperature oxidation and photo-oxidation processes, our knowledge about these transient species has been relatively limited due to difficulties in applying most of the powerful free radical monitoring techniques to them. This situation can be improved by making use of the unique property of specific electronic absorption bands in the 1 to 2 μm region for detection of peroxy radicals. We have found that these bands can be observed by phase sensitive detection of absorption when a modulated concentration of the radicals is generated in a mercury photosensitized reaction. This method has made it possible to observe the lowest excited electronic state of HO_2 with sufficient details of vibrational and rotational structure to estimate its geometry and illuminate its chemical nature.

More recently we have also observed analogous electronic band systems of CH_3O_2 , $\text{C}_2\text{H}_5\text{O}_2$, etc., and $\text{CH}_3\cdot\text{CO}\cdot\text{O}_2$, in the same frequency region but with characteristic shifts of the electronic term energies relative to HO_2 and interesting differences of vibronic structure. Just as for HO_2 these spectra are dominated by a progression of the O-O vibration, but additional structure due to internal rotation around C-O bond is introduced by changes of the internal rotational barrier between the ground and first excited electronic states.

Since these band systems occur in a generally empty spectral region and are specific for particular peroxy radicals, they are very useful for determining radical formation, reaction pathways and kinetics in photochemical and other types of processes. Applications of this kind will be illustrated with several examples.

REACTIONS OF HYDROGEN ATOMS WITH FLUORINATED KETONES

D. W. Grattan and K. O. Kutschke

Division of Chemistry
National Research Council of Canada
Ottawa, Canada K1A 0R6

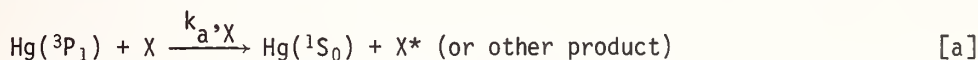
In an unpublished study of the reactions of CF_3 radicals, produced by the near uv photolysis of $(\text{CF}_3)_2\text{CO}$ (HFA), with H_2 , the product ratio $(\text{CF}_3\text{H} + \text{C}_2\text{F}_6)/2\text{CO}$ rose beyond the expected limit of one for some conditions. A radical exchange reaction between H atoms and the ketone, which formed CF_3 radicals, was thought to be responsible for this anomaly.

In order to study such a possible reaction, H atoms were generated in the presence of HFA by the Hg-sensitized decomposition of H_2 or of C_3H_8 . Attempts were made to evaluate relative rate constants by competitive methods. Each competition studied yielded unexpected kinetic results; possible mechanistic explanations are suggested.

The constants for the quenching of $\text{Hg}(^3\text{P}_1)$ by C_2H_4 , C_3H_8 , $n\text{-C}_4\text{H}_{10}$ and HFA were determined with the nitrous oxide method.

Experimental. A conventional apparatus was employed which contained a quartz reaction cell ($\sim 200 \text{ cm}^3$, optical path 10 cm) illuminated by a low pressure Hg lamp. The cell was part of a loop consisting of a glass circulating piston pump, U-tube cold trap and a second U-tube thermostatted at 26°C and containing a drop of Hg. The loop was connected to apparatus for volume measurement, and for chromatographic and/or mass analysis.

Results. (1) Quenching Constants. Those for C_2H_4 , C_3H_8 and $n\text{-C}_4\text{H}_{10}$ were determined by the N_2O method in the usual way [1,2]¹. The method measures the total quenching constant, $k_{q,X} = k_{a,X} + k_{b,X}$, for compound X, and is based on the diminution in the rate



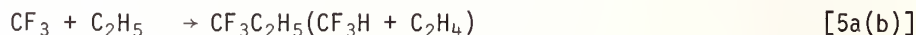
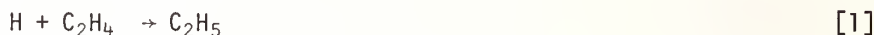
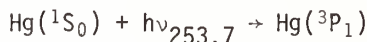
of formation of $\text{N}_2(r_{\text{N}_2})$ when an addend is present during the photodecomposition of N_2O [1, 2].

For HFA, the determination was made in the presence of C_2H_4 , at three ratios of $[\text{C}_2\text{H}_4]/[\text{N}_2\text{O}]$, in order to scavenge the O atoms formed. The kinetic analysis yields [c]; results are collected in Table 1.

¹Figures in brackets indicate literature references at the end of this paper.

$$\frac{I_a}{r_{N_2}} = \frac{k_{q,N_2O}}{k_{a,N_2O}} + \frac{k_{q,C_2H_4}}{k_{a,N_2O}} \frac{[C_2H_4]}{[N_2O]} + \frac{k_{q,HFA}}{k_{a,N_2O}} \frac{[HFA]}{[N_2O]} \quad [c]$$

(2) $H + HFA$; method I. A method which had been devised by Cvetanovic [3] for the determination of the rates of addition of H atoms to olefins relative to that for $H + C_2H_4$ was employed. H atoms were generated by the $Hg(^3P_1)$ decomposition of 600 torr of H_2 and their addition to a constant amount of C_2H_4 was in competition with that to other olefins (here to HFA). The yield of $n-C_4H_{10}$, produced by combination of the C_2H_5 formed in the addition $H + C_2H_4$, was measured as a function of $[HFA]/[C_2H_4]$. The standard [3] mechanism and treatment is shown below.



Assuming that all radical-radical interaction rates are equal, and that there is no direct quenching of $Hg(^3P_1)$ by either C_2H_4 or HFA, then, representing the rate of formation of $n-C_4H_{10}$ in the presence and in the absence of HFA by (rBu) and $(rBu)_0$ respectively,

$$((rBu)_0^{1/2} - (rBu)^{1/2})/(rBu)^{1/2} = k_2[HFA]/k_1[C_2H_4].$$

The results (Figure 1), obtained at four pressures of C_2H_4 , show that this function depends on the absolute pressures of C_2H_4 and/or HFA and not solely on their ratio. Presumably this arises from the neglect of [6].



Resolving the kinetics including [6] and deleting [2] yields:

$$(rBu)_0^{1/2}((rBu)_0^{1/2} - (rBu)^{1/2})/(rBu)^{1/2} = ((1/2)k_6k_3^{1/2}/k)[HFA]$$

where $2k \equiv 2(k_{3a} + k_{3b}) = k_{5a} + k_{5b} = k_4$. This plot also is shown in Figure 1 which shows that the points now all coalesce about a single line. If $\log k$ is taken as $13.5(\ell \text{ mol}^{-1} \text{ s}^{-1} \text{ units})$, $k_6 = 1.0 \times 10^8 \ell \text{ mol}^{-1} \text{ s}^{-1}$.

During prolonged photolyses more C_2H_4 and HFA were consumed than is predicted by the mechanism; this is evidence of some additional reaction(s) between HFA and C_2H_4 .

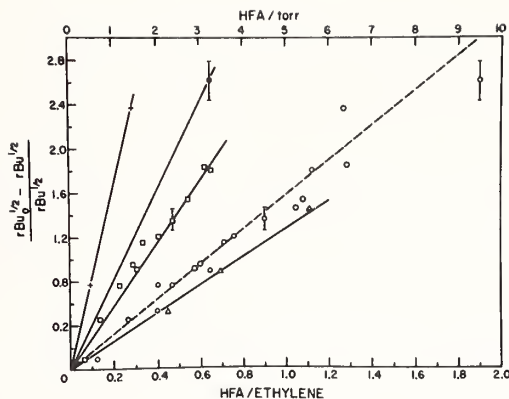
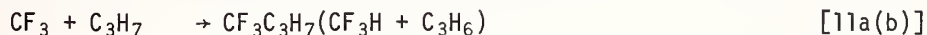
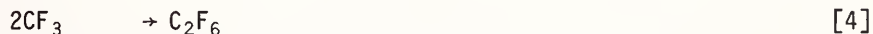
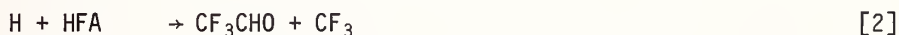
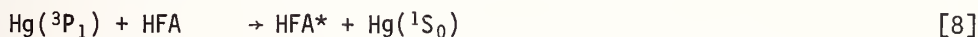
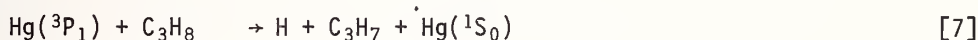


Figure 1. Points refer to $[C_2H_4] = 20$ (+), 15 (), 10 () and 5 (Δ) torr, lower abscissa. Open circles refer to upper abscissa.

(3) H + HFA; method II. In an attempt to overcome the disadvantages of the previous method, H atoms were generated from the quenching of $Hg(^3P_1)$ by C_3H_8 [4,5]. The rate of H_2 formation was studied as a function of $[HFA]/[C_3H_8]$; the following mechanism was expected to apply.



$$\frac{r_{H_2}^0}{r_{H_2}} = (1 + k_2[HFA]/k_9[C_3H_8])(1 + k_7[HFA]/k_8[C_3H_8]).$$

From (1), k_7/k_8 is 10.2 and Baldwin [6] gives $k_9 = 1.27 \times 10^5 \text{ l mol}^{-1} \text{ s}^{-1}$. At low $[HFA]/[C_3H_8]$ the measured k_9/k_2 were reasonably constant and give $k_2 = 8.5 \times 10^5 \text{ l mol}^{-1} \text{ s}^{-1}$.

Above $[HFA]/[C_3H_8] \approx 0.04$, the k_9/k_2 so deduced increase very rapidly; presumably additional processes become important at higher $[HFA]/[C_3H_8]$ ratios.

(4) Product Analysis. Heavier products of the overall reaction (600 torr H_2 , 10 torr HFA) were studied. Many products were detected, most due to secondary processes; F_3CHO was identified.

Conclusions. The values of the quenching constants agree well with those of other workers. This gives some confidence to the $k_{q,HFA} = 13 \times 10^{10} \text{ l mol}^{-1} \text{ s}^{-1}$; cf the much larger value of $39 \times 10^{10} \text{ l mol}^{-1} \text{ s}^{-1}$ for acetone measured by Cvetanović [1].

The result that addition of C_2H_5 to HFA proceeds at some 1000 times the rate of that of H atoms also is consistent with other work [7].

Table 1. Quenching Constants, $k_q^{(a)}$

Cmpd.	This work ^(b)	Others ^(b)	Others ^(c)
HFA	13.0	-	-
C_2H_4	31.0	30.0 ^(b)	-
C_3H_8	1.27	1.13 ^(d)	1.28 ^(a)
$n-C_4H_{10}$	3.35	3.65 ^(b)	3.75 ^(e) , 3.83 ^(f)

(a) k_q in $10^{-10} \text{ l mol}^{-1} \text{ s}^{-1}$.

(b) Based on $k_{q,N_2O} = 14.3$, reference [2].

(c) Based on $k_{q,C_2H_4} = 30.0$, reference [2].

(d) Reference [8].

(e) Reference [9].

(f) Reference [10].

REFERENCES

- [1] R. J. Cvetanović, J. Chem. Phys. 23, 1208 (1955).
- [2] R. J. Cvetanović in Progress in Reaction Kinetics, ed. G. Porter, vol. 2, p. 39. MacMillan Co., New York, 1964.
- [3] R. J. Cvetanović and L. C. Doyle, J. Chem. Phys. 50, 4705 (1969).
- [4] R. A. Back, Can. J. Chem. 37, 1834 (1959).
- [5] R. J. Cvetanović, W. E. Falconer and K. R. Jennings, J. Chem. Phys. 35, 1225 (1961); K. R. Jennings and R. J. Cvetanović, J. Chem. Phys. 35, 1233 (1961).
- [6] R. R. Baldwin, Trans. Farad. Soc. 60, 527 (1964).
- [7] A. S. Gordon, W. P. Norris, R. H. Knipe and J. H. Johnston, Int. J. Chem. Kinetics 7, 15 (1975).
- [8] Y. Rousseau and H. E. Gunning, Can. J. Chem. 41, 465 (1963).
- [9] G. London, A. C. Vikis and D. J. Le Roy, Can. J. Chem. 48, 1420 (1970).
- [10] J. V. Michael and G. N. Suess, J. Phys. Chem. 78, 5 (1974).

THE REACTION OF NH_2 WITH OLEFINS STUDIED BY FLASH PHOTOLYSIS

R. Lesclaux and Pham Van Khê

Laboratoire de Chimie Physique A
Universite de Bordeaux I
33405 Talence (France)

In spite of the large amount of studies on the photochemistry or radiochemistry of ammonia, little attention has been given to the reactivity of NH_2 radical, even though this radical is generally an intermediate in the dissociation processes of ammonia. However, the few available data concerning the NH_2 reactivity, indicate that this radical is weakly reactive compared to the isoelectronic OH radical.

In our first experiments, we have studied the reactions $\text{NH}_2 + \text{NO}$ [1]¹ and $\text{NH}_2 + \text{NH}_2 + \text{M}$ [2] which are fast processes, by using a conventional flash photolysis apparatus. It is particularly important to know the kinetics of the recombination process since it often competes with other NH_2 slower reactions. The rate constants of this process were determined in the fall off region (0-1000 Torr of N_2), by using different third bodies (NH_3 , N_2 and Ar) and in the temperature range 300-500 K [2].

The reaction of NH_2 with olefins was studied by flash photolysis, the NH_2 absorption being measured by using a CW dye laser operated in single mode. The reaction being fairly slow, it was never possible to completely eliminate the radical-radical recombination processes by using the conventional apparatus (white analysing light source + monochromator) because the NH_2 concentration was too high. The CW dye laser was then used in order to increase the sensitivity of radical detection by resonance absorption (laser spectral width narrower than the absorption line).

The flash photolysis set up is essentially the same as the one previously described [1]. NH_2 radicals are produced by photolysis of ammonia, using two flash lamps delivering 40-60 joules in 20 μs . An absorption optical path of about 30 m is obtained by placing the reaction cell in a multipass system. The temperature can be varied from room temperature up to 240°C.

The single mode CW dye laser, Spectra Physics model 580 has a spectral width lower than 50 MHz. Absorption measurements were performed at 597.73 nm which corresponds to one of the strongest NH_2 absorption line.

The signals are detected by using two photodiodes and a differential amplifier on the oscilloscope. One of the photodiodes measures the absorption signal, the other, the reference laser intensity. This system reduced considerably the perturbations due to the laser intensity variations and allows good measurements of absorption less than 10%.

An important increase in the sensitivity of NH_2 radical detection was obtained by comparison to the experiments using an analysing light source. For an equivalent absorp-

¹Figures in brackets indicate literature references at the end of this paper.

tion and signal to noise ratio the NH_2 concentration was about 30 times smaller with the laser. Moreover, the measured optical density is now a linear function of the radical concentration.

The initial concentration was evaluated by measuring the second order kinetics of NH_2 recombination which rate constant was determined in various conditions [2]. The NH_2 concentration was found to be from $2 \cdot 10^{-9}$ to 10^{-8} M for 10% of light absorption, according to the pressure broadening of the absorption line, for pressures up to 700 Torr.

This important increase in the sensitivity of radical detection is essentially due to the fact that absorption measurements can be made at the maximum of the absorption line and also to the large number of pass in the cell possible with the laser beam. A new increase in the sensitivity should be obtained by averaging the signals from a large number of flashes.

The sensitivity of detection obtained in our system is in the same range as that of most other methods of radical detection with the exception of the laser excited fluorescence which is much more sensitive at low pressure. However, the very efficient collisional quenching of the $\text{NH}_2(^2\text{A}_1)$ excited state reduces considerably the fluorescence intensity at high pressure [3]. The advantage of resonance absorption is that it is not too sensitive to experimental conditions and can then be applied to various systems (atmospheric conditions, flames etc ...).

The reaction kinetics of NH_2 with ethylene, propylene and 1-butene were determined in the temperature range 300-500 K. The pressure of olefins were varied from 10 to 100 Torr. In all conditions the disappearance kinetics of NH_2 were first order and the reciprocal lifetimes were a linear function of the olefin pressure (figure 1). Thus no radical recombination contributed to the NH_2 disappearance. The temperature dependence of the rate constants (figure 2) is accounted for by the following Arrhenius expressions:

$$k_{\text{NH}_2 + \text{C}_2\text{H}_4} = 1.2 \cdot 10^8 \exp - 3.95 (\pm 0.2)/RT \quad \text{M}^{-1}\text{s}^{-1}$$

$$k_{\text{NH}_2 + \text{C}_3\text{H}_6} = 2.9 \cdot 10^8 \exp - 4.3 (\pm 0.2)/RT \quad \text{M}^{-1}\text{s}^{-1}$$

$$k_{\text{NH}_2 + 1-\text{C}_4\text{H}_8} = 2.8 \cdot 10^8 \exp - 4.1 (\pm 0.2)/RT \quad \text{M}^{-1}\text{s}^{-1}$$

which correspond to the following room temperature rate constants. 1.6×10^5 , 2.2×10^5 , $3.0 \times 10^5 \text{ M}^{-1}\text{s}^{-1}$ for C_2H_4 , C_3H_6 , and $1-\text{C}_4\text{H}_8$ respectively. Activation energies are given in kcal/mole and the errors on the rate constants are estimated to be smaller than 20%.

The reaction is thus fairly slow at room temperature compared to the equivalent reaction of the isoelectronic OH radical. The difference is essentially due to the significant activation energy found in the case of NH_2 radicals whereas there is no activation energy and even a slight negative temperature coefficient in the case of OH radical [4].

No information is given in this work about the products of the reaction. However, the addition reaction is the most likely to occur since hydrogen abstraction reactions from hydrocarbons by NH_2 radicals seem to be very slow: $< 10^3 \text{ M}^{-1}\text{s}^{-1}$ [5].

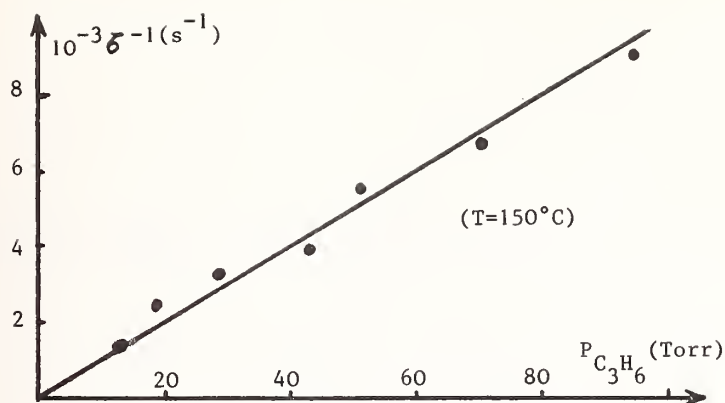


Figure 1. Reciprocal NH_2 lifetime as a function of propylene pressure.

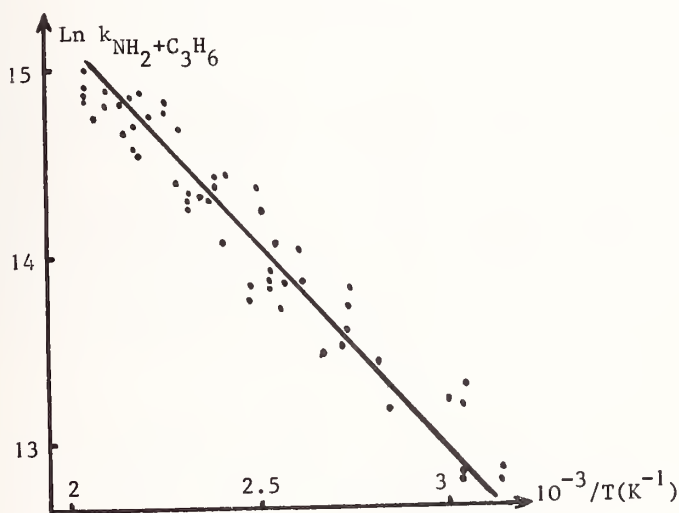


Figure 2. Arrhenius plot for the reaction of NH_2 with propylene.

Experiments are still in progress in order to extend this study to a series of unsaturated hydrocarbons.

REFERENCES

- [1] R. Lesclaux, P. V. Khé, P. Dezaudier, and J. C. Soullignac, *Chem. Phys. Letters* **35**, 493 (1975).
- [2] P. V. Khé, J. C. Soullignac, and R. Lesclaux - to be published.
- [3] J. B. Halpern, G. Hancock, M. Lenzi, and K. H. Welge, *J. Chem. Phys.* **63**, 4808 (1975).
- [4] R. Atkinson and J. N. Pitts, Jr., *J. Chem. Phys.* **63**, 3591 (1975).
- [5] R. Lesclaux and P. V. Khé, *J. Chem. Phys.* **70**, 119 (1973).

DETECTION AND REACTIONS OF $\text{NH}(\text{X}^3\Sigma^-)$ RADICALS IN THE VACUUM UV FLASH
PHOTOLYSIS OF NH_3 USING RESONANCE FLUORESCENCE

I. Hansen, K. Hoinghaus, C. Zetzsch and F. Stuhl

Physikalische Chemie I
Ruhr-Universität
4630 Bochum, West Germany

In the course of an investigation of the kinetics of imino radicals we have recently studied the quenching of metastable NH and ND radicals in their ($\text{b}^1\Sigma^+$) state [1]¹. In the present paper we would like to describe a method to study the kinetics of ground state $\text{NH}(\text{X}^3\Sigma^-)$ radicals.

Kinetic data on reactions of $\text{NH}(\text{X}^3\Sigma^-)$ radicals are sparse. There are only a few estimates of rate constants in the literature which are based on experimental work such as those for the reactions with NH_3 , N_2H_4 , NH , NO , HN_3 , O_2 , C_2H_4 and C_3H_6 . None of these rate constants have been obtained from more than one experiment. In the most direct studies, previously $\text{NH}(\text{X}^3\Sigma^-)$ was generated either by electron bombardment or flash photolysis of NH_3 or HN_3 and was detected by time resolved absorption spectroscopy. With these techniques concentrations of NH in the approximate range of $3 \times 10^{13} \text{ cm}^{-3}$ to $2 \times 10^{15} \text{ cm}^{-3}$ were produced and lifetimes $\tau^{1/2} \leq 0.2 \text{ ms}$ were observed. In the presence of NH_3 it was concluded that NH is removed efficiently by NH_3 [2] and even more efficiently by NH [3].

In the present study the apparatus consisted of a pulsed light source, a reaction chamber, an NH emission lamp and a resonance fluorescence detection system. A similar photolysis apparatus for the study of the kinetics of OH has been described previously [4]. Vacuum uv light pulses ($\tau^{1/2} = 1.5 \mu\text{s}$) were generated by discharging a capacitor (5 to 60 J) with a repetition frequency of about 0.5 Hz. $\text{NH}(\text{X}^3\Sigma^-)$ radicals were produced by photolysing mixtures of NH_3 , inert gas and reactive gas through a LiF window ($\lambda > 105 \text{ nm}$). The approximate range of the initial concentration of NH was estimated to be from $2 \times 10^{11} \text{ cm}^{-3}$ to $2 \times 10^{12} \text{ cm}^{-3}$.

The NH resonance emission was generated by passing a small flow of a mixture of NH_3 at 0.35 Torr and Ar at 1.6 Torr through a microwave discharge. The $\text{NH}(\text{A}^3\Pi \rightarrow \text{X}^3\Sigma^-)$ - emission of the lamp is shown in Figure 1. The dominant feature of this spectrum is the Q-branch of the (0;0)-band. Furthermore the R- and P-branches of this band and the Q-branch of the (1;1)-band are clearly observed in this spectrum. Care had to be taken to avoid generation of $\text{N}_2(\text{C}^3\Pi; \nu'=0 \rightarrow \text{B}^3\Pi; \nu''=0)$ emission at 337 nm in the discharge. It should be noted also that under the present conditions emission from $\text{NH}(\text{c}^1\Pi \rightarrow \text{a}^1\Delta)$ at 325 nm appears to be absent.

¹Figures in brackets indicate literature references at the end of this paper.

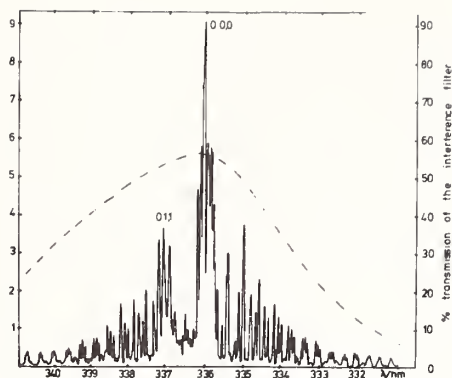


Figure 1. Emission spectrum of the NH lamp. The transmission of the interference filter used is included.

The resonance fluorescence from NH radicals was monitored at right angles to the incident flash light and to the NH resonance light. It was detected by a photomultiplier through an interference filter, the transmission of which is included in Figure 1 (dashed line). The signal of the photomultiplier was fed to a multichannel scaler where up to 64 single runs were accumulated and averaged.

Several experiments were performed to show that the observed fluorescence signal indeed originates from the presence of $\text{NH}(\text{X}^3\Sigma^-)$ radicals. In the present system NH radicals can be observed up to 1 s after the light pulse. In the presence of NH_3 the removal of $\text{NH}(\text{X}^3\Sigma^-)$ appears to be rather complex. Figure 2 shows two decay curves of the NH resonance fluorescence under the same experimental conditions but with and without inert gas present. The semilogarithmic plot shows that the decay of NH cannot be accounted for by a single first order reaction. In Figure 3 the inverse of the intensity of the fluorescence is plotted vs. time for these two runs. Similarly this figure shows that no

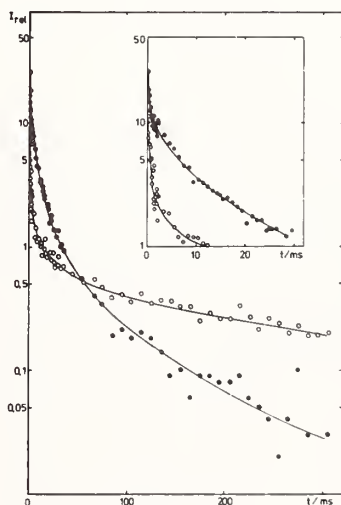


Figure 2. Semilogarithmic plot of the resonance fluorescence intensity (arb. units) vs. time. Experimental conditions: 0.15 Torr NH_3 ; 0.15 Torr NH_3 + 700 Torr He.

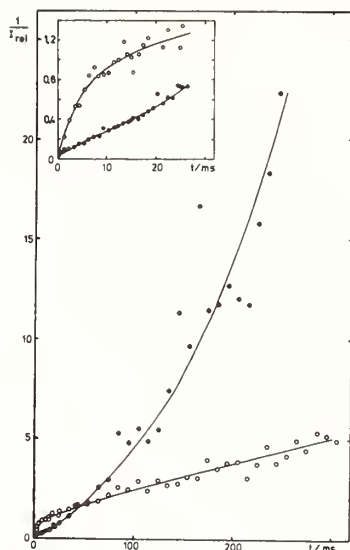


Figure 3. Plots of the inverse of the resonance fluorescence intensity (arb. units) vs. time. Experimental conditions: 0.15 Torr NH_3 ; 0.15 Torr NH_3 + 700 Torr He.

single second order process causes the removal of $\text{NH}(\chi^3\Sigma^-)$. From decay curves like these, limits of rate constants can be obtained for the reactions of NH with NH and with NH_3 . Furthermore, it seems to be likely that NH can survive collisions with the reactor walls during its long lifetime.

Upon addition of NO to this system the NH lifetime decreases resulting in a rate constant for the reaction $\text{NH} + \text{NO}$ [5] in agreement with a value previously reported [6]. These and other results will be discussed.

REFERENCES

- [1] C. Zetzsch, F. Stuhl, Chem. Phys. Letts. 33, 375 (1975).
- [2] K. A. Mantei, E. J. Bair, J. Chem. Phys. 49, 3248 (1968).
- [3] G. M. Meaburn, S. Gordon, J. Phys. Chem. 72, 1592 (1968).
- [4] F. Stuhl, H. Niki, J. Chem. Phys. 57, 3671 (1972).
- [5] C. Zetzsch, F. Stuhl, Chem. Phys. Letts., to be published.
- [6] S. Gordon, W. Mulac, P. Nangia, J. Phys. Chem. 75, 2087 (1971).

INTERPRETATION OF THE ARRHENIUS PLOTS FOR REACTIONS OF OXYGEN ATOMS WITH OLEFINS

R. J. Cvetanovic

Division of Chemistry
National Research Council of Canada
Ottawa, Canada

Relative rates of the ground state oxygen atom, $O(^3P)$, reactions with a number of representative olefins and their variation with temperature were determined in this laboratory almost two decades ago [1]¹. Since that time, and in particularly in the last few years, several techniques have been developed and used to measure the absolute values of the rate constants of these reactions and of their temperature dependences [2-5]. As a result of these developments, the absolute values of the rate constants are now known with great accuracy. However, the reactions are very fast and are therefore generally not affected strongly by temperature. As a consequence, determinations of the Arrhenius parameters are experimentally very demanding. Nevertheless, temperature dependence studies reported in the literature indicate for some of these reactions two somewhat unexpected features: 1) negative values of the Arrhenius energy parameters [2a, 2b] and 2) curved logarithmic Arrhenius plots [3c, 5]. A definitive confirmation of these two observations, especially of the curvatures of the Arrhenius plots, requires precise determinations of the reaction rates over relatively wide temperature intervals. The present paper will report the final results of the recent study [2d] in this laboratory by D. L. Singleton and R. J. Cvetanovic of the temperature dependence of the rates of oxygen atom reactions with several olefins. The major part of the oral presentation will be devoted to a discussion of the observed negative values of the Arrhenius energy parameters and the curvatures of the Arrhenius plots and of the broader implications of these observations. The background experimental information will be briefly summarized in the following.

The determinations of the rate constants have been made by the phase-shift technique [2]. Study of the temperature dependence of the rates was made possible by a considerable further improvement [2c, 2d] in the precision of the measurements, with the standard deviation reduced to about 3%. The reactions of the following olefins were studied: ethylene, propylene, 1-butene, 3-methyl-1-butene, isobutene, cis-2-butene and tetramethylethylene. (The results for tetramethylethylene have been published [2c] and those for the other olefins have been submitted for publication [2d]). When (least squares) linear logarithmic Arrhenius plots are imposed on the experimental points, negative values of the Arrhenius activation energy parameter are obtained for tetramethylethylene, cis-2-butene and isobutene (-0.77, -0.27 and -0.10 kcal/mole, respectively). For ethylene, propylene, 1-butene and 3-methyl-1-butene the Arrhenius activation energies are positive (1.68, 0.72, 0.66 and 0.53 kcal/mole, respectively). For the olefins studied so far by the phase-shift technique the preexponential factors are all very similar (1.2×10^{10} for tetramethylethylene and close to 7×10^9 l.mole⁻¹.sec⁻¹ for the other olefins studied). These results are in very good agreement with the relative data from competitive experiments [1] and, with minor exceptions, with the resonance fluorescence results [3].

¹Figures in brackets indicate literature references at the end of this paper.

Although for the temperature interval (298 - 480 K) of these experiments [2c, 2d] the observed temperature dependences can be approximately expressed empirically by the Arrhenius equation, the data seem to be correlated better by slightly curved logarithmic Arrhenius plots. This is particularly noticeable for the reactions of 3-methyl-1-butene, 1-butene, propylene and isobutene. A theoretical treatment based on the transition state theory shows that the curvatures can be explained by the temperature dependence of the entropies of activation and do not therefore require the postulate [3c] that abstraction of the allylic hydrogen from the olefins competes efficiently with the oxygen atom addition to the olefinic double bond. Great similarity of the overall behavior and of the apparent Arrhenius parameters for propylene, 1-butene and 3-methyl-1-butene in spite of the vastly different lability of the allylic CH bonds rules out an important contribution from the hydrogen abstraction reaction. Product analysis study [2e] for the reactions of oxygen atoms with 1-butene and 3-methyl-1-butene supports this conclusion.

Several explanations have been suggested in the literature for the observed negative values of the Arrhenius activation energy parameter. There is at the moment no conclusive evidence in support of one of these suggestions to the exclusion of the alternative possibilities. One of the potential explanations, suggested originally in connection with the oxygen atom studies in this laboratory, [1, 2a] postulates formation of intermediate molecular complexes ("charge transfer" complexes) between oxygen and olefins. It seems to be consistent with all the currently available experimental observations and will be discussed in some detail.

REFERENCES

- [1] R. J. Cvetanovic, J. Chem. Phys. 30, 19 (1959); *ibid* 33, 1063 (1960); Can. J. Chem. 38, 1678 (1960); Adv. Photochem. 1, 115 (1963).
- [2a] R. Atkinson and R. J. Cvetanovic, J. Chem. Phys. 55, 659 (1971); *ibid* 56, 432 (1972); b) S. Furuyama, R. Atkinson, A. Colussi and R. J. Cvetanovic, Int. J. Chem. Kinet. 6, 741 (1974); c) D. L. Singleton, S. Furuyama, R. J. Cvetanovic, and R. S. Irwin, J. Chem. Phys. 63, 1003 (1975); d) D. L. Singleton and R. J. Cvetanovic (submitted for publication); e) R. J. Cvetanovic and L. C. Doyle (to be published).
- [3a] D. D. Davis, R. E. Huie, J. T. Herron, M. J. Kurylo, and W. Braun, J. Chem. Phys. 56, 4868 (1972); b) D. D. Davis, R. E. Huie, and J. T. Herron, J. Chem. Phys. 59, 628 (1973); c) R. E. Huie, J. T. Herron, and D. D. Davis, J. Phys. Chem., 76, 3311 (1972); d) M. J. Kurylo, Chem. Phys. Lett. 14, 117 (1972).
- [4] F. Stuhl and H. Niki, J. Chem. Phys. 55, 3954 (1971).
- [5] A. A. Westenberg and N. de Haas, Twelfth (International) Symp. Combust., Poitiers, France, 289 (1969).

ABSOLUTE RATE OF THE REACTION OF $O(^3P)$ WITH HYDROGEN SULPHIDE

D. A. Whytock [1]¹ and R. B. Timmons

Department of Chemistry
The Catholic University of America
Washington, DC 20017

and

J. H. Lee [2], J. V. Michael [3], W. A. Payne and L. J. Stief

Astrochemistry Branch
NASA/Goddard Space Flight Center
Greenbelt, Maryland 20771

The rate constant for the reaction of $O(^3P)$ with H_2S has been the subject of considerable interest (K. Schofield, J. Phys. Chem. Ref. Data 2, 25 (1973); I. R. Slagle, F. Biaocchi and D. Gutman, Abstracts of the 12th Int. Symp. on Free Radicals, Laguna Beach, California (1976)), arising in part from the possible importance of this reaction in the chemistry of combustion processes, in polluted terrestrial atmospheres and in the atmosphere of Venus.

Previous investigations, all employing the discharge-flow technique give room temperature rate constants which vary by more than a factor of 3. The results from the two variable temperature studies also do not agree. Gutman and co-workers obtained $k = 3.3 \times 10^{-11} \exp(-4000/1.987 T) \text{ cm}^3 \text{ molecule}^{-1} \text{ sec}^{-1}$ between 250 and 500 K, whereas Hollinden, Kurylo and Timmons (J. Phys. Chem. 74, 988 (1970)) reported $k = 2.9 \times 10^{-13} \exp(-1500/1.987 T) \text{ cm}^3 \text{ molecule}^{-1} \text{ sec}^{-1}$ from 205 to 300 K.

The disagreements noted above, which probably result from inaccurate assessment of the overall reaction stoichiometry, have motivated the present study using the flash photolysis-resonance fluorescence technique for the temporal measurement of $[O]$. This technique allows very low atom concentrations to be used ($< 10^{11} \text{ cm}^{-3}$) and afford experimental conditions under which the first step in a reaction scheme may be isolated. Thus uncertain stoichiometric corrections do not complicate the analysis even in systems like the present where fast secondary reactions can contribute to O atom removal.

The apparatus and techniques have been described in detail previously (R. B. Klemm and L. J. Stief, J. Chem. Phys. 61, 4900 (1974)). In the present study, 3-component mixtures of H_2S , O_2 and argon diluent were flash photolyzed at $\lambda < 136 \text{ nm}$ to produce $O(^3P)$ ($\sim 10^{11} \text{ cm}^{-3}$) in an excess of both H_2S and the source compound, O_2 . Under the pseudo-first-order conditions employed here, with $[H_2S] \gg [O]$, the decay of O atoms may be expressed experimentally as

$$\ln [O] = -k_{\text{observed}} t + \ln [O]_0 \quad (1)$$

¹Figures in brackets indicate literature references at the end of this paper.

where the observed pseudo-first-order rate constant is given by

$$k_{\text{observed}} = k_{bi} [H_2S] + K^* \quad (2)$$

k_{bi} is the bimolecular rate constant which is equal to k_3 in the limit of unit stoichiometry



and K^* is a correction term arising from loss of O atoms by the reaction



and from diffusional loss of O out of the reaction viewing zone. The correction term ($K^* = k_4[O_2][M] + k_d$) was determined independently by flash photolyzing mixtures of O_2 and Ar at the various experimental temperatures and pressures employed in this study. K^* was typically $\sim 15\%$ of k_{observed} .

The evidence of previous work that secondary reactions are important at low $[H_2S]/[O]$ ratios suggested that k_{observed} would exhibit dependence on flash intensity. Preliminary experiments showed that k_{observed} over a range of flash energies equation (1) was strictly followed, with plots of $\ln[O]$ vs t exhibiting good linearity. At higher flash energies, k_{observed} and hence k_{bi} was observed to increase and at the upper limit of flash energy clear bending in the $\ln[O]$ vs t plots was apparent. The increase in k_{bi} at high flash energies is direct evidence of the onset of secondary reactions contributing to the O atom decays. Whichever reactions cause the rate constant k_{bi} to increase, the low intensity limiting k_{bi} is obtained under conditions which are unaffected by competing secondary reactions of O atoms and corresponds to k_3 . Intensity-independent values of k_3 were obtained over a wide range of experimental conditions, a typical example of the data for 400 K being as follows.

Rate Data for the Reaction $O + H_2S$ at 400 K

$\frac{P_{\text{total}}}{\text{torr}}$	$\frac{P_{O_2}}{\text{mTorr}}$	$\frac{P_{H_2S}}{\text{mTorr}}$	Flash Energy J	Number of Experiments	k_3^b $10^{-14} \text{ cm}^3 \text{ molecule}^{-1} \text{ sec}^{-1}$
10	1000	100	9.0-81	6	10.6 ± 1.0
20	2000	200	9.0-56	5	11.7 ± 0.8
50	500	75	9.0-36	4	12.0 ± 0.6
100	1000	150	9.0-20	3	11.9 ± 0.7
200	2000	300	14 -36	3	11.5 ± 0.7
200	667	100	9.0-56	4	11.4 ± 1.1
300	1000	150	9.0-20	2	11.5 ± 1.1
400	1000	100	8.1-81	7	11.3 ± 1.2
					11.4 ± 1.0^a

a - mean value of k_3 at 400 K.

b - error limit in k_3 is the standard deviation.

Mean k_3 values at other temperatures were as follows: 495 K, $(27.4 \pm 2.7) \times 10^{-14}$; 450 K, $(17.1 \pm 1.8) \times 10^{-14}$; 345 K, $(5.42 \pm 0.30) \times 10^{-14}$; 298 K, $(2.97 \pm 0.23) \times 10^{-14}$; 263 K, $(1.31 \pm 0.21) \times 10^{-14}$. The values of k_3 provide the Arrhenius equation $k_3 = (7.24 \pm 1.07) \times 10^{-12} \exp(-3300 \pm 100/1.987 T) \text{ cm}^3\text{molecule}^{-1}\text{sec}^{-1}$. Comparable experiments with D_2S showed that the reaction exhibits a primary isotope effect, in support of a hydrogen abstraction mechanism.

REFERENCES

- [1] On leave from Department of Chemistry, University of Essex, Colchester.
- [2] NAS/NRC Postdoctoral Research Associate.
- [3] NAS/NRC Senior Postdoctoral Research Associate.

KINETICS OF THE REACTION: $\text{OH} + \text{NO}_2 (+\text{M}) \rightarrow \text{HNO}_3 (+\text{M})$
OVER A WIDE RANGE OF TEMPERATURE AND PRESSURE

C. Anastasi and I. W. M. Smith

Department of Physical Chemistry
University Chemical Laboratories
Cambridge CB2 1EP, England

and

R. Zellner

Institut für Physikalische Chemie der
Universität Göttingen
34 Göttingen, West Germany

Because of its importance in atmospheric chemistry, the reaction



has been studied several times just recently [1]¹. It also attracts interest because the changeover between second- and third-order kinetics occurs in a range of [M] that is easily accessible. The present paper reports measurements of effective second-order rate constants, $k_1 = (-d \ln[\text{OH}]/dt)/[\text{NO}_2]$, through the ranges: $3 \times 10^{16} \leq [\text{M}] \leq 1.6 \times 10^{19}$ molecule cm^{-3} and $220 < T < 550$ K. The observed 'fall-off' behaviour is compared with predictions made by RRKM theory.

Experimental Method and Results

Most of our measurements have been made using the flash photolysis resonance absorption (FPRA) technique that we have described elsewhere [1,2]. At $T < 358$ K, OH radicals were generated by photolysis of $\sim 1 \times 10^{16}$ molecule cm^{-3} of HNO_3 , while at higher temperatures H_2O was used. For each combination of T and [M], experiments were carried out for several NO_2 concentrations producing values of $k_{1st} = -d \ln[\text{OH}]/dt$ between $\sim 10^3$ and 10^4 s^{-1} .

At room temperature and below some rate measurements were also made using the discharge flow resonance fluorescence (DFRF) method [3]. These extended the range of [M] that has been covered down to 3×10^{16} molecule cm^{-3} and were particularly useful at the lowest temperatures, since some allowance had to be made in the FPRA experiments for the dimerisation of NO_2 .

The observed values of k_1 were neither proportional to nor independent of [M], showing that reaction (1) was passing through its transition region in the range of [M] and T covered by our experiments. This behaviour is shown clearly by the data for 296 K which is plotted in figure 1.

¹Figures in brackets indicate literature references at the end of this paper.

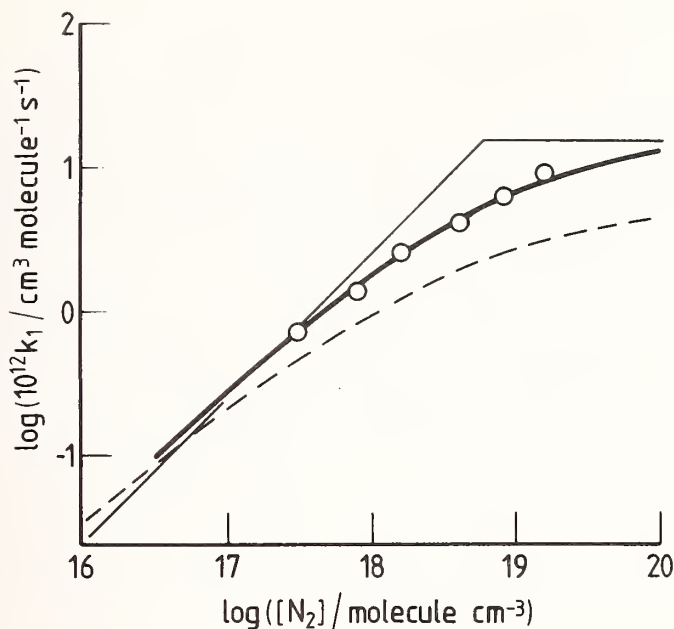


Figure 1. Comparison of experimental and theoretical results. The continuous curve shows the results of our RRKM calculations and the dashed curve those of Tsang [7]. The straight lines indicate the limiting behaviour at low and high $[M]$.

The rate constants in the limit of low $[M]$, k_1^0 , and of high $[M]$, k_1^∞ , were obtained by following the empirical procedure proposed by Troe [4]. Both the absolute magnitude and the temperature dependence of k_1 that we find is in good agreement with other work [1, 3]. The kinetics at high pressure has been studied much less extensively but the present value of k_1^∞ at 296 K is in fair agreement with Morley and Smith's [5] earlier estimate.

Table 1. Values of k_1^0 and k_1^∞

T/K	$10^{30} k_1^0 / \text{cm}^6 \text{ molecule}^{-2} \text{ s}^{-1}$			$10^{11} k_1^\infty / \text{cm}^3 \text{ molecule}^{-1} \text{ s}^{-1}$	
	$M = \text{N}_2$		$M = \text{He}$	expt.	calc.
	(FPRA)	(FPRA)	(DFRF)	(FPRA)	
220	6.3	2.5	3.0	2.0	1.45
296	2.6 ₅	0.91	1.05	1.6	1.6
358	1.6 ₇	-	-	1.3	-
450	1.0 ₉	-	-	0.38	-
550	0.61	-	-	0.44	2.6
1000	-	-	-	0.19 [6]	-

RRKM Calculations and Discussion

Including the shock tube experiments [6] on its reverse, reaction (1) has now been studied over a wide range of T and $[M]$ and can therefore provide a good test of unimolecular reaction rate theories. We have carried out conventional RRKM calculations along the lines followed previously by Morley and Smith [5] and by Tsang [7]. A model for the transition state was chosen to yield a partition function given by $Q^\ddagger = k_1^\infty Q_{OH} Q_{NO_2} / (kT/h)$, where k_1 was the observed rate constant in the limit of high pressure and the other symbols have their usual meanings. This (based on model B of Morley and Smith) had frequencies of 3550, 1650, 1325, 800, 135 and 135 cm^{-1} , two active internal rotations (moments of inertia = 1.5×10^{-40} g cm^2), and inactive overall rotations (moments of inertia = 65, 434, and 499×10^{-40} g cm^2). With the collisional efficiency (β) for N_2 assumed to be 0.3, the calculated fall-off curve at 296 K agrees quite well with the experimental results (see figure 1). The transition state model chosen to fit the fall-off behaviour at 296 K does not, however, predict the correct variation of k_1 with T (see Table 1). This is not peculiar to this particular model but probably constitutes an example of a general failure of 'conventional' transition state theory when it is applied to systems where motions in the transition state should not be treated as separable, small amplitude vibrations.

REFERENCES

- [1] C. Anastasi, P. P. Bemand and I. W. M. Smith, Chem. Phys. Letters, 37, 370 (1976), and references therein.
- [2] I. W. M. Smith and R. Zellner, J. C. S. Faraday II, 70, 1045 (1974).
- [3] J. G. Anderson, J. J. Margitan and F. Kaufman, J. Chem. Phys., 60, 3310 (1974).
- [4] J. Troe, Ber. Bunsenges, Phys. Chem., 78, 478 (1974).
- [5] C. Morley and I. W. M. Smith, J. C. S. Faraday II, 68, 1016 (1972).
- [6] K. Glanzer and J. Troe, Ber. Bunsenges. Phys. Chem., 78, 71 (1974).
- [7] W. Tsang, Int. J. Chem. Kinetics, 5, 947 (1973).

VACUUM UV FLASH PHOTOLYSIS OF PHOSPHINE: RATE OF THE REACTION $H + PH_3$ AND IMPLICATIONS FOR THE PHOTOCHEMISTRY OF THE ATMOSPHERE OF JUPITER³

J. H. Lee, [1]¹ J. V. Michael, [2] W. A. Payne, D. A. Whytock [3] and
L. J. Stief

Astrochemistry Branch, Laboratory for
Extraterrestrial Physics, NASA/
Goddard Space Flight Center
Greenbelt, Maryland

Phosphine has been detected as a minor constituent of the atmospheres of Jupiter [4] and Saturn [5]. Prinn and Lewis [6] have proposed that the Great Red Spot on Jupiter may be due to red phosphorous formed as a final product of the photodissociation of PH_3 . Notably absent from their model is the abstraction reaction



Their neglect of reaction (1) is based on the work of Norrish and Oldershaw [7] who studied the flash photolysis of PH_3 and concluded that reaction (1) is important only at high temperatures. Their arguments are not compelling. Furthermore, there are qualitative results from three separate studies which are not consistent with reaction (1) being negligibly slow at room temperature. These include product analysis in a flow system, [8] product analysis in gamma radiolysis [9] and an ESR-fast flow study [10]. To our knowledge there has not been a single determination of the rate constant k_1 and, although the primary processes $PH_3 + h\nu \rightarrow PH_2 + H$ is plausible and consistent with experimental results, [7, 11] the formation of H is not established by direct detection. We have obtained information on both of these questions by monitoring Lyman- α resonance fluorescence in the vacuum UV flash photolysis of phosphine.

The apparatus and techniques have been described previously [12]. Dilute mixtures of PH_3 in He were flash photolyzed at $\lambda > 105$ nm to produce H-atom concentrations of the order 10^{11} cm^{-3} or less while the PH_3 reactant concentration was $\sim 10^{13} \text{ cm}^{-3}$ or larger. In order to minimize photodecomposition of the reactant and to avoid accumulation of reaction products, reaction mixtures were flowed through the reaction cell at a rate just sufficient to replenish the sample between subsequent pulses of vacuum UV radiation. Under the conditions employed here, with $[PH_3] \gg [H]$, H-atoms detected by the pulse counting resonance fluorescence technique decayed exponentially with time due to reaction with PH_3 and to diffusion out of the reaction viewing zone:

$$\ln[H] = -k_{\text{observed}} t + \ln[H]_0 \quad (2)$$

where the observed pseudo-first order rate constant is given by

$$k_{\text{observed}} = k_1[PH_3] + k_d. \quad (3)$$

Figures in brackets indicate literature references at the end of this paper.

The diffusion term k_d was determined independently using mixtures of CH_4 and He at the appropriate pressures and temperatures employed in this study. Typically k_d was of the order of 20% of k_{observed} .

It was observed under all conditions employed that equation (2) was obeyed and the decay of H was first order over at least two decay lifetimes. In addition, plots of $k_{\text{obs.}}$ vs $[\text{PH}_3]$ exhibited good linearity as required by equation (3) and the intercepts yielded diffusion rate constants k_d which agreed with those obtained independently. Rate data were obtained at seven temperatures in the range 209 to 495 K over a wide range of experimental conditions, i.e. $[\text{PH}_3]$, total pressure and flash energy (atom and radical concentration). An example of the range of experimental conditions employed is shown in the table for data at 298 K. Mean values of k_1 (units $\text{cm}^3 \text{ molecule}^{-1} \text{ sec}^{-1}$) at the other temperatures were: $(10.3 \pm 0.6) \times 10^{-12}$ at 495 K, $(7.64 \pm 0.95) \times 10^{-12}$ at 420 K $(5.93 \pm 0.41) \times 10^{-12}$ at 353 K, $(2.21 \pm 0.25) \times 10^{-12}$ at 250 K, $(1.77 \pm 0.19) \times 10^{-12}$ at 228 K and $(1.37 \pm 0.11) \times 10^{-12}$ at 209 K. A least squares treatment of the data leads to the Arrhenius expression $k_1 = (4.52 \pm 0.39) \times 10^{-11} \exp(-1470 \pm 50/1.987 T) \text{ cm}^3 \text{ molecule}^{-1} \text{ sec}^{-1}$.

Rate Data for H + PH_3 at 298 K

$\frac{\text{PH}_3}{\text{mTorr}}$	$\frac{\text{He}}{\text{torr}}$	$\frac{\text{Flash Energy}}{\text{J}}$	$\frac{\text{No. of Expt.}}{\text{No. of Expt.}}$	$\frac{k_1^a}{10^{-12} \text{ cm}^3 \text{ molec}^{-1} \text{ sec}^{-1}}$
0.8	20	20-144	5	2.99 ± 0.61
1.0	50	183	1	4.37
2.0	50	20-144	9	3.43 ± 0.47
4.0	100	20-183	12	3.38 ± 0.32
6.0	10,20	110-183	3	4.14 ± 0.20
8.0	200,400	36-144	7	3.41 ± 0.25
9.0	15,30	81-183	4	3.59 ± 0.09
(av).				3.45 ± 0.46

a. uncertainty in k_1 is the standard deviation

REFERENCES

- [1] NAS/NRC Resident Research Associate.
- [2] NAS/NRC Senior Resident Research Associate.
- [3] Department of Chemistry, University of Essex, Colchester; on leave at Catholic University of America, Washington, D.C.
- [4] S. T. Ridgway, *Bull. Am. Astron. Soc.*, **6**, 376 (1974).
- [5] J. D. Bregman, D. F. Lester, and D. M. Rank, *Astrophys. J.*, **202**, L55 (1975).
- [6] R. G. Prinn and J. S. Lewis, *Bull. Am. Astron. Soc.*, **7**, 381 (1975); R. G. Prinn and J. S. Lewis, *Science*, **190**, 274 (1975).
- [7] R. G. W. Norrish and G. A. Oldershaw, *Proc. Roy. Soc.*, **A262**, 1 (1961).
- [8] D. M. Wiles and C. A. Winkler, *J. Phys. Chem.*, **61**, 620 (1975).

- [9] J. W. Buchanan and R. J. Hanrahan, Radiation Research, 42, 244 (1970) *ibid*, 44, 305 (1970).
- [10] R. B. Timmons, Private communication.
- [11] D. Kley and K. H. Welge, Z. Naturforschg. 20a, 124 (1965).
- [12] R. B. Klemm and L. J. Stief, J. Chem. Phys., 61, 4900 (1974); W. A. Payne, Jr. and L. J. Stief, J. Chem. Phys., 64, 1150 (1976).

Energy-Dependent Cross Sections for Quenching of Li(²P) and Na(²P)¹

John R. Barker,² Shen-Maw Lin, and Ralph E. Weston, Jr.

Chemistry Department
Brookhaven National Laboratory
Upton, New York 11973

Li(²P) and Na(²P) atoms were produced with varying amounts of translational energy by photodissociation of LiI with light of wavelengths from 200-230 nm or NaI with wavelengths of 215-240 nm. In the presence of a quenching gas of concentration [Q], the lifetime τ_Q of an excited metal atom is related to the bimolecular quenching rate constant by

$$\tau_Q^{-1} = \tau_0^{-1} + k_Q[Q], \quad (1)$$

where τ_0 is the natural lifetime of the excited atom. The single-photon time-correlation apparatus used to determine lifetimes is illustrated in figure 1. The light source has a pulse width of ~ 4 nsec (FWHM) and a pulse repetition rate of ~ 10 -20 kHz. Each light pulse generates a start pulse for the TAC, and a stop pulse is generated if a fluorescence photon is detected by photomultiplier P2 before the next start pulse. A voltage proportional to the time elapsed between start and stop pulses is stored in the multichannel analyzer, and after many pulses have accumulated, the number of counts in each channel is proportional to the population of excited atoms at the corresponding time. Thus, a fluorescence decay curve is obtained directly. Due to the finite width of the exciting light pulse relative to τ_Q , numerical deconvolution methods were used to calculate lifetimes.

From the measured values of k_Q , cross sections for quenching (S_Q) can be calculated from the relation

$$k_Q = \int_0^{\infty} S_Q(g)P(g)gdg \quad (2)$$

where g is the relative collision speed and $P(g)$ is the speed distribution function. The latter quantity is calculated from Franck-Condon factors for transitions from populated vibrational levels of the ground state to the upper dissociative state of the alkali iodide. The Franck-Condon factors are derived from observed fluorescence spectra.

Because eq. (2) cannot be uniquely deconvoluted, a "phenomenological" cross section, $\langle S_Q \rangle$, is defined in terms of the velocity g_{mp} corresponding to the maximum in $P(g)$ by the expression

$$\langle S_Q \rangle = k_Q/g_{mp}. \quad (3)$$

For both Li(²P) and Na(²P), the cross sections were found to be inversely dependent on relative collision energy; this is particularly obvious in the case of Na when our results are combined with those obtained at lower temperatures in experiments with Na vapor. Using

¹ This research sponsored by the U.S. Energy Research and Development Administration.

² Present address: Stanford Research Institute, Menlo Park, CA 94025.

eqs. (2) and (3), we compared experimental cross sections with those calculated from two models for two-body collisions: (1) The orbiting collision model for particles subject to a long-range attractive potential $V(R) = -C_6/R^6$, which leads to a cross section

$$S_Q(E) = w(3\pi/2)(2C_6E)^{1/3}, \quad (4)$$

where w is a quenching efficiency. (2) The absorbing-sphere model, in which it is assumed that every incoming trajectory reaching a capture radius R_c leads to quenching, with a cross section given by

$$S_Q(E) = \pi R_c^2 [1 - V(R_c)/E]. \quad (5)$$

Results of this analysis are given in Table I.

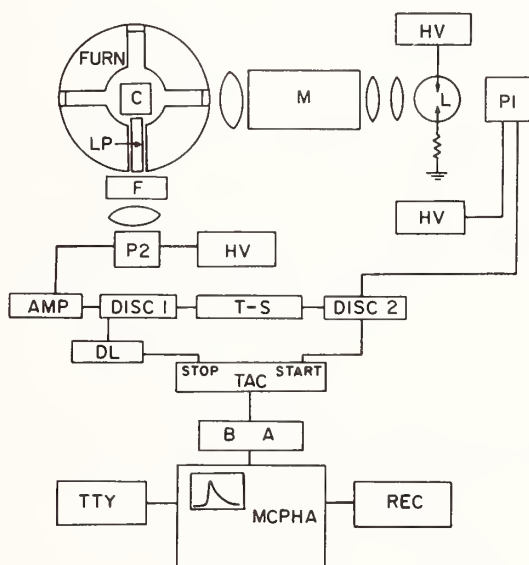


Figure 1. Block diagram of single-photon time-correlation apparatus. HV, high voltage supplies; L, lamp; P1 and P2, photomultipliers; M, monochromator; FURN, furnace; C, sample cell; LP, light pipe; F, interference filter; AMP, amplifier; DISC1 and DISC2, discriminators; T-S, time-scaler; DL, delay line; TAC, time-to-amplitude converter; BA, biased amplifier; MCPHA, multichannel pulse-height analyzer; TTY, teletype printer and papertape punch; REC, recorder.

The orbiting-trajectory model gives reasonable agreement with our results for Li and , but in the latter case it fails to predict the large cross sections observed by other workers at low energies. The cross sections calculated from the absorbing sphere formula are in better agreement over a large energy range. The physical basis for this is the "harpooning" or curve-crossing model, in which the potential curves for the covalent states $2P + Q$ and $M(^2S) + Q$ intersect a strongly attractive curve for the ionic state M^+Q^- . The quantities R_c and $V(R_c)$ of eq. (5) can then be identified with the distance at which the covalent and ionic curves cross, and the potential energy at this distance. A more detailed calculation, based on the Landau-Zener probabilities of non-adiabatic transitions, is in agreement with this.

Table 1. Parameters for quenching cross section expressions

Gas	Orbiting collision model ^a				Absorbing-sphere model ^b			
	Li(2 ² P)		Na(3 ² P)		Li(2 ² P)		Na(3 ² P)	
	C ₆	w	C ₆	w	R _c	V(R _c)	R _c	V(R _c)
H ₂	0.86	0.55	1.29	0.20	2.33	- 40	1.13	-125
D ₂	0.86	0.52	1.29	0.15	2.22	- 43	1.26	- 50
N ₂	2.00	0.52	2.95	0.28	2.18	-133	1.54	-173
CO	2.20	0.73	3.26	0.50	2.98	- 50	2.46	- 90
CO ₂	3.00	0.67	4.46	0.63	2.58	-200	2.52	-200
C ₂ H ₄	4.70	0.74	7.05	0.52	3.66	- 24	3.45 ^c	- 40 ^c
I ₂	10.00	1.80	15.43	2.2 ^c	6.56	19	6.6 ^c	- 98 ^c

^a S_Q given by eq. (4); C₆ in units of 10⁻⁵⁸ erg cm⁶.

^b S_Q given by eq. (5); R_c in Å, V(R_c) in meV.

^c Ref. 6.

Our results fit qualitatively into the pattern of quenching and reactive cross sections obtained for other alkali metal atoms with a variety of quenching gases.

References

- [1] Barker, J. R. and Weston, R. E., Jr., J. Chem. Phys. 65, (1976).
- [2] Lin, S.-M. and Weston, R. E., Jr., J. Chem. Phys. 65, (1976).
- [3] Isenberg, I., Dyson, R. D., and Hanson, R., Biophys. J. 13, 1090 (1973).
- [4] Magee, J. L. and Ri, T., J. Chem. Phys. 9, 638 (1941).
- [5] Barker, J. R., Chem. Phys., to be published.
- [6] Earl, B. L., Herm, R. R., Lin, S.-M., and Mims, C. A., J. Chem. Phys. 56, 867 (1972).
- [7] Earl, B. L. and Herm, R. R., Chem. Phys. Lett. 22, 95 (1973).
- [8] Earl, B. L. and Herm, R. R., J. Chem. Phys. 60, 4568 (1974).
- [9] Brodhead, D. C., Davidovits, P., and Edelstein, S. A., J. Chem. Phys. 51, 3601 (1969); Edelstein, S. A. and Davidovits, P., *ibid.*, 55, 5164 (1971); Gedeon, A., Edelstein, Davidovits, P., *ibid.*, 59, 3143 (1973); Maya, J. and Davidovits, P., *ibid.*, 61, 1082 (1974).

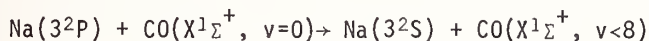
ELECTRONIC-TO-VIBRATIONAL ENERGY TRANSFER REACTIONS:
 $\text{Na}(3^2\text{P}) + \text{CO}(X^1\Sigma^+, v=0)$

D.S.Y. Hsu¹ and M.C. Lin

Physical Chemistry Branch, Chemistry Division
Naval Research Laboratory
Washington, D. C. 20375

Extensive experimental data exist on the quenching of excited Na atoms by various gases. Most of these studies deal with overall quenching cross sections [1]². To understand the mechanism by which the electronic energy is released during collisions, it would be extremely helpful to have detailed microscopic data. Hassler and Polanyi [2] have previously indicated that CO vibrational excitation up to $v=3$ was observed in the $\text{Na}^* + \text{CO}$ reaction, employing the infrared chemiluminescence method. However, no detailed vibrational distribution was given.

Using an infrared laser resonance absorption method, we have obtained the initial vibrational population distribution of CO produced from the $E \rightarrow V$ energy transfer reaction,



$$\Delta E = -48.5 \text{ kcal/mole}$$

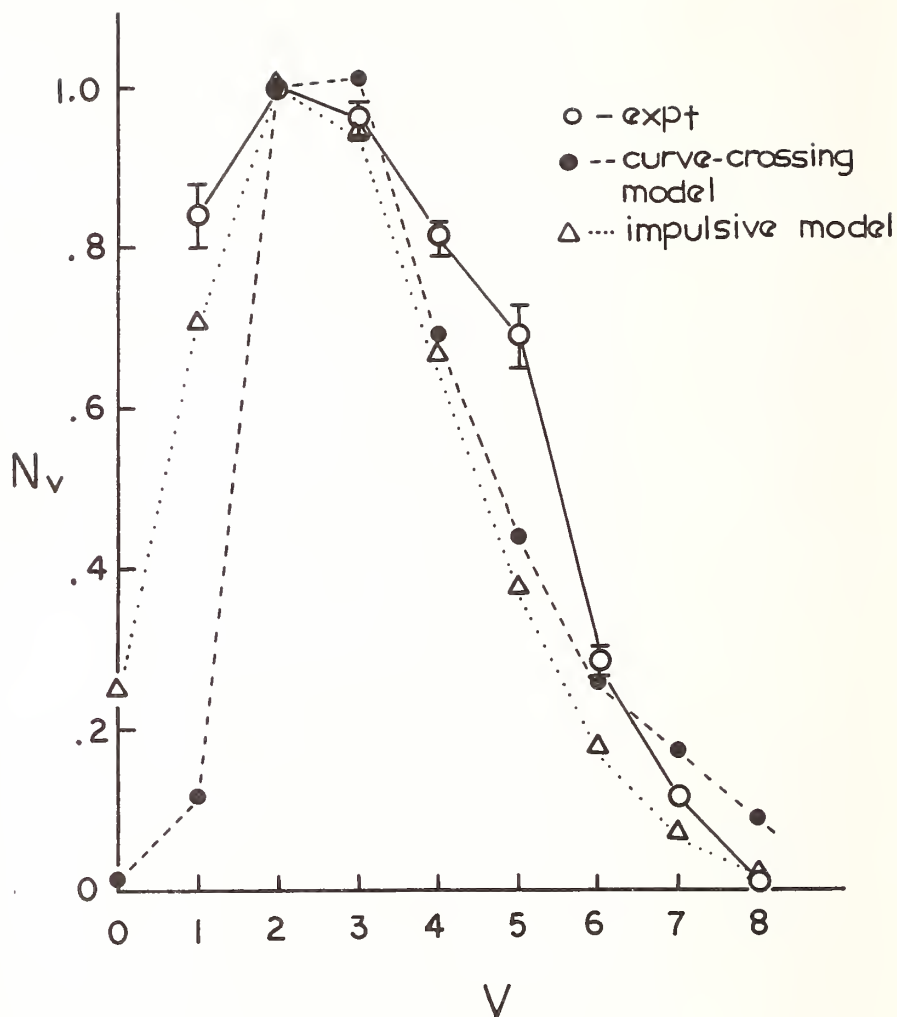
Our results are found to be consistent with the curve-crossing model [3] by Bauer, Fisher and Gilmore and the impulsive model [4] by Levine and Bernstein.

In order to measure the initial vibrational population distribution of the CO, a stabilized cw CO laser (preset at the various vibrational-rotational CO lines) and a Comatix CMX-4 dye laser (tuned to one of the Na doublets) were directed colinearly along the axis of a low-carbon stainless steel reaction tube, which contained Na vapor and CO in Ar. An aluminum block oven is used to maintain a constant temperature. Time-resolved absorption curves, signal-averaged over 1024 shots of the dye laser, were used to obtain the initial vibrational population distribution. The population distributions obtained from using different pumped Na states and CO concentrations (0.5 percent, 1 percent, 2 percent) agree closely with one another. The fact that the distributions differ very little regardless of whether the $3^2\text{P}_{1/2}$ or $3^2\text{P}_{3/2}$ state of Na is pumped indicates that both states are effectively in equilibrium, due to the large cross sections for doublet pumping [5,6], before appreciable energy transfer to CO has taken place. The lack of dependence on CO concentration is evidence that the excited CO is indeed produced in the primary step, and not by secondary reactions. Figure 1 presents the average of these four sets of experimental vibrational population distributions at 528 °K.

Our results show unequivocally that in the $\text{Na}^* + \text{CO}$ reaction, the $E \rightarrow V$ transfer process is nonresonant; a resonant transfer would result in a narrow distribution peaking at $v=8$. CO vibrational excitation was observed up to $v=8$ clearly indicates that CO is vibrationally excited up to the limit of the available electronic energy. The nonstatistical distribution, as revealed by the existence of a maximum at $v=2$, suggest strongly that the

¹NRL Resident Research Associate (September 1975-present).

Numbers in brackets indicate literature references at the end of this paper.



E→V energy transfer process occurs through an impulsive mechanism. In fact, our experimental distribution can be correlated satisfactorily with the "near-collinear" impulsive model by Levine and Bernstein [4], using $\langle \Delta E \rangle / h\nu = 2.83$ as the average vibrational quanta transferred in their Poisson distribution. Our experimental distribution also agrees surprisingly well with the prediction of the curve-crossing model by Fisher and Smith [3b]. It can be concluded that the $\text{Na}^* + \text{CO}$ E→V energy transfer reaction occurs impulsively, with 18.2 kcal/mole of its 48.5 kcal/mole of electronic energy channeling into vibrational and the remaining into translation and/or rotation.

References

- [1] Alkemade, C. Th. J and Zeeger, P. J. Th., in *Spectro-Chemical Methods of Analysis*, ed. by Winefordner, J. D., Wiley Interscience, New York, 1971. This review summarizes earlier work on the total quenching cross sections of excited alkali atoms.

- [2] Hassler, J. C. and Polanyi, J. C., Disc. Faraday Soc. 44, 182 (1967).
- [3] (a) Bauer, E., Fisher, E. R. and Gilmore, F. R., J. Chem. Phys. 51, 4173 (1969);
(b) Fisher, E. R. and Smith, G. K., Appl. Opt. 10, 1803 (1971).
- [4] Levine, R. D. and Bernstein, R. B., Chem. Phys. Letters 15, 1 (1972).
- [5] (a) Pitre, J., F.S.C. and Krause, L., Can. J. Phys. 46, 125 (1968); (b) 45, 2671 (1967).
- [6] Chen, H. L. and Fried, S., IEEE J. Quantum Electron. QE-11, 669 (1975).

ENERGY TRANSFER IN THE COLLISION OF METASTABLE EXCITED
 $\text{Ar } ^3\text{P}_2$ ATOMS WITH GROUND STATE $\text{H } ^2\text{S}$ ATOMS

Penelope B. Monkhouse, Kyle D. Bayes* and Michael A. A. Clyne

Department of Chemistry
Queen Mary College
London E1 4NS, U.K.

The interaction of metastable excited argon ($^3\text{P}_{2,0}$) atoms with ground state $\text{H } ^2\text{S}$ atoms presents a very fundamental problem in energy transfer. Conservation of energy and momentum show that H should receive almost the full energy defect (1.34 eV). From a study of the shape and width of the H atom Lyman- α (121.6 nm) line emission profile, information was derived regarding the nature of the collision process, what kinetic energy is actually present in the H atom, and whether any thermalization occurs. In addition, we have compared our results for the $\text{Ar } ^3\text{P}_2 + \text{H}$ system with the line profiles of Lyman- α lines obtained from a microwave discharge plasma.

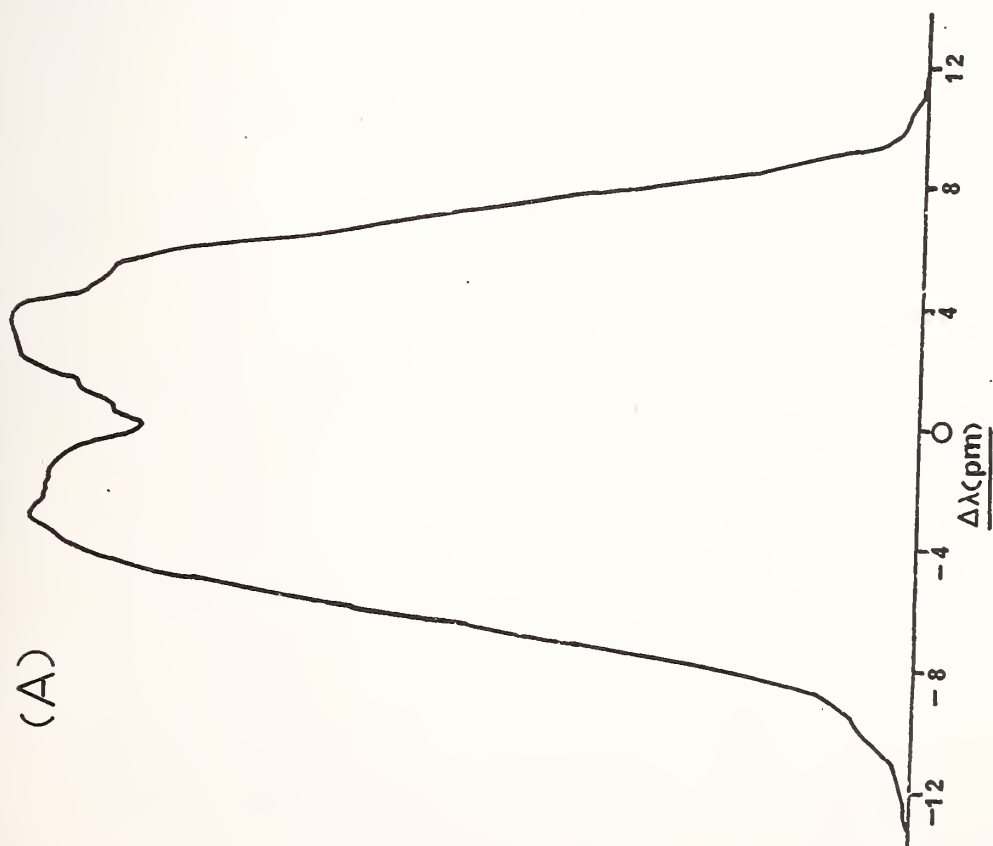
Metastable argon atoms were produced by flowing purified argon through a low-power (220 v, 5 mA) hollow cathode discharge which has been described [1]¹. Total pressures were near 1.3 Torr. H_2 was diluted to the required strength ($\leq 10\%$) in argon and passed with argon carrier gas through a microwave discharge. The reagent flow was mixed coaxially with the metastable Ar flow downstream of the hollow-cathode discharge, in front of a LiF observation window.

The Lyman- α 121.6 nm line, $\text{H } 2\text{p}^2\text{P} - ^2\text{S}$, was examined using a 1.5 m Fastie-Ebert vacuum monochromator (Jarrell-Ash) in the fourth order of a 1200 line mm^{-1} grating blazed at 500 nm and using a slit width of 30 μm . The Lyman- α line from the $\text{Ar } ^3\text{P}_{2,0} + \text{H}$ interaction was found to be broadened (HBW = 0.013 nm), and to possess a profile close to a boxcar (rectangular) shape. The edges of this line are steep, as expected from the instrumental profile (Figure 1). The $\text{Cl } (^4\text{P}_{3/2} - ^2\text{P}_{3/2})$ emission line at 138.0 nm from the reaction $\text{Ar } ^3\text{P}_{0,2} + \text{Cl}_2$ was chosen to determine the slit function; it was unreversed, near Gaussian shape, and thermal (HBW = 0.003 nm). The top of the Lyman- α profile was effectively flat, with only limited self reversal at relatively high atom particle densities in the order of 10^{13} cm^{-3} .

The Lyman- α and chlorine line profiles were then digitized manually and after iterative smoothing to remove random noise, were processed computationally through a deconvolution program which utilized an iterative routine [2]. The resulting spectrum (Figure 2B) confirmed our preliminary estimations of an essentially rectangular profile.

¹Figures in brackets indicate literature references at the end of this paper.

(A)



(B)

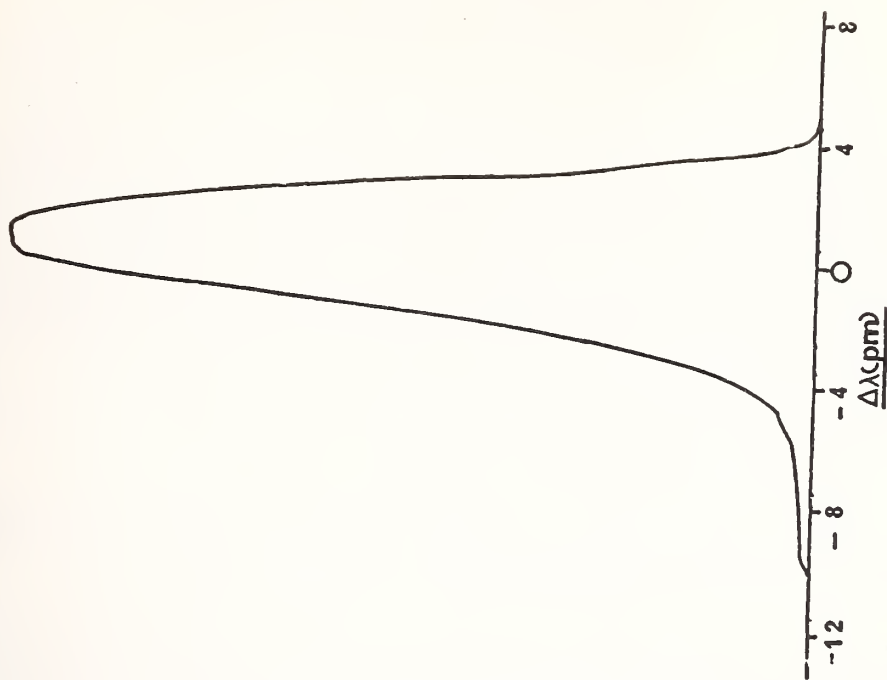
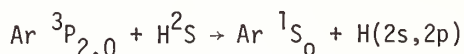


Figure 1

The results will be discussed in terms of the model proposed by Biondi and Connor [3] in studies of non-thermal line shapes of Ne produced by electron-ion recombination. Deconvolution of the observed line shape has led to the conclusion that all ($\geq 90\%$) of the excess energy (1.34 eV for Ar 3P_2) in the Ar* + H interaction is found as kinetic energy of the H atom, allowing for the very small fraction that is transferred to the Ar 1S_0 atom. This indicates that negligible thermalization had occurred under our conditions. Figure 2 compares the experimental deconvoluted result (B) with the calculated Biondi profile for the Ar (3P_2) + H system. (A)

The overall rate constant for the process



has been measured using the Ar 3P_2 + Kr reaction as a standard [4]. The value obtained was $(2.8 \pm 1.5) \times 10^{-10} \text{ cm}^3 \text{ molecule}^{-1} \text{ s}^{-1}$, i.e. close to unit collisional efficiency at 298 K.

Lyman- α profiles from microwave plasmas operating in pure argon and helium have also been investigated. In the case of argon, a very broad profile (Figure 3) similar to that obtained from the Ar(3P_2) + H reaction was observed. These results suggest that a major excitation process for Lyman- α in the microwave discharge in argon is by collision of H with metastable argon atoms. The helium plasmas showed much narrower H atom line profiles tending towards the limit of the instrumental line width at low [H]. Thus it would seem likely that either the predominant excitation of H(2p) in helium plasmas did not involve metastables or that H(2s) was formed and then partly thermalized by collisions with He, before quenching to the 2p state could occur.

* On sabbatical leave from University of California at Los Angeles.

REFERENCES

- [1] D. W. Setser, D. H. Stedman and J. A. Coxon, J. Chem. Phys. (1970), 53, 1004.
- [2] Unpublished data of M. Heaven, Queen Mary College.
- [3] R. T. Connor and M. A. Biondi, Phys. Rev. (1965), 140A, 778.
- [4] L. A. Gundel, D. W. Setser, W. S. Nip, M. A. A. Clyne and J. A. Coxon, J. Chem. Phys., 64, 4390 (1976).

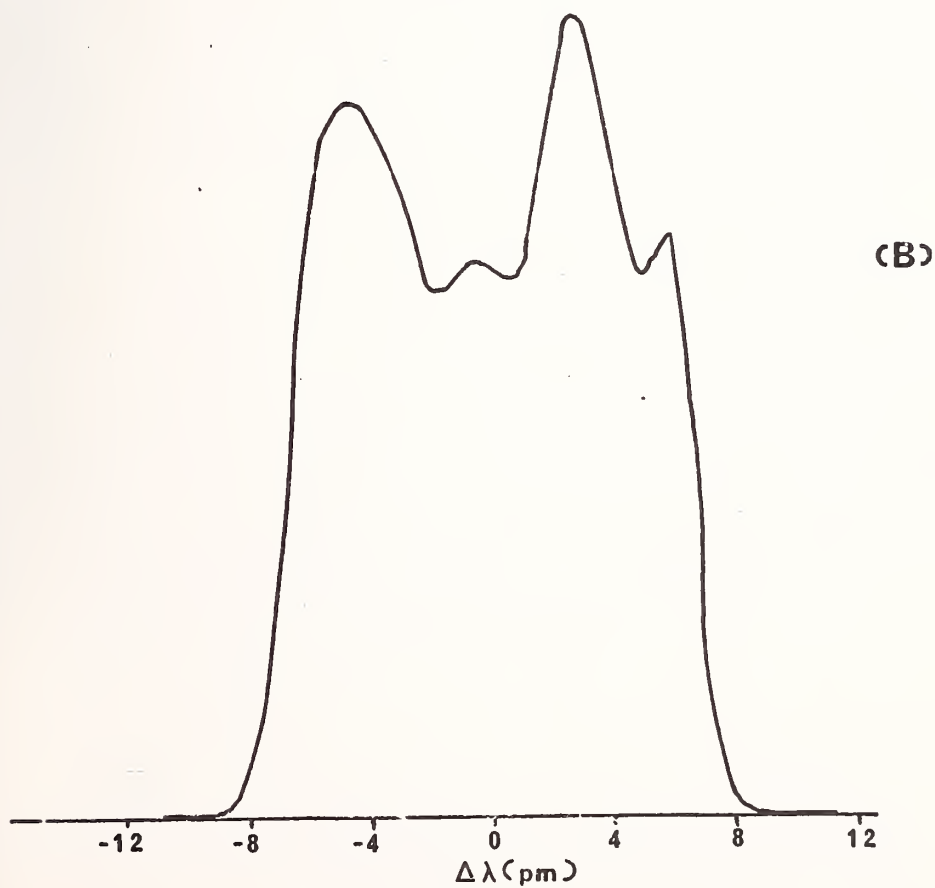
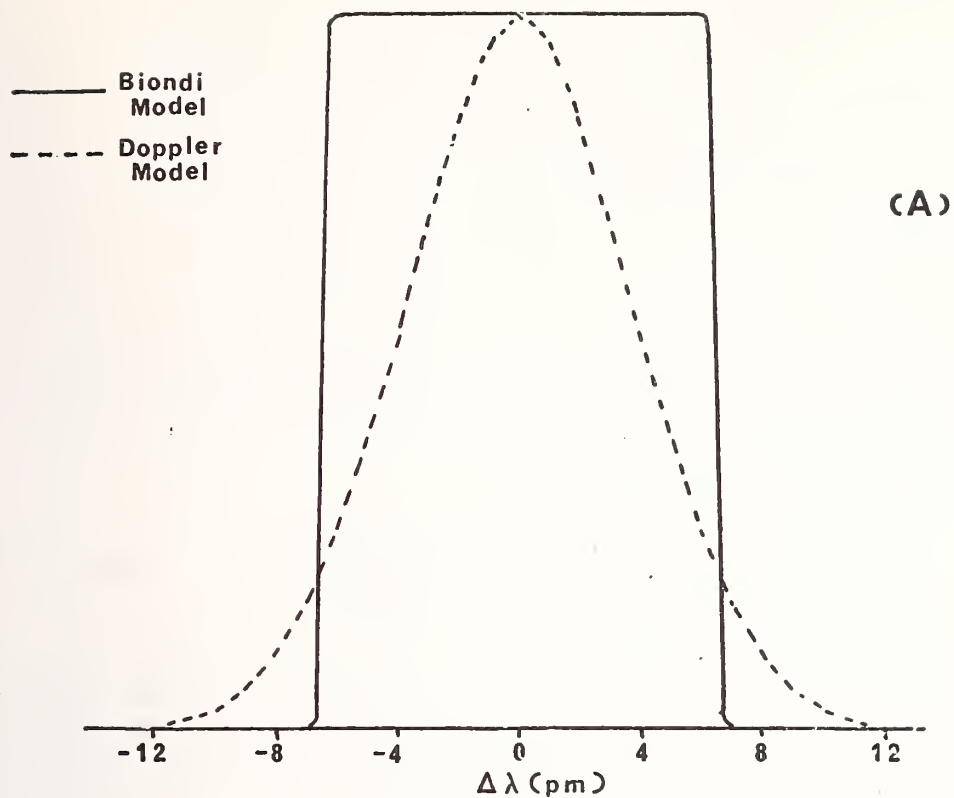
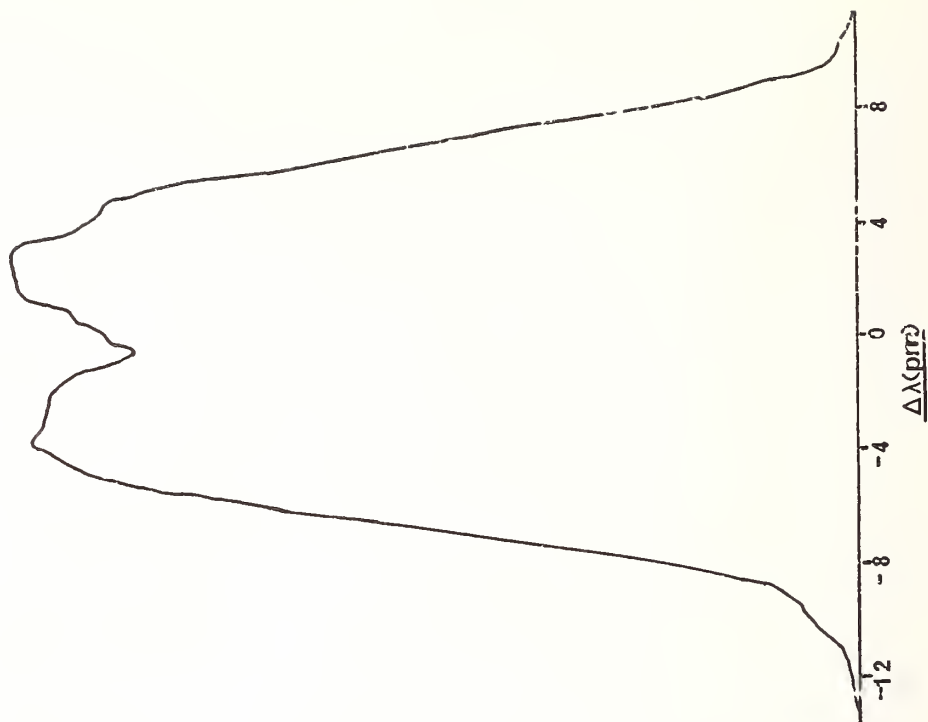


Figure 2

(B)



(A)

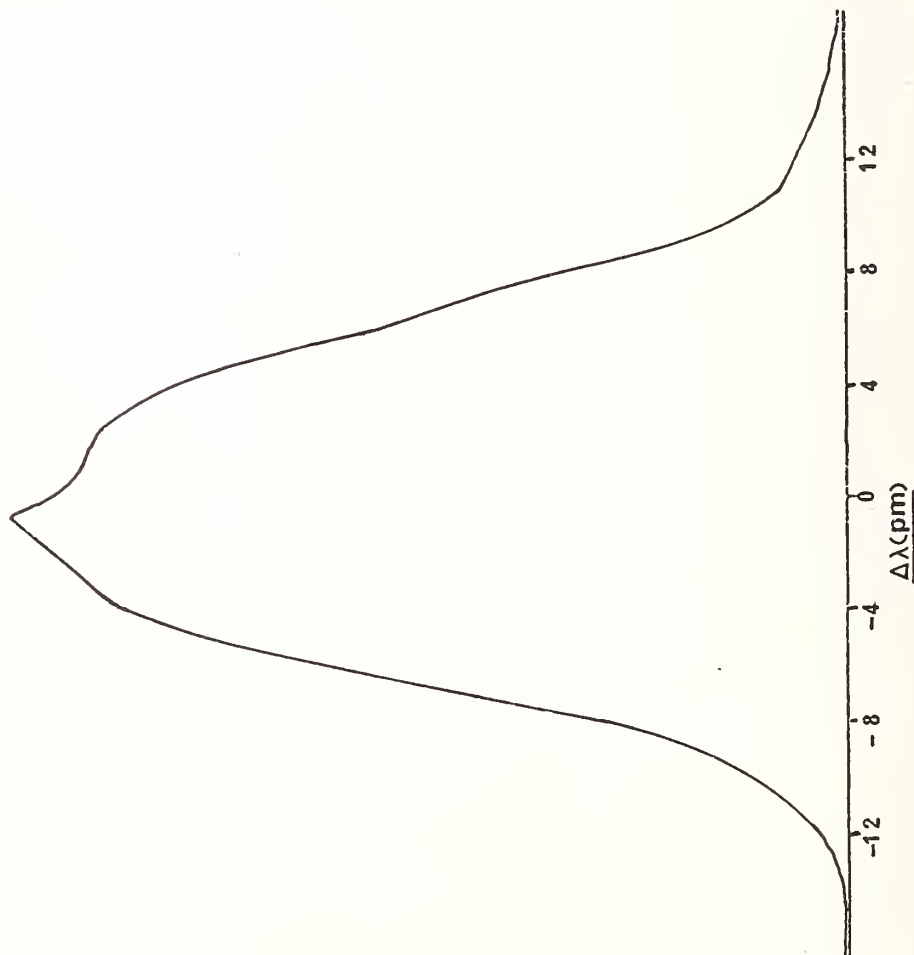


Figure 3

QUENCHING RATE CONSTANTS FOR $\text{Ar}(^3\text{P}_2)$, $\text{Kr}(^3\text{P}_2)$ AND $\text{Xe}(^3\text{P}_2)$
BY HALOGEN-CONTAINING MOLECULES, AND BRANCHING RATIOS FOR
 XeF AND KrF FORMATION*

J. E. Velazco, H. E. Kolts and D. W. Setser

Department of Chemistry
Kansas State University
Manhattan, Kansas 66506

The discovery [1,2]¹ of rare gas-halogen excimer formation from the reaction of rare gas metastable atoms with halogen or halogen-containing molecules, has led to the development of a new class of ultraviolet lasers [3]. However, scaling-up of these prototype devices faces some practical as well as theoretical problems: halogen donors must be found that give excimer formation with high efficiency, do not absorb at the laser frequency and are reasonably easy to handle. Modeling of these systems requires the knowledge of the rate constants (and branching ratios) for the relevant steps. In this work total (thermal) quenching rate constants for $\text{Ar}(^3\text{P}_2)$, $\text{Kr}(^3\text{P}_2)$, and $\text{Xe}(^3\text{P}_2)$ with a variety of fluorine donor reagents are reported; also, the branching ratios for the formation of KrF^* and XeF^* were measured. Emission from a second excimer state of XeF , XeCl , KrCl and KrF , which correlated with the $(^2\text{P}_{1/2})$ state of the rare gas ion will be reported, as will the observation of vibrational relaxation of the excimers in the 1-10 torr pressure range.

Total quenching rate constant (k_Q) were measured using a flowing after-glow apparatus [4] with a linear flow velocity of $\sim 80 \text{ msec}^{-1}$. The Ar metastable atoms were produced by passing a flow of purified Ar through a hollow cathode discharge. Total metastable concentrations $\sim 5 \times 10^{10} \text{ cc}^{-1}$, were measured at the first observation point, with $\text{Ar}(^3\text{P}_2)$ and $\text{Ar}(^3\text{P}_0)$ in a $\sim 6:1$ ration. The $\text{Kr}(^3\text{P}_2)$ or $\text{Xe}(^3\text{P}_2)$ metastables were produced by energy transfer reactions from $\text{Ar}(^3\text{P}_0)$ by adding small quantities ($\sim 0.3\%$) of Kr or Xe to the Ar flow before the discharge. The decay of the metastables along the tubular reactor as a function of quencher concentration was followed by atomic absorption using Pen Ray source lamps: the Ar 811.5 nm, Kr 811.2 nm, Xe 881.9 nm lines are used. Fluorine donors were diluted in Ar and stored in a passivated stainless vessel connected to the inlet part of the flow reactor by 1/4" ss tubing. Less reactive reagents were stored and metered through glass lines. The quenching rate constants, k_Q , from these experiments are listed in Table I. The reproducibility of k_Q for the highly corrosive F-donors is $\pm 20\%$ due mainly to difficulties in purification of samples. For chlorine and fluorides that do not attack glass, the reproducibility is $\pm 10\%$.

Figures in brackets indicate literature references at the end of this paper.

TABLE I. Rate Constant Summary

Reagent	$k_Q (10^{11} \text{ cm}^3 \text{ molec}^{-1} \text{ sec}^{-1})$			Relative k_{MX}	
	Ar(3P_2)	Kr(3P_2)	Xe(3P_2)	k_{KrCl}	k_{XeCl}
Cl ₂	71	73	72	100 ^a	100 ^a
F ₂	75	72	75	100	100
Br ₂	65		60		
ClF ₃				62 ^b	33 ^b
ICl	61		50		
OF ₂	57	53	57	82	80
CF ₃ OF	43	42	47	35	25
SF ₆	16		28	~ 0	~ 0
SeF ₆	71		65	0	0
TeF ₆	58		63	0	0
SO ₂ F ₂	42			0	0
NF ₃	14	16	9	7	14
N ₂ F ₄	31	33		22	27
NOF	36	47	30	< 5	40;(43) ^d
NOCl	48		51		
HCl	37		56		
HBr	57		61		
HI	75				
CF ₃ I			52		
BrF ₅				0;(33) ^e	0;(23) ^e

a. Cl₂ was used as the reference reaction for assigning k_{MX} .

b. Both chloride and fluoride excimer emission was observed.

c. NO (γ) and (β) emissions were the main product. This value is based on an estimate of the KrF emission intensity.

d. NO (γ) bands were also observed. This value includes the contribution of the γ -bands.

e. MBr rather than MF was the product.

A comparison technique was developed to measure the branching ratio for excimer formation, k_{MX}/k_Q , which eliminates the need of a direct and absolute measurement of k_{MX} . In the absence of quenching or non-radiative processes, the excimer emission intensity is given by (1).

$$I_{MX}^{RX} = k_{MX}[M^*][RX] \quad (1)$$

Hence, if k_{MX} is assigned for a reference reaction, and if experiments are done for the same $[M^*]$, we can obtain other k_{MX}' from (2),

$$k_{MX}' = k_{MX} \frac{I_{MX}^{R'X}/[R'X]}{I_{MX}^{RX}/[RX]}, \quad (2)$$

by simply comparing the relative emission intensities for known RX and RX' concentrations. In order to perform these intensity comparisons, a system was built that consists of two gas handling sections (one grease-free but of glass and the other stainless steel and the flow reactor section. Pressures and flow rates were monitored with a pressure transducer. Emission from the reaction of $Kr(^3P_2)$ or $Xe(^3P_2)$ (produced as described above) with added halogen donor, was detected by a computer controlled 0.75 m Jarrell-Ash monochromator equipped with a cooled photomultiplier tube and SSR photon counter. For low pressure spectra, the intensity (counts/sec) was recorded at 1 Å intervals; whereas, for high pressure spectra shorter intervals were used. The data were stored in magnetic tapes and subsequently corrected for spectral response. Integrated emission intensities were obtained by simple addition of the counts in each interval.

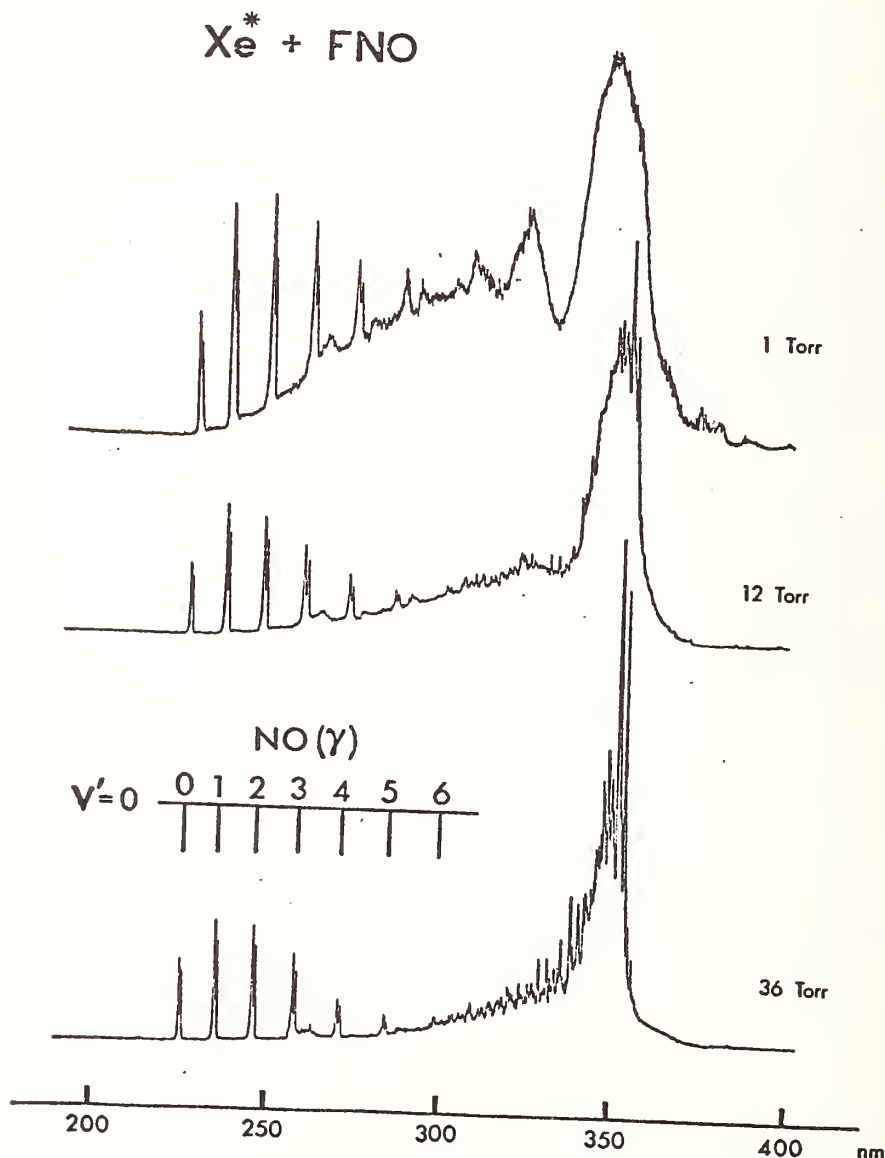
Molecular chlorine was selected as the reference donor (RX) because the absolute values of k_{KrCl} and k_{XeCl} could be estimated, and also because Cl_2 can be handled in a relatively simple and reliable way. Columns 4 and 5 of Table I list the rate constants for excimer formation relative to Cl_2 (see equation (2)). The absolute value of k_{KrCl} from the $Kr^* + Cl_2$ reaction was calculated by using the absolute rate constant for the formation of the Cl_2^* 257 nm continuum from $Ar^* + Cl_2$ (1.7×10^{-11} cc molec $^{-1}$ sec $^{-1}$). Comparing the emission intensities of the Cl_2^* 257 nm continuum and the $KrCl$ excimer emission gives (3).

$$\frac{I_{Cl_2}^*}{I_{KrCl}^*} = \frac{k_{Cl_2}^{Ar}}{k_{KrCl}} \frac{[Cl_2]}{[Cl_2]} \frac{[Ar(^3P_{0,2})]}{[Kr(^3P_2)]} \quad (3)$$

The ratio of Ar and Kr metastable concentrations was determined and the results for equal $[Cl_2]$ was $k_{KrCl} = 52 \times 10^{-11}$ ml molec $^{-1}$ sec $^{-1}$. This value gives a branching ratio of 0.7 for excimer formation from $Kr^* + Cl_2$. This value however, may have an uncertainty of as much as $\pm 50\%$ because the intensity comparisons required to determine $k_{Cl_2}^*$ are at the extreme ends of our calibrated spectral response curved. Furthermore, it is likely that some $KrCl^*$ emission extends into the v.u.v. and, therefore, is not included in I_{KrCl}^* .

Careful recalibration experiments now under way will decrease the uncertainty of this branching ration. The lack of reliable oscillator strengths for transitions in the 6s-6p manifold precludes a determination of k_{XeCl} by the method outlined above. However, evidence will be presented that supports the assignment of unity branching ratio for excimer formation from $Xe^* + Cl_2$.

Extensive vibrational relaxation of the excimers occur in the 1-40 Torr pressure range as shown in Figure 1 for XeF from Xe* + ONF. Similar results were obtained for XeCl*, KrCl* and KrF*. Since significant relaxation is evident even at < 5 Torr, simple consideration of the gas-kinetic collision frequency at these pressure ($\sim 4.3 \times 10^7$ at 5 Torr) suggest a lifetime > 50 ns for the rare gas-halide excimers. Figure 1 also shows the XeF emission at ~ 265 nm, originating from an upper excimer excited state ($^2\pi_{1/2}$) that correlated with the ($^2P_{1/2}$) state of the rare gas ion [5]. The state responsible for the main excimer emission correlates with the $^2P_{3/2}$ ion state. Emission from the upper state was also identified for XeCl*, KrF* and KrCl*. The separation between the maximum of the primary emission and that due to this new state is 9422 cm^{-1} (1.17 eV) for XeF, 9867 cm^{-1} (1.22 eV) for XeCl, 5050 cm^{-1} (0.63 eV) for KrF and 5380 cm^{-1} (0.67 eV) for KrCl. The dynamics of these reactions as deduced from the emission spectra of the excimers will be briefly discussed in terms of analogy to alkali metal atom reactions.



REFERENCES

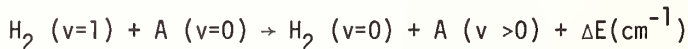
- * This work was supported by U. S. Army Research Office (DAHC04-75-60018) and by U. S. Energy Research and Development Administration (E(11-1-2807).
- [1] a. J. E. Velazco and D. W. Setser 4th Conference on Chemical and Molecular Lasers October 21-23, 1974; IEEE J. Quant. Electron. QE-11, 708 (1975).
b. J. E. Velazco and D. W. Setser, J. Chem. Phys. 62, 1990 (1974).
- [2] M. F. Golde and B. A. Thrush, Chem. Phys. Lett. 29, 486 (1974).
- [3] a. K. Searles and G. A. Hart, Appl. Phys. Lett. 27, 243 (1975).
b. J. J. Ewing and C. A. Brau, Appl. Phys. Lett. 27, 350 (1975).
c. E. R. Ault, R. S. Bradfor and M. L. Bhaumik, Appl. Phys. Lett. 27, 413 (1975).
d. G. C. Tisone, A. K. Hays, and J. M. Hoffman, Opt. Commen. 15, 188 (1975).
- [4] L. G. Piper, J. E. Velazco and D. W. Setser, J. Chem. Phys. 59, 3323 (1973).
- [5] C. A. Brau and J. J. Ewing, J. Chem. Phys. 63, 4640 (1975).

V-V ENERGY TRANSFER IN H₂ - ADDITIVE GAS MIXTURES USING A STIMULATED RAMAN EXCITATION TECHNIQUE

Richard G. Miller^{*} and J. K. Hancock

Chemistry Division
Naval Research Laboratory
Washington, DC 20375

We have measured gas phase vibrational energy transfer rates for the following inelastic collision process,



where A was various heteronuclear diatomics and triatomics. A measurable population in the H₂ (v=1) state was produced using a stimulated Raman excitation technique. Ducuing, Joffrin, and Coffinet [1]¹ demonstrated the utility of this technique in measuring V-T deactivation rates in H₂ gas. Matsui, Resler, and Bauer [2] have more recently measured V-V energy transfer rates in H₂-CO and D₂-CO gas mixtures using a stimulated Raman - IR fluorescence technique. We have extended this excitation scheme to our system utilizing two cells which has enabled us to observe V-V energy transfer in H₂-A gas mixtures at pressures much less than an atmosphere.

Experimental

Our experimental apparatus is depicted in the accompanying diagram. The excitation source was a doubled Nd³⁺: YAG laser (International Laser Systems, Inc.) with a TEM₀₀ mode output of ~ 85 mJoules/pulse and a 15 nsec pulse duration. The 532.0 nm beam was bent and focused into the center of Cell 1 which contained 50 psi of H₂. Stimulated Stokes-shifted beams (at 683.2 nm) and anti-Stokes-shifted beams (at 435.6 nm) subsequently propagated from Cell 1 in both directions coaxially with the laser beam. The Stokes-shifted beam and the laser beam are then re-focused into the center of the second cell resulting in the excitation of the H₂ (v=1) state. (Figure 1).

Energy transfer rates from H₂ (v=1) to the additive molecules A were obtained by monitoring the IR fluorescence from the IR-active vibrational modes of the A species. The A species which we have studied include, HCl, DCl, HBr, CO₂, N₂O, ¹²CO, ¹³CO, and NO. The IR-fluorescence from these species was monitored with an InSb photoconductive detector. The temporal profile of the fluorescence was processed with a Biomation 8100 transient digitizer interfaced with a Nicolet 1072 signal averager. The respective V-V and V-T rates were such that the desired V-V rate was contained in the fall time of the fluorescence from the additive molecule.

¹Figures in brackets indicate literature references at the end of this paper.

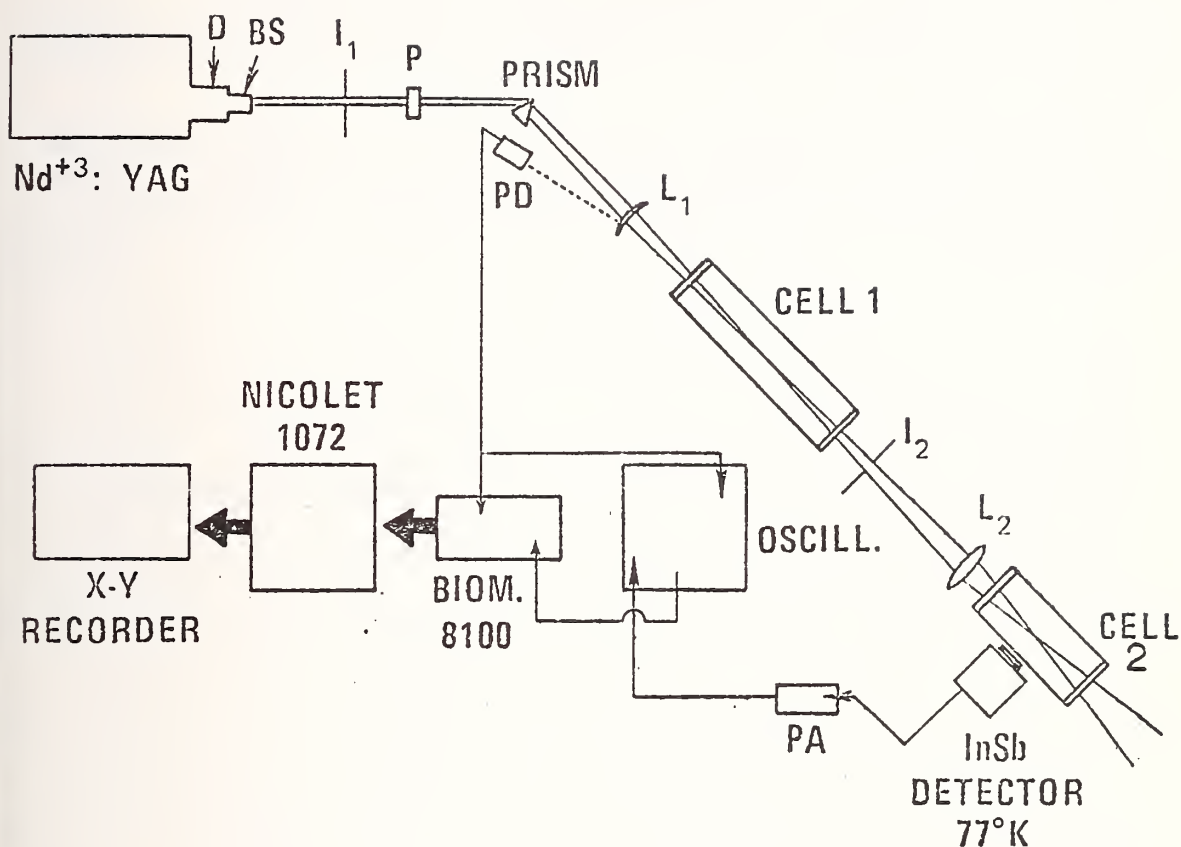


Figure 1

Results

The $\text{H}_2\text{-HCl}$ gas mixtures were studied extensively. Pressures of 85 to 692 torr and 1.06 to 73 torr of H_2 and HCl , respectively, were irradiated. The $(P_T \tau_s)^{-1}$ values ranged from 20 to $310 \text{ sec}^{-1} \text{ torr}^{-1}$. The composite V-V and V-T energy transfer rate constant $(k_e^{VV} + k_e^{VT})$ for the H_2 to HCl transfer was evaluated to be $1510 \pm 210 \text{ sec}^{-1} \text{ torr}^{-1}$. Two other groups [3,4] have obtained H_2 to HCl $k_e^{VV} + k_e^{VT}$ values by exciting a mixture of H_2

and HCl containing a trace of HF with an HF laser. Bott's [3] value was 1250 ± 150 $\text{sec}^{-1} \text{ torr}^{-1}$ and Pirkle and Cool [4] reported a value of $1730 \pm 250 \text{ sec}^{-1} \text{ torr}^{-1}$. We have also made some measurements on the HF-H₂-HCl system using HF laser excitation and obtained $(P_T \tau_S)^{-1}$ values that were in good agreement with our results obtained with the stimulated Raman pumping scheme.

The complete results shown in the accompanying table will be compared further with available results of others. The importance of V-V transfer to the overtone and combination bands of the A species studied will be discussed. Reasonable correlations of our H₂-H(D)X results with V-V results on various homonuclear diatomic - H(D)X gas mixtures can be shown.

REFERENCES

* NRC Postdoctoral Fellow.

- [1] J. Ducuing, C. Joffrin, and J. P. Coffinet, Opt. Comm., 2, 6 (1970).
- [2] H. Matsui, E. L. Resler, Jr., and S. H. Bauer, J. Chem. Phys., 63, 4171 (1975).
- [3] J. F. Bott, preprint.
- [4] R. J. Pirkle and T. A. Cool, preprint.

Vibrational Energy Transfer Rates in $\text{H}_2(v=1) +$
Additive $\text{M} \rightarrow \text{H}_2(v=0) + \text{M}(v=1,2) + \Delta E$
Mixtures at 296°K

Additive Molecule M	Energy ₁ Defect cm	$k_{\text{H}_2-\text{m}}^{v_v + v_t}$ (sec ⁻¹ torr ⁻¹)	Probability
HC1	1274 -1508(v=2)	1510 ± 210	8.62 × 10 ⁻⁵
DC1	2069 34(v=2)	689 ± 30	3.95 × 10 ⁻⁵
HBr	1604 - 865(v=2)	224 ± 18	1.26 × 10 ⁻⁵
DBr	2321 527(v=2)	212 ± 36	1.19 × 10 ⁻⁵
CO ₂	1811(001) 551(021) 444(101)	497 ± 30	2.01 × 10 ⁻⁵
N ₂ O	1936(001) 795(021) 679(101)	462 ± 14	1.82 × 10 ⁻⁵
¹² CO	2017 - 100(v=2)	12.3 ± 9.5	6.02 × 10 ⁻⁷
¹³ CO	2069 - 6(v=2)	9.7 ± 1.9	
NO(² Π _{1/2})	2284 436(v=2)	42 ± 17	2.47 × 10 ⁻⁶
NO(² Π _{3/2})	2159 311(v=2)		

EXPERIMENTS CONCERNING THE LASER ENHANCED REACTION BETWEEN O_3^+ AND NO

Kin-Kwok Hui and Terrill A. Cool

School of Applied and Engineering Physics
Cornell University
Ithaca, New York 14853

Several recent studies of the laser-enhanced reaction of nitric oxide with vibrationally excited ozone



and



have been reported [1-5]¹. In these studies the visible chemiluminescence from $NO_2^*(^2B_1)$ has been observed to be significantly enhanced in response to the laser-induced vibrational excitation of ozone, i.e.,



The initial experiments of Gordon and Lin [1] revealed a lag in the rise of fluorescence from $NO_2^*(^2B_1)$ produced in reaction (1a). It was suggested that this lag was associated with the $\nu_3 \rightarrow \nu_2$ coupling of vibrational modes in O_3 . However, later experiments [6] showed that the $\nu_3 \rightarrow \nu_2$ coupling time was an order of magnitude longer than that necessary to explain the fluorescence lag reported by Gordon and Lin.

Other puzzling aspects of the experimental measurements on reactions (1a) and (1b) have been reported [4,7]. Kurylo et al., [4] measured the rate sum for reactions (1a) and (1b) as a function of temperature and observed a complicated temperature dependence which could not be expressed with a single choice of Arrhenius parameters. Kurylo et al., [4] have suggested that an understanding of this temperature dependence requires the resolution of the influences of intermode vibrational transfer in O_3 , of vibrational deactivation of O_3 , and the relative temperature dependence of the two reaction channels (1a) and (1b).

We have performed experimental measurements with an apparatus designed to yield new information concerning reactions (1a) and (1b). A Q-switched CO_2 laser operated on the P(30) transition of the 9.5 micron band is employed for laser excitation of O_3 . The laser produces 1 mJ pulses of 1 μ sec (FWHM) pulse width and 170 Hz repetition rate. A continuous flow reactor has been employed which was carefully designed for more rapid and uniform gas mixing than had been accomplished in previous work. The apparatus was designed for operation over the range 150-400 °K, and permits observations of vibrational fluorescences from O_3 and NO_2 in addition to the electronic fluorescence previously observed. Measurements have been performed of the temporal variations in fluorescence from the $NO_2^*(^2B_1)$ and $NO_2^+(^2A_1)$ states as a function of gas composition over a wide range of parameters.

¹. Figures in brackets indicate literature references at the end of this paper.

The fluorescence from the $\text{NO}_2^*(^2\text{B}_1)$ molecules does not show a delayed rise, of the type reported by Gordon and Lin, under any experimental conditions we have explored to date. These include both high and low partial pressures of O_3 with and without large amounts of various diluents. Conditions for which all three modes of O_3 should be equilibrated and conditions for which only the ν_1 and ν_3 modes participate were examined. We believe the delayed fluorescence rise reported by Gordon and Lin was not of kinetic origin, but rather was caused by incomplete gas mixing. The dependence of the decay of $\text{NO}_2^*(^2\text{B}_1)$ on NO pressure gives a value of $(7.5 \pm 0.8) \times 10^{10} \text{ cm}^3\text{mole}^{-1}\text{sec}^{-1}$ for the sum of rate constants for reactions (1a) and (1b) at a temperature of $308 \pm 3 \text{ }^\circ\text{K}$ in good agreement with recent measurements [4,5].

Observations of vibration fluorescence from the $\text{NO}_2^+(^2\text{A}_1)$ state at 3.7 microns show a rise time determined by collisional quenching of $\text{NO}_2^+(^2\text{A}_1)$ and a characteristic decay rate determined by the combined rate of reactions (1a) and (1b). A rate constant for these combined reactions of $(8.6 \pm 0.8) \times 10^{10} \text{ cm}^3\text{mole}^{-1}\text{sec}^{-1}$ at $308 \pm 3 \text{ }^\circ\text{K}$ is obtained from the $\text{NO}_2^+(^2\text{A}_1)$ fluorescence decay, in agreement with the value found from the relaxation of $\text{NO}_2^*(^2\text{B}_1)$. The rise time data for $\text{NO}_2^+(^2\text{A}_1)$ fluorescence give values of $(1.1 \pm 0.2) \times 10^{12} \text{ cm}^3\text{mole}^{-1}\text{sec}^{-1}$ for the quenching of $\text{NO}_2^+(^2\text{A}_1)$ by NO and $(3.1 \pm 0.8) \times 10^{11} \text{ cm}^3\text{mole}^{-1}\text{sec}^{-1}$ for the quenching of $\text{NO}_2^+(^2\text{A}_1)$ by O_2 . These values are in good agreement with the results of previous measurements [8].

Results for the AC/DC fluorescence ratios for both the $\text{NO}_2^*(^2\text{B}_1)$ and $\text{NO}_2^+(^2\text{A}_1)$ states indicate a surprisingly low yield of $\text{NO}_2^+(^2\text{A}_1)$ by reaction (1b) which suggests that products of the laser enhanced reaction are predominantly excited in the translational and rotational degrees of freedom rather than in vibration.

Measurements currently in progress devoted toward an understanding of reactions (1a) and (1b) will be discussed.

References

- [1] Gordon, R. J. and Lin, M. C., Chem. Phys. Lett. 22, 262 (1973).
- [2] Kurylo, M. j., Braun, W., Kaldor, A., Freund, S. M. and Wayne, R. P., J. Photochem. 3, 71 (1974/1975).
- [3] Braun, W., Kurylo, M. j., Kaldor, A. and Wayne, R. P., J. Chem. Phys. 61, 461 (1974).
- [4] Kurylo, M. J., Braun, W., Xuan, C. N. and Kaldor, A., J. Chem. Phys. 62, 2065 (1975).
- [5] Gordon, R. J. and Lin, M. C., J. Chem. Phys. 64, 1058 (1976).
- [6] Hui, K. K., Rosen, D. I. and Cool, T. A., Chem. Phys. Lett. 32, 141 (1975).
- [7] Redpath, A. E. and Menzinger, M., J. Chem. Phys. 62, 1987 (1975).
- [8] Golde, M. F. and Kaufman, F., Chem. Phys. Lett. 29, 480 (1974).

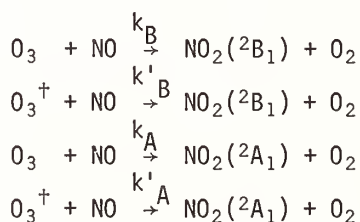
INFRARED LASER ENHANCED REACTIONS: CHEMISTRY OF NO(v=1) WITH O₃*

J. C. Stephenson and S. M. Freund

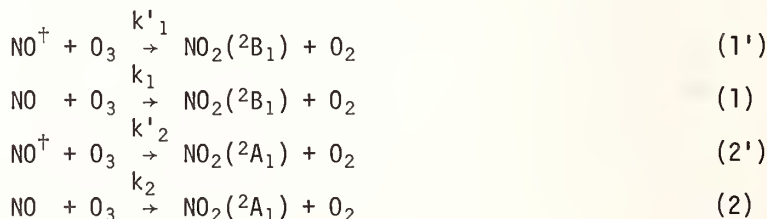
National Bureau of Standards
Washington, D.C. 20234

A variety of recent experiments demonstrates that bimolecular chemical reaction rates may be enhanced by optically exciting the vibrational levels of the reactant molecules with an infrared laser. The molecular system studied in greatest detail is the reaction of ozone with nitric oxide to give nitrogen dioxide and molecular oxygen, a process of importance in the atmosphere. The thermal reaction rate constant has been thoroughly investigated. The enhancement of the reaction rate following excitation of the O₃(001) vibrational level by a CO₂ laser was first reported by Gordon and Lin [1]¹, and then studied in greater detail by Kurylo et al., and Freund and Stephenson [2-4].

The present work continues the investigation of the laser-enhanced reaction between NO and O₃. Because it is the ozone O₂-O bond which breaks during the reaction, it was expected and then proven [2-4] that vibrational excitation of the O₃ asymmetric stretching motion increases the rate. For the reactions



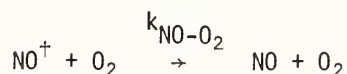
where O₃⁺ represents vibrationally excited ozone, the room temperature rate constant enhancement factors k'_B/k_B = 4.1 ± 2 and k'_A/k_A = 17.1 ± 4.3 were determined [2]. Since the NO bond does not break in the reaction, it was not obvious that there would be any increase in rate for the analogous reactions



where NO⁺ denotes NO(v=1). However, in the experiment described below, we excited the NO(v=1) state with a CO laser, and found k'₁/k₁ = 5.7 ± 1.4 and (k'₂ + k_{NO-O₃})/k₂ ≤ 22. A

¹Figures in brackets indicate literature references at the end of this paper.

necessary part of the experiment was the determination of the rate at which NO is vibrationally deactivated by O₂



for which $k_{\text{NO-O}_2} = 920 \pm 80 \text{ sec}^{-1} \text{ Torr}^{-1}$.

All of the experimental measurements were performed on mixtures of gases flowing in a pyrex cell. The reactants were monitored by means of calibrated flow meters and were admitted to the cell through concentric glass tubing which terminated in a "shower head" configuration. The laser excitation beam traversed the center of the cell perpendicular to the gas flow and visible and infrared fluorescence was viewed in a direction perpendicular to both the flow direction and the laser beam. The distance between the fluorescence viewing window and the mixing jet could be easily adjusted by sliding the glass tubing in or out through an O-ring connector to the desired position. Polished BaF₂ windows were fastened to the cell with epoxy at the Brewster angle laser entrance and exit positions and at the central fluorescence viewing port. The pressure drop ΔP along the cell was small (less than 5 percent of the total pressure for conditions under which data was taken). The commercially obtained reactant gases were used directly from the cylinders without further purification. The ozone was produced in a commercial generator which gave a maximum mole fraction of O₃ in O₂ of 0.045.

The ¹⁴N¹⁶O molecules were pumped by radiation from a liquid-nitrogen-cooled cw CO laser which produced about 3 watts of power on the fundamental (TEM₀₀) mode of the 1884 cm⁻¹ line (P(13) transition of the 9-8 ¹²C¹⁶O band). The beam was focused by a 10 cm focal length BaF₂ lens and was chopped at the focal point by a servo-controlled chopping wheel which produced a square-wave modulated beam (100 percent modulation) at a frequency of about 100 Hz. It was then collimated by a second BaF₂ lens and directed into the cell by three front-surface-reflecting mirrors. The beam diameter at the entrance to the reaction cell was approximately the same size as the tubing through which it subsequently passed.

Since the center of this laser line is 732 MHz above the transition in nitric oxide, NO(v=0, J=3/2) ²Π_{3/2} → NO(v=1, J=5/2) ²Π_{3/2}, the molecular transition must be tuned into coincidence by applying a magnetic field. The polarization of the laser was such that E (laser) was parallel to B (magnet). The magnetic field required to maximize the absorption was 760 gauss; this field was measured to be homogeneous to ± 10 gauss over the region of the cell near the fluorescence port. Measurements of the laser power absorbed in a short cell containing NO placed at the center of the magnetic coils gave an absorption coefficient at room temperature of 0.0209 cm⁻¹ Torr⁻¹ (standard deviation of 0.0003 cm⁻¹ Torr⁻¹) for absorption of the 1884 cm⁻¹ laser line in the pressure region P < 4 Torr. The laser frequency was not stabilized by locking to the top of the gain profile or to an external cavity. The reproducibility of the laser absorption coefficient measurements showed that any drift in laser frequency was small compared to the Doppler width of the NO transition.

Visible fluorescence from the NO₂^{*}(²B₁) product, hereafter designated NO₂^{*}, was detected with a photomultiplier tube cooled to -30 °C. The NO(v=1) fluorescence was monitored with a large area photovoltaic InSb detector. The analog signals which developed across appropriate load resistors were amplified by low noise amplifiers (DC to 1 MHz band pass), processed by a transient recorder which digitized the signal in real time (minimum 10⁻⁸ sec/channel), and stored in a multichannel analyzer. The electronics were triggered by the signal from an InSb detector which monitored the laser light transmitted through the cell. In a typical $\Delta I/I_0$ experiment, 40,000 cycles of the square wave signal were summed.

References

- [1] Gordon, R. J. and Lin, M. C., Chem. Phys. Lett. 22, 262 (1973).
- [2] Kurylo, M. J., Braun, W., Kaldor, A., Freund, S. M. and Wayne, R. P., J. Photochem. 3, 71 (1974).

- [3] Kurylo, M. J. Braun, W., Xuan, C. N. and Kaldor, A., J. Chem. Phys. 62, 2065 (1975).
- [4] Freund, S. M. and Stephenson, J. C., "Laser Enhanced Chemical Reaction Between $O_3(001)$ and NO," Chem. Phys. Letters 41, 157 (1976).

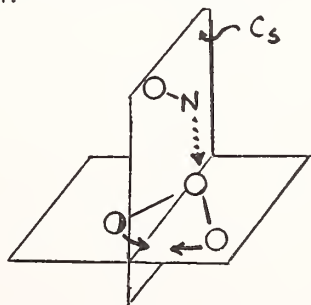
KINETIC ENERGY - AND INTERNAL STATE DEPENDENCE OF THE $\text{NO} + \text{O}_3 \rightarrow \text{NO}_2^* + \text{O}_2$ REACTION

Anthony E. Redpath and Michael Mensinger

Department of Chemistry
University of Toronto
Toronto, ON

The numerous degrees of freedom of nuclear and electronic motion of both reactants and products make the title reaction rich in dynamical detail. Associated with the problem of Energy Consumption are the questions of influence of (a) reactant kinetic energy E , (b) of the $\text{NO}(^2\Pi_{1/2,3/2})$ spin-orbit states and (c) of $\text{O}_3(\nu_1, \nu_2, \nu_3)$ vibrational excitation, on the dynamics and rates of the different product channels. (d) The effects of NO vib-rotational and O_3 rotational energy are believed to be small and we have not investigated them. The problem of Energy Disposal has its spicy sides since (e) at least two electronic NO_2 states (2A_1 groundstate and an excited state, presumably 2B_1) are populated, but primary vibrational state distribution are unavailable due to the complexity of the electronic NO_2^* chemiluminescence spectrum and to extensive vib-rotational quenching in the 2A_1 groundstate. (f) Furthermore, the $\text{O}_2(^1\Delta_g, ^1\Sigma_g^+)$ states are energetically accessible, but Gauthier and Snelling have shown [1]¹ them to be produced with negligible probability in the thermal reaction. (g) Given the long radiative lifetimes of $\text{NO}_2^*(\tau_R^* \sim 10^{-4} \text{ sec})$ and $\text{NO}_2^\pm(\tau_R^\pm \sim 10^{-2} \text{ sec?})$ it has to be kept in mind that bulk experiments are usually conducted at pressures where secondary collisions dominate the kinetics. In our "single collision" beam/gas experiments, a He or H_2 seeded supersonic NO beam issues from a heatable nozzle (300-650 K), is skimmed, chopped and shot through an O_3 filled scattering chamber (variable temperature 150-300 K to populate O_3 vibration) and monitored. Using lock-in techniques chemiluminescence is detected by [1] a bare photomultiplier [2] a monochromator/photomultiplier combination [3] a PbS infrared detector plus filter for electronic NO_2^* emission (1-3 μm) and [4] PbS detector and another filter for vibrational NO_2^\pm (3-4 μm) emission. The beam energy is varied via (a) the seeding ratio and (b) the nozzle temperature. Beams are velocity analyzed by time-of-flight.

It is found that NO beams from a heated (600 K) nozzle yield ca. 4x more visible CL than beams of the same nominal velocity issuing from a room temperature nozzle. It is shown that the former have a higher population of the $\text{NO}(^2\Pi_{3/2})$ spin-orbit component than the latter. We conclude that $\text{NO}(^2\Pi_{3/2}) + \text{O}_3$ yields primarily electronically excited NO_2^* , while $\text{NO}(^2\Pi_{1/2}) + \text{O}_3$ leads to groundstate $\text{NO}_2(^2A_1)$. The only $(\text{NO} \cdot \text{O}_3)$ collision complex which correlates with $\text{NO}_2^*(^2B_1) + \text{O}_2(^3\Sigma_g^-)$ and $\text{NO}_2^\pm(^2A_1) + \text{O}_2(^3\Sigma_g^-)$ rather than with $\text{O}_2(^1\Delta_g, ^1\Sigma_g^+)$ [1] has C_5 symmetry: NO approaches along the $\text{O}-\text{O}-\text{O}$ bisecting plane and attacks the central rather than an end-standing O-atom. This " C_5 " reaction pathway is expected to be greatly facilitated by the O_3 bending mode ν_2 , [2] which furthers bond formation between the end-standing oxygen:



¹Figures in brackets indicate literature references at the end of this paper.

A cyclic O_3 isomer of very similar energy as the "classical" bent O_3 groundstate, that has been predicted on theoretical grounds [3,4] supports this view. However, competing channels in which end-standing O may be transferred cannot be ruled out on the basis of the circumstantial evidence presented here. We observe enhancement of the CL crosssection through thermally populating O_3 internal modes.

The excitation functions for production of visible and for IR (1-3 μm) electronic emission are almost identical: till ~ 3 kcal above threshold they are well represented by

$$\begin{aligned}\sigma_{CL}(E) &= C(E - E_0)^n & E > E_0 \\ &= 0 & E < E_0\end{aligned}$$

with $C = 7.1 \times 10^{-5} \text{ Å}^2$, $E_0 = 3.0 \pm .3$ kcal/mole and $n = 2.3 \pm .3$. This yields an activation energy in good agreement with measured values [5].

The CL spectra, recorded at $\bar{E} = 15 \pm 1.5$ and 12 ± 1.2 kcal/mole and at thermal energies show a strong blue shift with increasing collision energy: the short wavelength cutoff invariably agrees with the total available energy, demonstrating that in a small (unknown) fraction of collisions the total energy is funneled into internal NO_2^* and subsequently emitted as light. The energy dependence of the vibrational IR emission is markedly distinct from electronic emission: no threshold is discernible even at the lowest collision energy $E_{min} = 1.1$ kcal/mole, and the signal rises less rapidly as E increases.

In the spirit of information theory [6] $\sigma_{CL}(E)$ or rather

$$k_{CL}(E) = v\sigma(E) = \rho(E')\omega(E)$$

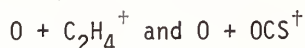
is decomposed [7] into a calculable (*a priori*) product phasespace density $\rho(E')$ and the dynamical "averaged state to state transition probability" $\omega(E)$. It comes somewhat as a surprise that the time-honoured hard sphere/line-of-center model for reaction crosssections [8] gives an excellent representation of $\omega(E) \propto (1 - E_0/E)$. For the penta-atomic title reaction, the phasespace factor dominates $\sigma(E)$.

We express our thanks to Dr. Akimichi Yokozeki for the information theoretical analysis, and to Professor Tucker Carrington for the correlation diagrams and for numerous chemiluminating discussions in the course of this work. Financial support stems from the National Research Council of Canada and is gratefully acknowledged.

References

- [1] Gauthier, M. and Snelling, D. R., Chem. Phys. Lett., 20, 178 (1973).
- [2] (a) Gordon, R. J. and Lin, M. C., Chem. Phys. Lett., 22, 262 (1973).
(b) Gordon, R. J. and Lin, M. C., J. Chem. Phys., 64, 1058 (1976).
- [3] Wright, J. S., Can. J. Chem., 51, 139 (1973).
- [4] Shih, S., Buenker, R. J. and Peyerimhoff, S. D., Chem. Phys. Lett., 28, 463 (1974).
- [5] Clough, P. N. and Thrush, B. A., Trans. Far. Soc., 63, 915 (1967).
- [6] Bernstein, R. B. and Levine, R. D.: "Role of Energy in Reactive Molecular Scattering: An Information Theoretic Approach" in Advances in Atomic and Molecular Physics, Vol. II. Ed. Bates, D. R., Academic Press, 1975.
- [7] Pruett, J. G., Grabiner, F. R. and Brooks, P. R., J. Chem. Phys., 63, (75) 1173.
- [8] Levine, R. D. and Bernstein, R. B., Molecular Reaction Dynamics, Oxford U.P., 1974.

THE EFFECT OF INFRARED LASER EXCITATION ON REACTION DYNAMICS:



Ronald G. Manning, Walter Braun, and Michael J. Kurylo

National Bureau of Standards
Washington, DC 20234

A variety of experiments have been reported in the literature recently regarding the energetics and dynamics of atom exchange processes ($A + BC \rightarrow AB + C$). These studies have utilized the infrared arrested fluorescence technique to analyze the energy distribution in the diatomic product [1]¹ and thermal [2], microwave [3], chemical [4], and infrared laser [5] excitation methods to investigate the effect of internal energy in the diatomic reactant on the reaction rate. Calculations for these systems show that, depending on the nature of the reaction hypersurface, reactant vibrational energy can be very effective or virtually ineffective in influencing the rate of chemical reaction [6]. A number of more complex systems have also been investigated using either IR laser excitation of a reactant molecule [7,8,9] or chemical or flash photolytic production of an excited transient (i.e. $OH(v>0)$ [10, 11] and $CN(v>0)$) [12]. Most of these systems exhibited rate constant enhancements of factors of three to four for reaction of the vibrationally excited species when compared with the thermal process. In the molecular system studied in greatest detail ($O_3^+ + NO$), it was found that the temperature coefficient remained essentially identical to that for the Boltzman reaction [7]. These results indicate that while there appears to be little coupling between the reactant vibrational energy and the reaction coordinate in the ($O_3^+ + NO$) system a small but significant effect can be observed on the overall reaction rate.

In this study we have investigated the effect of vibrational energy on the reactions of $O(^3P)$ atoms with OCS and C_2H_4 :



Experimental

The experimental apparatus for the kinetic measurements (depicted schematically in Figure 1) consists of a flash photolysis resonance fluorescence (FPRF) apparatus modified

¹Figures in brackets indicate literature references at the end of this paper.

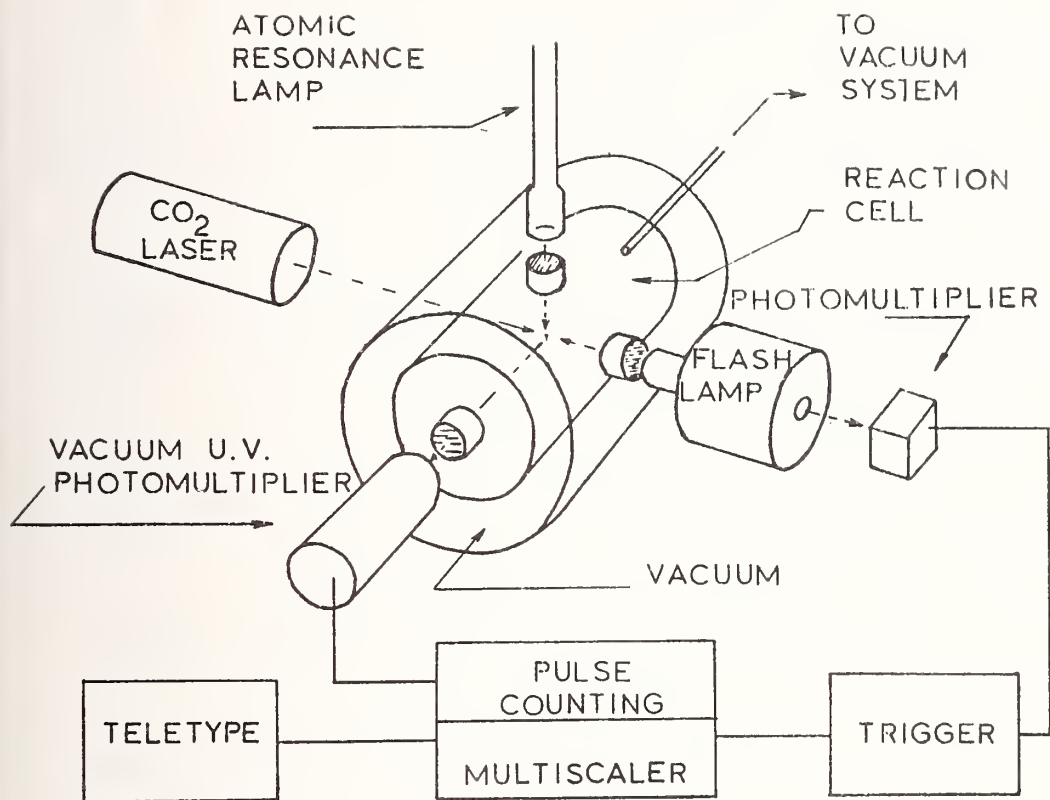


Figure 1. Schematic diagram of the flash photolysis-resonance fluorescence (FPRF) apparatus modified for IR laser reactant excitation.

to allow passage of IR laser radiation. The basic FPRF assembly consists of a reaction cell of arbitrary geometry to which are attached a flash lamp, resonance lamp, and fluorescence detecting photomultiplier on perpendicular axes. The sensitivity and precision of the FPRF method enable one to discern changes in experimental conditions which cause perturbation of the measured decay rate by several percent. The CO₂ laser shown in the diagram can be operated cw over numerous lines in the 9-10 μ region with a power level of 3-6 watts. Consequently, under conditions which minimize vibrational deactivation, steady state concentrations of vibrationally excited species can be achieved such that $([S]_v > 0 / [S]_v = 0) > 0.05$. By comparing the atom decay rate for laser on vs. laser off conditions, any significant change in the rate constant due to reactant vibrational excitation can be detected. The limiting value of the laser enhancement that can be discerned depends ultimately on two factors: 1) the equilibrium concentration of vibrationally excited reactant that can be experimentally realized (i.e. absorption of laser flux vs. deactivation losses) and 2) the magnitude of the activation energy for the thermal reaction. This determines the extent of a purely thermal (heating) effect.

Results

The excited substrate molecules (S^+) can be formed by two methods: direct IR absorption and V-V transfer from another molecule which is pumped by the laser. Such V-V

transfer is generally much faster than V-T deactivation in the system and this latter scheme is often successful in achieving high enough concentrations of S^+ to facilitate measuring the smallest possible change in k^+/k^{13} . In these experiments CH_3F^+ has been used as a transfer agent because of its strong absorption of the P20 line, 9.6 μ band CO_2 laser radiation.

Under these conditions we observed little or no effect of vibrational energy in C_2H_4 on the rate of reaction with O atoms. Because of a somewhat higher activation energy, it was considerably more difficult to measure an effect in the $O + OCS$ reaction. Within the limits of detectability, all observations in this system could be attributed to heating effects. A factor of 1.5 increase in the rate constant for $O + C_2H_4^+$ over that for $O + C_2H_4$ and a factor of 3 for $O + OCS^+$ over $O + OCS$ would have been detectable in these experiments. The results seem to indicate that there is little or no coupling of vibrational energy to the reaction coordinate leading to activated complexes in these two reaction systems. Experiments are in progress to determine the effect of vibrational energy on other reaction systems.

REFERENCES

- [1] K. G. Anlauf, P. J. Kuntz, D. H. Maylotte, P. D. Pacey, and J. C. Polanyi, *Disc. Faraday Soc.* 44, 183 (1967).
- [2a] L. J. Kirsch and J. C. Polanyi, *J. Chem. Phys.* 57, 4498 (1972).
- [b] J. H. Birely, J. V. V. Kasper, F. Hai, and L. A. Darnton, *Chem. Phys. Letters* 31, 220 (1975).
- [3a] R. F. Heidner and J. V. V. Kasper, *Chem. Phys. Letters* 15, 179 (1972).
- [b] L. B. Sims, L. R. Dosser, and P. S. Wilson, *Chem. Phys. Letters* 32, 150 (1975).
- [4] D. J. Douglas, J. C. Polanyi, and J. J. Sloan, *J. Chem. Phys.* 59, 6679 (1973).
- [5a] T. J. Odiorne, P. R. Brooks, and J. V. V. Kasper, *J. Chem. Phys.* 55, 1980 (1971).
- [b] D. Arnoldi, K. Kaufman, and J. Wolfrum, *Phys. Rev. Letters* 34, 1597 (1975).
- [c] Z. Karny, B. Katz, and A. Szoke, *Chem. Phys. Letters* 35, 100 (1975).
- [d] S. R. Leone, R. G. Macdonald and C. B. Moore, *J. Chem. Phys.* 63, 4735 (1975).
- [6] J. C. Polanyi, *Accounts of Chemical Research* 5, 161 (1972).
- [7] M. J. Kurylo, W. Braun, C. Nguyen Xuan, and A. Kaldor, *J. Chem. Phys.* 62, 2065 (1975); 63, 1042 (1975).
- [8] R. J. Gordon and M. C. Lin, *J. Chem. Phys.* 64, 1058 (1976).
- [9] E. N. Chesnokov, V. P. Strunin, N. K. Serdyuk, and V. N. Panfilov, *Reaction Kinetics and Catalysis Letters* 3, 131 (1975).
- [10] S. D. Worley, R. N. Coltharp, and A. E. Potter, *J. Phys. Chem.* 76, 1511 (1972).
- [11] G. E. Streit and H. S. Johnston, *J. Chem. Phys.* 64, 95 (1976).

- [12] V. H. Schacke, K. J. Schmatjko, and J. Wolfrum, Ber. Buns. Phys. Chem. 77, 248 (1973).
- [13a] M. J. Kurylo, W. Braun, and A. Kaldor, Chem. Phys. Letters 27, 249 (1974).
- [b] W. Braun, M. J. Kurylo, and A. Kaldor, Chem. Phys. Letters 28, 440 (1974).
- [c] D. I. Rosen and T. A. Cool, J. Chem. Phys. 62, 466 (1975).

REACTION OF FLASH PHOTOLYTICALLY PRODUCED $\text{CN}(X^2\Sigma^+, v)$ RADICALS WITH $\text{O}(^3\text{P})$ ATOMS

K. J. Schmatjko and J. Wolfrum

MPI fur Stromungsforschung
D-3400 Gottingen
West Germany

The reaction (1) $\text{CN}(X^2\Sigma^+, v) + \text{O}(^3\text{P}) \rightarrow \text{CO}(X^1\Sigma^+, v) + \text{N}(^4\text{S}, ^2\text{D})$ was studied using a flash-photolysis arrangement combined with a discharge-flow reactor. CN-radicals were produced by flash-photolysis of C_2N_2 diluted in He and their concentrations monitored by visible absorption spectroscopy. The flash discharge (17 kV, 0.2 μF) is switched by a thyatron with a repetition rate up to 5 Hz. $\text{O}(^3\text{P})$ atoms present in excess with respect to the CN radicals are continuously generated in a microwave discharge. The concentrations of the $\text{CO}(X^1\Sigma^+, v)$ molecules formed in reaction (1) were obtained from time-resolved infrared laser absorption spectroscopy (see Figure 1).

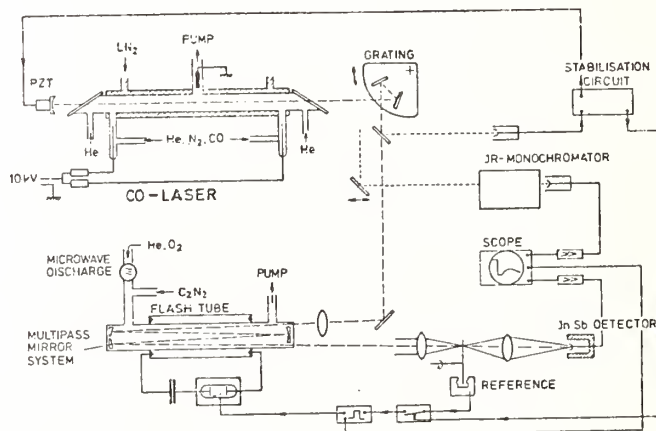


Figure 1. Schematic of the experimental apparatus for infrared laser resonance absorption-gain measurements

The CO-laser could be tuned by a grating on single rotational lines of the vibrational transitions of $\text{CO}(v)$ between (1, 0), and (26, 25). For transitions below (3, 2) the laser output had to be stabilized continuously between measurements.

To maintain isothermal conditions and to avoid the rapid exchange of vibrational energy during the formation of the $\text{CO}(v)$ molecules very low concentrations have to be applied. This was achieved by using an internal multi-pass mirror system. The adjustable mirrors allowed up to 60 traversals of the analysis laser beam along the flow tube.

From the absorption or gain signals the absolute concentration of $\text{CO}(v)$ formed in the reaction was evaluated starting with the highest vibrational transition of $\text{CO}(v)$ where $[\text{CO}(v+1)] = 0$ was found. No absorption or gain was observed for lines in the (26, 25) to the (15, 14) bands. From the measured concentration-time profile (see Figure 2a) the

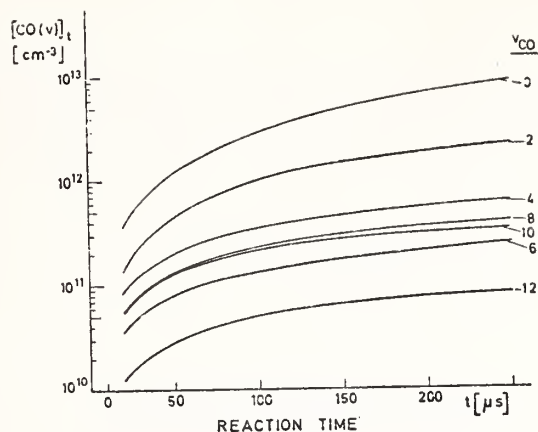


Figure 2a. Formation of CO(v) in Reaction (1).

distribution of CO(v) molecules formed in reaction (1) could be obtained directly. The shape of the distribution measured at early times (see Figure 2b) shows only small changes

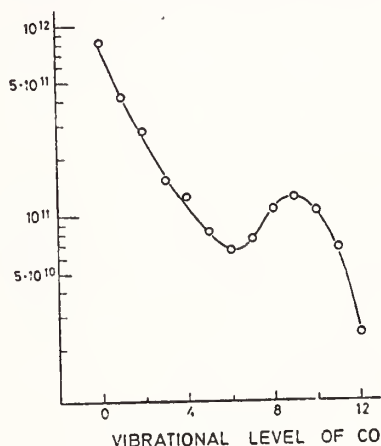


Figure 2b. Distribution of CO(v) formed in Reaction (1).

as the reaction time proceeds. The rate constant $k_1 = (1, 1 \pm 0, 3) \cdot 10^{13} \text{ cm}^3 \text{ mol}^{-1} \text{ s}^{-1}$ at 295 K could be obtained from the CO(v,t) profiles. No systematic variation was found using different CO(v) levels.

The observed energy distribution (see Figure 2b) shows two different parts which can be understood by considering the correlation diagram of reaction (1). As can be seen in Figure 3 several pathways exist: one reaction path direct to CO($X^1 \Sigma^+$) and N(4S) atoms and two reaction paths to N(2D) atoms and CO($X^1 \Sigma^+$) either directly or via the stable intermediate NCO($X^2 \Pi$). To stimulate the dynamics of reaction (1) three-dimensional classical trajectory calculations were carried out using two different empirical adiabatic potential energy surfaces. The trajectory calculations show that on the path to N(4S) atoms the reaction energy is predominantly channeled into vibrational excitation of the CO molecule.

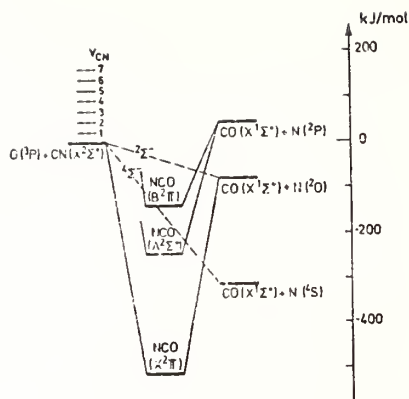
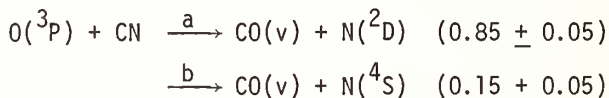


Figure 3. Correlation diagram for Reaction (1).

On the path to $N(^2D)$ via $NCO(X^2\Pi)$ the formation of $CO(v = 0)$ predominates and the reaction energy is mainly converted into electronic excitation of the metastable $N(^2D)$ atom. If one sums up the measured absolute population of the CO vibrational levels according to the shapes of the distribution predicted by the trajectory calculations one obtains.



Observation of the electron state of the nitrogen atoms produced in reaction (3) provides an independent way to obtain information on the importance of the two pathways (1a) and (1b).

Observation of the nitrogen atoms produced in the reaction was made by time-resolved resonance absorption in the vacuum UV (see Figure 4).

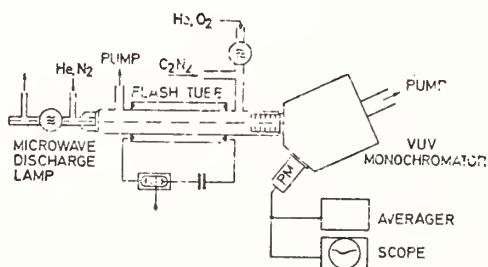


Figure 4. Detection of nitrogen atoms formed in Reaction (1) by resonance absorption.

Figure 5 shows the measured time-resolved absorption signals from the $N(^2D)$ atoms produced in (1). While the concentration of $N(^4S)$ remains nearly constant during the observation time a decay of the $N(^2D)$ concentration due to quenching of the metastable $N(^2D)$ atoms by the components of the reaction mixture is observed.

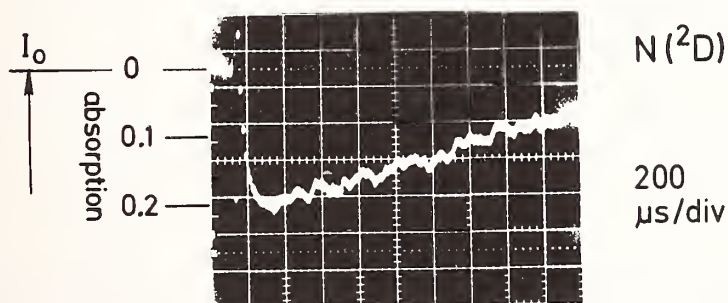


Figure 5. Oscilloscope of the vacuum ultraviolet absorption of $N(^2D)$ formed in Reaction (1).

From the measured absorption signals a ratio of 5:1 for $N(^2D)$ versus $N(^4S)$ formation in reaction (1) in good agreement with the result from the $CO(v)$ distribution is obtained.

VIBRATIONAL PHOTOCHEMISTRY: THE RELAXATION OF $\text{HCl}(v=1)$ and $\text{DCl}(v=1)$ BY BROMINE ATOMS

R. D. H. Brown, I. W. M. Smith and S. W. J. Van der Merwe

Department of Physical Chemistry
University Chemical Laboratories
Cambridge CB2 1EP, England

The atom-transfer reaction



is establishing itself as the prototype of endoergic reactions whose rates are selectively enhanced by vibrational excitation of the bond that is broken in the reaction. Recently the relative rates of (1) for $1 < v \leq 4$ have been determined using a 'chemiluminescence depletion' method [1]¹ and the total rates for reactive plus inelastic processes, i.e.



have been measured for $v=1,2$ in laser induced vibrational fluorescence experiments at room temperature [2]. This paper reports measurements by the second technique of $(k_1 + k_2)$ for $\text{HCl}(v=1)$ and $\text{DCl}(v=1)$. The experimental results are interpreted in the light of the results of Monte Carlo trajectory calculations.

Experimental Method and Results

A description of our general experimental method has been given elsewhere [3]. Gas samples were prepared in a flow-discharge system and some of the HCl contained in this mixture was excited to $v=1$ with the output from a pulsed HCl chemical laser. The decay of the vibrational fluorescence was measured with different concentrations of Br atoms present. These were prepared by means of the reactions



that convert O atoms quantitatively to Br . The atomic oxygen was produced by partial dissociation of O_2 in a microwave discharge and its concentration was determined, prior to addition of Br_2 , by titration with NO_2 .

¹Figures in brackets indicate literature references at the end of this paper.

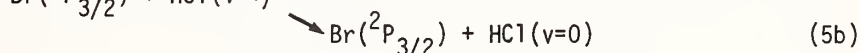
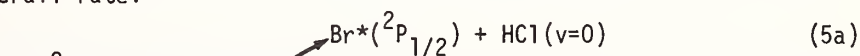
By measuring the energy absorbed from the laser it was shown that 1 - 1.5% of the HCl was excited to $v=1$. The degree of excitation was purposely kept this low to avoid problems that might arise through fast V-V exchange of vibrational energy followed by rapid removal of HCl from levels with $v > 1$.

Table 1 summarizes the results obtained in our experiments.

Table 1. Summary of Observed Rate Constants

Excited molecule	T K	$k_{5a} + k_{5b}$	k_{5b}	
		$10^{-13} \text{ cm}^3 \text{ molecule}^{-1} \text{ s}^{-1}$	$10^{-13} \text{ cm}^3 \text{ molecule}^{-1} \text{ s}^{-1}$	
HCl($v=1$)	210	2.8	2.6	2.8^{2a}
HCl($v=1$)	295	5.6	4.8	2.7^{2b}
HCl($v=1$)	371	9.5	7.7	2.6^{2c}
DC1($v=1$)	295	9.4	9.4	

Chemical reaction between Br and HCl($v=1$) is so endoergic that it cannot remove HCl($v=1$) at low temperatures. There remain, however, two energy transfer processes that may contribute to the overall rate:



Process (5a) is 2.3 kcal/mole endoergic but it can provide a route for loss of HCl($v=1$) in our experiments as Br^* is rapidly quenched by O_2 . The rate constant k_{5a} can be calculated from k_{-5a} for the reverse process [4]. Assuming k_{-5a} to be independent of temperature, the values of k_{5b} listed in the last column of Table 1 are obtained.

Our value of k_{5b} at 295 K is almost twice that determined in other recent investigations. In these Br atoms were formed by partial dissociation of Br_2 in a discharge. Because Br_2 deactivates HCl($v=1$) efficiently, [2a] the acceleration brought about by the atoms was only ~ 40% as against a threefold increase in our experiments. Nevertheless it appears that an as yet unidentified systematic error may cause the difference between these two sets of results.

Theoretical Results and Discussion

To assist with the interpretation of the experimental data a three-dimensional quasiclassical trajectory study is now being made of the dynamics of $\text{Br} + \text{HCl}(v)$ and $\text{Br} + \text{DC1}(v)$ collisions. These allow one to examine the electronically adiabatic routes for removal of HCl(v).

The computations are being carried out using procedures that have been described previously [5] with a single parameter LEPS potential. Calculations have been carried

out on collisions between Br and HCl ($1 \leq v \leq 4$) with translational and rotation energy distributions corresponding to temperatures of 333.3 and 1000 K. The results are summarized in Table 2.

Table 2. Calculated Rate Constants

$\frac{T}{K}$	v	$k_1 + k_2$	k_1	$100k_1$
		$10^{-11} \text{ cm}^3 \text{ molecule}^{-1} \text{ s}^{-1}$	$10^{-11} \text{ cm}^3 \text{ molecule}^{-1} \text{ s}^{-1}$	$k_1 + k_2$
1000	4	8.6	5.6	66.7
	3	7.1	4.5	63.4
	2	2.7	1.5	56.5
	1	~ 0.1	~ 0.05	50
333.3	4	4.6	2.1	46.7
	3	2.3	1.2	51.5
	2	0.3 ₂	0.09	28
	1			

The relative values of the rate constants for different v are in reasonable agreement with the experimental results of Douglas *et al* [1]. For $v \geq 2$ processes (1) and (2) have roughly equal rates with relaxation becoming more effective than reaction as v and T are lowered. Energy transfer occurs in collisions where at some stage in the trajectory $(r_{\text{HCl}}/r_{e,\text{HCl}}) > (r_{\text{HBr}}/r_{e,\text{HBr}})$, i.e. reaction 'nearly' takes place.

The calculations provide strong evidence that process (5b) does not occur in electronically adiabatic collisions. The absolute magnitude of the observed rate constant, and the fact that k_{5b} for DCI is greater than for HCl, indicate that relaxation proceeds via the kind of curve-crossing process that has been proposed by Nikitin [6]. The rate of this process should be approximately proportional to v [7]. Consequently three detailed mechanisms may make roughly equal contributions to the removal of HCl($v=2$) by Br atoms, although this proposal is at variance with the conclusions reached by Douglas, Polanyi and Sloan [1].

REFERENCES

- [1] (a) D. J. Douglas, J. C. Polanyi and J. J. Sloan, *J. Chem. Phys.*, **59**, 6679 (1973) and *Chem. Phys.*, **13**, 15 (1976).
- [2] (a) S. R. Leone, R. G. Macdonald and C. B. Moore, *J. Chem. Phys.*, **63**, 4735 (1975);
 (b) D. Arnoldi, K. Kaufman and J. Wolfrum, *Phys. Rev. Letters*, **34**, 1597 (1975);
 (c) Z. Karny and B. Katz, *Chem. Phys. Letters*, **38**, 382 (1976).
- [3] (a) R. D. H. Brown, G. P. Glass and I. E. M. Smith, *Chem. Phys. Letters*, **32**, 517 (1975) and (b) *J. C. S. Faraday II*, **71**, 1963 (1975).

- [4] S. R. Leone and F. J. Wodarczyk, *J. Chem. Phys.*, 60, 314 (1974).
- [5] (a) I. W. M. Smith and P. M. Wood, *Mol. Phys.*, 25, 441 (1973); (b) I. W. M. Smith, *J. C. S. Faraday II*, 71, 1970 (1975).
- [6] E. E. Nikitin and S. Ya. Umanski, *Faraday Disc. Chem. Soc.*, 53, 7 (1972).
- [7] I. W. M. Smith, *Acct. Chem. Res.*, 9, 161 (1976).

VIBRATIONAL RELAXATION OF HF($v = 1,2,3$) IN THE PRESENCE
OF H_2 , N_2 , AND CO_2

J. F. Bott

The Aerospace Corporation
P. O. Box 92957
Los Angeles, California 90009

The study of vibrational relaxation has greatly increased in the last few years because of the interest in chemical laser. In addition, these chemical lasers have provided the means for performing the experimental studies. Until recently, experiments have been largely confined to relaxation rate measurements for molecules in the first vibrational levels because of the difficulties involved in the controlled production of the higher levels so that specific upper level processes could be isolated. The techniques of direct laser pumping of the second vibrational level, low-pressure combustion with spectroscopic diagnostics, reactive flows in medium-pressure flow tubes, and laser-induced fluorescence by sequential absorption have been used to study upper vibrational level deactivation. Laser-induced fluorescence was used in this study to measure the relaxation rates of HF($v = 1,2,3$) in H_2 , N_2 , O_2 , HCl, and CO_2 .

A laser-induced fluorescence experiment in which the sequential absorption of photons produces the higher vibrational levels in relatively easy to perform, and the interpretation of the data is straightforward. The experiments can be performed with a large ratio of the collision partner to HF, thereby reducing the HF-HF V-V deactivation processes to negligible contributions.

A knowledge of the upper level deactivation rates is important for understanding and modeling the performance of the HF chemical laser since the $F + H_2$ pumping reaction directly populates levels $v = 1, 2$, and 3 . The values for HF(v)- CO_2 deactivation obtained in this experiment can be compared with the theoretical calculations of Dillon and Stephenson and the measured values obtained in more complicated experiments.

The apparatus for this experiment included a HF TEA laser, a fluorescence cell, and several detectors. The TEA laser operated on SF_6 and H_2 and produced laser pulses of a few millijoules with time durations of approximately 100 to 300 nsec. The laser was operated at a repetition rate of ~ 3 Hz without substantial degradation of the fluorescence signal. A concave mirror and a partially transmitting flat formed the laser cavity. No spectral line selection was necessary, and the laser output contained various lines of the $3 \rightarrow 2$, $2 \rightarrow 1$, and $1 \rightarrow 0$ vibrational bands. By appropriate adjustments in the pressures of SF_6 and H_2 , the laser was made to pump the HF to vibrational levels $v = 1, 2$, and 3 or just $v = 1$ and 2 . The pressure tuning determined whether the $1 \rightarrow 0$, $2 \rightarrow 1$, and $3 \rightarrow 2$ laser transitions occurred in the proper sequence or overlapped sufficiently to produce upper level pumping of the HF in the fluorescence cell.

The fluorescence from HF($v = 3$) and HF($v = 2$) were monitored with a RCA C-31034 GaAs photomultiplier and a RCA 7102 (S-1) photomultiplier, respectively. An InSb detector was used to monitor the fluorescence from HF($v = 1$). Spectral filters were used to pass only the desired $3 \rightarrow 0$, $2 \rightarrow 0$, or $1 \rightarrow 0$ fluorescence from HF. The signals from the detector or photomultiplier were recorded with a Biomation 805 transient recorder and transferred to a Nicolet Model 1072 signal averager in which 32 to 512 experiments could be stored and averaged before being displayed on an X-Y recorder.

The relaxation rates of $\text{HF}(v = 3)$ were measured in gas mixtures containing 0.02% HF, 0 to 99.98% H_2 , and a balance of Ar at a total pressure of 20 Torr. The slope of the rates plotted versus H_2 concentration was interpreted as the sum of the V-V transfer rates from $\text{HF}(v = 3)$ to H_2 and the V-R, T deactivation rate of $\text{HF}(v = 3)$ by H_2 . The measured relaxation rates extrapolated to zero H_2 concentration indicated a value that is compatible with the $\text{HF}(v = 3)$ -HF deactivation rate obtained by Osgood and coworkers. Data were also obtained for $\text{HF}(v = 1)$ and $\text{HF}(v = 2)$. Similar data were obtained for the deactivation of $\text{HF}(v)$ by N_2 , O_2 , HCl , and CO_2 .

Although this technique is not applicable to the study of all molecules, it has many advantages for those diatomic molecules capable of laser action on several vibrational, rotational transitions. This technique can most likely be extended to $\text{HF}(v > 3)$ by the use of such fuels as HBr or HI in the pumping laser.

The rates of vibrational energy transfer from the upper vibrational levels of HF to N_2 , O_2 , HCl , and CO_2 increase faster with v than the predicted rates for harmonic oscillators having no energy defect. Part of this increase can be attributed to the decrease in the energy defect, $\Delta E(v)$, with v so that less energy must be absorbed by the rotational and translational degrees of freedom for the transfer of a quantum of energy. However, the dependence of the rates on v can be explained only qualitatively in terms of the anharmonicity of HF and the resulting energy defect dependence on v .

QUENCHING OF $\text{NO}(\text{B}^2\Pi_r)_{v'=0}$ PRODUCED BY THE REACTION OF $\text{N}(^2\text{D})$ WITH N_2O

G. Black, R. L. Sharpless, and T. G. Slanger

Stanford Research Institute
Menlo Park, California 94025

Very little information is available on the quenching of $\text{NO}(\text{B}^2\Pi_r)$, largely because the state has not been observed in NO fluorescence [1]¹. However, $\text{NO}(\text{B}^2\Pi_r)$ can be made and its quenching studied in many other ways. We have used the reaction



as the source of $\text{NO}(\text{B}^2\Pi_r)$, generating the $\text{N}(^2\text{D})$ by photodissociation of N_2O [2]. This reaction produces most of the $\text{NO}(\text{B}^2\Pi_r)$ in the $v'=0$ level [3].

The apparatus for these measurements has been fully described [2]. Previously, [2] we have shown that over the region 1100-1500 Å, the largest quantum yield of $\text{N}(^2\text{D})$ from N_2O occurs between 1150 Å and 1200 Å. Most of the measurements were therefore made at 1175 Å. A Wratten No. 18A filter was used to isolate the 3000-4000 Å region in which the strongest (0, v'') NO β bands occur. For these measurements, a cooled EMI 9635AM was used (dark count at -20°C , ~ 20 counts/sec). The experiments were performed in a very similar way to those described previously [2]. Figure 1 shows plots obtained for $\text{N}_2 = 0$ and 17.2 torr.

In all cases, single exponential decays were observed covering at least one decade change in intensity. Figure 1 shows two effects of adding N_2 --the decay rate increases and the intercept decreases.

The increasing decay rate with quenching gas addition has previously been used [4-6] to determine rate coefficients for quenching $\text{N}(^2\text{D})$. The decay rates shown in Figure 1 give a rate coefficient of $1.96 \times 10^{-14} \text{ cm}^3 \text{ molec}^{-1} \text{ sec}^{-1}$ for the quenching of $\text{N}(^2\text{D})$ by N_2 , in good agreement with the two most recently reported [6,7] values of $(1.5 \pm 0.1) \times 10^{-14}$ and $(1.85 \pm 0.15) \times 10^{-14} \text{ cm}^3 \text{ molec}^{-1} \text{ sec}^{-1}$.

Our main purpose here is to determine rate coefficients for quenching $\text{NO}(\text{B}^2\Pi_r)$ from the decrease in the intercept with quenching gas addition (Figure 1). (Recently, we used similar measurements [8] to study the quenching of $\text{Se}_2(\text{B}^3\Sigma_u^-)$). Absorption by the added gas was always negligible over the ~ 10 cm from the LiF window to the center of the region viewed by the photomultiplier. Therefore, for plots like those shown in

¹Figures in brackets indicate literature references at the end of this paper.

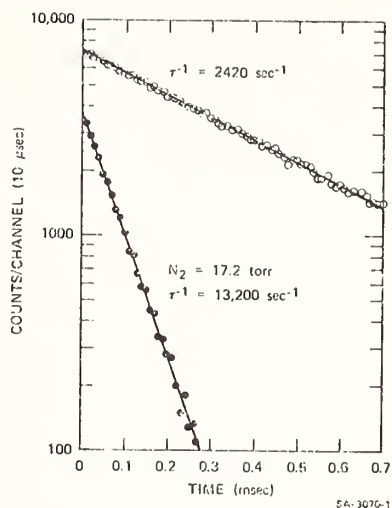


Figure 1. Quenching of $N(^2D)$ and $NO(B^2\Pi_r)_{v'=0}$. Ar = 3 torr; N_2O = 28 mtorr. 20 min. experiments at 1175 Å.

Figure 1, we can write

$$\frac{I_0}{I} = 1 + \frac{\tau k_Q [Q]}{1 + \tau k_{Ar} [Ar] + \tau k_{N_2O} [N_2O]} \quad (2)$$

where I_0 is the intercept at time zero (the time the lamp is pulsed with no quenching gas, I is the intercept with quenching gas addition $[Q]$, τ is the radiative lifetime of $NO(B^2\Pi_r)_{v'=0}$ (3.0×10^{-6} sec), $[Q]$ and k_Q , k_{Ar} , and k_{N_2O} are the rate coefficients for quenching $NO(B^2\Pi_r)_{v'=0}$ by Q , Ar, and N_2O , respectively.

Figure 1 gives $I_0/I = 1.91 \pm 0.09$ for $N_2 = 17.2$ torr. This point and values of I_0/I at several other nitrogen pressures are shown plotted as suggested by Equation (2) in Figure 2. The straight line predicted by Equation (2) is indeed observed. The slope S of this Stern-Volmer plot can be written

$$S = \frac{\tau k_{N_2}}{1 + \tau k_{Ar} [Ar] + \tau k_{N_2O} [N_2O]} \quad (3)$$

To determine k_{N_2} , we must know k_{Ar} and k_{N_2O} . The rate coefficient k_{Ar} was determined with sufficient accuracy for substitution in Equation (3) by making measurements similar to those described above in argon- N_2O mixtures containing N_2O = 15 mtorr and neglecting quenching by N_2O . Below, we described how k_{N_2O} was determined.

The quenching of the intercept by CO_2 was studied at several N_2O pressures from 40 to 760 mtorr. For these experiments, Equation (3) was rearranged:

$$S^{-1} = \frac{1}{\tau k_{\text{CO}_2}} + \frac{k_{\text{Ar}}[\text{Ar}]}{k_{\text{CO}_2}} + \frac{k_{\text{N}_2\text{O}}[\text{N}_2\text{O}]}{k_{\text{CO}_2}} \quad (4)$$

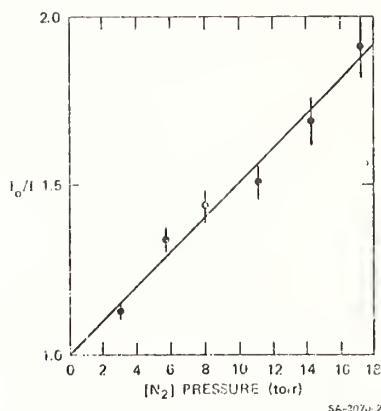


Figure 2. Stern-Volmer plot for N_2 quenching of $\text{NO}(\text{B}^2\Pi_r)_{v'=0}$. Ar = 3 torr; N_2O = 28 mtorr.

where S^{-1} , the reciprocal slope of the Stern-Volmer plots, is the half-quenching pressure. The data for the CO_2 experiments are shown plotted as suggested by Equation (4) in Figure 3. The slope of this graph gives $k_{\text{N}_2\text{O}}/k_{\text{CO}_2} = 4.5 \pm 0.5$, and the intercept, after correcting for the small argon contribution, gives a "true" half-quenching pressure (the pressure at which the rate of quenching by CO_2 equals the rate of radiation) for CO_2 of 1.47 ± 0.2 torr. Hence, $k_{\text{CO}_2} = (7.0 \pm 1.0) \times 10^{-12} \text{ cm}^3 \text{ molec}^{-1} \text{ sec}^{-1}$ (since $\tau = 3.0 \times 10^{-6} \text{ sec}$) and $k_{\text{N}_2\text{O}} = (3.2 \pm 0.8) \times 10^{-11} \text{ cm}^3 \text{ molec}^{-1} \text{ sec}^{-1}$. Table 1 shows true half-quenching pressures and corresponding rate coefficients for several gases, together with the values of Campbell and Thrush [10] for CO_2 , H_2 , and N_2O , and the value of Melton and Klemperer [11] for the quenching of $\text{NO}(\text{B}^2\Pi_r)_{v'=0}$ by NO.

Table 1

Quenching of $\text{NO}(\text{B}^2\Pi_r)_{v'=0}$ at 298°K
 Half-Quenching Pressures and Rate Coefficients

Gas	Half-Quenching Pressure (torr)	Rate Coefficient ($\text{cm}^3 \text{ molec}^{-1} \text{ sec}^{-1}$)	Other values [10,11] ($\text{cm}^3 \text{ molec}^{-1} \text{ sec}^{-1}$)
He	36 ± 6	$(2.9 \pm 0.5) \times 10^{-13}$	
Ar	36 ± 5	$(2.9 \pm 0.4) \times 10^{-13}$	
N_2	17 ± 3	$(6.1 \pm 1.1) \times 10^{-13}$	
CO_2	1.47 ± 0.2	$(7.0 \pm 1.0) \times 10^{-12}$	1.0×10^{-11}
H_2	1.0 ± 0.25	$(1.03 \pm 0.26) \times 10^{-11}$	2.0×10^{-11}
CH_4	0.41 ± 0.09	$(2.5 \pm 0.6) \times 10^{-11}$	
CO	0.36 ± 0.04	$(2.9 \pm 0.3) \times 10^{-11}$	
N_2O		$(3.2 \pm 0.8) \times 10^{-11}$	4.5×10^{-11}
NO			$(1.4 \pm 0.1) \times 10^{-10}$
O_2	0.064 ± 0.013	$(1.6 \pm 0.3) \times 10^{-10}$	
NH_3	0.038 ± 0.009	$(2.7 \pm 0.6) \times 10^{-10}$	
C_2H_4	0.032 ± 0.008	$(3.2 \pm 0.8) \times 10^{-10}$	

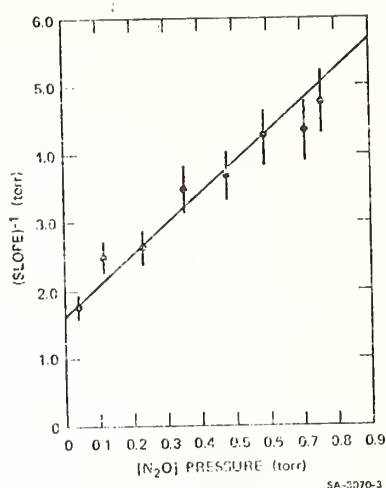


Figure 3. CO₂ quenching data. The reciprocal of the slope of Stern-Volmer graphs vs [N₂O]. Ar = 3 torr.

REFERENCES

- [1] A. B. Callear and I. E. M. Smith, Trans. Faraday Soc. 59, 1720 (1963).
- [2] G. Black, R. L. Sharpless, T. G. Slanger, and D. C. Lorents, J. Chem. Phys. 62, 4266 (1975).
- [3] K. H. Becker and K. H. Welge, Z. Naturforsch., 20a, 442 (1965).
- [4] G. Black, T. G. Slanger, G. A. St. John, and R. A. Yound, J. Chem. Phys. 51, 116 (1969).
- [5] T. G. Slanger, B. J. Wood, and G. Black, J. Geophys. Res. 76, 8430 (1971).
- [6] T. G. Slanger and G. Black, J. Chem. Phys. 64, xxxx (1976).
- [7] D. Husain, S. K. Mitra, and A. N. Yound, J. Chem. Soc. Farad. II 70, 1721 (1974).
- [8] G. Black, R. L. Sharpless, and T. G. Slanger, J. Chem. Phys. 64, 3993 (1976).
- [9] M. Jeunehomme and A. B. F. Duncan, J. Chem. Phys. 41, 1692 (1964).
- [10] I. M. Capbell and B. A. Thrush, J. Quant. Spectrosc. Radiat. Transfer 8, 1571 (1968).
- [11] L. A. Melton and W. Klemperer, J. Chem. Phys. 59, 1099 (1973).

CW INFRARED LASER ISOTOPE SEPARATION:
 $\text{Cl} + \text{CH}_3\text{Br} (\nu_6) \rightarrow \text{HCl} + \text{CH}_2\text{Br}$

T. J. Manuccia and M. D. Clark

Naval Research Laboratory
Washington, DC

and

E. R. Lory

Cornell University
Ithaca, NY

Using a novel CW IR scheme, either Br^{79} or Br^{81} is enriched by vibrational enhancement of the above reaction whose rate is slow compared to the CH_3Br interisotope VV rate. Data from this first reaction studied indicated excellent electrical efficiencies and throughputs should be possible using this scheme to separate a variety of isotopes.

Summary

The attractiveness of the infrared for laser induced chemistry (LIC) and laser isotope separation (LIS) has been stated for some time and stems from the availability of very efficient, scalable lasers, and considerations such as the number of photons per joule and reactivity changes upon excitation of reagent vibrational modes. For example, the large changes in reaction rates associated with shorter wavelength excitation may be of little use in applications such as some LIS schemes where net enrichment is limited by factors such as spectroscopic selectivity or interisotope energy energy exchange.

A serious obstacle to IR gas-phase photochemistry has been distinguishing vibrational enhancements from purely thermal effects. We obviate this problem by observing isotope separation: the non-absorbing isotope serves as a reference reaction, monitoring any temperature rise. Unfortunately, excitation of the non-absorbing isotope can also occur by fast near resonant energy transfer. To overcome this, it is usually stated that the chemistry of the excited state must be fast compared to the rate of VV transfer. This very severe constraint is met by very few reactions and has seriously limited single IR photon LIS work.

We circumvent this difficulty by VT deactivation of the excited states of both isotopic species of the reagent. For the absorbing species, deactivation competes with absorption of photons, but relative rates can be adjusted to allow the absorbing transition to ensure saturation and hence maximize the excited state density. For the non-absorbing isotope, deactivation competes with the rate of resonant energy transfer and can be made to dominate it by reducing the density of the reagent in the reaction vessel. Thus, in principle, one can prepare on a CW basis a sample of reagent with one isotope excited and the other arbitrarily close to thermal equilibrium. With this "competing deactivation" method, we have avoided the constraint of fast chemistry and allowed vibrational enhancement of quite slow reactions to be studied. This may be of interest in itself, or if isotope separation is the goal, this technique allows a controlled trade-off between separation factor and quantum efficiency. In the IR where photons are relatively cheap, this may be economically interesting.

Using this technique, we have studied v_6 mode vibrational enhancement of the reaction $\text{Cl} + \text{CH}_3\text{Br} \rightarrow \text{HCl} + \text{CH}_2\text{Br}$ in a low pressure discharge/flow reactor intracavity to a line selected CW CO_2 laser. The radical produced by the above reaction reacts quickly with excess molecular chlorine to produce the stable product CH_2BrCl which is then detected by an on-line mass spectrometer. A boxcar integrator is used to average the output of the mass spectrometer and calculate isotope ratios. The radical chain formed by the above two reactions is not a priori detrimental to isotopic specificity. It is terminated by heterogeneous recombination before the reaction mixture leaves the irradiation zone. Argon was chosen as the carrier gas and deactivating agent. The available intracavity flux of about 100 W/cm^2 and published deactivation rates set the maximum argon pressure in the 1 to 5 torr range to ensure saturation of the absorbing transition. Assuming an interisotope VV rate of 10 collisions, CH_3Br pressures below 5μ will provide for a large difference in the degree of excitation between the two isotopic species. Under such conditions, the power absorbed per unit volume will be low and thermal effects should be negligible.

With the laser operating on R(14) of the $10 \mu \text{ CO}_2$ band, and the reactor at -100°C , Br^{79} in the CH_2BrCl product is enriched by $3.0 \text{ percent} \pm 0.5 \text{ percent}$, tuning to P(10) of the same band enriches the Br^{81} by $2.0 \text{ percent} \pm 0.5 \text{ percent}$. Other lines produce little effect as expected from small signal absorption measurements we have performed using a spectraphone. The data seem consistent with a single IR photon mechanism. The component of the rate enhancement which is not isotopically selective is only somewhat larger than the selective component and may reflect residual thermal heating, VV exchange or chemical scrambling between enriched products and depleted reagents. The enrichment drops only by a factor of 2 going from -100°C to 20°C , but drops rapidly to zero above room temperature.

With this lab-scale apparatus, throughput of enriched bromine was 122 mg/day with 5.9 MeV of electrical energy (including pumps) spent per product molecule. As the reactor was optically thin and the path included non-reacting gas, improvements of 10^3 in both numbers should be possible by simply changing to a folded optical path without making any other changes.

From the point of view of pressures, flow rates, absorption, coefficients, and in particular, scaling factors, this first reaction studied seems typical of many reactions one might investigate using the method of competing deactivation. As an isotope separation scheme, many reactions exhibit considerably larger vibrational enhancements than $\text{Cl} + \text{CH}_3\text{Br}$ and promise excellent electrical efficiencies and throughputs. As a scheme for investigating the reactivity of vibrationally excited states we have demonstrated sensitivity to changes of less than 1 percent in reaction rate. This scheme has the further advantage that it is reasonably state selective within a given molecule. For example, $v_6 = 2$ of $\text{CH}_3^{79}\text{Br}$ which could be populated by VV processes is not because of the competing VT deactivation. With the exception of one early experiment whose interpretation has been questioned, this seems to be the first demonstration of isotope separation using a cw IR photochemical technique.

APPENDIX I

AUTHOR INDEX

(Underscoring indicates author presentation)

Abramowitz, S.	<u>B2</u>	Corkum, R.	C3
Adamson, A. W.	<u>G1</u>	Crutzen, P. J.	F6
Addington, J. W.	G4	Cu, A.	D3
Akimoto, H.	H8, K8	Curran, A. H.	E3
Albery, W. J.	I1	Cvetanovic, R. J.	F8, <u>P5</u>
Albrecht, A. C.	<u>E8</u>	Damon, E.	K3
Allen, E. R.	<u>K7</u>	Darnall, K. R.	N1, N4
Anastasi, C.	<u>P7</u>	Davidson, J. A.	F5
Anderson, J. G.	F1	Davis, D. D.	<u>F3</u> , <u>N3</u>
Anderson, L. G.	<u>O1</u>	De Armond, M. K.	G3
Archer, M. D.	I1	De Mare, G. R.	<u>O7</u>
Asprey, L. B.	<u>L2</u>	Demas, J. N.	<u>A4</u> , <u>G4</u>
Atkinson, G. H.	<u>O2</u>	DeMore, W. B.	M4
Atkinson, R.	<u>N1</u>	Despres, A.	L5
Ausloos, P.	M3	Dismukes, G. C.	L6
Austin, E. R.	H7	Dodge, M. C.	K9
Back, M. H.	<u>C3</u>	Donnelly, V. M.	E2
Back, R. A.	C3, H6	Donovan, R. J.	<u>M5</u>
Baldwin, G. C.	<u>C8</u>	Dwyer, P.	D5
Balzani, V.	<u>G6</u>	El-Manguch, M.	O4
Barker, J. R.	<u>Q1</u>	El-Sayed, M. A.	L7
Baronavski, A.	E5	Eyler, J. R.	<u>E6</u>
Bass, A. M.	<u>M2</u>	Fajer, J.	<u>J4</u>
Bauer, S. H.	<u>C4</u>	Felder, W.	<u>B1</u>
Bayes, K. D.	<u>Q3</u>	Ferreira, M. I. C.	I1
Bergmark, W. R.	I2	Finkenberg, E.	G7
Bergström, S.	J3	Fisher, P.	G7
Bersohn, R.	H5	Fontijn, A.	B1
Black, G.	F2, <u>R8</u>	Fournier, J.	H9
Bogan, D. J.	<u>B4</u>	Frazier, G. F.	A5
Bolletta, F.	<u>G6</u>	Freund, S. M.	C6, <u>R2</u>
Bondybey, V. E.	L1	Gafney, H. D.	G7
Bott, J. F.	<u>R7</u>	Gandini, A.	<u>H6</u>
Bottenheim, J.	<u>K1</u> , <u>K3</u> , K4	Gay, B. W.	K5
Bowman, W. D.	A4	Gillespie, H. M.	<u>M5</u>
Bowmen, W. R.	I1	Grätzel, M.	I5
Braun, W.	B2, R4	Graham, R. E.	H4
Breitenbach, L.	N2	Grattan, D. W.	P2
Bremer, N.	L3	Gregory, T. A.	O6
Brown, B. J.	L3	Groth, W.	D1
Brown, R. D. H.	R6	Gutierrez, A. R.	<u>G1</u>
Brune, D. C.	J4	Gutman, D.	<u>H4</u>
Brus, L. E.	<u>L1</u>	Hackett, P. A.	<u>H6</u>
Bufalini, J. J.	<u>K5</u>	Hager, S. L.	L6
Calvert, J. G.	<u>K1</u> , K3	Hakala, D.	C8
Campion, A.	<u>L7</u>	Hancock, J. K.	Q5
Carter, W. P. L.	N4	Hansen, I.	P4
Chameides, W. L.	<u>F4</u>	Hanst, P. L.	K5
Chien, K. R.	C4	Harris, E. W.	A4, G4
Cicerone, R. J.	F4	Harvey, R. B.	F4
Clark, H. M.	C8	Heicklen, J.	<u>K6</u>
Clyne, M. A. A.	E3, Q4	Henry, M. S.	<u>D4</u>
Cody, R. J.	<u>E4</u>	Hoffman, M. Z.	<u>D4</u> , I3
Coleman, W. F.	<u>L2</u>	Hoggard, P. E.	<u>G5</u>
Cool, T. A.	<u>RT</u>	Hogo, H.	K9

Höinghaus, K.	P4	McDermid, I. S.	E3
Holmström, B.	J3	McDonald, J. R.	E5
Hoshino, M.	K8	McDowell, R. S.	L2
Howard, C. J.	F5	Menzinger, M.	R3
Hsu, D.S.Y.	Q2	Merrill, J.	G3
Hui, K-K	R1	Michael, J. V.	F7, P6, P8
Hunziker, H. E.	P1	Migirdicyan, E.	L5
Inoue, G.	K8	Miller, R. G.	C2, Q5
Ishiwata, T.	H8	Molina, M. J.	M1
Jacox, M. E.	L9	Monkhouse, P. B.	Q3
Jaffe, S.	M4	Mori, T.	J2
Janda, K.	D5	Morine, G. H.	L3, L6
Janson, T. R.	I4	Niki, H.	N2
Jones, G.	I2	Noonan, R. C.	K5
Jones, L. H.	L2	Noyes, W. A.	O3
Juris, A.	G6	O'Connor, D. V.	J1
Kaduk, B.	B3	Okada, T.	J2
Katz, J. J.	I4	Okuda, M.	K8
Kaufman, F.	E2	Ors, J. A.	D7
Kaufman, K.	M5	Ott, W. R.	A3
Kawasaki, M.	H5	Overend, R.	K2
Keifer, W.	N3	Paine, R. T.	L2
Khe, P. V.	P3	Paraskevopoulos, G.	K2
Killus, J. P.	K9	Parmenter, C. S.	O1
Kirk, A. D.	G5	Parsons, J. M.	H6
Klapthor, R.	D5	Pasch, N. F.	D6
Klose, J. Z.	C7	Paulson, J. F.	E7
Klosterman, N. E.	A2	Payne, W. A.	F7, P6, P8
Knight, A. E. W.	O1	Perry, R.	N1
Koepe, M.	D5	Peterson, S.	G4
Kolts, J. H.	Q4	Philen, D. L.	F3
Krauss, M.	B2	Phillips, D.	O5
Kurylo, M. J.	B2, R4	Pitts, J. N.	N1, N4
Kutschke, K. O.	P2	Plummer, B. F.	D8
Lahmani, F.	D2	Porter, G. B.	G5
Lampe, F. W.	H7	Rebbert, R. E.	M3
Larson, H. B.	J3	Redpath, A. E.	R3
Ledford, A. E.	M2	Reeves, R. R.	C8
Lee, E. K. C.	C2, E1	Ritter, J. J.	C6
Lee, J. H.	P6, P8	Rockley, M. G.	G5
Lee, S. A.	O3	Rockwood, S. D.	C5
Lee, S.-J.	H5	Sabety-Dzvonik, M.	E4
Lejeune, V.	L5	Santhanam, M.	I2
Lesclaux, R.	P3	Savage, C.	N2
Levine, S. Z.	K1	Schiff, H. I.	F5
Lewis, R. B.	L2	Schmatjko, K. J.	R5
Lewis, R. S.	C2	Schmeltekopf, A. L.	F5
Lichtin, N. N.	I3	Schwerzel, R. E.	A2
Lin, D. P.	L6	Scott, L. J.	D8
Lin, M. C.	H2, Q2	Serpone, N.	G6
Lin, S-M	Q1	Setser, D. W.	Q4
Lindsay, J. M.	A5	Sharpless, R. L.	R8
Lipsky, S.	O6	Shedd, A.	D5
Litvak, H.	H5	Shortridge, R. G.	H2
Lloyd, A. C.	N1, N4	Simons, J. P.	H1
Lyman, J. L.	C5	Singleton, D. L.	F8
Maestri, M.	G6	Slanger, T. G.	F2, R8
Maker, P.	N2	Smith, I. W. M.	P7, R6
Manning, R. G.	R4	Spears, K. G.	O4
Martin, T. W.	G2	Srinivasan, R.	D2
Masanet, J.	H9	Stedman, D. H.	F4
Mataga, N.	J2	Stephenson, J. C.	R2
McAfee, J.	F6	Stevens, B.	D7
McBride, R. P.	A4, G4	Stevens, M. V.	G2

Stief, L. J.	P6, <u>P8</u>
Stratton, K.	D5
Streit, G. E.	F5
Stuhl, F.	<u>P4</u>
Su, F.	<u>K3</u>
Swords, M. D.	<u>O5</u>
Tanaka, I.	<u>H8</u>
Tang, K. Y.	<u>E1</u>
Taylor, D. G.	<u>A4</u>
Tchernev, D. I.	<u>I6</u>
Tedder, S. H.	<u>L4</u>
Termonia, M.	07
Testa, A. C.	<u>D3</u>
Thomas, T. F.	<u>E7</u>
Thorsell, D. L.	<u>K3</u>
Timmons, R. B.	P6
Toby, F. S.	B3
Toby, S.	B3
Trappen, N.	<u>L8</u>
Umstead, M. E.	<u>H2</u>
Van, S. P.	<u>J4</u>
Van der Merwe, S. W. J.	R6
Velazco, J. E.	<u>O4</u>
Venkatesh, C. G.	<u>O2</u>
Verber, C. M.	A2
Vermeil, C.	H9
Walters, R. T.	<u>G1</u>
Wampler, F. B.	<u>K4</u>
Ware, W. R.	<u>J1</u>
Washida, N.	<u>K8</u>
Watson, R. T.	<u>F3</u>
Webber, S. E.	D6, <u>L4</u>
Welge, K. H.	<u>C1</u>
Weston, R. E.	<u>Q1</u>
Wettack, F. S.	<u>D5</u>
Whitbeck, M. R.	<u>K1</u>
White, J. M.	03
Whitten, G. Z.	<u>K9</u>
Whytock, D. A.	<u>F7</u> , P6, P8
Wijnen, M. H. J.	H3
Wildes, P. D.	<u>I3</u>
Wilkerson, T. D.	<u>A5</u>
Willard, J. E.	<u>L3</u> , <u>L6</u>
Willis, C.	<u>C3</u>
Windsor, M. W.	<u>G5</u>
Winer, A. M.	N1, N4
Wolfrum, J.	M5, <u>R5</u>
Wright, R. E.	G1
Yardwood, A. J.	07
Zalewski, E. F.	A1
Zellner, R.	<u>P7</u>
Zetzsch, C.	P4

U.S. DEPT. OF COMM. BIBLIOGRAPHIC DATA SHEET	1. PUBLICATION OR REPORT NO. NBS SP-526	2. Gov't Accession No.	3. Recipient's Accession No.
4. TITLE AND SUBTITLE 12th Informal Conference on Photochemistry Proceedings of the 12th Informal Conference on Photochemistry Held at the National Bureau of Standards, Gaithersburg, MD June 28-July 1, 1976		5. Publication Date October 1978	6. Performing Organization Code
7. AUTHOR(S) Michael J. Kurylo and Walter Braun		8. Performing Organ. Report No.	
9. PERFORMING ORGANIZATION NAME AND ADDRESS NATIONAL BUREAU OF STANDARDS DEPARTMENT OF COMMERCE WASHINGTON, D.C. 20234		10. Project/Task/Work Unit No.	11. Contract/Grant No.
12. Sponsoring Organization Name and Complete Address (Street, City, State, ZIP) National Bureau of Standards Department of Transportation Department of Energy National Science Foundation		13. Type of Report & Period Covered	14. Sponsoring Agency Code
15. SUPPLEMENTARY NOTES Library of Congress Catalog Card Number: 78-600105			
16. ABSTRACT (A 200-word or less factual summary of most significant information. If document includes a significant bibliography or literature survey, mention it here.) The 12th Informal Conference on Photochemistry was held at the National Bureau of Standards Laboratories in Gaithersburg, Maryland, from June 28-July 1, 1976. Nearly 300 members of the international scientific community attended the 123 individual research papers presented. Extended abstracts of these presentations (many revised after the Conference) comprise the present proceedings. The wide range of highly specialized topics include Environmental Chemistry (both Photochemical Smog and Upper Atmosphere/Ozone Layer), Laser Photochemistry, Photochemical Isotope Separation, Photochemical Conversion of Solar Energy, Actinometric and Radiometric Measurements, Chemiluminescent Processes, Primary Photochemical and Photophysical Processes, Inorganic Photochemistry, and Elementary Reaction Processes.			
17. KEY WORDS (six to twelve entries; alphabetical order; capitalize only the first letter of the first key word unless a proper name; separated by semicolons) Chemical kinetics; energy transfer; fluorescence; lasers; photochemistry; solar energy; spectra			
18. AVAILABILITY <input checked="" type="checkbox"/> Unlimited <input type="checkbox"/> For Official Distribution. Do Not Release to NTIS <input checked="" type="checkbox"/> Order From Sup. of Doc., U.S. Government Printing Office Washington, D.C. 20402, SD Stock No. SN003-003- <input type="checkbox"/> Order From National Technical Information Service (NTIS) Springfield, Virginia 22151		19. SECURITY CLASS (THIS REPORT) UNCLASSIFIED	21. NO. OF PAGES 411
		20. SECURITY CLASS (THIS PAGE) UNCLASSIFIED	22. Price \$6.00

NBS TECHNICAL PUBLICATIONS

PERIODICALS

JOURNAL OF RESEARCH—The Journal of Research of the National Bureau of Standards reports NBS research and development in those disciplines of the physical and engineering sciences in which the Bureau is active. These include physics, chemistry, engineering, mathematics, and computer sciences. Papers cover a broad range of subjects, with major emphasis on measurement methodology, and the basic technology underlying standardization. Also included from time to time are survey articles on topics closely related to the Bureau's technical and scientific programs. As a special service to subscribers each issue contains complete citations to all recent NBS publications in NBS and non-NBS media. Issued six times a year. Annual subscription: Domestic \$17.00; foreign \$21.25. Single copy, \$3.00 domestic; \$3.75 foreign.

Note: The Journal was formerly published in two sections: Section A "Physics and Chemistry" and Section B "Mathematical Sciences."

DIMENSIONS/NBS

This monthly magazine is published to inform scientists, engineers, businessmen, industry, teachers, students, and consumers of the latest advances in science and technology, with primary emphasis on the work at NBS. The magazine highlights and reviews such issues as energy research, fire protection, building technology, metric conversion, pollution abatement, health and safety, and consumer product performance. In addition, it reports the results of Bureau programs in measurement standards and techniques, properties of matter and materials, engineering standards and services, instrumentation, and automatic data processing.

Annual subscription: Domestic, \$11.00; Foreign \$13.75

NONPERIODICALS

Monographs—Major contributions to the technical literature on various subjects related to the Bureau's scientific and technical activities.

Handbooks—Recommended codes of engineering and industrial practice (including safety codes) developed in cooperation with interested industries, professional organizations, and regulatory bodies.

Special Publications—Include proceedings of conferences sponsored by NBS, NBS annual reports, and other special publications appropriate to this grouping such as wall charts, pocket cards, and bibliographies.

Applied Mathematics Series—Mathematical tables, manuals, and studies of special interest to physicists, engineers, chemists, biologists, mathematicians, computer programmers, and others engaged in scientific and technical work.

National Standard Reference Data Series—Provides quantitative data on the physical and chemical properties of materials, compiled from the world's literature and critically evaluated. Developed under a world-wide program coordinated by NBS. Program under authority of National Standard Data Act (Public Law 90-396).

NOTE: At present the principal publication outlet for these data is the Journal of Physical and Chemical Reference Data (JPCRD) published quarterly for NBS by the American Chemical Society (ACS) and the American Institute of Physics (AIP). Subscriptions, reprints, and supplements available from ACS, 1155 Sixteenth St. N.W., Wash., D.C. 20056.

Building Science Series—Disseminates technical information developed at the Bureau on building materials, components, systems, and whole structures. The series presents research results, test methods, and performance criteria related to the structural and environmental functions and the durability and safety characteristics of building elements and systems.

Technical Notes—Studies or reports which are complete in themselves but restrictive in their treatment of a subject. Analogous to monographs but not so comprehensive in scope or definitive in treatment of the subject area. Often serve as a vehicle for final reports of work performed at NBS under the sponsorship of other government agencies.

Voluntary Product Standards—Developed under procedures published by the Department of Commerce in Part 10, Title 15, of the Code of Federal Regulations. The purpose of the standards is to establish nationally recognized requirements for products, and to provide all concerned interests with a basis for common understanding of the characteristics of the products. NBS administers this program as a supplement to the activities of the private sector standardizing organizations.

Consumer Information Series—Practical information, based on NBS research and experience, covering areas of interest to the consumer. Easily understandable language and illustrations provide useful background knowledge for shopping in today's technological marketplace.

Order above NBS publications from: Superintendent of Documents, Government Printing Office, Washington, D.C. 20402.

Order following NBS publications—NBSIR's and FIPS from the National Technical Information Services, Springfield, Va. 22161.

Federal Information Processing Standards Publications (FIPS PUB)—Publications in this series collectively constitute the Federal Information Processing Standards Register. Register serves as the official source of information in the Federal Government regarding standards issued by NBS pursuant to the Federal Property and Administrative Services Act of 1949 as amended, Public Law 89-306 (79 Stat. 1127), and as implemented by Executive Order 11717 (38 FR 12315, dated May 11, 1973) and Part 6 of Title 15 CFR (Code of Federal Regulations).

NBS Interagency Reports (NBSIR)—A special series of interim or final reports on work performed by NBS for outside sponsors (both government and non-government). In general, initial distribution is handled by the sponsor; public distribution is by the National Technical Information Services (Springfield, Va. 22161) in paper copy or microfiche form.

BIBLIOGRAPHIC SUBSCRIPTION SERVICES

The following current-awareness and literature-survey bibliographies are issued periodically by the Bureau:

Cryogenic Data Center Current Awareness Service. A literature survey issued biweekly. Annual subscription: Domestic, \$25.00; Foreign, \$30.00.

Liquefied Natural Gas. A literature survey issued quarterly. Annual subscription: \$20.00.

Superconducting Devices and Materials. A literature survey issued quarterly. Annual subscription: \$30.00. Send subscription orders and remittances for the preceding bibliographic services to National Bureau of Standards, Cryogenic Data Center (275.02) Boulder, Colorado 80302.

U.S. DEPARTMENT OF COMMERCE
National Bureau of Standards
Washington, D.C. 20234

OFFICIAL BUSINESS

Penalty for Private Use, \$300

POSTAGE AND FEES PAID
U.S. DEPARTMENT OF COMMERCE
COM-215



SPECIAL FOURTH-CLASS RATE
BOOK









